

NISTIR 8271 DRAFT SUPPLEMENT

Face Recognition Vendor Test (FRVT) Part 2: Identification

Patrick Grother
Mei Ngan
Kayee Hanaoka
*Information Access Division
Information Technology Laboratory*

This document is a draft supplement of [NIST Interagency Report 8271](#)

2022/09/26



NISTIR 8271 DRAFT SUPPLEMENT

Face Recognition Vendor Test (FRVT) Part 2: Identification

Patrick Grother
Mei Ngan
Kayee Hanaoka
*Information Access Division
Information Technology Laboratory*

This document is a draft supplement of [NIST Interagency Report 8271](#)

February 2022



U.S. Department of Commerce
Gina M. Raimondo, Secretary

National Institute of Standards and Technology
Laurie E. Locascio, NIST Director and Undersecretary of Commerce for Standards and Technology

RELEASE NOTES

2022-09-23: The 1:N track of the FRVT remains open.

- ▷ This document is the seventeenth draft update to [NIST Interagency Report 8271](#). It contains results for one first-time participant: Intema-LGL Group and T4iSB.
- ▷ The document also includes results for algorithms from two returning developers: Cloudwalk - Moontime Smart Technology, Dermalog, Griaule, Hangzhuo Allu Network Information Technology, Intellivision, Line Corporation, NEC, Sensetime Group, Realnetworks Inc and Vietnam Posts and Telecommunications Group.

2022-07-28: The 1:N track of the FRVT remains open.

- ▷ This document is the seventeenth draft update to [NIST Interagency Report 8271](#). It contains results for one first-time participant: Maxvision.
- ▷ The document also includes results for algorithms from two returning developers: Rank One Computing, and Viettel Group.
- ▷ We have replaced the probe set used in the visa-border benchmark. It was previously comprised of 80 000 images; it now has size 1 212 892 - see amended entries in Table 1. False negative identification rates have increased.
- ▷ We have added images to the probe set used in the visa-kiosk benchmark. It was previously comprised of 21 016 mates and the same number of non-mates; it now has 31 579 mates and 45 460 non-mates - see amended and entries in Table 1. False negative identification rates are improved (reduced) slightly.

2022-06-08: The 1:N track of the FRVT remains open.

- ▷ This document is the seventeenth draft update to [NIST Interagency Report 8271](#). It includes results for algorithms submitted by three first-time participants: Digidata, DiluSense Technology, and Vietnam Posts and Telecommunications Group.
- ▷ The document also includes results for algorithms from five returning developers: Canon Inc, Imagus Technology, Neurotechnology, Thales, and Samsung S1.

2022-04-28: The 1:N track of the FRVT remains open.

- ▷ This document is the sixteenth draft update to [NIST Interagency Report 8271](#). It includes results for algorithms submitted by one first-time participants: Hangzhuo Allu Network Information Technology.
- ▷ The document also includes results for algorithms from three returning developers: HyperVerge Inc, Qnap Security, and Realnetworks Inc.
- ▷ The [1:N results page](#) has been updated.

2022-03-30: The 1:N track of the FRVT remains open.

- ▷ This document is the sixteenth draft update to [NIST Interagency Report 8271](#). It includes results for algorithms submitted by two first-time participants: Intellivision, and Pangiam.
- ▷ The document also includes results for algorithms from three returning developers: Fujitsu Research and Development Center, Idemia, and Gorilla Technology.
- ▷ The [1:N results page](#) has been updated.

2022-02-23: The 1:N track of the FRVT remains open.

- ▷ This document is the fifteenth draft update to [NIST Interagency Report 8271](#). It includes results for algorithms submitted by four first-time participants: Cloudwalk - Moontime Smart Technology, Decatur Industries Inc, NotionTag Technologies Private Limited, and Reveal Media Ltd.

- ▷ The document also includes results for algorithms from three returning developers: Cognitec Systems GmbH, Sensetime Group, and Viettel Group
- ▷ The [1:N results page](#) has been updated.

2022-01-20: The 1:N track of the FRVT remains open.

- ▷ This document is the fourteenth draft update to [NIST Interagency Report 8271](#). It includes results for algorithms recently submitted by two first-time participants: Daon and SQIsoft.
- ▷ The document also includes results for algorithms from five returning developers: Cyberlink Corp, NEC, Neurotechnology, Paravision, and Rank One Computing.
- ▷ The [1:N results page](#) has been updated.

2021-12-16: The 1:N track of the FRVT remains open.

- ▷ This document is the thirteenth draft update to [NIST Interagency Report 8271](#). It includes results for algorithms from six returning developers: Dahua Technology, Imagus Technology, Line Corporation, N-Tech Lab, Qnap Security, and Realnetworks Inc.
- ▷ The [1:N results page](#) has been updated.

2021-11-22: The 1:N track of the FRVT remains open.

- ▷ This document is the twelfth draft update to [NIST Interagency Report 8271](#). It includes results for algorithms recently submitted by three first-time participants Clearview AI, Griaule, and Mantra Softech India.
- ▷ This document and the [1:N results page](#) also include results for algorithms from six returning developers: Acer Incorporated, Canon, Dermalog, Samsung S1, VisionLabs, and Veridas Digital Authentication.

2021-10-28: The 1:N track of the FRVT remains open.

- ▷ This document is the eleventh draft update to [NIST Interagency Report 8271](#). It includes results for algorithms recently submitted by three first-time participants (20Face, Fujitsu Research and Development Center, and Vision-Box), and five returning participants (Alchera, Gorilla Technology, Tevian, Thales-Cogent, and Visidon).
- ▷ Both the main [1:N results page](#) and the small-gallery [paperless travel page](#) have been updated.

2021-09-21: The 1:N track of the FRVT remains open. Three news items:

- ▷ This document is the tenth draft update to [NIST Interagency Report 8271](#). It includes results for algorithms recently submitted by six first-time developers: Cubox, Fincore, HyperVerge, Qnap Security, Staqu Technologies, and Tripleize (Aize, 3-ize).
- ▷ It includes results also for four returning developers: Cognitec Systems, Incode Technologies, Innovatrics, Neurotechnology, and Rank One Computing.

2021-08-02: The 1:N track of the FRVT remains open. Three news items:

- ▷ This document is the ninth draft update to [NIST Interagency Report 8271](#). It includes results for algorithms recently submitted by eight participants: Cyberlink Corp, NEC Corp, N-Tech Lab, Realnetworks Inc., Sensetime Group, Veridas Digital, Viettel Group, and Vigilant Solutions.
- ▷ Algorithms submitted since July 24 will be included in the next update scheduled for September 9, 2021.

- ▷ A new report, NIST Interagency Report 8381 - FRVT Part 7: Identification for Paperless Travel and Immigration, has been released [[PDF](#), [webpage](#)]. It documents the use of FRVT 1:N algorithms in positive access control and immigration status update travel applications where the enrolled population size is as low as 420 people for aircraft boarding, and 42 000 for an airport security line. These population sizes are much smaller than those used in the main [1:N evaluation](#). Going forward, we will update the report and webpage with results for new algorithms.

2021-07-07: The 1:N track of the FRVT remains open. One update:

- ▷ This document is the eighth draft update to [NIST Interagency Report 8271](#). It include results for an algorithm from one participant: Kakao Enterprises.

2021-06-22: The 1:N track of the FRVT remains open. Three updates:

- ▷ This is the seventh draft of the update to [NIST Interagency Report 8271](#). It includes results for algorithms from three new participants: Line Corporation, Rendip, and Samsung S1 Corp.
- ▷ We have also added results for algorithms from five returning developers: Imagus Technology, Kneron, Tevian, Visidon, and Xforward AI Technology.
- ▷ The algorithm-specific report cards (examples: [1](#), [2](#), and [3](#)) now include figures showing how low threshold values can be used to reduce candidate list lengths for human review, while (usually) elevating miss rates (FNIR) only modestly. The reports also feature some minor additions and clarifications.

2021-03-26: The 1:N track of the FRVT remains open. Three updates:

- ▷ This is the sixth draft of the update to [NIST Interagency Report 8271](#). It includes results for algorithms from three returning developers: Neurotechnology, Guangzhou Pixel Solutions, and Tech5 SA.
- ▷ We have added results on the webpage and in the report for a new ageing dataset in which border crossing photos are searched against a gallery of border crossing photos collected between 10 and 15 years prior to the mated search photos. See section 2 for a description of the images. Table 1 has a new entry describing the experiment.
- ▷ We will mostly discontinue running the mugshot ageing test, reserving it for algorithms that show high accuracy on the new border-crossing set.

2021-03-26: Regarding the fifth draft of the update to [NIST Interagency Report 8271](#):

- ▷ In addition have added results for first algorithms from two new participants: Viettel Group and Veridas Digital Authentication Solutions.
- ▷ We have added results for algorithms from two returning developers: Idemia and Cognitec Systems.
- ▷ In addition to the report, the [results page](#) and its hyperlinked [report cards](#) have been updated.

2021-02-08: Regarding the fourth draft of the update to [NIST Interagency Report 8271](#):

- ▷ We have added results for eight algorithms submitted by eight developers: Cyberlink, Dermalog, Imagus, Paravision, Sensetime, Trueface, Vigilant Solutions, and X-Forward AI. With the exception of Trueface, all of these developers have participated previously.
- ▷ We anticipate updating this report again in the first week of March 2021.
- ▷ The main [results page](#) has been revised with tabs for the investigative and lights-out identification tables, and a new tab dedicated to speed and resource consumption.
- ▷ The report cards (example [here](#)) hyperlinked from the [results page](#) have been revised to improve content and format.

2020-12-14: Regarding third draft of the update to [NIST Interagency Report 8271](#):

- ▷ We have added results for fifteen algorithms submitted by thirteen developers. The four first-time participants are: Acer, Akurat Satu Indonesia, Canon, and Xforward AI Technology. The ten returning developers are: AllGoVision, Cyberlink Corp, Dahua Technology, Deepglint, Guangzhou Pixel Solutions, IIT Vision, Innovatrics, Rank One Computing, Scanovate, Sensetime Group, Synesis, and VisionLabs.
- ▷ We have added two new datasets to the evaluation: First a set of “visa-border” photos, representing search of an airport immigration lane photo against a database of closely ISO standard portraits; second a “visa-kiosk” set representing search of a photo collected in a registered traveller kiosk against the same ISO portrait gallery. The images are described in section 2.1.
- ▷ As in previous reports, we include results for searching mugshots against a mugshot gallery containing a single image of each of 12 million people. However we have suspending running searches against a gallery in which multiple lifetime photos per person are present, because this is computationally expensive. We retain a $N = 3$ million search test dedicated to ageing in which mugshots taken up to 18 years after the first photograph are searched - see Table 7.
- ▷ Tables containing computational resource information, Table 2 . . . , now include duration of the finalization step, in which search algorithms can, at their option, build fast-search data structures.
- ▷ We have linked revised per-algorithm PDF report cards from the main [results page](#).
- ▷ We have regenerated all figures and tables to drop algorithms submitted before June 2018. Results for prior algorithms appear in [archived editions](#) of this report.
- ▷ Going forward, we anticipate producing more frequent updates to this report. Developers may submit one algorithm to this evaluation every four calendar months.

2020-03-24: Regarding the second draft of the update to [NIST Interagency Report 8271](#):

- ▷ Adds results for three algorithms from three developers, Dermalog, Innovatrics, and Synesis.
- ▷ Adds Table 7 on ageing showing the increase in false negative rates with time elapsed between two photos. Some of the results were contained in graphs in prior editions of this report, but the table adds results for some newly submitted algorithms.
- ▷ Adjusts frontal mugshot results (for recent and lifetime consolidated galleries) to include the effect of removing some images that should not have been included in image test sets. These images were mostly profile views, images of tattoos containing faces, images of faces on tee shirts, and images of photographs on walls behind the intended subject. This affects many tables and reduces false negative identification rates for all algorithms. The reduction is larger for “recent” enrollments than for “lifetime consolidated” ones with the consequence that accuracy on recent images is now superior.

2020-02-26: Regarding the first draft of the update to [NIST Interagency Report 8271](#):

- ▷ Adds results for 38 algorithms from 31 different developers, eleven of whom are entirely new to the 1:N track of FRVT. These are Allgovision, Cyberlink, Deepsea Tencent, Farbar F8, Imperial College London, Intsys MSU, Kedacom, Kneron, Pixelall, and Scanovate.

DISCLAIMER

Specific hardware and software products identified in this report were used in order to perform the evaluations described in this document. In no case does identification of any commercial product, trade name, or vendor, imply recommendation or endorsement by the National Institute of Standards and Technology, nor does it imply that the products and equipment identified are necessarily the best available for the purpose.

INSTITUTIONAL REVIEW BOARD

The National Institute of Standards and Technology's Research Protections Office reviewed the protocol for this project and determined it is not human subjects research as defined in Department of Commerce Regulations, 15 CFR 27, also known as the Common Rule for the Protection of Human Subjects (45 CFR 46, Subpart A).

ACKNOWLEDGMENTS

The authors are grateful for the support and collaboration of the the Department of Homeland Security's Science & Technology Directorate (S&T), Office of Biometric Identity Management (OBIM), and Customs and Border Protection (CBP).

Additionally, the authors are grateful to staff in the NIST Biometrics Research Laboratory for infrastructure supporting rapid evaluation of algorithms.

Executive Summary

This document is a draft revision of the September 2019 report [NIST Interagency Report 8271](#). That report gave extensive documentation of face recognition applied to mugshots. This report extends that by adding more two more challenging datasets containing images with serious departures from canonical frontal image standards. The report also adds results for algorithms submitted to NIST since in 2019 and 2020. The algorithms, which implement one-to-many identification of faces appearing in two-dimensional images, are prototypes from the research and development laboratories of mostly commercial suppliers, and are submitted to NIST as compiled black-box libraries implementing a NIST-specified C++ test interface. The report therefore does not describe how algorithms operate. The report lists accuracy results alongside developer names and will therefore be useful for comparison of face recognition algorithms and assessment of absolute capability. The report is accompanied by a [webpage](#) with sortable results.

The evaluation uses six datasets: frontal mugshots, profile view mugshots, desktop webcam photos, visa-like immigration application photos, immigration lane photos, and registered traveler kiosk photos. These datasets are sequestered at NIST, meaning that developers do not have access to them for training or testing. This aspect is important because face recognition algorithms are very often deployed without the developer having access to the customers image data. A possible exception to this would be in a cloud-based application where the operational image data is uploaded to a cloud operated by a face recognition developer.

The major result in NIST IR 8271 was that massive gains in accuracy have been achieved in the years 2013 to 2018 and these far exceed improvements made in the prior period, 2010 to 2013. While the industry gains were broad - at least 30 developers' algorithms outperformed the most accurate algorithm from late 2013, there remains a wide range of capability. While this report shows accuracy gains only over the period 2018-2020, the most accurate algorithm reported here is substantially more accurate than anything reported in NIST IR 8271. This is evidence that face recognition development continues apace, and that FRVT reports are but a snapshot of contemporary capability.

From discussion with developers, the accuracy gains stem from the adoption of deep convolutional neural networks. As such, face recognition has undergone an industrial revolution, with algorithms increasingly tolerant of poorly illuminated and other low quality images, and poorly posed subjects. One related result is that a few algorithms correctly match side-view photographs to galleries of frontal photos, with search accuracy approaching that of the best c. 2010 algorithms operating on purely frontal images. The capability to recognize under a 90-degree change in viewpoint - pose invariance - has been a long-sought milestone in face recognition research.

With good quality portrait photos, the most accurate algorithms will find matching entries, when present, in galleries containing 12 million individuals, with rank one miss rates of approaching 0.1%. The remaining errors are in large part attributable to long-run ageing, facial injury and poor image quality. Given this impressive achievement - close to perfect recognition - an advocate might claim that cooperative face recognition is a solved problem, a statement that can be refuted with the following context and caveats:

- ▷ **Mugshots vs. less constrained captures:** The low error rates reported here are attained using mostly excellent cooperative live-capture mugshot images collected with an attendant present. Recognition in other circumstances, particularly those without a dedicated photographic environment and human or automated quality control checks, will lead to declines in accuracy. This is documented here for side-view images, poorer quality webcam images, and, particularly, for newly introduced ATM-style kiosk photos that were not originally intended for automated face recognition. In this case, recognition error rates are much higher, often in excess of 20% even with the more accurate algorithms which variously remain intolerant of face cropping (at image edge) and of large downward head pitch.
- ▷ **Algorithm accuracy spectrum:** Recognition accuracy is very strongly dependent on the algorithm and, more

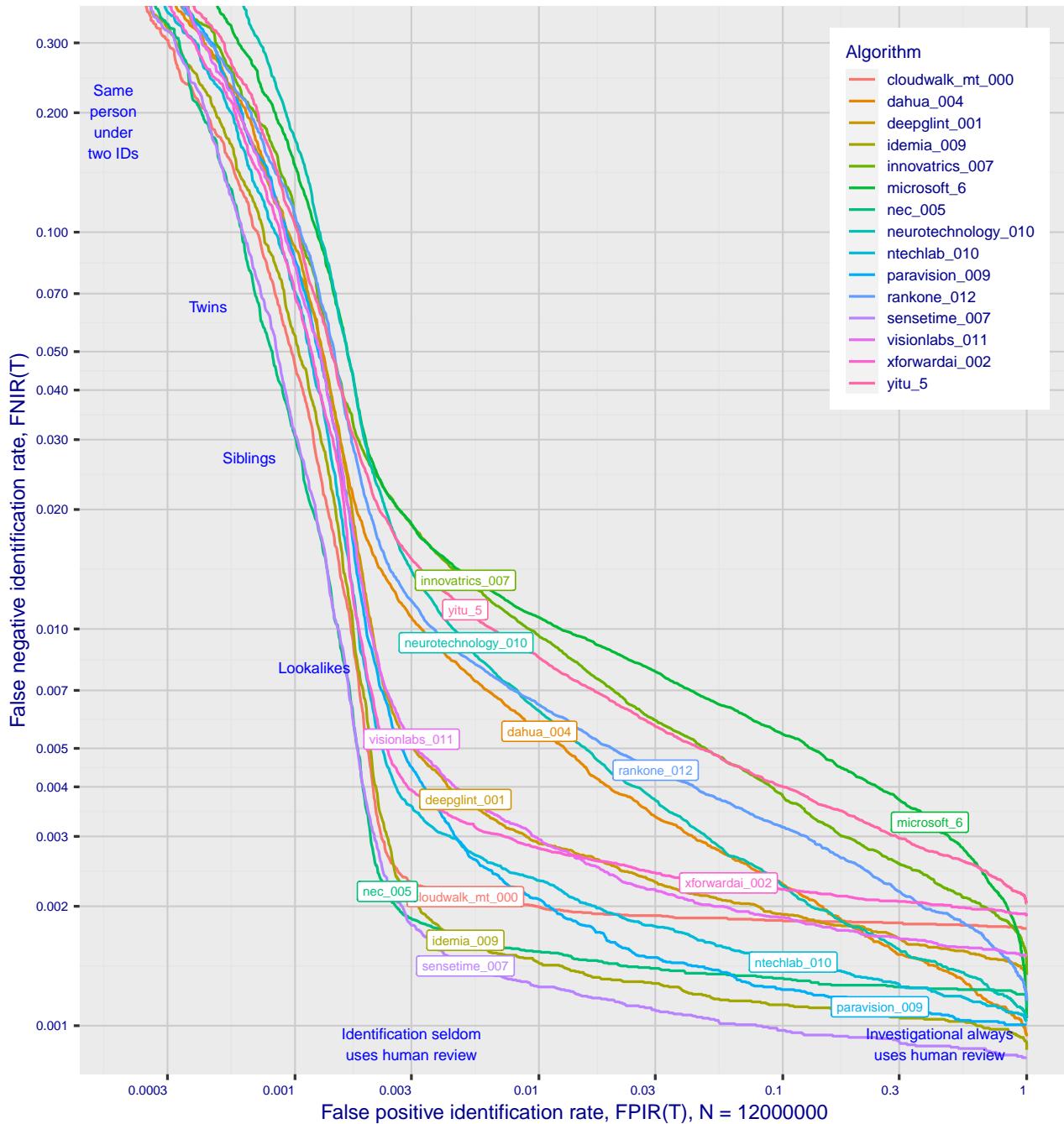


Figure 1: Identification miss rates across the false positive range. $N = 12$ million individuals are enrolled with one recent image.

generally, on the developer of the algorithm. False negative error rates in a particular scenario range from a few tenths of one percent to beyond fifty percent. This is tabulated exhaustively later: For example Table 11 shows accuracy across datasets. Figure 1 here compares algorithms on mugshot searches in a consolidated gallery of 12 million subjects and 12 million photos. Many algorithms do not achieve the low error rates noted above, and while many of those may still be useful and valuable to end-users, only the most accurate excel on poor quality images and those collected long after the initial enrollment sample.

▷ **Versioning:** While results for up to ten algorithms from each developer are reported here, the intra-provider

accuracy variations are usually smaller than the inter-provider variations. That said different versions give an order of magnitude fewer misses. Some developers demonstrate speed-accuracy tradeoffs¹. See Figs. 18, 19.

- ▷ **Low similarity scores:** In thousands of mugshot cases the correct gallery image is returned at rank 1 but its similarity score is nevertheless low, below some operationally required score threshold. This is not so important when face recognition is used for “lead generation” in investigational applications because human reviewers are specifically required to review potentially long candidate lists and the threshold is effectively 0. In applications where search volumes are higher and labor is not available to review the results from searches, a higher threshold must be applied. This reduces the length of candidate lists and false positive identification rates at the expense of increased false negative miss rates. The tradeoff between the two error rates is reported extensively later.
- ▷ **Population size:** As the number of enrolled subjects grows, some mates are displaced from rank one, decreasing accuracy. As tabulated later for N up to 12 million, false negative rates generally rise slowly with population size. This enables use of face recognition in very large populations. However in most positive and negative identification applications², a score threshold is set to limit the rate at which non-mate searches produce false positives. This has the consequence that some mated searches will report the mate below threshold, i.e. a miss, even if it is at rank 1. The utility of this is that many non-mated searches will return no candidate identities at all. As the error-tradeoff characteristic shows, investigational miss rates on the right side are very low but then rise steadily (in the center region) as threshold is increased to support “lights-out” applications, and ultimately rise quickly (left side) as discussed below. Thus, if we demand that just one in one thousand non-mate searches produce any false positives, the most accurate algorithms there (Sensetime-004 and NEC-3) would fail on between 3 and 5% of mated searches. Even though the graph shows results for the most accurate algorithms, all but two would fail to find the mate in more than 8% of mated searches. While the two most accurate algorithms produce a relatively flat error tradeoff until the threshold is raised to limit false positives to about 1 in 400 non-mated searches³.

Thereafter, as the threshold is raised to further reduce false positives, miss rates rise rapidly. This means that low false positive identification rates are inaccessible with these algorithms, a result that does not apply for ten-finger identification algorithms. The rapid rise occurs because the lower mate scores are mixed with very high non-mate scores, the low scores from poor image quality and ageing, the high non-mates from the presence of lookalikes persons (doppelgangers), twins (discussed next) and, ultimately, the presence of a few unconsolidated subjects i.e. persons present under multiple IDs.

- ▷ **False negatives from ageing:** A large source of error in long-run applications where subjects are not re-enrolled on a set schedule is ageing. Changes in facial appearance increase with the time elapsed between photographs. These will depress similarity scores and eventually cause false negatives. All faces age and while this usually proceeds in a graceful and progressive manner, drug use can accelerate this [28]. Elective surgery may be effective in delaying it although this has not been formally quantified with face recognition. As ageing is essentially unavoidable, it can only be mitigated by scheduled re-capture, as in passport re-issuance. To quantify ageing effects, we used the more accurate algorithms to enroll the earliest image of 3.1 million adults and then search

¹For example, NEC-0 prepares templates much faster than NEC-2 but gives twenty times more misses. Dermalog-5 executes a template search much more quickly than Dermalog-6 but is also much less accurate.

²In a positive identification application such as a registered traveler system, a user is making an implicit claim to be enrolled in the system - most users will be. In a negative application, such as with deportees, the implicit claim is that the subject is not enrolled - most will not be.

³The gallery size here is 12 million people, one image per person. Given 331 201 non-mated searches, an exhaustive implementation of one-too-many search would execute almost 4 trillion comparisons. At a false positive identification rate of 0.0025 the number of false positives is, to first order, 828 corresponding to single-comparison false match rate of $828 / 4 \text{ trillion} = 2.1 \times 10^{-10}$ i.e. about 1 in 5 billion. Strictly this FMR computation is meaningful only for algorithms that implement 1:N search using N 1:1 comparisons, which is not always the case.

with 10.3 million newer photos taken up to 18 years after the initial enrollment photo. Figure 2 puts ageing into context by contrasting it with the increase in false negatives that occurs when the number of individuals in an enrollment database becomes larger and the chance of a false positive increases such that higher thresholds may become necessary⁴.

The Figure shows, from top to bottom, increases in false negative identification rates (FNIR) with the algorithm being tested. This applies to increases due to N on the left side, and increases due to ageing on the right side. The relative spacing of the dots shows that for all algorithms the dependency of FNIR on N (up to 12 million) is considerably less than on ΔT (up to 18 years).

In the inset table, accuracy is seen to degrade progressively with time, as mate scores decline and non-mates displace mates from rank 1 position. More accurate algorithms tend to be less sensitive to ageing. The more accurate algorithms give fewer errors after 18 years of ageing than middle tier algorithms give after four. Note also we do not quantify an ageing rate - more formal methods [2] borrowed from the longitudinal analysis literature have been published for doing so (given suitable repeated measures data). See Figures 60, 87 and 100.

⁴Some algorithms implement strategies to automatically adjust scores to account for increased population size. This relieves the system owner of having to increase thresholds as N increases.

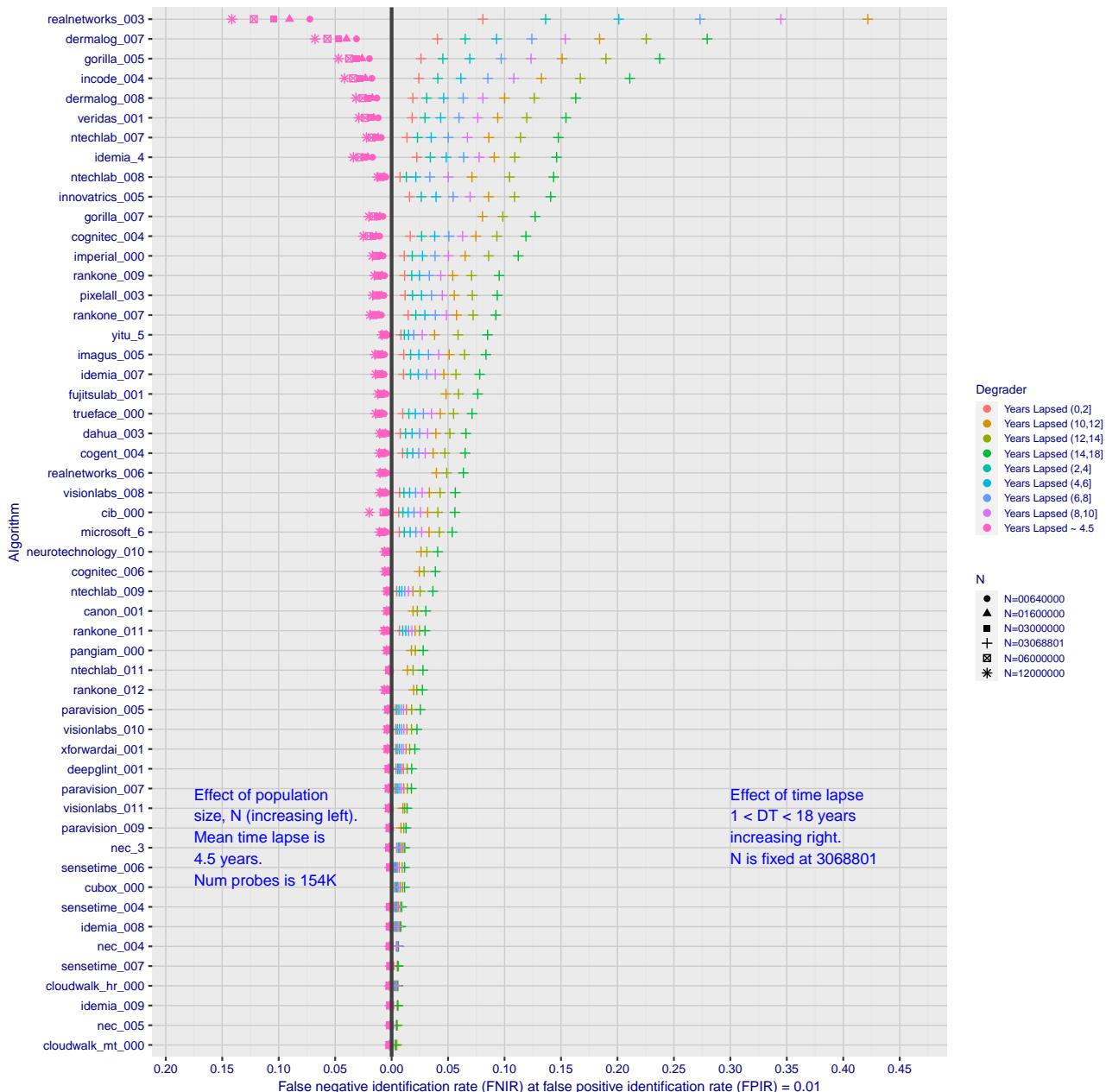
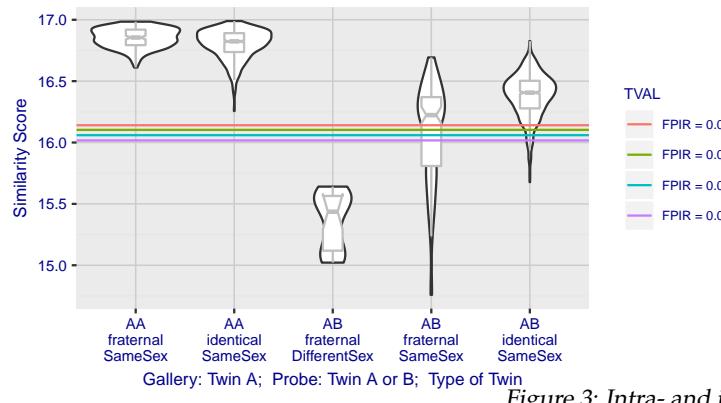


Figure 2: Identification miss rates as a function of enrolled population size, N , and time-lapse, ΔT .



▷ **False positives from twins:** By enrolling 640 000 mugshots, adding photos of one twin, and then searching photos of those subjects and their twin the inset figure shows, for one typical algorithm, the similarity is generally greater when searching twins against themselves (A) than when searching twins against their sibling (B) but very often still above even stringent thresholds i.e. those corresponding to one in one thousand searches producing a false positive. Thus twins will very often produce a high-scoring non-match on a candidate list and a false alarm in an online identification system. The plot of Fig. 3 shows that fraternal twins are sometimes correctly rejected at those thresholds - including most different sex twins (at center). Figure ?? shows substantially similar behavior for all algorithms tested. In an investigative search, a twin would typically appear at rank 1, or rank 2 if their sibling happened to also be the gallery. Twins (and triplets etc.) constituted 3.3% of all live births [17] in recent years⁵, and because that number is higher today than when the individuals in current adult databases were born, the false positives that arise from twins are now, and will increasingly be, an operational problem. Relative to the United States, twins are born with considerable regional variation. For example they are much less common in East Asia, and much more common in Sub-Saharan Africa [21].

The presence of twins in the mugshot database is inevitable given its size, around 12.3 million people. As this is not an insignificant sample of the domestic United States population, people with other familial ties will be present also. The data was collected over an extended period and because location information is not available, we are unable to estimate the proportion of the domestic population that is present in the dataset. However, if we assume twins are neither more or less disposed to arrest than the general population, we can estimate that hundreds of thousands of individuals in the dataset are twins. This will affect false positive rates because we randomly set aside 331 201 individuals for nonmate searches, and some proportion of those will be twins with siblings in the gallery.

▷ **Database integrity:** An operational error rate should be added to all false negative rates in this report reflecting the proportion of images in a real database that are un-matchable. Such anomalies arise from images that: do not contain a face; include multiple persons; cannot be decoded; are rotated by 90° or 180°; depict a face on clothing; and others introduced by a long tail of various clerical errors. While the mugshot trials in this report have been constructed to minimize such effects, they are a real problem in actual operations.

This report is being updated continuously as new algorithms are submitted to FRVT, and run on new datasets. Participation in the [one-to-many identification track](#) is independent of participation in the [one-to-one verification track](#) of FRVT.

⁵See the CDC's National Vital Statistics Report for 2017: https://www.cdc.gov/nchs/data/nvsr/nvsr67/nvsr67_08-508.pdf

Scope and Context

Audience: This report is intended for developers, integrators, end users, policy makers and others who have some familiarity with biometrics applications. The methods and metrics documented here will be of interest to organizations engaged in tests of face recognition algorithms. Some of these have been incorporated in the ISO/IEC 19795 Part 1 Biometric Testing and Reporting Framework standard, now nearing publication.

Prior benchmarks: Automated face recognition accuracy has improved massively in the two decades since initial commercialization of the various technologies. NIST has tracked that improvement through its conduct of regular independent, free, open, and public evaluations. These have fostered improvements in the state of the art. This report serves as an update to the [NIST Interagency Report 8271](#) on performance of face identification algorithms, published in September 2019.

Demographics: In December 2019, NIST published a first report on demographic dependencies in face recognition, [NIST Interagency Report 8280](#) that documented age, sex and race differentials in one-to-one and one-to-many false positive and false negative rates.

Scope: NIST IR 8271 documented recognition results for four databases containing in excess of 30.2 million still photographs of 14.4 million individuals. That constituted the largest public and independent evaluation of face recognition ever conducted. It includes results for accuracy, speed, investigative vs. identification applications, scalability to large populations, use of multiple images per person, images of cooperative and non-cooperative subjects.

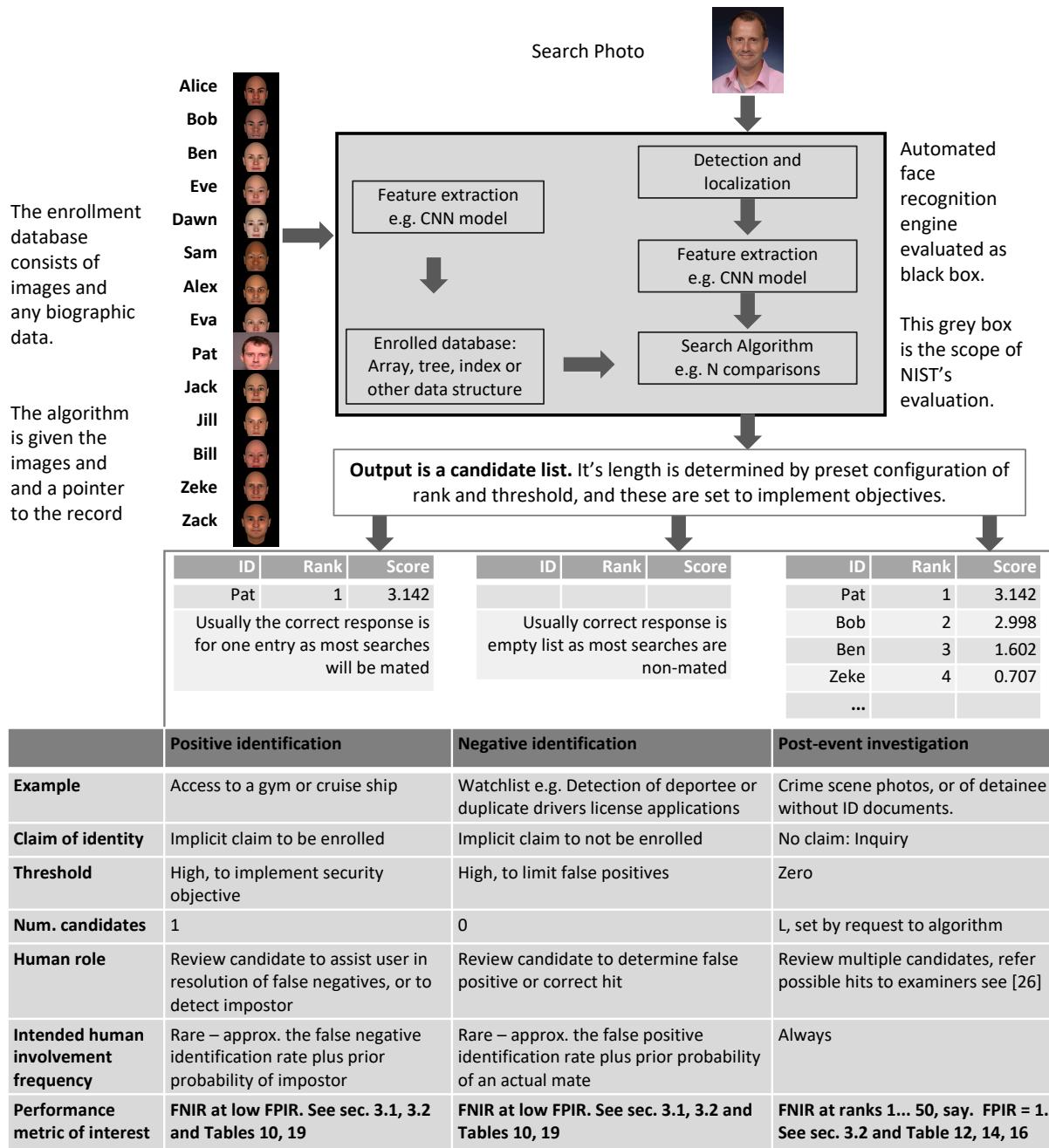
The report also includes results for ageing, recognition of twins, and recognition of profile-view images against frontal galleries. It otherwise does not address causes of recognition failure, neither image-specific problems nor subject-specific factors including demographics. Separate reports on demographic dependencies in face recognition will be published in the future. Additionally out of scope are: performance of live [human-in-the-loop transactional systems](#) like automated border control gates; human recognition accuracy as used in forensic applications; and recognition of persons in video sequences (which NIST evaluated separately [9]). Some of those applications share core matching technologies that *are* tested in this report.

Images: Five kinds of images are employed; these are either compared with images of the same kind, or against others from different capture environments as follows. The primary dataset is a set of law enforcement mugshot images (Fig. 5) which are enrolled and then searched with three kinds of images: other mugshots (i.e. within-domain); profile-view photographs (90 degree cross-view); and lower quality webcam images (Fig. 6) collected in similar detention operations (cross-domain). Additionally we compare high quality visa-like photos collected in immigration offices, with: medium quality border crossing images collected in primary immigration lanes; poor quality images collected in ATM-like registered traveller kiosks.

Participation and industry coverage: The report includes performance figures for prototype algorithms from the research laboratories of commercial developers and a few universities. This represents a substantial majority of the face recognition industry, but only a tiny minority of the academic community. Participation was open worldwide. While there is no charge for participation, developers incur some software engineering expense in implementing their algorithms behind the NIST application programming interface (API). The test is a black-box test where the function of the algorithm, and the intellectual property associated with it, is hidden inside pre-compiled libraries.

Recent technology development: Most face recognition research with deep convolutional neural networks (CNNs) has been aimed at achieving invariance to pose, illumination and expression variations that characterize photojournalism and social media images. The initial research [18, 22] employed large numbers of images of relatively few ($\sim 10^4$) individuals to learn invariance. Inevitably much larger populations ($\sim 10^7$) were employed for training [11, 20] but the benchmark, Labeled Faces in the Wild with (essentially) an equal error rate metric [12], represents an easy task,

one-to-one verification at very high false match rates. While a larger scale identification benchmark duly followed, Megaface [15], its primary metric, rank one hit rate, contrasts with the high threshold discrimination task required in most large-population applications of face recognition, namely credential de-duplication, and background checks. There, identification in galleries containing up to 10^8 individuals must be performed using a) very few images per individual and b) stringent thresholds to afford very low false positive identification rates. This track of FRVT was launched to measure the capability of the new technologies, including in these two cases. FRVT has included open-set identification tests since 2002, reporting both false negative and positive identification rates [7].



Performance metrics for applications: This report documents the performance of one-to-many face recognition algorithms. The word "performance" here refers to recognition accuracy and computational resource usage, as measured

by executing those algorithms on massive sequestered datasets.

This report includes extensive tabulation of recognition error rates germane to the main use-cases for face search technology. The Figure below, inspired by the Figure 1 in [23] differentiates different applications of the technolgy. The last row directs readers to the main tables relevant to those applications, respectively threshold-based and rank-based metrics that are special cases of the metrics given in section 3. The terms negative identification and positive identification are taken from the ISO/IEC 2382-37:2017 standardized biometrics vocabulary.

The algorithms are specifically configured for these applications by setting thresholds and candidate list lengths. Both rank-based metrics and threshold-based metrics include tradeoffs. In investigation, overall accuracy will be reduced if labor is only available to review a few candidates from the automated system. Note that when a fixed number of candidates are returned, the false positive identification rate of the automated face recognition engine will be 100%, because a probe image of anyone not enrolled will still return candidates. In identification applications where false positives must be limited to satisfy reviewer labor availability or a security objective, higher false negative rates are implied. This report includes extensive quantification of this threshold-based tradeoff.

See Sec. 3

Template diversity: The FRVT is designed to evaluate black-box technologies with the consequence that the templates that hold features extracted from face images are entirely proprietary opaque binary data that embed considerable intellectual property of the developer. Despite migration to CNN-based technologies there is no consensus on the optimal feature vector dimension. This is evidenced by template sizes ranging from below 100 bytes to more than four kilobytes. This diversity of approaches, suggests there is no prospect of a standard template something that would require a common feature set to be extracted from faces. Interoperability in automated face recognition remains solidly based on images and documentary standards for those, in particular the ICAO portrait [27] specification deriving from the ISO/IEC 19794-5 Token frontal [24] standard, which are similar to certain ANSI/NIST Type 10 [26] formats.

Training: The algorithms submitted to NIST have been developed using image datasets that developers do not disclose. The development will often include application of machine learning techniques and will additionally involve iterative training and testing cycles. NIST itself does not perform any training and does not refine or alter the algorithm in any way. Thus the model, data files, and libraries that define an algorithm are fixed for the duration of the tests. This reflects typical operational reality where recognition software, once installed, is fixed and constant until upgraded. This situation persists because on-site training of algorithms on customer data is atypical essentially because training is not a turnkey process.

Automated search and human review: Virtually all applications using automated face search require human review of the outputs at some frequency: Always for investigational applications; rarely in positive identification applications, after rejection (false or otherwise); and rarely in negative identification applications, after an alarm (false or otherwise). The human role is usually to compare a reference image with the query image or the live-subject if present, to render either a definitive decision on “exclusion” (different subjects), or “identification” (same subject), or a declaration that one or both images have “no value” and that no decision can be made. Note that automated face recognition algorithms are not built to do exclusion - low scores from a face comparison arise from different faces *and* poor quality images of the same face.

Human reviewers make recognition errors [5, 19, 25] and are sensitive to image acquisition and quality. Accurate human review is supported by high resolution - as specified in the Type 50, 51 acquisition profiles of the ANSI/NIST Type 10 record [26], and by multiple non-frontal views as specified in the same standard. These often afford views of the ear. Organizations involved in image collection should consider supporting human adjudication by collecting high-resolution frontal and non-frontal views, preparing low resolution versions for automated face recognition [24], and retaining both for any subsequent resolution of candidate matches. Along these lines, the ISO/IEC Joint Technical

Committee 1 subcommittee 37 on biometrics has just initiated projects on image quality assessment and face-aware capture.

Release Notes

FRVT Activities: Since February 2017, NIST has been evaluating one-to-one verification algorithms on an ongoing basis. NIST then restarted FRVT's one-to-many track in February 2018, inviting participants to send up to prototype algorithms. Both tracks allows developers to submit updated algorithms to NIST at any time but no more frequently than four calendar months. This more closely aligns development and evaluation schedules. Results are posted to the web within a few weeks of submission. Details and full report are linked from the [Ongoing FRVT site](#).

FRVT Reports: The results of the FRVT appear in the series NIST Interagency Reports tabulated below. The reports were developed separately and released on different schedules. In prior years NIST has mostly reported FRVT results as a single report; this had the disadvantage that results from completed sub-studies were not published until all other studies were complete.

Date	Link	Title	No.
2014-03-20	PDF	FRVT Performance of Automated Age Estimation Algorithms	7995
2015-04-20	PDF	Face Recognition Vendor Test (FRVT) Performance of Automated Gender Classification Algorithms	8052
2014-05-21	PDF	FRVT Performance of face identification algorithms	8009
2017-03-07	PDF	Face In Video Evaluation (FIVE) Face Recognition of Non-Cooperative Subjects	8173
2017-11-23	PDF	The 2017 IARPA Face Recognition Prize Challenge (FRPC)	8197
2018-11-27	PDF	Face Recognition Vendor Test - Part 2: Identification	8271
2019-09-11	PDF	Face Recognition Vendor Test - Part 2: Identification	8271
2019-12-11	PDF	Face Recognition Vendor Test - Part 3: Demographic Effects	8280
2020-01-03	WWW	Face Recognition Vendor Test (FRVT) - Part 1 Verification	Draft

Details appear on pages linked from <https://www.nist.gov/programs-projects/face-projects>.

Appendices: This report is accompanied by appendices which present exhaustive results on a per-algorithm basis. These are machine-generated and are included because the authors believe that visualization of such data is broadly informative and vital to understanding the context of the report.

Typesetting: Virtually all of the tabulated content in this report was produced automatically. This involved the use of scripting tools to generate directly type-settable L^AT_EX content. This improves timeliness, flexibility, maintainability, and reduces transcription errors.

Graphics: Many of the Figures in this report were produced using the **ggplot2** package running under **R**, the capabilities of which extend beyond those evident in this document.

Contents

Release Notes	1
Disclaimer	5
Institutional Review Board	5
Acknowledgments	5
Executive Summary	6
Scope and Context	12
Release Notes	16
1 Introduction	18
2 Evaluation datasets	19
3 Performance metrics	25
4 Results	41
Appendices	81
A Accuracy on large-population FRVT 2018 mugshots	81
B Effect of time-lapse: Accuracy after face ageing	126
C Effect of enrolling multiple images	249
D Accuracy with poor quality webcam images	256
E Accuracy for profile-view to frontal recognition	266
F Search duration	270
G Gallery Insertion Timing	280

1 Introduction

One-to-many identification represents the largest market for face recognition technology. Algorithms are used across the world in a diverse range of biometric applications: detection of duplicates in databases, detection of fraudulent applications for credentials such as passports and driving licenses, token-less access control, surveillance, social media tagging, lookalike discovery, criminal investigation, and forensic clustering.

This report contains a breadth of performance measurements relevant to many applications. Performance here refers to accuracy and resource consumption. In most applications, the core accuracy of a facial recognition algorithm is the most important performance variable. Resource consumption will be important also as it drives the amount of hardware, power, and cooling necessary to accommodate high volume workflows. Algorithms consume processing time, they require computer memory, and their static template data requires storage space. This report documents these variables.

1.1 Open-set searches

FRVT tested open-set identification algorithms. Real-world applications are almost always “open-set”, meaning that some searches have an enrolled mate, but some do not. For example, some subjects have truly not been issued a visa or drivers license before; some law enforcement searches are from first-time arrestees⁶. In an “open-set” application, algorithms make no prior assumption about whether or not to return a high-scoring result, and for a mated search, the ideal behaviour is that the search produces the correct mate at high score and first rank. For a non-mate search, the ideal behavior is that the search produces zero high-scoring candidates.

Many academic benchmarks execute only closed-set searches. The proportion of mates found in the rank one position is the default accuracy metric. This hit rate metric ignores the score with which a mate is found; weak hits count as much as strong hits. This ignores the real-world imperative that in many applications it is necessary to elevate a threshold to reduce the number of false positives.

⁶Operationally closed-set applications are rare because it is usually not the case that all searches have an enrolled mate. One counter-example, however, is a cruise ship in which all passengers are enrolled and all searches should produce exactly one identity. Another example is forensic identification of dental records from an aircraft crash.

2 Evaluation datasets

This report documents accuracy for four kinds of images - mugshots, webcam, profiles and wild - as described in the following sections.

2.1 Immigration-related images

This report includes benchmark tests sharing a common enrollment of high quality frontal portrait images collected while subject make applications for various immigration benefits. We then search that with two kinds of images, webcam images collected during in-bound immigration and also images collected from registered travelers using a ATM-style kiosk. These are described below and depicted in Figure 4.



Figure 4: Example photos.

- ▷ **Application reference photos:** The images are collected in an attended interview setting using dedicated capture equipment and lighting. The images, at size 300x300 pixels, are smaller than normally indicated by ISO. The images are all high-quality frontal portraits collected in immigration offices and with a white background. As such, potential quality related drivers of high false match rates (such as blur) can be expected to be absent. The images are encoded as ISO/IEC 10918-1 i.e. JPEG. Older images had a compression ration of about 16:1, while newer images, since 2010, are more lightly compressed at 4:1. When these images are provided as input into the algorithm, they are labeled with the type "iso". This report enrols 1 600 000 application images, one per person.
- ▷ **Border crossing photos:** Most images are have width 320 and height 240 pixels. They are JPEG compressed at 16:1 i.e. filesize just below 15KB. The images present challenges for face recognition in that subjects often exhibit non-zero yaw and pitch (associated with the rotational degrees of freedom of the camera mount), low contrast (due to varying and intense background lights), and poor spatial resolution (due to inexpensive cameras). There are often subjects standing in the background, usually at very low resolution (see Figure 4b). In such cases, algorithms should detect all faces and determine which is the largest and most centered. When these images are provided as input into the algorithm, they are labeled with the type "wild".
- ▷ **Kiosk photos:** These photos were collected from subjects whose attention was focused on interaction with an immigration kiosk. They images were not intended for use with automated face recognition. The camera is situated above a display which the user touches, and is triggered either without directing the subject to look at it, or without waiting for the subject to comply. The images are therefore characterized by pitch-down pose, sometimes exceeding 45 degrees, as in Figure 4c. Yaw-angle variation is mild, with most images close to frontal. The images

have width 320 pixels and height 240 pixels and therefore tall individuals are sometimes cropped. This is often just above the eyes and can occur at the nose or mouth. Conversely, short individuals are sometimes cropped such that only the top part of the face is visible. In a quite small number of cases, there other subjects standing just behind the primary subject such that algorithms should detect all faces and determine which is the largest and most centered. Background ceiling lighting is often visible and this sometimes leads to under-exposure of the face. When these images are provided as input into the algorithm, they are labeled with the type "wild".

2.2 Law enforcement images

The main mugshot dataset used is referred to as the FRVT 2018 set. This set was collected over the period 2002 to 2017 in routine United States law enforcement operations. This set yields three subsets

- ▷ **Mugshots:** Mugshots comprise about 86% of the database. They have reasonable compliance with the ANSI/NIST ITL1-2011 Type 10 standard's subject acquisition profiles levels 10-20 for frontal images [26]. The most common departure from the standard's requirements is the presence of mild pose variations around frontal - the images of Figure 5 are typical. The images vary in size, with many being 480x600 pixels with JPEG compression applied to produce filesizes of between 18 and 36KB with many images outside this range, implying that about 0.5 bits are being encoded per pixel. When these images are provided as input into the algorithm, they are labeled with the type "mugshot".

Example images appear in Fig. 5

[NIST Interagency Report 8238](#) includes a comparison of this set of mugshots with the smaller and easier sets of mugshots used in tests run in 2010 and 2014.

- ▷ **Profile images:** Profile-view images have been collected in law enforcement for more than 100 years, as human capability is improved with orthogonal information. The profile images used in this report were collected during the same session as the frontal mugshot photograph, in the same standardized photographic setup. These would not therefore be used with automated face recognition. A small subset, 200 000 images, were set aside for testing. When these images are provided as input into the algorithm, they are labeled with the type "wild".

Example images appear in Fig. 7

- ▷ **Webcam images:** The remaining 14% of the images were collected using an inexpensive webcam attached to a flexible operator-directed mount. These images are all of size 240x240 pixels, that are in considerable violation of most quality-related clauses of all face recognition standards. As evident in the figure, the most common defects are non-frontal pose (associated with the rotational degrees of freedom of the camera mount), low contrast (due to varying and intense background lights), and poor spatial resolution (due to inexpensive camera optics) - see examples in Fig 6. The images are overly JPEG compressed, to between 4 and 7KB, implying that only 0.5 to 1 bits are being encoded per color pixel. When these images are provided as input into the algorithm, they are labeled with the type "wild".

Example images appear in Fig. 6

These are drawn from NIST Special Database 32 which may be downloaded [here](#).

These images were partitioned in galleries and probesets for the various experiment listed in Table 1.

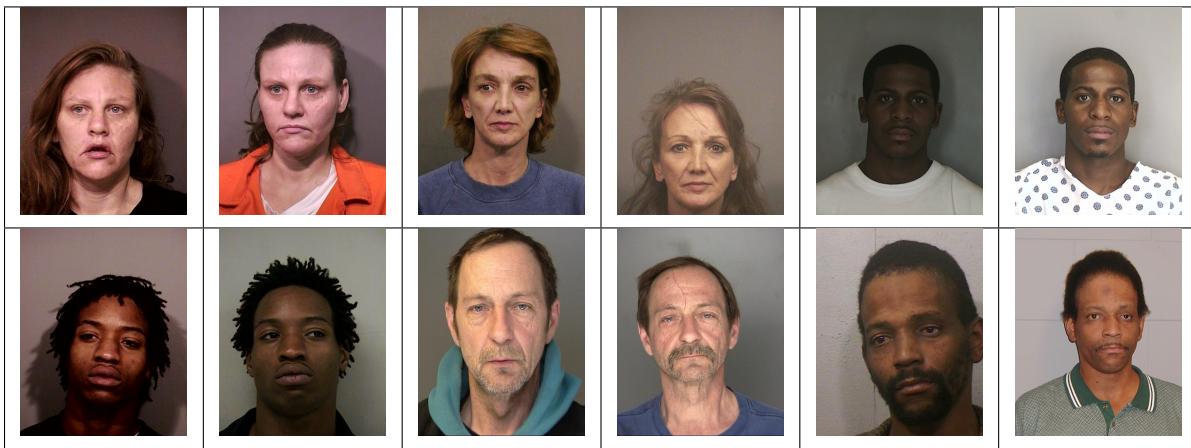


Figure 5: Six mated mugshot pairs representative of the FRVT-2014 (LEO) and FRVT-2018 datasets. The images are collected live, i.e. not scanned from paper. Image source: NIST Special Database 32 the Multiple Encounter Deceased Subjects dataset.



Figure 6: Twelve webcam images representative of probes against the FRVT-2018 mugshot gallery. The first eight images are four mated pairs. Such images present challenges to recognition including pose, non-uniform illumination, low contrast, compression, cropping, and low spatial sampling rate. Image source: NIST Special Database 32 the Multiple Encounter Deceased Subjects dataset.



Figure 7: **[Profile views]** The three images are a frontal enrollment, subsequent frontal probe, and same-session ninety degree profile view. While collection of both frontal and profile views has been typical in law enforcement for more than a century, the recognition of profile to frontal views has essentially been impossible. However, reasonably high accuracy results is now possible - see section E.

Image				
Encounter	1	...	$K_i - 1$	K_i
Capture Time	T_1	...	$T_{K_i - 1}$	T_{K_i}
Role RECENT	Not used	Not used	Enrolled	Search
Role LIFETIME	Enrolled	Enrolled	Enrolled	Search

Figure 8: Depiction of the “recent” and “lifetime” enrollment types. Image source: NIST Special Database 32

2.3 Enrollment strategies

Many operational applications include collection and enrollment of biometric data from subjects on more than one occasion. This might be done on a regular basis, as might occur in credential (re-)issuance, or irregularly, as might happen in a criminal recidivist situation [4]. The number of images per person will depend on the application area. In civil identity credentialing (e.g. passports, driver’s licenses), the images will be acquired approximately uniformly over time (e.g. ten years for a passport). While the distribution of dates for such images of a person might be assumed uniform, a number of factors might undermine this assumption⁷. In criminal applications, the number of images would depend on the number of arrests. The distribution of dates for arrest records for a person (i.e. the recidivism distribution) has been modeled using the exponential distribution but is recognized to be more complicated⁸.

In any case, the 2010 NIST evaluation of face recognition showed that considerable accuracy benefits accrue with retention and use of *all* historical images [6].

To this end, the FRVT API document provides $K \geq 1$ images of an individual to the enrollment software. The software is tasked with producing a single proprietary undocumented “black-box” template⁹ from the K images. This affords the algorithm an ability to generate a *model* of the individual, rather than to simply extract features from each image on a sequential basis.

As depicted in Figure 8, the i -th individual in the FRVT 2018 dataset has K_i images. These are labelled as x_k for $k = 1 \dots K_i$ in chronological order of capture date. To measure the utility of having multiple enrollment images, this report evaluates three kinds of enrollment:

- ▷ **Recent:** Only the second most recent image, $x_{K_i - 1}$ is enrolled. This strategy of enrollment mimics the operational policy of retaining the imagery from the most recent encounter. This might be done operationally to ameliorate the effects of face ageing. Obviously retaining only the most recent image should only be done if the identity of the person is trusted to be correct. For example, in an access control situation retention of the most recent successful *authentication* image would be hazardous if it could be a false positive.
- ▷ **Lifetime-consolidated:** All but the most recent image are enrolled, $x_1 \dots x_{K_i - 1}$. This subject-centric strategy might be adopted if quality variations exist where an older image might be more suitable for matching, despite the ageing effect.

⁷For example, a person might skip applying for a passport for one cycle, letting it expire. In addition, a person might submit identical images (from the same photography session) to consecutive passport applications at five year intervals.

⁸A number of distributions have been considered to model recidivism, see for example [3].

⁹There are no formal face template standards. Template standards only exist for fingerprint minutiae - see ISO/IEC 19794-2:2011.

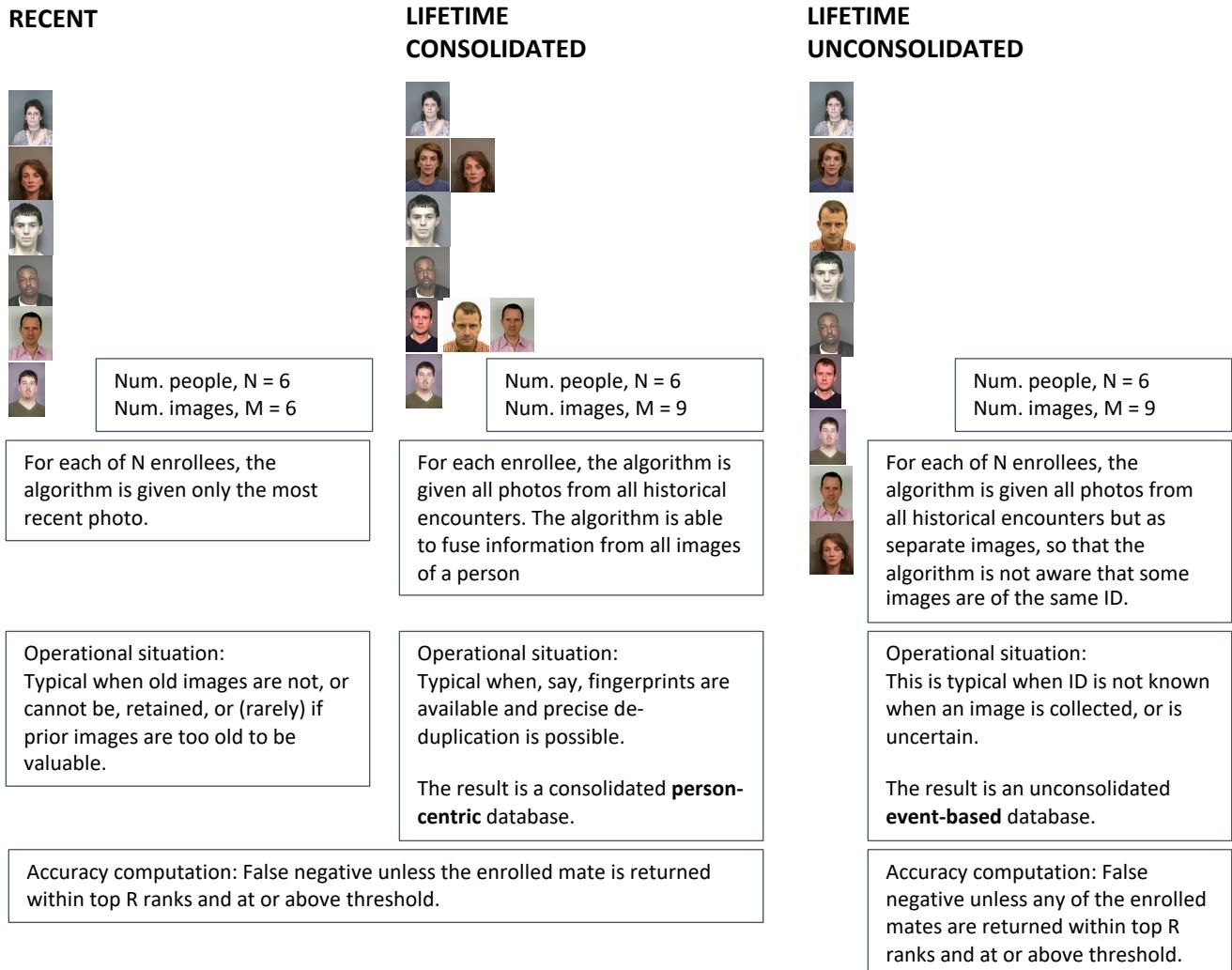


Figure 9: Enrollment strategies. The figure shows the three kinds of enrollment databases examined in this report. Image source: NIST Special Database 32

	ENROLLMENT				SEARCH			
	TYPE SEE SECTION 2.3	POPULATION FILTER	N-SUBJECTS	N-IMAGES	MATE N-SUBJECTS	NON-MATE N-IMAGES	N-SUBJECTS	N-IMAGES
Mugshot trials from enrollment of single images								
1	RECENT	NATURAL	640 000	640 000	154 549	154 549	331 254	331 254
2	RECENT	NATURAL	1 600 000	1 600 000				
3	RECENT	NATURAL	3 000 000	3 000 000				
4	RECENT	NATURAL	6 000 000	6 000 000				
5	RECENT	NATURAL	12 000 000	12 000 000				
Cross-domain								
13	MUGSHOTS AS ON ROW 2				82 106 WEBCAM	82 106 WEBCAM	331 254 WEBCAM	331 254 WEBCAM
Cross-view								
14	MUGSHOTS AS ON ROW 2				100 000 PROFILE	100 000 PROFILE	100 000 PROFILE	100 000 PROFILE
Mugshot ageing								
17	OLDEST	NATURAL	3 068 801	3 068 801	2 853 221	10 951 064	0	0
Border crossing ageing								
18	OLDEST	NATURAL	1 600 000	1 600 000	903 655	1 922 393	1 393 076	1 680 000
Visa-border								
19	PRIOR	NATURAL	1 600 000 VISA	1 600 000 VISA	577 444 BORDER	1 212 892 BORDER	79 769 BORDER	80 000 BORDER
20	VISA AS ON ROW 18				14 004 BORDER	31 579 BORDER	42 474 BORDER	45 460 BORDER

Table 1: Enrollment and search sets. Each row summarizes one identification trial. Unless stated otherwise, all entries refer to mugshot images. The term “natural” means that subjects were selected without heed to demographics, i.e. in the distribution native to this dataset. The probe images were collected in a different calendar year to the enrollment image. Missing values in rows 2-12 are the same as in row 1.

▷ **Lifetime-unconsolidated:** Again all but the most recent image are enrolled $x_1 \dots x_{K_i-1}$ but now separately, with different identifiers, such that the algorithm is not aware that the images are from the same face. This kind of event- or encounter-centric enrollment is very common when operational constraints preclude reliable consolidation of the historical encounters into a single identity. This aspect also prevents the recognition algorithm from a) building a holistic model of identity (as is common in speaker recognition systems) and b) implementing fusion, for example template-level fusion of feature vectors, or post-search score-level fusion. The result is that searches will typically yield more than one image of a person in the top ranks. This has consequences for appropriate metrics, as detailed in section 3.2.1

NIST first evaluated this kind of enrollment in mid 2018, and the results tables include some comparison of accuracy available from all three enrollment styles.

In all cases, the most recent image, x_{K_i} , is reserved as the search image. For the 1.6 million subject enrollment partition of the FRVT 2018 data, $1 \leq K_i \leq 33$ with $K_i = 1$ in 80.1% of the individuals, $K_i = 2$ in 13.4%, $K_i = 3$ in 3.7%, $K_i = 4$ in 1.4%, $K_i = 5$ in 0.6%, $K_i = 6$ in 0.3%, and $K_i > 6$ is 0.2% for everyone else. This distribution is substantially dependent on United States recidivism rates.

We did not evaluate the case of retaining only the highest quality image, since automated quality assessment is out of scope for this report. We do not anticipate that such strategies will prove beneficial when the quality assessment apparatus is imperfect and unvalidated.

3 Performance metrics

This section gives specific definitions for accuracy and timing metrics. Tests of open-set biometric algorithms must quantify frequency of two error conditions:

- ▷ **False positives:** Type I errors occur when search data from a person who has never been seen before is incorrectly associated with one or more enrollees' data.
- ▷ **Misses:** Type II errors arise when a search of an enrolled person's biometric does not return the correct identity.

Many practitioners prefer to talk about "hit rates" instead of "miss rates" - the first is simply one minus the other as detailed below. Sections 3.1 and 3.2 define metrics for the Type I and Type II performance variables.

Additionally, because recognition algorithms sometimes fail to produce a template from an image, or fail to execute a one-to-many search, the occurrence of such events must be recorded. Further because algorithms might elect to not produce a template from, for example, a poor quality image, these failure rates must be combined with the recognition error rates to support algorithm comparison. This is addressed in section 3.5.

Finally, section 3.7 discusses measurement of computation duration, and section 3.8 addresses the uncertainty associated with various measurements. Template size measurement is included with the results.

3.1 Quantifying false positives

It is typical for a search to be conducted into an enrolled population of N identities, and for the algorithm to be configured to return the closest L candidate identities. These candidates are ranked by their score, in descending order, with all scores required to be greater than or equal to zero. A human analyst might examine either all L candidates, or just the top $R \leq L$ identities, or only those with score greater than threshold, T . The workload associated with such examination is discussed later, in 3.6.

False alarm performance is quantified in two related ways. These express how many searches produces false positives, and then, how many false positives are produced in a search.

False positive identification rate: The first quantity, FPIR, is the proportion of non-mate searches that produce an adverse outcome:

$$\text{FPIR}(N, T) = \frac{\text{Num. non-mate searches where one or more enrolled candidates are returned with score at or above threshold}}{\text{Num. non-mate searches attempted.}} \quad (1)$$

Under this definition, FPIR can be computed from the highest non-mate candidate produced in a search - it is not necessary to consider candidates at rank 2 and above. FPIR is the primary measure of Type I errors in this report.

Selectivity: However, note that in any given search, several non-mate may be returned above threshold. In order to quantify such events, a second quantity, selectivity (SEL), is defined as the *number* of non-mates returned on a candidate list, averaged over all searches.

$$\text{SEL}(N, T) = \frac{\text{Num. non-mate enrolled candidates returned with score at or above threshold}}{\text{Num. non-mate searches attempted.}} \quad (2)$$

where $0 \leq \text{SEL}(N, T) \leq L$. Both of these metrics are useful operationally. FPIR is useful for targeting how often an

adverse false positive outcome can occur, while SEL as a number is related to workload associated with adjudicating candidate lists. The relationship between the two quantities is complicated - it depends on whether an algorithm concentrates the false alarms in the results of a few searches or whether it disburses them across many. This was detailed in FRVT 2014, NISTIR 8009. It has not yet been detailed in FRVT 2018.

3.2 Quantifying hits and misses

If L candidates are returned in a search, a shorter candidate list can be prepared by taking the top $R \leq L$ candidates for which the score is above some threshold, $T \geq 0$. This reduction of the candidate list is done because thresholds may be applied, and only short lists might be reviewed (according to policy or labor availability, for example). It is useful then to state accuracy in terms of R and T , so we define a “miss rate” with the general name **false negative identification rate** (FNIR), as follows:

$$\text{FNIR}(N, R, T) = \frac{\text{Num. mate searches with enrolled mate found outside top } R \text{ ranks or score below threshold}}{\text{Num. mate searches attempted.}} \quad (3)$$

This formulation is simple for evaluation in that it does not distinguish between causes of misses. Thus a mate that is not reported on a candidate list is treated the same as a miss arising from face finding failure, algorithm intolerance of poor quality, or software crashes. Thus if the algorithm fails to produce a candidate list, either because the search failed, or because a search template was not made, the result is regarded as a miss, adding to FNIR.

Hit rates, and true positive identification rates: While FNIR states the “miss rate” as how often the correct candidate is either not above threshold or not at good rank, many communities prefer to talk of “hit rates”. This is simply the **true positive identification rate**(TPIR) which is the complement of FNIR giving a positive statement of how often mated searches are successful:

$$\text{TPIR}(N, R, T) = 1 - \text{FNIR}(N, R, T) \quad (4)$$

This report does not report true positive “hit” rates, preferring false negative miss rates for two reasons. First, costs rise linearly with error rates. For example, if we double FNIR in an access control system, then we double user inconvenience and delay. If we express that as decrease of TPIR from, say 98.5% to 97%, then we mentally have to invert the scale to see a doubling in costs. More subtly, readers don’t perceive differences in numbers near 100% well, becoming inured to the “high nineties” effect where numbers close to 100 are perceived indifferently.

Reliability is a corresponding term, typically being identical to TPIR, and often cited in automated (fingerprint) identification system (AFIS) evaluations.

An important special case is the **cumulative match characteristic**(CMC) which summarizes accuracy of mated-searches only. It ignores similarity scores by relaxing the threshold requirement, and just reports the fraction of mated searches returning the mate at rank R or better.

$$\text{CMC}(N, R) = 1 - \text{FNIR}(N, R, 0) \quad (5)$$

We primarily cite the complement of this quantity, $\text{FNIR}(N, R, 0)$, the fraction of mates *not* in the top R ranks.

The **rank one hit rate** is the fraction of mated searches yielding the correct candidate at best rank, i.e. $\text{CMC}(N, 1)$. While this quantity is the most common summary indicator of an algorithm’s efficacy, it is not dependent on similarity scores, so it does not distinguish between strong (high scoring) and weak hits. It also ignores that an adjudicating reviewer is often willing to look at many candidates.

3.2.1 False negative rates for unconsolidated galleries

As detailed in section 2.3 a common type of gallery, here referred to as the lifetime unconsolidate type, is populated with all images of an individual without any association between them. That is, the gallery construction algorithm is not provided with any ID labels that would support processing of a person's images jointly. This contrasts with the lifetime consolidate type where an algorithm may explicitly fuse features from multiple images of a person, or select a best image. In such cases, where the number of enrolled images is a random variable, we define two false negative rates as follows.

The first demands that the algorithm place any of the K_i mates in the top $R \geq 1$ ranks. The proportion of searches for which this does not occur forms a false negative identification rate:

$$\text{FNIR}_{\text{any}}(N, R, T) = 1 - \frac{\text{Num. mate searches where any enrolled mate is found in the top } R \text{ ranks and at-or-above threshold}}{\text{Num. mate searches attempted.}} \quad (6)$$

The second demands that the algorithm place all K_i mates in the top $R \geq K_i$ ranks. The proportion of searches for which this does not occur forms a false negative identification rate:

$$\text{FNIR}_{\text{all}}(N, R, T) = 1 - \frac{\text{Num. mate searches where all enrolled mates are found in the top } R \text{ ranks and at-or-above threshold}}{\text{Num. mate searches attempted.}} \quad (7)$$

Placing all mates in the top ranks is a more difficult task than correctly retrieving any image, so it holds that: $\text{FNIR}_{\text{all}} \geq \text{FNIR}_{\text{any}}$. This is evident in the results presented for November 2018 algorithms in Tables starting at ??.

The information retrieval community might prefer to compute and plot *precision* and *recall*; this is a valid approach, but we advance the two metrics above because they relate to our normal definition of consolidated FNIR, and they cover the two extreme use-cases of wanting any hit vs. all hits.

3.3 DET interpretation

In biometrics, a false negative occurs when an algorithm fails to match two samples of one person – a Type II error. Correspondingly, a false positive occurs when samples from two persons are improperly associated – a Type I error.

Matches are declared by a biometric system when the native comparison score from the recognition algorithm meets some threshold. Comparison scores can be either similarity scores, in which case higher values indicate that the samples are more likely to come from the same person, or dissimilarity scores, in which case higher values indicate different people. Similarity scores are traditionally computed by fingerprint and face recognition algorithms, while dissimilarities are used in iris recognition. In some cases, the dissimilarity score is a distance possessing metric properties. In any case, scores can be either mate scores, coming from a comparison of one person's samples, or nonmate scores, coming from comparison of different persons' samples.

The words "genuine" or "authentic" are synonyms for mate, and the word "impostor" is used as a synonym for non-mate. The words "mate" and "nonmate" are traditionally used in identification applications (such as law enforcement search, or background checks) while genuine and impostor are used in verification applications (such as access control).

An error tradeoff characteristic represents the tradeoff between Type II and Type I classification errors. For identification this plots false negative vs. false positive identification rates i.e. FNIR vs. FPIR parametrically with T. Such plots

are often called detection error tradeoff (DET) characteristics or receiver operating characteristic (ROC). These serve the same function – to show error tradeoff – but differ, for example, in plotting the complement of an error rate (e.g. $TPIR = 1 - FNIR$) and in transforming the axes, most commonly using logarithms, to show multiple decades of FPIR. More rarely, the function might be the inverse of the Gaussian cumulative distribution function.

The slides of Figures 10 through 15 discuss presentation and interpretation of DETs used in this document for reporting face identification accuracy. Further detail is provided in formal biometrics testing standards, see the various parts of ISO/IEC 19795 Biometrics Testing and Reporting. More terms, including and beyond those to do with accuracy, appear in ISO/IEC 2382-37 Information technology – Vocabulary – Part 37: Harmonized biometric vocabulary.

2022/09/26
18:06:18FNIR(N, R, T) = False neg. identification rate
FPIR(N, T) = False pos. identification rateN = Num. enrolled subjects
R = Num. candidates examined

T = Threshold

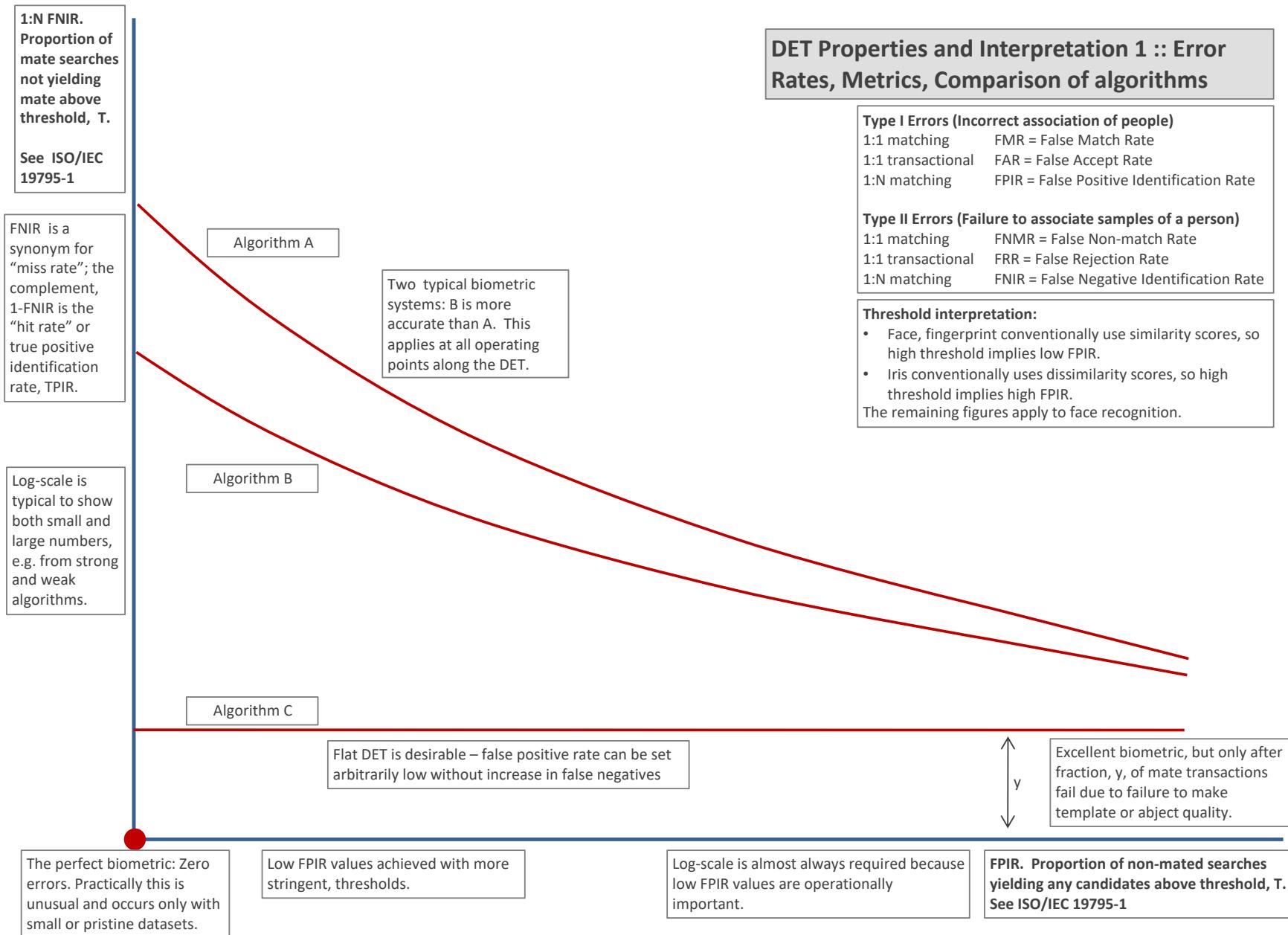
T = 0 → Investigation
T > 0 → Identification

Figure 10: DET as the primary performance reporting mechanism.

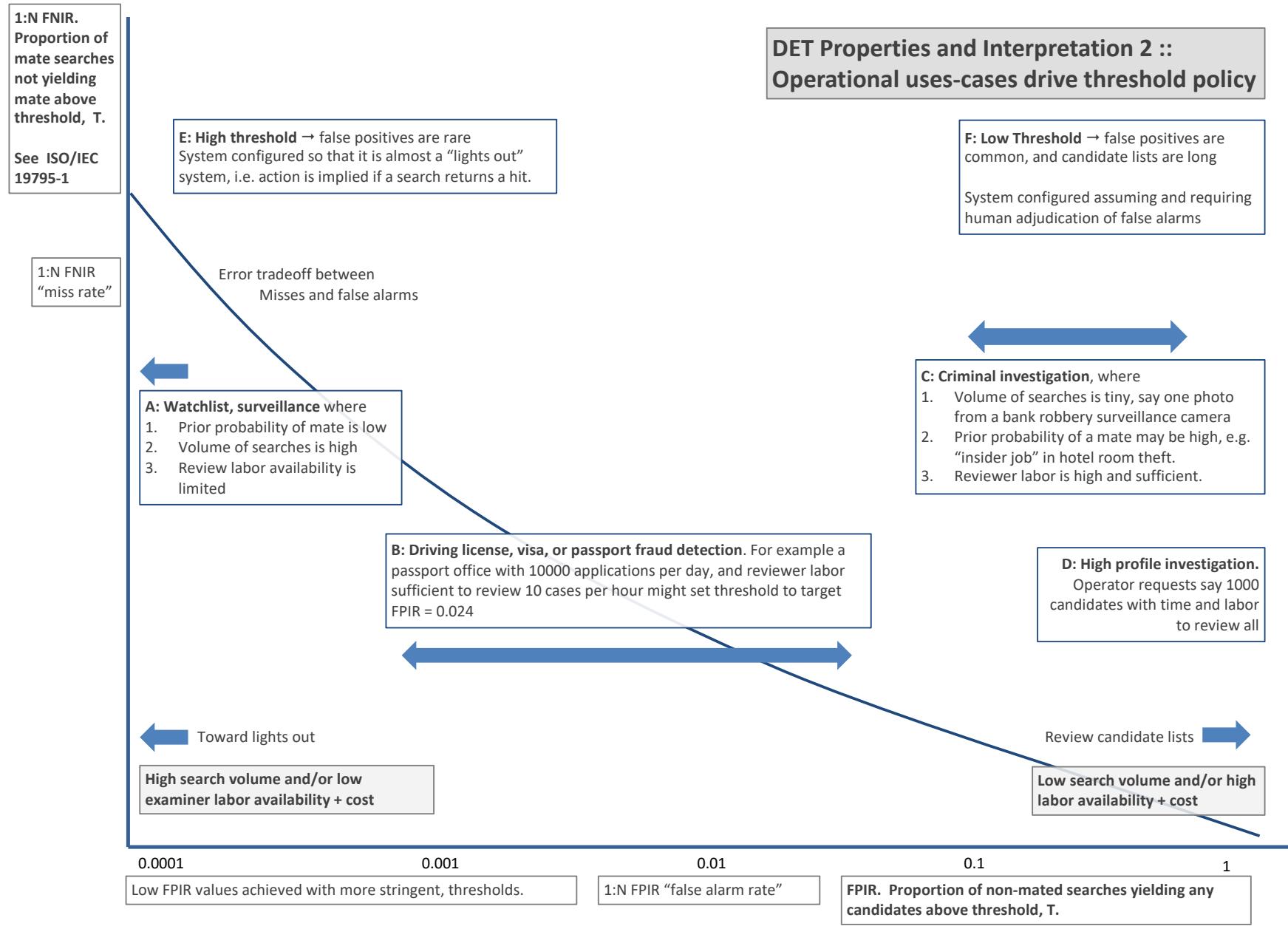
2022/09/26
18:06:18FNIR(N, R, T) = False neg. identification rate
FPIR(N, T) = False pos. identification rate
N = Num. enrolled subjects
R = Num. candidates examined
T = ThresholdT = 0 → Investigation
T > 0 → Identification

Figure 11: DET as the primary performance reporting mechanism.

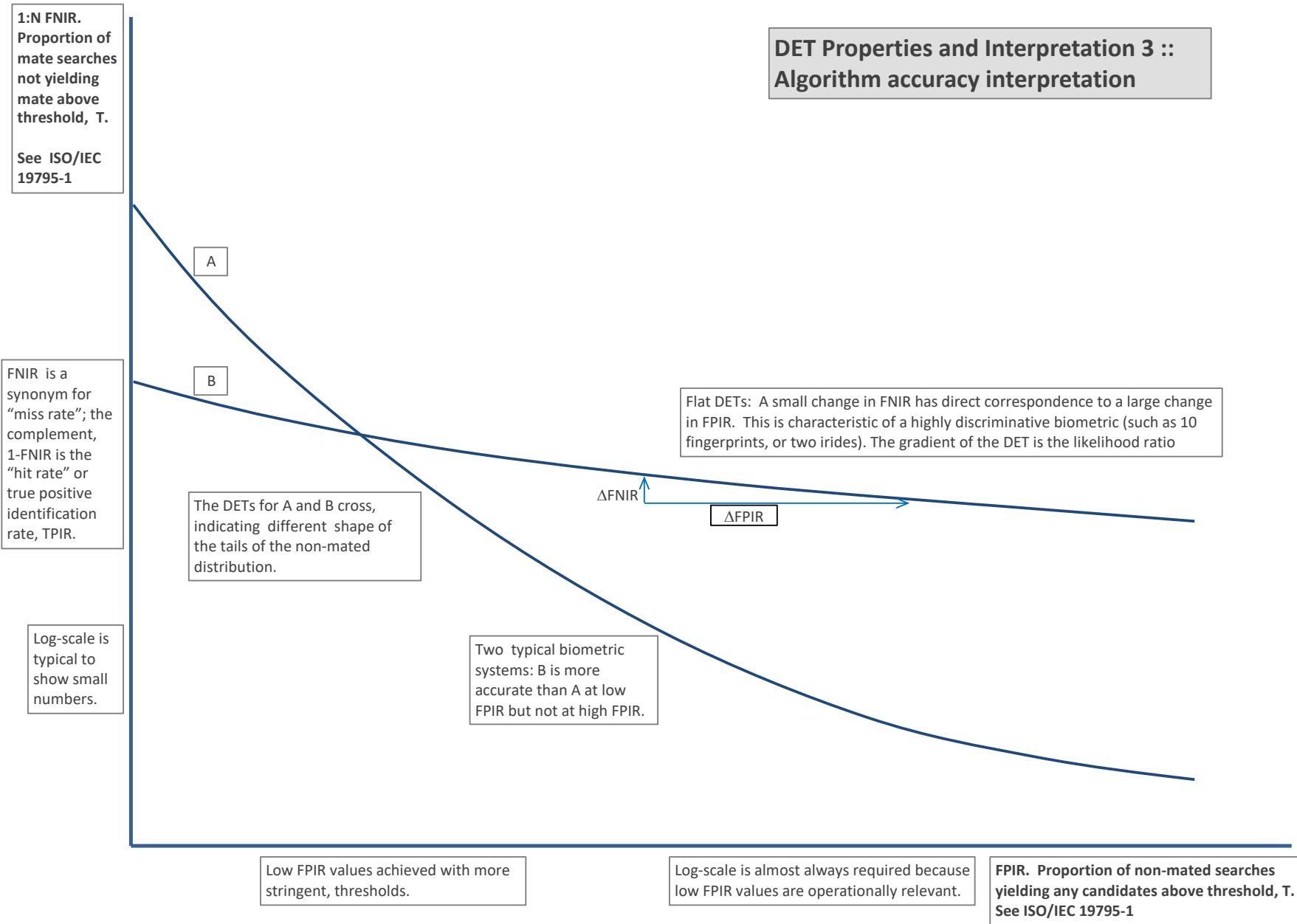
2022/09/26
18:06:18FNIR(N, R, T) = False neg. identification rate
FPIR(N, T) = False pos. identification rateN = Num. enrolled subjects
R = Num. candidates examinedT = Threshold
T = 0 → Investigation
T > 0 → Identification

Figure 12: DET as the primary performance reporting mechanism.

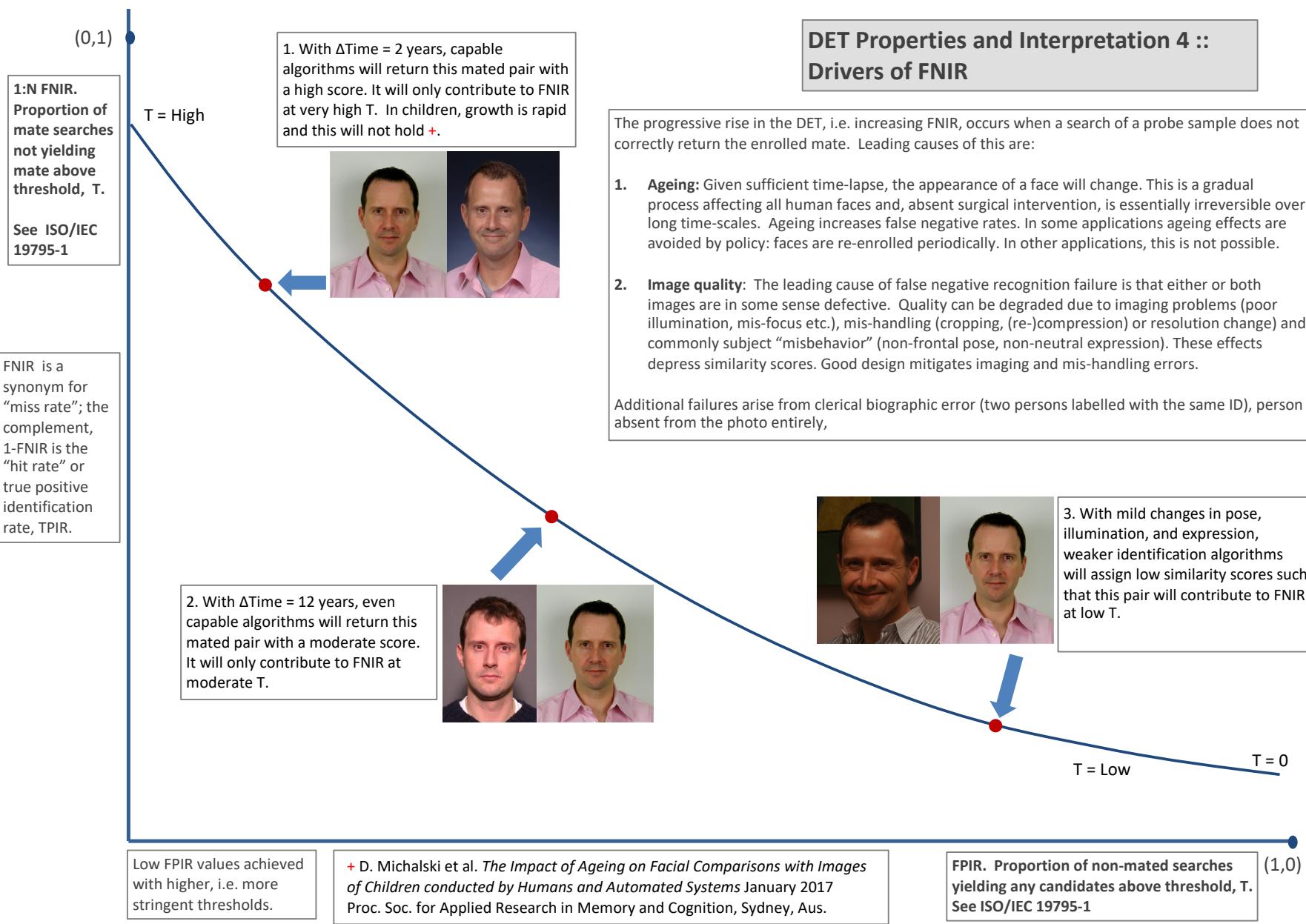
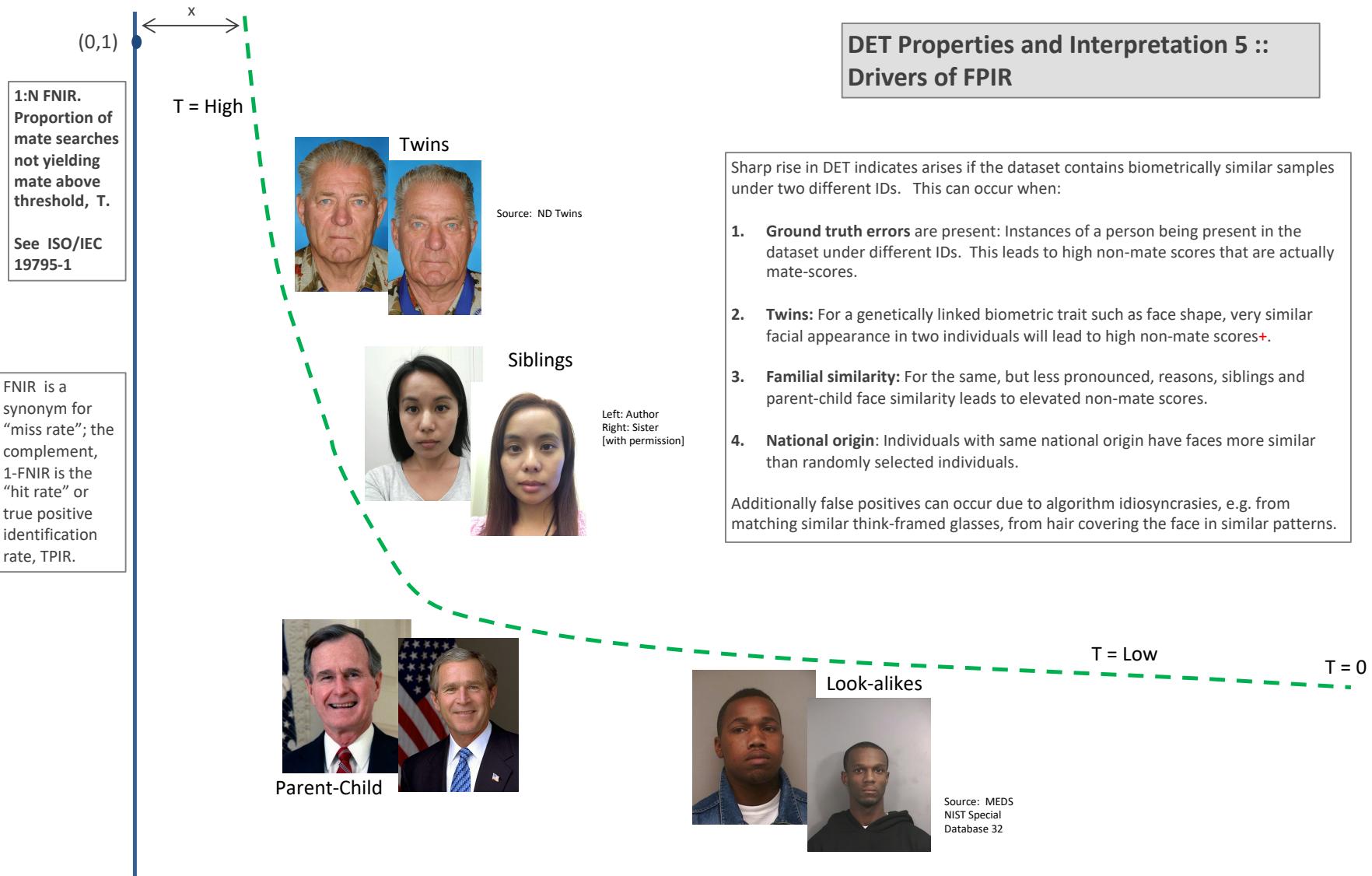


Figure 13: DET as the primary performance reporting mechanism.

2022/09/26
18:06:18FNIR(N, R, T) = False neg. identification rate
FPIR(N, T) = False pos. identification rate

T = Threshold

T = 0 → Investigation
T > 0 → Identification

Low FPIR values achieved with higher, i.e. more stringent thresholds.

+ NOTE: While most algorithms will not recognize twins correctly, there is at least one face recognition algorithm that can correctly distinguish twins [US Patent: [US7369685B2](#)].

FPIR. Proportion of non-mated searches yielding any candidates above threshold, T.
See ISO/IEC 19795-1

Figure 14: DET as the primary performance reporting mechanism.

2022/09/26
18:06:18

$\text{FNIR}(N, R, T) =$ False neg. identification rate
 $\text{FPIR}(N, T) =$ False pos. identification rate

N = Num. enrolled subjects
 R = Num. candidates examined

T = Threshold

$T = 0 \rightarrow$ Investigation
 $T > 0 \rightarrow$ Identification

1:N FNIR.
Proportion of mate searches not yielding mate above threshold, T .
See ISO/IEC 19795-1

Algorithm X,
Condition 1

Algorithm X,
Condition 2

If system X is used with images of different properties, say from different imaging systems, or from different populations, generally both FNIR and FPIR will change. The dotted line joins points of the same threshold. Horizontal (vertical) lines indicate change in FPIR (FNIR) only. Two cases concerning population size are shown below (A and B), for the blue curves.

FNIR is a synonym for "miss rate"; the complement, 1-FNIR is the "hit rate" or true positive identification rate, TPIR.

Log-scale is typical to show small numbers.

Algorithm Y,
Condition 1

Algorithm Y,
Condition 2

If DETs are computed for two categories (men and women) or (cameras A and B) or (indoor vs. outdoor), generally the Type I and Type II errors will differ and the line of constant threshold will be neither horizontal nor vertical.

The ideal situation in most applications is that a fixed threshold yields a fixed FPIR so that system owners see no change in false alarms across populations or conditions.

Low FPIR values achieved with higher, i.e. more stringent, thresholds.

Log-scale is often required because low FPIR values are operationally relevant.

FPIR. Proportion of non-mated searches yielding any candidates above threshold, T . See ISO/IEC 19795-1

Figure 15: DET as the primary performance reporting mechanism.

2022/09/26
18:06:18FNIR(N, R, T) = False neg. identification rate
FPIR(N, T) = False pos. identification rateN = Num. enrolled subjects
R = Num. candidates examined

T = Threshold

T = 0 → Investigation
T > 0 → Identification

1:N FNIR.
Proportion of mate searches not yielding mate above threshold, T.
See ISO/IEC 19795-1

FNIR is a synonym for "miss rate"; the complement, 1-FNIR is the "hit rate" or true positive identification rate, TPIR.

Log-scale is typical to show small numbers.

A: Typical case: In theory, and often in practice, a 1:N search is implemented by executing N 1:1 comparisons independently and then sorting by similarity score:

Mate scores: A mate comparison score is independent of the rest of enrollment data, and so independent of N. This implies the horizontal line above $\text{FNIR}(T, N) = \text{FNMR}(T, 1)$.

Non-mate scores: FPIR increases linearly with N from binomial theory: $\text{FPIR}(N, T) = 1 - (1 - \text{FMR}(T))^N \rightarrow N \text{ FMR}(T)$ for small FPIR.

Pop. N1



Pop. N2 > N1

B: Special case: An enrollment database is not just a linear data structure, it could be an index, or tree, then search is not simply N 1:1 comparisons and a sort. In that case:

Mate scores become dependent on the enrollment data, either its size or actual content, then generally $\text{FNIR}(T, N) \neq \text{FNIR}(T, 1)$.

Non-mate scores are normally no longer just the highest 1:1 comparison score. Instead, for example, scores may be normalized as the implementation attempts to make FPIR independent of N will yield the vertical line linking points of equal threshold.

Low FPIR values achieved with higher, i.e. more stringent, thresholds.

Log-scale is often required because low FPIR values are operationally important.

DET Properties and Interpretation 7 :: Effect of enrolled population size.

FPIR. Proportion of non-mated searches yielding any candidates above threshold, T.
See ISO/IEC 19795-1

Figure 16: DET as the primary performance reporting mechanism.

DET Properties and Interpretation 8 :: Non-ideal tests, datasets or systems

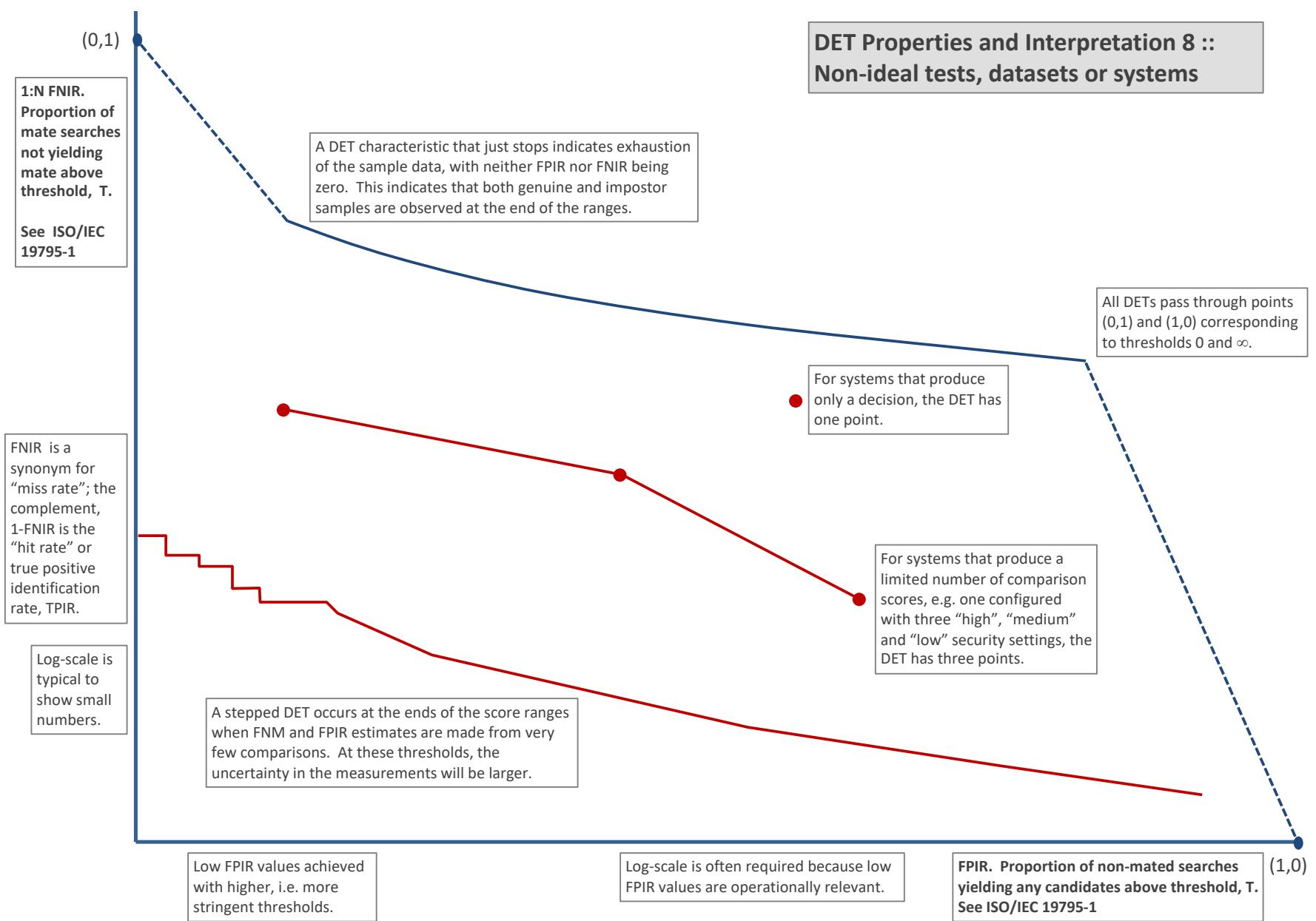


Figure 17: DET as the primary performance reporting mechanism.

3.4 Best practice testing requires execution of searches with and without mates

FRVT embeds 1:N searches of two kinds: Those for which there is an enrolled mate, and those for which there is not. The respective numbers for these types of searches appear in Table 1. However, it is common to conduct only mated searches¹⁰. The cumulative match characteristic is computed from candidate lists produced in mated searches. Even if the CMC is the only metric of interest, the actual trials executed in a test should nevertheless include searches for which no mate exists. As detailed in Table 1 the FRVT reserved disjoint populations of subjects for executing true non-mate searches.

3.5 Failure to extract features

During enrollment some algorithms fail to convert a face image to a template. The proportion of failures is the failure-to-enroll rate, denoted by FTE. Similarly, some search images are not converted to templates. The corresponding proportion is termed failure-to-extract, denoted by FTX.

We do not report FTX because we assume that the same underlying algorithm is used for template generation for enrollment and search.

Failure to extract rates are incorporated into FNIR and FPIR measurements as follows.

- ▷ **Enrollment templates:** Any failed enrollment is regarded as producing a zero length template. Algorithms are required by the API [10] to transparently process zero length templates. The effect of template generation failure on search accuracy depends on whether subsequent searches are mated, or non-mated: Mated searches will fail giving elevated FNIR; non-mated searches will not produce false positives so, to first order, FPIR will be reduced by a factor of $1 - \text{FTE}$.
- ▷ **Search templates and 1:N search:** In cases where the algorithm fails to produce a search template from input imagery, the result is taken to be a candidate list whose entries have no hypothesized identities and zero score. The effect of template generation failure on search accuracy depends on whether searches are mated, or non-mated: Mated searches will fail giving elevated FNIR; Non-mated searches will not produce false positives, so FPIR will be reduced. Thus given a measurement of false negative and positive rates made over only those where failures-to-extract did not occur, those rates - call them FNIR^\dagger and FPIR^\dagger - could be adjusted by an explicit measurement of FTX as follows

$$\text{FNIR} = \text{FTX} + (1 - \text{FTX})\text{FNIR}^\dagger \quad (8)$$

$$\text{FPIR} = (1 - \text{FTX})\text{FPIR}^\dagger \quad (9)$$

This approach is the correct treatment for positive-identification applications such as access control where cooperative users are enrolled and make attempts at recognition. This approach is not appropriate to negative identification applications, such as visa fraud detection, in which hostile individuals may attempt to evade detection by submitting poor quality samples. In those cases, template generation failures should be investigated as though a false alarm had occurred.

¹⁰For example, the [Megaface benchmark](#). This is bad practice for several reasons: First, if a developer knows, or can reasonably assume, that a mate always exists, then unrealistic gaming of the test is possible. A second reason is that it does not put FPIR on equal footing with FNIR and that matters because in most applications, not all searches have mates - not everyone has been previously enrolled in a driving license issuance or a criminal justice system - so addressing between-class separation becomes necessary.

3.6 Fixed length candidate lists, threshold independent workload

Suppose an automated face identification algorithm returns L candidates, and a human reviewer is retained to examine up to R candidates, where $R \leq L$ might be set by policy, preference or labor availability. For now, assume also that the reviewer is not provided with, or ignores, similarity scores, and thresholds are not applied. Given the algorithm typically places mates at low (good) ranks, the number of candidates a reviewer can be expected to review can be derived as follows. Note that the reviewer will:

- ▷ Always inspect the first ranked image Frac. reviewed = 1
- ▷ Then inspect those candidates where mate not confirmed at rank 1 Frac. reviewed = 1-CMC(1)
- ▷ Then inspect those candidates where mate not confirmed at rank 1 or 2 Frac. reviewed = 1-CMC(2)

etc. Thus if the reviewer will stop after a maximum of R candidates, the expected number of candidate reviews is

$$M(R) = 1 + (1 - CMC(1)) + (1 - CMC(2)) + \dots + (1 - CMC(R - 1)) \quad (10)$$

$$= R - \sum_{r=1}^{R-1} CMC(r) \quad (11)$$

A recognition algorithm that front-loads the cumulative match characteristic will offer reduced workload for the reviewer. This workload is defined only over the searches for which a mate exists. In the cases where there truly is no mate, the reviewer would review all R candidates. Thus, if the proportion of searches for which a mate does exist is β , which in the law enforcement context would be the recidivism rate [3], the full expression for workload becomes:

$$M(R) = \beta \left(R - \sum_{r=1}^{R-1} CMC(r) \right) + (1 - \beta)R \quad (12)$$

$$= R - \beta \sum_{r=1}^{R-1} CMC(r) \quad (13)$$

3.7 Timing measurement

Algorithms were submitted to NIST as implementations of the application programming interface(API) specified by NIST in the Evaluation Plan [10]. The API includes functions for initialization, template generation, finalization, search, gallery insert, and gallery delete. Two template generation functions are required, one for the preparation of an enrollment template, and one for a search template.

In NIST's test harness, all functions were wrapped by calls to the C++ std::chrono::high_resolution_clock which on the dedicated timing machine counts 1ns clock ticks. Precision is somewhat worse than that however.

3.8 Uncertainty estimation

3.8.1 Random error

This study leverages operational datasets for measurement of recognition error rates. This affords several advantages. First, large numbers of searches are conducted (see Table 1) giving precision to the measurements. Moreover, for the two mugshot datasets, these do not involve reuse of individuals so binomial statistics can be expected to apply to recognition error counts. In that case, an observed count of a particular recognition outcome (i.e. a false negative or false positive) in M trials will sustain 95% confidence that the actual error rate is no larger than some value.

As an example, the minimum number of mugshot searches conducted in this report is $M = 154\,549$, and for an observed FNIR around 0.002, the measurement supports a conclusion that the actual FNIR is no higher than 0.00228 at 99% confidence level. On the false positive side, we tabulate FNIR at FPIR values as low as 0.001. Given estimates based on 331 254 non-mate trials, the actual FPIR values will be below 0.00115 at 99% confidence. In conclusion, large scale evaluation, without reuse of subjects, supports tight uncertainty bounds on the measured error rates.

3.8.2 Systematic error

The FRVT 2018 dataset includes anomalies discovered as a result of inspecting images involved in recognition failures from the most accurate algorithms. Two kinds of failure occur: False negatives (which, for the purpose here, include failures to make templates) and false positives.

False negative errors: We reviewed 600 false negative pairs for which either or both of the leading two algorithms did not put the correct mate in the top 50 candidates. Given 154 549 searches, this number represents 0.39% of the total, resulting in $\text{FNIR} \sim 0.0039$. Of the 600 pairs:

- ▷ **A: Poor quality:** About 20% of the pairs included images of very low quality, often greyscale, low resolution, blurred, low contrast, partially cropped, interlaced, or noisy scans of paper images. Additionally, in a few cases, the face is injured or occluded by bandages or heavy cosmetics.
- ▷ **B: Ground truth identity label bugs:** About 15% of the pairs are not actually mated. We only assigned this outcome when a pair is clearly not mated.
- ▷ **C: Profile views:** About 35% included an image of a profile (side) view of the face, or, more rarely, an image that was rotated 90 degrees in-plane (roll).
- ▷ **D: Tattoos:** About 30% included an image of a tattoo that contained a face image. These arise from mis-labelling in the parent dataset metadata.
- ▷ **E: Ageing:** There is considerable time-lapse between the two captures.

All these estimates are approximate. Of these, the tattoo and mislabeled images can never be matched. These constitute an accuracy floor in the sample implying that FNIR cannot be below 0.0018¹¹. The profile-views, low-quality images, and images with considerable ageing can, in principle, be successfully matched - indeed some algorithms do so - so are not part of the accuracy floor.

¹¹This value is the sum of two partial false negative rates: $\text{FNIR}_B = 0.15 * 0.0039$ plus $\text{FNIR}_D = 0.3 * 0.0039$

For the microsoft-4 algorithm the lowest miss rate from (recent entry in Table 25) is $\text{FNIR}(640\,000, 50, 0) = 0.0018$. This is close to the value estimated from the inspection of misses. It is below the 0.0039 figure because the algorithm does match some profile and poor quality images, that the yitu-2 algorithm does not.

For many tables (e.g. Table 25), the FNIR values obtained for the FRVT-2018 mugshots could be corrected by reducing them by 0.0018. The best values would then be indistinct from zero. The results in this report *were not* adjusted to account for this systematic error.

False positive errors: As shown in Figure 1 and discussed in Figure 14 many of the DET characteristics in this report exhibit a pronounced turn upward at low false positive rates. The shape can be caused by identity labelling errors in the ground truth of a dataset, specifically persons present in the database under two IDs such that some proportion of non-mate pairs are actually mated. To look for such possibilities, we merged the highest 1000 non-mate pairs produced by three different algorithms which resulted in 1839 unique pairs. This constitutes 0.56% of all non-mate searches. We assert that it is *very* difficult for human reviewers to assign the pairs into the following three categories: twins; doppelgangers; or ground-truth errors (instances of the same person under two IDs). Given this difficulty we made no attempt to correct any possible ground truth errors except by removing 57 pairs in the following categories:

- ▷ **A: Profile views:** Thirteen pairs included one or two profile-view images. As described in Figure 195, these can cause false positives.
- ▷ **B: Same-session photographs:** For twelve pairs, the images were identical or trivially altered (e.g. cropped) versions of the same photo. These were present under a different ID likely due to some clerical or procedural mistake.
- ▷ **C: Tattoos of faces:** There were fourteen instances of tattoo photographs that contained faces causing false matches.
- ▷ **D: T-shirt faces:** There were six instances of T-shirt photographs (of Bob Marley and Che Guevara) being detected instead of the face and causing false positives.
- ▷ **E: Background faces:** There were twelve instances of one subject appearing in the background of two otherwise correct portrait photos.

Note we did not remove any images where there was a chance that the pair was actually a different person.

In any case, the results in this report have not been adjusted for this systematic error.

4 Results

This section gives extensive results for algorithms submitted to FRVT 2018. Three page “report cards” for each algorithm are contained in a [separate supplement](#). Performance metrics were described in section 3. The main results are summarized in tabular form with more exhaustive data included as DET, CMC and related graphs in appendices as follows:

- ▷ The three tables 2-4 list algorithms alongside full developer names, acceptance date, size of the provided configuration data, template size and generation time, and search duration data.
 - The **template generation duration** is most important to applications that require fast response. For example, an eGate taking more than two seconds to produce a template might be unacceptable. Note that GPUs may be of utility in expediting this operation for some algorithms, though at additional expense. Two additional factors should be considered¹²¹³.
 - The **search duration** is the time taken for a search of a search template into a gallery of N enrollment templates. This performance variable, together with the volume of searches, is influential on the amount of hardware needed to sustain an operational deployment. This is measured here with the algorithm running on a single core of a contemporary CPU. Search is most simply implemented as N computations of a distance metric followed by a sort operation to find the closest enrollments. However, considerable optimization of this process is possible, up to and including fast-search algorithms that, by various means, avoid computation of all N distances.
 - The **template size** is the size of the extracted feature vector (or vectors) and any needed header information. Large template sizes may be influential on bus or network bandwidth, storage requirements, and on search duration. While the template itself is an opaque data blob, the feature dimensionality might be estimated by assuming a four-bytes-per-float encoding. There is a wide range of encodings. For the more accurate algorithm, sizes range from 256 bytes to about 2KB bytes, indicating essentially no consensus on face modeling and template design.
 - The **template size multiplier** column shows how, given k input images, the size of the template grows. Most implementations internally extract features from each image and concatenate them, and implement some score-level fusion logic during search. Other implementations, including many of the most accurate algorithms, produce templates whose size does not grow with k . This could be achieved via selection of the best quality image - but this is not optimal in handling ageing where the oldest image could be the best quality. Another mechanism would be feature-level fusion where information is fused from all k inputs. In any case, as a black-box test, the fusion scheme is proprietary and unknown.
 - The size of the **configuration data** is the total size of all files resident in a vendor-provided directory that contains arbitrary read-only files such as parameters, recognition models (e.g caffe). Generally a large value for this quantity may prohibit the use of the algorithm on a resource-constrained device.

¹²The FRVT 2018 API prohibited threading, so some gains from parallelism may be available on multiple-cores or multiple processors, if the feature extraction code could be distributed across them.

¹³Note also that factors of two or more may be realizable by exploiting modern vector processing instructions on CPUs. It is not clear in our measurements whether all developers exploited Intel’s AVX2 instructions, for example. Our machine was so equipped, but we insisted that the same compiled library should also run on older machines lacking that instruction. The more sophisticated implementations may have detected AVX2 presence and branched accordingly. The less sophisticated may be defaulted to the reduced instruction set. Readers should see the FRVT 2018 API document for the specific chip details.

▷ Tables 25-26 report core rank-based accuracy for mugshot images. The population size is limited to $N = 1.6$ million identities because this is the largest gallery size on which all algorithms were executed. Notable observations from these tables are as follows:

- **Accuracy gains since 2018:** NIST Interagency Report 8238 documented massive gains over those reported in the FRVT 2014 report, NIST Interagency Report 8009. Further gains are documented in this report. Comparing the most accurate algorithm in November 2018, NEC-3, the value of $\text{FNIR}(N, L, T)$ reduced from 0.0031 to 0.0024 for the Sensetime-004 algorithm with $N = 12$ million recent images. The tables show broader gains: many developers have made advances since 2018 with between two and five-fold reduction in errors.
- **Wide range in accuracy:** The rank-1 miss rates vary from $\text{FNIR}(N, 1, 0) = 0.0012$ for sensetime-004 up to about 0.5 for the very fast but inaccurate microfocus-x algorithms. Among the developers who are superior to NEC in 2013, the range is from 0.002 to 0.035 for camvi-3. This large accuracy range is consistent with the buyer-beware maxim, and indicates that face recognition software is far from being commoditized.

▷ Tables 30-31 report threshold-based error rates, $\text{FNIR}(N, L, T)$, for $N = 1.6$ million for mugshot-mugshot accuracy on FRVT 2014, FRVT 2018, and also (in pink) mugshot-webcam accuracy using FRVT 2018 enrollments. Notable observations from these tables are as follows:

- **Order of magnitude accuracy gains since 2014:** As with rank-based results, the gains in accuracy are substantial, though somewhat reduced. At $\text{FPIR} = 0.01$, the best improvement over NEC in 2014 is a 27 fold reduction in FNIR using the NEC_2 algorithm. At $\text{FPIR} = 0.001$, the largest gain is a six-fold reduction in FNIR via the NEC_3 algorithm.
- **Broad gains across the industry:** About 19 companies realize accuracy better than the NEC benchmark from 2014. This is somewhat lower than the 28 developers who succeeded on the rank-1 metric. This may be due to the ubiquity of, and emphasis on, the rank-1 metric in many published algorithm development papers.
- **Webcam images:** Searches of webcam images give $\text{FNIR}(N, T)$ values around 2 to 3 times higher than mugshot searches. Notably the leading developers with mugshots are approximately the same with poorer quality webcams. But some developers e.g. Camvi, Megvii, TongYi, and Neurotechnology do improve their relative rankings on webcams, perhaps indicating their algorithms were tailored to less constrained images.

▷ Tables 18, 21, 22 and show, respectively, high-threshold, rank 1, and rank 50 FNIR values for all algorithms performing searches into five different gallery sizes, $N = 640\,000$, $N = 1\,600\,000$, $N = 3\,000\,000$, $N = 6\,000\,000$ and $12\,000\,000$. The $\text{FPIR} = 0.001$ table is included to inform high-volume duplicate detection applications. The Rank-1 table is included as a primary accuracy indicator. The Rank-50 table is included to inform agencies who routinely produce 50 candidates for human-review. The notable results are:

- **Slow growth in rank-based miss rates:** $\text{FNIR}(N, R)$ generally grows as a power law, aN^b . From the straight lines of many graphs of Figure 20 this is clearly a reasonable model for most, but not all, algorithms. The coefficient a can be interpreted as FNIR in a gallery of size 1. The more important coefficient b indicates scalability, and often, $b \ll 1$, implies very benign growth in FNIR. The coefficients of the models appear in the Tables 21 and 22.
- **Slow growth in threshold-based miss rates:** $\text{FNIR}(N, T)$ also generally grows as a power law, aN^b except at the high threshold values corresponding to low FPIR values. This is visible in the plots of Figure 36 which

show straight lines except for $FPIR = 0.001$, which increase more rapidly with N above 3 000 000. Each trace in those figures shows $FNIR(N, T)$ at fixed $FPIR$ with both N and T varying. Thus at large N , it is usually necessary to elevate T to maintain fixed $FPIR$. This causes increased $FNIR$. Why that would no-longer obey a power-law is not known. However, if we expect large galleries to contain individuals with familial relations to the non-mate search images - in the most extreme case, twins - then suppression of false positives becomes more difficult. This is discussed in the Figures starting at Fig. 10

▷ Figure ?? shows false positives from twins against their enrolled siblings, broken out by type of twin: fraternal or identical. The Figure is based on the enrollment of 104 single images on one of a pair of twins, and then the search of 2354 second images. Note that the dataset is heavily skewed towards identical twins which is not representative of the true population. There is also a skew towards same sex fraternal twin pairs compared to different sex fraternal twin pairs again not representative of the true population.

The notable results are:

- For all algorithms tested, the 1087 mated searches (Twin A vs. Twin A) produce scores almost always above typical operational thresholds, with (not shown) matches at rank 1. The images are of good quality, so this is the result expected from the rest of this report.
- For the 1066 identical twin searches (AB), almost all produce the twin at rank 1, with a few producing the mate at further down the candidate lists rank and low score.
- For the 169 fraternal searches (AB) from same sex pairs, most algorithms give a large number of very high scores, implying false positives at all thresholds. However, there are long tails containing lower scores that are correctly below threshold. In general, scores that are higher in this distribution are all rank 1 whereas the lower scores have much higher ranks.
- (Not shown) Of the 169, there are 24 fraternal searches (AB) involving different sex twins. Here most algorithms correctly report scores well below the lowest threshold, and usually not on the candidate list at all.

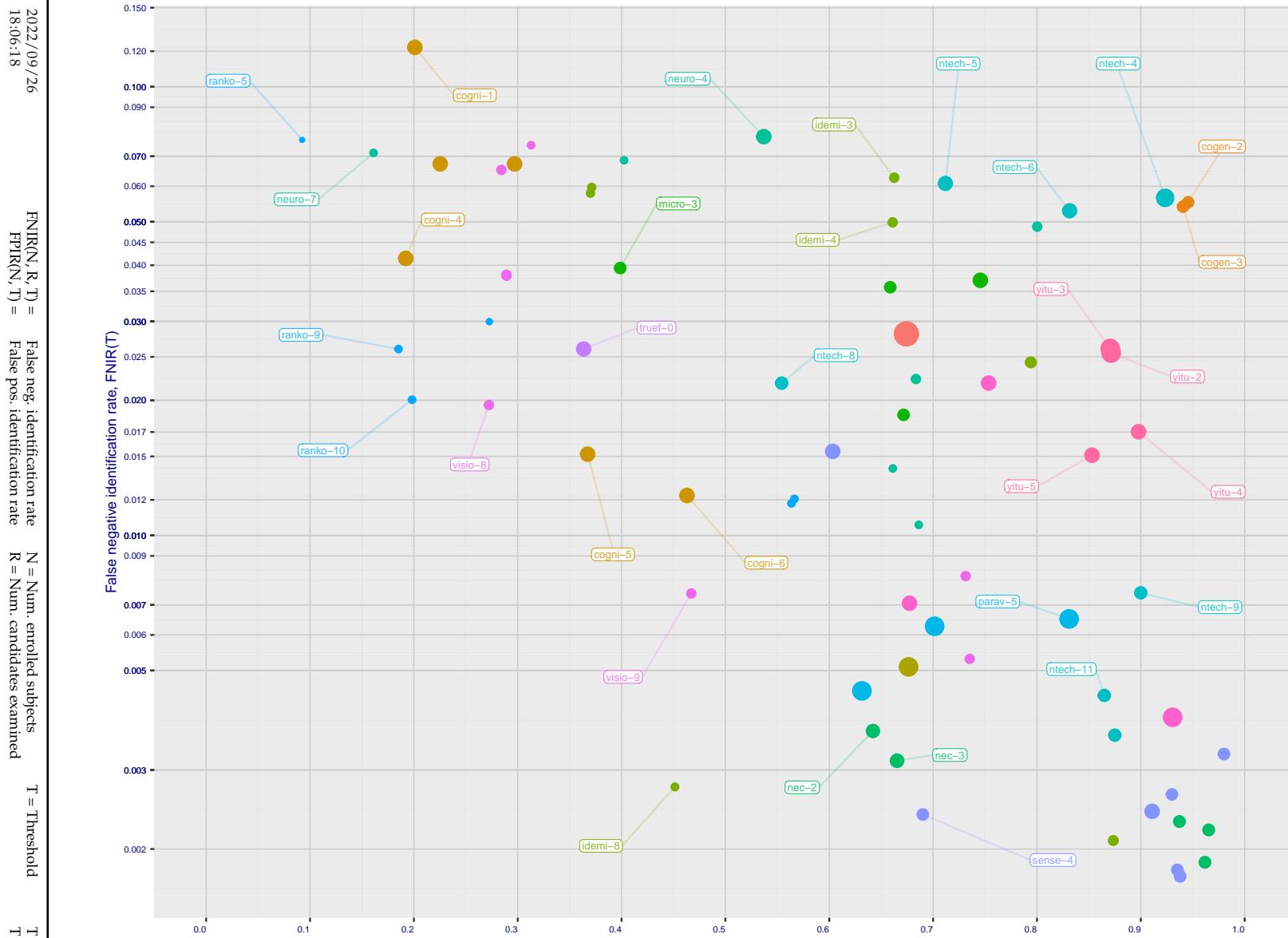


Figure 18: [Mugshot Dataset] Speed-accuracy tradeoff. For developers of the more accurate algorithms the plot shows the tradeoff of high-threshold recognition miss-rates, $\text{FNIR}(N, N, T)$ for $\text{FPIR}(N, T) = 0.003$, and template generation time. Developers are coded by color. Template size is encoded by the size of the circle. Some labels are quite distant from the respective point, to avoid superposing text. Without any other influences, the assumption would be that taking time to localize the face, and extract features, would lead to better accuracy. The most notable result, for NEC, is that their slower algorithms are much more accurate than the version that extract features in fewer than 90 milliseconds.

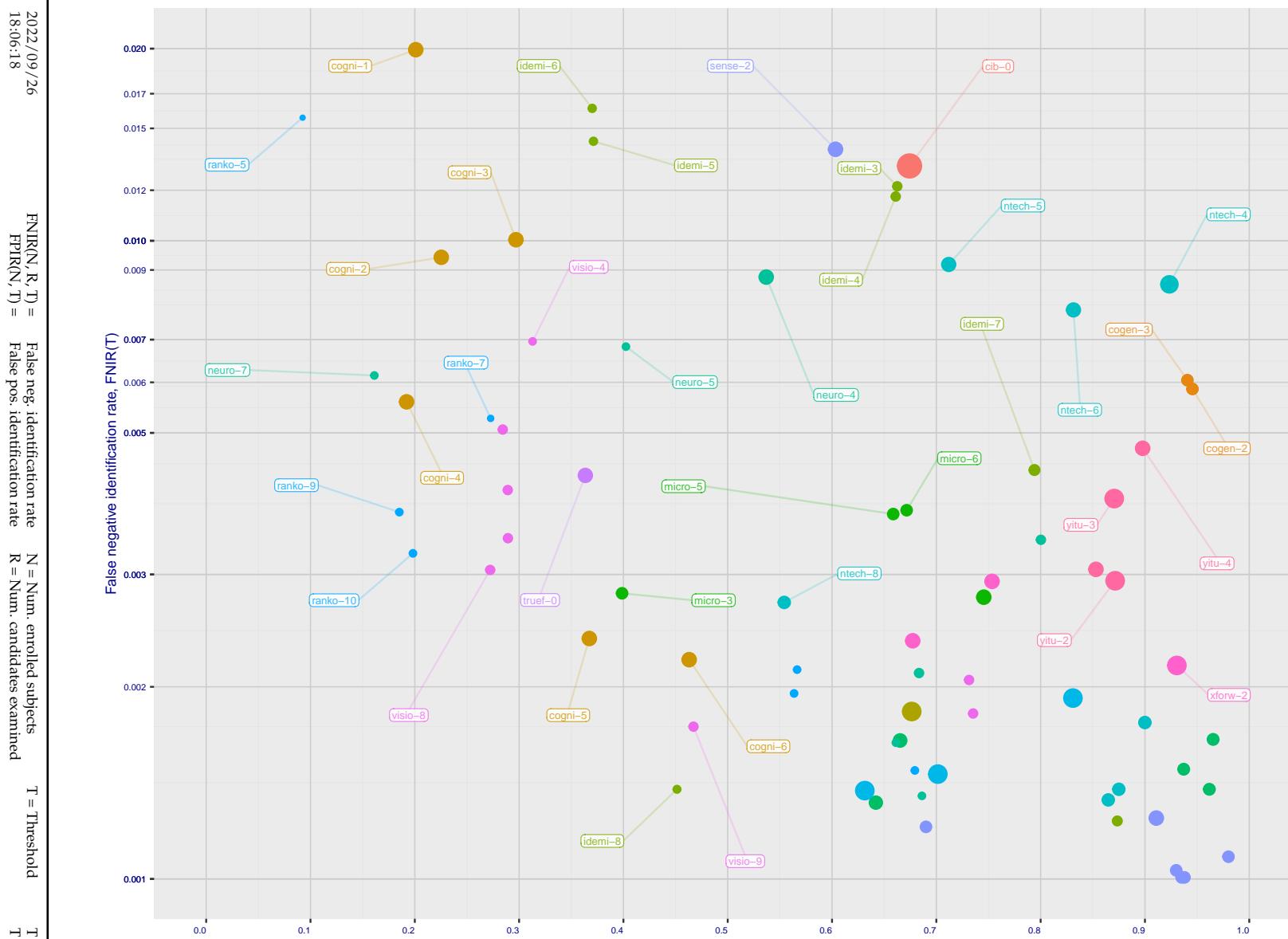


Figure 19: [Mugshot Dataset] Speed-accuracy tradeoff. For developers of the more accurate algorithms the plot shows the tradeoff of rank-one recognition miss-rates, $\text{FNIR}(N, 1, 0)$, and template generation time. Developers are coded by color. Template size is encoded by the size of the circle. Some labels are quite distant from the respective point, to avoid superposing text. Without any other influences, the assumption would be that taking time to localize the face, and extract features, would lead to better accuracy. This occurs for NEC with their slower algorithm being much accurate than the version that extract features in fewer than 90 milliseconds.

	DEVELOPER	SHORT	SEQ.	VALIDATION	CONFIG ¹	LIB ¹	TEMPLATE GENERATION			FINALIZE ²	SEARCH DURATION ⁵ MILLISEC					
							DATA (MB)	DATA (MB)	SIZE (B)		N=1.6M	N=1.6M	N=3M	N=6M	N=12M	(μ s)
	FULL NAME	NAME	NUM.	DATE												
1	20Face	20face	000	2021-10-01	112	319	141	2048	-	21.236	71.9	(227)6355	(229)6341	-	-	-
2	3Divi	3divi	5	2018-10-26	186	51	218	4096	k	116.638	189.28	(101)538	(101)537	(94)1377	(90)2614	(85)5530
3	3Divi	3divi	6	2018-10-26	187	51	41	528	k	117.640	29.5	(14)33	(14)33	-	-	-
4	Acer Incorporated	acer	000	2020-08-12	35	67	34	512	-	17.198	19.4	(65)295	(64)295	(54)623	(84)2302	(77)4915
5	Acer Incorporated	acer	001	2021-11-08	42	610	121	2048	-	12.184	68.9	(115)619	(110)575	-	-	-
6	Akurat Satu Indonesia	ptakuratsatu	000	2020-10-23	0	572	44	538	-	223.905	242	28633	(7)15	(6)16	(5)17	(4)17
7	Alchera Inc	alchera	2	2018-10-30	7	14	145	2048	k	6.114	220.63	(202)2923	(205)2929	-	-	-
8	Alchera Inc	alchera	3	2018-10-30	251	14	125	2048	k	91.531	221.63	(203)2955	(206)2956	(177)6546	(178)15013	(178)35262
9	Alchera Inc	alchera	004	2021-09-17	476	24	118	2048	-	198.853	204.35	(225)6657	(235)6851	-	-	-
10	Alivia / Innovation Sys	isystems	3	2018-10-30	350	784	108	2048	1	187.825	152.16	(78)385	(81)389	(94)979	(71)1822	(116)9348
11	AllGoVision	allgogvision	000	2019-07-30	168	150	97	2048	k	55.404	102.12	(206)3226	(209)3193	(179)6129	(178)12449	(174)25835
12	AllGoVision	allgogvision	001	2020-07-14	283	126	169	2048	-	172.777	108.13	(205)3174	(208)3183	(174)6073	(173)12284	(173)25701
13	Anke Investments	anke	0	2018-10-30	779	27	205	2072	k	63.429	149.16	(118)675	(124)748	(101)1483	(99)2968	(94)6148
14	Anke Investments	anke	1	2018-10-30	779	27	206	2072	k	64.430	142.15	(123)707	(127)769	-	-	-
15	Anke Investments	anke	002	2019-06-27	341	401	199	2056	k	108.623	120.13	(116)624	(118)682	(91)1306	(86)2403	(82)5082
16	Aware	aware	5	2018-10-30	368	27	215	3100	k	177.792	201.34	(18)95	(23)98	(22)203	(19)371	(14)252
17	Aware	aware	6	2018-10-30	368	27	2	124	k	176.789	4.2	(35)158	(35)162	-	-	-
18	Ayonix	ayonix	1	2018-10-29	74	2	68	1036	k	2.12	94.11	(61)279	(60)279	-	-	-
19	Ayonix	ayonix	2	2018-10-30	74	2	67	1036	1	1.11	126.14	(60)279	(59)276	(43)535	(43)1087	(43)2284
20	Camvi Technologies	camvitech	4	2018-10-30	233	220	52	1024	1	136.686	197.31	(15)33	(13)32	(12)38	(10)40	(7)48
21	Camvi Technologies	camvitech	5	2018-10-30	257	220	56	1024	1	161.751	197.31	(13)31	(10)30	-	-	-
22	Canon Inc	cib	000	2020-10-19	426	127	243	8196	-	128.674	227.113	(207)3589	(211)3604	(178)6738	(176)13495	(175)27114
23	Canon Inc	canon	001	2021-10-27	1139	91	222	4096	-	212.885	175.21	(230)6804	(233)6789	(196)12741	(192)25650	(189)51922
24	Canon Inc	canon	002	2022-04-26	1231	111	237	6200	-	218.897	218.58	(232)7673	(236)7599	(194)12416	(194)28503	(192)57633
25	Clearview AI Inc	clearviewai	000	2021-11-12	358	316	228	4096	-	166.765	194.30	(129)802	(115)657	(82)1134	(79)1939	(69)3889
26	Cloudwalk - Hengrui AI Technology	hr	000	2021-02-10	501	392	167	2048	-	222.905	135.15	(62)282	(56)276	(45)539	(52)1268	(61)3177
27	Cloudwalk - Moontime Smart Technology	cloudwalk	000	2022-01-31	716	573	135	2048	-	204.869	86.10	(89)440	(77)371	(47)547	(42)1065	(55)2902
28	Cloudwalk - Moontime Smart Technology	cloudwalk	mtt	2022-07-27	797	574	136	2048	-	238.953	130.14	(26)273	(28)427	(63)784	(63)1601	(63)3341
29	Cognitec Systems GmbH	cognitec	2	2018-10-30	463	26	176	2052	k	20.225	184.27	(177)1733	(179)1763	(157)3660	(152)7279	(148)13895
30	Cognitec Systems GmbH	cognitec	3	2018-10-30	465	26	188	2052	k	32.297	147.16	(176)1719	(180)1791	(155)3638	(151)7277	(155)14904
31	Cognitec Systems GmbH	cognitec	004	2021-03-08	384	60	175	2052	-	15.192	118.13	(175)1673	(177)1727	(142)2904	(140)5801	(138)11707
32	Cognitec Systems GmbH	cognitec	005	2021-07-30	460	61	173	2052	-	42.367	73.9	(167)1556	(169)1551	(144)2916	(148)6561	(149)13958
33	Cognitec Systems GmbH	cognitec	006	2022-02-10	689	61	177	2052	-	74.463	83.10	(144)1006	(140)1002	(119)2097	(115)4312	(105)7624
34	Cubox	cubox	000	2021-08-24	529	298	160	2048	-	226.917	82.10	(208)3646	(213)4076	(180)7605	(179)15871	-
35	Cyberlink Corp	cyberlink	000	2019-06-12	217	93	180	2052	1	121.654	193.30	(230)696	(230)701	(95)1379	(91)2639	(96)6214
36	Cyberlink Corp	cyberlink	001	2019-10-07	459	102	186	2052	1	61.423	198.28	(211)698	(119)700	(93)1350	(138)5524	(141)12031
37	Cyberlink Corp	cyberlink	002	2020-07-31	333	109	235	4140	-	152.724	232.6875	(164)1353	(210)3198	(176)6138	(172)12205	(146)13106
38	Cyberlink Corp	cyberlink	003	2021-01-05	333	100	240	6212	-	139.691	206.35	(95)488	(121)723	(98)1415	(97)2886	(87)5643
39	Cyberlink Corp	cyberlink	004	2021-07-16	371	100	239	6212	-	154.728	179.23	(95)492	(98)504	(72)923	(59)1448	(64)3350
40	Cyberlink Corp	cyberlink	005	2022-01-07	371	100	238	6212	-	156.733	196.30	(97)501	(94)498	(87)1193	(92)2672	(89)5693
41	DAON	daon	000	2021-12-23	274	2	202	2069	-	98.583	51.8	(100)524	(111)625	(99)1454	(102)3097	(98)6316
42	Dahua Technology Co Ltd	dahua	0	2018-10-29	276	167	163	2048	k	47.374	177.22	-	(50)258	-	-	(127)1.16N ^{1.1}
43	Dahua Technology Co Ltd	dahua	1	2018-10-29	276	167	110	2048	k	43.369	186.28	-	(54)257	(52)602	(49)1202	(58)3007
44	Dahua Technology Co Ltd	dahua	002	2019-12-02	607	137	128	2048	k	134.685	169.19	(48)243	(57)269	(85)1189	(98)2950	(102)6732
45	Dahua Technology Co Ltd	dahua	003	2020-11-18	889	154	102	2048	-	151.723	161.18	(63)283	(53)249	(40)468	(40)935	(38)1871
46	Dahua Technology Co Ltd	dahua	004	2021-11-18	812	116	115	2048	-	164.758	88.11	(86)423	(85)411	(66)871	(62)1568	(60)3174
47	Decatur Industries Inc	decatur	000	2022-02-09	411	383	185	2052	-	200.863	75.9	(178)1761	(187)2023	(150)3361	(153)7283	(152)14592
48	Deepglint	deepglint	001	2019-11-15	448	265	229	4096	-	130.676	203.35	(119)677	(167)1495	(110)1724	(94)2747	(97)6246
49	Dermalog	dermalog	5	2018-10-26	0	440	3	128	1	90.528	231.3155	(31)0	(1)0	(1)0	(1)0	(1)0
50	Dermalog	dermalog	6	2018-10-26	0	453	14	256	1	85.507	5.2	(32)142	(32)144	(27)269	(26)531	(25)1294
51	Dermalog	dermalog	007	2020-02-12	0	424	4	128	1	58.410	2.1	(24)98	(24)218	(22)429	(22)1013	(156)0.011N ^{1.1}
52	Dermalog	dermalog	008	2021-01-25	0	531	33	512	-	44.370	21.4	(71)335	(48)246	(39)462	(39)924	(37)1849

Notes																
1 Configuration size does not capture static data present in libraries. Libraries are included but the size also includes any ancillary libraries for image processing (e.g. openCV) or numerical computation (e.g. blas).																
2 Finalization is the processing of converting N = 1600000 templates into a searchable data structure an operation which can be a simple copy, or the building of an index or tree, for example. The duration of the operation may be data dependent, and may not be linear in the number of input templates.																
3 This multiplier expresses the increase in template size when k images are passed to the template generation function.																
4 All durations are measured on Intel®Xeon®@CPU E5-2630 v4 @ 2.20GHz processors. Estimates are made by wrapping the API function call in calls to std::chrono::high_resolution_clock which on the machine in (3) counts 1ns clock ticks. Precision is somewhat worse than that however.																
5 Search durations are measured as in the prior note. The power-law model in the final column mostly fits the empirical results in Figure 196. However in certain cases the model is not correct and should not be used numerically.																

Table 2: Summary of algorithms and properties included in this report. The blue

	DEVELOPER	SHORT	SEQ.	VALIDATION	CONFIG ¹	LIB ¹	TEMPLATE GENERATION			FINALIZE ²	SEARCH DURATION ³ MILLISEC													
							NAME	NUM.	DATE	DATA (MB)	DATA (MB)	SIZE (B)	MULT ³	TIME (MS) ⁴	TIME (S)	L=1	L=50	L=50	L=50	L=50	POWER LAW (μ s)			
	FULL NAME						N=1.6M	N=1.6M	N=1.6M	N=3M	N=6M	N=12M												
53	Dermalog	dermalog	009	2021-11-09	0	318	36	512	-	38	347	15	3	(53)	253	(49)	246	(38)	461	(36)	1846	³⁷ 0.16N ^{1.0}		
54	Dermalog	dermalog	010	2022-07-25	0	514	30	512	112	633	17	3	(47)	241	(47)	242	(37)	454	(35)	910	(35)1823	⁴⁰ 0.15N ^{1.0}		
55	Digidata	digidata	000	2022-06-03	248	33	139	2048	-	94	560	230	2444	(2)	0	(18)	95	-	-	-	-			
56	DiluSense Technology	dilusense	000	2022-05-26	311	56	129	2048	-	24	247	183	26	(182)	1904	(182)	1898	(154)	3597	(150)	7256	(153)14689	⁸⁵ 0.88N ^{1.0}	
57	FarBar Inc	f8	001	2019-10-03	266	19	168	2048	k	182	810	123	14	-	-	-	-	-	-	-	-			
58	Fincore Ltd	fincore	000	2021-08-18	250	224	96	2048	-	77	475	62	9	(109)	562	(106)	560	-	-	-	-	-		
59	Fujitsu Research and Development Center	fujitsulab	000	2021-10-12	497	337	63	1032	-	236	945	31	5	(174)	1668	(173)	1657	(148)	3140	(145)	6320	(144)12723	⁸³ 0.78N ^{1.0}	
60	Fujitsu Research and Development Center	fujitsulab	001	2022-03-15	675	386	62	1032	-	211	882	63	9	(180)	1854	(181)	1817	(151)	3451	(149)	6986	(150)14166	¹⁰² 0.72N ^{1.0}	
61	Gorilla Technology	gorilla	2	2018-10-29	91	1252	76	1132	k	37	338	181	24	(33)	145	(33)	146	(29)	293	(27)	612	(29)1509	¹⁵⁴ 0.02N ^{1.1}	
62	Gorilla Technology	gorilla	3	2018-10-26	94	1252	208	2156	k	93	559	236	2020	-	(188)	2047	-	-	-	-	-	-		
63	Gorilla Technology	gorilla	004	2020-01-06	182	1244	209	2192	k	50	388	208	41	(64)	286	(63)	285	(96)	1191	(87)	2416	(81)5036	¹⁹³ 0.00N ^{1.3}	
64	Gorilla Technology	gorilla	005	2021-02-22	306	1420	241	6288	-	81	483	223	78	(128)	802	(128)	799	(103)	1514	(118)	4454	(112)8820	¹⁷⁸ 0.05N ^{1.2}	
65	Gorilla Technology	gorilla	006	2021-09-30	377	691	244	8336	-	167	767	226	99	(170)	1626	(170)	1612	(128)	2422	(117)	4422	(117)9363	⁸² 0.59N ^{1.0}	
66	Gorilla Technology	gorilla	007	2022-02-16	392	322	242	6290	-	89	526	225	89	(126)	765	(123)	745	(97)	1408	(96)	2823	(90)5764	⁶⁵ 0.42N ^{1.0}	
67	Griaule	griaule	000	2021-11-01	0	584	174	2052	-	60	417	45	8	(222)	5827	(226)	6150	(188)	11473	(186)22952	(183)46070	³⁴ 3.89N ^{1.0}		
68	Griaule	griaule	001	2022-07-26	0	615	182	2052	-	245	1102	97	12	(223)	5866	(227)	6181	(190)	11629	(187)23175	(184)46504	⁵¹ 3.74N ^{1.0}		
69	Guangzhou Pixel Solutions Co Ltd	pixelall	002	2019-07-01	0	165	210	2560	k	14	190	139	15	(161)	1296	(163)	1334	(155)	2526	(130)	5136	(134)11045	¹⁰⁷ 0.52N ^{1.0}	
70	Guangzhou Pixel Solutions Co Ltd	pixelall	003	2019-11-05	0	690	213	2560	k	145	703	178	22	(158)	1273	(159)	1307	(132)	2474	(131)	5198	(135)11141	¹¹¹ 0.46N ^{1.0}	
71	Guangzhou Pixel Solutions Co Ltd	pixelall	004	2020-07-02	0	538	212	2560	k	66	449	161	17	(157)	1259	(158)	1300	(131)	2465	(136)	5492	(136)11443	¹³³ 0.34N ^{1.1}	
72	Guangzhou Pixel Solutions Co Ltd	pixelall	005	2021-03-23	0	717	211	2560	-	193	840	92	11	(169)	1606	(168)	1528	(157)	2609	(127)	4926	(139)11770	⁷⁰ 0.73N ^{1.0}	
73	Hangzhou Allu Network Information Technology	hzailu	000	2022-03-18	855	97	53	1024	-	119	649	93	11	(199)	2609	(203)	2551	(172)	4813	(170)	9702	(169)19338	⁵⁸ 1.50N ^{1.0}	
74	Hangzhou Allu Network Information Technology	hzailu	001	2022-08-18	273	162	98	2048	-	171	777	99	12	(211)	4537	(217)	4637	(183)	8666	(181)	17109	(180)39805	¹⁰⁹ 1.79N ^{1.0}	
75	Hikvision Research Institute	hikvision	5	2018-10-29	593	9	81	1408	1	103	607	145	16	(137)	883	(138)	895	(114)	1908	(108)	3792	(118)9387	¹⁶⁵ 0.10N ^{1.1}	
76	Hikvision Research Institute	hikvision	6	2018-10-29	593	9	82	1408	1	101	598	148	16	(135)	871	(137)	877	-	-	-	-	-		
77	HyperVerge Inc	hyperverge	001	2021-08-11	1791	212	55	1024	-	196	845	27	5	(122)	705	(117)	681	(92)	1346	(93)	2681	(88)5680	⁹³ 0.32N ^{1.0}	
78	HyperVerge Inc	hyperverge	002	2022-04-13	1140	1118	51	1024	-	229	934	67	9	(117)	661	(116)	659	(90)	1292	(80)	2188	(41)2181	¹⁷ 11.29N ^{0.8}	
79	Idemia	idemia	5	2018-10-29	417	48	24	352	1	46	371	25	5	(29)	137	(30)	138	(34)	437	(32)	724	(31)1630	¹⁸ 0.01N ^{1.2}	
80	Idemia	idemia	6	2018-10-29	417	48	25	352	1	45	370	25	4	(30)	137	(29)	138	(35)	442	(35)	827	(32)1646	¹⁸⁹ 0.01N ^{1.2}	
81	Idemia	idemia	007	2020-01-17	738	113	50	860	1	178	794	124	14	(34)	151	(34)	152	(58)	683	(61)	1481	(59)3022	¹⁹⁸ 0.00N ^{1.4}	
82	Idemia	idemia	008	2021-03-15	378	65	23	300	-	68	451	16	3	(28)	132	(28)	131	(25)	247	(24)	501	(23)1013	⁶⁸ 0.07N ^{1.0}	
83	Idemia	idemia	009	2022-03-01	735	68	48	636	-	206	873	39	7	(43)	211	(42)	205	(33)	389	(34)	787	(30)1615	⁸⁰ 0.10N ^{1.0}	
84	Imagus Technology Pty Ltd	imagus	005	2021-01-15	222	311	157	2048	-	175	786	122	14	(46)	236	(67)	313	(56)	651	(56)	1361	(46)2461	¹⁶³ 0.03N ^{1.1}	
85	Imagus Technology Pty Ltd	imagus	006	2021-05-27	248	369	133	2048	-	221	904	76	9	(69)	317	(45)	234	(41)	499	(53)	1273	(50)2727	¹⁸⁴ 0.01N ^{1.2}	
86	Imagus Technology Pty Ltd	imagus	007	2021-11-16	248	366	109	2048	-	104	609	57	9	(49)	234	(46)	238	(36)	442	(36)	881	(34)1765	²⁹ 0.16N ^{1.0}	
87	Imagus Technology Pty Ltd	imagus	008	2022-05-26	204	335	146	2048	-	68	445	158	17	(107)	560	(109)	565	-	-	-	-	-		
88	Imperial College London	imperial	000	2019-08-28	461	15	120	2048	1	97	577	167	13	(73)	360	(80)	379	(107)	1626	(112)	4057	(132)10291	²⁰¹ 0.00N ^{1.5}	
89	Incode Technologies Inc	incode	2	2018-10-29	71	31	100	2048	1	30	289	144	15	(84)	411	(82)	404	-	-	-	-	-		
90	Incode Technologies Inc	incode	3	2018-10-29	133	31	116	2048	1	142	697	134	15	(80)	408	(86)	412	(65)	847	(64)	1608	(75)4486	¹⁵⁸ 0.05N ^{1.1}	
91	Incode Technologies Inc	incode	004	2019-06-24	254	50	103	2048	1	78	475	98	12	(76)	365	(79)	378	(100)	1482	(66)	1660	(57)2954	¹³¹ 0.12N ^{1.1}	
92	Incode Technologies Inc	incode	005	2021-07-29	259	21	123	2048	-	83	500	81	10	(68)	316	(91)	454	(70)	890	(72)	1843	(67)3640	¹⁴⁷ 0.07N ^{1.1}	
93	Innovatrics	innovatrics	4	2018-10-30	0	400	72	1076	k	51	399	233	10902	(6)	8	(4)	8	(4)	11	(2)	9	(3)	13	⁹ 668.38N ^{0.2}
94	Innovatrics	innovatrics	005	2019-09-30	0	455	43	538	1	189	827	235	11897	(5)	8	(5)	8	(3)	9	(3)	9	(2)	9	¹ 4055.65N ^{0.1}
95	Innovatrics	innovatrics	007	2021-08-16	175	58	42	538	-	170	777	125	14	(23)	97	(25)	100	(19)	188	(21)	378	(20)788	²⁶ 0.09N ^{1.0}	
96	Intellivision	intellivision	001	2022-03-08	62	130	194	2056	-	57	406	172	20	(79)	388	(78)	377	-	-	-	-	-		
97	Intellivision	intellivision	002	2022-07-28	114	128	195	2056	-	34	331	113	13	(23)	2052	(24)	20448	-	-	-	-	-		
98	Intema-LGL Group	intema	000	2022-08-24	1042	20	32	512	-	158	737	240	13809	(12)	27	(11)	31	(10)	36	(12)	44	(10)	54	¹¹ 791.50N ^{0.3}
99	IrexAI	irex	000	2021-02-09	724	46	214	3080	-	195	844	168	19	(114)	616	(111)	600	(81)	1120	(89)	2477	(91)	5863	¹³⁰ 1.13N ^{1.1}
100	Kakao Enterprise	kakao	000	2021-06-23	404	124	184	2052	-	192	835	47	8	(44)	213	(43)	215	(42)	510	(41)	971	(39)1955	¹⁴² 0.05N ^{1.1}	
101	Kakao Enterprise	kakao	001	2022-06-0																				

	DEVELOPER	SHORT	SEQ.	VALIDATION	CONFIG ¹	LIB ¹	TEMPLATE GENERATION	FINALIZE ²	SEARCH DURATION ⁵ MILLISEC							
									TIME (S)	L=1		L=50		L=50		
										N=1.6M	N=1.6M	N=1.6M	N=3M	N=6M	N=12M	
105	Line Corporation	line	000	2021-06-02	138	397	107 2048	-	79 481	52 8	(217) 5433	(221) 5418	(186) 10144	-	-	32 3.65N ^{1.0}
106	Line Corporation	line	001	2021-11-21	471	396	124 2048	-	234 907	53 8	(181) 1872	(185) 1934	(156) 3647	(157) 7675	-	121 0.64N ^{1.0}
107	Line Corporation	lineclova	002	2022-07-29	560	72	166 2048	-	186 824	114 13	(54) 262	(55) 257	-	-	-	-
108	Lomonosov Moscow State University	intsysmsu	000	2019-08-19	375	168	140 2048	1	106 614	115 13	(87) 430	(89) 431	(68) 860	(67) 1730	(84) 5353	173 0.03N ^{1.1}
109	Lookman Electroplast Industries	lookman	3	2018-10-28	203	24	21 292	1	36 336	14 3	(124) 739	(122) 745	(96) 1394	(95) 2817	(107) 8286	151 0.13N ^{1.1}
110	Lookman Electroplast Industries	lookman	4	2018-10-28	184	24	48 548	1	33 320	24 4	(141) 981	(142) 998	-	-	-	-
111	Lookman Electroplast Industries	lookman	005	2019-09-16	239	36	45 548	1	84 506	20 4	(143) 1005	(144) 1008	(136) 2597	(135) 5446	(113) 8939	149 0.19N ^{1.1}
112	Mantra Softech India	mantra	000	2021-10-28	460	61	183 2052	-	59 412	80 10	(139) 916	(139) 910	(109) 1714	(107) 3411	(103) 6841	38 0.57N ^{1.0}
113	Maxvision	maxvision	000	2022-06-17	167	60	105 2048	-	11 183	1 1	(216) 5044	(220) 5188	(185) 9663	(184) 19358	(179) 39552	84 2.41N ^{1.0}
114	Megvii/Face++	megvii	1	2018-10-28	1703	41	221 4096	1	110 631	209 32	(104) 552	(107) 561	(89) 1222	(85) 2321	(92) 5968	157 0.08N ^{1.1}
115	Megvii/Face++	megvii	2	2018-10-28	1735	42	226 4096	1	114 635	198 31	(105) 553	(104) 558	-	-	-	-
116	MicroFocus	microfocus	5	2018-10-29	94	26	8 256	k	26 262	9 2	(40) 182	(39) 186	(31) 354	(31) 708	(27) 1425	60 0.11N ^{1.0}
117	MicroFocus	microfocus	6	2018-10-29	94	26	11 256	k	25 262	11 2	(41) 183	(38) 186	-	-	-	-
118	Microsoft	microsoft	5	2018-10-29	381	155	54 1024	1	122 658	95 11	(168) 1606	(174) 1673	(147) 3076	(144) 6302	(147) 13160	81 0.79N ^{1.0}
119	Microsoft	microsoft	6	2018-10-29	478	155	57 1024	1	126 671	138 15	(171) 1642	(172) 1618	(158) 3710	(146) 6401	(145) 12892	101 0.68N ^{1.0}
120	N-Tech Lab	ntech	5	2018-10-30	1685	113	93 1940	k	149 711	217 55	(50) 243	(51) 246	(44) 538	(44) 1100	(53) 2867	169 0.02N ^{1.1}
121	N-Tech Lab	ntech	6	2018-10-30	1686	117	94 1940	k	191 831	217 63	(49) 243	(50) 246	(46) 546	(45) 1104	(54) 2873	171 0.02N ^{1.1}
122	N-Tech Lab	ntechlab	007	2019-06-25	2450	51	216 3348	k	179 795	222 73	(80) 393	(87) 427	(62) 780	(70) 1768	(66) 3499	111 0.16N ^{1.0}
123	N-Tech Lab	ntechlab	008	2020-01-06	1111	51	80 1300	k	92 554	207 36	(39) 179	(36) 184	(30) 341	(30) 683	(26) 1395	53 0.11N ^{1.0}
124	N-Tech Lab	ntechlab	009	2021-03-01	1208	42	79 1300	-	219 899	205 35	(38) 178	(37) 184	(29) 336	(29) 676	(33) 1704	132 0.05N ^{1.1}
125	N-Tech Lab	ntechlab	010	2021-06-24	351	213	78 1280	-	207 874	32 6	(88) 440	(90) 435	(64) 821	(65) 1645	(62) 3337	75 0.22N ^{1.0}
126	N-Tech Lab	ntechlab	011	2021-12-07	679	208	77 1280	-	201 864	34 6	(94) 488	(93) 483	(71) 912	(73) 1869	(79) 5003	153 0.07N ^{1.1}
127	NEC	nec	2	2018-10-30	705	35	89 1616	k	118 642	165 18	(81) 405	(84) 409	(79) 1072	(68) 1755	(74) 4255	160 0.06N ^{1.1}
128	NEC	nec	3	2018-10-30	774	110	90 1712	k	124 665	173 21	(4) 7	(3) 14	(9) 40	(11) 82	(179) 0.00N ^{1.2}	-
129	NEC	nec	004	2021-07-19	971	63	74 1104	-	242 965	35 7	(72) 349	(72) 351	(56) 662	(54) 1330	(48) 2685	63 0.20N ^{1.0}
130	NEC	nec	005	2021-12-13	922	88	73 1104	-	241 961	36 7	(92) 473	(102) 551	(77) 1017	(78) 2091	(72) 4242	72 0.28N ^{1.0}
131	NEC	nec	006	2022-08-10	701	54	75 1104	-	231 937	61 9	(73) 358	(73) 354	(57) 666	(55) 1331	(49) 2707	55 0.21N ^{1.0}
132	Neurotechnology	neurotech	5	2018-10-30	266	53	12 256	k	53 402	10 2	(132) 835	(134) 839	(108) 1690	(106) 3219	(114) 8955	139 0.19N ^{1.1}
133	Neurotechnology	neurotech	6	2018-10-30	564	53	12 256	k	153 726	8 2	(133) 839	(135) 842	-	-	-	-
134	Neurotechnology	neurotech	007	2019-10-03	57	51	10 256	k	7 161	7 2	(149) 1118	(149) 1110	(121) 2143	(116) 4397	(115) 9045	80 0.55N ^{1.0}
135	Neurotechnology	neurotechnology	008	2021-03-22	355	49	40 514	-	180 800	23 4	(152) 1167	(152) 1149	(123) 2266	(121) 4573	(122) 9586	89 0.55N ^{1.0}
136	Neurotechnology	neurotechnology	009	2021-09-01	246	82	36 513	-	133 683	12 3	(146) 1035	(146) 1049	(117) 1977	(114) 4270	(110) 8756	125 0.32N ^{1.1}
137	Neurotechnology	neurotechnology	010	2022-01-07	247	83	15 256	-	123 661	3 2	(142) 988	(140) 984	(112) 1897	(111) 3977	(108) 8048	116 0.36N ^{1.0}
138	Neurotechnology	neurotechnology	012	2022-06-07	247	84	8 256	-	135 686	13 3	(147) 1036	(148) 1063	(113) 4179	(109) 8624	(112) 411N ^{1.0}	-
139	Newland Computer Co Ltd	newland	2	2018-10-30	96	27	154 2048	-	199 855	140 15	(234) 8741	(239) 8854	(202) 17892	(199) 39356	-	155 1.32N ^{1.1}
140	Noblis	noblis	1	2018-10-30	114	176	106 2048	1	18 206	138 15	(159) 1273	(156) 1272	-	-	-	-
141	Noblis	noblis	2	2018-10-30	153	176	236 6144	1	87 517	210 43	(197) 2513	(202) 2522	(173) 5649	(174) 12432	(182) 44262	191 0.04N ^{1.3}
142	NotionTag Technologies Private Limited	notiontag	000	2022-01-14	265	945	207 2120	-	69 453	84 10	(233) 8619	(238) 8705	(201) 16652	(198) 38794	(195) 90607	159 1.15N ^{1.1}
143	Pangiam	pangiam	000	2022-02-22	453	23	159 2048	-	115 636	157 17	(57) 276	(66) 319	(51) 601	(50) 1210	(45) 2443	61 0.18N ^{1.0}
144	Paravision (EverAI)	everai	2	2018-10-30	224	304	138 2048	1	41 366	195 30	(59) 278	(62) 283	-	-	-	-
145	Paravision (EverAI)	everai	3	2018-10-30	438	304	112 2048	1	150 717	188 28	(58) 278	(61) 281	(48) 572	(46) 1146	(42) 2278	103 0.12N ^{1.0}
146	Paravision (EverAI)	everai-paravision	004	2019-06-19	527	128	217 4096	1	127 672	213 45	(106) 559	(105) 559	(138) 2611	(147) 6445	(151) 14519	199 0.00N ^{1.5}
147	Paravision (EverAI)	paravision	005	2019-12-11	543	154	223 4096	1	190 830	217 48	(108) 561	(108) 564	(78) 1056	(82) 2298	(79) 4966	129 0.16N ^{1.1}
148	Paravision (EverAI)	paravision	007	2021-02-01	529	235	219 4096	-	143 701	216 48	(110) 569	(103) 558	(80) 1086	(79) 2111	(73) 4254	23 1.11N ^{0.9}
149	Paravision	paravision	009	2021-12-14	672	300	230 4100	-	111 631	224 82	(209) 3690	(214) 4230	(181) 8037	(180) 16532	(176) 31422	105 1.62N ^{1.0}
150	Qnap Security	qnap	000	2021-07-28	182	15	144 2048	-	70 457	69 9	(154) 1231	(178) 1763	-	-	-	-
151	Qnap Security	qnap	001	2021-12-09	191	13	158 2048	-	105 613	48 8	(173) 1666	(166) 1429	(152) 3472	(154) 7375	(157) 15159	176 0.11N ^{1.2}
152	Qnap Security	qnap	002	2022-04-15	338	32	117 2048	-	185 822	156 17	(140) 958	(153) 1179	(120) 2312	(124) 4789	(129) 9791	141 0.24N ^{1.1}
153	Quantasoft	quantasoft	1	2018-10-30	276	452	143 2048	k	49 385	33 6	(235) 15422	(240) 14858	(199) 14717	-	(162) 18323	-
154	Rank One Computing	rankone	4	2018-10-09	0	101	185	k	3 36	37 7	(25) 101	(26) 101	(21) 190	-	-	30 0.07N ^{1.0}
155	Rank One Computing	rankone	5	2018-10-24	0	101	5 133	k	4 92	38 7	(31) 140	(31) 144	(26) 266	(25) 525	(24) 1049	27 0.11N ^{1.0}
156	Rank One Computing	rankone	006	2019-06-03	0	133	7 165	k	23 245	46 8	-	-	-	-	-	-

Notes
1 Configuration size does not capture static data present in libraries. Libraries are included but the size also includes any ancillary libraries for image processing (e.g. openCV) or numerical computation (e.g. blas).
2 Finalization is the processing of converting $N = 1600000$ templates into a searchable data structure an operation which can be a simple copy, or the building of an index or tree, for example. The duration of the operation may be data dependent, and may not be linear in the number of input templates.
3 This multiplier expresses the increase in template size when k images are passed to the template generation function.
4 All durations are measured on Intel® Xeon® CPU E5-2630 v4 @ 2.20GHz processors. Estimates are made by wrapping the API function call in calls to std::chrono::high_resolution_clock which on the machine in (3) counts 1ns clock ticks. Precision is somewhat worse than that however.
5 Search durations are measured as in the prior note. The power-law model in the final column mostly fits the empirical results in Figure 196. However in certain cases the model is not correct and should not be used numerically.

2022 / 09 / 26

18:06:18

FNIR(N, R, T) =

False neg. identification rate

N = Num. enrolled subjects

R = Num. candidates examined

	DEVELOPER	SHORT	SEQ.	VALIDATION	CONFIG ¹	LIB ²	TEMPLATE GENERATION			FINALIZE ³	SEARCH DURATION ⁵ MILLISEC											
							NAME	NUM.	DATE	DATA (MB)	DATA (MB)	SIZE (B)	MULT ⁴	TIME (MS) ⁴	TIME (S)	L=1	L=50	L=50	L=50	POWER LAW (μ s)		
N=1,6M	N=1,6M	N=1,6M	N=3M	N=6M	N=12M																	
157	Rank One Computing	rankone	007	2019-11-12	0	137	6	165	k	27	272	41	7	(27)	115	(23)	215	(23)	439	(21)	877	⁵⁹ 0.07N ^{1.0}
158	Rank One Computing	rankone	009	2020-06-26	0	105	16	260	k	13	185	91	11	(19)	95	(22)	96	(17)	181	(17)	362	⁴¹ 0.06N ^{1.0}
159	Rank One Computing	rankone	010	2020-11-05	0	135	17	261	-	18	198	85	10	(20)	95	(17)	95	(15)	178	(15)	357	³⁶ 0.06N ^{1.0}
160	Rank One Computing	rankone	011	2021-08-27	0	175	20	261	-	96	566	54	8	(22)	96	(19)	95	(18)	183	(18)	370	⁵⁰ 0.06N ^{1.0}
161	Rank One Computing	rankone	012	2021-12-27	0	257	19	261	-	95	563	48	8	(21)	95	(20)	95	(16)	179	(16)	361	³⁹ 0.06N ^{1.0}
162	Rank One Computing	rankone	013	2022-07-21	0	223	18	261	-	132	679	150	16	(26)	101	(24)	100	(20)	188	(20)	376	²² 0.20N ^{0.9}
163	Realnetworks Inc	realnetworks	2	2018-10-30	105	104	23	4104	k	27	241	187	28	(18)	208	(18)	2048	(16)	4194	(16)	8642	(156)15035
164	Realnetworks Inc	realnetworks	003	2019-06-12	93	102	91	1848	k	10	173	106	13	(15)	1145	(150)	1132	(120)	2142	(132)	5241	(133)10495
165	Realnetworks Inc	realnetworks	004	2019-10-17	94	102	92	1848	1	9	171	90	11	(150)	1143	(151)	1137	(122)	2149	(123)	4740	(125)9693
166	Realnetworks Inc	realnetworks	005	2021-06-23	168	209	193	2056	-	35	332	60	9	(172)	1654	(171)	1616	(146)	3030	(142)	6068	(124)12134
167	Realnetworks Inc	realnetworks	006	2021-12-02	250	56	190	2056	-	39	348	48	8	(103)	543	(100)	531	(76)	996	(77)	1998	(71)3991
168	Realnetworks Inc	realnetworks	007	2022-04-11	455	99	196	2056	-	113	634	157	17	(131)	815	(131)	812	(104)	1559	(103)	3159	(99)6361
169	Realnetworks Inc	realnetworks	008	2022-08-29	557	99	197	2056	-	245	668	100	12	(102)	538	(99)	525	(75)	986	(76)	1967	(86)5559
170	Remark Holdings	remarkai	000	2019-06-12	234	1092	148	2048	k	120	650	105	12	(221)	5776	(223)	5703	(189)	11604	(197)	32133	(196)91436
171	Remark Holdings	remarkai	0	2018-10-30	187	847	111	2048	k	99	593	128	14	(220)	5685	(224)	5723	-	-	-	-	-
172	Remark Holdings	remarkai	1	2018-10-30	187	847	113	2048	k	62	427	133	14	(219)	5680	(225)	5761	(193)	12475	(195)	28726	(193)59618
173	Rendip	rendip	000	2021-05-21	0	416	127	2048	-	214	890	72	9	(51)	249	(75)	368	(60)	697	(60)	1452	(56)2926
174	Reveal Media Ltd	revealmedia	000	2022-02-02	287	196	17	2052	-	48	383	79	10	(187)	2322	(186)	2019	(160)	3838	(159)	7816	(160)16559
175	SQLsoft	sqisoft	001	2021-12-20	271	377	191	2056	-	73	462	70	9	(162)	1310	(161)	1319	(130)	2456	(126)	4906	(128)9755
176	Samsung S1 Corp	s1	000	2021-06-03	257	196	227	4096	-	205	865	170	20	(229)	6715	(234)	6794	(197)	13032	(193)26372	(191)55723	
177	Samsung S1 Corp	s1	001	2021-11-01	240	198	161	2048	-	183	813	55	8	(189)	2415	(200)	2491	(170)	4718	(168)9614	(172)24472	(140)0.53N ^{1.1}
178	Samsung S1 Corp	s1	002	2022-05-04	244	93	165	2048	-	239	958	146	16	(159)	1234	(157)	1285	(127)	2411	(125)	4805	(126)9705
179	Scanova Ltd	scanovate	000	2020-01-15	250	446	97	2048	-	146	705	131	14	(166)	1419	(165)	1412	(145)	3008	(171)	11616	(140)12012
180	Scanova Ltd	scanovate	001	2020-09-10	250	446	164	2048	-	129	675	111	13	(163)	1321	(162)	1320	(133)	2502	(129)	5047	(130)10163
181	Sensetime Group	sensetime	0	2018-10-30	525	6	23	4104	k	14	693	209	41	(96)	498	(95)	501	(88)	1212	(81)	2281	(80)5032
182	Sensetime Group	sensetime	1	2018-10-30	525	6	234	4104	k	109	628	214	48	(99)	516	(96)	502	(83)	1146	(83)	2301	(76)4765
183	Sensetime Group	sensetime	002	2019-06-03	523	6	192	2056	k	102	603	163	18	(74)	359	(76)	370	(113)	1897	(110)	4508	(121)9543
184	Sensetime Group	sensetime	003	2019-12-02	769	76	198	2056	1	225	910	167	19	(214)	4885	(219)	4989	(192)	12325	(189)	24712	(186)49445
185	Sensetime Group	sensetime	004	2020-08-10	456	29	66	1032	-	130	690	104	12	(196)	2490	(196)	2477	(168)	4654	(167)	4402	(170)19651
186	Sensetime Group	sensetime	005	2020-12-17	631	39	65	1032	-	244	980	89	11	(192)	2459	(212)	3939	(179)	7398	(177)	14768	(160)19016
187	Sensetime Group	sensetime	006	2021-07-26	526	54	58	1032	-	227	929	42	7	(189)	2414	(195)	2422	(165)	4527	(163)	9128	(163)18640
188	Sensetime Group	sensetime	007	2022-01-15	526	37	59	1032	-	230	935	56	8	(190)	2432	(193)	2406	(163)	4513	(161)	8998	(166)18796
189	Sensetime Group	sensetime	008	2022-08-17	567	37	60	1032	-	232	937	66	9	(191)	2444	(194)	2419	(164)	4525	(162)	9114	(161)18279
190	Shaman Software	shaman	6	2018-10-26	0	200	10	2048	k	147	706	129	14	(113)	603	(112)	612	-	-	-	-	-
191	Shaman Software	shaman	7	2018-10-26	0	200	149	2048	k	148	707	132	14	(112)	602	(113)	614	(84)	1187	(88)	2448	(83)5083
192	Shanghai Yitu Technology	yitu	4	2018-10-30	2119	136	20	2070	1	21	897	212	45	(160)	1288	(159)	1203	(129)	2440	(130)	5241	(124)9671
193	Shanghai Yitu Technology	yitu	5	2018-10-30	2043	136	203	2070	1	197	853	211	44	(150)	1237	(154)	1199	(134)	2513	(128)	5013	(123)9620
194	Smilart	smilart	4	2018-10-30	65	89	27	512	k	167	167	24	4	(236)	16137	(241)	16333	-	-	-	-	-
195	Smilart	smilart	5	2018-10-30	562	89	156	2048	k	67	450	127	14	-	-	-	-	-	-	-	-	
196	Staqua Technologies	staqua	000	2021-08-30	1018	690	227	4096	-	188	826	182	24	(215)	4950	(218)	4933	-	-	-	-	-
197	Synesis	synesis	003	2019-07-04	143	17	150	2048	k	19	211	101	12	(98)	507	(97)	502	(124)	2297	(120)	4564	(119)9452
198	Synesis	synesis	3	2018-10-30	237	150	227	4096	k	5	99	191	29	(127)	789	(129)	801	(116)	1941	(110)	3888	(111)8810
199	Synesis	synesis	005	2020-09-08	494	24	232	4104	-	163	756	180	24	(136)	877	(136)	865	(149)	3182	(122)	4658	(127)9750
200	T4iSB	t4isb	000	2022-08-17	228	15	155	2048	-	160	741	117	13	(92)	250	(93)	250	-	-	-	-	-
201	Tech5 SA	tech5	001	2019-08-19	1394	116	89	1536	k	213	887	78	10	(77)	383	(126)	766	(140)	2767	(143)	6149	(95)6178
202	Tech5 SA	tech5	002	2021-04-07	727	112	39	513	-	234	940	18	4	(213)	4682	(232)	6689	(194)	12541	(190)	25145	(188)50239
203	Tencent Deepsea Lab	deepsea	001	2019-07-29	250	323	104	2048	1	159	737	103	12	(145)	1021	(141)	2774	(130)	5767	(143)	12341	¹⁸⁸ 0.06N ^{1.2}
204	Tevian	tevian	5	2018-10-30	773	15	130	2048	1	56	405	137	15	(82)	405	(83)	408	(66)	854	(69)	1757	(65)3380
205	Tevian	tevian	006	2021-04-16	769	19	61	1032	-	109	597	77	10	(66)	295	(65)	295	(49)	578	(48)	1187	(52)2741
206	Tevian	tevian	007	2021-10-12	703	19	61	1032	-	169	777	26	4	(66)	297	(66)	298	(50)	579	(47)	1179	(44)2418
207	Thales	cogent	2	2018-10-30	681	39	70	1043	k	235	945	185	27	(184)	2017	(191)	2144	(162)	4298	(159)	16429	⁷⁸ 1.08N ^{1.0}
208	Thales	cogent	3	2018-10-30	681	39	69	1043	k	233	940	74	9	(153)	1230	(160)	1311	(139)	2687	(130)	5398</td	

2022/09/26
18:06:18FNIR(N, R, T) = False neg. identification rate
FPIR(N, T) = False pos. identification rateN = Num. enrolled subjects
R = Num. candidates examined
T = ThresholdT = 0 → Investigation
T √ 0 → Identification

DEVELOPER	SHORT	SEQ.	VALIDATION	CONFIG ¹		LIB ¹	TEMPLATE GENERATION			FINALIZE ²	SEARCH DURATION ³ MILLISEC													
				NUM.	DATE		DATA (MB)	DATA (MB)	SIZE (B)	MULT ³	TIME (MS) ⁴	TIME (S)	L=1	L=50	L=50	L=50	POWER LAW							
FULL NAME	NAME										N=1.6M	N=1.6M	N=3M	N=6M	N=12M	(μ s)								
209 Thales	cogent	004	2021-02-10	1376	59	189	2053	-	237	947	121	14	(20)	2903	(183)	1911	(153)	3566	(155)	7498	(158)	16370	122	0.64 N ^{1.0}
210 Thales	cogent	005	2021-09-13	1043	56	71	1062	-	168	769	30	5	(138)	912	(141)	996	(111)	1872	(109)	3845	(104)	7555	92	0.44 N ^{1.0}
211 Thales	cogent	006	2022-05-14	508	70	47	550	-	194	843	44	8	(111)	587	(132)	820	(105)	1564	(104)	3173	(108)	8290	144	0.16 N ^{1.1}
212 TigerIT Americas LLC	tiger	2	2018-10-29	416	518	172	2052	k	71	461	141	15	(179)	1816	(184)	1921	(159)	3833	(156)	7526	(154)	14820	97	0.83 N ^{1.0}
213 TigerIT Americas LLC	tiger	3	2018-10-30	416	518	181	2052	k	72	461	244	37431	(42)	191	(40)	189	-	-	-	-	-	-	-	
214 Toshiba	toshiba	0	2018-10-30	961	105	88	1548	k	209	876	96	12	(226)	6153	(228)	6236	(191)	12221	(191)	25355	(187)	49448	127	0.36 N ^{1.2}
215 Toshiba	toshiba	1	2018-10-30	961	105	201	2060	k	208	875	245	44701	(225)	6007	(230)	6355	-	-	-	-	-	-	-	
216 Tripleize	aize	001	2021-08-06	262	150	134	2048	-	52	402	65	9	(204)	3087	(207)	3080	-	-	-	-	-	-	-	
217 Trueface.ai	trueface	000	2021-01-27	247	119	95	2000	-	40	363	109	13	(55)	271	(71)	327	(53)	614	(51)	1239	(47)	2678	87	0.15 N ^{1.0}
218 Veridas Digital Authentication Solutions S.L.	veridas	001	2021-03-05	347	875	114	2048	-	205	872	110	13	(218)	5493	(222)	5469	(187)	10350	(185)	20655	(181)	41264	47	3.40 N ^{1.0}
219 Veridas Digital Authentication Solutions S.L.	veridas	002	2021-07-06	347	870	153	2048	-	210	877	80	10	(70)	322	(69)	325	(59)	685	(57)	1365	(51)	730	130	0.09 N ^{1.1}
220 Veridas Digital Authentication Solutions S.L.	veridas	003	2021-11-09	346	870	122	2048	-	203	867	58	9	(90)	440	(70)	327	(61)	699	(58)	1401	(70)	3954	180	0.02 N ^{1.2}
221 Vietnam Posts and Telecommunications Group	vnpt	001	2022-05-05	361	235	137	2048	-	216	892	171	20	(130)	813	(130)	804	(102)	1514	(101)	3037	(93)	6128	45	0.50 N ^{1.0}
222 Vietnam Posts and Telecommunications Group	vnpt	002	2022-09-08	547	235	152	2048	-	181	808	157	16	(134)	857	(133)	835	(106)	1576	(105)	3183	(108)	6412	70	0.44 N ^{1.0}
223 Viettel Group	vts	000	2021-03-12	250	257	132	2048	-	82	492	229	2295	(3)	4	(2)	4	(2)	6	(4)	11	-	-	14	0.61 N ^{0.6}
224 Viettel Group	vts	001	2021-07-16	352	600	151	2048	-	215	891	176	21	(193)	2477	(199)	2487	(166)	4644	(165)	9313	(165)	18713	48	1.53 N ^{1.0}
225 Viettel Group	vts	002	2022-02-08	244	600	147	2048	-	220	903	192	29	(195)	2485	(198)	2485	(169)	4678	(166)	9370	(167)	18833	56	1.49 N ^{1.0}
226 Viettel Group	vts	003	2022-07-14	493	468	162	2048	-	144	702	202	34	(194)	2482	(197)	2480	(167)	4649	(164)	9302	(164)	18651	49	1.52 N ^{1.0}
227 Vigilant Solutions	vigilant	5	2018-10-30	335	122	87	1544	k	165	762	166	19	-	(176)	1720	-	-	-	-	-	-	-	-	
228 Vigilant Solutions	vigilant	6	2018-10-30	337	122	86	1544	k	184	816	174	21	-	(175)	1713	-	-	-	-	-	-	-	-	
229 Vigilant Solutions	vigilantsolutions	007	2021-01-08	340	51	85	1544	-	107	616	154	16	(165)	1354	(164)	1352	(143)	2911	(141)	5966	(137)	11466	143	0.27 N ^{1.1}
230 Vigilant Solutions	vigilantsolutions	008	2021-07-23	340	51	84	1544	-	54	403	116	13	(148)	1062	(147)	1061	(126)	2330	(137)	5520	(120)	4999	166	0.11 N ^{1.1}
231 Visidon	visidon	1	2018-10-30	166	42	178	2052	k	125	667	143	15	(210)	4370	(216)	4472	(182)	8454	(182)	17262	(177)	34288	69	2.40 N ^{1.0}
232 Visidon	vd	002	2021-05-18	248	42	171	2052	-	137	687	59	9	(188)	2089	(192)	2336	-	-	-	-	-	-	-	
233 Visidon	vd	003	2021-10-12	497	43	187	2052	-	140	692	50	8	(186)	2095	(190)	2082	-	-	-	-	-	-	-	
234 Visiob-Box	visionbox	000	2021-09-17	252	274	200	2059	-	80	481	153	16	(85)	422	(74)	359	(67)	855	(28)	631	(40)	2096	18	2.46 N ^{0.8}
235 VisionLabs	visionlabs	6	2018-10-30	360	17	35	512	1	31	289	241	20290	(16)	36	(15)	36	(13)	39	(11)	44	(9)	53	8	3211.93 N ^{0.2}
236 VisionLabs	visionlabs	7	2018-10-30	360	17	29	512	1	29	289	243	34666	(17)	63	(16)	63	(14)	72	(14)	80	(12)	115	10	2076.32 N ^{0.2}
237 VisionLabs	visionlabs	008	2019-06-18	348	17	26	512	1	28	272	238	12747	(10)	23	(8)	24	(7)	26	(6)	29	(5)	33	6	2539.61 N ^{0.2}
238 VisionLabs	visionlabs	009	2020-08-04	689	20	28	512	-	75	467	239	13245	(11)	23	(9)	29	(9)	34	(13)	61	(13)	145	13	8.88 N ^{0.6}
239 VisionLabs	visionlabs	010	2021-02-05	1042	20	31	512	-	155	731	234	11837	(8)	21	(12)	32	(11)	36	(8)	39	(6)	43	7	3183.79 N ^{0.2}
240 VisionLabs	visionlabs	011	2021-10-20	1042	20	37	512	-	157	735	237	12255	(9)	21	(7)	23	(8)	26	(7)	34	(8)	51	12	301.26 N ^{0.3}
241 Vocord	vocord	5	2018-10-30	1035	185	49	768	k	173	780	40	7	(36)	158	(41)	204	(32)	383	(33)	767	(28)	1466	52	0.12 N ^{1.0}
242 Vocord	vocord	6	2018-10-30	1035	185	245	10240	k	174	785	228	243	(37)	170	(44)	216	-	-	-	-	-	-	-	
243 Xforward AI Technology	xforwardai	000	2020-07-24	236	171	119	2048	-	162	753	119	13	(212)	4603	(237)	7647	(200)	15723	(188)	23900	(190)	53729	167	0.56 N ^{1.1}
244 Xforward AI Technology	xforwardai	001	2021-01-21	332	50	142	2048	-	131	677	151	16	(224)	5887	(215)	4384	(184)	8798	(183)	18553	(185)	48993	174	0.32 N ^{1.1}
245 Xforward AI Technology	xforwardai	002	2021-05-24	691	50	224	4096	-	228	930	164	18	(231)	6957	(231)	6400	(195)	12659	(196)	31077	(194)	65158	172	0.52 N ^{1.1}

Notes
1 Configuration size does not capture static data present in libraries. Libraries are included but the size also includes any ancillary libraries for image processing (e.g. openCV) or numerical computation (e.g. blas).
2 Finalization is the processing of converting $N = 1600000$ templates into a searchable data structure an operation which can be a simple copy, or the building of an index or tree, for example. The duration of the operation may be data dependent, and may not be linear in the number of input templates.
3 This multiplier expresses the increase in template size when k images are passed to the template generation function.
4 All durations are measured on Intel®Xeon®CPU E5-2630 v4 @ 2.20GHz processors. Estimates are made by wrapping the API function call in calls to std::chrono::high_resolution_clock which on the machine in (3) counts 1ns clock ticks. Precision is somewhat worse than that however.
5 Search durations are measured as in the prior note. The power-law model in the final column mostly fits the empirical results in Figure 196. However in certain cases the model is not correct and should not be used numerically.

Table 6: Summary of algorithms and properties included in this report. The blue superscripts give ranking for the quantity in that column. Missing search durations, denoted by “-”, are absent because those runs were not executed, usually because we did not run on the larger galleries. Caution: The power-law model is sometimes an incorrect model. It is included here only to show broad sublinear behavior, which is flagged in green. The models should not be used for prediction.

MISS RATES		INVESTIGATION, FNIR(N, R = 1, T = 0)								IDENTIFICATION, FNIR(N, R = L, T ≥ 0) FOR FPPIR = 0.001							
#	ALGORITHM	(0, 2]	(2, 4]	(4, 6]	(6, 8]	(8, 10]	(10, 12]	(12, 14]	(14, 18]	(0, 2]	(2, 4]	(4, 6]	(6, 8]	(8, 10]	(10, 12]	(12, 14]	(14, 18]
1	3DIVI-005	98.0207	97.0304	97.0415	97.0533	97.0646	132.0735	132.0884	133.1148	101.1580	98.2316	98.3033	98.3740	98.4285	130.4742	131.5329	129.5975
2	ANKE-000	95.0162	95.0245	95.0333	95.0428	95.0515	130.0615	130.0780	129.1028	96.1132	96.1761	96.2402	96.3057	95.3640	122.4200	127.4928	127.5680
3	ANKE-002	49.0055	50.0074	50.0090	49.0103	48.0116	82.0135	81.0162	80.0202	54.0329	54.0560	56.0843	57.1169	57.1481	88.1820	89.02280	88.02831
4	AWARE-005	10.0328	10.0519	10.0712	10.0910	10.1078	139.1235	139.1457	144.1831	106.3605	107.4949	107.5948	107.6783	108.7393	146.7905	146.8408	141.8831
5	AWARE-006	110.0702	110.1110	110.1502	110.1899	110.2253	147.2614	146.3045	146.3659								
6	AYONIX-002	115.0360	115.04389	115.05144	115.05814	115.06340	150.06818	150.07297	155.0774	110.08288	111.09013	111.09375	111.09603	111.09744	144.09837	144.09893	144.09927
7	CAMVI-004	109.0623	109.0944	109.1243	109.1548	108.1812	144.02056	144.02344	142.02672	91.0810	91.1267	88.01721	88.02203	88.02619	118.03040	117.03543	113.04124
8	CAMVI-005	111.0849	111.09255	111.06311	111.01989	111.02298	146.02585	145.02915	144.03246								
9	CANON-001								34.0052	35.0057	27.0042						
10	CANON-002								48.0062	48.0070	48.0070						
11	CIB-000	14.0022	14.0030	15.0037	15.0044	17.0049	41.0057	42.0069	42.0062	25.0139	26.0240	27.0373	28.0525	28.0689	52.0859	53.1109	53.1454
12	CLEARVIEWAI-000	4.0017	4.0023	4.0028	3.0034	11.0039	28.0046	35.0056	35.0047	16.0066	18.0121	18.0194	19.0287	19.0385	38.0493	42.0662	42.0873
13	CLOUDWALK-HR-000	8.0019	7.0024	8.0029	6.0032	5.0032	6.0036	7.0041	5.0020	1.0029	1.0041	1.0054	1.0064	2.0073	6.0085	6.0102	6.0112
14	CLOUDWALK-MT-000								3.0037	3.0038	2.0013						
15	CLOUDWALK-MT-001								7.0037	1.0037	1.0012						
16	COGENT-000	90.0128	90.0184	93.0250	92.0327	93.0407	124.0488	125.0611	127.0794	78.0559	78.0923	77.1342	77.2243	75.2675	10.3240	110.3992	
17	COGENT-001	91.0128	91.0184	92.0250	93.0327	92.0407	125.0488	124.0611	122.0794	77.0559	77.0923	76.1342	76.2243	76.2675	10.3240	109.3992	
18	COGENT-002	69.0081	66.0105	63.0123	64.0137	62.0157	95.0175	93.0215	93.0280	69.0499	68.0827	67.1207	67.1639	67.2037	98.2432	99.2972	100.3638
19	COGENT-003	77.0082	67.0108	65.0128	67.0145	66.0168	101.0191	101.0239	99.0312	80.0582	80.0971	80.1417	80.1918	80.2380	113.2836	115.3440	116.4207
20	COGENT-004	59.0066	53.0080	45.0085	39.0080	31.0083	61.0092	62.0106	63.0130	63.0410	65.0720	63.1099	65.1539	64.1974	99.2443	102.3043	102.3757
21	COGENT-006								2.0045	2.0049	2.0038					30.0370	26.0448
22	COGNITEC-000	105.0265	103.0423	103.0588	102.0757	102.0894	137.1014	137.1169	136.1381	100.1522	99.2330	99.3051	99.3751	99.4300	131.4779	130.5307	128.5913
23	COGNITEC-001	93.0149	94.0228	94.0312	94.0399	94.0479	127.0546	126.0656	124.0806	92.0963	93.1562	93.2157	93.2771	93.3287	125.3771	124.4343	123.4959
24	COGNITEC-002	77.0101	80.0138	81.0170	81.0201	81.0237	113.0264	111.0309	110.0389	72.0517	71.0879	72.1269	73.2098	71.2098	108.2463	98.2919	98.3535
25	COGNITEC-003	78.0104	81.0140	82.0174	82.0205	82.0238	114.0266	112.0311	112.0401	21.0504	20.0855	20.1235	20.1662	20.2045	97.2403	97.2854	96.3451
26	COGNITEC-004	64.0073	63.0099	62.0118	59.0130	59.0147	94.0163	99.0189	89.0239	53.0325	53.0548	53.0798	51.1074	50.1325	80.1591	77.1952	76.2414
27	COGNITEC-006								55.0081	53.0081	54.0090					49.0777	49.0926
28	CUBOX-000	7.0019	5.0024	5.0028	4.0031	4.0032	3.0037	15.0044	14.0027	8.0039	8.0059	7.0083	8.0111	8.0141	17.0185	18.0252	18.0339
29	CYBERLINK-002	50.0055	45.0068	41.0075	35.0078	32.0084	62.0094	63.0107	61.0114	32.0180	33.0302	33.0460	32.0643	33.0837	61.1058	62.1370	60.1787
30	CYBERLINK-003	35.0041	34.0052	27.0057	25.0058	20.0061	35.0068	40.0078	51.0078	17.0109	18.0175	20.0259	21.0356	21.0468	44.0594	46.0787	40.1072
31	DAHUA-002	50.0035	28.0047	28.0058	22.0067	28.0074	28.0082	50.0100	50.0108	30.0169	32.0294	31.0449	30.0635	30.0817	58.1013	57.1291	56.1638
32	DAHUA-003	19.0026	19.0036	19.0043	20.0050	20.0055	40.0062	51.0080	46.0073	29.0160	30.0280	29.0432	29.0615	29.0794	56.0987	56.1270	55.1587
33	DEEPLINT-001	17.0024	16.0032	14.0037	13.0040	13.0043	30.0049	38.0060	37.0052	12.0058	10.0087	11.0119	11.0155	11.0199	21.0249	21.0338	22.0463
34	DEEPSA-001	70.0081	70.0116	73.0149	76.0182	76.0216	112.0260	114.0332	114.0432	66.0458	66.0752	64.1086	63.1460	63.1812	95.2186	95.2663	93.3213
35	DERMALOG-006	82.0113	82.0142	78.0163	77.0183	74.0200	106.0218	104.0251	102.0329	75.0545	73.0889	73.1271	72.1697	70.2090	102.1031	101.3670	
36	DERMALOG-007	88.0125	88.0170	88.0214	88.0264	87.0309	119.0356	120.0432	120.0579	92.0910	92.1453	92.2009	92.2602	92.3134	124.3649	124.4289	124.5007
37	DERMALOG-008	52.0057	52.0077	54.0095	54.0110	53.0128	88.0148	87.0180	88.0223	70.0501	69.0850	70.1247	71.1692	72.2105	103.2541	103.3102	103.3762
38	DERMALOG-010								30.0056	30.0059	28.0043					41.0519	41.0643
39	DILUSENSE-000								74.0123	73.0146	76.0180					87.0184	83.0249
40	FUJITSULAB-001								60.0089	58.0098	60.0111					70.1403	69.1723
41	GORILLA-002	103.0213	103.0359	103.0528	102.0716	103.0895	138.01088	138.01367	138.01765	103.1828	104.02787	104.03654	104.04485	104.05168	134.05823	134.06508	134.7180
42	GORILLA-005	38.0044	47.0070	58.0102	62.0136	67.0170	104.0204	107.0272	109.0373	29.0566	81.0973	82.0432	81.0937	81.0393	115.02862	114.03437	114.04150
43	GORILLA-007								71.0108	69.0128	69.0145					90.1862	88.02198
44	GRIAULE-001								25.0046	21.0050	23.0038						

Table 7: Accuracy for the FRVT 2018 mugshot sets under ageing. The second row shows the time lapse between gallery and subsequent probe images, in years. The first two columns identify the algorithm. The next 8 values give rank-based FNIR with $R = 1$, $T = 0$ and FPIR = 1. All these are relevant to investigational uses where candidates from all searches would need human review. The second 8 values give threshold-based FNIR with $T \geq 0$, FPIR = 0.001 and no rank criterion. The shaded cells indicate the three most accurate algorithms for that elapsed time. The gallery size is 3068801. The total number of searches is 10951064.

2022/09/26
18:06:18

$FNIR(N, K, T) =$ False neg. identification rate
 $FPIR(N, T) =$ False pos. identification rate

N = Num. enrolled subjects
 R = Num. candidates examined

1 = 1 threshold

$I \equiv 0 \rightarrow$ Investigation
 $T > 0 \rightarrow$ Identification

MISS RATES		INVESTIGATION, FNIR($N, R = 1, T = 0$)								IDENTIFICATION, FNIR($N, R = L, T \geq 0$) FOR FPIR = 0.001								
#	ALGORITHM	(0, 2]	(2, 4]	(4, 6]	(6, 8]	(8, 10]	(10, 12]	(12, 14]	(14, 18]	(0, 2]	(2, 4]	(4, 6]	(6, 8]	(8, 10]	(10, 12]	(12, 14]	(14, 18]	
45	HZAILU-001																	
46	IDEMIA-003	⁸¹ 0.0110	⁸⁶ 0.0151	⁸⁶ 0.0196	⁸⁵ 0.0238	⁸⁴ 0.0281	¹¹⁷ 0.0313	¹¹⁷ 0.0368	¹¹⁶ 0.0504	⁸² 0.0717	⁸⁶ 0.1147	⁸⁶ 0.1614	⁸⁶ 0.2113	⁸⁵ 0.2553	¹¹⁷ 0.2976	¹¹⁶ 0.3537	¹¹⁷ 0.4334	
47	IDEMIA-004	⁸¹ 0.0107	⁸⁴ 0.0148	⁸⁵ 0.0192	⁸⁴ 0.0233	⁸³ 0.0277	¹¹⁶ 0.0312	¹¹⁶ 0.0367	¹¹⁷ 0.0512	⁸⁵ 0.0733	⁸⁵ 0.0587	⁸⁴ 0.0833	⁸⁵ 0.1100	⁵¹ 0.1340	⁷⁹ 0.1580	⁷⁶ 0.1911	⁷⁷ 0.2482	
48	IDEMIA-005	⁸⁴ 0.0118	⁸⁷ 0.0167	⁹⁰ 0.0218	⁸⁹ 0.0270	⁸⁸ 0.0317	¹²⁰ 0.0357	¹¹⁹ 0.0425	¹¹⁹ 0.0579	⁶⁵ 0.0440	⁶⁴ 0.0689	⁶⁰ 0.0964	⁵⁹ 0.1254	⁵⁸ 0.1513	⁸⁶ 0.1762	⁸¹ 0.2113	⁸³ 0.2698	
49	IDEMIA-006	⁸¹ 0.0124	⁸⁷ 0.0171	⁸⁹ 0.0218	⁸⁷ 0.0263	⁸⁶ 0.0302	¹¹⁸ 0.0321	¹¹⁵ 0.0356	¹¹⁵ 0.0471	⁶² 0.0409	⁵⁹ 0.0620	⁵⁸ 0.0850	⁵⁸ 0.1097	⁴¹ 0.1309	⁷³ 0.1486	⁷¹ 0.1738	⁷⁰ 0.2200	
50	IDEMIA-007	⁴⁷ 0.0050	⁴⁸ 0.0071	⁴⁸ 0.0089	⁵⁰ 0.0106	⁵¹ 0.0124	⁸⁴ 0.0142	⁸⁴ 0.0171	⁸⁶ 0.0220	³⁶ 0.0202	³⁶ 0.0335	³⁴ 0.0491	³³ 0.0663	³¹ 0.0825	⁵⁷ 0.0999	⁵⁴ 0.1240	⁵⁷ 0.1645	
51	IDEMIA-008	³ 0.0018	⁶ 0.0024	⁶ 0.0029	⁵ 0.0032	⁷ 0.0035	¹¹ 0.0039	¹⁷ 0.0044	¹⁸ 0.0033	³ 0.0034	³ 0.0051	⁵ 0.0069	⁵ 0.0087	¹¹ 0.0123	¹⁰ 0.0146	¹⁰ 0.0186		
52	IDEMIA-009																	
53	IMAGUS-005	³³ 0.0039	³³ 0.0052	³¹ 0.0061	²⁹ 0.0067	³⁰ 0.0077	⁵⁹ 0.0088	⁶⁰ 0.0103	⁵⁹ 0.0109	³⁹ 0.0212	³⁹ 0.0357	⁴⁰ 0.0539	⁴⁰ 0.0755	³⁸ 0.0967	⁶⁶ 0.1183	⁶⁵ 0.1485	⁶³ 0.1893	
54	IMAGUS-008																	
55	IMPERIAL-000	³⁴ 0.0040	³⁵ 0.0054	³⁶ 0.0067	³⁸ 0.0079	⁴⁰ 0.0093	⁷² 0.0112	⁷¹ 0.0139	⁷⁴ 0.0178	⁴⁹ 0.0286	⁵¹ 0.0503	⁵¹ 0.0779	⁵⁴ 0.1116	⁵⁶ 0.1455	⁸⁷ 0.1844	⁹² 0.2341	⁹¹ 0.2951	
56	INCODE-003	⁹¹ 0.0155	⁹⁶ 0.0247	⁹⁶ 0.0348	⁹⁶ 0.0463	⁹⁶ 0.0571	¹³¹ 0.0674	¹³¹ 0.0856	¹³² 0.1114	¹⁰² 0.1627	¹⁰² 0.2507	¹⁰² 0.3322	¹⁰⁰ 0.4122	¹⁰⁰ 0.4772	¹³ 0.5368	¹³ 0.6059	¹³ 0.6766	
57	INCODE-004	⁵⁶ 0.0061	⁵⁹ 0.0087	⁵⁹ 0.0110	⁶¹ 0.0136	⁶⁴ 0.0161	⁹⁷ 0.0185	¹⁰⁰ 0.0236	⁹⁸ 0.0309	⁷³ 0.0532	⁷⁴ 0.0908	⁷⁵ 0.1334	⁷⁵ 0.1809	⁷⁷ 0.2245	¹⁰⁸ 0.2675	¹⁰⁷ 0.3249	¹⁰⁶ 0.3932	
58	INNOVATRICS-004	¹¹⁴ 0.3594	¹¹⁵ 0.3629	¹¹⁵ 0.3688	¹¹⁵ 0.3754	¹¹⁵ 0.3813	¹⁴⁸ 0.3870	¹⁴⁸ 0.3960	¹⁴⁸ 0.4135	¹⁰² 0.4234	¹⁰⁶ 0.4642	¹⁰⁶ 0.5073	¹⁰⁶ 0.5522	¹⁰⁵ 0.5902	¹³ 0.6274	¹³ 0.6736	¹³ 0.7253	
59	INNOVATRICS-005	⁴¹ 0.0046	⁴¹ 0.0063	⁴² 0.0078	⁴⁵ 0.0092	⁴⁵ 0.0106	⁷⁵ 0.0124	⁷⁶ 0.0149	⁷⁵ 0.0178	³⁵ 0.0343	⁵⁶ 0.0590	⁵⁸ 0.0886	⁵⁸ 0.1222	⁵⁷ 0.1544	⁹¹ 0.1881	⁸⁹ 0.2874		
60	INTELLIVISION-002																	
61	INTEMA-000																	
62	IREX-000	²⁴ 0.0031	²⁴ 0.0042	²⁵ 0.0051	²⁶ 0.0060	²⁶ 0.0068	⁵⁴ 0.0080	⁵⁶ 0.0095	⁵⁰ 0.0107	⁵² 0.0313	⁵² 0.0539	⁵³ 0.0815	⁵⁶ 0.1137	⁵⁵ 0.1442	⁸⁵ 0.1755	⁸⁷ 0.2181	⁸⁵ 0.2718	
63	ISYSTEMS-002	⁷⁶ 0.0101	⁷⁹ 0.0135	⁸⁰ 0.0169	⁷⁹ 0.0197	⁸⁰ 0.0228	¹¹⁰ 0.0256	¹¹⁰ 0.0304	¹¹¹ 0.0398	⁹⁰ 0.0779	⁹⁰ 0.1258	⁹¹ 0.1759	⁹⁰ 0.2299	⁹⁰ 0.2758	¹²¹ 0.3204	¹²¹ 0.3763	¹¹⁹ 0.4401	
64	ISYSTEMS-003	⁷⁷ 0.0089	⁶⁹ 0.0115	⁶⁹ 0.0139	⁶⁹ 0.0158	⁷⁰ 0.0177	¹⁰⁵ 0.0198	⁹⁹ 0.0234	⁹⁸ 0.0303	⁸⁴ 0.0647	⁸⁴ 0.1056	⁸⁴ 0.1502	⁸¹ 0.1986	⁸¹ 0.2402	¹¹ 0.2819	¹¹ 0.3351	¹⁰ 0.3976	
65	KAKAO-001																	
66	KEDACOM-001	⁸¹ 0.0116	⁷⁵ 0.0130	⁶⁷ 0.0135	⁶⁰ 0.0133	⁵⁷ 0.0135	⁸³ 0.0141	⁷⁷ 0.0151	⁷¹ 0.0176	⁴¹ 0.0241	⁴¹ 0.0360	³⁹ 0.0513	³⁴ 0.0689	³¹ 0.0866	⁶² 0.1060	⁵⁸ 0.1327	⁵⁸ 0.1694	
67	LOOKMAN-003	⁸⁶ 0.0123	⁸³ 0.0144	⁷⁷ 0.0158	⁷⁰ 0.0168	⁷¹ 0.0178	⁹⁹ 0.0188	⁹² 0.0212	⁹² 0.0260	⁶⁴ 0.0438	⁶² 0.0687	⁶¹ 0.0978	⁶¹ 0.1296	⁶⁰ 0.1581	⁹¹ 0.1879	⁹⁰ 0.2294	⁸⁷ 0.2756	
68	LOOKMAN-005	⁸¹ 0.0118	⁷⁷ 0.0134	⁷⁰ 0.0142	⁶⁶ 0.0144	⁶¹ 0.0150	⁹³ 0.0160	⁸⁰ 0.0131	⁸² 0.0164	⁷⁸ 0.0185	⁴³ 0.0243	⁴⁴ 0.0432	⁴⁴ 0.0658	⁴⁴ 0.0913	⁴⁷ 0.1172	⁷² 0.1476	⁷⁴ 0.1874	⁷² 0.2272
69	MAXVISION-000																	
70	MICROFOCUS-005	¹¹⁵ 0.4269	¹¹⁵ 0.5527	¹¹⁵ 0.6355	¹¹⁶ 0.7024	¹¹⁶ 0.7503	¹⁵² 0.7876	¹⁵² 0.8234	¹⁵³ 0.8601	¹¹¹ 0.8338	¹¹² 0.9113	¹¹² 0.9468	¹¹² 0.9667	¹¹² 0.9771	¹⁴ 0.9836	¹⁴ 0.9880	¹⁴ 0.9924	
71	MICROSOFT-003	²⁸ 0.0034	³² 0.0050	³³ 0.0064	³⁶ 0.0078	³⁸ 0.0092	⁶⁸ 0.0107	⁷⁰ 0.0135	⁷¹ 0.0166	⁵⁰ 0.0288	⁵⁰ 0.0503	⁵⁰ 0.0763	⁵⁰ 0.1067	⁵⁴ 0.1359	⁸² 0.1680	⁸² 0.2116	⁸¹ 0.2644	
72	MICROSOFT-004	²⁹ 0.0032	²⁷ 0.0047	²⁹ 0.0060	³² 0.0075	³⁵ 0.0087	⁶⁵ 0.0103	⁶⁹ 0.0131	⁶⁹ 0.0159	⁴⁷ 0.0268	⁴⁸ 0.0470	⁴⁸ 0.0716	⁴⁸ 0.1007	⁴⁸ 0.1291	⁸¹ 0.1610	⁸⁰ 0.2052	⁷⁹ 0.2590	
73	MICROSOFT-005	²² 0.0031	²⁹ 0.0047	³⁸ 0.0066	⁴³ 0.0084	⁴³ 0.0103	⁸⁰ 0.0131	⁸² 0.0164	⁷⁸ 0.0185	⁴³ 0.0243	⁴⁴ 0.0432	⁴⁴ 0.0658	⁴⁴ 0.0913	⁴⁷ 0.1172	⁷² 0.1476	⁷⁴ 0.1874	⁷² 0.2272	
74	MICROSOFT-006	²⁹ 0.0032	³¹ 0.0049	³⁴ 0.0065	⁴² 0.0081	⁴⁰ 0.0096	⁷³ 0.0117	⁷² 0.0144	⁷⁰ 0.0160	²⁴ 0.0134	²⁴ 0.0233	²⁵ 0.0346	²³ 0.0462	²² 0.0578	⁴⁸ 0.0713	⁴⁸ 0.0903	⁴⁸ 0.1156	
75	NEC-000	⁹¹ 0.0195	⁹⁹ 0.0316	⁹⁹ 0.0445	⁹⁹ 0.0581	⁹⁸ 0.0699	¹³⁴ 0.0817	¹³⁴ 0.0998	¹³⁴ 0.1237	⁸⁹ 0.0759	⁸⁹ 0.1245	⁸⁹ 0.1729	⁸⁹ 0.2240	⁸⁹ 0.2671	¹²⁰ 0.3117	¹¹⁸ 0.3639	¹¹⁸ 0.4348	
76	NEC-001	¹⁰⁴ 0.0246	¹⁰² 0.0382	¹⁰³ 0.0524	¹⁰⁷ 0.0672	¹⁰⁷ 0.0793	¹³⁶ 0.0904	¹³⁵ 0.1076	¹³⁵ 0.1317	⁹⁴ 0.1019	⁹⁴ 0.1623	⁹⁴ 0.2214	⁹⁴ 0.2834	⁹⁴ 0.3341	¹²⁵ 0.3844	¹²⁵ 0.4440	¹²⁵ 0.5183	
77	NEC-002	²⁹ 0.0033	²² 0.0041	¹⁸ 0.0043	¹⁶ 0.0044	¹⁵ 0.0045	²⁹ 0.0049	³¹ 0.0056	²⁹ 0.0061	¹⁵ 0.0066	¹¹ 0.0090	¹⁰ 0.0111	¹⁰ 0.0131	⁹ 0.0149	¹⁴ 0.0171	¹⁵ 0.0207	¹⁵ 0.0267	
78	NEC-003	³¹ 0.0036	²⁶ 0.0046	²⁴ 0.0051	²⁴ 0.0055	²⁴ 0.0059	⁴⁷ 0.0067	⁴⁷ 0.0077	⁴⁹ 0.0073	⁹ 0.0056	⁹ 0.0076	⁹ 0.0091	⁷ 0.0105	⁶ 0.0119	¹³ 0.0137	¹² 0.0162	¹² 0.0209	
79	NEC-004	³ 0.0039	²⁵ 0.0045	²² 0.0047	¹⁸ 0.0046	¹⁴ 0.0044	²⁸ 0.0046	²⁸ 0.0052	²¹ 0.0036	⁷ 0.0046	⁵ 0.0057	⁴ 0.0063	¹ 0.0069	⁴ 0.0076	⁴ 0.0105			
80	NEC-005														⁵ 0.0080	⁵ 0.0091	⁵ 0.0107	
81	NEC-006														¹ 0.0030	¹ 0.0033	¹ 0.0012	
82	NEUROTECHNOLOGY-003	¹⁰¹ 0.0234	¹⁰¹ 0.0379	¹⁰² 0.0549	¹⁰¹ 0.0682	¹⁰⁸ 0.0720	¹³³ 0.0747	¹³³ 0.0886	¹³¹ 0.1066	¹⁰⁸ 0.6802	¹⁰⁸ 0.8187	¹¹⁰ 0.8920	¹¹⁰ 0.9355	¹¹⁰ 0.9594	¹⁴² 0.9738	¹⁴² 0.9828	¹⁴² 0.9885	
83	NEUROTECHNOLOGY-004	⁷⁹ 0.0104	⁷⁸ 0.0134	⁷⁶ 0.0156	⁷³ 0.0173	⁷² 0.0195	¹⁰³ 0.0212	¹⁰³ 0.0245	¹⁰⁸ 0.0320	⁸³ 0.0642	⁸² 0.1015	⁸¹ 0.1426	⁷⁹ 0.1881	⁷⁹ 0.2299	¹⁰⁷ 0.3537	¹⁰⁷ 0.4334		
84	NEUROTECHNOLOGY-005	⁷⁹ 0.0089	⁷¹ 0.0116	⁶⁸ 0.0136	⁶⁸ 0.0152	⁶⁹ 0.0173	^{102</}											

#	ALGORITHM	INVESTIGATION, FNIR(N, R = 1, T = 0)								IDENTIFICATION, FNIR(N, R = L, T ≥ 0) FOR FPIR = 0.001							
		(0, 2]	(2, 4]	(4, 6]	(6, 8]	(8, 10]	(10, 12]	(12, 14]	(14, 18]	(0, 2]	(2, 4]	(4, 6]	(6, 8]	(8, 10]	(10, 12]	(12, 14]	(14, 18]
89	NTECHLAB-003	⁶⁵ 0.0078	⁷⁰ 0.0131	⁸⁷ 0.0202	⁹⁶ 0.0295	⁹¹ 0.0405	¹²⁵ 0.0543	¹²⁹ 0.0761	¹³⁰ 0.1035	⁶⁸ 0.0491	⁷² 0.0881	⁷⁹ 0.1384	⁸³ 0.1985	⁸⁹ 0.2594	¹²² 0.3270	¹²² 0.4065	¹²² 0.4891
90	NTECHLAB-004	⁶² 0.0068	⁶⁸ 0.0110	⁷⁹ 0.0167	⁸⁶ 0.0239	⁸⁹ 0.0330	¹²³ 0.0447	¹²⁵ 0.0641	¹²⁷ 0.0891	⁶⁰ 0.0379	⁶³ 0.0688	⁶⁶ 0.1108	⁶³ 0.1629	⁷³ 0.2192	¹¹⁴ 0.2846	¹¹⁹ 0.3657	¹²¹ 0.4524
91	NTECHLAB-006	⁵¹ 0.0056	⁶⁵ 0.0095	⁷⁵ 0.0148	⁸³ 0.0218	⁸⁵ 0.0301	¹²¹ 0.0413	¹²² 0.0591	¹²⁵ 0.0814	⁵⁶ 0.0349	⁶⁰ 0.0636	⁶³ 0.1023	⁶⁴ 0.1506	⁶⁶ 0.2024	¹⁰⁴ 0.2617	¹¹¹ 0.3374	¹¹⁵ 0.4185
92	NTECHLAB-007	³⁷ 0.0044	⁴³ 0.0066	⁴⁹ 0.0089	⁵² 0.0118	⁶⁰ 0.0150	¹⁰⁸ 0.0189	¹⁰⁵ 0.0255	¹⁰⁵ 0.0342	⁴⁵ 0.0256	⁴⁶ 0.0450	⁴⁸ 0.0705	⁴⁹ 0.1012	⁵¹ 0.1334	⁸³ 0.1692	⁸⁴ 0.2170	⁸⁶ 0.2752
93	NTECHLAB-008	³⁰ 0.0025	²⁵ 0.0038	²⁸ 0.0052	³¹ 0.0074	⁴⁴ 0.0104	⁸⁵ 0.0146	¹⁰¹ 0.0236	²⁶ 0.0143	²⁸ 0.0267	³² 0.0459	³⁰ 0.0733	⁴⁰ 0.1062	⁷¹ 0.1469	⁷³ 0.2044	⁸² 0.2698	
94	NTECHLAB-009	¹⁵ 0.0022	¹⁵ 0.0031	¹⁶ 0.0038	¹⁷ 0.0045	¹⁹ 0.0055	⁴⁹ 0.0067	⁵⁴ 0.0088	⁵⁶ 0.0100	¹⁸ 0.0073	¹⁷ 0.0117	¹⁷ 0.0170	¹⁷ 0.0238	¹⁸ 0.0319	³⁰ 0.0419	³¹ 0.0577	⁴⁰ 0.0833
95	NTECHLAB-011						⁴⁰ 0.0056	⁴⁰ 0.0066	⁴⁷ 0.0073						²⁶ 0.0351	²⁷ 0.0475	³¹ 0.0724
96	PANGIAM-000						³² 0.0051	³⁰ 0.0055	³¹ 0.0046						⁴⁰ 0.0503	³⁹ 0.0617	³⁸ 0.0810
97	PARAVISION-002	⁵³ 0.0058	⁵⁸ 0.0083	⁶⁰ 0.0111	⁶³ 0.0137	⁶⁵ 0.0162	⁹⁸ 0.0187	⁹⁷ 0.0229	⁹⁵ 0.0295								
98	PARAVISION-003	⁴⁴ 0.0048	⁴¹ 0.0067	⁵¹ 0.0090	⁵² 0.0109	⁵⁴ 0.0128	⁸⁶ 0.0148	⁸⁶ 0.0178	⁸⁵ 0.0219	⁵⁷ 0.0354	⁵⁸ 0.0618	⁵⁹ 0.0931	⁶⁰ 0.1290	⁶¹ 0.1625	⁶³ 0.1964	⁶⁵ 0.2408	⁶⁰ 0.2924
99	PARAVISION-004	¹⁶ 0.0024	¹⁷ 0.0032	¹⁷ 0.0040	¹⁹ 0.0047	¹⁸ 0.0053	⁴³ 0.0061	⁴⁵ 0.0073	⁴⁵ 0.0072	²⁰ 0.0118	²³ 0.0209	²⁴ 0.0327	²⁴ 0.0465	²⁴ 0.0613	³⁰ 0.0779	⁵⁰ 0.1008	⁵⁰ 0.1285
100	PARAVISION-005	¹² 0.0021	¹³ 0.0028	¹⁵ 0.0035	¹⁴ 0.0041	¹⁶ 0.0046	³⁸ 0.0054	⁴¹ 0.0067	⁴⁴ 0.0070	¹¹ 0.0057	¹² 0.0093	¹² 0.0144	¹⁴ 0.0207	¹³ 0.0278	²⁹ 0.0368	³⁰ 0.0508	³⁰ 0.0715
101	PARAVISION-007	⁶ 0.0019	⁸ 0.0025	⁷ 0.0029	⁸ 0.0033	⁸ 0.0036	¹⁹ 0.0042	¹⁹ 0.0049	¹⁶ 0.0030	¹⁰ 0.0057	¹³ 0.0094	¹⁴ 0.0144	¹⁵ 0.0206	¹⁴ 0.0275	²⁷ 0.0357	²⁸ 0.0485	²⁷ 0.0652
102	PARAVISION-009						¹⁷ 0.0041	¹⁵ 0.0046	¹⁵ 0.0026						²³ 0.0283	²⁴ 0.0371	²⁴ 0.0525
103	PIXELALL-002	⁷² 0.0085	⁷³ 0.0119	⁷¹ 0.0147	⁷² 0.0172	⁷³ 0.0198	¹⁰⁷ 0.0225	¹⁰⁸ 0.0270	¹⁰⁷ 0.0349	⁹⁷ 0.1193	⁹⁷ 0.1900	⁹⁷ 0.2601	⁹⁷ 0.3322	⁹⁷ 0.3955	¹²⁹ 0.4565	¹²⁹ 0.5268	¹³⁰ 0.6030
104	PIXELALL-003	⁴⁰ 0.0050	⁴² 0.0063	³⁶ 0.0072	³⁴ 0.0077	³⁵ 0.0085	⁶³ 0.0095	⁶⁴ 0.0113	⁶² 0.0119	⁴⁴ 0.0248	⁴⁵ 0.0418	⁴³ 0.0622	⁴³ 0.0861	⁴¹ 0.1104	⁶⁸ 0.1723		
105	PIXELALL-004	⁴⁵ 0.0049	⁴⁰ 0.0063	⁴⁰ 0.0072	³⁷ 0.0079	³⁶ 0.0089	⁶⁷ 0.0103	⁶⁷ 0.0127	⁶⁷ 0.0146	³⁸ 0.0211	⁴⁰ 0.0360	⁴² 0.0553	⁴² 0.0792	³⁹ 0.1045	⁶⁷ 0.1317	⁶⁷ 0.1700	⁷¹ 0.2246
106	PTAKURATSATU-000	⁵⁴ 0.0061	⁵⁹ 0.0082	⁵⁶ 0.0097	⁵³ 0.0109	⁴⁹ 0.0120	⁷⁹ 0.0131	⁷⁴ 0.0146	⁷⁷ 0.0180	⁵⁹ 0.0375	⁵⁷ 0.0596	⁵⁵ 0.0842	⁵⁵ 0.1116	⁵³ 0.1357	⁷³ 0.1553	⁷⁴ 0.1820	⁷⁴ 0.2326
107	RANKONE-002	⁹⁹ 0.0212	⁹⁸ 0.0313	⁹⁸ 0.0431	⁹⁸ 0.0562	⁹⁹ 0.0712	¹³ 0.0881	¹³ 0.1130	¹³ 0.1543	⁹⁵ 0.1111	⁹⁵ 0.1707	⁹⁵ 0.2305	⁹⁵ 0.2968	⁹⁶ 0.3646	¹²⁸ 0.4345	¹²⁸ 0.5172	¹³¹ 0.6110
108	RANKONE-004	¹⁰⁸ 0.0424	¹⁰⁷ 0.0643	¹⁰⁷ 0.0875	¹⁰⁷ 0.1127	¹⁰⁷ 0.1364	¹⁴⁰ 0.1579	¹⁴¹ 0.1914	¹⁴¹ 0.2378	¹⁰⁴ 0.1855	¹⁰⁵ 0.2681	¹⁰³ 0.3431	¹⁰¹ 0.4155	¹⁰¹ 0.4785	¹³² 0.5350	¹³² 0.5980	¹³² 0.6722
109	RANKONE-005	⁹² 0.0136	⁹³ 0.0192	⁹¹ 0.0246	⁹¹ 0.0303	⁹⁰ 0.0362	¹²² 0.0422	¹²¹ 0.0521	¹²¹ 0.0694	⁸¹ 0.0582	⁷⁵ 0.0910	⁷¹ 0.1260	⁶⁸ 0.1645	⁶⁵ 0.2005	⁹⁶ 0.2353	⁹⁷ 0.2816	⁹⁷ 0.3522
110	RANKONE-007	⁶⁷ 0.0078	⁶⁴ 0.0099	⁶¹ 0.0113	⁵⁸ 0.0123	⁵⁸ 0.0139	⁹² 0.0156	⁹¹ 0.0191	⁹⁰ 0.0242	⁴² 0.0242	⁴² 0.0376	⁴¹ 0.0542	³⁸ 0.0737	³⁷ 0.0935	⁶⁴ 0.1130	⁶² 0.1416	⁶² 0.1811
111	RANKONE-009	⁴⁸ 0.0054	⁴⁹ 0.0072	⁴⁶ 0.0085	⁴⁷ 0.0098	⁴⁷ 0.0113	⁷⁸ 0.0130	⁸³ 0.0169	⁸⁷ 0.0220	³⁷ 0.0208	³⁸ 0.0345	³⁷ 0.0504	³⁶ 0.0706	³⁶ 0.0930	⁶⁷ 0.1174	⁶⁵ 0.1504	⁶⁵ 0.2002
112	RANKONE-010	⁴² 0.0047	³⁸ 0.0061	³⁸ 0.0070	³³ 0.0076	³⁴ 0.0087	⁶⁴ 0.0098	⁶⁵ 0.0113	⁶³ 0.0120	³¹ 0.0177	²⁹ 0.0269	²⁶ 0.0368	²⁶ 0.0479	²⁵ 0.0590	⁴⁷ 0.0688	⁴⁷ 0.0803	⁴⁵ 0.0991
113	RANKONE-011	²³ 0.0031	²⁵ 0.0041	²³ 0.0047	²³ 0.0053	²² 0.0058	⁵⁰ 0.0067	⁴⁶ 0.0077	⁴⁸ 0.0073	²³ 0.0127	²⁰ 0.0194	²¹ 0.0265	²⁰ 0.0345	²⁰ 0.0422	³⁹ 0.0499	³⁶ 0.0611	³⁴ 0.0756
114	RANKONE-012							⁴⁶ 0.0065	⁴³ 0.0069	³⁸ 0.0053					³⁹ 0.0460	³¹ 0.0540	²⁸ 0.0672
115	RANKONE-013							³³ 0.0051	²⁵ 0.0051	¹⁹ 0.0035					²⁴ 0.0306	²³ 0.0355	²⁰ 0.0405
116	REALNETWORKS-002	¹⁰⁷ 0.0381	¹⁰⁸ 0.0687	¹⁰⁸ 0.1062	¹⁰⁸ 0.1495	¹⁰⁹ 0.1963	¹⁴⁵ 0.2515	¹⁴⁷ 0.3206	¹⁴⁷ 0.3927	¹⁰⁸ 0.2153	¹⁰⁸ 0.3323	¹⁰⁸ 0.4444	¹⁰⁵ 0.5485	¹⁰⁶ 0.6355	¹³⁸ 0.7132	¹³⁹ 0.7855	¹³⁹ 0.8437
117	REALNETWORKS-003	¹⁰³ 0.0245	¹⁰⁵ 0.0437	¹⁰⁵ 0.0686	¹⁰⁵ 0.0975	¹⁰⁶ 0.1312	¹⁴³ 0.1719	¹⁴³ 0.2294	¹⁴⁴ 0.2907	⁹⁸ 0.1468	¹⁰⁰ 0.2370	¹⁰¹ 0.3313	¹⁰³ 0.4269	¹⁰³ 0.5142	¹³⁶ 0.5979	¹³⁷ 0.6815	¹³⁷ 0.7567
118	REALNETWORKS-004	¹⁰² 0.0244	¹⁰⁴ 0.0428	¹⁰⁴ 0.0663	¹⁰⁵ 0.0939	¹⁰³ 0.1251	¹⁴³ 0.1634	¹⁴² 0.2170	¹⁴³ 0.2785	⁹⁹ 0.1484	¹⁰¹ 0.2377	¹⁰² 0.3303	¹⁰² 0.4249	¹⁰² 0.5106	¹³⁵ 0.5924	¹³⁶ 0.6758	¹³⁶ 0.7534
119	REALNETWORKS-006							⁵³ 0.0069	⁴⁸ 0.0077	⁵² 0.0080					⁵⁹ 0.1022	⁵⁷ 0.1253	⁵⁷ 0.1622
120	REALNETWORKS-008							³¹ 0.0049	²⁹ 0.0054	³⁴ 0.0047					³⁶ 0.0462	³⁴ 0.0577	³⁵ 0.0745
121	S1-002						²⁷ 0.0046	²⁴ 0.0051	²⁴ 0.0038					³⁶ 0.0482	³⁶ 0.0597	³⁵ 0.0788	
122	SCANOVATE-001	⁶⁸ 0.0079	⁷² 0.0117	⁷⁵ 0.0151	⁷⁸ 0.0185	⁷⁸ 0.0221	¹¹¹ 0.0259	¹¹³ 0.0321	¹¹³ 0.0427	⁸⁸ 0.02727	⁸⁸ 0.1169	⁸⁷ 0.1650	⁸⁷ 0.2115	⁸⁴ 0.2528	¹¹⁶ 0.2925	¹¹³ 0.3437	¹¹⁴ 0.4084
123	SENSETIME-002	⁹⁶ 0.0186	⁹² 0.0191	⁸⁴ 0.0183	⁷⁹ 0.0179	⁸⁸ 0.0173	⁸¹ 0.0133	⁸⁵ 0.0089	⁴¹ 0.0059	⁴⁰ 0.0220	²⁵ 0.0236	¹⁹ 0.0237	¹⁸ 0.0240	¹² 0.0245	¹⁹ 0.0219	¹³ 0.0222	
124	SENSETIME-003	¹¹ 0.0021	¹² 0.0028	¹¹ 0.0031	⁷ 0.0033	⁶ 0.0035	¹⁴ 0.0040	¹⁸ 0.0047	¹⁷ 0.0033	⁸ 0.0046	⁸ 0.0064	⁶ 0.0076	⁶ 0.0086	⁶ 0.0101	¹⁰ 0.0122	¹¹ 0.0155	¹¹ 0.0196
125	SENSETIME-004	³ 0.0016	³ 0.0022	³ 0.0025	³ 0.0028	³ 0.0030	⁵ 0.0035	¹³ 0.0043	¹² 0.0025	⁴¹ 0.0036	⁴ 0.0052	³ 0.0066	³ 0.0081	³ 0.0099	¹² 0.0126	¹⁴ 0.0169	¹⁴ 0.0230
126	SENSETIME-005	² 0.0015															

MISS RATES		INVESTIGATION, FNIR(N, R = 1, T = 0)								IDENTIFICATION, FNIR(N, R = L, T ≥ 0) FOR FPIR = 0.001								
#	ALGORITHM	(0, 2]	(2, 4]	(4, 6]	(6, 8]	(8, 10]	(10, 12]	(12, 14]	(14, 18]	(0, 2]	(2, 4]	(4, 6]	(6, 8]	(8, 10]	(10, 12]	(12, 14]	(14, 18]	
133	T41SB-000																	
134	TECH5-001	⁵⁷ 0.0061	⁶¹ 0.0093	⁶⁶ 0.0128	⁷¹ 0.0171	⁷⁷ 0.0221	¹¹⁵ 0.0289	¹¹⁸ 0.0560		⁸⁶ 0.0660	⁸⁷ 0.1156	⁹⁰ 0.1733	⁹¹ 0.2385	⁹¹ 0.2998	¹²³ 0.3629	¹²⁵ 0.4424	¹²⁶ 0.5284	
135	TOSHIBA-001	⁷³ 0.0086	⁷⁴ 0.0119	⁷⁴ 0.0150	⁷⁴ 0.0178	⁷⁸ 0.0209	¹⁰⁹ 0.0241	¹⁰⁹ 0.0292	¹⁰⁸ 0.0365									
136	TRUEFACE-000	³⁶ 0.0043	³⁶ 0.0057	³⁸ 0.0061	²⁸ 0.0067	²⁷ 0.0073	⁵⁷ 0.0084	⁵⁷ 0.0097	⁵⁵ 0.0099	³⁵ 0.0200	³⁷ 0.0338	³⁸ 0.0504	³⁵ 0.0705	³⁵ 0.0904	⁶³ 0.1112	⁶¹ 0.1401	⁶¹ 0.1792	
137	VERIDAS-001	⁵⁸ 0.0063	⁵⁶ 0.0083	⁵⁶ 0.0099	⁵⁶ 0.0113	⁵⁶ 0.0132	⁸⁷ 0.0148	⁸⁸ 0.0184	⁸⁴ 0.0219	⁶¹ 0.0403	⁶¹ 0.0684	⁶² 0.1012	⁶² 0.1386	⁶² 0.1741	⁹⁴ 0.2113	⁹³ 0.2611	⁹³ 0.3233	
138	VISIONLABS-004	⁴³ 0.0048	⁴⁶ 0.0069	⁵² 0.0091	⁵⁵ 0.0111	⁵⁵ 0.0130	⁹⁰ 0.0152	⁸⁹ 0.0187	⁹¹ 0.0242	⁷⁴ 0.0540	⁷⁷ 0.0916	⁷⁸ 0.1358	⁷⁸ 0.1855	⁷⁹ 0.2303	¹¹⁰ 0.2745	¹⁰⁹ 0.3312	¹⁰⁵ 0.3913	
139	VISIONLABS-005	³⁹ 0.0044	³⁹ 0.0063	⁴³ 0.0081	⁴⁶ 0.0095	⁴⁶ 0.0109	⁷⁶ 0.0125	⁷⁸ 0.0151	⁷⁹ 0.0187	⁶⁷ 0.0479	⁶⁷ 0.0812	⁶⁸ 0.1212	⁷⁰ 0.1664	⁶⁹ 0.2078	¹⁰¹ 0.2473	¹⁰⁰ 0.2999	⁹³ 0.3577	
140	VISIONLABS-006	²⁹ 0.0035	³⁰ 0.0048	³² 0.0061	³⁰ 0.0069	²⁹ 0.0077	⁵⁸ 0.0087	⁶¹ 0.0105	⁶⁴ 0.0120	⁴⁸ 0.0273	⁴⁷ 0.0465	⁴⁷ 0.0702	⁴⁷ 0.0970	⁴⁷ 0.1228	⁷⁴ 0.1486	⁷³ 0.1847	⁷³ 0.2295	
141	VISIONLABS-008	²¹ 0.0028	²⁰ 0.0037	²¹ 0.0047	²⁰ 0.0053	²⁹ 0.0058	⁴⁶ 0.0067	⁵² 0.0081	⁵³ 0.0085	²⁷ 0.0143	²⁷ 0.0241	²⁸ 0.0373	²⁷ 0.0519	²⁷ 0.0677	³¹ 0.0850	³¹ 0.1104	³¹ 0.1444	
142	VISIONLABS-009	¹⁰ 0.0020	¹⁰ 0.0026	¹⁰ 0.0030	¹⁰ 0.0034	¹⁰ 0.0038	²¹ 0.0044	²⁷ 0.0052	³² 0.0046	¹⁴ 0.0065	¹⁵ 0.0105	¹⁵ 0.0156	¹⁵ 0.0217	¹⁶ 0.0289	²⁹ 0.0368	²⁹ 0.0499	²⁶ 0.0681	
143	VISIONLABS-010	⁹ 0.0020	⁹ 0.0025	⁹ 0.0030	¹¹ 0.0034	⁹ 0.0036	²⁹ 0.0043	²² 0.0051	³³ 0.0047	¹⁷ 0.0069	¹⁶ 0.0113	¹⁶ 0.0170	¹⁶ 0.0238	¹⁷ 0.0316	³¹ 0.0411	³² 0.0557	³² 0.0740	
144	VISIONLABS-011								¹⁸ 0.0042	¹⁶ 0.0046	²⁰ 0.0036							
145	VNPT-002								³⁶ 0.0053	³⁷ 0.0059	³⁰ 0.0044							
146	VTS-000	¹¹⁸ 0.5878	¹¹⁶ 0.6312	¹¹⁶ 0.6602	¹¹⁵ 0.6863	¹¹⁵ 0.7073	¹³¹ 0.7246	¹³⁵ 0.7458	¹³⁰ 0.7747	¹⁰⁸ 0.5929	¹⁰⁸ 0.6397	¹⁰⁸ 0.6729	¹⁰⁸ 0.7034	¹⁰⁷ 0.7279	¹³⁹ 0.7493	¹³⁸ 0.7739	¹³⁸ 0.8076	
147	VTS-003								³⁷ 0.0054	³⁴ 0.0059	⁴⁰ 0.0054					⁴⁵ 0.0597	⁴⁴ 0.0731	⁴⁴ 0.0950
148	XFORWARDAI-000	²⁰ 0.0027	¹⁸ 0.0034	²⁰ 0.0044	²¹ 0.0052	²¹ 0.0058	⁵¹ 0.0067	⁵⁰ 0.0079	⁵⁰ 0.0076	²⁸ 0.0157	³¹ 0.0281	³⁶ 0.0443	³¹ 0.0635	³² 0.0834	⁶⁰ 0.1050	⁵⁹ 0.1330	⁵⁹ 0.1714	
149	XFORWARDAI-001	¹⁵ 0.0023	¹¹ 0.0028	¹² 0.0034	¹² 0.0037	¹² 0.0039	²⁴ 0.0045	²⁶ 0.0052	²⁹ 0.0043	¹³ 0.0060	¹⁴ 0.0096	¹³ 0.0144	¹² 0.0200	¹³ 0.0260	²⁵ 0.0334	²⁵ 0.0435	²⁵ 0.0586	
150	YITU-002	⁶⁰ 0.0066	⁵⁷ 0.0083	⁵⁵ 0.0094	⁴⁸ 0.0101	⁵⁰ 0.0121	⁸⁹ 0.0150	⁹⁴ 0.0223	¹⁰¹ 0.0326	³¹ 0.0189	³⁴ 0.0317	³⁵ 0.0494	³⁹ 0.0750	⁴¹ 0.1066	⁷⁶ 0.1494	⁸¹ 0.2171	⁹² 0.2958	
151	YITU-003	⁶³ 0.0072	⁶⁰ 0.0089	⁵⁷ 0.0100	⁵¹ 0.0107	⁵² 0.0125	⁹¹ 0.0153	⁹⁶ 0.0226	¹⁰⁴ 0.0334	³⁴ 0.0194	³⁵ 0.0321	³⁶ 0.0500	⁴¹ 0.0756	⁴² 0.1071	⁷⁷ 0.1500	⁸⁶ 0.2177	⁹³ 0.2964	
152	YITU-004	⁵⁵ 0.0061	⁵¹ 0.0075	⁴⁴ 0.0081	⁴¹ 0.0081	³⁹ 0.0092	⁶⁷ 0.0107	⁸⁰ 0.0154	⁸² 0.0207	²⁸ 0.0125	²² 0.0204	²³ 0.0314	²⁵ 0.0469	²⁶ 0.0671	²⁹ 0.0955	⁶⁹ 0.1421	⁶⁹ 0.2006	
153	YITU-005	⁶¹ 0.0067	⁵⁴ 0.0080	⁴⁷ 0.0087	⁴⁴ 0.0085	⁴¹ 0.0094	⁷⁰ 0.0108	⁷⁹ 0.0151	⁸¹ 0.0204	²¹ 0.0124	²¹ 0.0198	²² 0.0308	²³ 0.0462	²⁵ 0.0667	³⁴ 0.0953	⁶³ 0.1418	⁶⁴ 0.1930	

Table 10: **Accuracy for the FRVT 2018 mugshot sets under ageing.** The second row shows the time lapse between gallery and subsequent probe images, in years. The first two columns identify the algorithm. The next 8 values give rank-based FNIR with $R = 1$, $T = 0$ and FPIR = 1. All these are relevant to investigational uses where candidates from all searches would need human review. The second 8 values give threshold-based FNIR with $T \geq 0$, FPIR = 0.001 and no rank criterion. The shaded cells indicate the three most accurate algorithms for that elapsed time. The gallery size is 3068801. The total number of searches is 10951064.

2022 / 09 / 26

18:06:18

FNIR(N, R, T) = False neg. identification rate

FPIR(N, T) = False pos. identification rate

T = Threshold

 $T = 0 \rightarrow$ Investigation
 $T > 0 \rightarrow$ Identification

#	ALGORITHM	INVESTIGATION MODE						IDENTIFICATION MODE						FAILURE TO EXTRACT FEATURES						
		RANK ONE MISS RATE, FNIR(N, 0, 1)						HIGH T → FPIR = 0.001, FNIR(N, T, L)												
		N=1.6M						N=1.6M												
GALLERY	MUGSHOT	MUGSHOT	MUGSHOT	VISA	BORDER	BOR ₁ 10YR	KIOSK	MUGSHOT	MUGSHOT	MUGSHOT	VISA	BORDER	BOR ₁ 10YR	KIOSK	MUGSHOT	MUGSHOT	MUGSHOT	VISA	BORDER	KIOSK
PROBE	MUGSHOT	WEBCAM	PROFILE	BORDER	BOR ₁ 10YR	KIOSK		MUGSHOT	WEBCAM	PROFILE	BORDER	BOR ₁ 10YR	KIOSK		MUGSHOT	WEBCAM	PROFILE	BORDER	BOR ₁ 10YR	KIOSK
1	20FACE-000	²⁶ 0.055	²⁵⁹ 0.085	¹⁷⁰ 0.736	¹⁹ 0.056	¹²¹ 0.239	¹⁸⁹ 0.243	²⁶ 0.348	²⁶² 0.450	²⁴² 1.000	¹⁹ 0.424	¹¹ 0.772	¹⁹ 0.938	0.000	0.000	0.000	0.000	0.000		
2	3DIVI-003	²⁷⁸ 0.083	²⁷⁶ 0.206		²⁰⁷ 0.141		²¹³ 0.474	²⁷⁴ 0.400	²⁷⁶ 0.626		²⁰⁷ 0.605		¹⁷⁶ 0.821	0.002	0.005					
3	3DIVI-004	²³ 0.018	²⁴⁷ 0.062		¹⁸ 0.035		¹⁹³ 0.279	²⁴ 0.169	²⁵² 0.343		¹⁸ 0.277		¹⁵ 0.607	0.002	0.005					
4	3DIVI-005	²³⁸ 0.018	²⁴⁶ 0.062	²¹⁷ 0.930	²²⁷ 0.821		¹⁹⁴ 0.279	²⁴² 0.166	²⁵⁰ 0.339	¹⁶⁰ 0.996	²¹⁶ 0.864		¹⁵⁰ 0.597	0.002	0.005	0.442				
5	3DIVI-006	²⁴ 0.024	²⁵⁴ 0.074		¹⁹ 0.047		²⁰² 0.312	²⁴ 0.168	²⁵¹ 0.342		¹⁸⁰ 0.283		¹⁵ 0.615	0.002	0.005					
6	ACER-000	²¹⁴ 0.011	²¹⁰ 0.036	¹⁹ 0.827	¹⁷ 0.025		¹⁷⁷ 0.209	²³⁴ 0.146	²²⁹ 0.246	¹¹¹ 0.981	¹⁸² 0.201		¹³⁵ 0.490	0.000	0.000	0.042				
7	ACER-001	¹⁶ 0.005	¹⁵⁹ 0.020	¹¹⁵ 0.422	¹³⁶ 0.008	¹⁰³ 0.050	⁸¹ 0.098	¹⁷ 0.056	¹⁵⁷ 0.109	¹⁹⁶ 0.999	¹⁴ 0.068	⁹⁹ 0.406	¹³ 0.479	0.001	0.001	0.041	0.000			
8	AIZE-001	¹⁷⁴ 0.006	¹⁷³ 0.022	¹⁶⁰ 0.683	¹⁶ 0.016	¹⁰⁵ 0.050	¹⁶⁰ 0.165	¹⁹⁶ 0.077	¹⁸⁵ 0.143	¹³⁷ 0.994	¹⁵⁹ 0.101	⁹³ 0.364	¹¹⁵ 0.387	0.001	0.001	0.047				
9	ALCHERA-000	²³³ 0.016	²³⁴ 0.047	²⁰⁴ 0.870	¹⁸⁹ 0.046		¹⁹⁹ 0.292	²³¹ 0.138	²¹⁴ 0.216	¹⁷⁶ 0.999	¹⁷⁰ 0.176		¹² 0.803	0.006	0.014	0.328				
10	ALCHERA-001	³⁰⁷ 0.987	³⁰³ 1.000		²²⁹ 1.000		²⁹⁶ 1.000	³⁰¹ 0.999	³⁰² 1.000		²⁸¹ 1.000		²⁵⁶ 1.000	0.006	0.013	0.324				
11	ALCHERA-002	²⁸⁰ 0.095	²⁷⁵ 0.166	²³¹ 0.954	²²³ 0.668		²¹¹ 0.446	²⁸¹ 0.486	²⁷³ 0.591	²⁰³ 1.000	²¹⁵ 0.827		¹⁷³ 0.811	0.001	0.002	0.106				
12	ALCHERA-003	²¹ 0.010	²⁰⁸ 0.035	¹⁷¹ 0.741	¹⁶⁵ 0.016		¹⁷⁵ 0.206	²³⁸ 0.155	²²⁶ 0.239	¹⁸⁸ 0.999	¹⁷⁵ 0.172		¹³ 0.464	0.001	0.002	0.106				
13	ALCHERA-004	²¹⁷ 0.011	²¹³ 0.038	¹⁰⁷ 0.345	¹⁶³ 0.017	¹¹⁴ 0.088	¹⁴⁹ 0.144	²⁷³ 0.394	²⁶⁸ 0.529	¹³² 0.991	¹⁹⁸ 0.424	¹⁰⁶ 0.708	¹⁴⁶ 0.546	0.001	0.001	0.046	0.000			
14	ALLGOVISION-000	²² 0.011	²⁰⁴ 0.033	²⁰⁷ 0.894	¹⁶⁷ 0.021		¹⁹⁶ 0.282	²⁰⁹ 0.088	²⁰¹ 0.166	¹²⁹ 0.990	¹⁵⁰ 0.117		¹⁴ 0.526	0.002	0.003	0.122				
15	ALLGOVISION-001	²⁰¹ 0.009	²¹⁹ 0.038	¹⁵⁶ 0.661	¹⁶⁸ 0.021		¹⁸⁷ 0.241	²¹⁴ 0.102	²¹⁸ 0.221	¹¹⁸ 0.986	¹⁷⁰ 0.150		¹³⁶ 0.491	0.001	0.001	0.042				
16	ANKE-000	²² 0.013	²¹⁴ 0.038	²²⁰ 0.931	²⁴⁷ 1.000		²⁹¹ 1.000	²¹⁹ 0.117	²¹⁶ 0.220	¹³⁸ 0.994	²⁸⁴ 1.000		²⁶ 1.000	0.000	0.001	0.080				
17	ANKE-001	²² 0.013	²¹⁵ 0.038	²²⁸ 0.946	²³⁷ 1.000		³⁰⁴ 1.000	²²² 0.119	²¹⁷ 0.220	¹⁴⁴ 0.994	²⁷⁴ 1.000		²⁷⁸ 1.000	0.000	0.001	0.080				
18	ANKE-002	¹² 0.003	¹³⁵ 0.016	¹³⁴ 0.522	¹⁰⁸ 0.005		¹²³ 0.119	¹³ 0.032	¹² 0.079	⁸¹ 0.948	¹⁰² 0.034		⁸ 0.245	0.001	0.001	0.049				
19	AWARE-003	²⁵⁵ 0.031	²⁶⁰ 0.090	²⁴³ 0.966	²¹³ 0.316		¹⁹⁸ 0.290	²²⁶ 0.128	²⁴⁴ 0.298	¹¹⁵ 0.984	¹⁹⁹ 0.428		¹⁴⁴ 0.530	0.004	0.003	0.874				
20	AWARE-004	²² 0.068	²⁷⁵ 0.176	²⁵¹ 0.976	²⁰ 0.122		²⁰⁹ 0.414	²⁵⁹ 0.269	²⁶⁷ 0.509	²⁰⁷ 1.000	¹⁹⁴ 0.397		¹⁷⁴ 0.816	0.003	0.003	0.776				
21	AWARE-005	²⁵⁶ 0.031	²⁴⁸ 0.067	²⁵² 0.978	¹⁹ 0.048		²⁰¹ 0.308	²⁶⁸ 0.364	²³¹ 0.253	²¹⁰ 1.000	¹⁸⁶ 0.255		¹⁸⁸ 0.916	0.001	0.002	0.189				
22	AWARE-006	²⁷⁵ 0.070	²⁶⁹ 0.128	²⁵⁴ 0.983	²⁰⁴ 0.111		²¹⁰ 0.421	²⁵⁹ 0.276	²³⁵ 0.398	¹⁹⁹ 0.999	¹⁹² 0.368		¹⁶⁶ 0.749	0.001	0.002	0.189				
23	AYONIX-000	²⁹ 0.450	²⁹⁸ 0.685	²⁶³ 0.996	²² 0.607		²²⁶ 0.867	²⁹ 0.811	²⁹² 0.939	¹⁶⁸ 0.998	²²⁹ 0.954		²⁰² 0.982	0.010	0.031	0.939				
24	AYONIX-001	²⁹⁴ 0.341	²⁹⁰ 0.527	²⁵⁸ 0.993	²²⁸ 0.994		²²² 0.778	²⁹³ 0.824	²⁸⁷ 0.920	¹⁹⁵ 0.999	²²⁴ 0.999		¹⁹⁹ 0.969	0.010	0.031	0.939				
25	AYONIX-002	²⁹ 0.341	²⁹¹ 0.527	²⁵⁹ 0.993	²¹⁷ 0.464		²²³ 0.778	²⁹ 0.824	²⁸⁸ 0.920	¹⁹⁷ 0.999	²¹⁷ 0.915		¹⁹⁹ 0.969	0.010	0.031	0.939				
26	CAMVI-003	²⁶⁸ 0.052	²⁶¹ 0.090	²¹⁰ 0.911	²⁰¹ 0.093		²⁰⁶ 0.360	¹⁹¹ 0.071	¹⁷⁷ 0.132	⁹² 0.970	¹⁵⁷ 0.114		¹¹⁸ 0.402	0.006	0.013	0.675				
27	CAMVI-004	²⁶ 0.047	²⁸⁵ 0.077	¹⁷³ 0.744	¹⁹ 0.072		²⁰⁰ 0.296	¹⁹⁷ 0.072	¹⁷⁹ 0.136	¹⁹¹ 0.999	¹⁵⁴ 0.100		¹⁷ 0.787	0.000	0.000	0.000				
28	CAMVI-005	²⁷ 0.065	²⁶⁷ 0.103	¹⁷⁵ 0.746	²⁰ 0.098		²⁰⁵ 0.341	²¹² 0.099	²⁰⁸ 0.179	²⁰² 1.000	¹⁷⁷ 0.156		²¹⁰ 0.999	0.000	0.000	0.000				
29	CANON-001	¹⁰ 0.001	³⁸ 0.066	³⁸ 0.088	²⁴ 0.001	²⁰ 0.007	²¹ 0.062	⁴ 0.005	²⁰ 0.023	²⁰ 0.365	²⁸ 0.008	²⁸ 0.068	³⁸ 0.139	0.001	0.000	0.042	0.000			
30	CANON-002	²⁵ 0.001	⁶ 0.006	⁴⁶ 0.106	¹⁴ 0.001	²⁴ 0.007	¹⁸ 0.059	³³ 0.005	²⁶ 0.020	²³ 0.407	⁵¹ 0.013	³³ 0.075	⁶⁷ 0.188	0.001	0.000	0.042	0.000			
31	CIB-000	⁵ 0.002	²⁹ 0.008	⁴⁴ 0.100	⁴⁰ 0.002	⁴⁷ 0.011	³² 0.069	⁷¹ 0.012	⁶⁷ 0.045	²¹⁷ 1.000	⁶¹ 0.017	⁵⁹ 0.141	¹⁸ 0.894	0.000	0.000	0.000	0.000			
32	CLEARVIEWAI-000	¹⁵ 0.001	¹⁴ 0.007	¹¹ 0.062	²³ 0.001	¹⁵ 0.006	¹³ 0.056	⁴² 0.006	³³ 0.025	⁹⁷ 0.974	²⁹ 0.008	²³ 0.057	⁹³ 0.268	0.000	0.000	0.037	0.000			
33	CLOUDWALK-HR-000	⁴ 0.001	⁵¹ 0.010	¹⁵ 0.064	³⁶ 0.002	¹⁸ 0.006	¹⁴ 0.057	¹ 0.002	¹² 0.013	³ 0.133	¹⁵ 0.005	¹⁰ 0.033	³⁸ 0.099	0.001	0.000	0.042	0.000			
34	CLOUDWALK-MT-000	²⁰ 0.002	⁷⁰ 0.011	⁵ 0.057	³ 0.001	⁵ 0.004	⁴ 0.051	¹² 0.002	¹¹ 0.013	² 0.109	¹ 0.002	⁴ 0.018	² 0.072	0.001	0.000	0.042	0.000			
35	CLOUDWALK-MT-001	⁶ 0.002	⁷¹ 0.011	² 0.053	¹ 0.001	¹ 0.003	¹ 0.042	¹⁰ 0.002	¹ 0.012	¹ 0.070	¹ 0.001	¹ 0.015	¹ 0.056	0.001	0.000	0.042	0.000			
36	COGENT-000	²¹² 0.010	²³² 0.046	²⁴¹ 0.965				¹⁶⁶ 0.053	¹⁸² 0.140	¹⁵¹ 0.995					0.000	0.000	0.000			
37	COGENT-001	²¹³ 0.010	²³¹ 0.046	²⁴² 0.965				¹⁶⁶ 0.053	¹⁸¹ 0.140	¹⁴⁹ 0.995					0.000	0.000	0.000			
38	COGENT-002	¹⁴⁴ 0.004	¹⁶¹ 0.020	²¹⁵ 0.925				¹⁵⁹ 0.044	¹⁴⁷ 0.098	¹⁶⁵ 0.998					0.000	0.000	0.000			
39	COGENT-003	¹⁴⁶ 0.004	¹⁶⁶ 0.021	²²⁴ 0.939				¹⁵⁸ 0.046	¹⁴¹ 0.095	¹⁶⁶ 0.998					0.000	0.000	0.000			
40	COGENT-004	⁹ 0.002	⁹⁹ 0.013	²¹⁴ 0.922	⁹⁰ 0.004		⁷⁰ 0.019	¹¹⁶ 0.113	¹³ 0.033	⁷³ 0.051	¹⁶³ 0									

#	ALGORITHM	INVESTIGATION MODE						IDENTIFICATION MODE						FAILURE TO EXTRACT FEATURES							
		RANK ONE MISS RATE, FNIR(N, 0, 1)						HIGH T → FPIR = 0.001, FNIR(N, T, L)													
		N=1.6M						N=1.6M													
	GALLERY	MUGSHOT	MUGSHOT	MUGSHOT	VISA	BORDER	VISA	MUGSHOT	MUGSHOT	MUGSHOT	VISA	BORDER	VISA	MUGSHOT	MUGSHOT	WEBCAM	PROFILE	BORDER	BOR _L 10YR	KIOSK	
PROBE	MUGSHOT	MUGSHOT	WEBCAM	PROFILE	BORDER	BOR _L 10YR	KIOSK	MUGSHOT	WEBCAM	PROFILE	BORDER	BOR _L 10YR	KIOSK	MUGSHOT	MUGSHOT	WEBCAM	PROFILE	BORDER	BOR _L 10YR	KIOSK	
47 COGNITEC-004	137 0.003	132 0.016	194 0.813	151 0.013	109 0.057	148 0.143	136 0.031	126 0.090	140 0.068	91 0.316	96 0.288	0.002	0.001	0.635	0.006						
48 COGNITEC-005	69 0.002	87 0.010	167 0.713	170 0.021	108 0.037	111 0.115	58 0.041	281 1.000	113 0.041	60 0.157	67 0.179	0.002	0.001	0.614	0.017						
49 COGNITEC-006	56 0.002	47 0.010	164 0.703	129 0.007	81 0.024	111 0.111	52 0.008	59 0.040	287 1.000	91 0.030	66 0.171	160 0.681	0.002	0.001	0.568	0.003					
50 CUBOX-000	47 0.001	84 0.010	8 0.058	27 0.002	7 0.004	3 0.049	21 0.003	22 0.019	6 0.168	11 0.004	9 0.028	3 0.073	0.001	0.000	0.042	0.000					
51 CYBERLINK-000	148 0.004	158 0.020	168 0.717	132 0.007	141 0.134	177 0.056	161 0.116	153 0.995	138 0.063	109 0.339	0.001	0.001	0.063								
52 CYBERLINK-001	144 0.004	146 0.018	169 0.731	125 0.007	144 0.133	170 0.054	150 0.109	148 0.995	135 0.062	159 0.652	0.000	0.000	0.040								
53 CYBERLINK-002	122 0.003	85 0.012	148 0.577	84 0.004	104 0.107	81 0.015	83 0.053	124 0.988	79 0.024	96 0.288	0.001	0.000	0.042								
54 CYBERLINK-003	58 0.002	38 0.009	125 0.474	63 0.003	48 0.012	59 0.082	53 0.008	50 0.035	95 0.972	48 0.012	41 0.100	112 0.368	0.000	0.000	0.039	0.000					
55 CYBERLINK-004	62 0.002	81 0.011	116 0.423	63 0.003	46 0.011	91 0.104	49 0.007	50 0.036	241 1.000	50 0.013	42 0.109	197 0.954	0.000	0.000	0.011						
56 CYBERLINK-005	74 0.002	64 0.011	72 0.209	43 0.002	41 0.010	82 0.098	62 0.010	60 0.041	208 1.000	53 0.014	37 0.089	193 0.926	0.000	0.000	0.034	0.000					
57 DAHUA-000	207 0.009	192 0.026	192 0.244	165 0.703	194 0.007	169 0.122	107 0.980	194 0.004	169 0.073	107 0.980	0.004	0.003									
58 DAHUA-001	183 0.007	184 0.024	165 0.703	194 0.007	169 0.122	107 0.980	194 0.004	169 0.073	107 0.980	0.002	0.002	0.346									
59 DAHUA-002	77 0.002	84 0.012	95 0.304	61 0.003	61 0.084	82 0.015	69 0.046	44 0.638	58 0.017	51 0.159	0.001	0.000	0.099								
60 DAHUA-003	29 0.001	16 0.007	70 0.206	38 0.002	39 0.009	38 0.073	76 0.014	62 0.041	39 0.579	49 0.013	35 0.081	37 0.134	0.000	0.000	0.000	0.000					
61 DAHUA-004	14 0.001	21 0.008	57 0.144	28 0.002	29 0.007	38 0.069	46 0.007	38 0.026	32 0.485	35 0.008	15 0.051	29 0.113	0.000	0.000	0.000	0.000					
62 DAON-000	151 0.004	140 0.017	137 0.530	103 0.005	72 0.020	129 0.125	111 0.023	97 0.061	209 1.000	80 0.025	68 0.173	181 0.846	0.002	0.002	0.108	0.001					
63 DECATUR-000	9 0.002	83 0.011	78 0.229	94 0.004	69 0.019	10 0.109	11 0.023	10 0.066	49 0.675	84 0.027	66 0.173	80 0.239	0.001	0.000	0.044	0.001					
64 DEEPLINT-001	47 0.001	15 0.007	68 0.200	52 0.002	39 0.073	29 0.003	13 0.014	201 1.000	21 0.006	50 0.159	0.000	0.000	0.038								
65 DEEPSA-001	156 0.004	150 0.016	195 0.814	141 0.010	14 0.140	157 0.046	140 0.101	116 0.985	145 0.077	108 0.326	0.000	0.001	0.047								
66 DERMALOG-003	284 0.126	278 0.217	212 0.296	216 0.560	289 0.482	278 0.655	213 0.677	183 0.870	0.002	0.002	0.103										
67 DERMALOG-004	28 0.125	27 0.215	218 0.930	206 0.135	21 0.467	27 0.480	27 0.657	154 0.995	208 0.603	188 0.856	0.001	0.002	0.107								
68 DERMALOG-005	23 0.015	21 0.037	163 0.701	21 0.242	208 0.384	20 0.088	192 0.154	128 0.990	189 0.300	150 0.614	0.001	0.002	0.102								
69 DERMALOG-006	196 0.008	188 0.024	154 0.619	142 0.010	156 0.155	164 0.052	152 0.105	110 0.981	133 0.059	108 0.318	0.003	0.006	0.181								
70 DERMALOG-007	207 0.009	193 0.027	158 0.675	157 0.014	162 0.170	209 0.086	193 0.152	127 0.990	153 0.099	148 0.557	0.001	0.002	0.102								
71 DERMALOG-008	130 0.003	123 0.015	132 0.516	122 0.007	95 0.029	146 0.139	153 0.045	138 0.094	243 1.000	130 0.057	97 0.382	195 0.940	0.000	0.000	0.002	0.000					
72 DERMALOG-009	12 0.003	11 0.014	64 0.167	130 0.007	12 0.999	98 0.106	104 0.021	10 0.066	223 1.000	93 0.031	12 0.999	178 0.840	0.001	0.001	0.018	0.003					
73 DERMALOG-010	101 0.002	78 0.011	20 0.066	188 0.038	118 0.124	117 0.113	47 0.007	87 0.055	184 0.999	151 0.089	121 1.000	141 0.522	0.001	0.001	0.018	0.003					
74 DIGIDATA-000	30 0.590	292 0.548	208 0.895	22 0.642	12 0.707	22 0.813	28 0.610	27 0.577	142 0.994	21 0.646	11 0.789	178 0.824	0.002	0.001	0.070	0.001					
75 DILUSENSE-000	103 0.002	90 0.012	93 0.297	135 0.008	92 0.028	86 0.099	134 0.030	121 0.078	45 0.655	110 0.039	105 0.664	71 0.203	0.001	0.001	0.219	0.006					
76 EYDEA-003	27 0.080	27 0.148	237 0.960	205 0.101	20 0.379	27 0.388	27 0.543	45 0.994	206 0.570	17 0.792	0.001	0.003	0.161								
77 F8-001	225 0.012	157 0.669	268 1.000	277 1.000	241 0.166	178 0.998	0.004	1.000													
78 FINCORE-000	216 0.011	207 0.034	181 0.767	181 0.032	117 0.117	171 0.191	236 0.134	215 0.217	214 1.000	177 0.187	104 0.598	128 0.458	0.000	0.001	0.043	0.000					
79 FUJITSULAB-000	104 0.002	110 0.014	119 0.440	89 0.004	75 0.023	83 0.098	103 0.021	90 0.056	77 0.024	69 0.177	81 0.240	0.000	0.001	0.016	0.000						
80 FUJITSULAB-001	81 0.002	103 0.013	121 0.455	91 0.004	84 0.026	10 0.106	95 0.018	134 0.092	78 0.024	10 0.739	81 0.247	0.000	0.003	0.150	0.002						
81 GLORY-000	288 0.178	284 0.320	262 0.994	210 0.228	218 0.678	269 0.367	271 0.547	147 0.995	201 0.453	0.001											
82 GLORY-001	28 0.127	281 0.267	257 0.992	205 0.178	21 0.594	26 0.305	26 0.537	135 0.993	196 0.408	178 0.819	0.011	0.013	0.988								
83 GORILLA-001	27 0.060	263 0.095	222 0.936	198 0.069	205 0.329	27 0.406	263 0.453	232 1.000	202 0.468	280 1.000	0.001	0.001	0.069								
84 GORILLA-002	244 0.020	228 0.044	177 0.753	173 0.027	182 0.214	248 0.188	238 0.268	224 1.000	185 0.250	214 1.000	0.001	0.001	0.069								
85 GORILLA-003	25 0.036	250 0.070	196 0.821	191 0.048	191 0.265	26 0.318	260 0.434	229 1.000	195 0.407	224 1.000	0.001	0.001	0.069								
86 GORILLA-004	180 0.006	188 0.024	162 0.697	146 0.012	159 0.162	210 0.089	198 0.160	83 0.959	164 0.135	124 0.438	0.000	0.001	0.042								
87 GORILLA-005	13 0.003	14 0.018	71 0.209	115 0.006	12 0.124	181 0.058	18 0.142	51 0.700	150 0.088	10 0.315	0.000	0.000	0.040								
88 GORILLA-006	68 0.002	87 0.012	50 0.122	73 0.003	65 0.018	97 0.105	126 0.027	133 0.089	37 0.531	85 0.028	64 0.166	74 0.218	0.000	0.000	0.041	0.000					
89 GORILLA-007	69 0.002	63 0.011	48 0.114	50 0.002	69 0.016	69 0.088	125 0.027	126 0.077	38 0.534	81 0.026	82 0.264	69 0.178	0.000	0.000	0.041	0.000					
90 GRIAULE-000	120 0.002	104 0.014	101 0.327	145 0.011	98 0.031	131 0.126	102 0.020	100 0.063	180 0.995	108 0.099	71 0.185	69 0.198	0.000	0.000	0.002	0.090	0.001				

#	ALGORITHM	INVESTIGATION MODE						IDENTIFICATION MODE						FAILURE TO EXTRACT FEATURES						
		RANK ONE MISS RATE, FNIR(N, 0, 1)						HIGH T → FPIR = 0.001, FNIR(N, T, L)												
		N=1.6M						N=1.6M												
GALLERY	MUGSHOT	MUGSHOT	MUGSHOT	VISA	BORDER	VISA		MUGSHOT	MUGSHOT	MUGSHOT	VISA	BORDER	VISA	MUGSHOT	MUGSHOT	MUGSHOT	VISA	BORDER	KIOSK	
PROBE	MUGSHOT	WEBCAM	PROFILE	BORDER	BOR _E 10YR	KIOSK		MUGSHOT	WEBCAM	PROFILE	BORDER	BOR _E 10YR	KIOSK	MUGSHOT	WEBCAM	PROFILE	BORDER	BOR _E 10YR	KIOSK	
93 HIK-004	21 ³ 0.011	19 ⁴ 0.027	17 ² 0.743	14 ⁵ 0.012	15 ⁵ 0.152	21 ¹ 0.099	19 ¹ 0.153	28 ⁶ 0.976	16 ⁷ 0.137	12 ³ 0.434	0.000	0.000	0.048							
94 HIK-005	16 ¹ 0.005	15 ⁵ 0.017	13 ⁹ 0.535	12 ² 0.007	11 ⁰ 0.111	15 ⁰ 0.044	11 ⁰ 0.077	19 ⁸ 0.999	13 ⁹ 0.068	14 ⁵ 0.541	0.000	0.000	0.000							
95 HIK-006	16 ⁰ 0.005	13 ⁴ 0.017	14 ⁰ 0.535			15 ⁹ 0.047	12 ⁹ 0.086	23 ⁵ 1.000			0.000	0.000	0.000							
96 HYPERVERGE-001	4 ⁰ 0.001	7 ³ 0.011	22 ⁶ 0.067	26 ⁰ 0.002	21 ⁰ 0.007	19 ⁰ 0.061	36 ⁰ 0.004	4 ⁰ 0.031	11 ⁰ 0.220	25 ⁰ 0.007	21 ¹ 0.053	22 ¹ 0.101	0.001	0.000	0.041		0.000			
97 HYPERVERGE-002	36 ⁰ 0.001	69 ⁰ 0.011	12 ⁰ 0.063	17 ⁰ 0.001	17 ⁰ 0.006	17 ⁰ 0.058	26 ⁰ 0.004	38 ⁰ 0.027	10 ⁰ 0.210	18 ⁰ 0.006	18 ⁰ 0.048	13 ⁰ 0.093	0.001	0.000	0.041		0.000			
98 HZAILU-000	10 ² 0.002	10 ² 0.013	82 ⁰ 0.244	66 ⁰ 0.003	69 ⁰ 0.015	69 ⁰ 0.090	10 ¹ 0.020	7 ¹ 0.051	88 ⁰ 0.967	68 ⁰ 0.020	96 ⁰ 0.316	4 ¹ 0.153	0.001	0.001	0.054	0.001				
99 HZAILU-001	88 ⁰ 0.002	72 ⁰ 0.011	47 ⁰ 0.106	46 ⁰ 0.002	115 ⁰ 0.113	72 ⁰ 0.092	54 ⁰ 0.009	20 ⁹ 0.183	121 ⁰ 0.986	181 ⁰ 0.196	283 ⁰ 1.000	159 ⁰ 0.679	0.000	0.000	0.039		0.000			
100 IDEMIA-003	18 ⁰ 0.007	26 ⁰ 0.034	23 ² 0.958	16 ⁵ 0.018		17 ⁰ 0.210	16 ⁰ 0.047	20 ⁶ 0.165		159 ⁰ 0.123		16 ¹ 0.766	0.000	0.000	0.041					
101 IDEMIA-004	18 ⁰ 0.007	29 ⁵ 0.032	22 ⁷ 0.947	16 ⁶ 0.018		17 ⁸ 0.210	14 ⁶ 0.037	16 ⁵ 0.118	96 ⁰ 0.973	160 ⁰ 0.123		16 ⁷ 0.766	0.000	0.000	0.041					
102 IDEMIA-005	19 ⁵ 0.008	22 ⁰ 0.039	23 ⁰ 0.954	17 ² 0.021		18 ³ 0.217	15 ² 0.044	18 ⁹ 0.150	102 ⁰ 0.978	161 ⁰ 0.130		184 ⁰ 0.879	0.000	0.000	0.041					
103 IDEMIA-006	20 ⁰ 0.010	25 ² 0.072	24 ⁵ 0.969	17 ⁰ 0.030		19 ⁰ 0.253	14 ⁹ 0.043	22 ² 0.226	112 ⁰ 0.982	168 ⁰ 0.144		16 ¹ 0.733	0.000	0.000	0.041					
104 IDEMIA-007	12 ¹ 0.003	12 ⁷ 0.015	28 ⁹ 1.000	116 ⁰ 0.006	99 ⁰ 0.036	137 ⁰ 0.131	94 ⁰ 0.018	86 ⁰ 0.055	257 ⁰ 1.000	125 ⁰ 0.052	71 ⁰ 0.182	30 ² 0.100	0.000	0.000	0.040	0.000				
105 IDEMIA-008	15 ⁰ 0.001	8 ⁰ 0.007	35 ⁰ 0.079	25 ¹ 0.001	25 ⁰ 0.007	4 ⁰ 0.075	9 ⁰ 0.002	10 ⁰ 0.13	9 ⁰ 0.204	14 ⁰ 0.005	14 ⁰ 0.036	21 ⁰ 0.106	0.000	0.000	0.040	0.000				
106 IDEMIA-009	3 ⁰ 0.001	7 ⁰ 0.006	17 ⁰ 0.065	8 ⁰ 0.001	11 ⁰ 0.005	6 ⁰ 0.051	3 ⁰ 0.002	3 ⁰ 0.011	4 ⁰ 0.141	5 ⁰ 0.003	8 ⁰ 0.027	6 ⁰ 0.074	0.000	0.000	0.040					
107 IMAGUS-002	29 ² 0.220	28 ² 0.301	25 ⁶ 0.988				28 ⁹ 0.749	28 ⁹ 0.816	240 ⁰ 1.000				0.004	0.008	0.550					
108 IMAGUS-003	29 ⁶ 0.356	28 ⁸ 0.513	26 ⁰ 0.993				29 ⁰ 0.807	28 ⁶ 0.909	222 ⁰ 1.000				0.004	0.008	0.550					
109 IMAGUS-005	8 ⁰ 0.002	28 ⁵ 0.048	98 ³ 0.319	114 ⁰ 0.006	73 ⁰ 0.022	139 ⁰ 0.132	98 ⁰ 0.018	10 ⁰ 0.066	67 ⁰ 0.838	87 ⁰ 0.029	63 ⁰ 0.161	77 ⁰ 0.231	0.000	0.000	0.000	0.000				
110 IMAGUS-006	9 ² 0.002	10 ⁷ 0.014	92 ⁰ 0.293	92 ⁰ 0.004	71 ⁰ 0.019	114 ⁰ 0.112	108 ⁰ 0.019	108 ⁰ 0.069	76 ⁰ 0.897	86 ⁰ 0.028	62 ⁰ 0.161	87 ⁰ 0.260	0.000	0.000	0.000	0.000				
111 IMAGUS-007	94 ⁰ 0.002	100 ⁰ 0.013	99 ⁰ 0.321	83 ⁰ 0.004	74 ⁰ 0.022	121 ⁰ 0.117	113 ⁰ 0.023	114 ⁰ 0.073	74 ⁰ 0.893	94 ⁰ 0.031	65 ⁰ 0.169	92 ⁰ 0.265	0.000	0.000	0.000	0.000				
112 IMAGUS-008	27 ⁹ 0.086	28 ² 0.093	96 ³ 0.305	171 ⁰ 0.021	113 ⁰ 0.081	12 ⁰ 0.119	29 ⁹ 0.974	28 ⁹ 0.774	156 ⁰ 0.996	204 ⁰ 0.520	122 ⁰ 1.000	140 ⁰ 0.518	0.000	0.000	0.000	0.000				
113 IMPERIAL-000	118 ⁰ 0.002	124 ⁰ 0.015	89 ⁰ 0.280	99 ⁰ 0.004	79 ⁰ 0.097	119 ⁰ 0.026	106 ⁰ 0.068	179 ⁰ 0.999	114 ⁰ 0.042	83 ⁰ 0.245	0.000	0.000	0.000							
114 INCODE-000	26 ⁰ 0.049	26 ⁵ 0.100	22 ⁹ 0.951				26 ⁰ 0.310	25 ⁹ 0.420	172 ⁰ 0.998				0.001	0.004	0.173					
115 INCODE-001	23 ⁵ 0.017	233 ⁰ 0.046	178 ⁰ 0.762				25 ¹ 0.212	241 ⁰ 0.296	238 ⁰ 1.000				0.001	0.004	0.173					
116 INCODE-002	23 ⁹ 0.018	235 ⁰ 0.048	199 ⁰ 0.843				24 ⁷ 0.184	23 ⁹ 0.269	136 ⁰ 0.993				0.000	0.001	0.066					
117 INCODE-003	22 ⁷ 0.013	222 ⁰ 0.040	179 ⁰ 0.764				24 ³ 0.167	23 ⁵ 0.264	194 ⁰ 0.999				0.000	0.001	0.066					
118 INCODE-004	14 ⁴ 0.004	14 ⁴ 0.017	126 ⁰ 0.475	139 ⁰ 0.008		143 ⁰ 0.135	173 ⁰ 0.054	16 ¹ 0.120	146 ⁰ 0.995	137 ⁰ 0.063	101 ⁰ 0.313	0.000	0.001	0.066						
119 INCODE-005	61 ⁰ 0.002	79 ⁰ 0.011	60 ⁰ 0.147	53 ⁰ 0.002	53 ⁰ 0.013	53 ⁰ 0.079	66 ⁰ 0.011	65 ⁰ 0.043	35 ⁰ 0.528	60 ⁰ 0.017	51 ⁰ 0.145	48 ⁰ 0.155	0.000	0.000	0.042	0.000				
120 INNOVATRICS-002	26 ⁰ 0.045	25 ³ 0.074	202 ⁰ 0.853				25 ⁰ 0.234	24 ⁶ 0.310	236 ⁰ 1.000				0.000	0.001	0.046					
121 INNOVATRICS-003	25 ¹ 0.026	238 ⁰ 0.055	201 ⁰ 0.845				25 ² 0.221	242 ⁰ 0.297	205 ⁰ 1.000				0.000	0.001	0.046					
122 INNOVATRICS-004	226 ⁰ 0.012	224 ⁰ 0.040	233 ⁰ 0.958				228 ⁰ 0.132	219 ⁰ 0.222	105 ⁰ 0.980				0.000	0.001	0.046					
123 INNOVATRICS-005	117 ⁰ 0.002	116 ⁰ 0.014	114 ⁰ 0.407	101 ⁰ 0.005		108 ⁰ 0.109	139 ⁰ 0.034	135 ⁰ 0.089	68 ⁰ 0.846	121 ⁰ 0.047		85 ⁰ 0.251	0.000	0.001	0.041					
124 INNOVATRICS-007	64 ⁰ 0.002	77 ⁰ 0.011	83 ⁰ 0.248	58 ⁰ 0.002	58 ⁰ 0.013	46 ⁰ 0.077	72 ⁰ 0.013	75 ⁰ 0.051	54 ⁰ 0.743	59 ⁰ 0.017	39 ⁰ 0.093	46 ⁰ 0.154	0.000	0.001	0.041	0.000				
125 INTELLIVISION-001	25 ⁹ 0.036	26 ⁶ 0.102	247 ⁰ 0.972	195 ⁰ 0.057	128 ⁰ 0.222	204 ⁰ 0.333	269 ⁰ 0.279	259 ⁰ 0.404	212 ⁰ 1.000	190 ⁰ 0.328	108 ⁰ 0.749	16 ¹ 0.685	0.001	0.000	0.044	0.000				
126 INTELLIVISION-002	21 ⁵ 0.011	202 ⁰ 0.031	225 ⁰ 0.942	164 ⁰ 0.018		112 ⁰ 0.080	173 ⁰ 0.200	233 ⁰ 0.154	210 ⁰ 0.196	182 ⁰ 0.999	163 ⁰ 0.134	101 ⁰ 0.437	129 ⁰ 0.460	0.001	0.000	0.043	0.000			
127 INTEMA-000	17 ⁰ 0.001	35 ⁰ 0.008	7 ⁰ 0.058	10 ⁰ 0.001	10 ⁰ 0.005	5 ⁰ 0.051	16 ⁰ 0.002	18 ⁰ 0.017	230 ⁰ 1.000	16 ⁰ 0.005	87 ⁰ 0.288	8 ⁰ 0.081	0.000	0.000	0.040	0.000				
128 INTSYSMSU-000	28 ⁶ 0.146	182 ⁰ 0.023	147 ⁰ 0.562	200 ⁰ 0.072		138 ⁰ 0.132	302 ⁰ 0.998	297 ⁰ 1.000	206 ⁰ 1.000	223 ⁰ 0.999		211 ⁰ 0.999	0.000	0.000	0.050					
129 IREX-000	15 ⁰ 0.004	44 ⁰ 0.010	159 ⁰ 0.681	51 ⁰ 0.002	49 ⁰ 0.012	59 ⁰ 0.082	130 ⁰ 0.028	96 ⁰ 0.060	82 ⁰ 0.957	117 ⁰ 0.044	89 ⁰ 0.302	57 ⁰ 0.170	0.000	0.000	0.042	0.000				
130 ISYSTEMS-002	18 ¹ 0.006	19 ¹ 0.026	200 ⁰ 0.844				18 ⁰ 0.078	12 ² 0.126	164 ⁰ 0.998				0.002	0.002	0.1					

#	ALGORITHM	INVESTIGATION MODE								IDENTIFICATION MODE								FAILURE TO EXTRACT FEATURES											
		RANK ONE MISS RATE, FNIR(N, 0, 1)								HIGH T → FPIR = 0.001, FNIR(N, T, L)								N=1.6M											
		GALLERY		MUGSHOT	MUGSHOT	MUGSHOT	VISA	BORDER	VISA	GALLERY		MUGSHOT	MUGSHOT	MUGSHOT	VISA	BORDER	VISA	GALLERY		MUGSHOT	MUGSHOT	MUGSHOT	VISA	BORDER	KIOSK				
139	LINECLOVA-002	³⁰⁵ 0.845	²⁰ 0.008	²⁷ 0.070	²² 0.716	¹²⁴ 0.981	²¹⁹ 0.697	²⁹⁵ 0.845	¹⁷⁴ 0.130	¹⁰⁹ 0.981	²¹ 0.717	¹¹⁶ 0.981	¹⁶⁵ 0.743	0.000	0.001	0.040	0.001												
140	LOOKMAN-003	²⁰⁰ 0.009	²¹⁸ 0.038	¹⁸⁶ 0.035		¹⁸⁶ 0.239	¹⁵¹ 0.044	¹⁶⁰ 0.112		¹⁴⁹ 0.084		¹¹⁰ 0.355	0.000	0.000															
141	LOOKMAN-004	²⁰² 0.009	²²¹ 0.039	²⁵⁰ 0.973				¹⁵⁴ 0.045	¹⁵⁴ 0.105	⁹⁹ 0.977			0.000	0.000	0.000														
142	LOOKMAN-005	¹⁹⁴ 0.008	²¹¹ 0.036	²⁴⁹ 0.972	¹⁸⁵ 0.035		¹⁸⁵ 0.237	¹³³ 0.030	¹²⁸ 0.086	¹⁰¹ 0.978	¹³⁶ 0.062		¹⁰⁰ 0.308	0.000	0.000	0.000													
143	MANTRA-000	⁶⁷ 0.002	⁵⁵ 0.010	¹⁶⁷ 0.709	¹²⁴ 0.007	⁸² 0.024	¹¹² 0.112	⁶³ 0.010	⁶¹ 0.041	²⁴⁸ 1.000	⁸⁸ 0.029	⁵⁸ 0.152	²¹³ 1.000	0.002	0.001	0.591	0.003												
144	MAXVISION-000	¹¹⁶ 0.002	¹²⁰ 0.015	¹⁰⁵ 0.327	⁹⁵ 0.004	¹⁰⁶ 0.051	⁸⁸ 0.101	¹³¹ 0.028	²³³ 0.237	⁵⁷ 0.767	¹⁶⁹ 0.149	¹¹⁹ 0.997	¹⁴⁹ 0.557	0.000	0.000	0.042	0.000												
145	MEGVII-001	²²³ 0.012	¹⁴³ 0.017	²⁶¹ 1.000				¹⁹³ 0.072	¹⁴⁶ 0.097										0.002	0.000									
146	MEGVII-002	²²⁴ 0.012	¹⁴⁵ 0.017	¹²⁰ 0.450	²⁴⁷ 1.000			¹⁹⁷ 0.077	¹⁴⁴ 0.096	¹⁷⁴ 0.998									0.002	0.000	0.033								
147	MICROFOCUS-003	³⁰⁴ 0.594	³⁰¹ 0.781	²² 0.708		²²⁸ 0.907	²⁹⁷ 0.931	²⁹⁶ 0.979		²²³ 0.982		²⁰⁶ 0.991	0.001	0.005															
148	MICROFOCUS-004	³⁰¹ 0.576	³⁰¹ 0.758	²²⁴ 0.701		²²⁷ 0.904	³⁰³ 0.999	²⁹⁴ 0.975		²²² 0.974		²⁰⁴ 0.989	0.001	0.005															
149	MICROFOCUS-005	²⁹⁹ 0.424	²⁹⁵ 0.601	²¹⁹ 0.494		²²¹ 0.777	²⁹⁴ 0.835	²⁹⁰ 0.928		²¹⁹ 0.935		²⁰³ 0.985	0.001	0.005															
150	MICROFOCUS-006	²⁹⁸ 0.427	²⁹⁴ 0.583	²¹⁸ 0.490		²²⁴ 0.782	³⁰⁰ 0.978	²⁸⁹ 0.923		²¹⁹ 0.923		²⁰⁰ 0.971	0.001	0.005															
151	MICROSOFT-003	⁵⁸ 0.002	⁹¹ 0.012	⁸² 0.004		¹⁰⁸ 0.109	¹²⁸ 0.028	¹³⁶ 0.091		¹⁰⁶ 0.036		⁷⁹ 0.233	0.000	0.001															
152	MICROSOFT-004	⁵⁰ 0.001	⁸⁹ 0.012	⁷⁶ 0.004		¹⁰⁹ 0.109	¹²⁰ 0.026	¹³⁰ 0.087		¹⁰⁷ 0.033		⁷⁵ 0.222	0.000	0.001															
153	MICROSOFT-005	⁸² 0.002	⁶⁸ 0.011	⁵⁸ 0.144	⁷⁰ 0.003		⁸⁴ 0.099	¹¹⁷ 0.026	¹¹⁰ 0.070	⁴⁰ 0.587	⁸² 0.027	⁶³ 0.180	0.000	0.001	0.049														
154	MICROSOFT-006	⁹⁰ 0.002	⁸² 0.011	⁶⁷ 0.150	⁸⁰ 0.004		⁸⁷ 0.100	⁶⁷ 0.012	⁵⁵ 0.037	²¹ 0.386	⁹⁷ 0.032	⁵⁹ 0.178	0.000	0.001	0.049														
155	NEC-000	³²⁶ 0.017	²²⁶ 0.041	²³⁰ 0.959	¹⁷³ 0.025		¹⁸⁸ 0.243	²⁰⁰ 0.079	¹⁸³ 0.140	¹⁰⁴ 0.979		¹³³ 0.474	0.001	0.002	0.890														
156	NEC-001	²⁴⁵ 0.021	²³⁹ 0.056	²⁴⁷ 0.967	¹⁸⁵ 0.033		¹⁹² 0.277	²¹⁷ 0.106	²¹² 0.197	¹¹⁹ 0.986	¹⁶² 0.133		¹³² 0.468	0.005	0.003	0.934													
157	NEC-002	¹¹ 0.001	³⁶ 0.009	¹¹⁰ 0.363	⁷⁵ 0.003		¹²⁰ 0.117	¹⁸ 0.003	²⁵ 0.020	¹⁹³ 0.999	³¹ 0.008		¹⁵⁸ 0.676	0.000	0.001	0.041													
158	NEC-003	³⁸ 0.001	⁵² 0.010	¹⁰⁷ 0.352	²⁸ 0.004	⁵¹ 0.013	¹²⁶ 0.120	¹⁵ 0.002	¹⁹ 0.017	⁶⁴ 0.824	³¹ 0.008	¹⁵ 0.036	¹⁵⁷ 0.668	0.000	0.001	0.041	0.001												
159	NEC-004	⁴⁵ 0.001	³⁵ 0.009	¹⁴⁴ 0.538	⁶⁸ 0.003	³⁰ 0.007	⁴³ 0.075	⁶ 0.002	⁹ 0.013	⁴³ 0.622	¹² 0.004	⁴ 0.019	²¹ 0.100	0.000	0.001	0.041	0.001												
160	NEC-005	²⁷ 0.001	²² 0.008	³⁶ 0.081	³¹ 0.002	¹⁰ 0.005	⁴⁰ 0.073	⁴ 0.002	⁵ 0.012	⁴⁸ 0.673	⁷ 0.003	³ 0.019	¹⁷ 0.099	0.000	0.001	0.040	0.001												
161	NEC-006	³² 0.001	³⁰ 0.008	¹⁵ 0.066	³⁵ 0.002	¹² 0.005	²⁶ 0.065	¹¹ 0.002	²¹ 0.018	²⁸ 0.463	⁸ 0.004	⁷ 0.026	¹⁴ 0.094	0.000	0.001	0.040	0.001												
162	NEUROTECHNOLOGY-003	²⁴⁶ 0.022	²²² 0.042	²³⁸ 0.961				²⁸⁷ 0.636	²³⁷ 0.266	²⁹⁴ 1.000																			
163	NEUROTECHNOLOGY-004	¹⁷¹ 0.006	¹⁵⁷ 0.020	²⁴⁹ 0.970				¹⁸⁷ 0.603	¹⁶² 0.117	¹⁴¹ 0.994																			
164	NEUROTECHNOLOGY-005	¹⁵⁵ 0.004	¹⁸⁷ 0.024	²⁰⁶ 0.893				¹⁷⁴ 0.054	¹⁷⁵ 0.130	¹⁶⁷ 0.998																			
165	NEUROTECHNOLOGY-006	²⁴⁰ 0.018	²³⁰ 0.045	¹⁵⁷ 0.606				²⁵⁷ 0.249	¹⁵⁷ 0.418																				
166	NEUROTECHNOLOGY-007	¹⁴⁷ 0.004	¹⁶⁵ 0.021	¹⁸⁷ 0.796	¹⁴⁰ 0.009		¹⁶⁸ 0.180	¹⁸⁶ 0.062	²⁰⁴ 0.173	²¹⁸ 1.000	¹⁹¹ 0.339		²²⁷ 1.000	0.001	0.001	0.041													
167	NEUROTECHNOLOGY-008	¹⁰⁰ 0.002	¹¹⁵ 0.014	¹²⁵ 0.457	⁸⁷ 0.004	⁷⁸ 0.023	⁹⁰ 0.101	¹⁶⁸ 0.053	¹²⁴ 0.080	²³¹ 1.000	¹⁰³ 0.035	⁸⁸ 0.293	⁷⁰ 0.203	0.000	0.001	0.052	0.001												
168	NEUROTECHNOLOGY-009	⁴⁶ 0.001	⁶⁵ 0.011	⁶⁷ 0.179	⁴¹ 0.002	⁵⁴ 0.013	⁵² 0.079	⁸⁵ 0.015	⁷⁹ 0.052	⁴¹ 0.588	⁶⁷ 0.020	⁵⁹ 0.153	⁵⁴ 0.165	0.001	0.000	0.046	0.000												
169	NEUROTECHNOLOGY-010	³⁰ 0.001	⁴³ 0.009	²⁸ 0.070	²⁰ 0.001	²⁹ 0.007	²⁹ 0.068	⁶¹ 0.010	⁵⁷ 0.037	¹⁶ 0.277	⁴⁴ 0.010	³⁴ 0.075	³² 0.126	0.000	0.000	0.041	0.000												
170	NEUROTECHNOLOGY-012	⁹ 0.001	²⁵ 0.008	¹⁷ 0.063	⁴ 0.001	¹³ 0.005	¹⁵ 0.057	¹⁰² 0.107	¹¹⁶ 0.026	¹⁰⁵ 0.067	⁵⁹ 0.750	⁹⁹ 0.032	⁷⁶ 0.223	0.000	0.000	0.042													
171	NEWLAND-002	²⁷⁶ 0.079	²⁶⁸ 0.117	²²¹ 0.936				²⁷⁷ 0.438	²⁶⁴ 0.466	¹⁸³ 0.999									0.007	0.012	0.200								
172	NOBLIS-001	²⁹³ 0.249	²⁸⁹ 0.522	²⁶ 0.993				³⁰⁵ 1.000	³⁰⁵ 1.000	²²⁶ 1.000									0.000	0.000	0.000								
173	NOBLIS-002	¹⁷⁹ 0.179	²⁸⁶ 0.392	²⁵³ 0.982				³⁰¹ 0.997	²⁹⁸ 1.000	²²⁸ 1.000									0.000	0.000	0.000								
174	NOTIONTAG-000	¹¹⁹ 0.002	⁹² 0.012	⁶⁷ 0.204	⁸⁸ 0.004	⁶¹ 0.016	⁷⁶ 0.095	⁸⁹ 0.017	⁹⁵ 0.059	⁴² 0.611	⁷² 0.021	⁵⁷ 0.150	⁵⁸ 0.176	0.000	0.000	0.000	0.000												
175	NTECHLAB-003	¹⁷⁷ 0.006	¹⁷⁶ 0.023	¹²⁸ 0.504				¹⁷² 0.054	¹																				

#	ALGORITHM	INVESTIGATION MODE							IDENTIFICATION MODE							FAILURE TO EXTRACT									
		RANK ONE MISS RATE, FNIR(N, 0, 1)							HIGH T → FPIR = 0.001, FNIR(N, T, L)							FEATURES									
		N=1.6M							N=1.6M																
	GALLERY	MUGSHOT	MUGSHOT	MUGSHOT	VISA	BORDER	VISA		MUGSHOT	MUGSHOT	MUGSHOT	VISA	BORDER	VISA		MUGSHOT	MUGSHOT	MUGSHOT	VISA	BORDER	KIOSK				
	PROBE	MUGSHOT	WEBCAM	PROFILE	BORDER	BOR _L 10YR	KIOSK		MUGSHOT	WEBCAM	PROFILE	BORDER	BOR _L 10YR	KIOSK		MUGSHOT	WEBCAM	PROFILE	BORDER	BOR _L 10YR	KIOSK				
185	PARAVISION-000	240	0.19	217	0.38	138	0.534	216	0.423	215	0.529	209	0.089	202	0.170	187	0.999	203	0.470	192	0.926	0.000	0.000		
186	PARAVISION-001	140	0.004	162	0.020	103	0.329	215	0.414	214	0.484	161	0.049	173	0.128	177	0.999	200	0.444	164	0.739	0.000	0.000		
187	PARAVISION-002	150	0.004	169	0.022	105	0.335	159	0.015	164	0.175	162	0.050	166	0.119	113	0.983	146	0.080	137	0.497	0.000	0.000		
188	PARAVISION-003	130	0.003	154	0.019	84	0.252	166	0.015	161	0.167	146	0.035	143	0.096	143	0.994	152	0.058	98	0.296	0.000	0.000		
189	PARAVISION-004	59	0.002	88	0.010	45	0.104	112	0.006	113	0.112	65	0.010	58	0.038	239	1.000	62	0.018	187	0.908	0.000	0.000		
190	PARAVISION-005	56	0.002	48	0.010	34	0.079	126	0.007	96	0.106	28	0.004	31	0.024	106	0.980	45	0.011	32	0.132	0.000	0.000		
191	PARAVISION-007	29	0.001	28	0.008	19	0.066	108	0.005	42	0.010	89	0.101	27	0.004	32	0.025	234	1.000	39	0.009	44	0.113	290	1.000
192	PARAVISION-009	8	0.001	17	0.007	21	0.067	19	0.001	7	0.004	10	0.054	20	0.003	23	0.019	53	0.735	0.003	11	0.073	0.000	0.025	
193	PIXELALL-002	159	0.005	172	0.022	192	0.810	144	0.011	169	0.187	219	0.105	254	0.388	229	1.000	207	0.602	267	1.000	0.000	0.000		
194	PIXELALL-003	98	0.002	114	0.014	131	0.515	121	0.006	152	0.151	108	0.022	113	0.073	204	1.000	109	0.037	147	0.554	0.000	0.000		
195	PIXELALL-004	95	0.002	121	0.015	135	0.523	108	0.005	154	0.152	97	0.018	12	0.079	221	1.000	121	0.051	207	0.994	0.000	0.000		
196	PIXELALL-005	81	0.002	67	0.011	86	0.264	148	0.012	89	0.028	150	0.146	69	0.012	72	0.050	227	1.000	83	0.027	75	0.203	212	1.000
197	PTAKURATSATU-000	136	0.003	158	0.017	151	0.605	108	0.005	87	0.027	96	0.105	141	0.037	171	0.124	78	0.924	126	0.046	77	0.206	78	0.232
198	QNAP-000	192	0.008	198	0.027	133	0.522	158	0.013	107	0.054	157	0.158	227	0.129	225	0.238	246	1.000	178	0.191	103	0.539	209	0.998
199	QNAP-001	150	0.004	170	0.022	127	0.498	126	0.006	106	0.041	115	0.112	171	0.054	18	0.137	79	0.928	147	0.081	96	0.368	108	0.331
200	QNAP-002	168	0.005	164	0.021	66	0.172	93	0.004	97	0.031	130	0.125	121	0.026	155	0.106	59	0.772	127	0.052	86	0.281	94	0.272
201	QUANTASOFT-001	29	0.218	29	0.727							28	0.639												
202	RANKONE-002	240	0.019	251	0.071							229	0.118	233	0.261										
203	RANKONE-003	240	0.019	249	0.068							221	0.118	232	0.255										
204	RANKONE-004	26	0.041	270	0.141							249	0.193	259	0.426										
205	RANKONE-005	206	0.009	225	0.041	255	0.986					183	0.059	205	0.173	169	0.998							0.489	
206	RANKONE-006	167	0.005			189	0.797					143	0.037			100	0.977							0.167	
207	RANKONE-007	139	0.003	151	0.019	186	0.796					110	0.022	140	0.095	87	0.967							0.001	0.102
208	RANKONE-009	112	0.002	86	0.013	142	0.549	111	0.006	142	0.134	96	0.018	17	0.076	91	0.969	134	0.062	107	0.328	0.000	0.000		
209	RANKONE-010	106	0.002	49	0.010	112	0.374	108	0.005	85	0.027	132	0.126	77	0.014	93	0.058	62	0.802	126	0.052	78	0.208	86	0.259
210	RANKONE-011	51	0.002	80	0.011	76	0.223	78	0.004	68	0.019	60	0.082	55	0.009	70	0.048	108	0.037	70	0.182	201	0.977	0.000	0.000
211	RANKONE-012	37	0.001	61	0.010	53	0.127	69	0.003	58	0.014	31	0.069	51	0.008	84	0.053	89	0.029	58	0.144	131	0.465	0.000	0.000
212	RANKONE-013	13	0.001	10	0.007	33	0.076	13	0.001	35	0.008	9	0.054	31	0.005	52	0.034	159	0.996	63	0.018	51	0.141	41	0.142
213	REALNETWORKS-000	26	0.040	258	0.078							25	0.234	24	0.319									0.001	
214	REALNETWORKS-001	262	0.040	257	0.078							255	0.234	249	0.319									0.001	
215	REALNETWORKS-002	259	0.039	256	0.078							251	0.231	24	0.315									0.001	
216	REALNETWORKS-003	240	0.024	245	0.062	182	0.771	180	0.031	176	0.209	239	0.159	236	0.266	173	0.998	173	0.164	138	0.500	0.001	0.000		
217	REALNETWORKS-004	247	0.024	243	0.059	188	0.797	179	0.031	181	0.213	238	0.158	234	0.263	189	0.999	174	0.170	132	0.613	0.001	0.000		
218	REALNETWORKS-005	108	0.002	101	0.013	118	0.433	96	0.004	76	0.023	92	0.102	127	0.028	115	0.074	93	0.971	102	0.037	78	0.223	75	0.215
219	REALNETWORKS-006	42	0.001	50	0.010	91	0.287	58	0.002	43	0.010	50	0.078	79	0.015	81	0.053	108	0.980	53	0.016	45	0.120	47	0.154
220	REALNETWORKS-007	36	0.001	42	0.009	87	0.267	36	0.002	39	0.009	37	0.072	59	0.010	66	0.043	103	0.979	47	0.012	106	0.463	39	0.140
221	REALNETWORKS-008	21	0.001	24	0.008	39	0.089	32	0.002	27	0.007	70	0.091	44	0.006	45	0.029	89	0.968	36	0.008	29	0.068	35	0.129
222	REMARKAI-000	141	0.003	147	0.018	155	0.660	133	0.008	151	0.148	175	0.055	16	0.120	186	0.999	142	0.069	162	0.717	0.000	0.000		
223	REMARKAI-000	197	0.009	201	0.030							223	0.128	213	0.203									0.000	
224	REMARKAI-002	197	0.008	200	0.029	190	0.802					224	0.124	211	0.196	131	0.991								0.001
225	RENDIP-000	56	0.002	122	0.015	117	0.424	117	0.006	88	0.028	63	0.084	69	0.012	94	0.059	75	0.894	73	0.022	72	0.185	85	0.167
226	REVEALMEDIA-000	89	0.002	46	0.010	88	0.275	43	0.002	50	0.012	41	0.074	79	0.012	64	0.042	50	0.680	71	0.021	40	0.093	42	0.143
227	S1-000	111	0.002	137	0.017	85	0.258	110	0.005	80	0.025	68	0.090	12	0.085	244	1.000	122	0.047	188	1.000	0.000	0.000	0.040	0.000
228	S1-001	134	0.003	111	0.014	75	0.215	62	0.003	66	0.018	45	0.077	86	0.016	78	0.052	117	0.985	64	0.019	47	0.136	43	0.148
229	S1-002	41	0.001	40	0.009	43	0.003	111	0.001	41	0.010	12	0.055	41	0.006	45	0.031	89	0.196	26	0.007	118	0.792	188	0.841
230	SCANOVATE-000	166	0.005	229	0.045	146	0.560	184	0.035	180	0.211	190	0.067	228	0.240	73	0.893	183	0.215	117	0.400	0.000	0.001	0.057	

Table 15: **Miss rates by dataset**: At left, rank 1 miss rates relevant to investigations; at right, with threshold set to target FPIR = 0.01 for higher volume, low prior, uses. Yellow indicates most accurate algorithm. Throughout blue superscripts indicate the rank of the algorithm for that column.

2022/09/26
18:06:18

FNIR(N, R, T) = False neg. identification rate
FPIR(N, T) = False pos. identification rate

N = Num. enrolled subjects
 R = Num. candidates examined

T = Threshold

$T = 0 \rightarrow$ Investigation
 $T > 0 \rightarrow$ Identification

#	ALGORITHM	INVESTIGATION MODE										IDENTIFICATION MODE										FAILURE TO EXTRACT FEATURES												
		RANK ONE MISS RATE, FNIR(N, 0, 1)										HIGH T → FPIR = 0.001, FNIR(N, T, L)																						
		N=1.6M					N=1.6M					N=1.6M					N=1.6M					N=1.6M					N=1.6M							
		GALLERY	MUGSHOT	MUGSHOT	MUGSHOT	VISA	BORDER	BOR _C 10YR	KIOSK		MUGSHOT	MUGSHOT	MUGSHOT	VISA	BORDER	BOR _C 10YR	KIOSK	MUGSHOT	MUGSHOT	WEBCAM	PROFILE	BORDER	BOR _C 10YR	KIOSK	MUGSHOT	MUGSHOT	WEBCAM	PROFILE	BORDER	BOR _C 10YR	KIOSK			
231	SCANOVATE-001	¹⁷⁰ 0.005	²²³ 0.040	¹⁵⁰ 0.585	¹⁷⁸ 0.031		¹⁶⁷ 0.178				¹⁰⁶ 0.021	⁹⁹ 0.063	²⁹⁷ 1.000																					
232	SENSETIME-000	¹¹¹ 0.002	¹²⁸ 0.016	¹³⁶ 0.528							¹⁰⁹ 0.022	¹⁰¹ 0.064																						
233	SENSETIME-001																																	
234	SENSETIME-002	²³⁶ 0.014	¹⁹⁵ 0.020	¹¹³ 0.384	¹⁴³ 0.011		⁹⁴ 0.104				⁸⁰ 0.015	⁴¹ 0.028	¹⁴⁰ 0.994	⁹⁶ 0.032																				
235	SENSETIME-003	⁷ 0.001	⁹ 0.007	⁶¹ 0.150	⁶⁰ 0.003		⁷¹ 0.091				⁸ 0.002	⁶ 0.012	³⁰ 0.477	³² 0.008																				
236	SENSETIME-004	⁹ 0.001	¹² 0.007	³⁰ 0.072	⁴⁹ 0.002		⁶⁹ 0.084				⁵ 0.002	⁸ 0.013	¹³ 0.229	¹⁹ 0.006																				
237	SENSETIME-005	⁴ 0.001	⁴ 0.006	¹⁰ 0.059	⁴⁸ 0.002		²⁸ 0.007	³⁹ 0.082			¹⁴ 0.002	¹⁴ 0.014	⁷ 0.173	²³ 0.007	²⁹ 0.051	²³ 0.104																		
238	SENSETIME-006	³ 0.001	³ 0.006	⁴ 0.055	⁵ 0.001		³ 0.004	²³ 0.064			⁷ 0.002	⁷ 0.012	¹⁷¹ 0.998	⁹ 0.004	¹² 0.034	¹² 0.093																		
239	SENSETIME-007	² 0.001	² 0.006	¹ 0.052	³ 0.001		³ 0.003	²⁰ 0.062			² 0.001	⁷ 0.009	¹⁹² 0.999	⁴⁰ 0.003	⁸ 0.024	⁹ 0.085																		
240	SENSETIME-008	¹ 0.001	¹ 0.006	³ 0.054	² 0.001		² 0.003	²⁷ 0.067			¹ 0.001	¹ 0.009	²² 0.405	² 0.002	³ 0.021	⁷ 0.080																		
241	SHAMAN-003	²⁸¹ 0.124	²⁵⁴ 0.172								²⁷⁸ 0.451	²⁷⁷ 0.597																						
242	SHAMAN-004	²⁹² 0.222	²⁸³ 0.319								²⁸⁶ 0.615	²⁸¹ 0.754																						
243	SHAMAN-006	²⁶¹ 0.040	²⁴¹ 0.058	²²³ 0.938							²³² 0.141	²²⁸ 0.237	⁹⁴ 0.972																					
244	SHAMAN-007	²⁶⁰ 0.040	²⁴⁰ 0.057								²³³ 0.141	²²⁷ 0.240																						
245	SIAT-001	⁷³ 0.002	²⁸ 0.333		⁹⁷ 0.004			⁸⁵ 0.099			⁹⁰ 0.018	²⁵ 0.365			⁹² 0.031																			
246	SIAT-002	⁷⁶ 0.002	²⁸⁷ 0.446		²¹⁴ 0.348			⁹³ 0.102			¹⁰⁷ 0.022	²⁶⁸ 0.478			¹⁹³ 0.372			¹⁹¹ 0.923																
247	SIMILART-004	³⁰⁸ 0.965	³⁰² 0.974								²⁹⁸ 0.968	²⁹⁹ 0.976																						
248	SIMILART-005																																	
249	SQISOFT-001	¹⁵⁴ 0.004	¹⁵³ 0.019	⁹⁸ 0.282	¹⁰⁸ 0.005	⁸⁶ 0.027	⁸⁰ 0.097	²²⁹ 0.132	²³⁰ 0.252	⁶⁸ 0.797	¹¹² 0.040	⁹² 0.317	¹²² 0.420																					
250	STAQU-000	¹⁸⁸ 0.007	¹⁸⁰ 0.020	¹⁵³ 0.613	¹⁶⁷ 0.020	¹⁰⁸ 0.055	¹⁵⁸ 0.159	¹⁸⁴ 0.062	²⁶ 0.443	²¹³ 1.000	²⁰⁵ 0.535	¹¹⁵ 0.961	³⁰³ 1.000																					
251	SYNESIS-003	²⁸⁷ 0.170	²⁷⁹ 0.235								²⁸³ 0.582	²⁷⁷ 0.646																						
252	SYNESIS-003	²³⁴ 0.016	¹⁸⁰ 0.023	¹⁹⁸ 0.827	¹⁵¹ 0.013		¹⁴⁴ 0.136	¹⁸⁸ 0.065	¹⁷¹ 0.123	⁸⁸ 0.960	¹⁴⁴ 0.075																							
253	SYNESIS-005	¹⁹⁸ 0.009	⁹⁷ 0.013	¹⁷⁴ 0.744	⁷² 0.003		⁷² 0.092	¹¹⁵ 0.025	¹¹¹ 0.072	¹¹⁴ 0.984	⁹⁹ 0.032																							
254	T41SB-000	²¹⁰ 0.010	¹⁸³ 0.023	¹²³ 0.462	⁵⁹ 0.003	¹¹⁸ 0.115	⁵⁸ 0.081	⁸⁷ 0.016	⁸⁸ 0.053	³³ 0.510	⁶⁹ 0.021	²⁰⁸ 0.759	⁵⁶ 0.161																					
255	TECH5-001	¹⁴⁹ 0.004	¹³⁶ 0.017	¹⁴⁹ 0.584	¹²³ 0.007		¹⁰³ 0.107	¹⁷⁸ 0.057	²⁹¹ 0.935	²⁴⁵ 1.000	¹⁸⁴ 0.244																							
256	TECH5-002	¹²⁴ 0.003	⁶⁶ 0.011	⁹⁷ 0.312	⁷¹ 0.003	⁹⁴ 0.029	⁶⁷ 0.089	¹²⁴ 0.027	¹⁰⁸ 0.070	⁶³ 0.805	¹¹¹ 0.039	⁷⁶ 0.205	¹²⁵ 0.440																					
257	TEVIAN-003	²³¹ 0.015	²³⁶ 0.052							²⁴⁶ 0.177	²⁴³ 0.298																							
258	TEVIAN-004	²¹⁰ 0.011	²¹⁶ 0.038							²¹⁹ 0.117	²⁰⁸ 0.176																							
259	TEVIAN-005	¹⁸⁹ 0.007	¹⁹⁹ 0.028	¹²⁴ 0.467						²⁰⁶ 0.087	¹⁸⁸ 0.144	⁸⁶ 0.962																						
260	TEVIAN-006	¹¹⁵ 0.002	⁷⁵ 0.011	⁵¹ 0.123	⁶⁴ 0.003	⁵⁷ 0.013	³⁵ 0.071	⁶⁰ 0.010	⁴⁸ 0.032	²⁴ 0.425	⁵⁶ 0.016	³⁸ 0.093	¹⁹⁶ 0.951																					
261	TEVIAN-007	⁷² 0.002	⁴¹ 0.009	⁴² 0.093	³⁹ 0.002	⁴⁸ 0.009	²⁸ 0.067	³⁹ 0.005	²⁹ 0.022	¹⁸ 0.301	⁴² 0.009	²⁷ 0.065	³⁰ 0.122																					
262	TIGER-000	²⁷¹ 0.062	²⁶⁴ 0.095							²⁷² 0.390	²⁶⁶ 0.500																							
263	TIGER-002	¹⁷⁷ 0.006	¹⁷ 0.023	¹³⁰ 0.514						²⁰² 0.086	¹⁹⁷ 0.158	¹⁸¹ 0.999																						
264	TIGER-003	¹⁷² 0.006	¹⁷⁸ 0.023							²⁰³ 0.086	¹⁹⁶ 0.158																							
265	TONGYITRANS-000	¹⁸⁴ 0.007	¹⁷⁴ 0.022							¹⁹⁵ 0.074	¹⁵⁹ 0.112																							
266	TONGYITRANS-001	¹⁸⁵ 0.007	¹⁷⁵ 0.022							¹⁸⁹ 0.066	¹⁵⁰ 0.101																							
267	TOSHIBA-000	¹⁵⁸ 0.004	¹⁶ 0.022	¹⁸⁰ 0.766						¹⁸³ 0.062	¹⁶⁸ 0.118	¹⁵² 0.995																						
268	TOSHIBA-001	¹⁶³ 0.005	¹⁷¹ 0.022							¹⁸⁰ 0.058	¹³⁹ 0.092																							
269	TRUEFACE-000	¹³⁸ 0.003	¹⁶⁵ 0.014	⁷⁹ 0.230	¹²⁸ 0.007	⁸⁰ 0.																												

#	ALGORITHM	INVESTIGATION MODE										IDENTIFICATION MODE										FAILURE TO EXTRACT FEATURES													
		RANK ONE MISS RATE, FNIR(N, 0, 1)										HIGH T → FPIR = 0.001, FNIR(N, T, L)										N=1.6M													
		GALLERY	MUGSHOT	MUGSHOT	WEBCAM	PROFILE	BORDER	BOR _L 10YR	KIOSK	MUGSHOT	MUGSHOT	WEBCAM	PROFILE	BORDER	BOR _L 10YR	KIOSK	MUGSHOT	MUGSHOT	WEBCAM	PROFILE	BORDER	BOR _L 10YR	KIOSK												
277	VIGILANTSOLUTIONS-003	²⁷⁴ 0.069	²⁷² 0.151	²³⁷ 0.958						²⁷⁶ 0.408	²⁸⁰ 0.660	¹⁷⁸ 0.999						0.000	0.001	0.127															
278	VIGILANTSOLUTIONS-004	²⁸² 0.125	²⁸⁰ 0.244	²⁴⁰ 0.965						²⁸² 0.549	²⁸⁵ 0.817	¹⁵⁸ 0.996						0.000	0.001	0.127															
279	VIGILANTSOLUTIONS-005	²⁰³ 0.009		²¹⁷ 0.920						²⁷¹ 0.388		²²⁵ 1.000						0.000	0.001	0.127															
280	VIGILANTSOLUTIONS-006	²⁰⁹ 0.010		²¹³ 0.921						²⁶⁶ 0.353		²³³ 1.000						0.000	0.001	0.127															
281	VIGILANTSOLUTIONS-007	¹⁴⁰ 0.003	¹⁴¹ 0.017	²¹⁰ 0.925	¹⁵² 0.013	¹¹⁰ 0.068	¹⁶³ 0.175			¹³² 0.028	¹³¹ 0.088	¹⁵⁷ 0.996	¹⁴⁸ 0.081	⁹⁶ 0.371	¹¹⁶ 0.391		0.000	0.001	0.127		0.001														
282	VIGILANTSOLUTIONS-008	¹³² 0.003	¹⁴² 0.017	²¹⁰ 0.913	¹⁵⁶ 0.014	¹¹¹ 0.072	¹⁶⁶ 0.178			¹⁰³ 0.021	¹¹⁸ 0.077	¹⁸⁰ 0.999	¹⁵⁶ 0.104	⁹⁸ 0.398	¹³⁹ 0.511		0.000	0.001	0.127		0.001														
283	VISIONBOX-000	⁸⁵ 0.002	⁷⁶ 0.011	¹⁷⁷ 0.752	¹⁰⁰ 0.005	⁶⁴ 0.017	⁵¹ 0.078			⁹³ 0.018	⁹¹ 0.057	¹³⁰ 0.990	⁷⁰ 0.023	⁵⁵ 0.146	⁵³ 0.162		0.000	0.001	0.043		0.001														
284	VISIONLABS-004	¹²⁵ 0.003	¹⁵⁶ 0.020	¹⁰⁷ 0.343						¹⁷⁹ 0.058	¹⁹⁷ 0.159	⁷² 0.890						0.001	0.001	0.046															
285	VISIONLABS-005	¹¹³ 0.002	¹⁵⁰ 0.019	¹⁰⁴ 0.334						¹⁶³ 0.050	¹⁸⁷ 0.147	⁷¹ 0.888						0.001	0.001	0.046															
286	VISIONLABS-006	⁷⁸ 0.002	¹²⁶ 0.015	⁷¹ 0.211	⁸¹ 0.004					⁷⁸ 0.096	¹²³ 0.027	¹³⁵ 0.090	⁴⁶ 0.672					0.001	0.001	0.051															
287	VISIONLABS-007	⁷¹ 0.002	¹²⁵ 0.015	⁷³ 0.211	⁷⁷ 0.004					⁷⁷ 0.095	¹²² 0.027	¹³⁴ 0.090	⁴⁷ 0.672	⁹⁵ 0.031			⁶⁵ 0.185		0.001	0.001	0.051														
288	VISIONLABS-008	⁹² 0.002	¹⁰⁶ 0.014	⁵⁷ 0.141	⁴⁹ 0.002					⁵⁴ 0.081	⁷³ 0.013	⁷⁷ 0.051	³¹ 0.481	⁵⁷ 0.017			⁴⁴ 0.151		0.001	0.000	0.075														
289	VISIONLABS-009	²⁰ 0.001	³⁴ 0.008	⁴¹ 0.091	²¹ 0.001					³⁴ 0.071	³² 0.005	³⁴ 0.025	⁶¹ 0.799	³⁷ 0.008			²⁷ 0.113		0.000	0.000	0.060														
290	VISIONLABS-010	⁴¹ 0.001	⁶⁰ 0.010	²⁵ 0.069	¹⁸ 0.001	¹⁶ 0.006	³³ 0.069	³⁸ 0.005	³⁹ 0.027		³⁷ 0.008	²² 0.055	²⁶ 0.109				0.000	0.000	0.040		0.000														
291	VISIONLABS-011	²⁵ 0.001	³⁷ 0.009	¹⁷⁰ 0.064	¹⁵ 0.001	⁸ 0.004	²² 0.063	²⁴ 0.003	²⁴ 0.020		¹³ 0.004	¹³ 0.034	¹⁰ 0.090				0.000	0.000	0.032		0.000														
292	VNP-001	⁹⁹ 0.002	¹¹⁸ 0.014	⁵⁹ 0.145	⁵⁷ 0.002	⁷⁹ 0.023	³⁶ 0.071	⁷⁷ 0.014	¹⁰⁷ 0.068	⁵² 0.718	¹⁰⁴ 0.035	¹¹⁷ 0.990	¹¹¹ 0.362				0.001	0.000	0.042		0.000														
293	VNP-002	⁸³ 0.002	⁹³ 0.012	²⁷ 0.068	¹² 0.001	¹⁹ 0.006	¹¹ 0.054	⁴⁵ 0.007	⁴⁷ 0.032	¹⁷ 0.292	²⁷ 0.007	³¹ 0.072	¹⁵ 0.096				0.001	0.000	0.042		0.000														
294	VOCORD-003	¹⁷⁸ 0.006	¹⁸⁶ 0.024	¹⁹⁷ 0.804	¹⁹⁷ 0.061					¹⁷⁰ 0.188	²²³ 0.122	¹⁹³ 0.155	¹⁷⁸ 0.998	¹⁷² 0.157			¹¹⁹ 0.404		0.001	0.011	0.425														
295	VOCORD-004	¹⁹³ 0.008	¹⁶³ 0.021	¹⁸⁷ 0.792	¹⁸⁰ 0.012					¹³³ 0.127	²⁶⁷ 0.355	²⁰³ 0.173	²¹⁵ 1.000	¹⁸⁸ 0.193	²⁰⁵ 0.991			0.000	0.000	0.000															
296	VOCORD-005	¹⁸⁷ 0.007	¹⁸¹ 0.023	¹⁹³ 0.812	¹⁹³ 0.055					¹⁷⁴ 0.206	²³⁷ 0.158	¹⁷⁶ 0.130	¹⁶² 0.997	¹⁶⁶ 0.138	¹¹⁴ 0.381			0.001	0.009	0.554															
297	VOCORD-006	³⁰⁸ 1.000	³⁰⁹ 1.000	²⁷⁷ 1.000	³⁰² 1.000					²³⁹ 1.000	³⁰⁹ 1.000	³⁰⁸ 1.000	²⁷⁷ 1.000	²⁵⁹ 1.000	²⁴² 1.000			0.001	0.009	0.554															
298	VTS-000	³⁰³ 0.594	²⁹⁶ 0.608	²⁰⁹ 0.909	²²⁸ 0.607	¹²³ 0.724	²²⁰ 0.739	²⁸⁴ 0.598	²⁷⁸ 0.619	¹⁹⁰ 0.999	²¹⁰ 0.613	¹¹⁰ 0.760	¹⁶⁷ 0.761			0.000	0.001	0.047		0.000															
299	VTS-001	⁵⁴ 0.002	⁵³ 0.010	⁶ 0.167	¹¹³ 0.006	⁶⁷ 0.018	⁴⁸ 0.077	⁷⁴ 0.013	⁷⁶ 0.051	¹³⁹ 0.994	⁷⁴ 0.022	⁶² 0.141	⁶⁸ 0.192			0.000	0.000	0.040		0.000															
300	VTS-002	⁸⁷ 0.002	⁹⁸ 0.013	⁸⁰ 0.233	¹⁵⁸ 0.014	¹⁰¹ 0.038	¹²⁸ 0.125	¹¹⁸ 0.026	¹¹⁶ 0.075	²⁰⁸ 1.000	¹¹⁸ 0.045	⁸⁰ 0.231	¹²¹ 0.417			0.000	0.000	0.029																	
301	VTS-003	²² 0.001	¹⁵ 0.007	³⁷ 0.074	²⁹ 0.002	³⁷ 0.009	⁸ 0.053	⁵⁰ 0.007	⁵¹ 0.033	²²⁸ 1.000	³⁵ 0.014	¹¹⁴ 0.954	¹³⁵ 0.635			0.000	0.001	0.029		0.000															
302	XFORWARDAI-000	¹⁰⁷ 0.002	¹⁰⁹ 0.014	⁴⁰ 0.089	⁸³ 0.004	⁵⁹ 0.015	⁷⁵ 0.094	⁸³ 0.015	⁸⁵ 0.053	²⁶ 0.440	²⁰ 0.021	⁶¹ 0.159	⁵⁶ 0.169			0.000	0.000	0.000		0.000															
303	XFORWARDAI-001	⁹⁶ 0.002	⁹⁵ 0.013	²³ 0.067	⁶⁷ 0.003	³⁸ 0.009	⁵⁸ 0.082	³⁶ 0.005	⁴² 0.028	²⁷ 0.448	³² 0.008	²⁶ 0.062	³¹ 0.123			0.000	0.000	0.000		0.000															
304	XFORWARDAI-002	⁸⁹ 0.002	⁸⁸ 0.012	⁷ 0.059	⁵⁴ 0.002	²² 0.007	⁴⁷ 0.077	²³ 0.003	¹⁷ 0.016	³⁴ 0.525	¹⁷ 0.005	¹⁶ 0.041	²⁰ 0.099			0.000	0.000	0.000		0.000															
305	YISHENG-001	²⁵² 0.027	²⁴⁴ 0.060	¹⁹⁶ 0.058					¹⁹⁷ 0.287	²⁶⁴ 0.346	²⁸³ 0.808	²¹² 0.666	¹⁹⁰ 0.919			0.002	0.005																		
306	YITU-002	⁷⁹ 0.002	⁵⁶ 0.010						⁹¹ 0.018	⁷¹ 0.049							0.000	0.000																	
307	YITU-003	¹³¹ 0.003	¹³¹ 0.016						⁹⁹ 0.019	⁸⁰ 0.052								0.003	0.001																
308	YITU-004	³⁴ 0.001	³² 0.008	²⁰³ 0.866					⁵⁷ 0.010	³⁷ 0.027	⁸⁰ 0.936						0.000	0.000	0.000		0.000														
309	YITU-005	¹⁰⁹ 0.002	¹¹⁹ 0.014						⁶⁴ 0.010	⁴⁹ 0.032								0.003	0.001																

Table 17: **Miss rates by dataset:** At left, rank 1 miss rates relevant to investigations; at right, with threshold set to target FPIR = 0.01 for higher volume, low prior, uses. Yellow indicates most accurate algorithm. Throughout blue superscripts indicate the rank of the algorithm for that column.

2022 / 09 / 26

18:06:18

FNIR(N, R, T) = False neg. identification rate

#	ALGORITHM	MISSES BELOW THRESHOLD, T	ENROL MOST RECENT			
		DATASET: FRVT 2018 MUGSHOTS				
		N=0.64M	N=1.6M	N=3.0M	N=6.0M	N=12.0M
1	3DIVI-005	²⁴² 0.1358	²⁴² 0.1664	²¹² 0.1915	²⁰⁴ 0.2370	¹⁹⁶ 0.3054
2	ACER-000	²³⁵ 0.1185	²³⁴ 0.1455	²⁰⁶ 0.1714	¹⁹⁷ 0.2074	¹⁸⁹ 0.2537
3	ALCHERA-003	²³⁷ 0.1176	²³⁶ 0.1553	²⁰⁸ 0.1853	²⁰⁵ 0.2409	²⁰¹ 0.3553
4	ALLGOVISION-000	²⁰⁷ 0.0688	²⁰⁸ 0.0881	¹⁸⁹ 0.1084	¹⁸² 0.1389	¹⁶⁹ 0.2129
5	ALLGOVISION-001	²¹³ 0.0785	²¹⁴ 0.1017	¹⁹⁶ 0.1218	¹⁸⁹ 0.1584	¹⁷⁶ 0.2273
6	ANKE-000	²²⁰ 0.0942	²¹⁸ 0.1169	²⁰¹ 0.1404	¹⁹⁴ 0.1776	¹⁹⁰ 0.2559
7	ANKE-002	¹⁷ 0.0229	¹³⁷ 0.0318	¹³⁶ 0.0406	¹³¹ 0.0605	¹¹⁷ 0.1466
8	AWARE-003	²³⁰ 0.1098	²²⁶ 0.1283	²⁰² 0.1447	¹⁹² 0.1768	¹⁸¹ 0.2364
9	AWARE-005	²⁷ 0.3389	²⁶⁸ 0.3643	²¹⁷ 0.3993	²¹³ 0.4526	¹⁸⁸ 0.2531
10	AYONIX-002	²⁹² 0.7862	²⁹² 0.8242	²²⁵ 0.8508	²¹⁸ 0.8704	²¹² 0.8939
11	CAMVI-004	¹⁶³ 0.0367	¹⁹² 0.0716	¹⁸⁰ 0.0983	²⁰⁷ 0.2508	¹⁹⁴ 0.2701
12	CANON-001	⁴⁰ 0.0039	⁴⁰ 0.0054	³⁹ 0.0074	³⁸ 0.0158	⁴⁶ 0.0924
13	CANON-002	³⁸ 0.0036	³³ 0.0047	³⁴ 0.0061	²⁷ 0.0124	²⁸ 0.0808
14	CIB-000	⁶⁸ 0.0086	⁷¹ 0.0125	⁷⁰ 0.0160	⁷⁵ 0.0303	⁹² 0.1251
15	CLEARVIEWAI-000	⁴² 0.0040	⁴² 0.0058	⁴¹ 0.0078	³⁹ 0.0159	⁴⁹ 0.0971
16	CLOUDWALK-HR-000	¹⁵ 0.0019	¹³ 0.0020	¹⁰ 0.0023	¹⁵ 0.0072	²¹ 0.0701
17	CLOUDWALK-MT-000	¹⁴ 0.0019	¹² 0.0020	⁷ 0.0022	⁶ 0.0049	¹⁸ 0.0466
18	CLOUDWALK-MT-001	¹² 0.0018	¹⁰ 0.0019	⁸ 0.0020	⁷ 0.0052	¹⁵ 0.0555
19	COGENT-000	¹⁸ 0.0430	¹⁶⁷ 0.0527	¹⁶³ 0.0695	¹⁶⁸ 0.1133	¹⁵⁹ 0.1960
20	COGENT-001	¹⁸¹ 0.0430	¹⁶⁶ 0.0527	¹⁶⁸ 0.0695	¹⁶⁷ 0.1133	¹⁵⁷ 0.1960
21	COGENT-002	¹⁴⁹ 0.0322	¹⁵³ 0.0444	¹⁵¹ 0.0610	¹⁶⁵ 0.1116	¹⁷¹ 0.2180
22	COGENT-003	¹⁵⁰ 0.0328	¹⁵⁸ 0.0463	¹⁶³ 0.0683	¹⁷⁵ 0.1294	¹⁸⁸ 0.2445
23	COGENT-004	¹³⁴ 0.0210	¹³⁸ 0.0331	¹⁴⁶ 0.0527	¹⁷⁰ 0.1138	¹⁶⁸ 0.2119
24	COGENT-005	⁵⁸ 0.0064	⁵⁶ 0.0091	⁵⁶ 0.0123	⁷⁶ 0.0303	⁸⁴ 0.1233
25	COGENT-006	²⁹ 0.0032	²⁹ 0.0044	²⁹ 0.0057	²⁷ 0.0120	³² 0.0830
26	COGNITEC-000	²⁴ 0.1377	²⁴⁰ 0.1606	²¹¹ 0.1870	¹⁹⁹ 0.2176	¹⁹⁴ 0.2831
27	COGNITEC-001	²¹⁵ 0.0807	²¹³ 0.1017	¹⁹⁸ 0.1214	¹⁸⁵ 0.1513	¹⁷⁴ 0.2238
28	COGNITEC-002	¹²⁴ 0.0406	¹⁶⁹ 0.0531	¹⁵⁹ 0.0666	¹⁵³ 0.0935	¹³³ 0.1874
29	COGNITEC-003	¹⁷¹ 0.0400	¹⁶⁵ 0.0526	¹⁵⁸ 0.0650	¹⁴⁸ 0.0895	¹⁴⁶ 0.1772
30	COGNITEC-004	¹³⁶ 0.0222	¹³⁶ 0.0313	¹³² 0.0388	¹²³ 0.0540	⁷⁰ 0.1103
31	COGNITEC-005	⁵⁸ 0.0063	⁵⁸ 0.0096	⁶¹ 0.0144	⁶⁹ 0.0287	⁴⁸ 0.0967
32	COGNITEC-006	⁵⁰ 0.0053	⁵² 0.0077	⁵⁴ 0.0117	⁵⁷ 0.0254	⁴² 0.0919
33	CYBERLINK-000	¹⁷⁶ 0.0414	¹⁷⁷ 0.0565	¹⁷⁴ 0.0707	¹⁶¹ 0.1031	¹⁶ 0.2050
34	CYBERLINK-001	¹⁶⁷ 0.0392	¹⁷⁰ 0.0536	¹⁶⁴ 0.0695	¹⁵⁸ 0.0973	¹⁴⁷ 0.1794
35	CYBERLINK-002	⁷⁰ 0.0105	⁸¹ 0.0148	⁸⁰ 0.0202	⁹⁷ 0.0399	⁹ 0.1255
36	CYBERLINK-003	⁵² 0.0056	⁵³ 0.0077	⁴⁹ 0.0100	⁵³ 0.0235	⁸⁹ 0.1237
37	CYBERLINK-004	⁴⁸ 0.0051	⁴⁹ 0.0071	⁵¹ 0.0102	⁴⁵ 0.0199	⁹⁶ 0.1269
38	CYBERLINK-005	⁵⁹ 0.0067	⁶² 0.0099	⁶¹ 0.0138	⁹⁴ 0.0394	¹³ 0.1566
39	DAHUA-001	¹⁹⁶ 0.0569	¹⁹⁴ 0.0727	¹⁷⁸ 0.0878	¹⁷¹ 0.1148	¹⁵² 0.1867
40	DAHUA-002	⁸³ 0.0108	⁸² 0.0151	⁸⁰ 0.0191	⁷¹ 0.0291	⁸¹ 0.1153
41	DAHUA-003	⁷⁵ 0.0100	⁷⁶ 0.0139	⁷⁶ 0.0180	⁷² 0.0296	⁷⁵ 0.1130
42	DAHUA-004	⁴⁶ 0.0048	⁴⁸ 0.0069	⁴⁶ 0.0090	⁴¹ 0.0164	³⁵ 0.0853
43	DAON-000	¹¹¹ 0.0161	¹¹¹ 0.0226	¹¹¹ 0.0293	¹³⁰ 0.0562	¹⁴⁰ 0.1702
44	DECATUR-000	¹¹³ 0.0173	¹¹⁴ 0.0229	¹¹⁵ 0.0305	¹⁰⁷ 0.0464	¹¹ 0.1433
45	DEEPLINTL-001	²⁵ 0.0027	²⁵ 0.0033	²⁴ 0.0043	²⁸ 0.0121	⁴⁵ 0.0922
46	DEEPSA-001	¹⁵⁹ 0.0347	¹⁵⁷ 0.0462	¹⁵⁹ 0.0586	¹⁴⁶ 0.0802	¹⁴ 0.1708
47	DERMALOG-005	²¹¹ 0.0700	²⁰⁷ 0.0880	¹⁹¹ 0.1144	¹⁸⁸ 0.1578	¹⁸⁴ 0.2451
48	DERMALOG-006	¹⁶⁸ 0.0395	¹⁶⁴ 0.0517	¹⁵⁸ 0.0659	¹⁵⁷ 0.0973	¹⁴ 0.1745
49	DERMALOG-007	²⁰⁸ 0.0691	²⁰⁵ 0.0863	¹⁹⁰ 0.1107	¹⁸⁴ 0.1504	¹⁷⁹ 0.2299
50	DERMALOG-008	¹⁵⁵ 0.0338	¹⁵⁵ 0.0455	¹⁵⁰ 0.0626	¹⁶² 0.1060	¹²⁷ 0.2276
51	DERMALOG-009	¹⁰⁴ 0.0148	¹⁰⁴ 0.0206	¹⁰³ 0.0268	¹⁰¹ 0.0416	¹⁰ 0.1374
52	DERMALOG-010	⁴⁹ 0.0052	⁴⁷ 0.0069	⁴⁵ 0.0088	⁴⁶ 0.0207	⁵⁰ 0.0971
53	DILUSENSE-000	¹³⁵ 0.0208	¹³⁴ 0.0305	¹³⁰ 0.0377	¹²⁷ 0.0543	¹¹² 0.1429
54	FUJITSULAB-000	¹⁰⁵ 0.0148	¹⁰⁵ 0.0206	¹⁰⁷ 0.0277	¹²⁵ 0.0541	¹⁴⁴ 0.1739
55	FUJITSULAB-001	⁸⁸ 0.0126	⁹⁵ 0.0182	⁹⁸ 0.0251	¹³⁴ 0.0646	¹⁶ 0.2079
56	GORILLA-002	²⁴⁸ 0.1539	²⁴⁸ 0.1880	²¹⁵ 0.2184	²⁰⁸ 0.2596	²⁰³ 0.3398
57	GORILLA-004	²¹⁰ 0.0699	²¹⁰ 0.0892	¹⁸⁷ 0.1048	¹⁸⁰ 0.1370	¹⁶ 0.1969
58	GORILLA-005	¹⁸⁶ 0.0453	¹⁸¹ 0.0583	¹⁶⁹ 0.0704	¹⁵⁹ 0.0974	¹¹⁸ 0.1474
59	GORILLA-006	¹²⁶ 0.0196	¹²⁶ 0.0275	¹¹⁷ 0.0331	¹¹⁵ 0.0516	⁷⁴ 0.1113
60	GORILLA-007	¹²³ 0.0190	¹²⁵ 0.0271	¹²³ 0.0348	¹¹⁹ 0.0520	⁷⁴ 0.1129
61	GRIAULE-000	¹⁰¹ 0.0145	¹⁰² 0.0201	⁹⁹ 0.0253	⁹⁹ 0.0407	¹¹⁵ 0.1440
62	GRIAULE-001	³¹ 0.0033	³⁴ 0.0047	³⁶ 0.0153	³⁹ 0.0910	
63	HIK-003	²¹⁶ 0.0828	²¹⁵ 0.1028	¹⁹⁴ 0.1202	¹⁸⁷ 0.1525	¹⁸⁶ 0.2480
64	HIK-004	²¹⁴ 0.0796	²¹¹ 0.0988	¹⁹² 0.1147	¹⁸³ 0.1474	¹⁸ 0.2483
65	HIK-005	¹⁴⁷ 0.0312	¹⁵⁰ 0.0436	¹⁴⁹ 0.0560	¹⁵⁰ 0.0911	¹⁷⁰ 0.2129
66	HYPERVERGE-001	³⁰ 0.0033	³⁰ 0.0045	³⁰ 0.0059	²⁴ 0.0117	³¹ 0.0872
67	HYPERVERGE-002	²⁶ 0.0028	²⁶ 0.0037	²⁶ 0.0046	¹² 0.0064	¹ 0.0064
68	HZAILU-000	¹⁰⁶ 0.0143	¹⁰¹ 0.0197	¹⁰⁶ 0.0255	¹⁰⁰ 0.0411	⁸⁴ 0.1174
69	HZAILU-001	⁵⁸ 0.0066	⁵⁴ 0.0086	⁵² 0.0109	⁴⁷ 0.0207	⁶³ 0.1052
70	IDEARIA-003	¹⁵⁹ 0.0346	¹⁶⁰ 0.0471	¹⁷⁹ 0.0892	²¹⁰ 0.2789	²⁰ 0.4311
71	IDEARIA-004	¹⁴⁶ 0.0300	¹⁴⁶ 0.0373	¹³⁸ 0.0447	¹³² 0.0617	¹³⁹ 0.1635
72	IDEARIA-005	¹⁶² 0.0360	¹⁵² 0.0440	¹⁴⁷ 0.0537	¹⁴⁵ 0.0764	¹⁵ 0.1915

Table 18: Identification-mode: Effect of N on FNIR at high threshold. Values are threshold-based miss rates i.e. FNIR at FPIR = 0.001 for five enrollment population sizes, N. The right six columns apply for enrollment of one image. Missing entries usually apply because another algorithm from the same developer was run instead. Some developers are missing because less accurate algorithms were not run on galleries with $N \geq 3\,000\,000$. Throughout blue superscripts indicate the rank of the algorithm for that column.

#	ALGORITHM	MISSES BELOW THRESHOLD, T FNIR(N, T > 0, R > L)		ENROL MOST RECENT DATASET: FRVT 2018 MUGSHOTS					
		N=0.64M	N=1.6M	N=3.0M	N=6.0M	N=12.0M			
73	IDEARIA-006	¹⁶⁰ 0.0351	¹⁴⁹ 0.0433	¹⁴⁵ 0.0525	¹⁴² 0.0734	¹⁷² 0.2201			
74	IDEARIA-007	⁹⁶ 0.0136	⁹⁴ 0.0181	⁸⁷ 0.0228	⁸⁷ 0.0357	¹¹¹ 0.1402			
75	IDEARIA-008	⁹ 0.0016	⁹ 0.0019	¹² 0.0024	⁸ 0.0053	¹¹ 0.0470			
76	IDEARIA-009	³ 0.0013	³ 0.0016	³ 0.0018	¹¹ 0.0061	¹⁴ 0.0550			
77	IMAGUS-005	⁹⁷ 0.0137	⁹⁸ 0.0185	⁹³ 0.0237	⁸⁹ 0.0368	⁶⁶ 0.1067			
78	IMAGUS-006	⁹⁸ 0.0137	¹⁰⁰ 0.0190	⁹⁶ 0.0244	⁹⁵ 0.0396	⁸⁸ 0.1159			
79	IMAGUS-007	¹⁰⁹ 0.0160	¹¹³ 0.0228	¹⁰⁹ 0.0284	¹¹⁴ 0.0444	⁸⁵ 0.1179			
80	IMPERIAL-000	¹¹⁹ 0.0187	¹¹⁹ 0.0259	¹²⁸ 0.0358	¹¹¹ 0.0733	¹⁴⁸ 0.1794			
81	INCODE-003	²⁴¹ 0.1324	²⁴³ 0.1672	²¹⁹ 0.1961	²⁰² 0.2345	¹⁹⁸ 0.3123			
82	INCODE-004	¹⁷² 0.0403	¹⁷³ 0.0538	¹⁵⁸ 0.0662	¹⁵² 0.0917	¹³⁶ 0.1619			
83	INCODE-005	⁶⁶ 0.0083	⁶⁶ 0.0113	⁶⁹ 0.0145	⁵⁴ 0.0247	⁴⁰ 0.0912			
84	INNOVATRICS-007	⁷² 0.0093	⁷² 0.0125	⁶⁹ 0.0159	⁵⁹ 0.0259	⁶⁷ 0.1092			
85	INTEMA-000	¹⁵ 0.0019	¹⁶ 0.0024	¹⁷ 0.0032	²¹ 0.0098	²⁵ 0.0745			
86	INTSYSMSU-000	³⁰⁴ 0.9982	³⁰² 0.9984	²²⁹ 0.9985	²²¹ 0.9987	²¹⁶ 0.9988			
87	IREX-000	¹²⁴ 0.0190	¹³⁰ 0.0280	¹³³ 0.0391	¹³⁷ 0.0677	¹²¹ 0.1479			
88	ISYSTEMS-002	¹⁹⁸ 0.0584	¹⁹⁸ 0.0783	¹⁸³ 0.0973	¹⁸¹ 0.1373	¹⁷⁸ 0.2295			
89	ISYSTEMS-003	¹⁸⁴ 0.0438	¹⁸² 0.0590	¹⁷⁶ 0.0807	¹⁷³ 0.1259	¹⁸⁰ 0.2357			
90	KAKAO-000	⁸⁴ 0.0109	⁸⁴ 0.0151	⁸² 0.0196	⁸² 0.0324	⁵⁴ 0.1010			
91	KAKAO-001	²⁹ 0.0021	¹⁹ 0.0026	¹⁸ 0.0032	¹⁹ 0.0085	²⁹ 0.0693			
92	KEDACOM-001	¹¹⁵ 0.0181	¹¹² 0.0227	¹⁰¹ 0.0265	¹⁰³ 0.0422	¹⁰⁴ 0.1340			
93	LOOKMAN-003	¹⁵⁸ 0.0346	¹⁵¹ 0.0437	¹⁴⁵ 0.0514	¹⁴⁰ 0.0724	¹⁵⁷ 0.1620			
94	LOOKMAN-005	¹³⁸ 0.0240	¹³³ 0.0301	¹²⁷ 0.0356	¹¹⁴ 0.0512	¹⁰³ 0.1334			
95	MANTRA-000	⁹ 0.0065	⁶³ 0.0101	⁶⁶ 0.0151	⁷⁷ 0.0308	⁵⁹ 0.1035			
96	MAXVISION-000	¹³² 0.0206	¹³¹ 0.0282	¹²⁴ 0.0355	¹¹⁶ 0.0517	¹⁰⁵ 0.1340			
97	MEGVII-001	¹⁹⁴ 0.0562	¹⁹³ 0.0722	¹⁷⁷ 0.0872	¹⁷⁷ 0.1309	¹⁹⁴ 0.2713			
98	MICROFOCUS-005	³⁰¹ 0.9732	²⁹⁴ 0.8354	²²⁶ 0.8555	²¹⁹ 0.8755	²¹³ 0.8954			
99	MICROSOFT-003	¹² 0.0198	¹²⁸ 0.0278	¹²⁸ 0.0356	¹²² 0.0538	¹² 0.1539			
100	MICROSOFT-004	¹¹⁸ 0.0185	¹²⁰ 0.0259	¹¹⁸ 0.0333	¹¹⁷ 0.0517	¹²⁵ 0.1510			
101	MICROSOFT-005	¹¹⁶ 0.0181	¹¹⁷ 0.0256	¹¹⁵ 0.0320	¹¹⁵ 0.0512	¹² 0.1491			
102	MICROSOFT-006	⁷¹ 0.0091	⁶⁷ 0.0120	⁷¹ 0.0162	⁷⁴ 0.0301	¹²² 0.1482			
103	NEC-000	²⁰² 0.0637	²⁰⁰ 0.0789	¹⁸⁹ 0.0933	¹⁷² 0.1163	¹⁵⁹ 0.1941			
104	NEC-001	²¹⁷ 0.0863	²¹⁷ 0.1055	¹⁹⁷ 0.1249	¹⁸⁶ 0.1519	¹⁷⁵ 0.2253			
105	NEC-002	¹⁸ 0.0020	¹⁸ 0.0026	¹⁹ 0.0033	³² 0.0135	¹⁸ 0.0653			
106	NEC-003	¹⁰ 0.0021	¹⁵ 0.0024	¹⁵ 0.0028	¹⁰ 0.0059	¹³ 0.0540			
107	NEC-004	¹⁰ 0.0017	⁶ 0.0018	⁷ 0.0020	³ 0.0037	⁷ 0.0329			
108	NEC-005	³ 0.0015	⁴ 0.0017	⁴ 0.0019	¹⁵ 0.0065	³ 0.0307			
109	NEC-006	¹¹ 0.0018	¹¹ 0.0020	¹³ 0.0026	²³ 0.0103	¹⁶ 0.0573			
110	NEUROTECHNOLOGY-003	²⁸ 0.5698	²⁸ 0.6362	²² 0.7035	²¹⁷ 0.7602	²¹ 0.8224			
111	NEUROTECHNOLOGY-004	¹⁸⁸ 0.0466	¹⁸⁷ 0.0629	¹⁷¹ 0.0779	¹⁶⁹ 0.1135	¹⁶⁷ 0.2102			
112	NEUROTECHNOLOGY-005	¹⁶⁹ 0.0396	¹⁷⁴ 0.0538	¹⁶¹ 0.0675	¹⁵⁶ 0.0950	¹⁶⁰ 0.1966			
113	NEUROTECHNOLOGY-007	¹⁸ 0.0436	¹⁸⁶ 0.0623	¹⁷¹ 0.0802	¹⁷⁸ 0.1320	¹⁸² 0.2393			
114	NEUROTECHNOLOGY-008	¹⁵⁶ 0.0339	¹⁶⁸ 0.0530	¹⁸⁰ 0.0893	¹⁹³ 0.1769	²⁰¹ 0.3288			
115	NEUROTECHNOLOGY-009	⁸ 0.0108	⁸⁵ 0.0152	⁸¹ 0.0196	⁸⁰ 0.0324	⁶⁹ 0.1102			
116	NEUROTECHNOLOGY-010	⁶² 0.0069	⁶¹ 0.0099	⁶² 0.0138	¹⁰⁶ 0.0449	¹⁴³ 0.1727			
117	NEUROTECHNOLOGY-012	⁴ 0.0047	⁴⁶ 0.0068	⁴⁶ 0.0097	⁶³ 0.0265	¹⁰ 0.1343			
118	NOTIONTAG-000	⁸⁹ 0.0128	⁸⁹ 0.0175	⁸⁸ 0.0228	⁸⁸ 0.0357	⁹⁷ 0.1270			
119	NTECHLAB-003	¹⁷⁸ 0.0421	¹⁷² 0.0537	¹⁶⁴ 0.0674	¹⁴⁹ 0.0907	¹³⁴ 0.1582			
120	NTECHLAB-004	¹⁴⁸ 0.0312	¹⁴⁷ 0.0405	¹⁴⁴ 0.0519	¹³⁹ 0.0722	¹²⁴ 0.1503			
121	NTECHLAB-005	¹⁵² 0.0334	¹⁴⁸ 0.0424	¹⁴⁶ 0.0537	¹⁴⁴ 0.0760	¹³⁰ 0.1543			
122	NTECHLAB-006	¹⁴⁴ 0.0288	¹⁴² 0.0367	¹⁴¹ 0.0471	¹³⁶ 0.0670	¹²⁶ 0.1523			
123	NTECHLAB-007	¹²⁰ 0.0188	¹¹⁶ 0.0256	¹¹³ 0.0317	¹¹² 0.0495	¹⁰² 0.1306			
124	NTECHLAB-008	⁸ 0.0107	⁷⁸ 0.0145	⁷⁸ 0.0187	⁶⁸ 0.0286	⁵⁹ 0.0995			
125	NTECHLAB-009	³⁷ 0.0037	³⁷ 0.0049	³⁵ 0.0062	³⁰ 0.0125	²⁴ 0.0735			
126	NTECHLAB-010	¹⁶ 0.0020	¹⁷ 0.0025	¹⁵ 0.0030	¹⁷ 0.0077	²¹ 0.0710			
127	NTECHLAB-011	²¹ 0.0022	²² 0.0030	²³ 0.0038	¹⁶ 0.0075	¹⁷ 0.0625			
128	PANGMIN-000	⁴ 0.0042	⁴³ 0.0060	⁴⁶ 0.0080	⁴⁰ 0.0160	³⁷ 0.0876			
129	PARAVISION-003	¹⁴⁰ 0.0260	¹⁴⁰ 0.0351	¹³⁹ 0.0447	¹³⁵ 0.0657	¹³⁸ 0.1630			
130	PARAVISION-004	⁶⁵ 0.0074	⁶⁵ 0.0101	⁶⁶ 0.0136	⁶⁴ 0.0267	⁶⁶ 0.1256			
131	PARAVISION-005	²⁸ 0.0032	²⁸ 0.0041	²⁸ 0.0057	⁴³ 0.0174	⁶⁰ 0.1037			
132	PARAVISION-007	²⁷ 0.0030	²⁷ 0.0040	²⁷ 0.0055	⁴⁸ 0.0211	⁶⁸ 0.1097			
133	PARAVISION-009	⁷ 0.0020	²⁰ 0.0026	²⁵ 0.0038	²² 0.0098	³⁴ 0.0857			
134	PIXELALL-002	²¹² 0.0716	²¹⁶ 0.1052	²⁰⁴ 0.1475	²⁰⁶ 0.2489	²⁰⁶ 0.3904			
135	PIXELALL-003	¹⁰⁸ 0.0158	¹⁰⁸ 0.0218	¹¹⁸ 0.0288	¹⁰⁸ 0.0474	²⁹ 0.1138			
136	PIXELALL-004	⁹² 0.0129	⁹⁷ 0.0183	⁹⁷ 0.0245	⁹⁶ 0.0378	¹⁰⁹ 0.1375			
137	PIXELALL-005	⁶⁹ 0.0087	⁶⁹ 0.0121	⁷¹ 0.0171	⁵⁶ 0.0250	⁶² 0.1052			
138	PTAKURATSATU-000	¹⁴¹ 0.0275	¹⁴¹ 0.0366	¹⁴⁰ 0.0458	¹²⁰ 0.0523	¹² 0.0523			
139	QNAP-001	¹⁷³ 0.0404	¹⁷¹ 0.0536	¹⁵⁷ 0.0661	¹⁵¹ 0.0916	¹³⁴ 0.1595			
140	QNAP-002	¹²⁸ 0.0200	¹²¹ 0.0265	¹¹⁸ 0.0327	¹¹⁰ 0.0490	¹⁰⁶ 0.1341			
141	QUANTASOFT-001	²⁸ 0.6387	²⁸ 0.6387	²² 0.6387		²⁰ 0.6387			
142	RANKONE-002	²²⁵ 0.0973	²²⁰ 0.1175	¹⁹⁸ 0.1359	¹⁹⁰ 0.1718	¹⁹¹ 0.2613			
143	RANKONE-003	²² 0.0973	²²¹ 0.1175	¹⁹ 0.1359	¹⁹¹ 0.1718	¹⁹¹ 0.2613			
144	RANKONE-005	¹⁸⁹ 0.0473	¹⁸³ 0.0592	¹⁶⁷ 0.0700	¹⁵⁴ 0.0944	¹⁶² 0.1998			

Table 19: Identification-mode: Effect of N on FNIR at high threshold. Values are threshold-based miss rates i.e. FNIR at FPIR = 0.001 for five enrollment population sizes, N. The right six columns apply for enrollment of one image. Missing entries usually apply because another algorithm from the same developer was run instead. Some developers are missing because less accurate algorithms were not run on galleries with $N \geq 3\ 000\ 000$. Throughout blue superscripts indicate the rank of the algorithm for that column.

#	ALGORITHM	MISSES BELOW THRESHOLD, T		ENROL, MOST RECENT				
		FNIR(N, T > 0, R > L)		DATASET: FRVT 2018 MUGSHOTS				
145	RANKONE-007	¹¹² 0.0168	¹¹⁰ 0.0222	¹⁰² 0.0266	⁹² 0.0381	⁷⁶ 0.1132		
146	RANKONE-009	⁹³ 0.0132	⁹² 0.0177	⁹⁰ 0.0230	⁸⁴ 0.0344	⁴⁴ 0.0921		
147	RANKONE-010	⁷⁹ 0.0106	⁷⁵ 0.0136	⁷⁴ 0.0174	⁶² 0.0265	²⁷ 0.0785		
148	RANKONE-011	⁵⁴ 0.0063	⁵⁵ 0.0087	⁵⁷ 0.0115	⁶⁵ 0.0269	⁷⁸ 0.1135		
149	RANKONE-012	⁵⁵ 0.0058	⁵¹ 0.0077	⁵⁰ 0.0100	⁴⁹ 0.0220	⁷² 0.1111		
150	RANKONE-013	²³ 0.0034	³¹ 0.0046	³¹ 0.0059	³¹ 0.0127	²⁶ 0.0875		
151	REALNETWORKS-002	²⁵⁴ 0.1943	²⁵³ 0.2314	²¹⁷ 0.2656	²¹² 0.3134	²⁰⁰ 0.3208		
152	REALNETWORKS-003	²⁴⁰ 0.1300	²³⁹ 0.1594	²¹⁰ 0.1858	²⁰⁰ 0.2246	¹⁹⁷ 0.3076		
153	REALNETWORKS-004	²³⁹ 0.1279	²³⁸ 0.1581	²⁰⁹ 0.1857	²⁰¹ 0.2329	¹⁹⁹ 0.3179		
154	REALNETWORKS-005	¹²⁹ 0.0202	¹²⁷ 0.0277	¹²⁵ 0.0355	¹²⁹ 0.0560	¹¹³ 0.1431		
155	REALNETWORKS-006	⁷⁴ 0.0097	⁷⁹ 0.0145	⁷⁷ 0.0182	⁷⁸ 0.0308	⁵¹ 0.0991		
156	REALNETWORKS-007	⁶¹ 0.0068	⁵⁹ 0.0097	⁵⁶ 0.0125	⁵¹ 0.0233	⁴¹ 0.0917		
157	REALNETWORKS-008	⁴⁴ 0.0044	⁴⁴ 0.0062	⁴⁸ 0.0082	³³ 0.0139	³⁰ 0.0824		
158	REMARKAI-000	¹⁷⁵ 0.0406	¹⁷⁸ 0.0552	¹⁶² 0.0676	¹⁶⁰ 0.1028	¹⁶³ 0.2003		
159	RENDIP-000	⁶⁹ 0.0085	⁶⁸ 0.0121	⁶⁷ 0.0156	⁶⁷ 0.0277	⁵⁶ 0.1182		
160	REVEALMEDIA-000	⁷⁰ 0.0090	⁷⁰ 0.0122	⁶⁸ 0.0158	⁶⁶ 0.0277	⁵⁶ 0.1019		
161	S1-000	¹³¹ 0.0204	¹²⁹ 0.0279	¹³¹ 0.0382	¹³³ 0.0630	¹⁴¹ 0.1707		
162	S1-001	⁸⁵ 0.0115	⁸⁶ 0.0156	⁸⁴ 0.0199	⁹³ 0.0392	⁹⁵ 0.1256		
163	S1-002	⁴¹ 0.0040	⁴¹ 0.0056	⁴⁰ 0.0077	⁶¹ 0.0264	³⁹ 0.1285		
164	SCANOVATE-000	¹⁹⁰ 0.0498	¹⁹⁰ 0.0667	¹⁷⁴ 0.0804	¹⁶⁴ 0.1097	⁷¹ 0.1109		
165	SCANOVATE-001	²⁰¹ 0.0630	²⁰¹ 0.0815	¹⁸⁵ 0.0993	¹⁷⁴ 0.1292	¹⁵⁹ 0.1960		
166	SENSETIME-000	¹⁰⁷ 0.0158	¹⁰⁶ 0.0208	¹⁰⁸ 0.0270	⁹⁶ 0.0398	⁸⁷ 0.1232		
167	SENSETIME-001	¹¹⁰ 0.0161	¹⁰⁹ 0.0219	¹⁰⁸ 0.0277	¹⁰² 0.0420	¹⁰⁰ 0.1304		
168	SENSETIME-002	¹⁰² 0.0146	⁸⁰ 0.0148	⁶⁶ 0.0153	⁵² 0.0234	¹⁹ 0.0657		
169	SENSETIME-003	⁷ 0.0016	⁸ 0.0018	⁸ 0.0021	⁹ 0.0054	⁸ 0.0451		
170	SENSETIME-004	¹ 0.0015	⁵ 0.0018	⁷ 0.0021	⁴ 0.0040	¹ 0.0354		
171	SENSETIME-005	⁸ 0.0016	¹⁴ 0.0022	¹⁶ 0.0031	²⁰ 0.0089	⁹ 0.0454		
172	SENSETIME-006	⁴ 0.0014	⁷ 0.0018	¹¹ 0.0023	⁵ 0.0047	⁷ 0.0372		
173	SENSETIME-007	² 0.0012	² 0.0014	² 0.0016	² 0.0036	⁴ 0.0316		
174	SENSETIME-008	¹ 0.0011	¹ 0.0013	¹ 0.0015	¹ 0.0031	² 0.0288		
175	SHAMAN-007	²⁵ 0.1212	²³³ 0.1413	²⁰⁹ 0.1587	¹⁹⁵ 0.1879	¹⁸ 0.2460		
176	SIAT-001	⁹⁵ 0.0136	⁹⁰ 0.0176	⁹¹ 0.0230	⁸³ 0.0344	⁵⁸ 0.1035		
177	SIAT-002	¹⁰⁶ 0.0154	¹⁰⁷ 0.0216	¹⁰⁸ 0.0273	⁹⁸ 0.0404	⁹⁸ 0.1283		
178	SQISOFT-001	²¹⁸ 0.0921	²²⁹ 0.1322	²⁰⁷ 0.1781	²⁰³ 0.2348	²¹⁴ 0.9271		
179	SYNESSIS-003	²⁸⁴ 0.5341	²⁸³ 0.5821	²²⁷ 0.6113	²¹⁶ 0.6479	²¹⁰ 0.6822		
180	SYNESSIS-003	¹⁹¹ 0.0499	¹⁸⁸ 0.0652	¹⁷⁵ 0.0804	¹⁶³ 0.1095	¹⁵⁵ 0.1916		
181	SYNESSIS-005	¹¹ 0.0181	¹¹⁵ 0.0248	¹¹¹ 0.0319	¹¹⁸ 0.0518	¹² 0.1580		
182	TECH5-001	¹⁷⁷ 0.0420	¹⁷⁸ 0.0574	¹⁸¹ 0.0911	¹⁹⁸ 0.2106	²⁰⁵ 0.3725		
183	TECH5-002	¹²⁵ 0.0194	¹²⁴ 0.0269	¹²² 0.0346	¹²¹ 0.0537	¹³⁵ 0.1607		
184	TEVIAN-005	²⁰⁹ 0.0692	²⁰⁶ 0.0873	¹⁸⁸ 0.1066	¹⁷⁶ 0.1301	¹⁵⁰ 0.1840		
185	TEVIAN-006	⁶⁵ 0.0078	⁶⁰ 0.0098	⁵⁸ 0.0130	⁶⁰ 0.0261	¹⁰¹ 0.1305		
186	TEVIAN-007	³⁹ 0.0038	³⁹ 0.0052	³⁶ 0.0065	³⁷ 0.0154	⁴⁷ 0.0957		
187	TIGER-002	²⁰⁴ 0.0647	²⁰² 0.0861	¹⁸⁶ 0.1036	¹⁷⁹ 0.1332	¹⁷³ 0.2231		
188	TOSHIBA-000	¹⁸ 0.0460	¹⁸⁵ 0.0620	¹⁷⁴ 0.0780	¹⁶⁶ 0.1117	¹⁶ 0.2082		
189	TRUEFACE-000	⁹⁴ 0.0134	⁹⁶ 0.0182	⁹⁴ 0.0238	⁹¹ 0.0380	¹¹⁰ 0.1385		
190	VD-001	²⁵⁰ 0.1642	²⁵⁰ 0.2015	²¹⁷ 0.2351	²⁰⁹ 0.2736	²⁰² 0.3293		
191	VERIDAS-001	¹⁴² 0.0278	¹⁴⁵ 0.0373	¹⁴² 0.0491	¹⁴³ 0.0753	¹²⁸ 0.1541		
192	VERIDAS-002	¹⁴³ 0.0278	¹⁴⁴ 0.0373	¹²⁸ 0.0373	¹¹¹ 0.0491	²⁶ 0.0753		
193	VERIDAS-003	⁸⁶ 0.0117	⁸⁸ 0.0166	⁸⁶ 0.0219	¹⁰⁵ 0.0446	¹²⁹ 0.1543		
194	VIGILANTSOLUTIONS-008	¹⁰³ 0.0146	¹⁰³ 0.0205	¹⁰⁸ 0.0269	¹⁰⁹ 0.0489	⁸³ 0.1164		
195	VISIONBOX-000	⁸⁷ 0.0122	⁹³ 0.0177	⁹⁵ 0.0239		²¹⁵ 0.9538		
196	VISIONLABS-004	¹⁸ 0.0427	¹⁷⁹ 0.0578	¹⁶⁷ 0.0703	¹⁵⁵ 0.0949	¹⁵ 0.1853		
197	VISIONLABS-005	¹⁶⁵ 0.0369	¹⁶³ 0.0502	¹⁵² 0.0626	¹⁴⁷ 0.0847	¹⁴⁹ 0.1815		
198	VISIONLABS-006	¹² 0.0188	¹²³ 0.0267	¹²⁸ 0.0336	¹²⁶ 0.0542	¹¹⁷ 0.1478		
199	VISIONLABS-007	¹²² 0.0188	¹²² 0.0266	¹¹⁹ 0.0335	¹²⁴ 0.0540	¹²⁰ 0.1479		
200	VISIONLABS-008	²³ 0.0096	⁷³ 0.0131	⁷² 0.0166	⁷⁰ 0.0291	⁹¹ 0.1247		
201	VISIONLABS-009	³⁴ 0.0034	³² 0.0046	³⁸ 0.0060	³⁴ 0.0140	³⁸ 0.0881		
202	VISIONLABS-010	³⁸ 0.0038	³⁸ 0.0051	³⁸ 0.0070	³⁵ 0.0149	⁴³ 0.0920		
203	VISIONLABS-011	²⁵ 0.0025	²⁴ 0.0033	²⁵ 0.0044	²⁶ 0.0120	³¹ 0.0825		
204	VNPT-001	⁷⁷ 0.0104	⁷⁷ 0.0143	⁷⁹ 0.0190	⁷³ 0.0296	⁵⁷ 0.1028		
205	VNPT-002	⁴ 0.0051	⁴⁵ 0.0065	⁴⁸ 0.0083	⁴² 0.0172	⁵³ 0.1005		
206	VCORD-005	²³⁴ 0.1179	²³⁷ 0.1577	²¹⁴ 0.2183	²¹¹ 0.3122	²⁰⁸ 0.4490		
207	VTS-001	⁷⁶ 0.0102	⁷⁴ 0.0133	⁷⁷ 0.0175	⁷⁹ 0.0322	⁹⁰ 0.1243		
208	VTS-002	¹¹⁷ 0.0185	¹¹⁸ 0.0259	¹²¹ 0.0344	¹²⁸ 0.0549	¹¹⁶ 0.1447		
209	VTS-003	³¹ 0.0053	⁵⁰ 0.0073	⁴⁷ 0.0096	⁴⁴ 0.0188	⁵¹ 0.1017		
210	XFORWARDAI-000	⁸⁰ 0.0107	⁸³ 0.0151	⁸¹ 0.0195	⁸¹ 0.0324	⁶⁴ 0.1057		
211	XFORWARDAI-001	³⁶ 0.0037	³⁶ 0.0049	³⁶ 0.0060	²⁵ 0.0120	²⁸ 0.0800		
212	XFORWARDAI-002	²⁴ 0.0026	²³ 0.0030	²¹ 0.0035	¹⁸ 0.0078	²² 0.0706		
213	YITU-002	⁹¹ 0.0129	⁹¹ 0.0177	⁸⁹ 0.0228	⁸⁸ 0.0345	⁷⁷ 0.1133		
214	YITU-003	⁹ 0.0138	⁹⁹ 0.0185	⁹⁹ 0.0236	⁸⁶ 0.0353	⁸⁰ 0.1148		
215	YITU-004	⁶⁰ 0.0067	⁵⁷ 0.0096	⁵⁷ 0.0129	⁵⁰ 0.0232	⁶¹ 0.1046		
216	YITU-005	⁶⁴ 0.0074	⁶⁴ 0.0101	⁵⁹ 0.0135	⁵⁸ 0.0255	⁶⁵ 0.1057		

Table 20: Identification-mode: Effect of N on FNIR at high threshold. Values are threshold-based miss rates i.e. FNIR at FPIR = 0.001 for five enrollment population sizes, N. The right six columns apply for enrollment of one image. Missing entries usually apply because another algorithm from the same developer was run instead. Some developers are missing because less accurate algorithms were not run on galleries with $N \geq 3\,000\,000$. Throughout blue superscripts indicate the rank of the algorithm for that column.

MISSES AT GIVEN RANK		ENROL MOST RECENT													
#	ALGORITHM	RANK 1					aN^b	RANK 50					aN^b		
		N=0.64M	N=1.6M	N=3.0M	N=6.0M	N=12.0M		N=0.64M	N=1.6M	N=3.0M	N=6.0M	N=12.0M			
1	3DIVI-005	²⁴⁰ 0.0137	²³⁸ 0.0176	²⁰⁵ 0.0210	²⁰⁰ 0.0253	¹⁹⁵ 0.0302	¹⁵³ 0.0004 N ^{0.271} ¹⁷⁷	²²⁰ 0.0040	²²⁰ 0.0049	¹⁹⁵ 0.0057	¹⁹² 0.0068	¹⁸⁷ 0.0081	⁴⁸ 0.0002 N ^{0.240} ¹⁸²		
2	ACER-000	²⁰⁷ 0.0081	²¹⁴ 0.0106	¹⁹³ 0.0128	¹⁹² 0.0157	¹⁸⁸ 0.0195	⁶³ 0.0001 N ^{0.299} ²⁰⁴	¹⁶⁵ 0.0020	¹⁸² 0.0026	¹⁷² 0.0031	¹⁷³ 0.0037	¹⁶⁹ 0.0045	¹⁹ 0.0000 N ^{0.284} ¹⁹⁵		
3	ALCHERA-003	²⁰³ 0.0079	²¹¹ 0.0104	¹⁹¹ 0.0123	¹⁹¹ 0.0147	¹⁸⁶ 0.0180	⁹⁵ 0.0002 N ^{0.278} ¹⁸⁸	²⁰¹ 0.0027	¹⁹⁹ 0.0032	¹⁷⁸ 0.0035	¹⁷⁶ 0.0042	¹⁷⁰ 0.0048	⁵⁸ 0.0002 N ^{0.199} ¹⁷²		
4	ALLGOVISION-000	²²² 0.0101	²²⁰ 0.0114	¹⁹² 0.0127	¹⁹⁰ 0.0145	¹⁸⁷ 0.0166	¹⁹⁰ 0.0010 N ^{0.171} ¹¹²	²⁴⁰ 0.0063	²³⁶ 0.0067	²⁰⁰ 0.0071	¹⁹⁵ 0.0075	¹⁸⁶ 0.0081	¹⁹⁸ 0.0020 N ^{0.086} ¹²⁹		
5	ALLGOVISION-001	¹⁹⁵ 0.0069	²⁰¹ 0.0094	¹⁸⁶ 0.0107	¹⁸⁵ 0.0128	¹⁸² 0.0157	⁸⁰ 0.0002 N ^{0.277} ¹⁸⁶	¹⁸⁷ 0.0023	¹⁸⁸ 0.0027	¹⁷³ 0.0031	¹⁶⁶ 0.0036	¹⁶⁴ 0.0043	⁴¹ 0.0001 N ^{0.211} ¹⁷⁷		
6	ANKE-000	²²⁵ 0.0102	²²⁸ 0.0132	²⁰ 0.0155	¹⁹⁷ 0.0188	¹⁹¹ 0.0225	¹³⁴ 0.0003 N ^{0.270} ¹⁷⁶	²¹⁰ 0.0032	²¹² 0.0040	¹⁹¹ 0.0046	¹⁸⁸ 0.0056	¹⁷⁸ 0.0066	⁴⁰ 0.0001 N ^{0.247} ¹⁸⁴		
7	ANKE-002	¹²⁸ 0.0024	¹²⁶ 0.0026	¹²⁸ 0.0032	¹²⁵ 0.0037	¹²⁸ 0.0043	⁷³ 0.0002 N ^{0.203} ¹²⁹	¹³⁵ 0.0016	¹³⁵ 0.0017	¹²⁷ 0.0017	¹²⁸ 0.0018	¹¹⁵ 0.0019	¹¹⁰ 0.0006 N ^{0.076} ¹¹⁶		
8	AWARE-003	²⁵⁷ 0.0238	²⁵⁵ 0.0306	²¹⁶ 0.0361	²¹¹ 0.0431	²⁰⁸ 0.0506	¹⁸⁶ 0.0008 N ^{0.258} ¹⁷¹	²³⁴ 0.0055	²⁴² 0.0075	²¹⁰ 0.0092	²⁰⁹ 0.0113	²⁰⁵ 0.0143	³⁰ 0.0001 N ^{0.323} ²⁰⁵		
9	AWARE-005	²⁵⁸ 0.0245	²⁵⁶ 0.0311	²¹⁷ 0.0366	²¹² 0.0434	¹⁹⁹ 0.0312	²⁰⁹ 0.0056 N ^{0.118} ⁶⁴	²⁸⁸ 0.0062	²⁴⁸ 0.0082	²¹² 0.0101	²⁰⁹ 0.0128	¹⁸⁹ 0.0089	¹³⁶ 0.0007 N ^{0.169} ⁶⁷		
10	AYONIX-002	²⁹⁴ 0.2935	²⁹ 0.3414	²² 0.3736	²²⁰ 0.4101	²¹⁴ 0.4465	²¹⁴ 0.0440 N ^{0.143} ⁸⁴	²⁹³ 0.0950	²⁹⁵ 0.1274	²²⁷ 0.1524	²¹⁷ 0.1828	²¹³ 0.2150	²⁰⁰ 0.023 N ^{0.279} ¹⁹³		
11	CAMVI-004	²³³ 0.0124	²⁶⁶ 0.0468	²²¹ 0.0719	²¹⁹ 0.2363	²¹³ 0.2367	¹⁷⁰ 0.0004 N ^{0.155} ²¹⁵	²⁶⁵ 0.0117	²⁸⁰ 0.0464	²²³ 0.0715	²²⁰ 0.2361	²¹⁴ 0.2364	³ 0.0000 N ^{0.371} ²¹⁷		
12	CANON-001	¹⁷ 0.0011	¹⁶ 0.0011	¹⁶ 0.0012	¹⁸ 0.0013	¹⁵ 0.0014	¹¹² 0.0002 N ^{0.113} ⁵⁷	²² 0.0009	²² 0.0009	²² 0.0009	²² 0.0009	²² 0.0010	¹⁰⁹ 0.0006 N ^{0.026} ⁵⁹		
13	CANON-002	²¹ 0.0011	²⁰ 0.0012	²² 0.0013	²⁹ 0.0014	²⁸ 0.0016	⁷² 0.0002 N ^{0.142} ⁸³	²³ 0.0009	²⁰ 0.0009	²⁰ 0.0009	¹⁹ 0.0009	¹⁸ 0.0009	¹³⁷ 0.0007 N ^{0.015} ³¹		
14	CIB-000	⁸⁷ 0.0014	⁵³ 0.0015	⁵¹ 0.0017	⁵⁷ 0.0019	¹⁷⁰ 0.0131	⁴ 0.0000 N ^{0.335} ²¹⁴	⁶⁶ 0.0012	⁵⁹ 0.0012	⁵⁸ 0.0012	⁵⁶ 0.0012	⁵⁰ 0.0012	⁴ 0.0000 N ^{0.647} ²¹⁴		
15	CLEARVIEW1-000	¹⁴ 0.0010	¹⁵ 0.0011	¹⁷ 0.0012	²⁰ 0.0013	¹⁹ 0.0015	⁸⁸ 0.0002 N ^{0.129} ⁷⁹	²⁵ 0.0009	²¹ 0.0009	²¹ 0.0009	¹⁹ 0.0009	¹⁹ 0.0010	¹²⁶ 0.0007 N ^{0.109} ⁴⁷		
16	CLOUDWALK-HR-000	⁶¹ 0.0015	⁴⁹ 0.0015	⁴⁸ 0.0015	³⁸ 0.0016	³⁴ 0.0017	¹⁸⁸ 0.0007 N ^{0.054} ¹²	¹¹⁹ 0.0014	¹⁰⁵ 0.0014	⁹⁴ 0.0014	⁸⁸ 0.0014	⁷⁰ 0.0014	¹⁷⁸ 0.0012 N ^{0.102} ²²		
17	CLOUDWALK-MT-000	⁸⁹ 0.0018	⁷⁰ 0.0018	⁶¹ 0.0018	⁵³ 0.0019	⁴⁵ 0.0020	¹⁹² 0.0011 N ^{0.036} ⁷	¹⁵⁰ 0.0018	¹⁴⁴ 0.0018	¹³² 0.0018	¹¹⁵ 0.0018	¹⁰³ 0.0018	¹⁹⁴ 0.0017 N ^{0.002} ⁴		
18	CLOUDWALK-MT-001	⁸⁸ 0.0018	⁶⁹ 0.0018	⁵⁸ 0.0018	⁵⁰ 0.0018	⁴⁵ 0.0019	¹⁹⁴ 0.0012 N ^{0.229} ⁴	¹⁴⁹ 0.0017	¹⁴⁵ 0.0018	¹³⁰ 0.0018	¹¹⁸ 0.0018	¹⁰¹ 0.0018	¹⁹³ 0.0017 N ^{0.003} ⁷		
19	COGENT-000	²²³ 0.0101	²¹² 0.0105	¹⁸⁸ 0.0109	¹⁸¹ 0.0115	¹⁷³ 0.0125	²⁰⁶ 0.0038 N ^{0.071} ¹⁷²	¹⁷⁶ 0.0021	¹⁶⁷ 0.0028	¹⁷¹ 0.0032	¹⁶⁹ 0.0036	¹⁶² 0.0036	⁸ 0.0000 N ^{0.466} ²¹⁰		
20	COGENT-001	²²⁴ 0.0101	²¹¹ 0.0105	¹⁸⁷ 0.0109	¹⁸¹ 0.0115	¹⁷⁴ 0.0125	²⁰⁷ 0.0038 N ^{0.071} ²³	¹⁷⁵ 0.0021	¹⁷⁶ 0.0024	¹⁶⁸ 0.0028	¹⁷⁰ 0.0036	¹⁶³ 0.0039	⁷ 0.0000 N ^{0.466} ²¹¹		
21	COGENT-002	¹⁴¹ 0.0029	¹⁴⁴ 0.0036	¹⁴¹ 0.0041	¹⁴⁰ 0.0049	¹³⁶ 0.0059	⁴³ 0.0001 N ^{0.244} ¹⁶³	¹¹⁶ 0.0014	¹²⁶ 0.0015	¹²¹ 0.0017	¹²⁷ 0.0019	¹²⁸ 0.0021	⁵³ 0.0002 N ^{0.144} ¹⁶¹		
22	COGENT-003	¹⁴⁷ 0.0031	¹⁴⁶ 0.0038	¹⁴⁶ 0.0043	¹⁴³ 0.0051	¹⁴⁰ 0.0060	⁵⁹ 0.0001 N ^{0.230} ¹⁵²	¹²⁸ 0.0015	¹³⁷ 0.0017	¹³⁸ 0.0018	¹³⁸ 0.0020	¹³⁶ 0.0022	⁵⁶ 0.0002 N ^{0.143} ¹⁶⁰		
23	COGENT-004	⁹⁰ 0.0018	⁹¹ 0.0020	⁸⁸ 0.0022	⁸⁹ 0.0025	⁸¹ 0.0028	¹⁰³ 0.0002 N ^{0.159} ¹⁰¹	¹⁰⁷ 0.0013	¹⁰³ 0.0014	⁹⁶ 0.0014	⁹² 0.0015	⁸² 0.0015	¹¹⁸ 0.0007 N ^{0.050} ⁹⁵		
24	COGENT-005	⁶⁸ 0.0016	⁶⁹ 0.0017	⁶² 0.0018	⁶⁰ 0.0020	⁵⁴ 0.0021	¹⁵⁶ 0.0004 N ^{0.108} ⁵²	¹¹⁰ 0.0013	⁹⁷ 0.0013	⁸⁷ 0.0014	⁸⁰ 0.0014	⁶⁹ 0.0014	¹⁷⁴ 0.0011 N ^{0.017} ³⁷		
25	COGENT-006	³³ 0.0012	³¹ 0.0012	²⁹ 0.0013	²⁶ 0.0014	²³ 0.0015	¹⁵¹ 0.0004 N ^{0.088} ³⁷	⁴⁹ 0.0011	⁴⁸ 0.0011	⁴³ 0.0011	³⁶ 0.0011	³³ 0.0011	¹⁵² 0.0008 N ^{0.109} ⁴⁴		
26	COGNITEC-000	²⁵¹ 0.0195	²⁵⁰ 0.0252	²¹³ 0.0297	²⁰³ 0.0352	¹⁸⁷ 0.0417	¹⁷⁸ 0.0006 N ^{0.259} ¹⁷²	²³⁰ 0.0050	²³⁴ 0.0065	²⁰⁷ 0.0077	²⁰⁸ 0.0097	²⁰⁰ 0.0122	³⁷ 0.0001 N ^{0.305} ¹⁹⁹		
27	COGNITEC-001	²¹⁸ 0.0090	²²² 0.0117	¹⁹⁸ 0.0139	¹⁹⁵ 0.0166	¹⁸⁹ 0.0199	¹²³ 0.0002 N ^{0.221} ¹⁷⁹	²⁰⁶ 0.0030	²⁰⁵ 0.0034	¹⁸⁶ 0.0040	¹⁸⁸ 0.0046	¹⁷⁴ 0.0054	³¹ 0.0002 N ^{0.207} ¹⁷⁶		
28	COGNITEC-002	¹⁷⁷ 0.0048	¹⁷⁵ 0.0057	¹⁶⁶ 0.0067	¹⁶¹ 0.0079	¹⁶⁰ 0.0094	¹⁰⁵ 0.0002 N ^{0.232} ¹⁵⁴	¹⁸⁹ 0.0024	¹⁸⁵ 0.0026	¹⁷⁰ 0.0028	¹⁷⁵ 0.0032	¹⁶³ 0.0034	⁹⁰ 0.0005 N ^{0.117} ¹⁴⁷		
29	COGNITEC-003	¹⁸⁰ 0.0053	¹⁷⁸ 0.0062	¹⁶⁷ 0.0072	¹⁶⁷ 0.0085	¹⁶⁷ 0.0100	¹³⁰ 0.0003 N ^{0.222} ¹⁴³	²⁰³ 0.0028	¹⁹⁷ 0.0030	¹⁸⁶ 0.0035	¹⁸⁷ 0.0037	¹⁸⁶ 0.0039	¹⁴⁸ 0.0008 N ^{0.097} ¹³⁷		
30	COGNITEC-004	¹³⁶ 0.0027	¹³⁶ 0.0032	¹³⁶ 0.0037	¹³⁶ 0.0045	¹³³ 0.0056	⁶³ 0.0001 N ^{0.253} ¹⁶⁹	¹⁰⁶ 0.0013	¹⁰⁷ 0.0014	¹⁰⁸ 0.0015	¹⁰⁹ 0.0017	¹⁰⁹ 0.0019	⁶² 0.0002 N ^{0.123} ¹⁵²		
31	COGNITEC-005	⁸⁸ 0.0014	⁶⁹ 0.0016	⁶⁷ 0.0018	⁶⁵ 0.0021	⁶⁵ 0.0024	⁶⁴ 0.0001 N ^{0.169} ¹⁰⁹	⁵⁵ 0.0011	⁵⁶ 0.0011	⁵⁶ 0.0011	⁵⁶ 0.0011	⁵⁶ 0.0011	¹¹⁶ 0.0007 N ^{0.037} ⁷³		
32	COGNITEC-006	⁵³ 0.0014	⁵⁶ 0.0016	⁵² 0.0017	⁵⁶ 0.0019	⁵⁶ 0.0022	⁸³ 0.0002 N ^{0.154} ⁹³	⁵⁶ 0.0011	⁵⁴ 0.0011	⁵³ 0.0011	⁵² 0.0011	⁵² 0.0011	¹¹⁷ 0.0007 N ^{0.035} ⁷²		
33	CYBERLINK-000	¹⁵³ 0.0034	¹⁴⁷ 0.0043	¹⁴² 0.0050	¹³⁹ 0.0060	¹⁴⁴ 0.0081	¹⁸ 0.0001 N ^{0.311} ²⁰⁴	⁸⁴ 0.0012	¹⁴⁰ 0.0017	¹³⁶ 0.0018	¹³¹ 0.0020	¹³¹ 0.0022	⁷⁰ 0.0004 N ^{0.104} ¹⁸⁶		
34	CYBERLINK-001	¹⁴⁴ 0.0030	¹⁴² 0.0035	¹⁴⁴ 0.0042	¹⁴² 0.0050	¹³⁹ 0.0060	⁴⁴ 0.0001 N ^{0.243} ¹⁶²	¹³⁸ 0.0016	¹⁴⁰ 0.0017	¹³⁶ 0.0018	¹³¹ 0.0020	¹³¹ 0.0022			

MISSES AT GIVEN RANK		ENROL MOST RECENT																							
#	FNIR(N, T= 0, R)	RANK 1					RANK 50																		
		N=0.64M	N=1.6M	N=3.0M	N=6.0M	N=12.0M	aN ^b	N=0.64M	N=1.6M	N=3.0M	N=6.0M	N=12.0M	aN ^b												
73	IDEMLA-006	201	0.0076	208	0.0096	190	0.0113	187	0.0135	184	0.0161	119	0.0002 N ^{0.259} 173	203	0.0028	209	0.0037	190	0.0046	187	0.0059	183	0.0076	15	0.0000 N ^{0.341} 207
74	IDEMLA-007	112	0.0021	121	0.0026	122	0.0030	123	0.0036	12	0.0044	25	0.0001 N ^{0.250} 167	54	0.0011	62	0.0012	60	0.0012	81	0.0015	63	0.0002 N ^{0.110} 144		
75	IDEMLA-008	8	0.0010	12	0.0011	12	0.0011	12	0.0013	12	0.0014	92	0.0002 N ^{0.121} 68	21	0.0009	18	0.0009	16	0.0009	18	0.0009	15	0.0007 N ^{0.116} 33		
76	IDEMLA-009	5	0.0009	5	0.0010	6	0.0010	3	0.0011	6	0.0012	125	0.0003 N ^{0.097} 44	14	0.0008	11	0.0009	10	0.0009	10	0.0009	7	0.0009	146	0.0008 N ^{0.007} 13
77	IMAGUS-005	87	0.0018	86	0.0019	87	0.0022	87	0.0025	29	0.0028	102	0.0002 N ^{0.158} 100	89	0.0013	95	0.0013	88	0.0014	87	0.0014	86	0.0016	94	0.0005 N ^{0.066} 115
78	IMAGUS-006	91	0.0018	93	0.0020	89	0.0022	89	0.0025	89	0.0026	100	0.0002 N ^{0.156} 94	114	0.0014	113	0.0014	105	0.0015	91	0.0016	129	0.0007 N ^{0.049} 94		
79	IMAGUS-007	84	0.0017	94	0.0020	92	0.0022	93	0.0026	87	0.0030	57	0.0002 N ^{0.189} 121	73	0.0012	74	0.0013	68	0.0013	68	0.0013	73	0.0015	95	0.0005 N ^{0.064} 113
80	IMPERIAL-000	121	0.0022	118	0.0024	112	0.0027	110	0.0030	106	0.0035	12	0.0003 N ^{0.157} 96	142	0.0016	136	0.0017	129	0.0017	117	0.0018	107	0.0018	165	0.0009 N ^{0.041} 81
81	INCODE-003	221	0.0098	227	0.0129	200	0.0154	198	0.0191	192	0.0233	91	0.0002 N ^{0.296} 198	198	0.0024	198	0.0031	188	0.0036	183	0.0046	176	0.0056	25	0.0001 N ^{0.285} 196
82	INCODE-004	142	0.0029	143	0.0035	143	0.0041	141	0.0049	138	0.0061	42	0.0001 N ^{0.244} 164	154	0.0018	150	0.0019	148	0.0020	145	0.0021	132	0.0022	168	0.0006 N ^{0.077} 123
83	INCODE-005	64	0.0015	61	0.0017	59	0.0018	60	0.0020	61	0.0023	114	0.0002 N ^{0.140} 81	80	0.0012	72	0.0013	73	0.0013	65	0.0014	128	0.0007 N ^{0.041} 78		
84	INNOVATRICS-007	70	0.0016	64	0.0017	66	0.0019	64	0.0021	66	0.0024	111	0.0002 N ^{0.143} 86	79	0.0012	70	0.0012	66	0.0013	64	0.0013	134	0.0007 N ^{0.037} 75		
85	INTEMA-000	23	0.0011	19	0.0011	19	0.0012	19	0.0013	28	0.0016	96	0.0002 N ^{0.124} 70	49	0.0010	42	0.0010	45	0.0011	40	0.0011	49	0.0013	75	0.0003 N ^{0.079} 124
86	INTSYSMSU-000	286	0.1395	286	0.1457	223	0.1498	216	0.1544	210	0.1591	216	0.0768 N ^{0.045} 9	293	0.1098	293	0.1163	226	0.1206	218	0.1252	212	0.1296	216	0.0519 N ^{0.056} 102
87	IREX-000	168	0.0043	157	0.0044	147	0.0044	136	0.0046	12	0.0048	203	0.0028 N ^{0.032} 6	223	0.0043	216	0.0043	189	0.0043	179	0.0043	164	0.0043	208	0.0042 N ^{0.002} 5
88	ISYSTEMS-002	182	0.0053	181	0.0064	170	0.0072	168	0.0083	161	0.0096	148	0.0003 N ^{0.204} 131	212	0.0033	206	0.0034	180	0.0036	174	0.0038	162	0.0041	183	0.0013 N ^{0.071} 118
89	ISYSTEMS-003	172	0.0046	169	0.0052	157	0.0057	150	0.0066	148	0.0076	160	0.0004 N ^{0.174} 114	209	0.0031	202	0.0033	176	0.0034	160	0.0037	184	0.0013 N ^{0.063} 112		
90	KAKAOU-000	89	0.0013	88	0.0015	89	0.0016	85	0.0019	88	0.0022	37	0.0001 N ^{0.192} 125	29	0.0009	29	0.0010	28	0.0010	31	0.0011	30	0.0011	86	0.0005 N ^{0.050} 96
91	KAKAO-001	48	0.0014	39	0.0014	39	0.0015	35	0.0016	35	0.0016	175	0.0000 N ^{0.060} 16	95	0.0013	84	0.0013	77	0.0013	69	0.0013	84	0.0013	176	0.0011 N ^{0.012} 21
92	KEDACOM-001	200	0.0076	191	0.0077	174	0.0079	164	0.0083	154	0.0087	208	0.0040 N ^{0.047} 10	245	0.0071	238	0.0072	204	0.0072	193	0.0073	180	0.0073	211	0.0063 N ^{0.009} 17
93	KNERON-000	176	0.0048	176	0.0059	167	0.0067	165	0.0079	159	0.0093	118	0.0002 N ^{0.226} 148	227	0.0048	229	0.0059	199	0.0067	198	0.0079	191	0.0093	61	0.0002 N ^{0.226} 180
94	LOOKMAN-003	211	0.0083	200	0.0088	182	0.0091	178	0.0096	165	0.0104	204	0.0030 N ^{0.166} 26	249	0.0072	241	0.0074	240	0.0075	196	0.0076	184	0.0077	209	0.0054 N ^{0.022} 50
95	LOOKMAN-005	202	0.0078	194	0.0080	177	0.0083	168	0.0086	159	0.0092	205	0.0038 N ^{0.053} 11	247	0.0072	205	0.0073	194	0.0073	181	0.0074	210	0.0060 N ^{0.013} 28		
96	MANTRA-000	65	0.0015	67	0.0017	69	0.0019	70	0.0022	70	0.0025	67	0.0002 N ^{0.171} 111	71	0.0012	63	0.0012	61	0.0012	60	0.0013	55	0.0013	114	0.0007 N ^{0.042} 82
97	MAXVISION-000	110	0.0021	116	0.0024	110	0.0027	115	0.0032	114	0.0038	54	0.0001 N ^{0.206} 134	96	0.0013	100	0.0014	97	0.0014	102	0.0015	100	0.0017	69	0.0003 N ^{0.100} 139
98	MEGVII-001	228	0.0105	223	0.0118	194	0.0128	189	0.0142	183	0.0161	198	0.0015 N ^{0.143} 85	251	0.0077	247	0.0080	208	0.0082	203	0.0086	190	0.0089	205	0.0040 N ^{0.048} 93
99	MICROFOCUS-005	297	0.3700	297	0.4242	226	0.4610	221	0.5000	211	0.5391	215	0.0674 N ^{0.128} 74	291	0.1300	298	0.1724	228	0.2046	221	0.2425	215	0.2810	204	0.0040 N ^{0.263} 190
100	MICROSOFT-003	36	0.0013	38	0.0016	64	0.0018	74	0.0022	80	0.0028	14	0.0000 N ^{0.227} 180	3	0.0006	3	0.0006	3	0.0007	7	0.0008	10	0.0009	28	0.0001 N ^{0.158} 166
101	MICROSOFT-004	34	0.0012	30	0.0015	31	0.0018	69	0.0021	28	0.0028	15	0.0000 N ^{0.281} 189	1	0.0006	1	0.0007	1	0.0007	6	0.0009	38	0.0001 N ^{0.139} 158		
102	MICROSOFT-005	63	0.0015	82	0.0019	96	0.0023	109	0.0030	109	0.0037	9	0.0000 N ^{0.320} 206	3	0.0006	3	0.0006	2	0.0007	2	0.0008	8	0.0009	39	0.0001 N ^{0.136} 157
103	MICROSOFT-006	67	0.0016	90	0.0020	100	0.0025	110	0.0030	110	0.0038	12	0.0000 N ^{0.305} 202	1	0.0006	4	0.0006	4	0.0007	4	0.0009	26	0.0010	24	0.0000 N ^{0.184} 169
104	NEC-000	236	0.0131	236	0.0170	204	0.0203	199	0.0244	194	0.0294	148	0.0003 N ^{0.226} 185	209	0.0029	211	0.0038	192	0.0048	188	0.0059	182	0.0074	16	0.0000 N ^{0.319} 203
105	NEC-001	248	0.0180	245	0.0209	206	0.0236	198	0.0304	206	0.0316	116	0.0001 N ^{0.179} 116	261	0.0109	256	0.0113	215	0.0116	201	0.0121	202	0.0122	208	0.0051 N ^{0.056} 100
106	NEC-002	66	0.0009	111	0.0010	110	0.0011	111	0.0012	110	0.0016	101	0.0002 N ^{0.113} 39	3	0.0008	3	0.0008	5	0.0008	5	0.0008	85	0.0005 N ^{0.138} 76		
107	NEC-003	42	0.0013	38	0.0014	36	0.0015	31	0.0016	31	0.0016	162	0.0005 N ^{0.079} 28	67	0.0012	61	0.0012	56	0.0012	53	0.0012	47	0.0012	161	0.0009 N ^{0.019} 46
108	NEC-004	51	0.0014	45	0.0014	39	0.0015	39	0.0016	32	0.0017	177	0.0005 N ^{0.099} 15	93	0.0013	80	0.0013	76	0.0013	74	0.0013	172	0.0010 N ^{0.016} 34		
109	NEC-005	31	0.0011	27	0.0012	23	0.0012	15	0.0013	14	0.0014	164	0.0005 N ^{0.066} 18	51	0.0011	47	0.0011	41	0.0011	37	0.0011	32	0.0011	160	0.0009 N ^{0.013} 27
110	NEC-006	35	0.0012	32	0.0013	31	0.0015	30	0.0016	104	0.0002 N ^{0.125} 72	42	0.0010	37	0.0010	30	0.0010	28	0.0010	27	0.0011	154	0.0008 N ^{0.014} 29		
111	NEUROTECHNOLOGY-003	247	0.0179	246	0.0225	206	0.0306	207	0.0361	185	0.0007 N ^{0.239} 160	224	0.0042	228	0.0057	203	0								

MISSES AT GIVEN RANK FNIR(N, T = 0, R)		ENROL MOST RECENT							RANK 50																
#	ALGORITHM	RANK 1					aN ^b	N=0.64M	N=1.6M	N=3.0M	N=6.0M	N=12.0M	aN ^b												
145	RANKONE-005	199	0.0075	206	0.0094	189	0.0110	188	0.0132	181	0.0156	127	0.0003 N ^{0.251} 168	199	0.0026	200	0.0032	184	0.0036	178	0.0043	171	0.0050	42	0.0001 N ^{0.221} 178
146	RANKONE-007	149	0.0028	139	0.0034	137	0.0038	138	0.0045	132	0.0053	79	0.0002 N ^{0.211} 138	138	0.0015	134	0.0017	130	0.0019	129	0.0021	67	0.0003 N ^{0.123} 151		
147	RANKONE-009	104	0.0020	112	0.0024	113	0.0027	118	0.0032	112	0.0038	41	0.0001 N ^{0.219} 141	111	0.0013	106	0.0014	103	0.0015	98	0.0016	104	0.0005 N ^{0.059} 106		
148	RANKONE-010	108	0.0020	106	0.0022	108	0.0025	108	0.0029	99	0.0032	108	0.0002 N ^{0.164} 108	122	0.0014	114	0.0015	109	0.0015	103	0.0016	97	0.0017	111	0.0006 N ^{0.058} 104
149	RANKONE-011	47	0.0014	51	0.0015	50	0.0017	51	0.0018	53	0.0021	87	0.0002 N ^{0.130} 91	63	0.0011	52	0.0012	54	0.0012	49	0.0012	44	0.0012	157	0.0008 N ^{0.023} 53
150	RANKONE-012	38	0.0013	37	0.0014	34	0.0015	41	0.0017	40	0.0020	89	0.0002 N ^{0.144} 87	51	0.0011	53	0.0011	48	0.0011	42	0.0011	36	0.0012	159	0.0009 N ^{0.016} 32
151	RANKONE-013	10	0.0010	13	0.0011	13	0.0012	16	0.0013	20	0.0015	58	0.0001 N ^{0.144} 88	16	0.0009	15	0.0009	14	0.0009	13	0.0009	11	0.0009	120	0.0007 N ^{0.17} 36
152	REALNETWORKS-002	263	0.0299	259	0.0393	239	0.0470	218	0.0562	209	0.0580	196	0.0013 N ^{0.226} 157	238	0.0054	243	0.0076	211	0.0097	208	0.0126	203	0.0132	23	0.0001 N ^{0.320} 204
153	REALNETWORKS-003	249	0.0183	249	0.0242	212	0.0291	208	0.0352	205	0.0423	158	0.0004 N ^{0.287} 193	222	0.0041	224	0.0054	198	0.0064	199	0.0080	195	0.0101	27	0.0001 N ^{0.307} 200
154	REALNETWORKS-004	246	0.0175	247	0.0236	211	0.0284	209	0.0347	204	0.0416	144	0.0003 N ^{0.295} 196	217	0.0040	221	0.0050	196	0.0061	197	0.0078	194	0.0099	20	0.0001 N ^{0.315} 201
155	REALNETWORKS-005	105	0.0020	108	0.0023	111	0.0026	108	0.0030	107	0.0037	49	0.0001 N ^{0.207} 135	69	0.0012	66	0.0012	75	0.0013	81	0.0014	74	0.0015	78	0.0004 N ^{0.081} 126
156	REALNETWORKS-006	40	0.0013	42	0.0014	46	0.0016	47	0.0018	48	0.0021	60	0.0001 N ^{0.163} 105	36	0.0010	32	0.0010	37	0.0010	38	0.0011	37	0.0012	81	0.0004 N ^{0.060} 108
157	REALNETWORKS-007	37	0.0013	35	0.0013	35	0.0014	39	0.0016	38	0.0018	117	0.0002 N ^{0.124} 69	39	0.0010	30	0.0010	32	0.0010	34	0.0011	34	0.0011	85	0.0004 N ^{0.057} 103
158	REALNETWORKS-008	18	0.0011	21	0.0011	24	0.0013	22	0.0014	25	0.0016	88	0.0002 N ^{0.131} 76	15	0.0009	14	0.0009	19	0.0009	19	0.0009	17	0.0009	97	0.0005 N ^{0.137} 74
159	REMARKAI-000	137	0.0027	141	0.0034	144	0.0040	139	0.0048	135	0.0058	36	0.0001 N ^{0.260} 174	125	0.0014	127	0.0015	120	0.0016	118	0.0018	116	0.0020	70	0.0003 N ^{0.108} 140
160	RENDIP-000	55	0.0014	55	0.0015	55	0.0017	58	0.0019	57	0.0022	78	0.0002 N ^{0.158} 98	61	0.0012	64	0.0012	59	0.0012	54	0.0012	48	0.0013	156	0.0008 N ^{0.25} 53
161	REVEALMEDIA-000	77	0.0017	80	0.0019	72	0.0022	79	0.0023	69	0.0025	132	0.0003 N ^{0.134} 77	77	0.0012	69	0.0012	63	0.0012	59	0.0013	53	0.0013	143	0.0007 N ^{0.35} 70
162	S1-000	111	0.0021	114	0.0024	118	0.0028	117	0.0032	111	0.0037	56	0.0001 N ^{0.203} 130	127	0.0014	121	0.0015	113	0.0015	107	0.0016	99	0.0017	119	0.0007 N ^{0.55} 99
163	S1-001	148	0.0031	134	0.0034	121	0.0036	117	0.0040	107	0.0049	187	0.0009 N ^{0.092} 41	180	0.0023	174	0.0023	160	0.0024	153	0.0024	141	0.0025	192	0.0017 N ^{0.223} 54
164	S1-002	49	0.0014	44	0.0014	40	0.0015	41	0.0016	37	0.0018	159	0.0004 N ^{0.085} 33	101	0.0013	91	0.0013	81	0.0013	66	0.0013	60	0.0013	177	0.0011 N ^{0.11} 20
165	SCANOVATE-000	163	0.0038	166	0.0050	165	0.0059	159	0.0073	144	0.0073	81	0.0002 N ^{0.235} 156	128	0.0014	125	0.0015	122	0.0020	122	0.0020	85	0.0002 N ^{0.142} 159		
166	SCANOVATE-001	166	0.0041	170	0.0064	164	0.0079	162	0.0098	160	0.0109	121	0.0001 N ^{0.299} 199	111	0.0013	124	0.0015	125	0.0017	143	0.0021	140	0.0024	36	0.0001 N ^{0.209} 175
167	SENSETIME-000	117	0.0022	110	0.0023	109	0.0026	108	0.0028	93	0.0032	149	0.0003 N ^{0.135} 78	147	0.0016	141	0.0017	135	0.0018	124	0.0018	118	0.0020	139	0.0007 N ^{0.060} 107
168	SENSETIME-001	116	0.0022	111	0.0023	106	0.0025	108	0.0029	108	0.0037	99	0.0002 N ^{0.177} 115	146	0.0016	130	0.0016	124	0.0017	121	0.0018	138	0.0024	66	0.0003 N ^{0.125} 153
169	SENSETIME-002	239	0.0136	230	0.0137	197	0.0137	188	0.0138	177	0.0139	212	0.0124 N ^{0.007} 2	269	0.0136	262	0.0136	215	0.0136	210	0.0136	204	0.0136	213	0.0135 N ^{0.001} 3
170	SENSETIME-003	9	0.0010	7	0.0010	7	0.0010	7	0.0011	7	0.0012	138	0.0003 N ^{0.085} 35	25	0.0009	25	0.0009	24	0.0010	20	0.0010	147	0.0008 N ^{0.135} 25		
171	SENSETIME-004	7	0.0010	6	0.0010	5	0.0010	6	0.0011	5	0.0012	140	0.0003 N ^{0.081} 30	12	0.0008	10	0.0009	11	0.0009	9	0.0009	113	0.0007 N ^{0.18} 43		
172	SENSETIME-005	4	0.0008	4	0.0009	4	0.0009	4	0.0010	4	0.0011	128	0.0003 N ^{0.085} 34	8	0.0008	6	0.0008	7	0.0008	5	0.0008	159	0.0008 N ^{0.002} 6		
173	SENSETIME-006	3	0.0008	2	0.0009	3	0.0009	2	0.0010	3	0.0010	142	0.0003 N ^{0.089} 20	8	0.0008	8	0.0008	8	0.0008	8	0.0008	127	0.0007 N ^{0.111} 19		
174	SENSETIME-007	2	0.0008	2	0.0008	1	0.0009	1	0.0009	1	0.0010	150	0.0004 N ^{0.061} 17	18	0.0008	9	0.0008	8	0.0008	8	0.0008	138	0.0007 N ^{0.08} 14		
175	SENSETIME-008	1	0.0008	1	0.0008	2	0.0009	2	0.0009	1	0.0010	143	0.0003 N ^{0.067} 19	7	0.0008	7	0.0008	6	0.0008	5	0.0008	115	0.0007 N ^{0.113} 24		
176	SHAMAN-007	267	0.0371	260	0.0396	218	0.0416	204	0.0443	211	0.0473	211	0.0122 N ^{0.083} 31	281	0.0308	276	0.0314	221	0.0319	214	0.0326	208	0.0337	214	0.0207 N ^{0.229} 66
177	SIAT-001	75	0.0017	73	0.0018	77	0.0020	70	0.0023	76	0.0027	71	0.0002 N ^{0.173} 113	47	0.0010	51	0.0011	52	0.0012	58	0.0013	57	0.0013	71	0.0003 N ^{0.085} 128
178	SIAT-002	74	0.0016	76	0.0018	78	0.0020	79	0.0023	73	0.0027	72	0.0002 N ^{0.171} 110	62	0.0011	67	0.0012	67	0.0013	67	0.0014	92	0.0005 N ^{0.162} 110		
179	SQISOFT-001	139	0.0028	154	0.0042	162	0.0059	168	0.0084	216	0.0207	202	0.0000 N ^{0.167} 216	39	0.0010	43	0.0010	44	0.0011	52	0.0012	216	0.9198	2	0.0000 N ^{0.883} 216
180	SYNESIS-003	287	0.0456	289	0.1700	234	0.1876	217	0.2088	212	0.2317	213	0.0177 N ^{0.188} 99	289	0.0828	289	0.0869	224	0.0920	217	0.0998	210	0.1104	215	0.218 N ^{0.098} 138
181	SYNESIS-003	245	0.0161	242	0.0162	202	0.0163	196	0.0165	193	0.0254	202	0.0002 N ^{0.127} 73	277	0.0160	267	0.0160	212	0.0160	207	0.0245	167	0.0009 N ^{0.192} 170		
182	SYNESIS-005	213	0.0085	198	0.0085	189	0.0086	156	0.0088	210	0.0088	210	0.0072 N ^{0.102} 3	255	0.0085	209	0.0085	188	0.0085	212	0.0085 N ^{0.000} 2				
183	TECH5-001	149	0.0042	151	0.0047	148	0.0057	140	0.0071	140	0.0071	31	0.0001 N ^{0.271} 178	136	0.0016	131	0.0017	130	0.0018	135	0.0020	88	0.0003 N ^{0.119} 148		
184	TECH5-002	106	0.0020	124	0.0027	130	0.0031	129	0.0040	124	0.0047	51	0.0000 N ^{0.224} 146	67	0.0012	59	0.0013								

MISSES AT GIVEN RANK		ENROL MOST RECENT											
FNIR(N, T= 0, R)		RANK 1					RANK 50						
#	ALGORITHM	N=0.64M	N=1.6M	N=3.0M	N=6.0M	N=12.0M	aN^b	N=0.64M	N=1.6M	N=3.0M	N=6.0M	N=12.0M	aN^b
217	YITU-005	¹²⁰ 0.0022	¹⁰⁹ 0.0023	¹⁰⁴ 0.0025	⁹⁵ 0.0027	⁹⁰ 0.0031	¹⁶⁸ 0.0005 N ^{-0.113} ⁵⁸	¹⁶³ 0.0020	¹⁵⁸ 0.0020	¹⁵⁰ 0.0020	¹³⁹ 0.0020	¹²³ 0.0020	¹⁹¹ 0.0017 N ^{-0.012} ²³

Table 24: Investigation-mode: Effect of N on FNIR on recent images For five enrollment population sizes, N , with $T = 0$ and $FPIR = 1$. The left five columns are rank 1 miss rates The right five columns are rank 50 miss rates Missing entries usually apply because another algorithm from the same developer was run instead. Some developers are missing because less accurate algorithms were not run on galleries with $N > 1\,600\,000$. Throughout blue superscripts indicate the rank of the algorithm for that column, and yellow highlighting indicates the most accurate value. Caution: The Power-low models are mostly intended to draw attention to the kind of behavior, not as a model to be used for prediction.

MISSES OUTSIDE RANK R		RESOURCE USAGE		ENROL MOST RECENT, N = 1.6M					
#	ALGORITHM	BYTES	MSEC	R=1	R=5	R=10	R=20	R=50	WORK=10
1	20FACE-000	18 ²⁰⁴⁸	73 ²⁴⁷	26 ^{0.0552}	26 ^{0.0269}	26 ^{0.0198}	26 ^{0.0146}	25 ^{0.0099}	26 ^{1.275}
2	3DIVI-003	67 ⁵¹²	174 ⁶²⁵	28 ^{0.0833}	27 ^{0.0444}	27 ^{0.0349}	26 ^{0.0270}	26 ^{0.0191}	27 ^{1.447}
3	3DIVI-004	281 ⁴⁰⁹⁶	175 ⁶²⁸	23 ^{0.0175}	29 ^{0.0091}	22 ^{0.0075}	22 ^{0.0061}	21 ^{0.0049}	23 ^{1.092}
4	3DIVI-005	278 ⁴⁰⁹⁶	184 ⁶⁵³	23 ^{0.0176}	23 ^{0.0091}	22 ^{0.0074}	22 ^{0.0061}	22 ^{0.0049}	23 ^{1.092}
5	3DIVI-006	87 ⁵²⁸	183 ⁶⁵³	24 ^{0.0240}	24 ^{0.0171}	25 ^{0.0160}	26 ^{0.0154}	26 ^{0.0148}	25 ^{1.162}
6	ACER-000	79 ⁵¹²	63 ²⁰¹	21 ^{0.0106}	19 ^{0.0051}	19 ^{0.0041}	19 ^{0.0034}	18 ^{0.0026}	19 ^{1.053}
7	ACER-001	163 ²⁰⁴⁸	54 ¹⁸⁴	16 ^{0.0051}	17 ^{0.0032}	16 ^{0.0028}	16 ^{0.0025}	16 ^{0.0022}	16 ^{1.031}
8	AIZE-001	196 ²⁰⁴⁸	113 ⁴⁰³	17 ^{0.0056}	17 ^{0.0037}	17 ^{0.0033}	18 ^{0.0030}	18 ^{0.0027}	17 ^{1.035}
9	ALCHERA-000	151 ²⁰⁴⁸	77 ²⁶³	23 ^{0.0161}	24 ^{0.0124}	24 ^{0.0117}	25 ^{0.0111}	25 ^{0.0105}	24 ^{1.116}
10	ALCHERA-001	219 ²⁰⁴⁸	39 ⁶⁶	30 ^{0.9869}	30 ^{0.9782}	30 ^{0.9735}	30 ^{0.9679}	30 ^{0.9590}	30 ^{9.811}
11	ALCHERA-002	201 ²⁰⁴⁸	47 ¹¹⁵	28 ^{0.0949}	28 ^{0.0555}	27 ^{0.0443}	27 ^{0.0354}	27 ^{0.0254}	27 ^{1.544}
12	ALCHERA-003	161 ²⁰⁴⁸	54 ¹⁸⁸	21 ^{0.0104}	20 ^{0.0054}	20 ^{0.0045}	20 ^{0.0038}	19 ^{0.0032}	20 ^{1.055}
13	ALCHERA-004	159 ²⁰⁴⁸	266 ⁸⁵⁴	27 ^{0.0110}	19 ^{0.0049}	18 ^{0.0038}	18 ^{0.0032}	18 ^{0.0025}	19 ^{1.051}
14	ALLGOVISION-000	211 ²⁰⁴⁸	123 ⁴²⁵	22 ^{0.0114}	22 ^{0.0084}	23 ^{0.0078}	23 ^{0.0073}	23 ^{0.0067}	23 ^{1.079}
15	ALLGOVISION-001	181 ²⁰⁴⁸	245 ⁷⁹²	20 ^{0.0090}	19 ^{0.0048}	19 ^{0.0040}	19 ^{0.0033}	18 ^{0.0027}	19 ^{1.048}
16	ANKE-000	259 ²⁰⁷²	125 ⁴³¹	22 ^{0.0132}	21 ^{0.0073}	21 ^{0.0060}	21 ^{0.0050}	21 ^{0.0040}	22 ^{1.072}
17	ANKE-001	260 ²⁰⁷²	126 ⁴³³	22 ^{0.0132}	21 ^{0.0073}	21 ^{0.0061}	21 ^{0.0050}	21 ^{0.0040}	22 ^{1.073}
18	ANKE-002	2056 ²⁰⁵⁶	178 ⁶⁴¹	12 ^{0.0028}	12 ^{0.0020}	12 ^{0.0018}	13 ^{0.0018}	13 ^{0.0017}	13 ^{1.019}
19	AWARE-003	261 ²⁰⁷⁶	219 ⁷¹⁶	25 ^{0.0306}	25 ^{0.0162}	24 ^{0.0127}	24 ^{0.0100}	24 ^{0.0075}	25 ^{1.163}
20	AWARE-004	35 ⁹²	216 ⁷¹²	22 ^{0.0679}	20 ^{0.0348}	26 ^{0.0274}	26 ^{0.0208}	26 ^{0.0145}	27 ^{0.134}
21	AWARE-005	271 ³¹⁰⁰	253 ⁸²⁷	25 ^{0.0311}	25 ^{0.0167}	24 ^{0.0134}	24 ^{0.0107}	24 ^{0.0082}	25 ^{1.167}
22	AWARE-006	36 ¹²⁴	249 ⁸¹⁸	27 ^{0.0697}	22 ^{0.0369}	26 ^{0.0288}	26 ^{0.0223}	26 ^{0.0158}	27 ^{1.371}
23	AYONIX-000	117 ¹⁰³⁶	34 ¹⁰	29 ^{0.4505}	30 ^{0.3540}	30 ^{0.3176}	30 ^{0.2834}	30 ^{0.2381}	30 ^{4.288}
24	AYONIX-001	116 ¹⁰³⁶	36 ¹²	29 ^{0.3414}	29 ^{0.2338}	29 ^{0.1977}	29 ^{0.1652}	29 ^{0.1274}	29 ^{3.226}
25	AYONIX-002	118 ¹⁰³⁶	35 ¹¹	29 ^{0.3414}	29 ^{0.2338}	29 ^{0.1977}	29 ^{0.1652}	29 ^{0.1274}	29 ^{3.226}
26	CAMVI-003	100 ¹⁰²⁴	212 ⁷⁰⁷	26 ^{0.0520}	27 ^{0.0517}	27 ^{0.0517}	28 ^{0.0517}	28 ^{0.0517}	27 ^{1.466}
27	CAMVI-004	102 ¹⁰²⁴	221 ⁷¹⁸	26 ^{0.0468}	25 ^{0.0465}	27 ^{0.0465}	27 ^{0.0464}	28 ^{0.0464}	27 ^{1.419}
28	CAMVI-005	104 ¹⁰²⁴	236 ⁷⁶⁹	27 ^{0.0652}	29 ^{0.0648}	28 ^{0.0648}	28 ^{0.0648}	28 ^{0.0647}	29 ^{1.584}
29	CANON-001	284 ⁴⁰⁹⁶	282 ⁸⁹³	18 ^{0.0011}	25 ^{0.0010}	28 ^{0.0010}	22 ^{0.0009}	22 ^{0.0009}	21 ^{1.009}
30	CANON-002	18 ⁰	33 ⁶	25 ^{0.0012}	22 ^{0.0010}	19 ^{0.0009}	18 ^{0.0009}	20 ^{0.0009}	18 ^{1.009}
31	CIB-000	307 ⁸¹⁹⁶	191 ⁶⁷⁴	32 ^{0.0015}	37 ^{0.0013}	35 ^{0.0012}	35 ^{0.0012}	39 ^{0.0012}	38 ^{1.012}
32	CLEARVIEWAI-000	289 ⁴⁰⁹⁶	233 ⁷⁶⁵	15 ^{0.0011}	23 ^{0.0010}	23 ^{0.0010}	20 ^{0.0009}	21 ^{0.0009}	19 ^{1.009}
33	CLOUDWALK-HR-000	216 ²⁰⁴⁸	289 ⁹⁰⁸	49 ^{0.0015}	77 ^{0.0014}	87 ^{0.0014}	95 ^{0.0014}	105 ^{0.0014}	72 ^{1.013}
34	CLOUDWALK-MT-000	194 ²⁰⁴⁸	273 ⁸⁷⁰	20 ^{0.0018}	108 ^{0.0018}	120 ^{0.0018}	130 ^{0.0018}	144 ^{0.0018}	103 ^{1.016}
35	CLOUDWALK-MT-001	10 ⁰	26 ²	69 ^{0.0018}	109 ^{0.0018}	118 ^{0.0018}	129 ^{0.0018}	145 ^{0.0018}	102 ^{1.016}
36	COGENT-000	83 ⁵²⁵	159 ⁵⁵¹	21 ^{0.0105}	23 ^{0.0096}	23 ^{0.0095}	184 ^{0.0032}	177 ^{0.0024}	231 ^{1.088}
37	COGENT-001	84 ⁵²⁵	160 ⁵⁵²	213 ^{0.0105}	234 ^{0.0096}	240 ^{0.0095}	185 ^{0.0032}	176 ^{0.0024}	230 ^{1.088}
38	COGENT-002	117 ¹⁰⁴³	307 ⁹⁸⁷	14 ^{0.0036}	139 ^{0.0022}	136 ^{0.0020}	131 ^{0.0018}	126 ^{0.0015}	140 ^{1.021}
39	COGENT-003	120 ¹⁰⁴³	304 ⁹⁶⁰	146 ^{0.0038}	150 ^{0.0024}	146 ^{0.0021}	147 ^{0.0019}	137 ^{0.0017}	148 ^{1.023}
40	COGENT-004	241 ²⁰⁵³	301 ⁹⁵²	91 ^{0.0020}	91 ^{0.0016}	95 ^{0.0015}	101 ^{0.0015}	103 ^{0.0014}	89 ^{1.015}
41	COGENT-005	121 ¹⁰⁶²	239 ⁷⁷⁴	63 ^{0.0017}	75 ^{0.0014}	77 ^{0.0014}	87 ^{0.0014}	97 ^{0.0013}	75 ^{1.013}
42	COGENT-006	27 ⁰	2 ⁰	3 ^{0.0012}	37 ^{0.0011}	36 ^{0.0011}	42 ^{0.0011}	48 ^{0.0011}	36 ^{1.010}
43	COGNITEC-000	230 ²⁰⁵²	52 ¹⁷⁶	25 ^{0.0252}	248 ^{0.0136}	246 ^{0.0107}	244 ^{0.0085}	234 ^{0.0065}	249 ^{1.136}
44	COGNITEC-001	239 ²⁰⁵²	221 ²⁰²	22 ^{0.0117}	28 ^{0.0062}	20 ^{0.0051}	20 ^{0.0042}	20 ^{0.0034}	20 ^{1.062}
45	COGNITEC-002	231 ²⁰⁵²	69 ²²⁷	17 ^{0.0057}	173 ^{0.0037}	174 ^{0.0032}	175 ^{0.0029}	183 ^{0.0026}	171 ^{1.035}
46	COGNITEC-003	236 ²⁰⁵²	87 ²⁹⁷	179 ^{0.0062}	182 ^{0.0040}	183 ^{0.0036}	189 ^{0.0033}	197 ^{0.0030}	181 ^{1.039}
47	COGNITEC-004	231 ²⁰⁵²	60 ¹⁹²	17 ^{0.0032}	131 ^{0.0020}	117 ^{0.0018}	110 ^{0.0015}	107 ^{0.0014}	134 ^{1.020}
48	COGNITEC-005	223 ²⁰⁵²	101 ³⁶⁷	60 ^{0.0016}	52 ^{0.0013}	51 ^{0.0012}	51 ^{0.0012}	56 ^{0.0011}	52 ^{1.012}
49	COGNITEC-006	225 ²⁰⁵²	135 ⁴⁶³	56 ^{0.0016}	51 ^{0.0013}	48 ^{0.0012}	54 ^{0.0011}	49 ^{0.0011}	51 ^{1.012}
50	CUBOX-000	218 ²⁰⁴⁸	293 ⁹¹⁸	45 ^{0.0014}	66 ^{0.0014}	75 ^{0.0014}	88 ^{0.0014}	99 ^{0.0014}	83 ^{1.012}
51	CYBERLINK-000	225 ²⁰⁵²	207 ⁶⁹⁹	14 ^{0.0040}	160 ^{0.0028}	164 ^{0.0026}	166 ^{0.0024}	167 ^{0.0022}	159 ^{1.027}
52	CYBERLINK-001	228 ²⁰⁵²	127 ⁴³³	142 ^{0.0035}	145 ^{0.0023}	144 ^{0.0021}	137 ^{0.0018}	140 ^{0.0017}	143 ^{1.022}
53	CYBERLINK-002	30 ⁴¹⁴⁰	229 ⁷³⁸	122 ^{0.0026}	141 ^{0.0023}	150 ^{0.0022}	158 ^{0.0021}	162 ^{0.0021}	138 ^{1.021}
54	CYBERLINK-003	30 ⁶²¹²	205 ⁶⁹⁶	59 ^{0.0016}	56 ^{0.0013}	57 ^{0.0013}	58 ^{0.0012}	58 ^{0.0012}	60 ^{1.012}
55	CYBERLINK-004	30 ⁶²¹²	225 ⁷³⁸	62 ^{0.0017}	83 ^{0.0015}	91 ^{0.0015}	97 ^{0.0014}	109 ^{0.0014}	79 ^{1.014}
56	CYBERLINK-005	30 ⁶²¹²	230 ⁷³⁹	71 ^{0.0018}	92 ^{0.0016}	98 ^{0.0015}	107 ^{0.0015}	110 ^{0.0014}	86 ^{1.015}
57	DAHUA-000	158 ²⁰⁴⁸	107 ³⁷⁸	205 ^{0.0093}	211 ^{0.0066}	215 ^{0.0061}	221 ^{0.0057}	225 ^{0.0054}	209 ^{1.062}
58	DAHUA-001	184 ²⁰⁴⁸	103 ³⁷¹	18 ^{0.0067}	183 ^{0.0040}	180 ^{0.0036}	187 ^{0.0033}	191 ^{0.0029}	181 ^{1.040}
59	DAHUA-002	157 ²⁰⁴⁸	206 ⁶⁹⁹	77 ^{0.0018}	80 ^{0.0015}	87 ^{0.0014}	92 ^{0.0014}	96 ^{0.0013}	80 ^{1.014}
60	DAHUA-003	217 ²⁰⁴⁸	224 ⁷²⁵	28 ^{0.0012}	13 ^{0.0010}	15 ^{0.0009}	14 ^{0.0009}	13 ^{0.0009}	16 ^{1.009}
61	DAHUA-004	156 ²⁰⁴⁸	232 ⁷⁵⁹	14 ^{0.0011}	16 ^{0.0010}	16 ^{0.0009}	17 ^{0.0009}	19 ^{0.0009}	14 ^{1.009}
62	DAON-000	259 ²⁰⁶⁹	165 ⁵⁸⁴	15 ^{0.0041}	175 ^{0.0038}	186 ^{0.0037}	196 ^{0.0037}	208 ^{0.0036}	171 ^{1.034}
63	DECATUR-000	232 ²⁰⁵²	276 ⁸⁷⁴	97 ^{0.0021}	93 ^{0.0016}	99 ^{0.0015}	94 ^{0.0014}	88 ^{0.0013}	99 ^{1.015}
64	DEEPLIGHT-001	29 ⁴⁰⁹⁶	196 ⁶⁸⁷	47 ^{0.0014}	65 ^{0.0014}	67 ^{0.0013}	73 ^{0.0013}	81 ^{0.0013}	62 ^{1.012}
65	DEEPSEA-001	169 ²⁰⁴⁸	242 ⁷⁸⁰	156 ^{0.0043}	140 ^{0.0022}	124 ^{0.0018}	117 ^{0.0016}	101 ^{0.0014}	144 ^{1.022}
66	DERMALOG-003	37 ¹²⁸	67 ²¹¹	28 ^{0.1259}	28 ^{0.0744}	28 ^{0.0603}	28 ^{0.0480}	29 ^{0.0347}	28 ^{1.}

MISSES OUTSIDE RANK R		RESOURCE USAGE		ENROL MOST RECENT, N = 1.6M								
FNIR(N, T=0, R)		TEMPLATE		FRVT 2018 MUGSHOTS								
#	ALGORITHM	BYTES	MSEC	R=1	R=5	R=10	R=20	R=50	WORK-10			
73	DERMALOG-010	1 0	212	101	0.0022	135	0.0021	143	0.0020	139	1.019	
74	DIGIDATA-000	150	222	103	0.0022	109	0.0015	82	0.0014	71	6.303	
75	DILUSENSE-000	150	222	103	0.0022	27	0.0800	27	0.0362	27	1.448	
76	EYEDEA-003	115	1036	385	27	0.0451	27	0.0289	27	0.0211	27	1.096
77	F8-001	191	2048	267	851	225	0.0120	237	0.0105	246	0.0100	
78	FINCORE-000	185	2048	140	477	216	0.0108	199	0.0052	193	0.0034	
79	FUJITSULAB-000	111	1032	300	950	104	0.0022	98	0.0016	107	0.0015	
80	FUJITSULAB-001	100	10	31	1	87	0.0019	96	0.0015	102	0.0014	
81	GLORY-000	65	418	48	160	288	0.1781	290	0.1391	290	0.1154	
82	GLORY-001	144	1726	116	405	280	0.1268	285	0.0967	286	0.0778	
83	GORILLA-001	264	2156	50	169	270	0.0603	263	0.0304	264	0.0174	
84	GORILLA-002	125	1132	96	341	24	0.0197	231	0.0092	227	0.0054	
85	GORILLA-003	263	2156	163	563	257	0.0361	250	0.0146	248	0.0078	
86	GORILLA-004	265	2192	111	395	180	0.0063	169	0.0032	165	0.0023	
87	GORILLA-005	306	6288	143	483	136	0.0032	116	0.0019	111	0.0017	
88	GORILLA-006	308	8336	234	768	68	0.0017	50	0.0013	47	0.0012	
89	GORILLA-007	25	0	32	6	65	0.0017	46	0.0012	41	0.0011	
90	GRIAULE-000	225	2052	122	419	120	0.0025	125	0.0020	129	0.0019	
91	GRIAULE-001	15	0	24	2	28	0.0012	31	0.0011	35	0.0010	
92	HIK-003	132	1408	176	633	222	0.0117	206	0.0060	205	0.0039	
93	HIK-004	126	1152	148	510	219	0.0113	205	0.0059	198	0.0037	
94	HIK-005	133	1408	173	619	161	0.0046	152	0.0025	146	0.0020	
95	HIK-006	131	1408	169	610	160	0.0046	153	0.0025	138	0.0020	
96	HYPERVERGE-001	101	1024	264	846	40	0.0014	53	0.0013	69	0.0013	
97	HYPERVERGE-002	15	0	5	1	35	0.0014	54	0.0013	61	0.0013	
98	HZAILU-000	22	0	8	1	102	0.0022	96	0.0016	107	0.0015	
99	HZAILU-001	5	0	29	2	88	0.0020	104	0.0017	109	0.0016	
100	IDEMIA-003	86	528	198	689	186	0.0069	190	0.0045	194	0.0034	
101	IDEMIA-004	85	528	189	669	182	0.0066	179	0.0038	175	0.0032	
102	IDEMIA-005	65	352	105	374	195	0.0081	188	0.0044	184	0.0036	
103	IDEMIA-006	64	352	104	373	208	0.0096	198	0.0052	196	0.0042	
104	IDEMIA-007	96	860	247	807	12	0.0026	94	0.0016	84	0.0014	
105	IDEMIA-008	62	300	130	451	12	0.0011	12	0.0009	14	0.0009	
106	IDEMIA-009	2	0	5	0	5	0.0010	5	0.0009	10	0.0009	
107	IMAGUS-002	71	512	40	76	291	0.2023	289	0.1342	288	0.0871	
108	IMAGUS-003	69	512	38	57	296	0.3559	296	0.2491	296	0.1791	
109	IMAGUS-005	160	2048	244	788	280	0.0019	95	0.0016	92	0.0013	
110	IMAGUS-006	204	2048	287	905	93	0.0020	100	0.0016	103	0.0015	
111	IMAGUS-007	187	2048	167	590	94	0.0020	82	0.0015	86	0.0013	
112	IMAGUS-008	28	0	15	2	29	0.0860	280	0.0701	282	0.0646	
113	IMPERIAL-000	200	2048	185	654	118	0.0024	118	0.0018	125	0.0018	
114	INCODE-000	106	1024	57	190	267	0.0489	262	0.0261	263	0.0160	
115	INCODE-001	165	2048	206	690	225	0.0166	225	0.0084	218	0.0055	
116	INCODE-002	135	2048	84	291	239	0.0178	228	0.0090	222	0.0070	
117	INCODE-003	152	2048	207	704	227	0.0129	210	0.0064	208	0.0051	
118	INCODE-004	178	2048	147	508	143	0.0035	146	0.0024	148	0.0020	
119	INCODE-005	154	2048	146	500	61	0.0017	68	0.0014	75	0.0013	
120	INNOVATRICS-002	88	530	75	255	265	0.0451	268	0.0342	271	0.0308	
121	INNOVATRICS-003	89	530	74	255	251	0.0263	243	0.0126	238	0.0074	
122	INNOVATRICS-004	122	1076	117	406	220	0.0123	209	0.0063	206	0.0050	
123	INNOVATRICS-005	92	538	261	842	117	0.0024	112	0.0018	113	0.0017	
124	INNOVATRICS-007	95	538	243	785	64	0.0017	73	0.0014	69	0.0013	
125	INTELLIVISION-001	35	0	12	2	258	0.0365	260	0.0199	258	0.0160	
126	INTELLIVISION-002	20	0	18	2	215	0.0107	202	0.0055	197	0.0037	
127	INTEMA-000	24	0	4	0	19	0.0011	29	0.0011	34	0.0011	
128	INTSYSMSU-000	184	2048	192	675	286	0.1457	288	0.1320	291	0.1272	
129	IREX-000	272	3080	305	2379	157	0.0044	184	0.0043	209	0.0043	
130	ISYSTEMS-002	207	2048	92	316	181	0.0064	185	0.0043	191	0.0037	
131	ISYSTEMS-003	195	2048	267	856	169	0.0052	180	0.0039	194	0.0034	
132	KAKAO-000	227	2052	259	840	48	0.0015	36	0.0011	34	0.0011	
133	KAKAO-001	1	0	27	2	39	0.0014	59	0.0013	69	0.0013	
134	KEDACOM-001	60	292	154	537	191	0.0077	217	0.0074	223	0.0073	
135	KNERON-000	174	2048	151	530	176	0.0059	204	0.0059	222	0.0059	
136	KNERON-001	197	2048	139	468	254	0.0295	264	0.0295	271	0.0295	
137	LINE-000	166	2048	142	482	16	0.0022	89	0.0015	79	0.0014	
138	LINE-001	164	2048	292	910	18	0.0011	24	0.0010	26	0.0010	
139	LINECLOVA-002	19	0	19	2	305	0.8451	305	0.8450	305	0.8450	
140	LOOKMAN-003	61	292	92	342	200	0.0088	221	0.0078	229	0.0076	
141	LOOKMAN-004	95	548	93	325	202	0.0091	222	0.0079	234	0.0075	
142	LOOKMAN-005	93	548	150	514	194	0.0080	219	0.0075	232	0.0073	
143	MANTRA-000	238	2052	119	412	60	0.0017	62	0.0013	61	0.0012	
144	MAXVISION-000	4	0	30	2	116	0.0024	105	0.0017	105	0.0016	
											109	

Table 26: Rank-based accuracy for the FRVT 2018 mugshot sets. In columns 3 and 4 are template size and template generation duration. Thereafter values are rank-based FNIR with $T = 0$ and FPIR = 1. This is appropriate to investigational uses but not those with higher volumes where candidates from all searches would need review. The next column is a workload statistic, a small value shows an algorithm front-loads mates into the first 10 candidates. Throughout, blue superscripts indicate the rank of the algorithm for that column, and the best value is highlighted in yellow.

#	ALGORITHM	MISSES OUTSIDE RANK R FNIR(N, T=0, R)		RESOURCE USAGE TEMPLATE		ENROL MOST RECENT, N = 1.6M FRVT 2018 MUGSHOTS					
		BYTES	MSEC	R=1	R=5	R=10	R=20	R=50	WORK-10		
145	MEGVII-001	²⁸⁵ 4096	¹⁸¹ 652	²²³ 0.0118	²³² 0.0093	²³² 0.0087	²⁴² 0.0084	²⁴⁷ 0.0080	²²⁷ 1.086		
146	MEGVII-002	²⁸⁸ 4096	¹⁸⁶ 656	²²⁴ 0.0118	²³¹ 0.0093	²³⁴ 0.0088	²⁴¹ 0.0084	²⁴⁶ 0.0080	²²⁸ 1.087		
147	MICROFOCUS-003	⁵⁰ 256	⁸⁰ 269	³⁰⁴ 0.5942	³⁰² 0.4692	³⁰⁷ 0.4204	³⁰² 0.3724	³⁰⁵ 0.3095	³⁰² 5.361		
148	MICROFOCUS-004	⁵⁴ 256	⁸¹ 270	³⁰¹ 0.5763	³⁰¹ 0.4519	³⁰¹ 0.4026	³⁰¹ 0.3560	³⁰¹ 0.2957	³⁰¹ 5.199		
149	MICROFOCUS-005	⁴⁹ 256	⁷⁹ 266	²⁹⁷ 0.4242	²⁹⁷ 0.3028	²⁹⁷ 0.2606	²⁹⁷ 0.2209	²⁹⁶ 0.1724	²⁹ 3.861		
150	MICROFOCUS-006	⁴⁸ 256	⁷⁹ 265	²⁹⁸ 0.4268	²⁹⁸ 0.3049	²⁹⁸ 0.2623	²⁹⁹ 0.2233	²⁹⁹ 0.1746	²⁹⁸ 3.880		
151	MICROSOFT-003	¹⁶⁵ 1024	¹¹⁴ 404	⁵⁸ 0.0016	²¹ 0.0010	³ 0.0009	³ 0.0008	² 0.0006	²⁵ 1.009		
152	MICROSOFT-004	¹⁷⁹ 2048	²³⁸ 773	⁵⁰ 0.0015	¹¹ 0.0009	¹ 0.0008	¹ 0.0007	¹ 0.0006	²³ 1.009		
153	MICROSOFT-005	⁹⁷ 1024	¹⁹⁶ 673	⁸² 0.0019	¹⁷ 0.0010	⁸ 0.0008	² 0.0008	³ 0.0006	³ 1.010		
154	MICROSOFT-006	¹⁰³ 1024	²⁰⁵ 695	⁹⁰ 0.0020	³⁸ 0.0011	²³ 0.0010	⁴ 0.0008	⁴ 0.0007	⁴³ 1.011		
155	NEC-000	²⁷⁰ 2592	⁴¹ 82	²³⁶ 0.0170	²²⁷ 0.0086	²¹⁸ 0.0066	²¹⁵ 0.0052	²¹¹ 0.0038	²²⁹ 1.087		
156	NEC-001	²⁷¹ 2592	⁴² 88	²⁴⁵ 0.0209	²⁴⁹ 0.0141	²⁵⁰ 0.0128	²⁵³ 0.0119	²⁵⁶ 0.0113	²⁴⁸ 1.135		
157	NEC-002	¹⁴² 1616	¹⁸² 653	¹¹ 0.0010	⁶ 0.0009	⁷ 0.0008	⁶ 0.0008	⁵ 0.0008	⁶ 1.008		
158	NEC-003	¹⁴³ 1712	¹⁹⁹ 690	³⁸ 0.0014	⁴⁹ 0.0012	⁵⁰ 0.0012	⁵⁹ 0.0012	⁶¹ 0.0012	⁴⁵ 1.011		
159	NEC-004	¹²⁴ 1104	³⁰⁶ 967	⁴⁵ 0.0014	⁶³ 0.0013	⁷⁴ 0.0013	⁷⁴ 0.0013	⁸⁰ 0.0013	⁶¹ 1.012		
160	NEC-005	¹²³ 1104	³⁰⁵ 964	²⁷ 0.0012	³⁵ 0.0011	⁴³ 0.0011	⁴⁷ 0.0011	⁴⁷ 0.0011	³⁵ 1.010		
161	NEC-006	²⁹ 0	⁷ 1	³² 0.0013	⁴⁴ 0.0012	⁴⁹ 0.0012	⁵² 0.0012	⁵⁵ 0.0011	⁴¹ 1.011		
162	NEUROTECHNOLOGY-003	¹⁷⁶ 2048	¹⁵⁷ 547	²⁴⁶ 0.0225	²⁴⁴ 0.0126	²⁴ 0.0100	²³⁹ 0.0078	²²⁸ 0.0057	²⁴ 1.125		
163	NEUROTECHNOLOGY-004	¹⁹⁹ 2048	¹⁵⁶ 543	¹⁷¹ 0.0056	¹⁷² 0.0036	¹⁷⁸ 0.0032	¹⁷⁹ 0.0029	¹⁷⁸ 0.0025	¹⁷³ 1.035		
164	NEUROTECHNOLOGY-005	⁵² 256	¹¹⁸ 412	¹³⁵ 0.0043	¹⁶² 0.0029	¹⁶⁶ 0.0027	¹⁶⁷ 0.0024	¹⁷² 0.0023	¹⁶³ 1.028		
165	NEUROTECHNOLOGY-006	⁴⁶ 256	²³¹ 746	²⁴⁰ 0.0180	²²³ 0.0079	²¹¹ 0.0059	²¹¹ 0.0046	²⁰⁹ 0.0033	²²⁵ 1.083		
166	NEUROTECHNOLOGY-007	⁴⁷ 256	⁵¹ 169	¹⁴⁷ 0.0039	¹⁵⁷ 0.0027	¹⁶² 0.0025	¹⁶³ 0.0023	¹⁶⁵ 0.0022	¹⁵⁵ 1.026		
167	NEUROTECHNOLOGY-008	⁸² 514	²⁴⁶ 804	¹⁰⁰ 0.0022	⁸⁴ 0.0015	⁸⁸ 0.0014	⁸⁹ 0.0014	⁸⁹ 0.0013	⁸ 1.015		
168	NEUROTECHNOLOGY-009	⁸⁰ 513	¹⁹⁵ 686	⁴⁶ 0.0014	⁴⁵ 0.0012	⁴⁶ 0.0012	⁴⁷ 0.0011	⁵⁰ 0.0011	⁴⁴ 1.011		
169	NEUROTECHNOLOGY-010	⁵³ 256	¹⁸⁰ 663	³⁰ 0.0012	²⁷ 0.0011	²⁹ 0.0010	³⁰ 0.0010	³⁷ 0.0010	²¹ 1.010		
170	NEUROTECHNOLOGY-012	²⁶ 0	³ 0	⁹ 0.0010	¹⁹ 0.0010	²² 0.0010	²⁵ 0.0009	²⁷ 0.0009	¹³ 1.009		
171	NEWLAND-002	²¹⁴ 2048	²⁷² 868	²⁶ 0.0786	²⁷⁶ 0.0480	²⁷⁵ 0.0397	²⁷⁵ 0.0332	²⁷² 0.0263	²⁷⁷ 1.468		
172	NOBLIS-001	¹⁹⁰ 2048	⁶⁶ 211	²⁹³ 0.2492	²⁹⁷ 0.1772	²⁹³ 0.1542	²⁹³ 0.1339	²⁹¹ 0.1112	²⁵³ 2.679		
173	NOBLIS-002	³⁶ 6144	¹⁵³ 535	²⁸⁹ 0.1794	²⁸⁶ 0.1108	²⁸⁸ 0.0903	²⁸⁵ 0.0722	²⁸⁴ 0.0535	²⁶ 2.077		
174	NOTIONTAG-000	²⁶² 2120	¹³⁴ 461	¹¹⁹ 0.0024	¹³⁶ 0.0021	¹⁴² 0.0021	¹⁵³ 0.0020	¹⁵⁷ 0.0019	¹⁵² 1.019		
175	NTechLab-003	²⁷⁰ 3484	²⁵¹ 831	¹⁷⁷ 0.0062	¹⁶⁵ 0.0029	¹⁵⁹ 0.0023	¹⁴⁸ 0.0019	¹²⁹ 0.0016	¹⁶⁸ 1.030		
176	NTechLab-004	²⁷⁵ 3484	²⁹⁴ 929	¹⁶⁴ 0.0048	¹⁴³ 0.0023	¹³¹ 0.0019	¹¹⁹ 0.0016	⁹³ 0.0013	¹⁵¹ 1.024		
177	NTechLab-005	¹⁴⁷ 1940	²²⁰ 717	¹⁶² 0.0047	¹³⁸ 0.0022	¹¹⁶ 0.0017	⁷⁶ 0.0013	⁴⁵ 0.0011	¹⁴⁶ 1.023		
178	NTechLab-006	¹⁴⁸ 1940	²⁶¹ 841	¹⁸² 0.0041	¹¹⁷ 0.0019	⁹⁶ 0.0015	³⁵ 0.0012	²³ 0.0009	¹⁵³ 1.019		
179	NTechLab-007	²⁷⁴ 3348	²⁵⁸ 834	¹²³ 0.0027	¹⁰¹ 0.0017	⁸⁶ 0.0014	⁸³ 0.0013	⁶⁸ 0.0012	¹⁰⁵ 1.016		
180	NTechLab-008	¹²⁹ 1300	¹⁶¹ 562	⁶⁶ 0.0017	⁴³ 0.0012	⁴⁶ 0.0012	⁴⁴ 0.0011	⁴¹ 0.0010	⁴⁸ 1.012		
181	NTechLab-009	¹³⁰ 1300	²⁸³ 900	³³ 0.0013	³⁰ 0.0011	³⁰ 0.0010	²⁷ 0.0010	²⁸ 0.0009	³³ 1.010		
182	NTechLab-010	¹² 1280	²⁷ 875	¹⁷ 0.0011	²⁶ 0.0010	²⁶ 0.0010	²⁹ 0.0010	³⁶ 0.0010	²⁴ 1.009		
183	NTechLab-011	¹²⁸ 1280	²⁷⁶ 865	¹⁰ 0.0010	⁹ 0.0009	¹⁵ 0.0009	¹⁶ 0.0009	¹⁷ 0.0009	⁹ 1.008		
184	PANGIAM-000	¹⁶ 0	²⁶ 2	²⁶ 0.0012	³⁵ 0.0011	³⁶ 0.0011	³⁴ 0.0010	³⁶ 0.0010	³² 1.010		
185	PARAVISION-000	¹⁶⁷ 2048	¹²⁹ 438	²⁴¹ 0.0188	²⁵³ 0.0171	²⁶⁰ 0.0167	²⁶³ 0.0165	²⁶⁸ 0.0164	²⁵¹ 1.156		
186	PARAVISION-001	²⁰² 2048	¹⁶⁶ 590	¹⁴⁵ 0.0038	¹⁴⁹ 0.0024	¹⁴⁹ 0.0022	¹⁵⁴ 0.0020	¹⁵¹ 0.0019	¹⁴⁹ 1.023		
187	PARAVISION-002	¹⁵⁹ 2048	¹⁰⁶ 377	¹⁵⁰ 0.0040	¹⁵⁴ 0.0025	¹⁵⁹ 0.0022	¹⁵⁷ 0.0021	¹⁵⁶ 0.0019	¹⁵² 1.025		
188	PARAVISION-003	²⁰³ 2048	²²⁶ 735	¹³⁵ 0.0031	¹³⁷ 0.0022	¹⁴¹ 0.0020	¹⁴⁴ 0.0019	¹³⁹ 0.0017	¹³⁷ 1.021		
189	PARAVISION-004	²⁷⁹ 4096	²²⁷ 720	⁵⁹ 0.0016	⁷⁰ 0.0014	⁷² 0.0013	⁸⁰ 0.0013	⁸⁷ 0.0013	⁶⁹ 1.013		
190	PARAVISION-005	²⁸³ 4096	²⁶⁸ 858	⁵² 0.0015	⁶⁷ 0.0014	⁷¹ 0.0013	⁸¹ 0.0013	⁹² 0.0013	⁶⁴ 1.013		
191	PARAVISION-007	²⁸⁹ 4096	²¹⁶ 706	²⁴ 0.0012	³² 0.0011	³¹ 0.0010	³² 0.0010	³⁶ 0.0010	²⁸ 1.010		
192	PARAVISION-009	²⁹³ 4100	¹⁷⁷ 638	⁸ 0.0010	¹⁴ 0.0010	²¹ 0.0010	²⁶ 0.0009	²⁶ 0.0009	¹¹ 1.009		
193	PIXELLALL-002	²⁵⁶ 2560	⁶¹ 198	¹⁵⁹ 0.0045	¹⁶³ 0.0029	¹⁶⁶ 0.0025	¹⁶⁰ 0.0022	¹⁵⁶ 0.0019	¹⁶¹ 1.028		
194	PIXELLALL-003	²⁶⁶ 2560	²²² 719	⁹⁸ 0.0021	⁹⁷ 0.0016	⁹⁸ 0.0015	⁹⁸ 0.0014	¹⁰⁸ 0.0014	⁹⁷ 1.015		
195	PIXELLALL-004	²⁶⁹ 2560	¹³¹ 453	⁹⁵ 0.0020	⁸⁶ 0.0016	⁹⁰ 0.0015	⁹⁶ 0.0014	⁹⁴ 0.0013	⁸⁵ 1.014		
196	PIXELLALL-005	²⁶⁷ 2560	²⁶³ 845	⁸⁴ 0.0019	¹⁰³ 0.0017	¹⁰⁸ 0.0016	¹¹⁸ 0.0016	¹²⁶ 0.0016	⁹⁵ 1.015		
197	PTAKURATSATU-000	⁹¹ 538	²⁹¹ 910	¹³³ 0.0030	¹³⁴ 0.0021	¹³⁵ 0.0019	¹²⁷ 0.0018	¹³¹ 0.0016	¹³⁵ 1.020		
198	QNAP-000	²¹³ 2048	¹³² 457	¹⁹² 0.0078	¹⁸⁶ 0.0044	¹⁸⁹ 0.0037	¹⁸⁸ 0.0033	¹⁹⁸ 0.0028	¹⁸⁸ 1.043		
199	QNAP-001	¹⁶² 2048	¹⁷⁰ 615	¹⁵³ 0.0041	¹⁶⁴ 0.0029	¹⁶⁷ 0.0027	¹⁶⁹ 0.0025	¹⁷⁵ 0.0023	¹⁶¹ 1.028		
200	QNAP-002	⁶ 0	²⁶ 2	¹⁶⁵ 0.0049	¹⁸⁷ 0.0044	¹⁹⁹ 0.0043	²¹⁰ 0.0043	²¹⁷ 0.0042	¹⁸ 1.040		
201	QUANTASOFT-001	²¹⁵ 2048	¹¹² 396	²⁹⁰ 0.2177	²⁹² 0.1643	²⁹² 0.1468	²⁹² 0.1312	²⁹² 0.1116	²⁹² 2.539		
202	RANKONE-002	⁴³ 133	⁴⁵ 113	²⁴³ 0.0194	²³⁸ 0.0112	²³⁵ 0.0093	²³⁷ 0.0077	²³¹ 0.0060	²³⁸ 1.111		
203	RANKONE-003	⁴¹ 133	⁴⁶ 114	²⁴² 0.0194	²³⁹ 0.0112	²³⁶ 0.0093	²³⁶ 0.0077	²³² 0.0060	²³⁹ 1.111		
204	RANKONE-004	³⁴ 85	³⁷ 36	²⁶⁴ 0.0145	²⁶¹ 0.0126	²⁶⁷ 0.0177	²⁵⁷ 0.0141	²⁵¹ 0.0102	²⁶ 1.225		
205	RANKONE-005	⁴² 133	⁴³ 94	²⁰⁶ 0.0094	²⁰¹ 0.0054	²⁰² 0.0046	²⁰³ 0.0039	²⁰⁶ 0.0032	²⁰¹ 1.054		
206	RANKONE-006	⁴⁴ 165	⁷⁶ 261	¹⁶⁷ 0.0050	¹⁶⁸ 0.0030	¹⁶⁸ 0.0027	¹⁶⁴ 0.0024	¹⁶⁷ 0.0021	¹⁶⁷ 1.030		
207	RANKONE-007	⁴⁵ 165	⁸³ 278	¹³⁹ 0.0034	¹⁴⁴ 0.0023	¹⁴⁵ 0.0021	¹⁴⁰ 0.0018	¹³⁴ 0.0017	¹⁴¹ 1.022		
208	RANKONE-009	⁵⁶ 260	⁵⁹ 191	¹¹² 0.0024	⁹⁹ 0.0016	¹⁰² 0.0015	¹⁰⁶ 0.0015	¹⁰⁶ 0.0014	¹⁰⁰ 1.015		
209	RANKONE-010	⁵⁶ 26									

MISSES OUTSIDE RANK R			RESOURCE USAGE		ENROL MOST RECENT, N = 1.6M					
FNIR(N, T=0, R)			TEMPLATE		R=1	R=5	R=10	R=20	R=50	WORK-10
#	ALGORITHM		BYTES	MSEC						
217	REALNETWORKS-004		148	1848	247	0.0236	240	0.0112	233	0.0068
218	REALNETWORKS-005		249	2056	95	337	108	0.0023	90	0.0016
219	REALNETWORKS-006		250	2056	99	350	42	0.0014	42	0.0012
220	REALNETWORKS-007		25	0	16	2	35	0.0013	39	0.0011
221	REALNETWORKS-008		11	0	25	2	21	0.0011	15	0.0010
222	REMARKAI-000		173	2048	201	691	141	0.0034	13	0.0021
223	REMARKAI-000		151	2048	171	615	199	0.0086	189	0.0044
224	REMARKAI-002		151	2048	122	434	197	0.0081	181	0.0040
225	RENDIP-000		208	2048	283	894	55	0.0015	55	0.0013
226	REVEALMEDIA-000		241	2052	108	385	80	0.0019	69	0.0013
227	S1-000		284	4096	271	865	114	0.0024	106	0.0018
228	s1-001		22	2048	248	814	134	0.0031	15	0.0025
229	S1-002		30	0	14	2	44	0.0014	61	0.0013
230	SCANOVATE-000		206	2048	215	712	166	0.0050	156	0.0026
231	SCANOVATE-001		177	2048	19	675	170	0.0053	159	0.0027
232	SENSETIME-000		296	4104	218	715	110	0.0023	129	0.0020
233	SENSETIME-001		29	4104	18	656	111	0.0023	122	0.0020
234	SENSETIME-002		251	2056	180	650	230	0.0137	247	0.0136
235	SENSETIME-003		248	2056	289	940	7	0.0010	18	0.0010
236	SENSETIME-004		108	1032	214	710	6	0.0010	7	0.0009
237	SENSETIME-005		111	1032	308	1007	4	0.0009	3	0.0008
238	SENSETIME-006		112	1032	302	956	3	0.0009	4	0.0008
239	SENSETIME-007		113	1032	303	958	1	0.0008	4	0.0008
240	SENSETIME-008		8	0	11	1	10	0.0008	1	0.0008
241	SHAMAN-003		198	2048	208	704	281	0.1243	284	0.0823
242	SHAMAN-004		171	2048	171	642	292	0.2211	29	0.1473
243	SHAMAN-006		171	2048	211	706	261	0.0398	269	0.0344
244	SHAMAN-007		188	2048	21	709	260	0.0396	26	0.0342
245	SIAT-001		233	2052	262	842	73	0.0018	72	0.0014
246	SIAT-002		24	2052	289	906	76	0.0018	69	0.0014
247	SMILART-004		77	512	49	167	306	0.9648	306	0.9640
248	SMILART-005		219	2048	139	464	198	0.0085	237	0.0085
249	SQISOFT-001		246	2056	153	460	154	0.0042	28	0.0014
250	STAUQ-000		28	4096	25	827	188	0.0071	20	0.0061
251	SYNESIS-003		29	4096	44	103	287	0.1700	287	0.1172
252	SYNESIS-003		180	2048	68	215	234	0.0162	25	0.0160
253	SYNESIS-005		295	4104	237	772	198	0.0085	226	0.0085
254	T4ISB-000		21	0	17	2	210	0.0104	244	0.0103
255	TECH5-001		134	1536	28	898	149	0.0040	147	0.0024
256	TECH5-002		81	513	299	941	124	0.0027	76	0.0014
257	TEVIAN-003		177	2048	90	300	231	0.1047	219	0.0744
258	TEVIAN-004		168	2048	88	299	218	0.0113	203	0.0057
259	TEVIAN-005		21	2048	12	416	189	0.0073	178	0.0038
260	TEVIAN-006		109	1032	168	599	115	0.0024	113	0.0018
261	TEVIAN-007		110	1032	24	779	72	0.0018	69	0.0014
262	TIGER-000		242	2052	124	428	271	0.0616	266	0.0310
263	TIGER-002		235	2052	138	464	172	0.0056	166	0.0029
264	TIGER-003		248	2052	157	464	173	0.0056	169	0.0029
265	TONGYTRANS-000		258	2070	58	190	184	0.0069	176	0.0038
266	TONGYTRANS-001		25	2070	56	189	185	0.0069	177	0.0032
267	TOSHIBA-000		141	1548	295	930	158	0.0045	155	0.0026
268	TOSHIBA-001		25	2060	29	931	163	0.0048	159	0.0027
269	TRUEFACE-000		149	2000	100	365	138	0.0033	161	0.0028
270	VD-000		107	1028	91	337	300	0.4737	29	0.3204
271	VD-001		226	2052	204	695	253	0.0276	256	0.0181
272	VD-002		24	2052	19	689	207	0.0095	22	0.0077
273	VD-003		239	2052	202	693	190	0.0076	213	0.0069
274	VERIDAS-001		196	2048	278	885	127	0.0028	122	0.0019
275	VERIDAS-002		222	2048	280	888	126	0.0028	121	0.0019
276	VERIDAS-003		186	2048	278	877	75	0.0018	81	0.0015
277	VIGILANTSOLUTIONS-003		136	1544	256	832	274	0.0694	277	0.0349
278	VIGILANTSOLUTIONS-004		135	1544	254	830	282	0.1249	28	0.0706
279	VIGILANTSOLUTIONS-005		138	1544	247	778	203	0.0092	197	0.0045
280	VIGILANTSOLUTIONS-006		140	1544	257	834	209	0.0099	193	0.0048
281	VIGILANTSOLUTIONS-007		139	1544	176	618	140	0.0034	124	0.0020
282	VIGILANTSOLUTIONS-008		137	1544	115	405	132	0.0029	115	0.0018
283	VISIONBOX-000		25	2059	14	482	85	0.0019	89	0.0015
284	VISIONLABS-004		51	256	91	315	125	0.0027	110	0.0018
285	VISIONLABS-005		78	512	89	300	113	0.0024	105	0.0017
286	VISIONLABS-006		66	512	85	292	78	0.0018	76	0.0015
287	VISIONLABS-007		70	512	86	293	71	0.0018	74	0.0014
288	VISIONLABS-008		74	512	82	277	92	0.0020	114	0.0018

Table 28: Rank-based accuracy for the FRVT 2018 mugshot sets. In columns 3 and 4 are template size and template generation duration. Thereafter values are rank-based FNIR with $T = 0$ and FPIR = 1. This is appropriate to investigational uses but not those with higher volumes where candidates from all searches would need review. The next column is a workload statistic, a small value shows an algorithm front-loads mates into the first 10 candidates. Throughout, blue superscripts indicate the rank of the algorithm for that column, and the best value is highlighted in yellow.

#	ALGORITHM	MISSES OUTSIDE RANK R		RESOURCE USAGE		ENROL MOST RECENT, N = 1.6M					
		FNIR(N, T=0, R)		TEMPLATE		FRVT 2018 MUGSHOTS					
		BYTES	MSEC	R=1	R=5	R=10	R=20	R=50	WORK-10		
289	VISIONLABS-009	76 512	145 494	20 0.0011	28 0.0011	29 0.0010	31 0.0010	31 0.0010	26 1.010		
290	VISIONLABS-010	72 512	225 732	41 0.0014	38 0.0013	60 0.0013	66 0.0013	73 0.0013	54 1.012		
291	VISIONLABS-011	68 512	227 736	29 0.0012	34 0.0011	39 0.0011	37 0.0011	46 0.0011	34 1.010		
292	VNPT-001	13 0	23 2	99 0.0022	119 0.0019	126 0.0018	135 0.0018	146 0.0018	116 1.017		
293	VNPT-002	3 0	31 2	83 0.0019	111 0.0018	121 0.0018	126 0.0018	143 0.0017	107 1.016		
294	VOCORD-003	97 896	217 714	179 0.0062	171 0.0035	171 0.0030	177 0.0026	173 0.0023	172 1.035		
295	VOCORD-004	98 896	155 538	193 0.0079	195 0.0049	197 0.0043	202 0.0038	204 0.0034	193 1.048		
296	VOCORD-005	95 768	250 822	187 0.0070	192 0.0046	194 0.0041	201 0.0038	207 0.0035	189 1.044		
297	VOCORD-006	309 10240	251 825	308 1.0000	309 1.0000	308 1.0000	308 1.0000	308 1.0000	309 10.000		
298	VTS-000	193 2048	144 492	305 0.5937	304 0.5936	304 0.5936	304 0.5936	304 0.5936	304 6.343		
299	VTS-001	220 2048	281 891	54 0.0015	40 0.0012	36 0.0011	37 0.0011	34 0.0010	42 1.011		
300	VTS-002	205 2048	286 903	87 0.0019	71 0.0014	59 0.0013	69 0.0012	52 0.0011	76 1.013		
301	VTS-003	31 0	13 2	22 0.0011	20 0.0010	18 0.0009	15 0.0009	16 0.0009	17 1.009		
302	XFORWARDAI-000	175 2048	238 768	106 0.0023	120 0.0020	127 0.0020	149 0.0019	135 0.0019	125 1.018		
303	XFORWARDAI-001	209 2048	194 681	96 0.0020	123 0.0019	134 0.0019	146 0.0019	154 0.0019	117 1.018		
304	XFORWARDAI-002	287 4096	297 935	89 0.0020	120 0.0019	132 0.0019	145 0.0019	153 0.0019	114 1.017		
305	YISHENG-001	277 3704	110 387	259 0.0265	246 0.0130	242 0.0102	240 0.0080	230 0.0059	247 1.134		
306	YITU-002	300 4138	274 870	79 0.0018	47 0.0012	42 0.0011	40 0.0011	39 0.0010	53 1.012		
307	YITU-003	299 4138	275 871	131 0.0029	142 0.0023	151 0.0022	157 0.0021	164 0.0021	139 1.021		
308	YITU-004	258 2070	250 910	34 0.0013	10 0.0009	12 0.0009	12 0.0009	12 0.0009	20 1.009		
309	YITU-005	256 2070	269 861	108 0.0023	132 0.0021	139 0.0020	157 0.0020	158 0.0020	127 1.019		

Table 29: Rank-based accuracy for the FRVT 2018 mugshot sets. In columns 3 and 4 are template size and template generation duration. Thereafter values are rank-based FNIR with $T = 0$ and FPIR = 1. This is appropriate to investigational uses but not those with higher volumes where candidates from all searches would need review. The next column is a workload statistic, a small value shows an algorithm front-loads mates into the first 10 candidates. Throughout, blue superscripts indicate the rank of the algorithm for that column, and the best value is highlighted in yellow.

MISSSES BELOW THRESHOLD, T		ENROL RECENT MUGSHOT, N = 1.6M												ENROL APPLICATION PORTRAIT, N = 1.6M																			
#	ALGORITHM	ENROL: MUGSHOT			ENROL: MUGSHOT			ENROL: WEBCAM			ENROL: PROFILE			ENROL: VISA			ENROL: BORDER			PROBE: BORDER			PROBE: BORDER 10+YR			PROBE: KIOSK							
		FPIR=0.0003	FPIR=0.001	FPIR=0.01	FPIR=0.0003	FPIR=0.001	FPIR=0.01	FPIR=0.0003	FPIR=0.001	FPIR=0.01	FPIR=0.0003	FPIR=0.001	FPIR=0.01	FPIR=0.0001	FPIR=0.001	FPIR=0.01	FPIR=0.0001	FPIR=0.001	FPIR=0.01	FPIR=0.0001	FPIR=0.001	FPIR=0.01	FPIR=0.0001	FPIR=0.001	FPIR=0.01								
1	20FACE-000	256	0.462	265	0.348	272	0.230	269	0.763	262	0.450	262	0.301	211	1.000	242	1.000	242	1.000	197	0.424	197	0.255	111	0.772	116	0.599	194	0.938	206	0.836		
2	3DIVI-003	258	0.482	274	0.400	278	0.282	264	0.685	276	0.626	278	0.497					209	0.605	209	0.445			176	0.821	199	0.717						
3	3DIVI-004	228	0.256	245	0.169	249	0.093	231	0.400	252	0.343	256	0.237					187	0.277	191	0.172			151	0.607	173	0.485						
4	3DIVI-005	227	0.255	242	0.166	249	0.093	235	0.395	253	0.339	253	0.234	153	0.998	160	0.996	172	0.990	216	0.864	218	0.846			150	0.597	174	0.484				
5	3DIVI-006	226	0.253	244	0.168	251	0.096	234	0.403	251	0.342	257	0.238					188	0.283	192	0.174			154	0.615	176	0.490						
6	ACER-000	212	0.208	234	0.146	238	0.074	215	0.300	222	0.246	231	0.157	99	0.987	111	0.981	140	0.955	182	0.201	187	0.114	135	0.490	160	0.363						
7	ACER-001	158	0.109	176	0.056	180	0.026	150	0.136	157	0.109	163	0.069	185	1.000	196	0.999	221	0.998	141	0.068	143	0.036	99	0.406	106	0.250	134	0.479	110	0.206		
8	AIZE-001	169	0.127	196	0.077	194	0.034	188	0.187	185	0.143	186	0.087	126	0.995	137	0.994	168	0.983	155	0.101	159	0.052	93	0.364	101	0.216	115	0.387	142	0.289		
9	ALCHERA-000	219	0.231	231	0.138	232	0.070	204	0.259	214	0.216	225	0.146	165	0.999	176	0.999	203	0.996	176	0.176	188	0.111			172	0.803	170	0.456				
10	ALCHERA-001	304	1.000	304	0.999	306	0.999	301	1.000	308	1.000									281	1.000	251	1.000			286	1.000	289	1.000				
11	ALCHERA-002	281	0.807	281	0.486	281	0.302	263	0.685	273	0.591	273	0.442	205	1.000	203	1.000	226	0.999	215	0.827	215	0.770	173	0.811	192	0.705						
12	ALCHERA-003	252	0.450	236	0.155	233	0.070	216	0.304	225	0.239	230	0.152	198	1.000	188	0.999	208	0.997	175	0.172	176	0.097	130	0.464	159	0.362						
13	ALCHERA-004	263	0.520	273	0.394	277	0.211	260	0.642	268	0.529	267	0.327	127	0.995	132	0.991	102	0.813	198	0.424	199	0.232	106	0.708	112	0.515	146	0.546	168	0.398		
14	ALLGOVISION-000	178	0.138	208	0.088	214	0.045	191	0.202	201	0.166	210	0.106	112	0.993	129	0.990	164	0.982	158	0.117	163	0.066			143	0.526	167	0.396				
15	ALLGOVISION-001	187	0.155	214	0.102	220	0.053	209	0.275	218	0.221	224	0.141	117	0.993	118	0.986	12	0.933	170	0.150	171	0.081			136	0.491	166	0.389				
16	ANKE-000	198	0.184	218	0.117	229	0.063	203	0.256	216	0.220	228	0.151	123	0.995	138	0.994	173	0.990	286	1.000	260	1.000			265	1.000	271	1.000				
17	ANKE-001	196	0.183	222	0.119	229	0.063	202	0.256	217	0.220	229	0.151	129	0.995	144	0.994	182	0.992	272	1.000	248	1.000			278	1.000	279	1.000				
18	ANKE-002	122	0.062	137	0.032	136	0.014	115	0.103	122	0.079	126	0.050	78	0.975	81	0.948	97	0.795	103	0.034	106	0.018			82	0.245	104	0.190				
19	AWARE-003	195	0.174	226	0.128	24	0.082	225	0.351	24	0.298	249	0.204	96	0.987	115	0.984	159	0.977	199	0.428	209	0.378			144	0.530	168	0.443				
20	AWARE-004	244	0.355	258	0.269	267	0.175	256	0.619	267	0.509	271	0.375	200	1.000	207	1.000	228	0.999	194	0.397	199	0.279			174	0.816	186	0.631				
21	AWARE-005	269	0.608	268	0.364	248	0.085	221	0.342	231	0.253	233	0.163	199	1.000	210	1.000	229	0.999	186	0.255	187	0.122			188	0.916	194	0.714				
22	AWARE-006	257	0.475	259	0.276	268	0.175	244	0.466	255	0.398	260	0.283	181	1.000	199	0.999	222	0.999	192	0.368	196	0.254			166	0.749	187	0.623				
23	AYONIX-000	285	0.846	291	0.811	29	0.724	282	0.956	29	0.939	294	0.892	154	0.998	168	0.998	209	0.995	220	0.954	228	0.891			202	0.982	212	0.959				
24	AYONIX-001	286	0.875	293	0.824	295	0.701	277	0.946	287	0.920	290	0.845	194	1.000	195	0.999	204	0.996	224	0.999			199	0.969	209	0.926						
25	AYONIX-002	287	0.876	292	0.824	296	0.702	278	0.946	288	0.920	289	0.845	193	1.000	197	0.999	205	0.996	217	0.915	216	0.821			198	0.969	208	0.926				
26	CAMVI-003	147	0.094	191	0.071	222	0.058	160	0.152	17	0.132	211	0.108	84	0.979	92	0.970	12	0.940	157	0.114	170	0.100			118	0.402	163	0.377				
27	CAMVI-004	156	0.107	192	0.072	223	0.054	199	0.240	179	0.136	200	0.100	184	1.000	191	0.999	212	0.998	154	0.100	173	0.081			170	0.787	177	0.507				
28	CAMVI-005	179	0.139	212	0.099	24	0.076	145	0.451	209	0.179	219	0.132	190	1.000	202	1.000	217	0.998	171	0.156	187	0.112			210	0.999	219	0.983				
29	CANON-001	33	0.012	40	0.005	40	0.02	29	0.031	30	0.015	31	0.013	163	0.999	20	0.365	33	0.217	28	0.008	30	0.004	28	0.068	32	0.034	38	0.139	29	0.092		
30	CANON-002	23	0.010	33	0.005	34	0.002	25	0.027	26	0.020	19	0.013	17	0.487	23	0.407	35	0.253	51	0.013	35	0.004	33	0.075	41	0.046	67	0.188	46	0.106		
31	CIB-000	91	0.044	71	0.012	66	0.005	86	0.077	57	0.045	66	0.025	231	1.000	217	1.000	238	1.000	61	0.017	53	0.008	50	0.141	53	0.068	188	0.894	178	0.521		
32	CLEARVIEWAI-000	37	0.013	42	0.006	38	0.002	38	0.036	35	0.025	34	0.016	168	0.999	97	0.974	10	0.149	29	0.008	25	0.004	23	0.057	25	0.027	93	0.268	17	0.080		
33	CLOUDWALK-HR-000	10	0.004	13	0.002	17	0.002	10	0.015	12	0.013	15	0.012	3	0.188	3	0.133	6	0.095	15	0.005	17	0.003	10	0.033	14	0.018	19	0.099	11	0.075		
34	CLOUDWALK-MT-000	6	0.003	12	0.002	22	0.002	7	0.015	11	0.013	17	0.012	20	0.169	2	0.109	2	0.077	3	0.002	2	0.002	2	0.018	3	0.009	2	0.072	5	0.063		
35	CLOUDWALK-MT-001	3	0.003	10	0.002	20	0.002	4	0.013	4	0.012	14	0.011	10	0.104	1	0.070	1	0.060	1	0.001	1	0.001	1	0.015	1	0.006	1	0.056	1	0.049		
36	COGENT-000	183	0.143	167	0.053	186	0.029	17	0.17																								

MISSES BELOW THRESHOLD, T		ENROL RECENT MUGSHOT, N = 1.6M												ENROL APPLICATION PORTRAIT, N = 1.6M																							
		ENROL: MUGSHOT				ENROL: MUGSHOT				ENROL: WEBCAM				ENROL: MUGSHOT				ENROL: PROFILE				ENROL: VISA		ENROL: BORDER		ENROL: BORDER 10+YR		ENROL: KIOSK									
#	ALGORITHM	FPIR=0.0003	FPIR=0.001	FPIR=0.01	FPIR=0.0003	FPIR=0.001	FPIR=0.01	FPIR=0.0003	FPIR=0.001	FPIR=0.01	FPIR=0.0003	FPIR=0.001	FPIR=0.01	FPIR=0.0003	FPIR=0.001	FPIR=0.01	FPIR=0.0003	FPIR=0.001	FPIR=0.01	FPIR=0.0003	FPIR=0.001	FPIR=0.01	FPIR=0.0003	FPIR=0.001	FPIR=0.01	FPIR=0.0003	FPIR=0.001										
47	COGNITEC-004	115	0.055	136	0.031	137	0.014	138	0.127	145	0.097	143	0.058	125	0.995	126	0.990	118	0.919	140	0.068	14	0.038	91	0.316	10	0.196	95	0.288	11	0.218						
48	COGNITEC-005	116	0.055	58	0.010	54	0.004	60	0.058	63	0.041	56	0.022	271	1.000	281	1.000	112	0.878	113	0.041	130	0.028	60	0.157	71	0.092	62	0.179	75	0.145						
49	COGNITEC-006	69	0.029	52	0.008	49	0.003	66	0.065	59	0.040	53	0.022	263	1.000	287	1.000	229	0.999	91	0.030	89	0.013	66	0.171	69	0.081	160	0.681	115	0.214						
50	CUBOX-000	13	0.005	21	0.003	24	0.002	20	0.022	22	0.019	26	0.014	8	0.276	6	0.168	11	0.104	11	0.004	12	0.003	9	0.028	9	0.014	3	0.073	3	0.062						
51	CYBERLINK-000	177	0.137	177	0.056	16	0.023	166	0.162	161	0.116	166	0.070	146	0.997	153	0.995	16	0.981	138	0.063	138	0.032	109	0.339	125	0.232										
52	CYBERLINK-001	148	0.096	170	0.054	165	0.022	153	0.138	158	0.109	159	0.067	144	0.997	148	0.995	166	0.984	138	0.062	134	0.031	156	0.652	127	0.239										
53	CYBERLINK-002	83	0.038	81	0.015	81	0.006	76	0.068	83	0.053	84	0.032	119	0.994	124	0.988	14	0.957	79	0.024	81	0.013	96	0.288	84	0.157										
54	CYBERLINK-003	95	0.045	53	0.008	45	0.004	53	0.035	50	0.021	120	0.995	95	0.972	106	0.845	48	0.012	51	0.007	41	0.100	45	0.051	112	0.368	53	0.120								
55	CYBERLINK-004	206	0.188	49	0.007	48	0.003	64	0.063	54	0.036	55	0.022	236	1.000	241	1.000	23	0.999	50	0.013	56	0.007	42	0.109	4	0.050	197	0.954	145	0.291						
56	CYBERLINK-005	213	0.208	62	0.010	59	0.004	60	0.041	68	0.026	209	1.000	208	1.000	113	0.888	53	0.014	52	0.007	37	0.089	38	0.043	193	0.926	138	0.266								
57	DAHUA-000	171	0.128	204	0.086	21	0.045	17	0.179	17	0.135	184	0.083																								
58	DAHUA-001	155	0.106	194	0.073	196	0.037	159	0.151	169	0.122	175	0.075	98	0.987	107	0.980	124	0.933																		
59	DAHUA-002	62	0.026	82	0.015	79	0.006	61	0.060	69	0.046	73	0.029	36	0.681	44	0.638	63	0.522	58	0.017	58	0.008			51	0.159	57	0.125								
60	DAHUA-003	61	0.025	76	0.014	70	0.005	54	0.054	62	0.041	63	0.024	32	0.647	39	0.579	53	0.447	49	0.013	49	0.006	35	0.081	39	0.043	37	0.134	41	0.109						
61	DAHUA-004	40	0.014	48	0.007	45	0.003	33	0.033	35	0.026	35	0.016	21	0.552	32	0.485	45	0.345	35	0.008	34	0.004	19	0.051	21	0.027	29	0.113	33	0.094						
62	DAON-000	175	0.135	111	0.023	10	0.009	90	0.079	97	0.061	102	0.039	203	1.000	209	1.000	21	0.998	80	0.025	81	0.013	68	0.173	70	0.091	181	0.846	92	0.172						
63	DECATUR-000	88	0.043	114	0.023	113	0.010	95	0.085	103	0.066	104	0.040	39	0.757	49	0.675	59	0.509	84	0.027	90	0.014	67	0.173	77	0.098	80	0.239	82	0.156						
64	DEEPLINT-001	26	0.010	25	0.003	25	0.002	15	0.018	15	0.014	9	0.010	225	1.000	201	1.000	35	0.503	21	0.006	35	0.004			50	0.159	35	0.097								
65	DEEPSEA-001	134	0.073	157	0.046	163	0.022	141	0.129	149	0.101	146	0.059	102	0.988	116	0.985	153	0.973	145	0.077	149	0.041			106	0.326	131	0.251								
66	DERMALOG-003	265	0.550	280	0.482	280	0.360	26	0.715	278	0.655	282	0.526											213	0.677	21	0.554			183	0.870	205	0.791				
67	DERMALOG-004	267	0.554	279	0.480	283	0.358	266	0.711	279	0.657	280	0.526	139	0.997	154	0.995	183	0.991	208	0.603	210	0.458			182	0.856	198	0.751								
68	DERMALOG-005	207	0.189	207	0.088	206	0.043	18	0.201	192	0.154	197	0.096	135	0.996	128	0.990	13	0.950	189	0.300	196	0.267			153	0.614	171	0.459								
69	DERMALOG-006	150	0.098	164	0.052	179	0.026	152	0.137	152	0.105	158	0.067	104	0.989	110	0.981	125	0.933	133	0.059	136	0.031			105	0.318	122	0.230								
70	DERMALOG-007	204	0.188	205	0.086	201	0.040	19	0.200	191	0.152	194	0.093	136	0.996	127	0.990	134	0.950	135	0.059	135	0.052			148	0.557	149	0.299								
71	DERMALOG-008	231	0.268	155	0.045	146	0.017	196	0.231	158	0.094	157	0.054	213	1.000	243	1.000	239	1.000	130	0.057	120	0.025	97	0.382	96	0.158	195	0.940	189	0.678						
72	DERMALOG-009	87	0.041	104	0.021	105	0.009	97	0.086	104	0.066	107	0.040	206	1.000	223	1.000	236	1.000	93	0.031	97	0.016	120	0.999	124	0.999	179	0.840	119	0.222						
73	DERMALOG-010	46	0.019	47	0.007	52	0.004	148	0.134	87	0.055	58	0.023	183	1.000	184	0.999	137	0.952	151	0.089	151	0.041	121	1.000	121	0.971	141	0.522	114	0.211						
74	DIGIDATA-000	270	0.620	285	0.610	293	0.598	272	0.577	283	0.560	170	0.999	142	0.994	131	0.942	211	0.646	213	0.643	112	0.789	118	0.722	177	0.824	204	0.816								
75	DILUSENS-000	110	0.053	134	0.030	131	0.012	111	0.100	121	0.078	123	0.047	51	0.852	45	0.655	35	0.488	110	0.039	120	0.022	105	0.664	104	0.242	71	0.203	81	0.154						
76	EYDEA-003	262	0.509	270	0.388	276	0.265	258	0.625	270	0.543	272	0.404	138	0.997	145	0.994	172	0.990	206	0.570	205	0.392			171	0.792	188	0.658								
77	F8-001	254	0.458	241	0.166	196	0.036							167	0.999	175	0.998	202	0.995																		
78	FINCORE-000	203	0.187	230	0.134	236	0.071	208	0.267	215	0.217	222	0.140	197	1.000	214	1.000	195	0.995	177	0.187	184	0.108	104	0.598	111	0.418	128	0.458	158	0.349						
79	FUJITSULAB-000	223	0.246	105	0.021	10	0.008	79	0.070	90	0.056	95	0.035							77	0.024	81	0.013	69	0.177	75	0.093	81	0.240	83	0.156						
80	FUJITSULAB-001	273	0.655	95	0.018	85	0.007	122	0.112	92	0.058	86	0.033	132	0.996	134	0.992	130	0.940	78	0.024	75	0.011	107	0.739	110	0.310	84	0.247	77	0.146						
81	GLORY-000																																				

MISSES BELOW THRESHOLD, T		ENROL RECENT MUGSHOT, N = 1.6M												ENROL APPLICATION PORTRAIT, N = 1.6M															
		ENROL: MUGSHOT				ENROL: MUGSHOT				ENROL: WEBCAM				ENROL: MUGSHOT				ENROL: PROFILE				ENROL: VISA		ENROL: BORDER		ENROL: BORDER 10+YR		ENROL: VISA	
#	ALGORITHM	FPIR=0.0003	FPIR=0.001	FPIR=0.01	FPIR=0.0003	FPIR=0.001	FPIR=0.01	FPIR=0.0003	FPIR=0.001	FPIR=0.01	FPIR=0.0003	FPIR=0.001	FPIR=0.01	FPIR=0.0003	FPIR=0.001	FPIR=0.01	FPIR=0.0001	FPIR=0.01	FPIR=0.0001	FPIR=0.01	FPIR=0.0001	FPIR=0.01	FPIR=0.0001	FPIR=0.01	FPIR=0.0001	FPIR=0.01			
93	HIK-004	¹⁸⁹ 0.156	²¹¹ 0.099	²²² 0.054	¹⁷⁸ 0.182	¹⁹¹ 0.153	²⁰⁶ 0.101	⁹² 0.983	⁹⁸ 0.976	¹³³ 0.947	¹⁶⁵ 0.137	¹⁷ 0.077	²¹ 0.053	²⁴ 0.027	²² 0.101	²⁰ 0.083								¹²³ 0.434	¹³⁶ 0.353				
94	HIK-005	¹⁵³ 0.102	¹⁵⁰ 0.044	¹⁵¹ 0.019	¹⁰⁷ 0.098	¹¹⁹ 0.077	¹²⁵ 0.048	¹⁸⁸ 1.000	¹⁹⁸ 0.999	²¹⁴ 0.998	¹³⁹ 0.068	¹⁴¹ 0.036												¹⁴⁵ 0.541	¹³³ 0.258				
95	HIK-006	¹⁸¹ 0.142	¹⁵⁹ 0.047	¹⁵⁴ 0.020	¹²⁰ 0.111	¹²⁹ 0.086	¹³¹ 0.052	²²⁰ 1.000	²³⁵ 1.000	²³⁵ 0.999																			
96	HYPERVERGE-001	²² 0.009	³⁰ 0.004	³⁵ 0.002	⁴⁰ 0.039	⁴⁶ 0.031	⁴⁹ 0.020	⁷ 0.275	¹¹ 0.220	¹⁷ 0.146	²⁵ 0.007	²⁹ 0.004	²¹ 0.053	²⁴ 0.027	²² 0.101	²⁰ 0.083													
97	HYPERVERGE-002	²⁰ 0.008	²⁶ 0.004	²² 0.002	³¹ 0.034	³⁸ 0.027	⁴¹ 0.018	¹⁰ 0.278	¹⁰ 0.210	¹³ 0.131	¹⁸ 0.006	¹⁸ 0.003	¹⁸ 0.048	¹⁸ 0.023	¹³ 0.093	¹⁴ 0.077													
98	HZAILU-000	⁷⁸ 0.035	¹⁰¹ 0.020	¹⁰⁴ 0.009	⁶⁵ 0.064	⁷⁴ 0.051	⁷⁸ 0.031	⁹⁰ 0.983	⁸⁸ 0.967	¹⁰³ 0.813	⁶⁸ 0.020	⁶⁴ 0.010	⁹⁰ 0.316	⁶⁰ 0.077	⁴⁵ 0.153	⁵⁶ 0.120													
99	HZAILU-001	⁴⁴ 0.016	⁵⁴ 0.009	⁶² 0.004	²³⁵ 0.414	²⁰⁹ 0.183	⁶⁵ 0.024	¹⁵⁷ 0.998	¹²¹ 0.986	³⁸ 0.282	¹⁸¹ 0.196	¹¹⁸ 0.021	²⁸³ 1.000	¹² 0.997	¹⁵⁹ 0.679	¹³⁰ 0.360													
100	IDEMIA-003	²⁶⁶ 0.552	¹⁶⁰ 0.047	¹⁵⁸ 0.021	²⁹⁷ 1.000	²⁰⁰ 0.165	¹⁷⁹ 0.079	⁸¹ 0.976	⁹⁶ 0.973	¹⁴ 0.968	¹⁶⁰ 0.123	¹⁶ 0.061												¹⁶⁸ 0.766	¹⁸¹ 0.630				
101	IDEMIA-004	¹¹⁴ 0.055	¹⁴⁶ 0.037	¹⁵⁹ 0.021	¹⁵⁰ 0.144	¹⁶⁵ 0.118	¹⁷⁸ 0.079																	¹⁶⁹ 0.766	¹⁸⁸ 0.630				
102	IDEMIA-005	¹²⁹ 0.066	¹⁵² 0.044	¹⁷⁸ 0.026	¹⁷⁷ 0.181	¹⁸⁹ 0.150	²⁰⁸ 0.102	⁸⁵ 0.979	¹⁰² 0.978	¹⁵¹ 0.973	¹⁶¹ 0.130	¹⁶⁷ 0.070												¹⁸⁴ 0.879	¹⁹⁶ 0.743				
103	IDEMIA-006	¹²⁷ 0.065	¹⁴⁵ 0.043	¹⁷⁴ 0.025	²⁰ 0.266	²² 0.226	²³² 0.161	⁹⁵ 0.984	¹¹² 0.982	¹⁶ 0.980	¹⁶⁸ 0.144	¹⁷ 0.090												¹⁶³ 0.733	¹⁷⁵ 0.531				
104	IDEMIA-007	⁷⁹ 0.035	⁹⁴ 0.018	⁹⁶ 0.008	⁸⁴ 0.073	⁸⁶ 0.055	⁸⁷ 0.033	²⁹⁷ 1.000	²⁵⁷ 1.000	²⁸⁵ 1.000	¹²⁵ 0.052	¹² 0.022	⁷¹ 0.182	⁸¹ 0.109	³⁰² 1.000	²¹⁰ 0.982													
105	IDEMIA-008	⁸ 0.004	⁹ 0.002	¹⁰ 0.001	¹² 0.016	¹⁰ 0.013	⁶ 0.009	⁹ 0.276	⁹ 0.204	¹⁴ 0.136	¹⁴ 0.005	¹⁴ 0.003	¹⁶ 0.019	⁸ 0.002	⁸ 0.027	⁸ 0.013	⁶ 0.074	⁶ 0.064											
106	IDEMIA-009	⁷ 0.004	³ 0.002	⁴ 0.001	³ 0.012	³ 0.011	³ 0.008	⁴ 0.202	⁴ 0.141	⁷ 0.099	⁵ 0.003	⁶ 0.002	⁸ 0.027	⁸ 0.013															
107	IMAGUS-002	²⁹⁰ 0.908	²⁸⁹ 0.749	²⁹¹ 0.564	²⁷⁶ 0.944	²⁸⁴ 0.816	²⁸⁶ 0.645	²¹⁴ 1.000	²⁴⁰ 1.000	²⁴⁴ 1.000																			
108	IMAGUS-003	²⁸⁹ 0.898	²⁹⁰ 0.807	²⁹ 0.669	²⁸ 0.954	²⁸ 0.909	²⁸⁸ 0.809	²¹⁵ 1.000	²²² 1.000	²⁴⁹ 1.000																			
109	IMAGUS-005	⁷⁶ 0.034	⁹⁸ 0.018	⁹⁷ 0.008	⁹⁸ 0.088	¹⁰² 0.066	¹⁰⁵ 0.040	⁶² 0.926	⁶⁷ 0.838	⁸² 0.647	⁸⁷ 0.029	⁹⁸ 0.016	⁶³ 0.161	⁷⁶ 0.094	⁷⁷ 0.231	¹⁰² 0.189													
110	IMAGUS-006	⁸⁴ 0.039	¹⁰⁰ 0.019	⁹⁸ 0.008	¹⁰⁶ 0.093	¹⁰⁸ 0.069	¹¹³ 0.042	⁸⁸ 0.980	⁷⁶ 0.897	⁷⁷ 0.621	⁸⁶ 0.028	⁹² 0.015	⁶² 0.161	⁷⁷ 0.092	⁸² 0.260	⁹⁶ 0.181													
111	IMAGUS-007	⁸⁹ 0.044	¹¹³ 0.023	¹¹² 0.010	¹¹⁰ 0.100	¹¹⁴ 0.073	¹¹⁷ 0.045	⁷⁶ 0.973	⁷⁴ 0.893	⁸³ 0.651	⁹⁴ 0.031	⁹⁸ 0.016	⁶⁵ 0.169	⁷⁸ 0.098	⁹² 0.265	⁹⁷ 0.181													
112	IMAGUS-008	²⁹⁹ 0.995	²⁹⁹ 0.974	²⁹⁰ 0.523	²⁸³ 0.958	²⁸² 0.774	²⁶¹ 0.285	¹⁹¹ 1.000	¹⁵⁶ 0.996	⁸⁹ 0.700	²⁰⁴ 0.520	¹⁶ 0.071	¹²² 1.000	¹¹⁴ 0.540	¹⁴⁰ 0.518	¹²⁹ 0.246													
113	IMPERIAL-000	¹⁸⁶ 0.154	¹¹⁹ 0.026	¹⁰⁸ 0.009	¹⁰⁰ 0.089	¹⁰⁶ 0.068	¹¹⁰ 0.041	²³⁰ 1.000	¹⁷⁹ 0.999	¹⁹⁴ 0.995	¹¹⁴ 0.042	¹¹⁵ 0.020												⁸³ 0.245	⁸⁹ 0.168				
114	INCODE-000	²⁵⁰ 0.423	²⁶² 0.310	²⁶⁹ 0.199	²⁴⁷ 0.486	²⁵⁸ 0.420	²⁶⁴ 0.304	¹⁹² 1.000	¹⁷² 0.998	¹⁹² 0.994																			
115	INCODE-001	²³⁹ 0.319	²⁵¹ 0.212	²⁵⁶ 0.112	²² 0.348	²⁴¹ 0.296	²⁴⁵ 0.198	²¹⁹ 1.000	²³⁸ 1.000	²³ 1.000														¹⁰¹ 0.313	¹²¹ 0.226				
116	INCODE-002	²³⁶ 0.285	²⁴¹ 0.184	²⁵⁴ 0.100	²¹⁹ 0.333	²³⁹ 0.269	²⁴¹ 0.176	¹⁴⁹ 0.998	¹³⁶ 0.993	¹⁵⁸ 0.976																			
117	INCODE-003	²⁵⁷ 0.286	²⁴³ 0.167	²⁴² 0.084	²³⁷ 0.372	²³⁵ 0.264	²³⁵ 0.164	²⁰² 1.000	¹⁹⁴ 0.999	²⁰⁶ 0.996																			
118	INCODE-004	¹⁵² 0.099	¹⁷³ 0.054	¹⁶⁹ 0.023	¹⁶⁸ 0.167	¹⁶⁸ 0.120	¹⁶⁷ 0.070	¹⁴⁵ 0.997	¹⁴⁶ 0.995	¹²³ 0.929	¹³⁷ 0.063	¹³⁵ 0.031																	
119	INCODE-005	⁵⁰ 0.021	⁶⁶ 0.011	⁶¹ 0.005	⁵⁹ 0.055	⁶⁵ 0.043	⁶⁹ 0.026	²⁹ 0.614	³⁵ 0.528	⁴⁰ 0.372	⁶⁰ 0.017	⁶¹ 0.009	⁵⁴ 0.145	⁵⁷ 0.073	⁴⁸ 0.155	⁴⁶ 0.116													
120	INNOVATRICS-002	²⁴⁸ 0.379	²⁵⁰ 0.234	²⁶⁴ 0.139	²³³ 0.403	²⁴⁶ 0.310	²⁵¹ 0.209	²¹¹ 1.000	²³⁶ 1.000	²³⁴ 0.999																			
121	INNOVATRICS-003	²⁹⁷ 0.297	²⁵² 0.221	²⁶⁰ 0.132	²³⁵ 0.351	²⁴² 0.297	²⁴⁸ 0.203	²⁰¹ 1.000	²⁰⁵ 1.000	²¹⁷ 0.998																			
122	INNOVATRICS-004	²⁰¹ 0.184	²²⁸ 0.132	²³⁹ 0.074	²⁰⁵ 0.262	²¹⁹ 0.222	²²⁶ 0.149	⁹⁴ 0.984	¹⁰⁵ 0.980	¹⁵⁰ 0.973	¹²¹ 0.047	¹²¹ 0.022												⁸⁵ 0.251	⁹⁹ 0.182				
123	INNOVATRICS-005	¹¹⁸ 0.057	¹³⁹ 0.034	¹³² 0.014	¹²⁴ 0.114	¹³² 0.089	¹³² 0.052	⁵⁶ 0.890	⁶⁸ 0.846	⁶⁸ 0.723	¹²¹ 0.047	¹²¹ 0.022																	
124	INNOVATRICS-007	⁵⁵ 0.024	⁷² 0.013	⁷¹ 0.005	⁶⁷ 0.065	⁷⁵ 0.051	⁸⁰ 0.032	⁴⁶ 0.806	⁵⁴ 0.743	⁶⁸ 0.567	⁵⁹ 0.017	⁶² 0.009	³⁹ 0.093	⁴⁷ 0.053	⁴⁶ 0.154	⁵⁹ 0.120													
125	INTELLIVISION-001	²⁶¹ 0.508	²⁶⁰ 0.279	^{266</sup}																									

MISSES BELOW THRESHOLD, T		ENROL RECENT MUGSHOT, N = 1.6M												ENROL APPLICATION PORTRAIT, N = 1.6M									
#	ALGORITHM	ENROL: MUGSHOT			ENROL: MUGSHOT			ENROL: MUGSHOT			ENROL: VISA			ENROL: BORDER			ENROL: VISA						
		FPIR=0.0003	FPIR=0.001	FPIR=0.01	FPIR=0.0003	FPIR=0.001	FPIR=0.01	FPIR=0.0003	FPIR=0.001	FPIR=0.01	FPIR=0.0001	FPIR=0.01	FPIR=0.01	FPIR=0.001	FPIR=0.01	FPIR=0.001	FPIR=0.01	FPIR=0.001	FPIR=0.01				
139	LINECLOVA-002	284	0.845	295	0.845	300	0.845	248	0.508	174	0.130	27	0.014	111	0.992	109	0.981	70	0.577	214	0.717	214	0.716
140	LOOKMAN-003	128	0.066	151	0.044	174	0.025	144	0.131	160	0.112	182	0.082							149	0.084	163	0.061
141	LOOKMAN-004	138	0.074	154	0.045	174	0.024	134	0.123	154	0.105	173	0.075	83	0.979	99	0.977	156	0.974				
142	LOOKMAN-005	106	0.050	133	0.030	144	0.017	111	0.102	125	0.086	135	0.063	87	0.980	101	0.978	152	0.973	136	0.062	154	0.047
143	MANTRA-000	130	0.066	63	0.010	59	0.004	62	0.063	61	0.041	54	0.022	301	1.000	248	1.000	230	0.999	88	0.029	87	0.014
144	MAXVISION-000	102	0.048	131	0.028	133	0.013	24	0.468	227	0.237	139	0.054	49	0.827	57	0.767	78	0.631	169	0.149	118	0.022
145	MEGVII-001	215	0.210	193	0.072	197	0.037	130	0.119	146	0.097	148	0.061							119	0.997	120	0.872
146	MEGVII-002	229	0.258	197	0.077	199	0.037	131	0.120	144	0.096	145	0.059	166	0.999	174	0.998	111	0.872				
147	MICROFOCUS-003	293	0.958	292	0.931	301	0.866	289	0.988	296	0.979	296	0.948							222	0.982	222	0.945
148	MICROFOCUS-004	302	0.999	303	0.999	307	0.999	288	0.984	294	0.975	295	0.940							221	0.974	221	0.935
149	MICROFOCUS-005	288	0.883	294	0.835	298	0.736	280	0.951	290	0.928	292	0.865							219	0.935	219	0.848
150	MICROFOCUS-006	297	0.983	300	0.978	302	0.963	279	0.950	287	0.923	291	0.885							218	0.923	217	0.843
151	MICROSOFT-003	104	0.049	128	0.028	126	0.012	128	0.117	136	0.091	142	0.056							106	0.036	112	0.019
152	MICROSOFT-004	98	0.046	120	0.026	115	0.011	121	0.111	130	0.087	135	0.053							101	0.033	102	0.018
153	MICROSOFT-005	100	0.047	117	0.026	116	0.010	101	0.090	110	0.070	111	0.041	126	0.999	40	0.587	46	0.354	82	0.027	84	0.013
154	MICROSOFT-006	59	0.025	67	0.012	78	0.006	49	0.048	58	0.037	64	0.024	16	0.452	21	0.386	37	0.281	97	0.032	93	0.015
155	NEC-000	161	0.113	200	0.079	219	0.047	169	0.171	183	0.140	192	0.093	91	0.983	104	0.979	147	0.969				
156	NEC-001	185	0.148	217	0.106	228	0.060	198	0.238	212	0.197	220	0.133	107	0.991	119	0.986	149	0.972	162	0.133	175	0.082
157	NEC-002	45	0.018	18	0.003	15	0.002	28	0.029	25	0.020	23	0.013	186	1.000	193	0.999	197	0.995	31	0.008	45	0.005
158	NEC-003	12	0.005	15	0.002	21	0.002	18	0.021	19	0.017	22	0.013	38	0.902	64	0.824	77	0.628	34	0.008	46	0.006
159	NEC-004	2	0.003	6	0.002	14	0.002	9	0.015	7	0.013	11	0.010	35	0.654	43	0.622	67	0.575	12	0.004	21	0.004
160	NEC-005	18	0.007	4	0.002	9	0.001	5	0.014	3	0.012	7	0.009	37	0.901	48	0.673	27	0.177	7	0.003	10	0.002
161	NEC-006	24	0.010	11	0.002	12	0.002	23	0.024	21	0.018	20	0.013	52	0.857	28	0.463	12	0.122	8	0.004	13	0.003
162	NEUROTECHNOLOGY-003	301	0.999	287	0.636	253	0.099	279	0.773	237	0.266	234	0.164	250	1.000	294	1.000	278	1.000				
163	NEUROTECHNOLOGY-004	162	0.120	182	0.063	183	0.028	156	0.146	162	0.117	169	0.073	137	0.996	141	0.994	174	0.990				
164	NEUROTECHNOLOGY-005	162	0.117	174	0.054	164	0.022	201	0.252	175	0.130	172	0.074	164	0.999	167	0.989						
165	NEUROTECHNOLOGY-006	298	0.987	257	0.249	258	0.121	298	1.000	257	0.418	250	0.206										
166	NEUROTECHNOLOGY-007	225	0.252	186	0.062	161	0.021	297	0.996	204	0.173	180	0.068	212	1.000	216	1.000	209	0.997	101	0.339	142	0.036
167	NEUROTECHNOLOGY-008	280	0.797	168	0.053	130	0.012	119	0.110	123	0.080	122	0.047	229	1.000	231	1.000	254	1.000	105	0.035	105	0.017
168	NEUROTECHNOLOGY-009	63	0.027	85	0.015	77	0.006	70	0.066	79	0.052	81	0.032	34	0.661	41	0.588	52	0.436	67	0.020	66	0.010
169	NEUROTECHNOLOGY-010	241	0.346	61	0.010	51	0.003	48	0.047	57	0.037	61	0.023	14	0.377	16	0.277	29	0.170	44	0.010	39	0.005
170	NEUROTECHNOLOGY-012	146	0.092	46	0.007	37	0.002	46	0.045	50	0.032	45	0.019	204	1.000	84	0.959	18	0.149	38	0.008	25	0.004
171	NEWLAND-002	264	0.523	277	0.438	279	0.294	249	0.535	261	0.466	268	0.335	174	0.999	185	0.999	216	0.998				
172	NOBLIS-001	305	1.000	305	1.000	303	0.991	309	1.000	303	1.000	304	1.000	235	1.000	226	1.000	248	1.000				
173	NOBLIS-002	303	1.000	301	0.997	289	0.488	305	1.000	299	1.000	309	1.000	228	1.000	259	1.000						
174	NOTIONTAG-000	74	0.032	89	0.017	93	0.007	85	0.076	98	0.059	99	0.036	35	0.671	42	0.611	53	0.467	72	0.021	74	0.011
175	NTECHLAB-003	138	0.080	172	0.054	184	0.028	157	0.148	163	0.118	174	0.075	34	0.873	66	0.837	96	0.752				
176	NTECHLAB-004	125	0.063	147	0.041	159	0.021	143	0.131	153	0.105	157	0.065	53	0.868	65	0.833	94	0.746	128	0.053	133	0.030
177	NTECHLAB-005	124	0.062	148	0.042	160	0.021	142	0.130	157	0.102	156	0.063	47	0.816	58	0.771	85	0.661	145	0.073	146	0.039
178	NTECHLAB-006	117	0.056	142	0.037	149	0.018	132	0.121	139	0.094	144	0.059	45	0.802	56	0.754	80	0.635	131	0.057	137	0.032
179	NTECHLAB-007	85	0.040	116	0.026	122	0.012	94	0.085	105	0.067	107	0.041	44	0.796	55	0.750	81	0.642	98	0.032	104	0.017
180	NTECHLAB-008	57	0.024	78	0.014	86	0.007	59	0.057	68	0.045	74	0.029	26	0.601	36	0.529	51	0.391	102	0.033	108	0.018
181	NTECHLAB-009	25	0.010	37	0.005	42	0.003	27	0.028	28	0.022	28	0.014	19	0.522	25	0.430	46	0.311	54	0.015	56	0.008
182	NTECHLAB-010	14	0.005	17	0.003	13	0.002	15	0.018	16	0.015	13	0.011	13	0.334	15	0.252	24	0.169	22	0.007	28	0.004
183	NTECHLAB-011	15	0.006	22	0.003	16	0.002	14	0.018	15	0.015	12	0.010	11	0.291	12	0.228	21	0.150	40	0.009	36	0.004
184	PANGIAM-000	39	0.014	43	0.006	41	0.003	45	0.039	44	0.030	43	0.018	77	0.974	19	0.318	26	0.175	43	0.009	38	0.005
														45	0.009	43	0.009	48	0.136	31	0.033	24	0.105

T = 0 → Investigation

T > 0 → Identification

FNIR(N, T, L) =

False neg. identification rate

MISSES BELOW THRESHOLD, T		ENROL RECENT MUGSHOT, N = 1.6M												ENROL APPLICATION PORTRAIT, N = 1.6M																	
#	ALGORITHM	ENROL: MUGSHOT			ENROL: MUGSHOT			ENROL: WEBCAM			ENROL: PROFILE			ENROL: VISA			ENROL: BORDER			ENROL: BORDER 10+YR			ENROL: KIOSK								
		FPIR=0.0003	FPIR=0.001	FPIR=0.01	FPIR=0.0003	FPIR=0.001	FPIR=0.01	FPIR=0.0003	FPIR=0.001	FPIR=0.01	FPIR=0.0003	FPIR=0.001	FPIR=0.01	FPIR=0.0001	FPIR=0.01	FPIR=0.001	FPIR=0.01	FPIR=0.0001	FPIR=0.01	FPIR=0.001	FPIR=0.01	FPIR=0.0001	FPIR=0.01	FPIR=0.01							
185	PARAVISION-000	234	0.278	209	0.089	213	0.045	240	0.447	202	0.170	202	0.100	216	1.000	187	0.999	207	0.997	203	0.470	208	0.443	192	0.926	201	0.779				
186	PARAVISION-001	180	0.140	161	0.049	156	0.020	192	0.207	173	0.128	171	0.074	232	1.000	177	0.999	19	0.994	200	0.444	209	0.428	164	0.739	182	0.573				
187	PARAVISION-002	143	0.085	162	0.050	166	0.022	161	0.152	166	0.119	176	0.076	110	0.992	113	0.983	95	0.748	146	0.080	153	0.043	137	0.497	138	0.268				
188	PARAVISION-003	126	0.063	140	0.035	140	0.016	137	0.124	143	0.096	147	0.060	143	0.997	143	0.994	96	0.733	132	0.058	140	0.034	98	0.296	124	0.232				
189	PARAVISION-004	58	0.025	65	0.010	63	0.004	51	0.049	58	0.038	62	0.024	218	1.000	239	1.000	100	0.797	62	0.018	70	0.011	187	0.908	113	0.211				
190	PARAVISION-005	42	0.014	28	0.004	31	0.002	30	0.031	31	0.024	37	0.016	141	0.997	106	0.980	23	0.181	45	0.011	57	0.008	35	0.132	52	0.120				
191	PARAVISION-007	101	0.048	27	0.004	25	0.002	250	0.560	32	0.025	32	0.015	227	1.000	234	1.000	251	1.000	39	0.009	48	0.006	44	0.113	20	0.024	290	1.000		
192	PARAVISION-009	19	0.007	20	0.003	8	0.001	24	0.026	20	0.019	16	0.012	43	0.778	53	0.735	60	0.550	6	0.003	11	0.002	10	0.015	4	0.073	2	0.061		
193	PIXELALL-002	274	0.664	216	0.105	187	0.030	285	0.974	254	0.388	183	0.083	229	1.000	245	1.000	207	0.602	156	0.047	267	1.000	222	1.000	147	0.554	132	0.255		
194	PIXELALL-003	103	0.049	108	0.022	106	0.009	111	0.102	117	0.073	114	0.043	204	1.000	219	0.998	109	0.037	111	0.020	207	0.994	211	0.942	188	0.232	116	0.179		
195	PIXELALL-004	164	0.120	97	0.018	90	0.007	27	0.783	123	0.079	100	0.037	221	1.000	222	0.999	123	0.051	91	0.015	212	1.000	217	0.983	187	0.232	116	0.179		
196	PIXELALL-005	137	0.079	69	0.012	65	0.005	242	0.456	72	0.050	71	0.027	227	1.000	235	0.999	83	0.027	100	0.017	75	0.203	54	0.071	212	1.000	217	0.983		
197	PTAKURATSATU-000	119	0.057	141	0.037	145	0.017	167	0.165	171	0.124	168	0.071	71	0.947	78	0.924	109	0.868	120	0.046	111	0.022	77	0.206	80	0.120	78	0.232	96	0.179
198	QNAP-000	296	0.972	227	0.129	219	0.052	294	0.998	225	0.238	214	0.117	237	1.000	246	1.000	250	1.000	178	0.191	166	0.068	103	0.539	108	0.263	209	0.998	219	0.985
199	QNAP-001	142	0.083	171	0.054	17	0.024	17	0.176	187	0.137	185	0.085	67	0.943	79	0.928	110	0.870	147	0.081	159	0.041	95	0.368	108	0.227	108	0.331	136	0.248
200	QNAP-002	94	0.045	121	0.026	134	0.013	151	0.136	155	0.106	162	0.068	48	0.820	59	0.772	74	0.622	122	0.052	126	0.025	86	0.281	97	0.171	94	0.272	116	0.214
201	QUANTASOFT-001	278	0.713	288	0.639	28	0.493	234	0.071	217	0.308	233	0.261	244	0.190																
202	RANKONE-002	199	0.184	220	0.118	234	0.071	217	0.308	233	0.261	244	0.190																		
203	RANKONE-003	200	0.184	221	0.118	235	0.071	214	0.300	232	0.255	242	0.187																		
204	RANKONE-004	224	0.250	249	0.193	259	0.124	246	0.482	259	0.426	266	0.324																		
205	RANKONE-005	149	0.096	183	0.059	192	0.033	192	0.212	207	0.173	215	0.119	175	0.999	169	0.998	193	0.994												
206	RANKONE-006	121	0.061	143	0.037	152	0.020	123	0.111	129	0.118	140	0.095	149	0.061	80	0.975	87	0.967	119	0.924										
207	RANKONE-007	75	0.034	110	0.022	123	0.011	129	0.118	140	0.095	149	0.061	89	0.987	100	0.977	126	0.937												
208	RANKONE-009	71	0.031	92	0.018	108	0.008	108	0.098	117	0.076	116	0.045	89	0.983	91	0.969	108	0.859	134	0.062	135	0.029	107	0.328	111	0.206				
209	RANKONE-010	52	0.023	75	0.014	91	0.007	87	0.077	93	0.058	98	0.036	59	0.905	62	0.802	84	0.652	126	0.052	129	0.027	78	0.208	84	0.119	86	0.259	108	0.194
210	RANKONE-011	159	0.109	55	0.009	69	0.004	91	0.079	70	0.048	75	0.029					108	0.037	105	0.017	70	0.182	71	0.092	201	0.977	172	0.465		
211	RANKONE-012	49	0.020	51	0.008	56	0.004	83	0.072	84	0.053	76	0.030	48	0.020	155	0.998	159	0.996	32	0.214	63	0.018	57	0.008	51	0.141	41	0.050	36	0.097
212	RANKONE-013	26	0.010	31	0.005	30	0.002	4	0.046	32	0.034	48	0.020	155	0.998	159	0.996	32	0.214	63	0.018	47	0.154	45	0.116	37	0.071	38	0.097		
213	REALNETWORKS-000	247	0.374	254	0.234	263	0.138	237	0.433	248	0.319	253	0.209																		
214	REALNETWORKS-001	246	0.374	255	0.234	26	0.138	238	0.433	249	0.319	252	0.209																		
215	REALNETWORKS-002	245	0.370	253	0.231	261	0.137	236	0.416	247	0.315	254	0.209																		
216	REALNETWORKS-003	232	0.273	239	0.159	245	0.090	222	0.342	236	0.266	240	0.172	171	0.999	173	0.998	168	0.987	173	0.164	180	0.103			138	0.500	161	0.364		
217	REALNETWORKS-004	222	0.242	238	0.158	244	0.090	222	0.353	231	0.263	237	0.169	187	1.000	189	0.999	188	0.992	174	0.170	181	0.103			152	0.613	162	0.370		
218	REALNETWORKS-005	109	0.052	122	0.028	129	0.012	104	0.094	115	0.074	121	0.047	93	0.984	92	0.971	114	0.896	107	0.037	101	0.017	79	0.223	87	0.123	73	0.215	87	0.165
219	REALNETWORKS-006	60	0.025	79	0.015	7	0.006	7	0.068	8	0.053	85	0.032	115	0.993	108	0.980	108	0.838	55	0.016	57	0.008	45	0.120	51	0.063	47	0.154	48	0.116
220	REALNETWORKS-007	48	0.019	59	0.010	58	0.004	58	0.057	66	0.043	70	0.027	108	0.992	103	0.979	107	0.855	47	0.012	44	0.005	102	0.463	52	0.063	39	0.140	37	0.100
221	REALNETWORKS-008	35	0.012	44	0.006	46	0.003	49	0.037	43	0.029	42	0.018	103	0.988	89	0.968	107	0.271	36	0.008	37	0.004	29	0.068	33	0.129	42	0.110		
222	REMARKAI-000	168	0.125	175	0.055	168	0.023	170	0.173	167	0.120	165	0.070	179	0.999	186	0.999	196	0.995	142	0.069	139	0.033								

MISSES BELOW THRESHOLD, T		ENROL RECENT MUGSHOT, N = 1.6M												ENROL APPLICATION PORTRAIT, N = 1.6M																										
#	ALGORITHM	ENROL: MUGSHOT			ENROL: MUGSHOT			ENROL: WEBCAM			ENROL: MUGSHOT			ENROL: PROFILE			ENROL: VISA			ENROL: BORDER			ENROL: BORDER 10+YR			ENROL: VISA														
		FPIR=0.0003	FPIR=0.001	FPIR=0.01	FPIR=0.0003	FPIR=0.001	FPIR=0.01	FPIR=0.0003	FPIR=0.001	FPIR=0.01	FPIR=0.0003	FPIR=0.001	FPIR=0.01	FPIR=0.0003	FPIR=0.001	FPIR=0.01	FPIR=0.001	FPIR=0.01	FPIR=0.001	FPIR=0.01	FPIR=0.001	FPIR=0.01	FPIR=0.001	FPIR=0.01	FPIR=0.001	FPIR=0.01														
231	SCANOVATE-001	170	0.128	201	0.081	200	0.037	212	0.281	221	0.227	223	0.140	66	0.935	77	0.911	104	0.834	179	0.192	182	0.103	142	0.523	86	0.160													
232	SENSETIME-000	80	0.036	106	0.021	107	0.009	88	0.078	99	0.063	106	0.040	233	1.000	297	1.000	169	0.988					36	0.133	44	0.115													
233	SENSETIME-001	81	0.036	105	0.022	111	0.010	92	0.080	101	0.064	112	0.041											28	0.113	36	0.100													
234	SENSETIME-002	82	0.037	80	0.015	139	0.014	136	0.124	41	0.028	59	0.023	140	0.997	140	0.994	160	0.979	96	0.032	102	0.017																	
235	SENSETIME-003	9	0.004	8	0.002	7	0.001	6	0.014	6	0.012	5	0.009	28	0.607	30	0.477	41	0.311	32	0.008	43	0.005																	
236	SENSETIME-004	5	0.003	5	0.002	6	0.001	8	0.015	10	0.010	12	0.031	13	0.229	20	0.149	19	0.006	23	0.004																			
237	SENSETIME-005	30	0.011	14	0.002	7	0.001	16	0.018	14	0.014	8	0.010	6	0.259	7	0.173	10	0.103	23	0.007	20	0.004	20	0.051	10	0.023													
238	SENSETIME-006	11	0.005	7	0.002	3	0.001	11	0.016	7	0.012	4	0.009	162	0.999	171	0.998	86	0.680	9	0.004	7	0.002	12	0.034	12	0.016													
239	SENSETIME-007	4	0.003	2	0.001	7	0.001	7	0.012	7	0.009	2	0.007	189	1.000	192	0.999	69	0.538	4	0.003	3	0.001	6	0.024	3	0.011													
240	SENSETIME-008	1	0.002	1	0.001	1	0.001	1	0.011	1	0.009	1	0.007	106	0.990	22	0.405	3	0.086	2	0.002	2	0.001	5	0.021	2	0.009													
241	SHAMAN-003	260	0.506	278	0.451	282	0.347	261	0.650	274	0.597	277	0.472																											
242	SHAMAN-004	275	0.679	286	0.615	289	0.488	277	0.812	28	0.754	285	0.639																											
243	SHAMAN-006	202	0.185	232	0.141	247	0.092	210	0.278	224	0.237	236	0.168	82	0.978	94	0.972	143	0.960																					
244	SHAMAN-007	197	0.183	233	0.141	246	0.092	21	0.280	22	0.240	238	0.169																											
245	SIAT-001	173	0.132	90	0.018	87	0.007	259	0.641	253	0.365	269	0.348							92	0.031	88	0.014																	
246	SIAT-002	249	0.417	107	0.022	92	0.007	275	0.942	265	0.478	275	0.460							193	0.372	202	0.356																	
247	SMILART-004	295	0.970	298	0.968	303	0.965	286	0.977	295	0.976	297	0.973																											
248	SMILART-005																																							
249	SQISOFT-001	218	0.226	229	0.132	210	0.044	220	0.340	230	0.252	212	0.111	73	0.956	60	0.797	72	0.608	112	0.040	111	0.019	92	0.317	93	0.150													
250	STAQU-000	240	0.334	184	0.062	16	0.022	22	0.848	261	0.443	150	0.061	208	1.000	213	1.000	22	0.999	205	0.535	14	0.039	115	0.961	93	1.000													
251	SYNESIS-003	272	0.648	283	0.582	286	0.443	265	0.708	277	0.646	279	0.524																											
252	SYNESIS-003	160	0.111	188	0.065	18	0.032	162	0.155	170	0.123	177	0.078	75	0.973	85	0.960	116	0.911	144	0.075	145	0.039			102	0.314	126	0.235											
253	SYNESIS-005	105	0.050	115	0.025	12	0.011	99	0.088	111	0.072	115	0.043	124	0.995	114	0.984	99	0.795	99	0.032	96	0.016			72	0.214	80	0.158											
254	T4ISB-000	64	0.027	87	0.016	121	0.011	75	0.068	92	0.053	92	0.034	21	0.566	33	0.510	54	0.463	69	0.021	67	0.010	109	0.759	98	0.177	52	0.161	58	0.125									
255	TECH5-001	282	0.807	178	0.057	148	0.018	291	0.994	291	0.935	141	0.055	276	1.000	245	1.000	241	1.000	184	0.244	13	0.028			208	0.994	205	0.817											
256	TECH5-002	112	0.053	124	0.027	128	0.012	103	0.094	109	0.070	108	0.040	55	0.874	63	0.805	76	0.627	111	0.039	110	0.019	76	0.205	82	0.111	125	0.440	108	0.182									
257	TEVIAN-003	221	0.239	246	0.177	250	0.096	22	0.346	24	0.298	246	0.198																											
258	TEVIAN-004	194	0.170	219	0.117	231	0.063	194	0.216	206	0.176	213	0.115																											
259	TEVIAN-005	172	0.129	206	0.087	21	0.045	170	0.180	18	0.144	189	0.089	100	0.988	86	0.962	99	0.796																					
260	TEVIAN-006	56	0.024	60	0.010	68	0.005	44	0.041	48	0.032	52	0.021	22	0.562	24	0.425	39	0.291	56	0.016	60	0.009	38	0.093	43	0.050	196	0.951	47	0.117									
261	TEVIAN-007	31	0.011	39	0.005	43	0.003	25	0.028	27	0.022	29	0.015	18	0.504	18	0.301	20	0.183	42	0.009	40	0.005	27	0.065	36	0.033	30	0.122	39	0.102									
262	TIGER-000	258	0.462	272	0.390	277	0.261	251	0.565	266	0.500	270	0.366																											
263	TIGER-002	190	0.158	202	0.086	203	0.039	190	0.202	195	0.158	196	0.095	180	0.999	181	0.999	157	0.975																					
264	TIGER-003	191	0.158	203	0.086	202	0.039	18	0.202	196	0.158	195	0.095																											
265	TONGYITRANS-000	157	0.107	195	0.074	201	0.038	154	0.141	159	0.112	164	0.069																											
266	TONGYITRANS-001	167	0.124	189	0.066	190	0.032	159	0.128	150	0.101	153	0.062																											
267	TOSHIBA-000	166	0.123	183	0.062	182	0.027	158	0.150	164	0.118	170	0.074	142	0.997	152	0.995	170	0.988																					
268	TOSHIBA-001	216	0.225	180	0.058	159	0.019	14	0.133	15	0.092	140	0.054																											
269	TRUEFACE-000	97	0.046	96	0.018	99	0.008	89	0.079	98	0.062	103	0.039	128	0.995	70	0.882	57	0.499	90	0.030	99	0.016	74	0.194	83	0.111	66	0.188	74	0.145									
270	VD-000	292	0.950	296	0.917	297	0.827	28	0.968	293	0.946	293	0.871																											
271	VD-001	233	0.278	250	0.201	257	0.116	218	0.331	240	0.281	243	0.188																											
272	VD-002	184	0.144	199	0.079	196	0.036	18	0.188</td																															

MISSES BELOW THRESHOLD, T			ENROL RECENT MUGSHOT, N = 1.6M												ENROL APPLICATION PORTRAIT, N = 1.6M															
#	ALGORITHM	FPIR=0.0003	ENROL: MUGSHOT			ENROL: MUGSHOT			ENROL: MUGSHOT			ENROL: VISA			ENROL: BORDER			ENROL: VISA			PROBE: BORDER			PROBE: BORDER 10+YR			PROBE: KIOSK			
			FPIR=0.001	FPIR=0.01	FPIR=0.003	FPIR=0.001	FPIR=0.01	FPIR=0.003	FPIR=0.001	FPIR=0.01	FPIR=0.003	FPIR=0.001	FPIR=0.01	FPIR=0.001	FPIR=0.01	FPIR=0.003	FPIR=0.001	FPIR=0.01	FPIR=0.001	FPIR=0.01	FPIR=0.001	FPIR=0.01	FPIR=0.001	FPIR=0.01	FPIR=0.001	FPIR=0.01	FPIR=0.001			
277	VIGILANTSOLUTIONS-003	²⁵⁹ 0.482	²⁷⁶ 0.408	²⁷⁷ 0.282	²⁶⁸ 0.730	²⁸⁰ 0.660	²⁸¹ 0.526	¹⁷³ 0.999	¹⁷⁸ 0.999	¹⁹⁸ 0.995																				
278	VIGILANTSOLUTIONS-004	²⁷¹ 0.624	²⁸² 0.549	²⁸⁸ 0.422	²⁷⁴ 0.858	²⁸³ 0.817	²⁸⁷ 0.709	¹⁵⁶ 0.998	¹⁵⁸ 0.996	¹⁷⁹ 0.991																				
279	VIGILANTSOLUTIONS-005	²⁹¹ 0.936	²⁷¹ 0.388	²⁰⁵ 0.043							²³⁴ 1.000	²²⁵ 1.000	²⁴⁹ 1.000																	
280	VIGILANTSOLUTIONS-006	²⁹⁴ 0.959	²⁶⁶ 0.353	²⁰⁸ 0.043							²²² 1.000	²³³ 1.000	²⁵⁷ 1.000																	
281	VIGILANTSOLUTIONS-007	¹³⁶ 0.076	¹³² 0.028	¹²⁴ 0.011	¹²³ 0.113	¹³¹ 0.088	¹³⁴ 0.053	¹⁴⁸ 0.997	¹⁵⁷ 0.996	¹⁸² 0.991	¹⁴⁸ 0.081	¹⁵⁵ 0.047	⁹⁶ 0.371	¹⁰⁵ 0.242	¹¹⁶ 0.391	¹⁴⁷ 0.295														
282	VIGILANTSOLUTIONS-008	¹⁰⁸ 0.051	¹⁰³ 0.021	¹¹⁶ 0.010	¹¹¹ 0.105	¹¹⁹ 0.077	¹¹⁹ 0.046	¹⁸² 1.000	¹⁸⁰ 0.999	¹⁷⁸ 0.991	¹⁵⁶ 0.104	¹⁶⁰ 0.054	⁹⁸ 0.398	¹⁰⁷ 0.259	¹³⁹ 0.511	¹⁵³ 0.316														
283	VISIONBOX-000	¹³³ 0.073	⁹³ 0.018	⁸⁹ 0.007	⁸¹ 0.071	⁹¹ 0.057	⁹⁶ 0.035	¹²¹ 0.995	¹³⁰ 0.990	¹⁵⁹ 0.974	⁷⁶ 0.023	⁷⁸ 0.012	⁵⁵ 0.146	⁶³ 0.081	⁵³ 0.162	⁵⁹ 0.126														
284	VISIONLABS-004	¹⁴⁵ 0.091	¹⁷⁹ 0.058	¹⁷¹ 0.024	¹⁸⁰ 0.199	¹⁹⁷ 0.159	¹⁹⁸ 0.097	⁶⁸ 0.944	⁷² 0.890	⁹² 0.742																				
285	VISIONLABS-005	¹⁴¹ 0.080	¹⁶³ 0.050	¹³⁵ 0.020	¹⁷⁰ 0.183	¹⁸⁷ 0.147	¹⁸⁷ 0.087	⁶⁹ 0.945	⁷¹ 0.888	⁹¹ 0.736																				
286	VISIONLABS-006	⁹³ 0.044	¹²³ 0.027	¹¹⁷ 0.010	¹²⁷ 0.117	¹³⁵ 0.090	¹³⁰ 0.051	⁴¹ 0.764	⁴⁶ 0.672	⁶² 0.511																				
287	VISIONLABS-007	⁹² 0.044	¹²² 0.027	¹¹⁴ 0.010	¹²² 0.117	¹³⁴ 0.090	¹²⁹ 0.051	⁴⁰ 0.764	⁴⁷ 0.672	⁶¹ 0.511	⁹⁵ 0.031	⁹¹ 0.014																		
288	VISIONLABS-008	⁶⁶ 0.028	⁷³ 0.013	⁷² 0.006	⁷⁴ 0.068	⁷⁷ 0.051	⁸³ 0.032	²⁵ 0.574	³¹ 0.481	⁴² 0.317	⁵⁷ 0.017	⁵³ 0.008																		
289	VISIONLABS-009	³⁴ 0.012	³² 0.005	²⁶ 0.002	³¹ 0.032	³⁴ 0.025	³⁸ 0.017	⁶⁴ 0.930	⁶¹ 0.799	³¹ 0.196	³⁷ 0.008	³⁵ 0.004																		
290	VISIONLABS-010	⁴¹ 0.014	³⁸ 0.005	³⁶ 0.002	³⁵ 0.034	³⁹ 0.027	⁴⁴ 0.019				²³ 0.169	³⁰ 0.008	²² 0.004	²² 0.055	²² 0.027	²⁶ 0.109	²⁶ 0.089													
291	VISIONLABS-011	³² 0.011	²⁴ 0.003	¹⁸ 0.002	²⁵ 0.024	²⁹ 0.020	²⁵ 0.014				³⁶ 0.194	¹⁵ 0.004	¹¹ 0.002	¹³ 0.034	¹³ 0.017	¹⁰ 0.090	¹⁵ 0.079													
292	VNPPT-001	⁶⁵ 0.027	⁷⁷ 0.014	⁸² 0.006	¹⁶³ 0.158	¹⁰⁷ 0.068	⁹⁷ 0.036	⁶⁰ 0.922	⁵² 0.718	⁵⁰ 0.373	¹⁰⁴ 0.035	⁷³ 0.011	¹¹⁷ 0.990	¹¹³ 0.537	¹¹¹ 0.362	⁶⁵ 0.134														
293	VNPPT-002	³⁸ 0.013	⁴⁵ 0.007	⁵⁶ 0.003	⁴⁷ 0.040	⁴⁷ 0.032	³¹ 0.021	²⁴ 0.568	¹⁷ 0.292	²² 0.154	²⁷ 0.007	²² 0.004	³¹ 0.072	²⁹ 0.031	¹² 0.096	¹² 0.075														
294	VOCORD-003	²⁴² 0.354	²²³ 0.122	²¹⁶ 0.048	¹⁸¹ 0.195	¹⁹³ 0.155	¹⁹³ 0.093	¹⁶³ 0.999	¹⁷⁰ 0.998	¹⁷⁶ 0.991	¹⁷² 0.157	¹⁸³ 0.105																		
295	VOCORD-004	²⁸³ 0.826	²⁶⁷ 0.355	²¹⁷ 0.051	²³⁵ 0.401	²⁰⁵ 0.173	¹⁹¹ 0.093	²²⁶ 1.000	²¹⁵ 1.000	²²⁹ 0.999	¹⁸⁰ 0.193	¹⁶⁴ 0.065																		
296	VOCORD-005	²⁷⁶ 0.689	²³⁷ 0.158	²⁰⁹ 0.044	¹⁶⁷ 0.161	¹⁷⁸ 0.130	¹⁸⁰ 0.080	¹⁶⁹ 0.999	¹⁶² 0.997	¹⁴⁶ 0.968	¹⁶⁶ 0.138	¹⁷⁷ 0.090																		
297	VOCORD-006	³⁰⁸ 1.000	³⁰⁹ 1.000	²⁹⁹ 1.000	³⁰⁸ 1.000	²⁹⁹ 1.000	²⁷⁰ 1.000	²⁷⁷ 1.000	²⁶⁶ 1.000	²⁵³ 1.000	²⁷⁵ 1.000																			
298	VTS-000	²⁶⁸ 0.605	²⁸⁴ 0.598	²⁹⁹ 0.595	²⁵⁷ 0.624	²⁷⁷ 0.619	²⁸⁴ 0.613	¹⁷⁸ 0.999	¹⁹⁰ 0.999	²²⁰ 0.998	²¹⁰ 0.613	²¹² 0.609	¹¹⁰ 0.760	¹¹⁹ 0.739	¹⁶ 0.761	¹⁹⁷ 0.749														
299	VTS-001	⁷⁷ 0.035	⁷⁴ 0.013	⁷³ 0.006	⁷³ 0.067	⁷⁶ 0.051	⁷⁷ 0.031	¹⁵⁰ 0.998	¹³⁹ 0.994	⁶⁰ 0.510	⁷⁴ 0.022	⁷⁹ 0.012	³² 0.141	⁶² 0.079	⁶⁸ 0.192	⁶⁰ 0.126														
300	VTS-002	¹¹¹ 0.053	¹¹⁸ 0.026	¹¹⁸ 0.010	¹⁰⁸ 0.098	¹¹⁹ 0.075	¹²⁰ 0.046	¹⁹⁵ 1.000	²⁰⁰ 1.000	¹³⁹ 0.953	¹¹⁸ 0.045	¹²² 0.026	⁸⁰ 0.231	⁸⁹ 0.133	¹² 0.417	¹⁰¹ 0.187														
301	VTS-003	⁴³ 0.015	⁵⁰ 0.007	⁴⁷ 0.003	⁵⁰ 0.048	⁵¹ 0.033	⁴⁶ 0.019	²²⁴ 1.000	²²⁰ 1.000	⁷⁹ 0.632	⁵² 0.014	⁴¹ 0.005	¹¹⁴ 0.954	⁴⁸ 0.060	¹⁵⁵ 0.635	²⁷ 0.089														
302	XFORWARDAI-000	⁶⁸ 0.029	⁸³ 0.015	⁸⁴ 0.006	⁷⁸ 0.070	⁸⁸ 0.053	⁹⁴ 0.034	³⁷ 0.698	²⁶ 0.440	³⁴ 0.250	⁷⁰ 0.021	⁶⁸ 0.011	⁶¹ 0.159	⁶⁶ 0.082	⁵⁶ 0.169	⁶⁴ 0.134														
303	XFORWARDAI-001	²⁷ 0.010	³⁶ 0.005	⁴⁴ 0.003	³⁷ 0.036	⁴² 0.028	⁴⁷ 0.020	⁵⁰ 0.838	²⁷ 0.448	¹⁵ 0.143	³³ 0.008	⁴² 0.005	²⁶ 0.062	²⁷ 0.030	³¹ 0.123	³⁸ 0.102														
304	XFORWARDAI-002	¹⁷ 0.007	²⁵ 0.003	³¹ 0.002	¹⁷ 0.018	¹⁷ 0.016	²⁴ 0.014	⁷⁹ 0.975	³⁴ 0.525	⁴ 0.095	¹⁷ 0.005	¹⁹ 0.003	¹⁶ 0.041	¹⁵ 0.018	²⁰ 0.099	²⁵ 0.089														
305	YISHENG-001	²⁵³ 0.452	²⁶⁴ 0.346	²⁷⁰ 0.206	²⁸⁷ 0.983	²⁸⁸ 0.808	²⁵⁹ 0.269				²¹² 0.666	²⁰⁸ 0.396																		
306	YITU-002	⁷² 0.031	⁹¹ 0.018	⁹⁴ 0.008	⁶ 0.063	⁷¹ 0.049	⁷² 0.028																							
307	YITU-003		⁷³ 0.032	⁹⁹ 0.019	¹⁰² 0.009	⁷¹ 0.067	⁸⁰ 0.052	⁸⁹ 0.033																						
308	YITU-004		⁴⁷ 0.019	⁵⁷ 0.010	⁶¹ 0.004	³⁶ 0.035	³⁷ 0.027	³⁹ 0.017	⁷² 0.948	⁸⁰ 0.936	¹¹⁷ 0.913																			
309	YITU-005		⁵¹ 0.022	⁶⁴ 0.010	⁶⁷ 0.005	⁴¹ 0.039	⁴⁹ 0.032	⁵⁷ 0.023																						

2022 / 09 / 26
18:06:18FNIR(N, R, T) = False neg. identification rate
FPIR(N, T) = False pos.

Appendices

Appendix A Accuracy on large-population FRVT 2018 mugshots

2022/09/26 18:06:18	$\text{FNIR}(N, R, T) =$ $\text{FPTR}(N, T) =$	False neg. identification rate False pos. identification rate	$N =$ Num. enrolled subjects $R =$ Num. candidates examined	$T =$ Threshold $T > 0 \rightarrow$ Identification	$T = 0 \rightarrow$ Investigation
------------------------	---	--	--	---	-----------------------------------

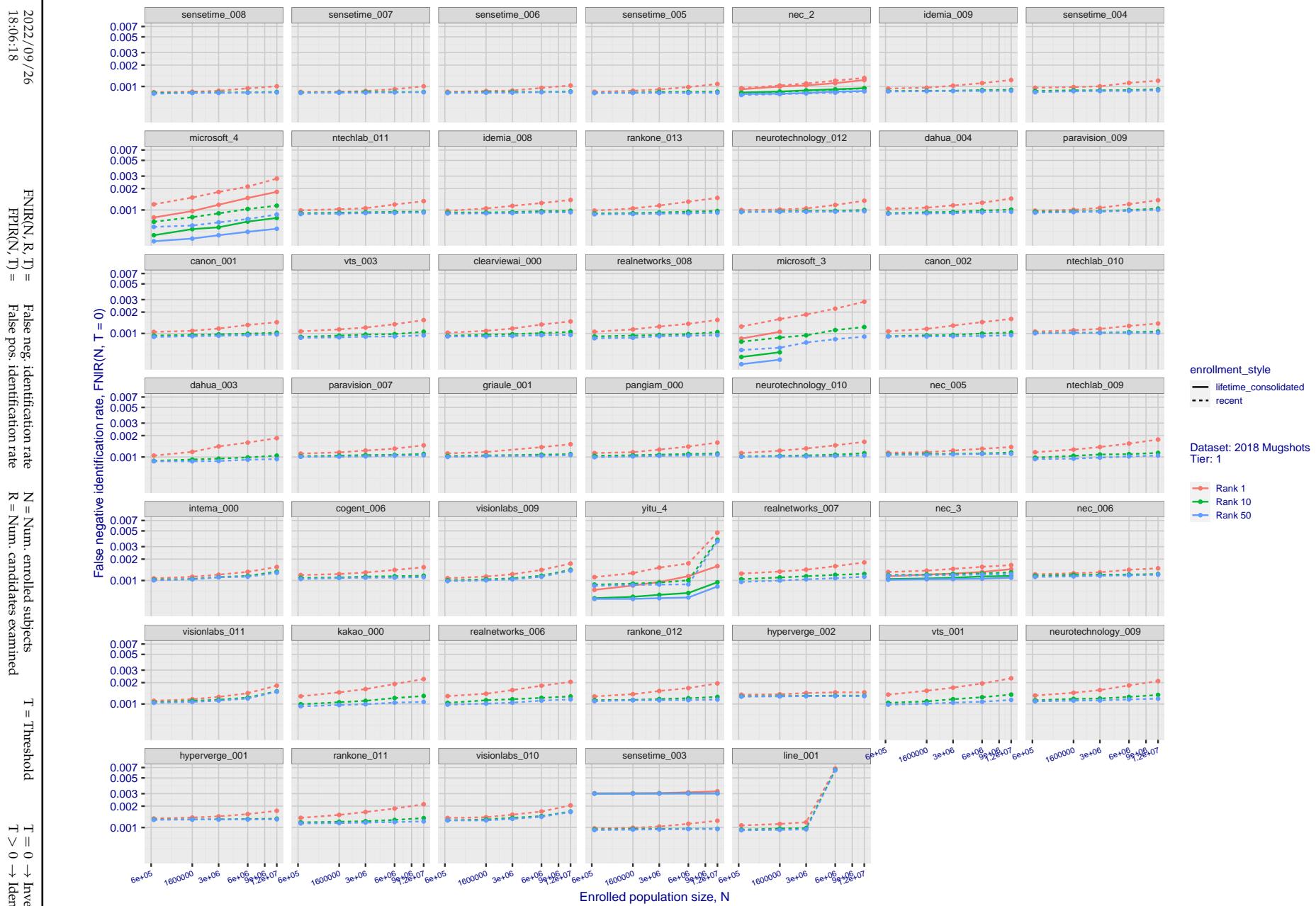


Figure 20: [FRVT-2018 Mugshot Dataset] Rank-based identification miss rates vs. number of enrolled subjects. The figure shows false negative identification rates, $\text{FNIR}(N, R)$, across various gallery sizes and ranks 1, 10 and 50. The threshold is set to zero, so this metric rewards even weak scoring rank 1 mates. This also means $\text{FPIR} = 1$, so any search without an enrolled mate will return non-mated candidates. For clarity, results are sorted and reported into tiers spanning multiple pages, the tiering criteria being rank 1 hit rate on a gallery size of 640 000.

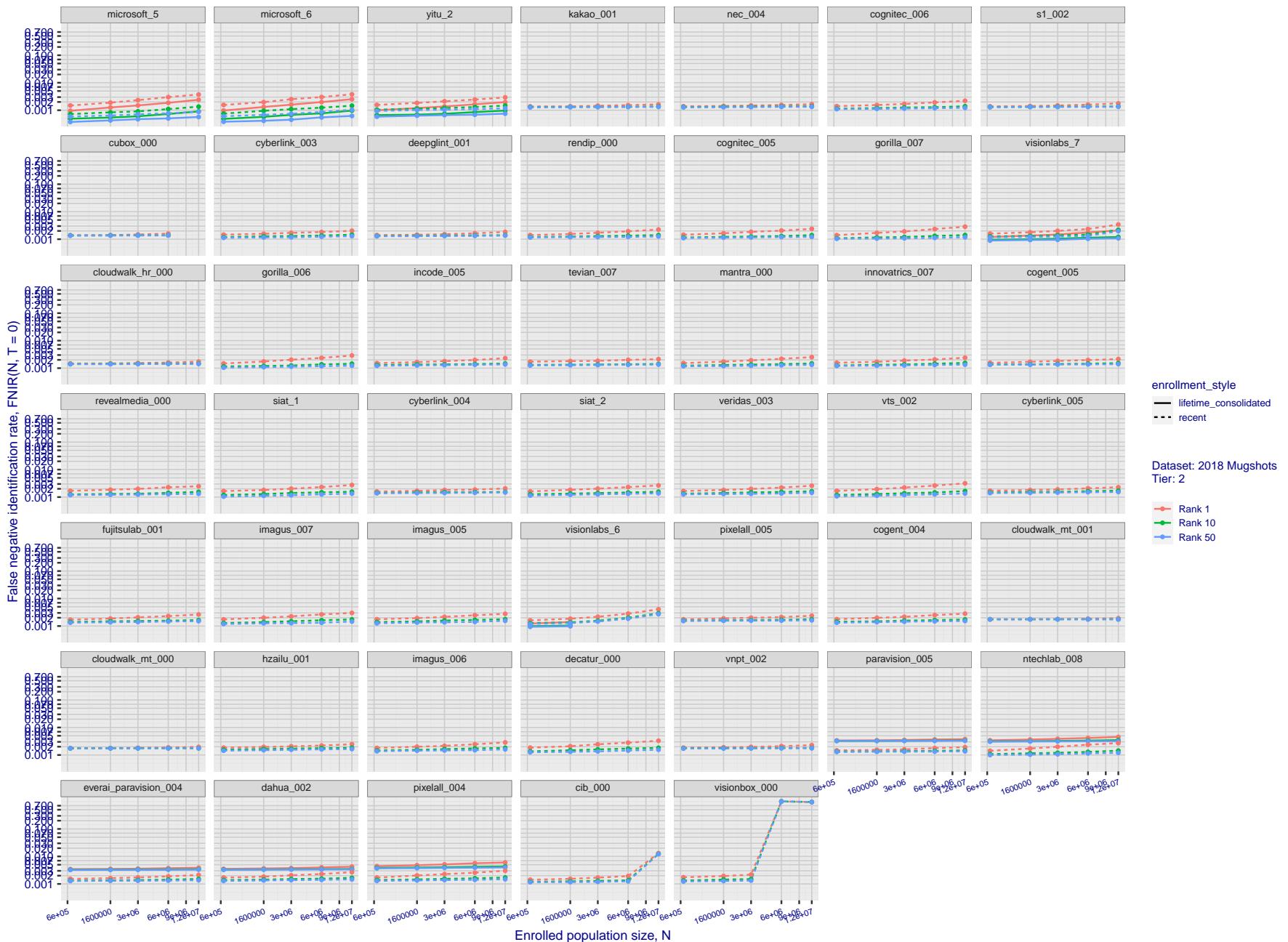


Figure 21: [FRVT-2018 Mugshot Dataset] Rank-based identification miss rates vs. number of enrolled subjects. The figure shows false negative identification rates, $\text{FNIR}(N, R)$, across various gallery sizes and ranks 1, 10 and 50. The threshold is set to zero, so this metric rewards even weak scoring rank 1 mates. This also means $\text{FPIR} = 1$, so any search without an enrolled mate will return non-mated candidates. For clarity, results are sorted and reported into tiers spanning multiple pages, the tiering criteria being rank 1 hit rate on a gallery size of 640 000.

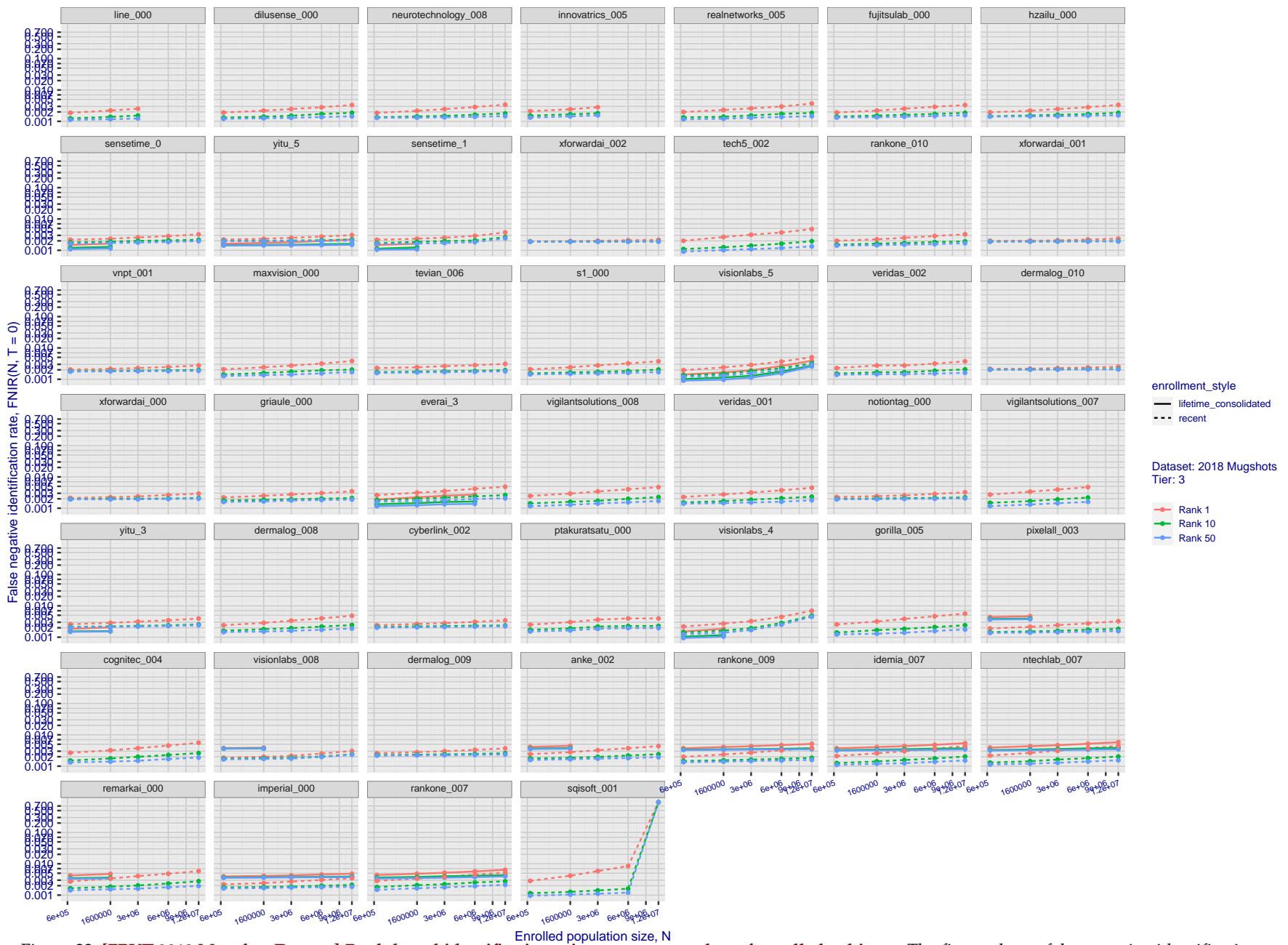


Figure 22: [FRVT-2018 Mugshot Dataset] Rank-based identification miss rates vs. number of enrolled subjects. The figure shows false negative identification rates, FNIR(N, R), across various gallery sizes and ranks 1, 10 and 50. The threshold is set to zero, so this metric rewards even weak scoring rank 1 mates. This also means FPIR = 1, so any search without an enrolled mate will return non-mated candidates. For clarity, results are sorted and reported into tiers spanning multiple pages, the tiering criteria being rank 1 hit rate on a gallery size of 640 000.

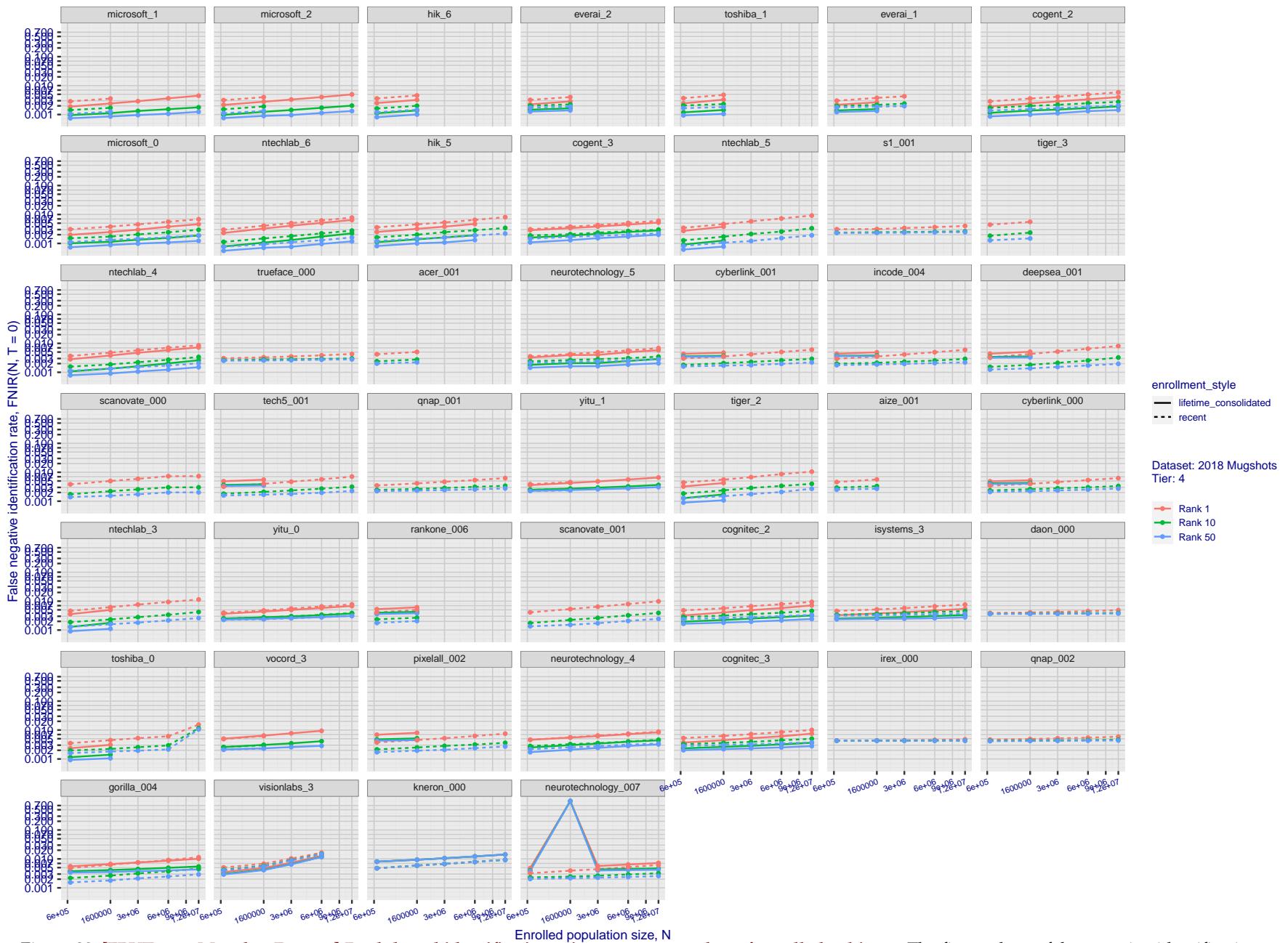


Figure 23: [FRVT-2018 Mugshot Dataset] Rank-based identification miss rates vs. number of enrolled subjects. The figure shows false negative identification rates, $\text{FNIR}(N, R)$, across various gallery sizes and ranks 1, 10 and 50. The threshold is set to zero, so this metric rewards even weak scoring rank 1 mates. This also means $\text{FPIR} = 1$, so any search without an enrolled mate will return non-mated candidates. For clarity, results are sorted and reported into tiers spanning multiple pages, the tiering criteria being rank 1 hit rate on a gallery size of 640 000.

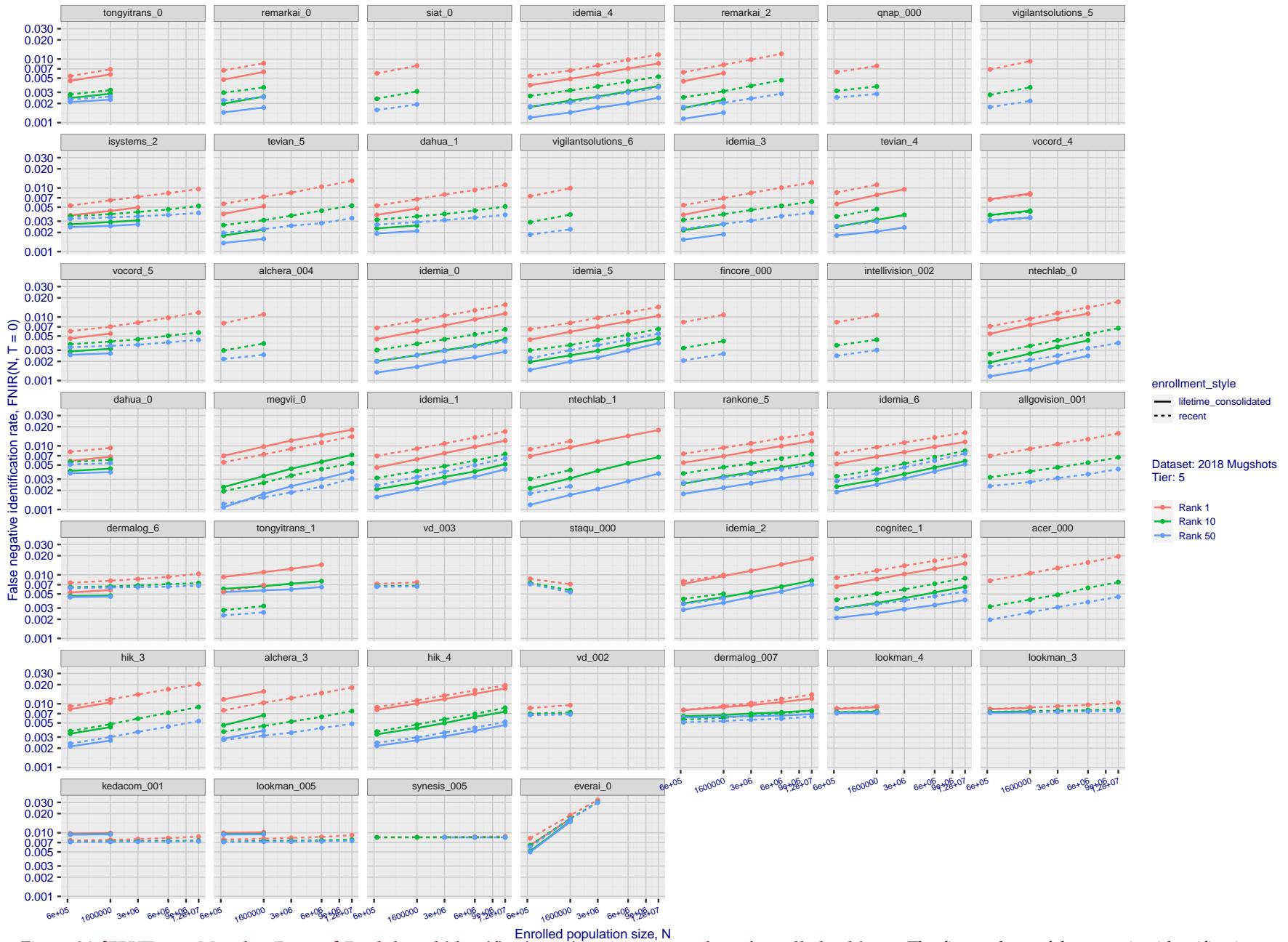
2022/09/26
18:06:18FNIR(N, R, T) = False neg. identification rate
FPIR(N, T) = False pos. identification rateN = Num. enrolled subjects
R = Num. candidates examinedT = Threshold
T = 0 → Investigation
T > 0 → Identification

Figure 24: [FRVT-2018 Mugshot Dataset] Rank-based identification miss rates vs. number of enrolled subjects. The figure shows false negative identification rates, $\text{FNIR}(N, R)$, across various gallery sizes and ranks 1, 10 and 50. The threshold is set to zero, so this metric rewards even weak scoring rank 1 mates. This also means $\text{FPIR} = 1$, so any search without an enrolled mate will return non-mated candidates. For clarity, results are sorted and reported into tiers spanning multiple pages, the tiering criteria being rank 1 hit rate on a gallery size of 640 000.

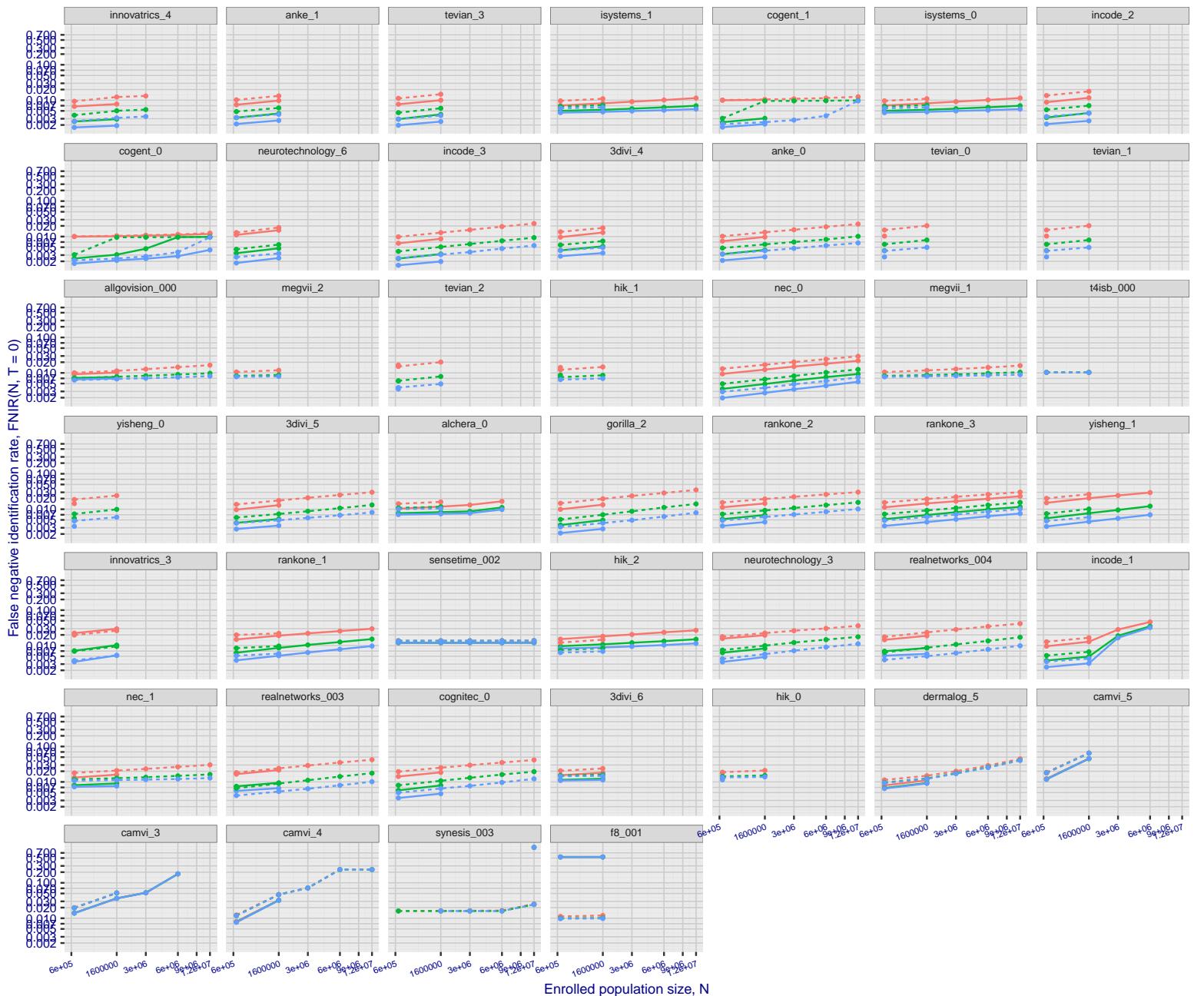


Figure 25: [FRVT-2018 Mugshot Dataset] Rank-based identification miss rates vs. number of enrolled subjects. The figure shows false negative identification rates, $\text{FNIR}(N, R)$, across various gallery sizes and ranks 1, 10 and 50. The threshold is set to zero, so this metric rewards even weak scoring rank 1 mates. This also means $\text{FPIR} = 1$, so any search without an enrolled mate will return non-mated candidates. For clarity, results are sorted and reported into tiers spanning multiple pages, the tiering criteria being rank 1 hit rate on a gallery size of 640 000.

2022 / 09 / 26

18:06:18

 $\text{FNIR}(N, R, T) = \text{False neg. identification rate}$ $N = \text{Num. enrolled subjects}$ $T = \text{Threshold}$ $R = \text{Num. candidates examined}$ $\text{FPIR}(N, T) = \text{False pos. identification rate}$ $T = 0 \rightarrow \text{Investigation}$ $T > 0 \rightarrow \text{Identification}$

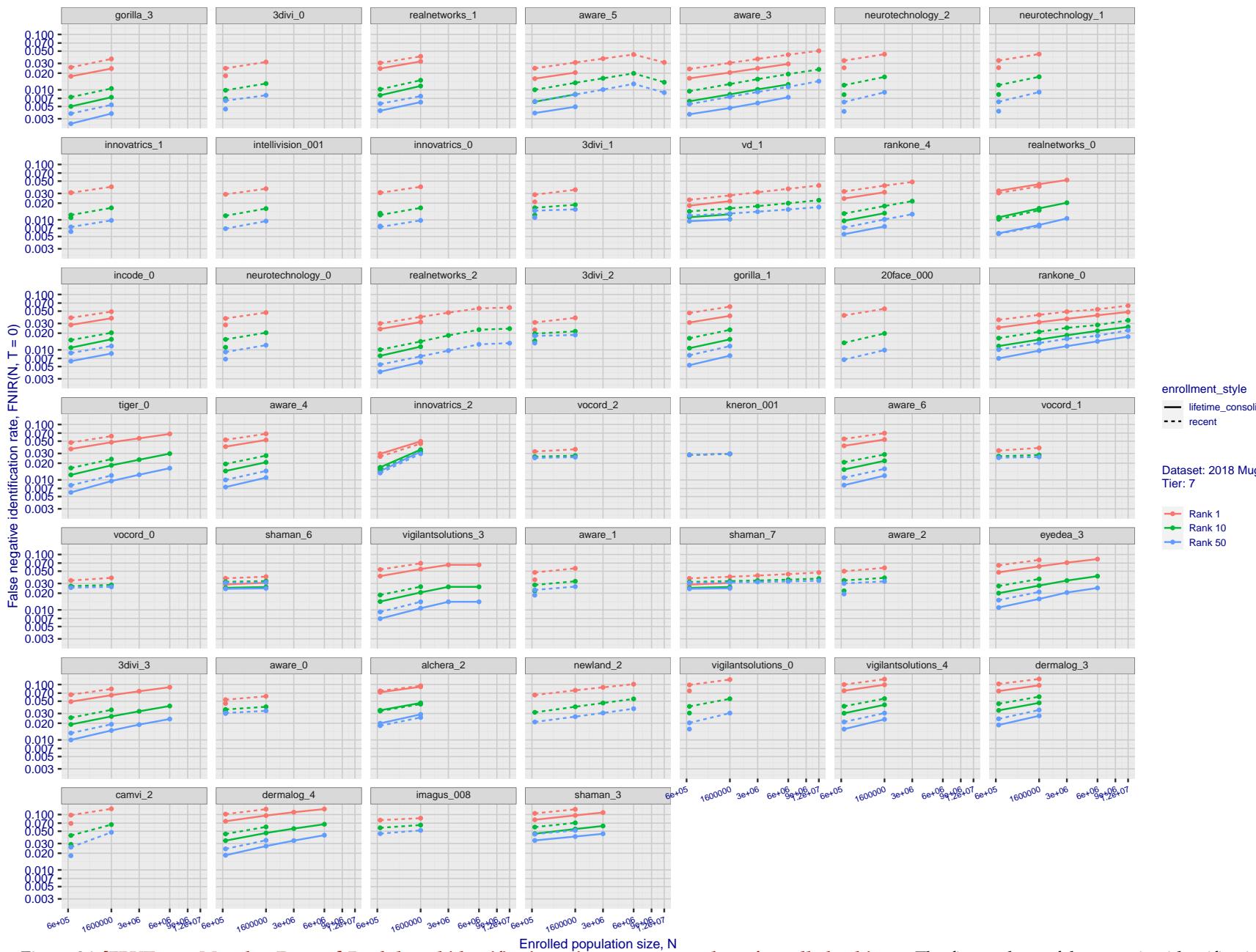


Figure 26: [FRVT-2018 Mugshot Dataset] Rank-based identification miss rates vs. number of enrolled subjects. The figure shows false negative identification rates, $\text{FNIR}(N, R)$, across various gallery sizes and ranks 1, 10 and 50. The threshold is set to zero, so this metric rewards even weak scoring rank 1 mates. This also means $\text{FPIR} = 1$, so any search without an enrolled mate will return non-mated candidates. For clarity, results are sorted and reported into tiers spanning multiple pages, the tiering criteria being rank 1 hit rate on a gallery size of 640 000.

2022/09/26
18:06:18FNIR(N, R, T) =
False neg. identification rate
FPIR(N, T) =
False pos. identification rateN = Num. enrolled subjects
R = Num. candidates examined

T = Threshold

T = 0 → Investigation
 $T > 0 \rightarrow$ Identification

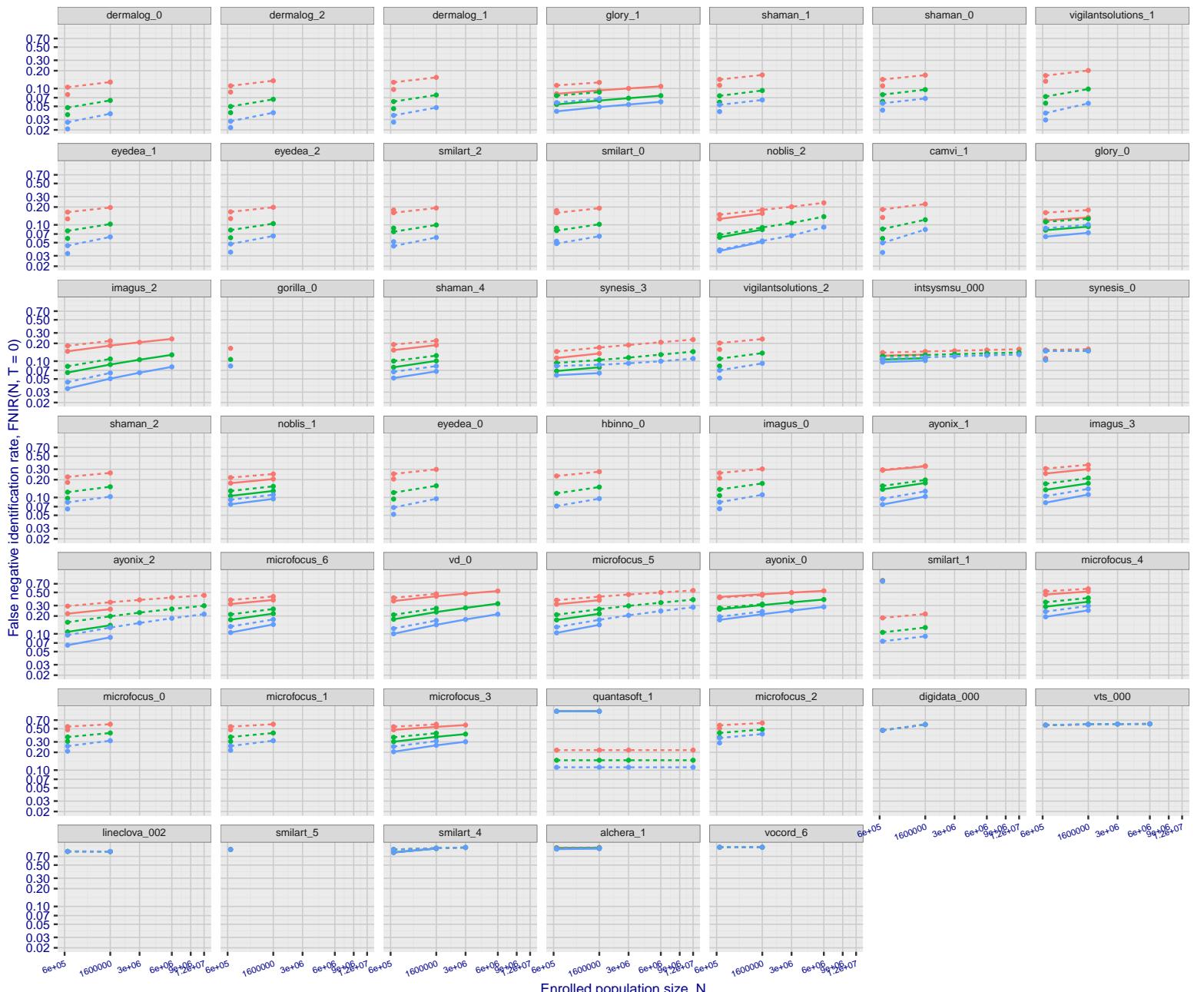


Figure 27: [FRVT-2018 Mugshot Dataset] Rank-based identification miss rates vs. number of enrolled subjects. The figure shows false negative identification rates, FNIR(N, R), across various gallery sizes and ranks 1, 10 and 50. The threshold is set to zero, so this metric rewards even weak scoring rank 1 mates. This also means FPIR = 1, so any search without an enrolled mate will return non-mated candidates. For clarity, results are sorted and reported into tiers spanning multiple pages, the tiering criteria being rank 1 hit rate on a gallery size of 640 000.

2022/09/26 18:06:18	$\text{FNIR}(N, R, T) =$ $\text{FPTR}(N, T) =$	False neg. identification rate False pos. identification rate	$N =$ Num. enrolled subjects $R =$ Num. candidates examined	$T =$ Threshold $T > 0 \rightarrow$ Identification	$T = 0 \rightarrow$ Investigation
------------------------	---	--	--	---	-----------------------------------

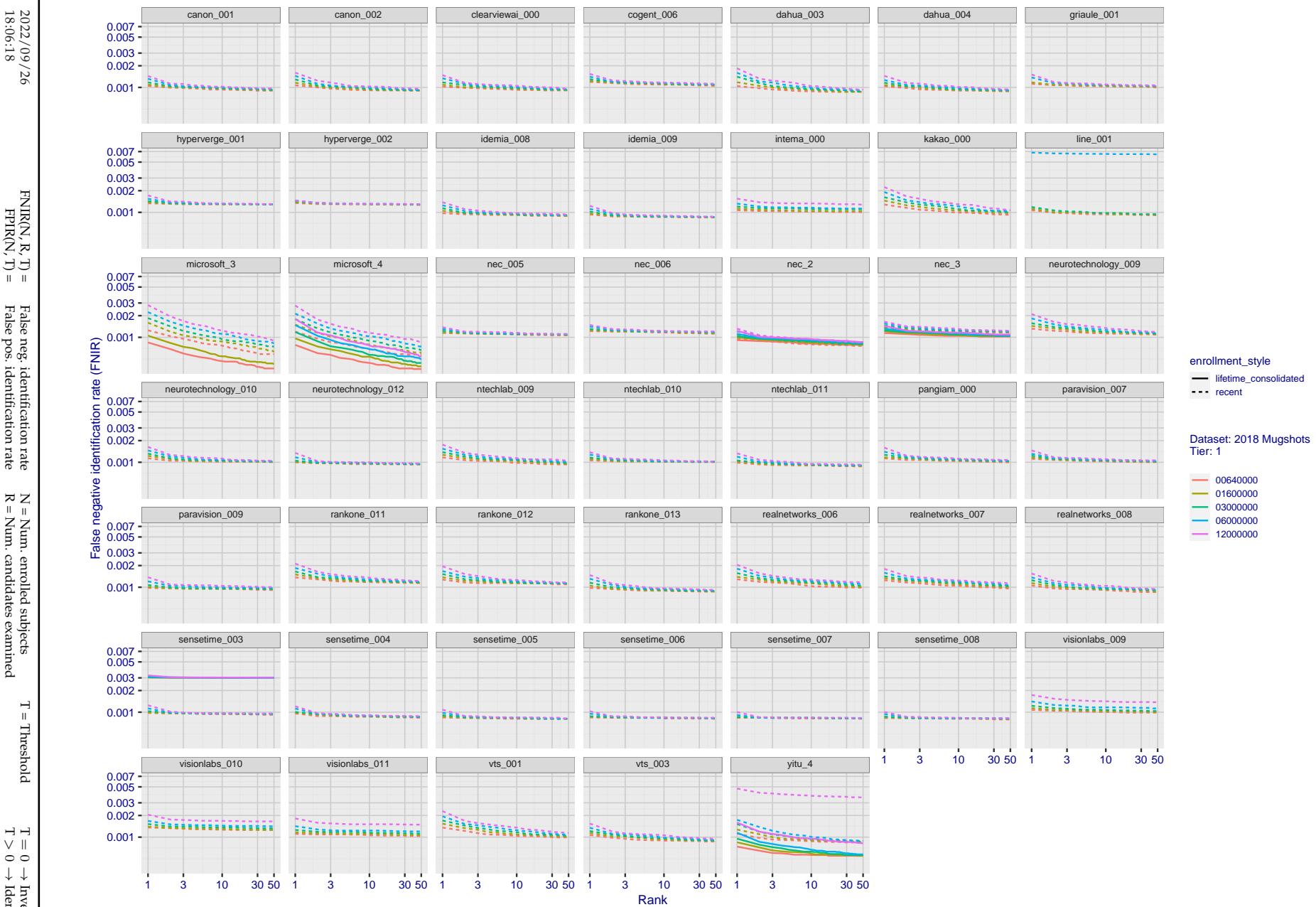


Figure 28: [FRVT-2018 Mugshot Dataset] Rank-based identification miss rates vs. rank. The figure shows false negative identification rates (FNIR) for ranks up to 50. This metric is appropriate to investigational applications where human reviewers will adjudicate sorted candidate lists. Note that with threshold set to zero, FPIR = 1, i.e. any search without an enrolled mate will return non-mated candidates. Results are sorted and reported into tiers for clarity, with the tiering criteria being rank 1 hit rate on a gallery size of $N = 640\,000$ subjects.

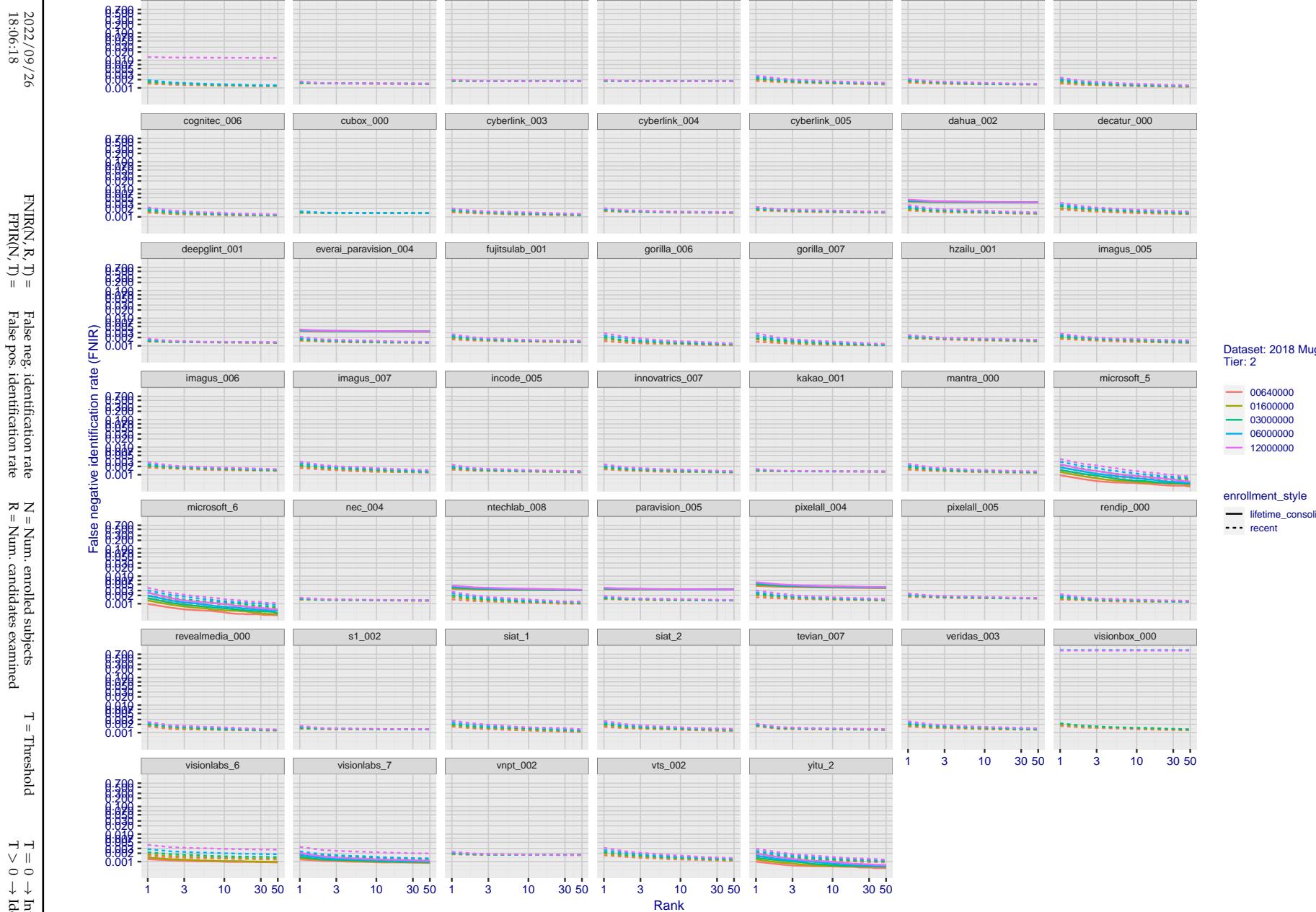


Figure 29: [FRVT-2018 Mugshot Dataset] Rank-based identification miss rates vs. rank. The figure shows false negative identification rates (FNIR) for ranks up to 50. This metric is appropriate to investigational applications where human reviewers will adjudicate sorted candidate lists. Note that with threshold set to zero, FPIR = 1, i.e. any search without an enrolled mate will return non-mated candidates. Results are sorted and reported into tiers for clarity, with the tiering criteria being rank 1 hit rate on a gallery size of N = 640 000 subjects.

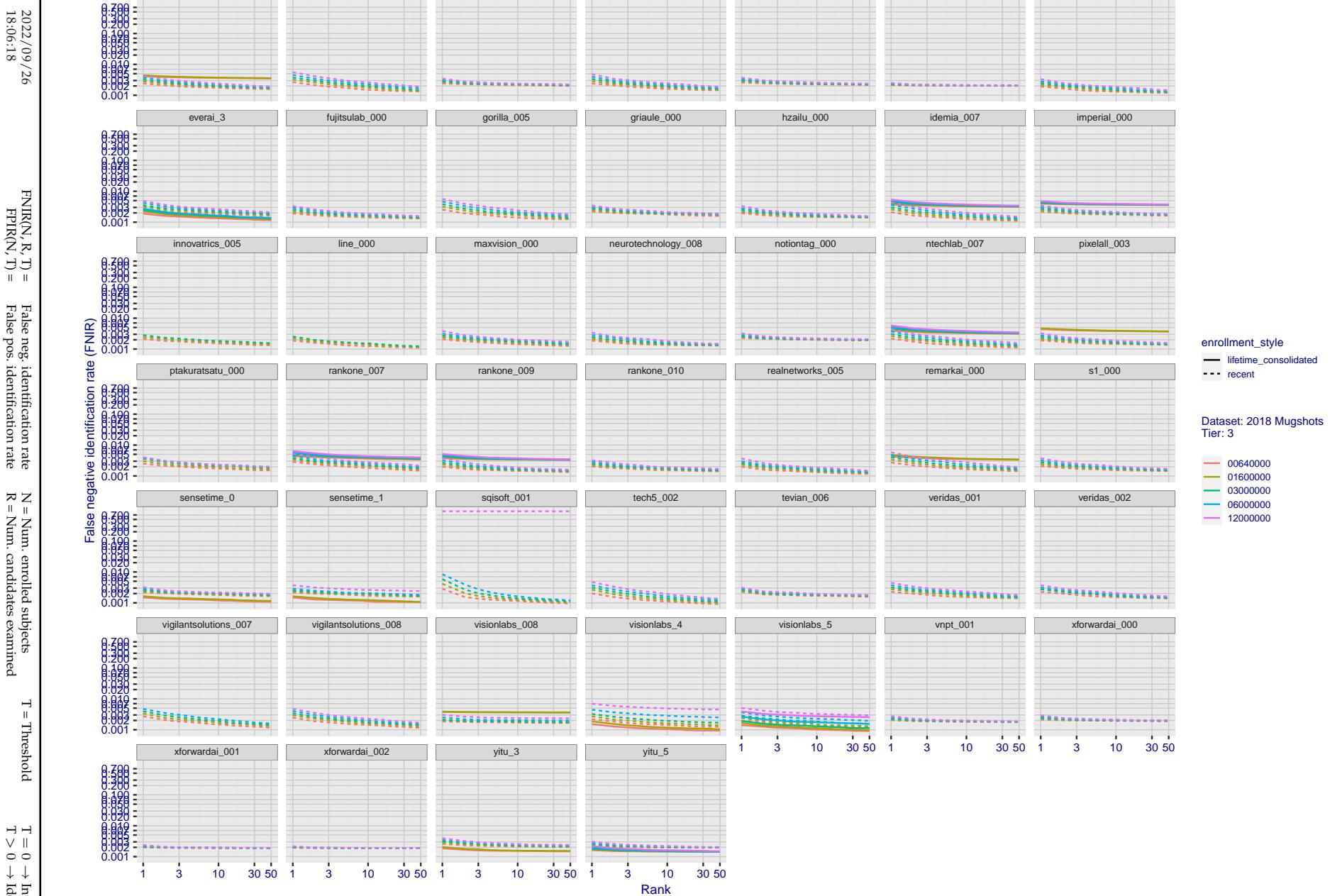


Figure 30: [FRVT-2018 Mugshot Dataset] Rank-based identification miss rates vs. rank. The figure shows false negative identification rates (FNIR) for ranks up to 50. This metric is appropriate to investigational applications where human reviewers will adjudicate sorted candidate lists. Note that with threshold set to zero, FPIR = 1, i.e. any search without an enrolled mate will return non-mated candidates. Results are sorted and reported into tiers for clarity, with the tiering criteria being rank 1 hit rate on a gallery size of N = 640 000 subjects.

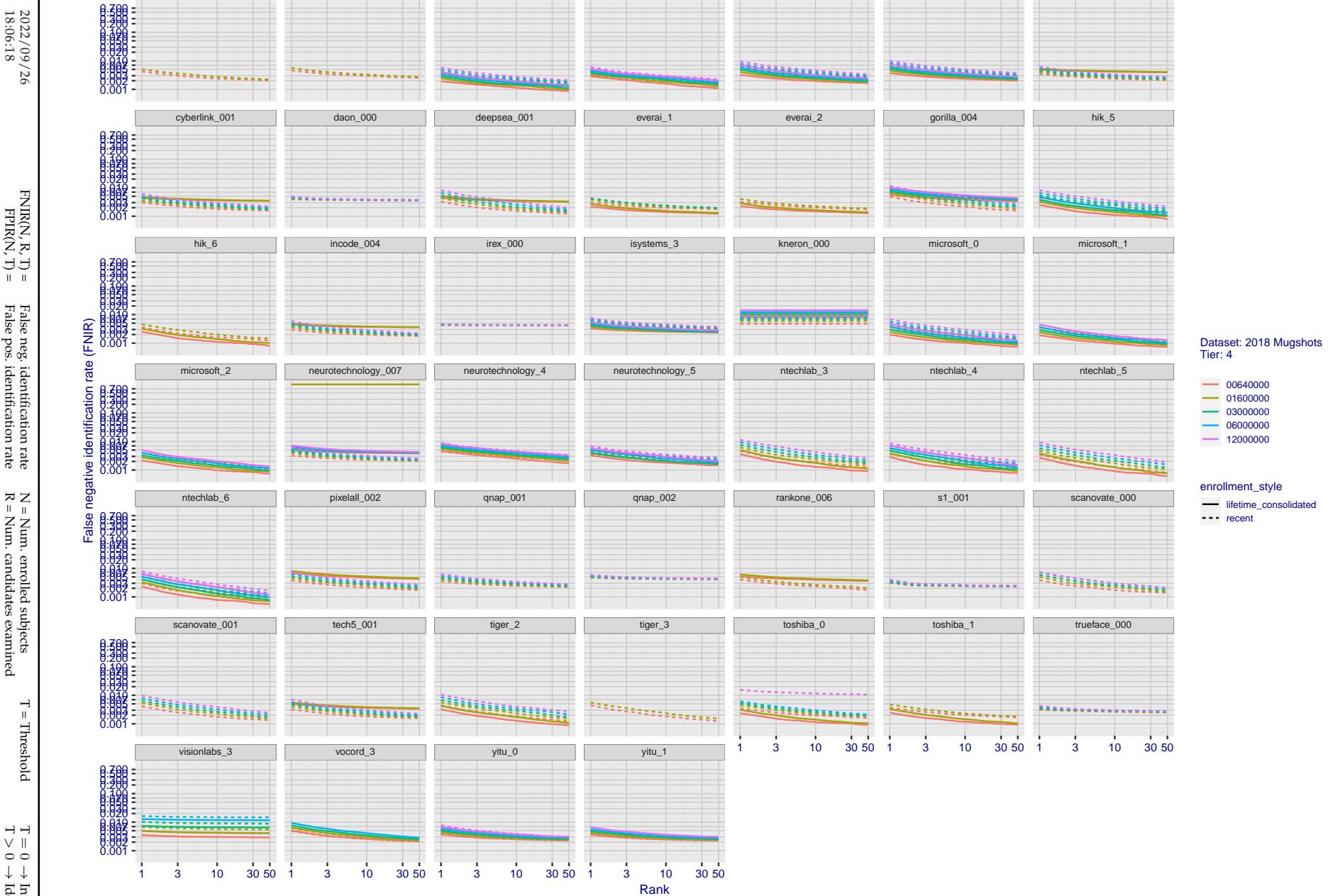


Figure 31: [FRVT-2018 Mugshot Dataset] Rank-based identification miss rates vs. rank. The figure shows false negative identification rates (FNIR) for ranks up to 50. This metric is appropriate to investigational applications where human reviewers will adjudicate sorted candidate lists. Note that with threshold set to zero, FPIR = 1, i.e. any search without an enrolled mate will return non-mated candidates. Results are sorted and reported into tiers for clarity, with the tiering criteria being rank 1 hit rate on a gallery size of N = 640 000 subjects.

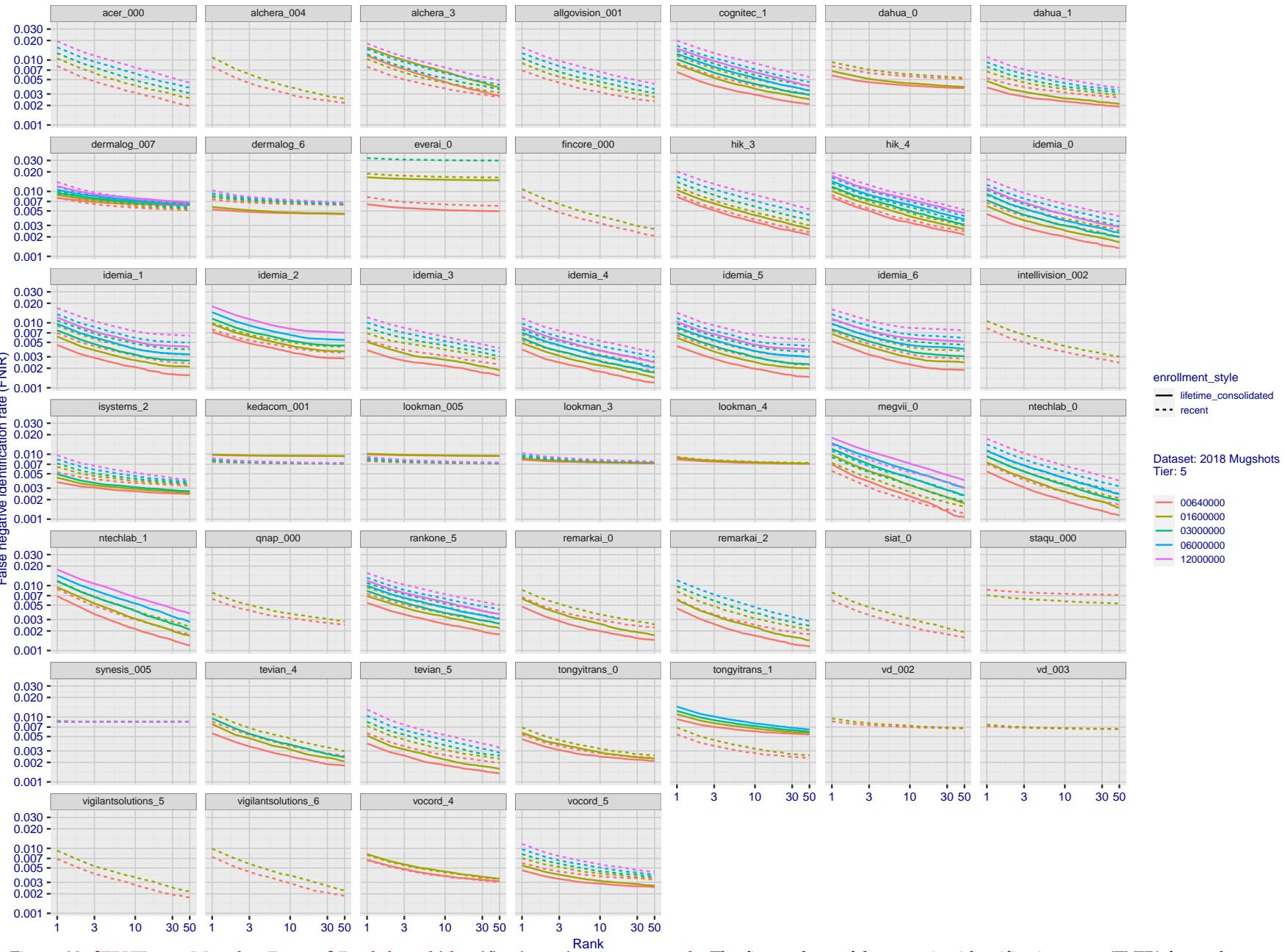
2022 / 09 / 26
18:06:18FNIR(N, R, T) = False neg. identification rate
FPIR(N, T) = False pos. identification rateN = Num. enrolled subjects
R = Num. candidates examined
T = ThresholdT = 0 → Investigation
 $T > 0 \rightarrow$ Identification

Figure 32: [FRVT-2018 Mugshot Dataset] Rank-based identification miss rates vs. rank. The figure shows false negative identification rates (FNIR) for ranks up to 50. This metric is appropriate to investigational applications where human reviewers will adjudicate sorted candidate lists. Note that with threshold set to zero, FPIR = 1, i.e. any search without an enrolled mate will return non-mated candidates. Results are sorted and reported into tiers for clarity, with the tiering criteria being rank 1 hit rate on a gallery size of N = 640 000 subjects.

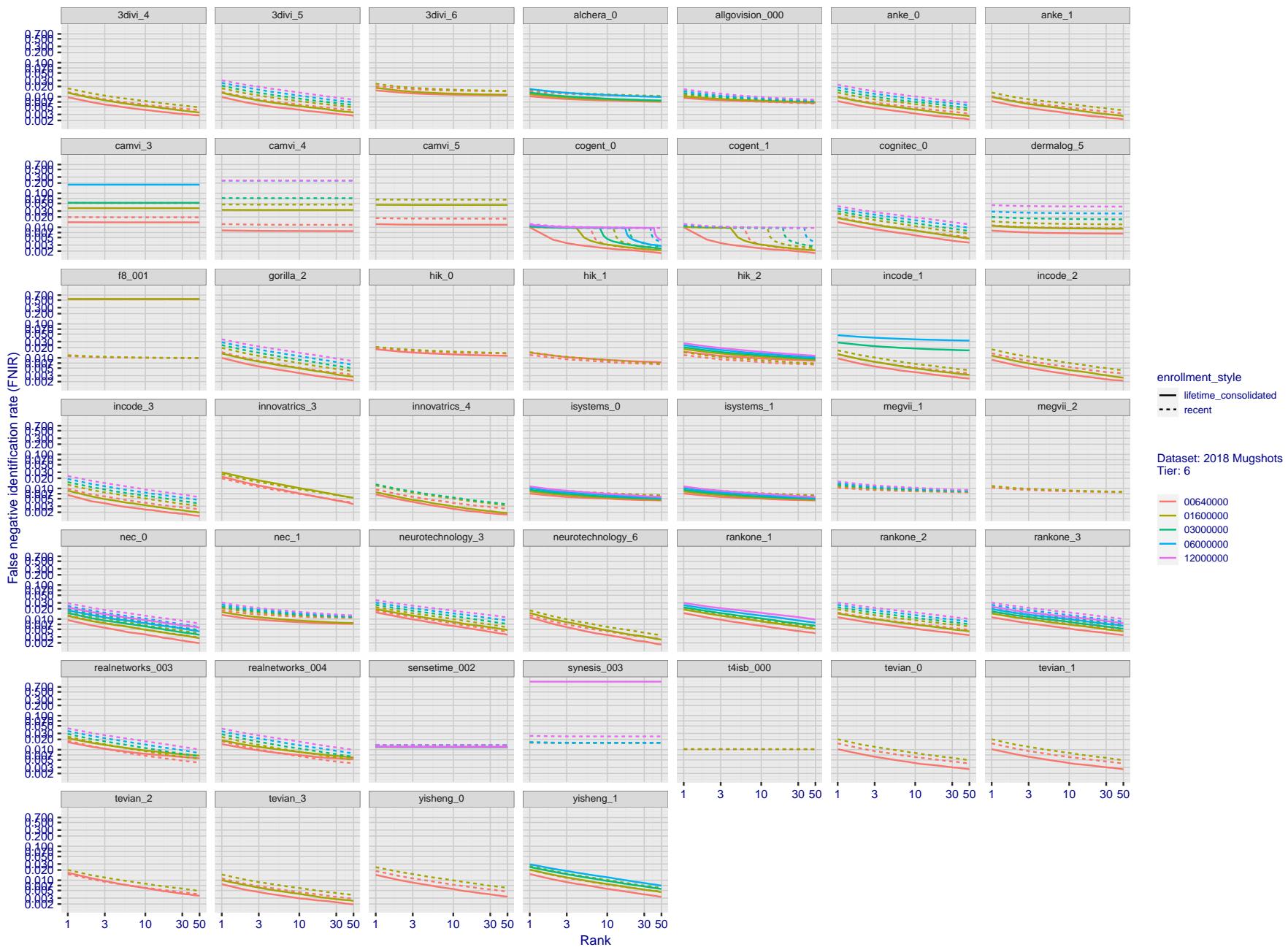


Figure 33: [FRVT-2018 Mugshot Dataset] Rank-based identification miss rates vs. rank. The figure shows false negative identification rates (FNIR) for ranks up to 50. This metric is appropriate to investigational applications where human reviewers will adjudicate sorted candidate lists. Note that with threshold set to zero, FPIR = 1, i.e. any search without an enrolled mate will return non-mated candidates. Results are sorted and reported into tiers for clarity, with the tiering criteria being rank 1 hit rate on a gallery size of $N = 640\,000$ subjects.

2022/09/26
18:06:18FNIR(N, R, T) = False neg. identification rate
FPIR(N, T) = False pos. identification rate N = Num. enrolled subjects
 R = Num. candidates examined T = Threshold $T = 0 \rightarrow$ Investigation
 $T > 0 \rightarrow$ Identification

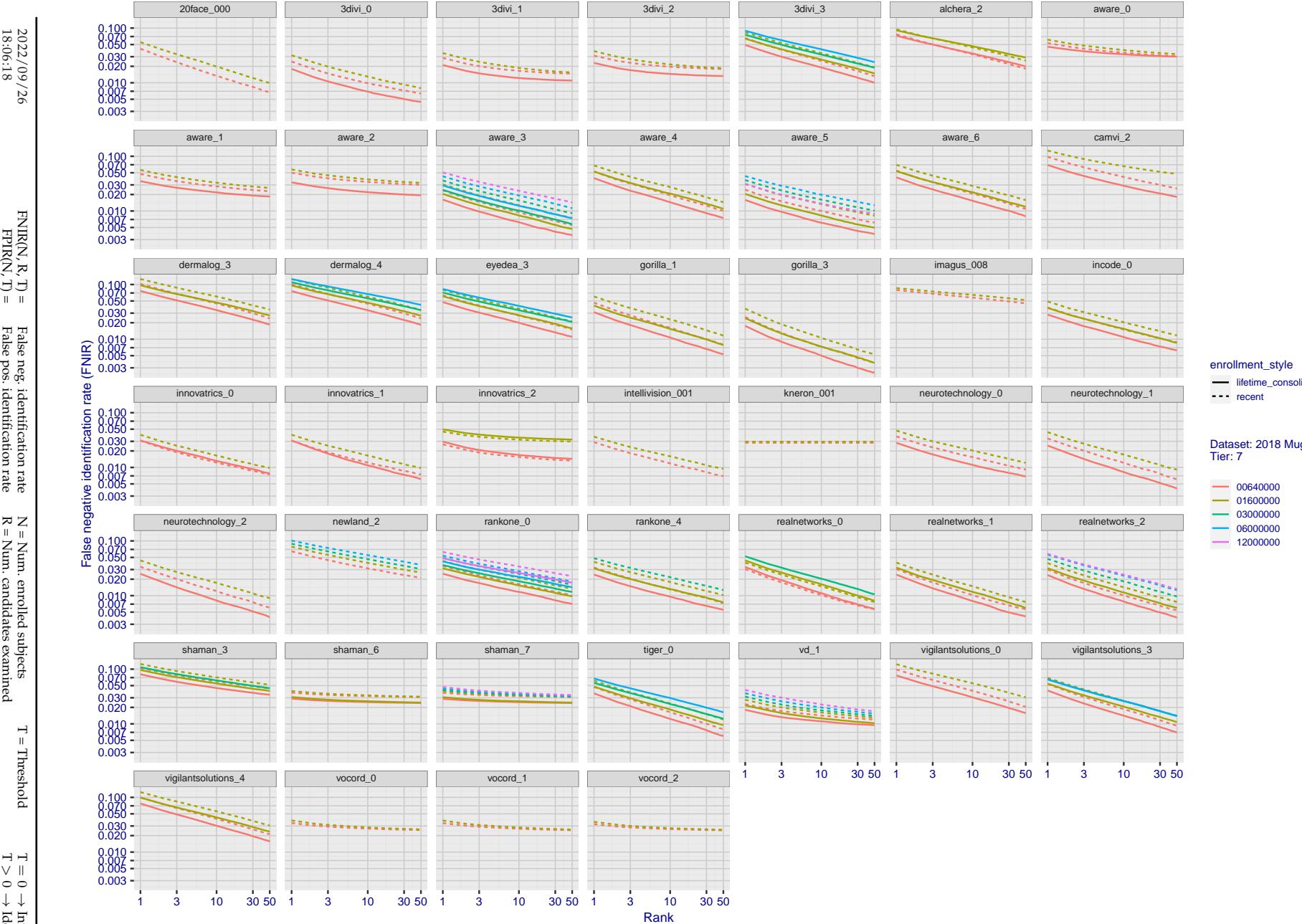


Figure 34: [FRVT-2018 Mugshot Dataset] Rank-based identification miss rates vs. rank. The figure shows false negative identification rates (FNIR) for ranks up to 50. This metric is appropriate to investigational applications where human reviewers will adjudicate sorted candidate lists. Note that with threshold set to zero, FPIR = 1, i.e. any search without an enrolled mate will return non-mated candidates. Results are sorted and reported into tiers for clarity, with the tiering criteria being rank 1 hit rate on a gallery size of N = 640 000 subjects.

2022 / 09 / 26
18:06:18FNIR(N, R, T) = False neg. identification rate
FPIR(N, T) = False pos. identification rateN = Num. enrolled subjects
R = Num. candidates examined

T = Threshold

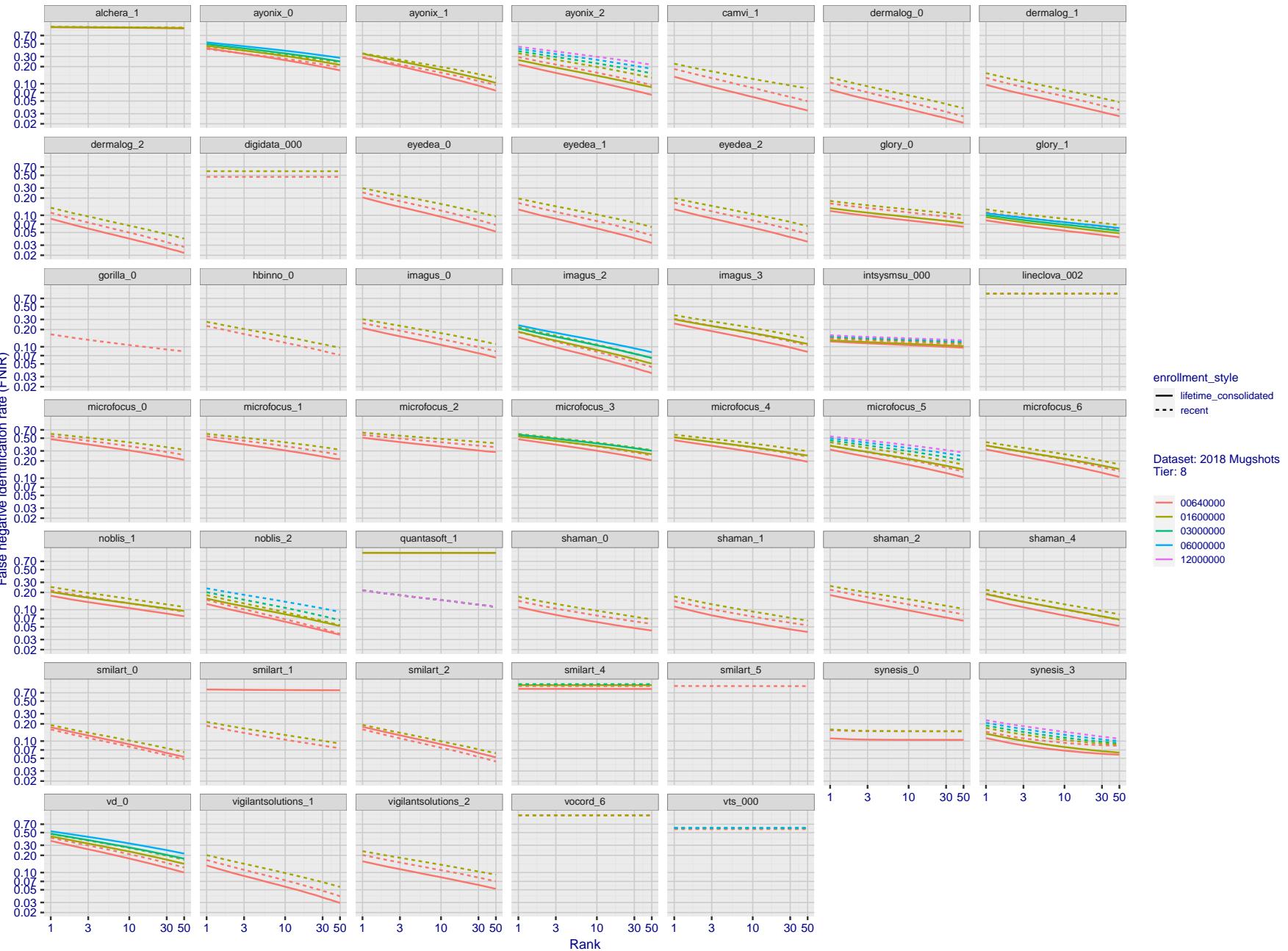
T = 0 → Investigation
T > 0 → Identification

Figure 35: [FRVT-2018 Mugshot Dataset] Rank-based identification miss rates vs. rank. The figure shows false negative identification rates (FNIR) for ranks up to 50. This metric is appropriate to investigational applications where human reviewers will adjudicate sorted candidate lists. Note that with threshold set to zero, FPIR = 1, i.e. any search without an enrolled mate will return non-mated candidates. Results are sorted and reported into tiers for clarity, with the tiering criteria being rank 1 hit rate on a gallery size of N = 640 000 subjects.

2022/09/26 18:06:18	$\text{FNIR}(N, R, T) =$ $\text{FPTR}(N, T) =$	False neg. identification rate False pos. identification rate	$N =$ Num. enrolled subjects $R =$ Num. candidates examined	$T =$ Threshold $T > 0 \rightarrow$ Identification	$T = 0 \rightarrow$ Investigation
------------------------	---	--	--	---	-----------------------------------

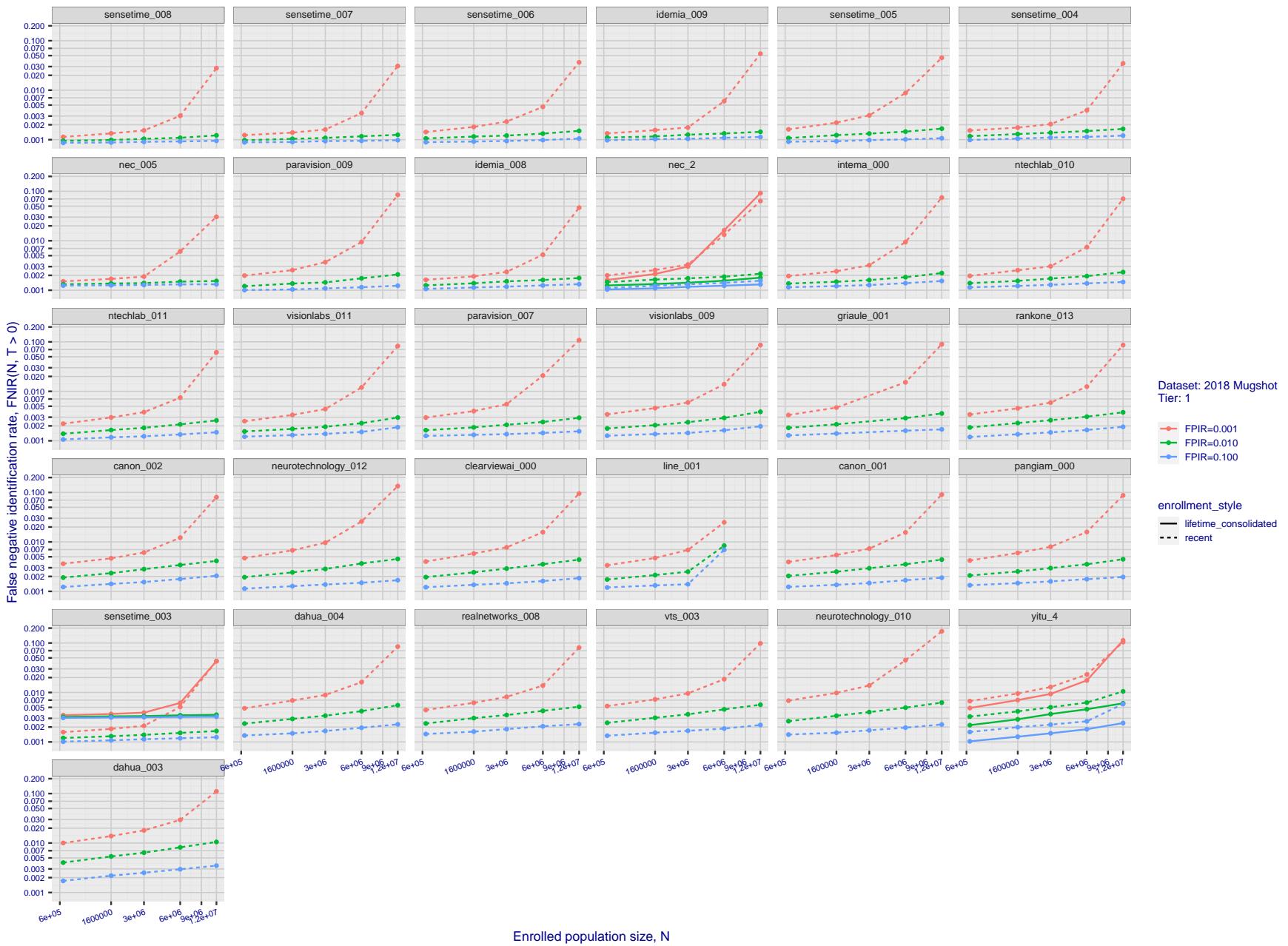


Figure 36: [FRVT-2018 Mugshot Dataset] Threshold-based identification miss rates vs. number of enrolled subjects. The figure shows $\text{FNIR}(N, T)$ across various gallery sizes when the threshold is set to achieve the given FPIRs. The rank criterion is irrelevant at high thresholds as mates are always at rank 1. The results are computed from the trials listed in rows 1-10 of Table 1. Less accurate algorithms were not run on large N , so results are missing. For clarity, results are sorted and reported into tiers spanning multiple pages. The tiering criteria is complicated: First paging by $\text{FNIR}(N_b, 1, 0)$, then sorting by median $\text{FNIR}(N_b, T)$, $N_b = 640\,000$.

2022/09/26
18:06:18FNIR(N, R, T) = False neg. identification rate
FPIR(N, T) = False pos. identification rateN = Num. enrolled subjects
R = Num. candidates examined

T = Threshold

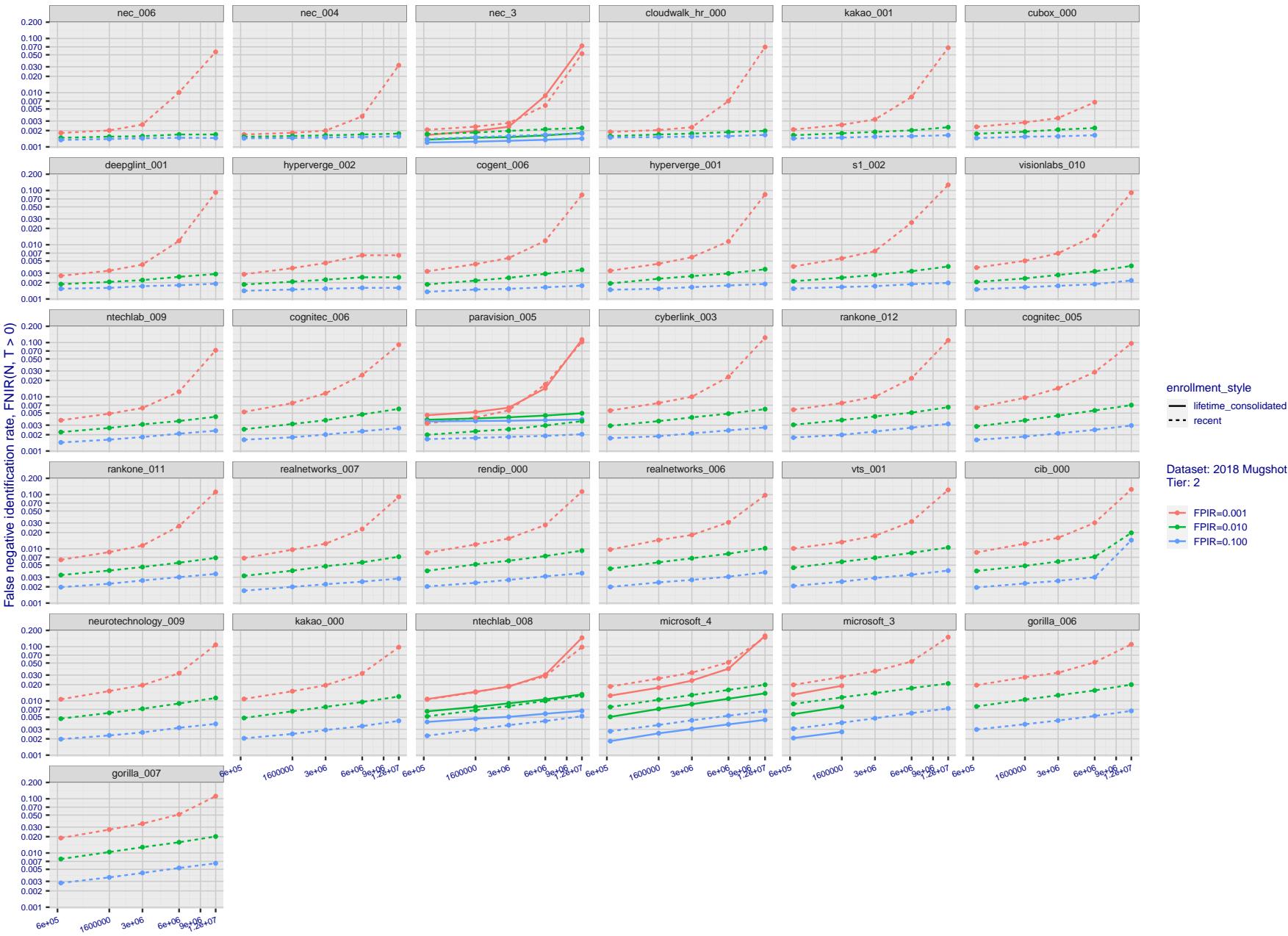
T = 0 → Investigation
T > 0 → Identification

Figure 37: [FRVT-2018 Mugshot Dataset] Threshold-based identification miss rates vs. number of enrolled subjects. The figure shows $\text{FNIR}(N, T)$ across various gallery sizes when the threshold is set to achieve the given FPIRs. The rank criterion is irrelevant at high thresholds as mates are always at rank 1. The results are computed from the trials listed in rows 1-10 of Table 1. Less accurate algorithms were not run on large N , so results are missing. For clarity, results are sorted and reported into tiers spanning multiple pages. The tiering criteria is complicated: First paging by $\text{FNIR}(N_b, 1, 0)$, then sorting by median $\text{FNIR}(N_b, T)$, $N_b = 640\,000$.

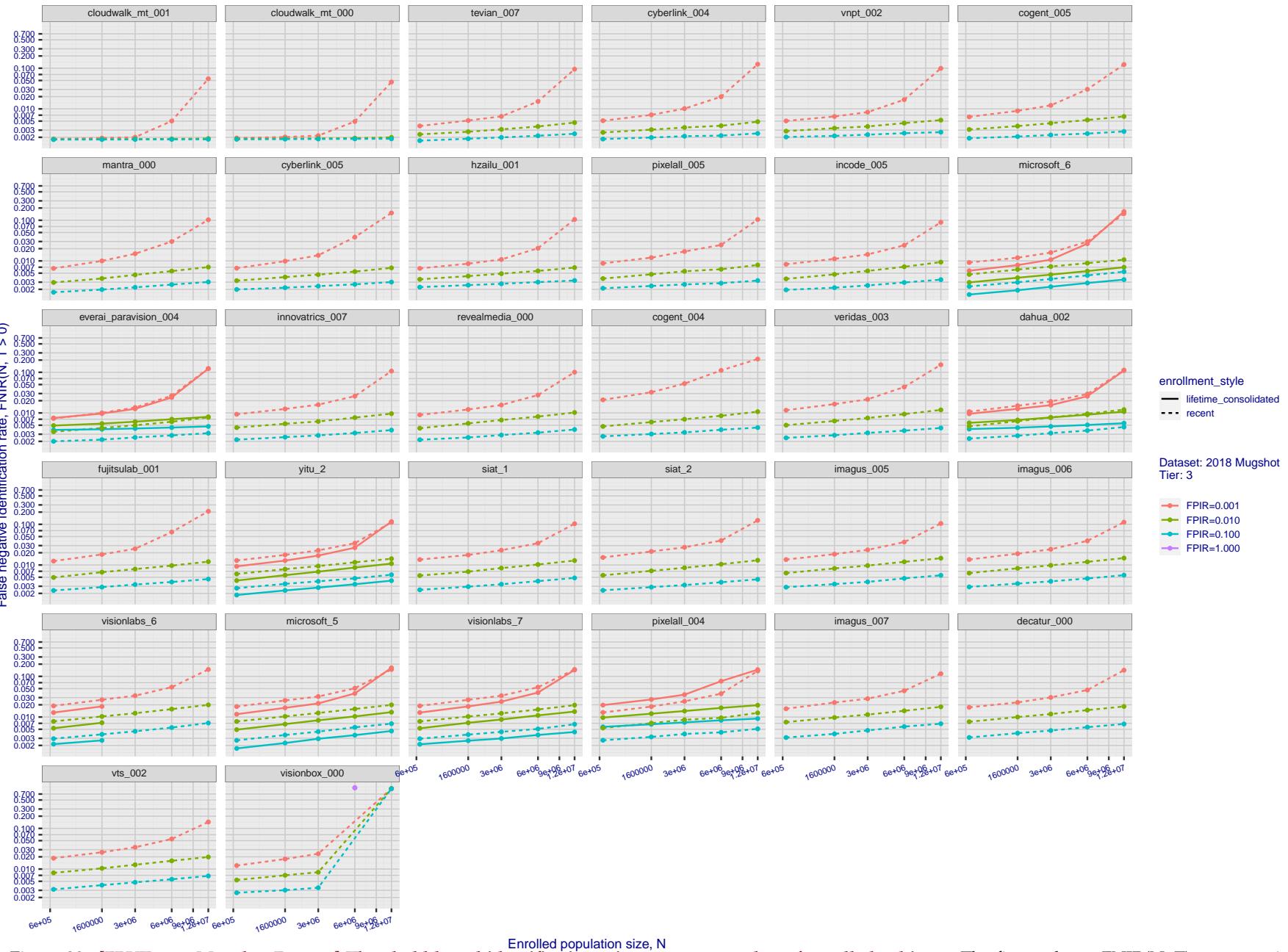
2022 / 09 / 26
18:06:18FNIR(N, R, T) = False neg. identification rate
FPIR(N, T) = False pos. identification rateN = Num. enrolled subjects
R = Num. candidates examined
T = ThresholdT = 0 → Investigation
T > 0 → Identification

Figure 38: [FRVT-2018 Mugshot Dataset] Threshold-based identification miss rates vs. number of enrolled subjects. The figure shows FNIR(N, T) across various gallery sizes when the threshold is set to achieve the given FPIRs. The rank criterion is irrelevant at high thresholds as mates are always at rank 1. The results are computed from the trials listed in rows 1-10 of Table 1. Less accurate algorithms were not run on large N , so results are missing. For clarity, results are sorted and reported into tiers spanning multiple pages. The tiering criteria is complicated: First paging by $\text{FNIR}(N_b, 1, 0)$, then sorting by median $\text{FNIR}(N_b, T)$, $N_b = 640\,000$.

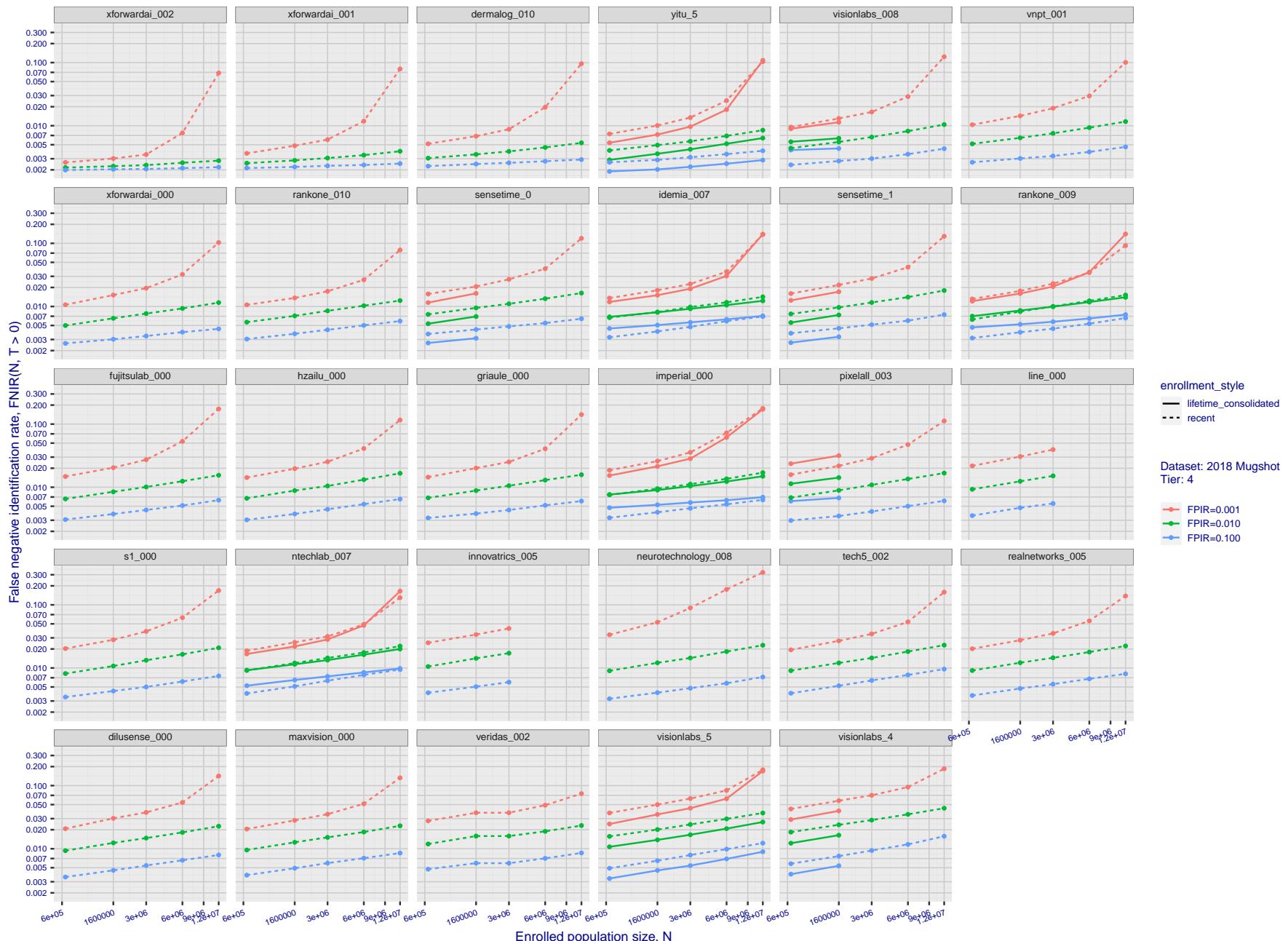


Figure 39: [FRVT-2018 Mugshot Dataset] Threshold-based identification miss rates vs. number of enrolled subjects. The figure shows $\text{FNIR}(N, T)$ across various gallery sizes when the threshold is set to achieve the given FPIRs. The rank criterion is irrelevant at high thresholds as mates are always at rank 1. The results are computed from the trials listed in rows 1-10 of Table 1. Less accurate algorithms were not run on large N , so results are missing. For clarity, results are sorted and reported into tiers spanning multiple pages. The tiering criteria is complicated: First paging by $\text{FNIR}(N_b, 1, 0)$, then sorting by median $\text{FNIR}(N_b, T)$, $N_b = 640\,000$.

2022 / 09 / 26
18:06:18FNIR(N, R, T) = False neg. identification rate
FPIR(N, T) = False pos. identification rateN = Num. enrolled subjects
R = Num. candidates examined

T = Threshold

T = 0 → Investigation
T > 0 → Identification

2022 / 09 / 26
18:06:18FNIR(N, R, T) = False neg. identification rate
FPIR(N, T) = False pos. identification rateN = Num. enrolled subjects
R = Num. candidates examined

T = Threshold

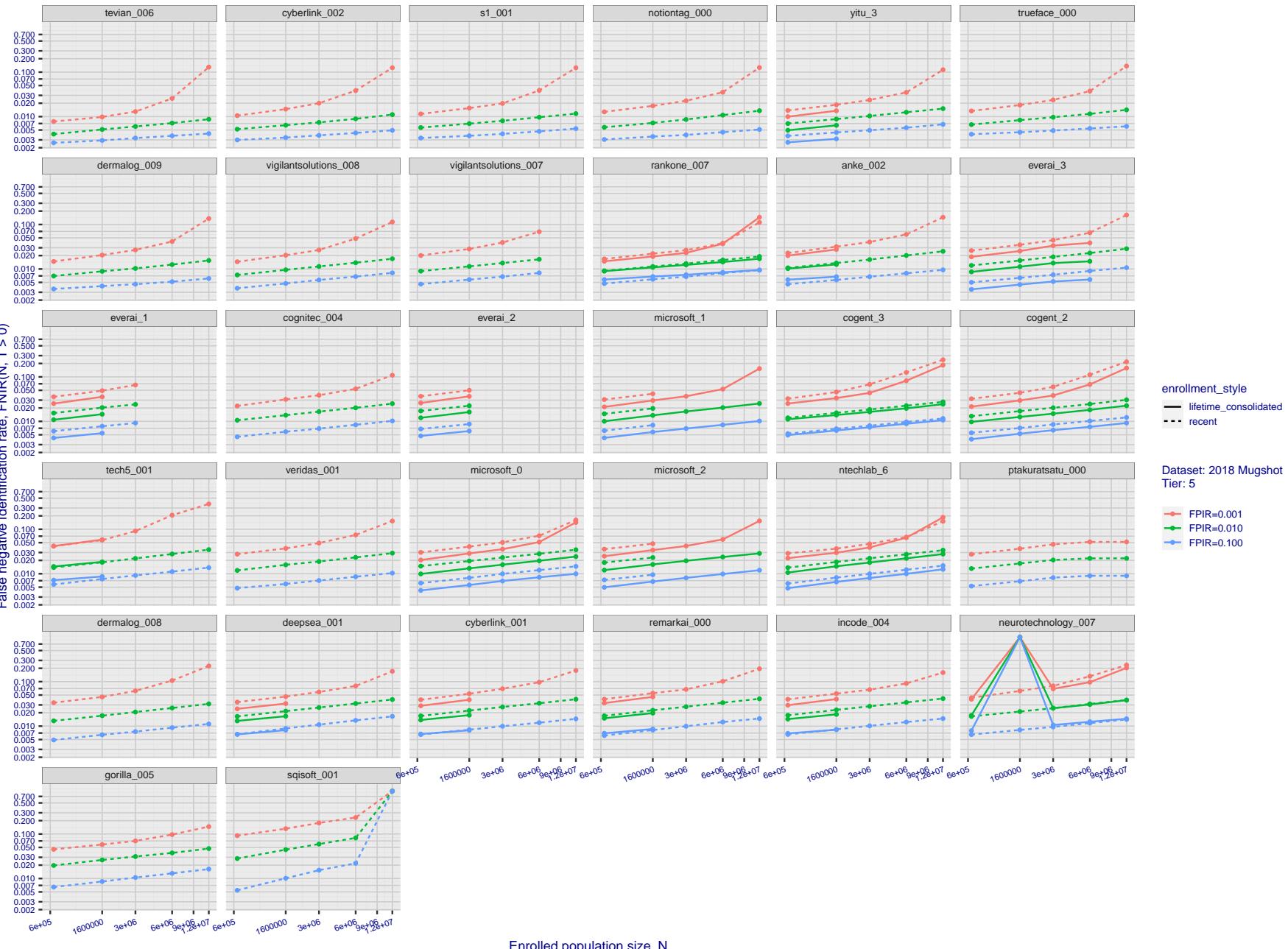
T = 0 → Investigation
T > 0 → Identification

Figure 40: [FRVT-2018 Mugshot Dataset] Threshold-based identification miss rates vs. number of enrolled subjects. The figure shows $\text{FNIR}(N, T)$ across various gallery sizes when the threshold is set to achieve the given FPIRs. The rank criterion is irrelevant at high thresholds as mates are always at rank 1. The results are computed from the trials listed in rows 1-10 of Table 1. Less accurate algorithms were not run on large N , so results are missing. For clarity, results are sorted and reported into tiers spanning multiple pages. The tiering criteria is complicated: First paging by $\text{FNIR}(N_b, 1, 0)$, then sorting by median $\text{FNIR}(N_b, T)$, $N_b = 640\,000$.

2022 / 09 / 26
18:06:18FNIR(N, R, T) = False neg. identification rate
FPFR(N, T) = False pos. identification rateN = Num. enrolled subjects
R = Num. candidates examined

T = Threshold

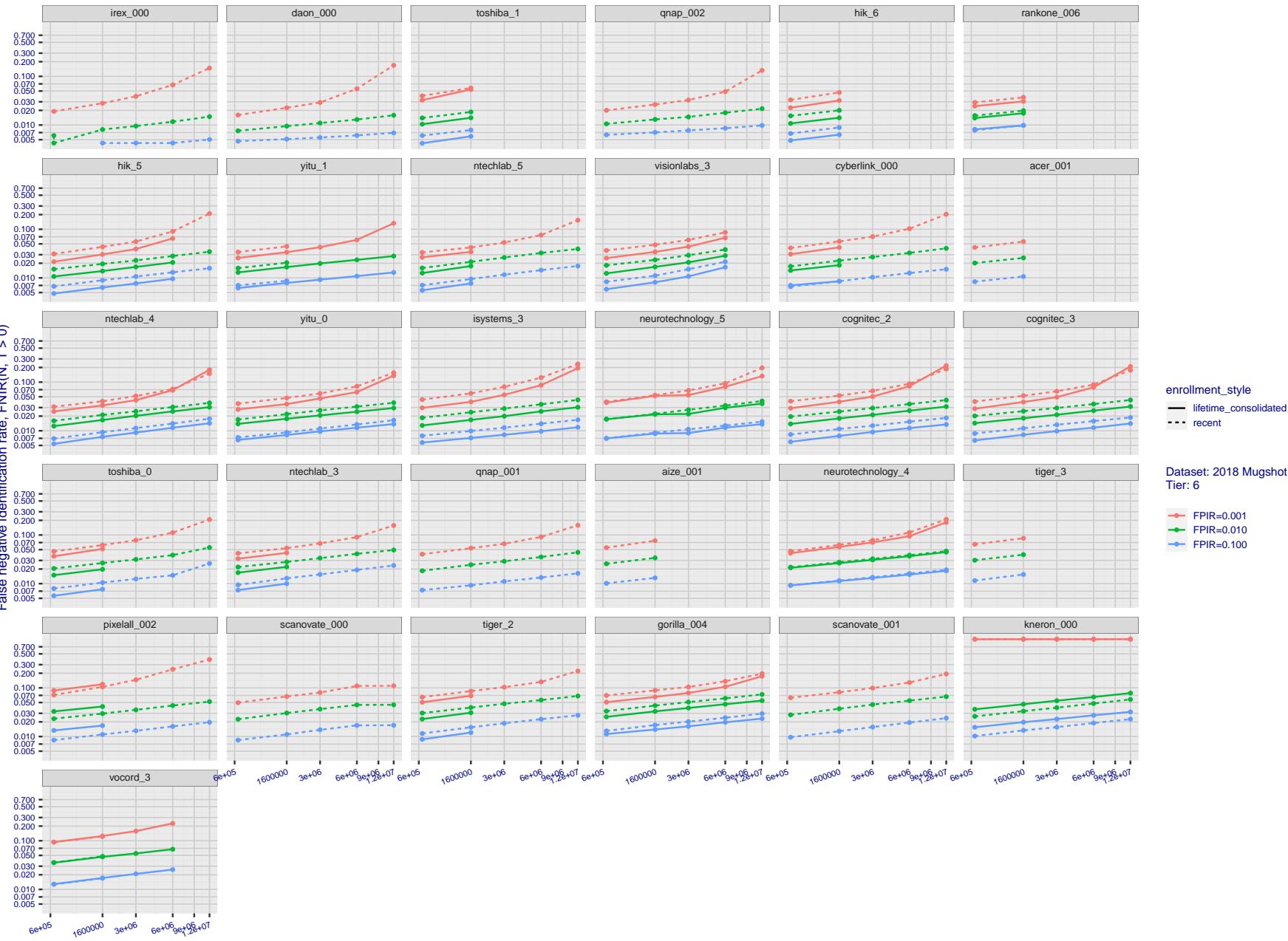
T = 0 → Investigation
T > 0 → Identification

Figure 41: [FRVT-2018 Mugshot Dataset] Threshold-based identification miss rates vs. number of enrolled subjects. The figure shows $\text{FNIR}(N, T)$ across various gallery sizes when the threshold is set to achieve the given FPIRs. The rank criterion is irrelevant at high thresholds as mates are always at rank 1. The results are computed from the trials listed in rows 1-10 of Table 1. Less accurate algorithms were not run on large N , so results are missing. For clarity, results are sorted and reported into tiers spanning multiple pages. The tiering criteria is complicated: First paging by $\text{FNIR}(N_b, 1, 0)$, then sorting by median $\text{FNIR}(N_b, T)$, $N_b = 640\,000$.

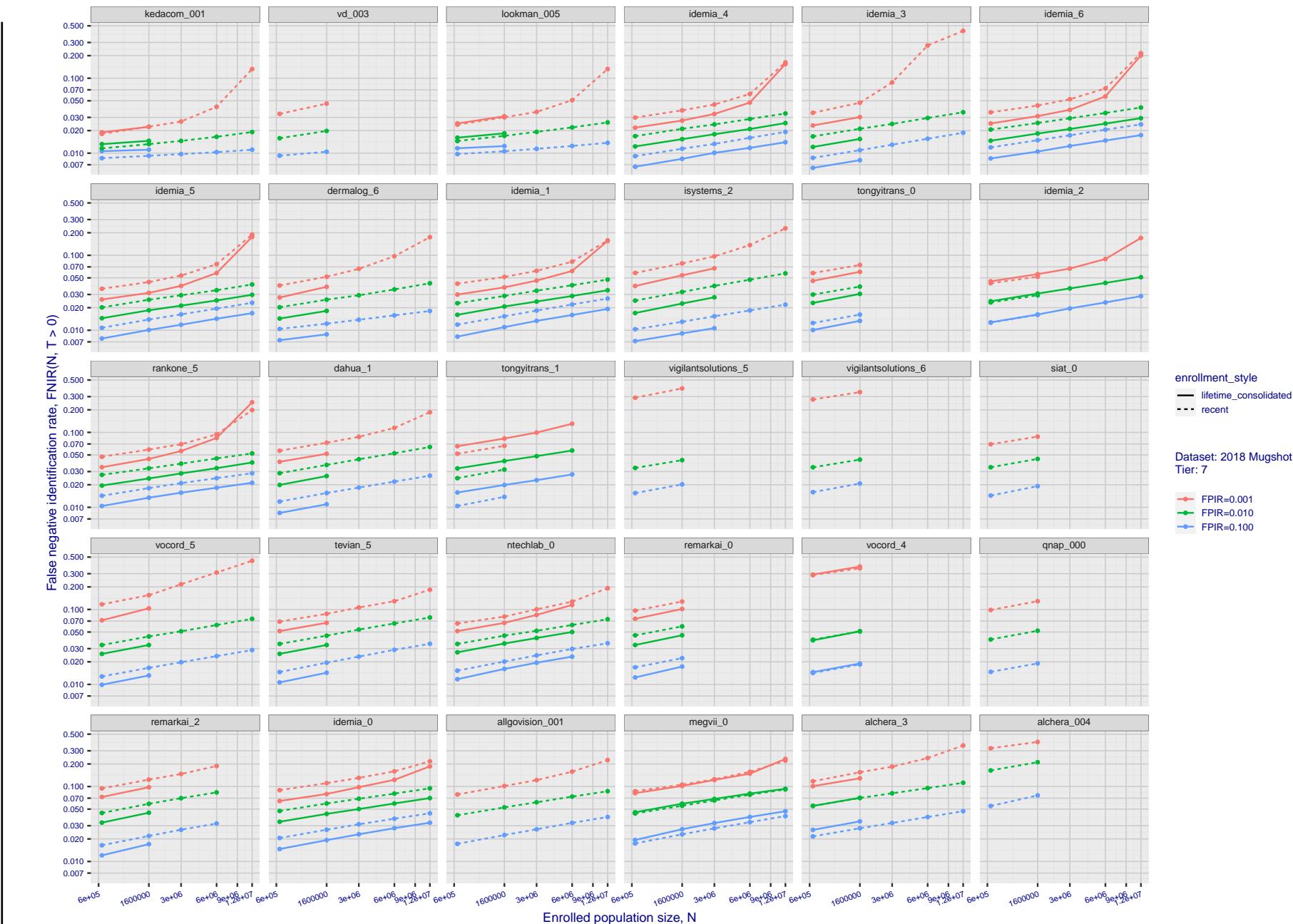
2022/09/26
18:06:18

Figure 42: [FRVT-2018 Mugshot Dataset] Threshold-based identification miss rates vs. number of enrolled subjects. The figure shows FNIR(N, T) across various gallery sizes when the threshold is set to achieve the given FPIRs. The rank criterion is irrelevant at high thresholds as mates are always at rank 1. The results are computed from the trials listed in rows 1-10 of Table 1. Less accurate algorithms were not run on large N , so results are missing. For clarity, results are sorted and reported into tiers spanning multiple pages. The tiering criteria is complicated: First paging by $\text{FNIR}(N_b, 1, 0)$, then sorting by median $\text{FNIR}(N_b, T)$, $N_b = 640\,000$.

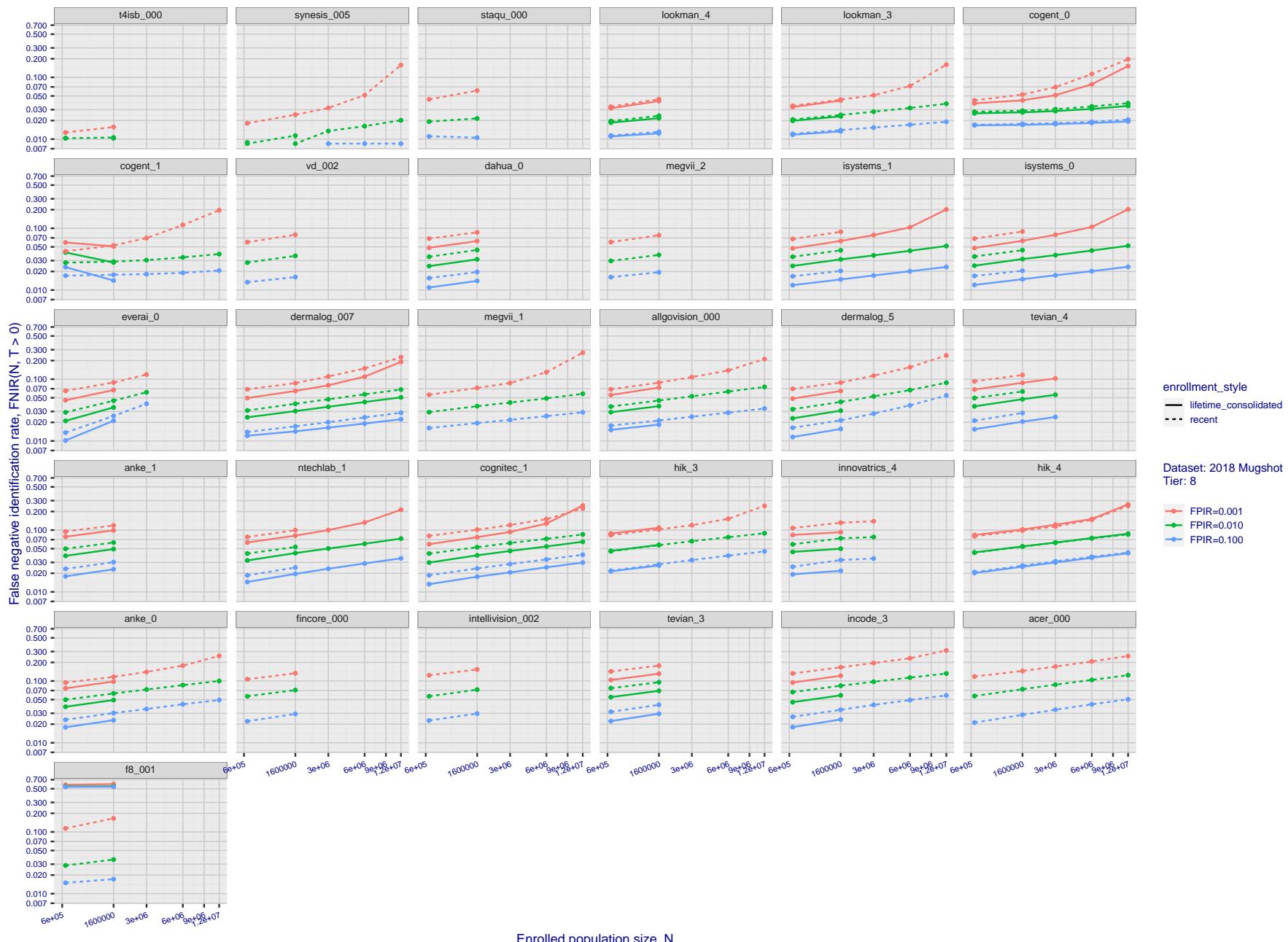


Figure 43: [FRVT-2018 Mugshot Dataset] Threshold-based identification miss rates vs. number of enrolled subjects. The figure shows $\text{FNIR}(N, T)$ across various gallery sizes when the threshold is set to achieve the given FPIRs. The rank criterion is irrelevant at high thresholds as mates are always at rank 1. The results are computed from the trials listed in rows 1-10 of Table 1. Less accurate algorithms were not run on large N , so results are missing. For clarity, results are sorted and reported into tiers spanning multiple pages. The tiering criteria is complicated: First paging by $\text{FNIR}(N_b, 1, 0)$, then sorting by median $\text{FNIR}(N_b, T)$, $N_b = 640\,000$.

2022/09/26
18:06:18FNIR(N, R, T) = False neg. identification rate
FPFR(N, T) = False pos. identification rateN = Num. enrolled subjects
R = Num. candidates examined

T = Threshold

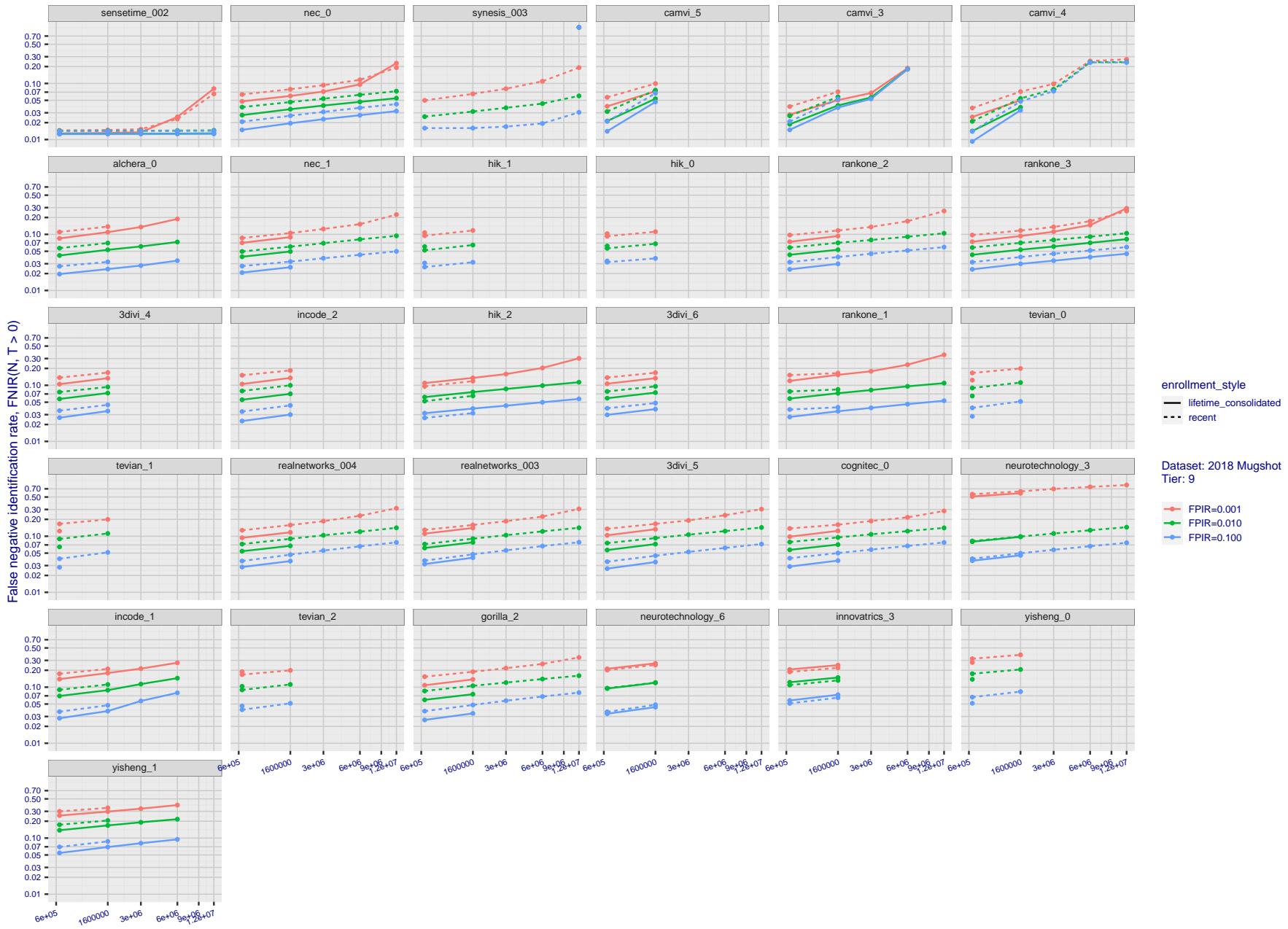
T = 0 → Investigation
T > 0 → Identification

Figure 44: [FRVT-2018 Mugshot Dataset] Threshold-based identification miss rates vs. number of enrolled subjects. The figure shows $\text{FNIR}(N, T)$ across various gallery sizes when the threshold is set to achieve the given FPIRs. The rank criterion is irrelevant at high thresholds as mates are always at rank 1. The results are computed from the trials listed in rows 1-10 of Table 1. Less accurate algorithms were not run on large N , so results are missing. For clarity, results are sorted and reported into tiers spanning multiple pages. The tiering criteria is complicated: First paging by $\text{FNIR}(N_b, 1, 0)$, then sorting by median $\text{FNIR}(N_b, T)$, $N_b = 640\,000$.

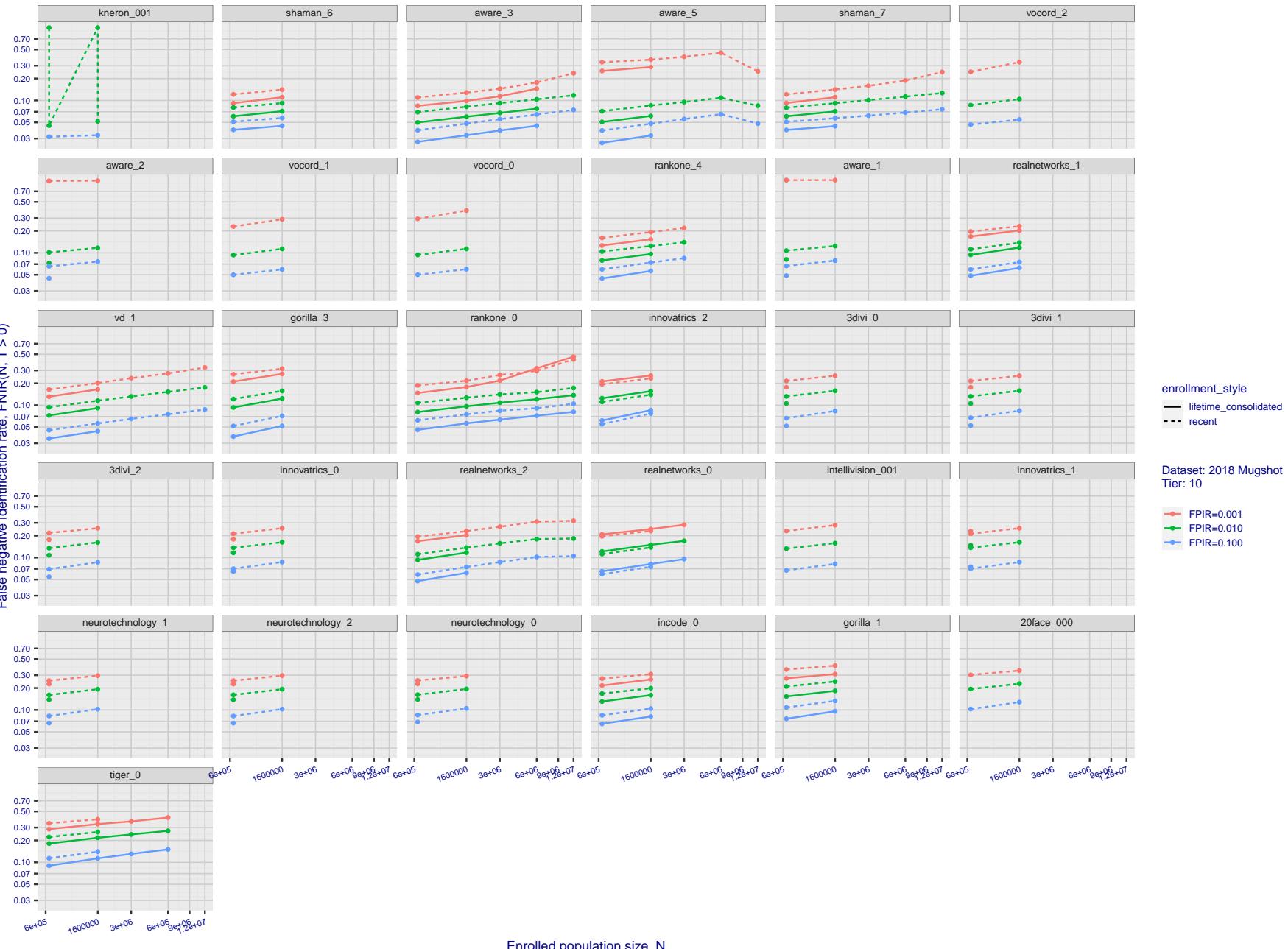
2022/09/26
18:06:18FNIR(N, R, T) = False neg. identification rate
FPFR(N, T) = False pos. identification rate
N = Num. enrolled subjects
R = Num. candidates examinedT = Threshold
T = 0 → Investigation
T > 0 → Identification

Figure 45: [FRVT-2018 Mugshot Dataset] Threshold-based identification miss rates vs. number of enrolled subjects. The figure shows $\text{FNIR}(N, T)$ across various gallery sizes when the threshold is set to achieve the given FPIRs. The rank criterion is irrelevant at high thresholds as mates are always at rank 1. The results are computed from the trials listed in rows 1-10 of Table 1. Less accurate algorithms were not run on large N , so results are missing. For clarity, results are sorted and reported into tiers spanning multiple pages. The tiering criteria is complicated: First paging by $\text{FNIR}(N_b, 1, 0)$, then sorting by median $\text{FNIR}(N_b, T)$, $N_b = 640\,000$.

2022/09/26
18:06:18FNIR(N, R, T) = False neg. identification rate
FPIR(N, T) = False pos. identification rateN = Num. enrolled subjects
R = Num. candidates examined

T = Threshold

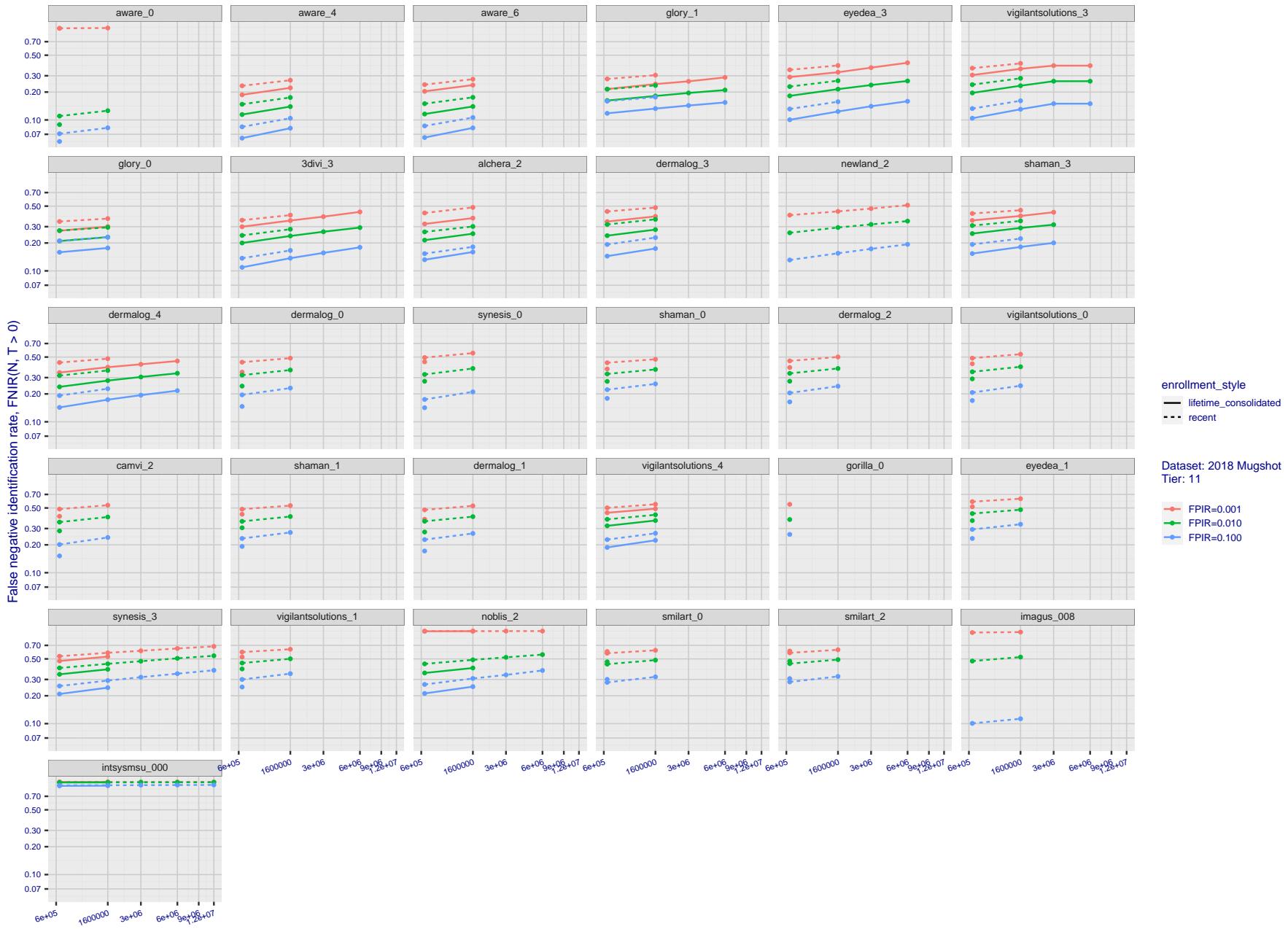
T = 0 → Investigation
T > 0 → Identification

Figure 46: [FRVT-2018 Mugshot Dataset] Threshold-based identification miss rates vs. number of enrolled subjects. The figure shows $\text{FNIR}(N, T)$ across various gallery sizes when the threshold is set to achieve the given FPIRs. The rank criterion is irrelevant at high thresholds as mates are always at rank 1. The results are computed from the trials listed in rows 1-10 of Table 1. Less accurate algorithms were not run on large N , so results are missing. For clarity, results are sorted and reported into tiers spanning multiple pages. The tiering criteria is complicated: First paging by $\text{FNIR}(N_b, 1, 0)$, then sorting by median $\text{FNIR}(N_b, T)$, $N_b = 640\,000$.

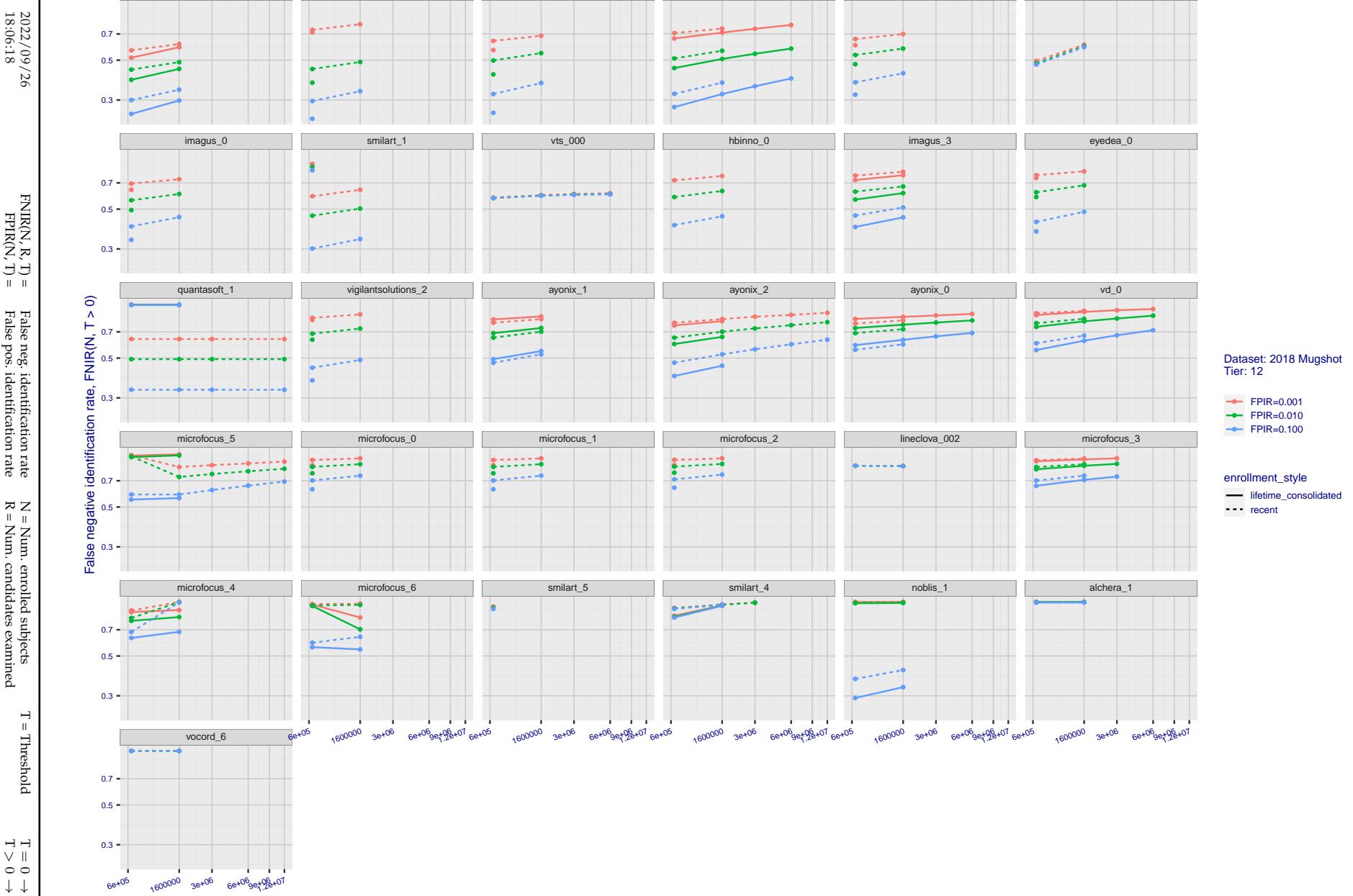


Figure 47: [FRVT-2018 Mugshot Dataset] Threshold-based identification miss rates vs. number of enrolled subjects. The figure shows $\text{FNIR}(N, T)$ across various gallery sizes when the threshold is set to achieve the given FPIRs. The rank criterion is irrelevant at high thresholds as mates are always at rank 1. The results are computed from the trials listed in rows 1-10 of Table 1. Less accurate algorithms were not run on large N , so results are missing. For clarity, results are sorted and reported into tiers spanning multiple pages. The tiering criteria is complicated: First paging by $\text{FNIR}(N_b, 1, 0)$, then sorting by median $\text{FNIR}(N_b, T)$, $N_b = 640\,000$.

2022/09/26 18:06:18	$\text{FNIR}(N, R, T) =$ $\text{FPTR}(N, T) =$	False neg. identification rate False pos. identification rate	$N =$ Num. enrolled subjects $R =$ Num. candidates examined	$T =$ Threshold $T > 0 \rightarrow$ Identification	$T = 0 \rightarrow$ Investigation
------------------------	---	--	--	---	-----------------------------------

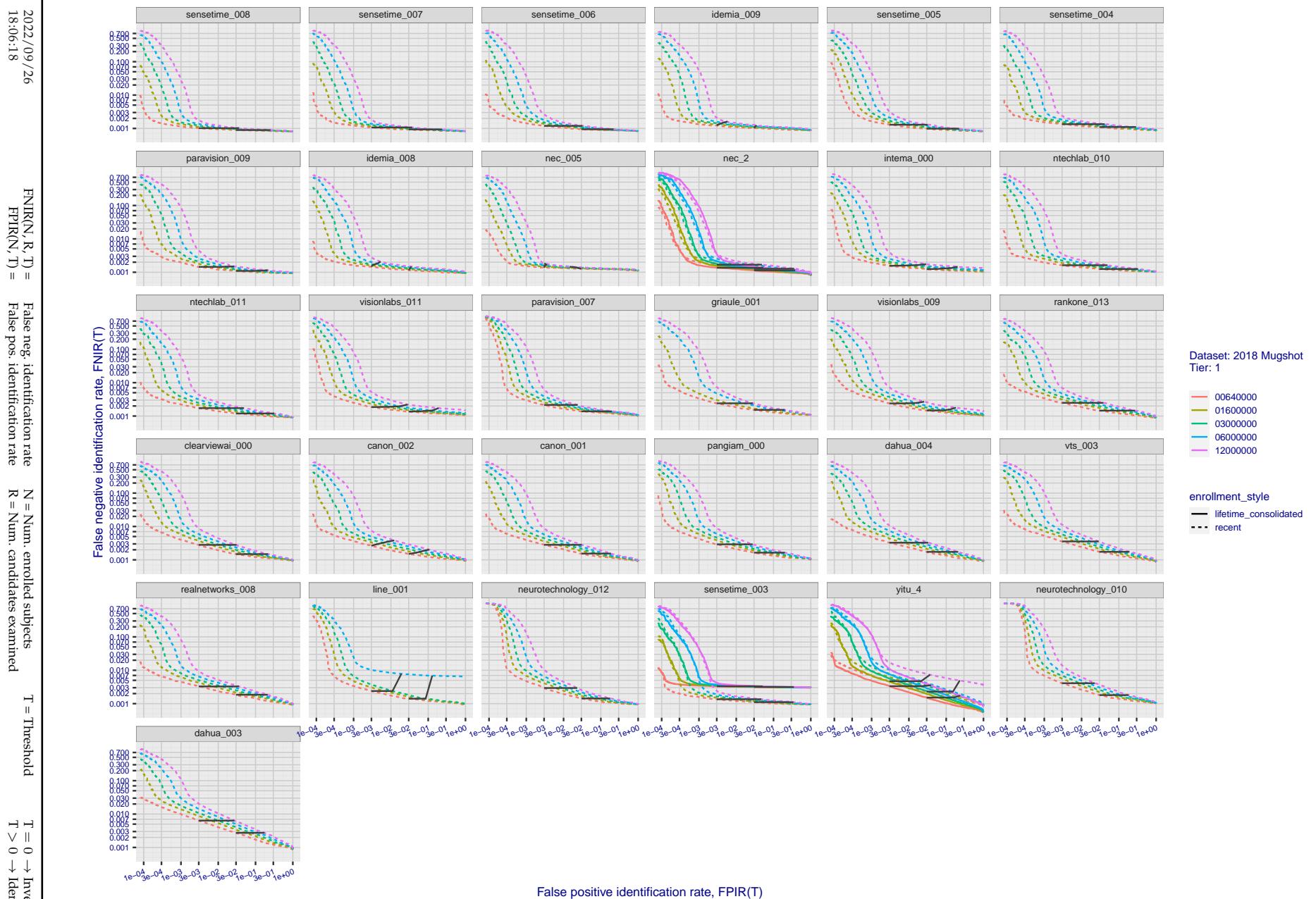


Figure 48: [FRVT-2018 Mugshot Dataset] Identification miss rates vs. false positive rates. The figure shows miss rates $\text{FNIR}(N, L, T)$ as a function of $\text{FPIR}(N, T)$, with N ranging from 640 000 to 12 000 000 as noted in rows 1-10 of Table 1. These error tradeoff characteristics are useful for applications where a threshold must be elevated to limit false positives, such as when human reviewer labor is not matched to the volume of searches. Dark lines join points of equal threshold: If horizontal, $\text{FPIR}(T)$ rises with N , and mate scores are independent of N . Other algorithms adjust scores in an attempt to make FPIR independent of N .

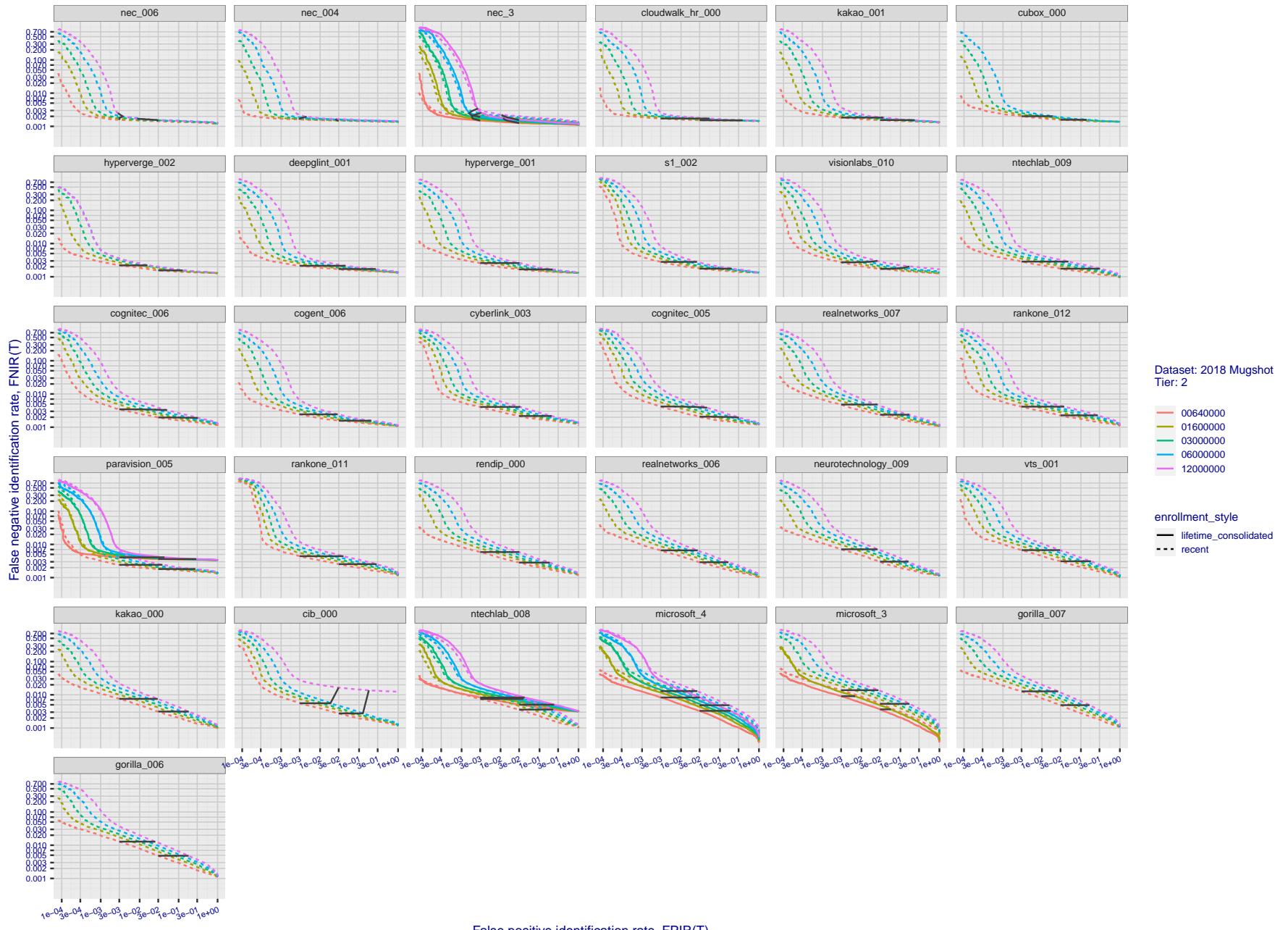


Figure 49: [FRVT-2018 Mugshot Dataset] Identification miss rates vs. false positive rates. The figure shows miss rates $\text{FNIR}(N, L, T)$ as a function of $\text{FPIR}(N, T)$, with N ranging from 640 000 to 12 000 000 as noted in rows 1-10 of Table 1. These error tradeoff characteristics are useful for applications where a threshold must be elevated to limit false positives, such as when human reviewer labor is not matched to the volume of searches. Dark lines join points of equal threshold: If horizontal, $\text{FPIR}(T)$ rises with N , and mate scores are independent of N . Other algorithms adjust scores in an attempt to make FPIR independent of N .

2022/09/26
18:06:18FNIR(N, R, T) = False neg. identification rate
FPIR(N, T) = False pos. identification rateN = Num. enrolled subjects
R = Num. candidates examined

T = Threshold

T = 0 → Investigation
 $T > 0 \rightarrow$ Identification

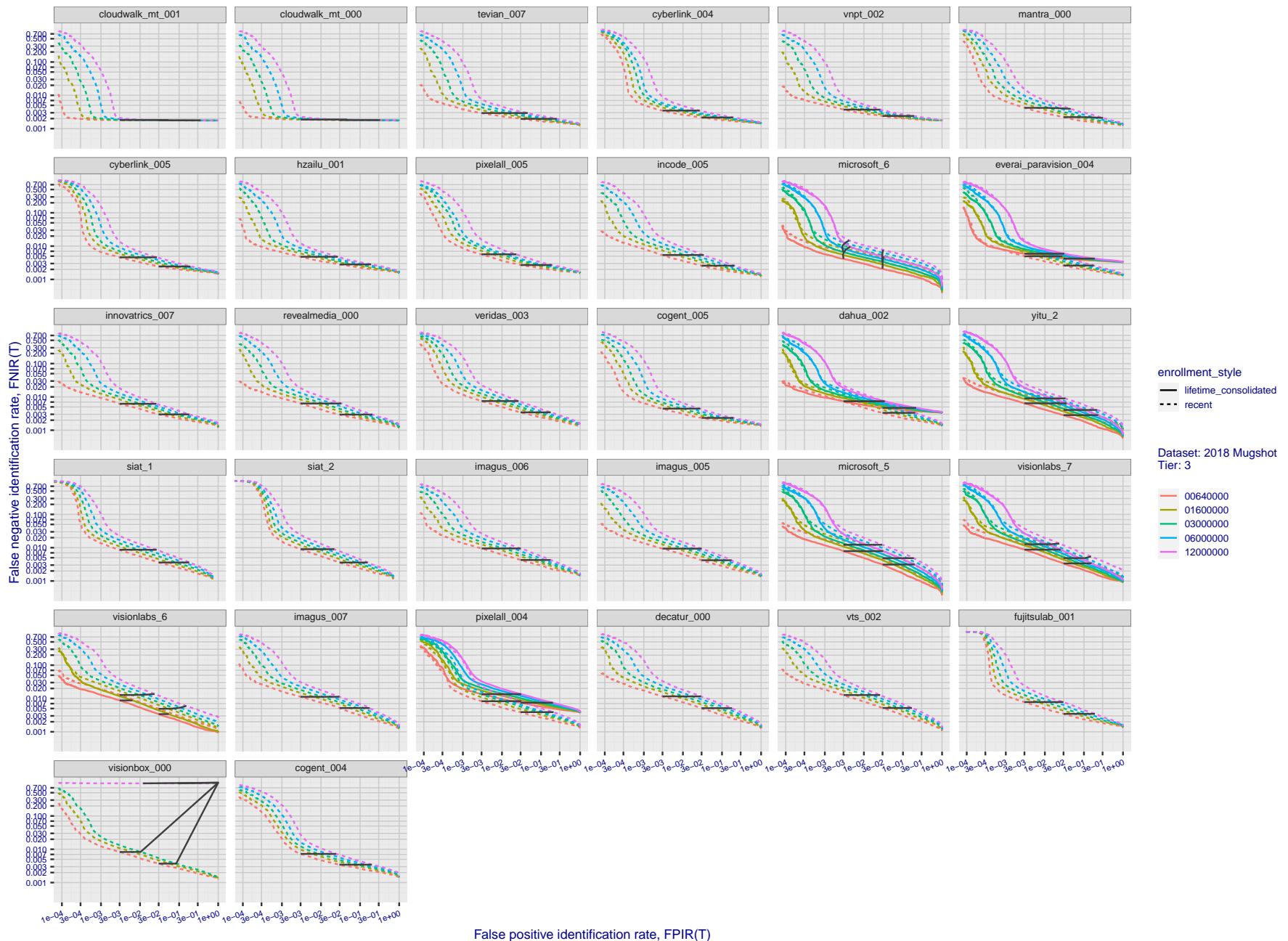


Figure 50: [FRVT-2018 Mugshot Dataset] Identification miss rates vs. false positive rates. The figure shows miss rates $\text{FNIR}(N, L, T)$ as a function of $\text{FPIR}(N, T)$, with N ranging from 640 000 to 12 000 000 as noted in rows 1-10 of Table 1. These error tradeoff characteristics are useful for applications where a threshold must be elevated to limit false positives, such as when human reviewer labor is not matched to the volume of searches. Dark lines join points of equal threshold: If horizontal, $\text{FPIR}(T)$ rises with N , and mate scores are independent of N . Other algorithms adjust scores in an attempt to make FPIR independent of N .

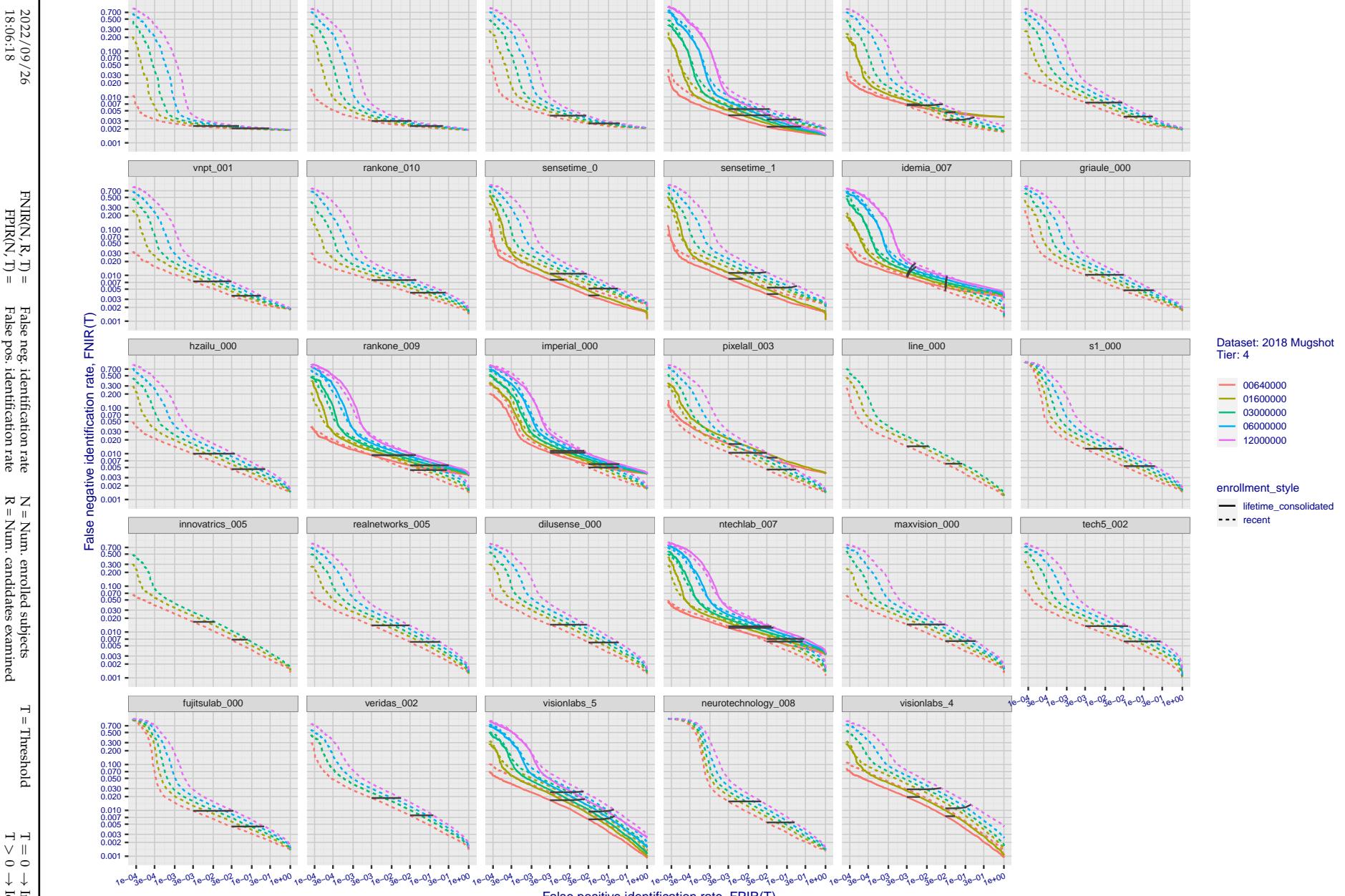


Figure 51: [FRVT-2018 Mugshot Dataset] Identification miss rates vs. false positive rates. The figure shows miss rates $\text{FNIR}(N, L, T)$ as a function of $\text{FPIR}(N, T)$, with N ranging from 640 000 to 12 000 000 as noted in rows 1-10 of Table 1. These error tradeoff characteristics are useful for applications where a threshold must be elevated to limit false positives, such as when human reviewer labor is not matched to the volume of searches. Dark lines join points of equal threshold: If horizontal, $\text{FPIR}(T)$ rises with N , and mate scores are independent of N . Other algorithms adjust scores in an attempt to make FPIR independent of N .

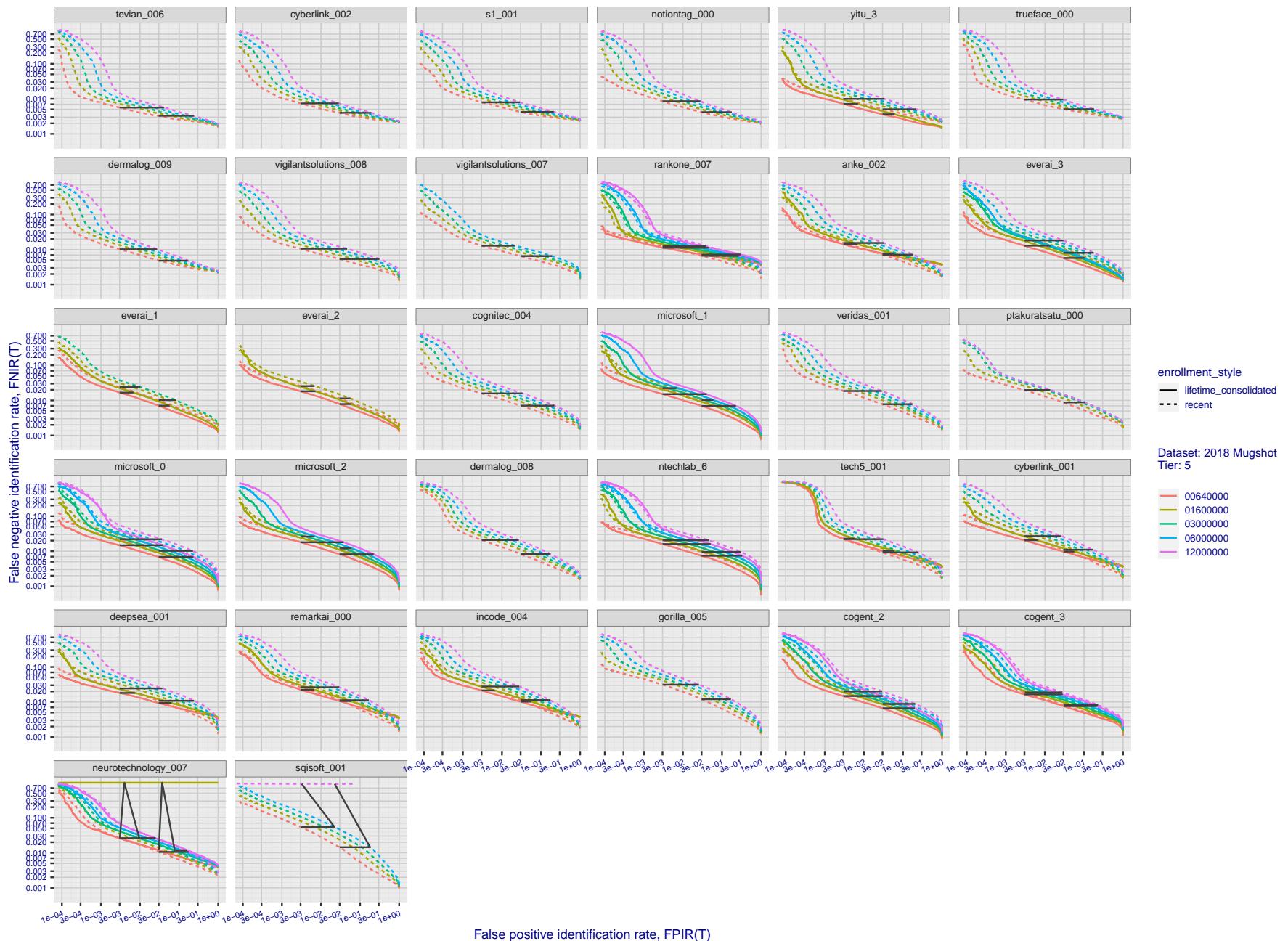


Figure 52: [FRVT-2018 Mugshot Dataset] Identification miss rates vs. false positive rates. The figure shows miss rates $\text{FNIR}(N, L, T)$ as a function of $\text{FPIR}(N, T)$, with N ranging from 640 000 to 12 000 000 as noted in rows 1-10 of Table 1. These error tradeoff characteristics are useful for applications where a threshold must be elevated to limit false positives, such as when human reviewer labor is not matched to the volume of searches. Dark lines join points of equal N . Other algorithms adjust scores in an attempt to make FPIR independent of N .

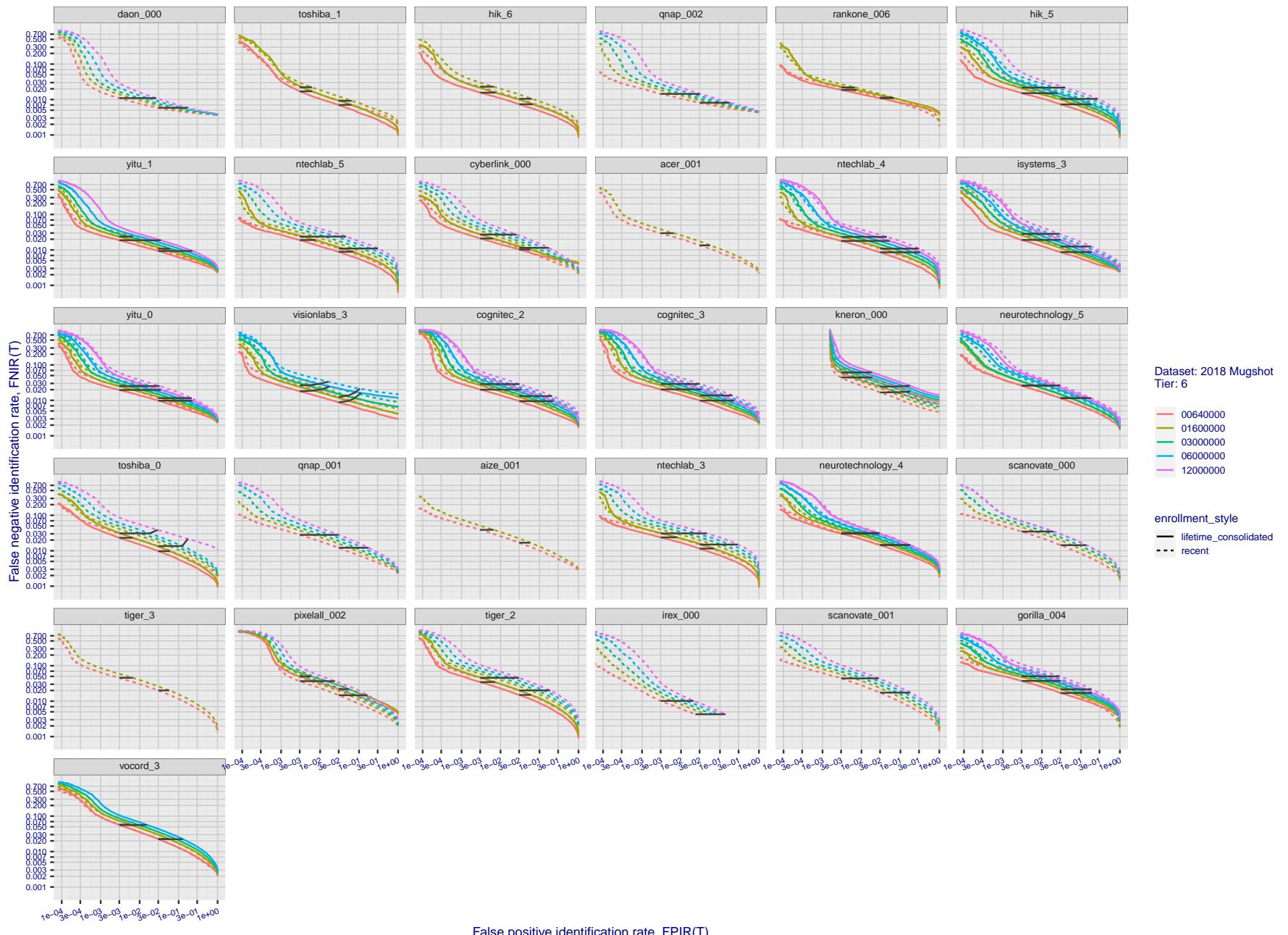


Figure 53: [FRVT-2018 Mugshot Dataset] Identification miss rates vs. false positive rates. The figure shows miss rates $\text{FNIR}(N, L, T)$ as a function of $\text{FPIR}(N, T)$, with N ranging from 640 000 to 12 000 000 as noted in rows 1-10 of Table 1. These error tradeoff characteristics are useful for applications where a threshold must be elevated to limit false positives, such as when human reviewer labor is not matched to the volume of searches. Dark lines join points of equal threshold: If horizontal, $\text{FPIR}(T)$ rises with N , and mate scores are independent of N . Other algorithms adjust scores in an attempt to make FPIR independent of N .

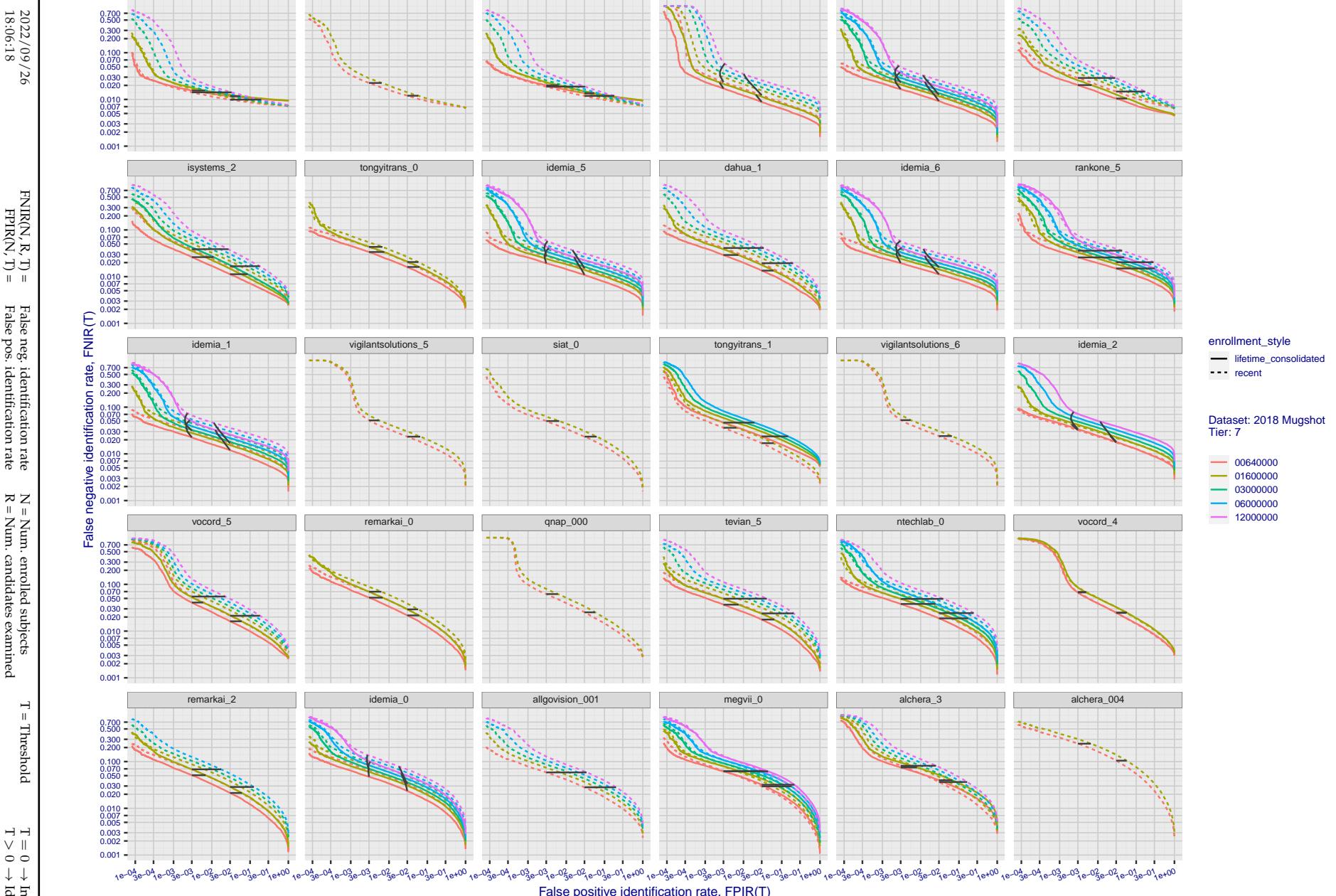


Figure 54: [FRVT-2018 Mugshot Dataset] Identification miss rates vs. false positive rates. The figure shows miss rates $\text{FNIR}(N, L, T)$ as a function of $\text{FPIR}(N, T)$, with N ranging from 640 000 to 12 000 000 as noted in rows 1-10 of Table 1. These error tradeoff characteristics are useful for applications where a threshold must be elevated to limit false positives, such as when human reviewer labor is not matched to the volume of searches. Dark lines join points of equal N . Other algorithms adjust scores in an attempt to make FPIR independent of N .

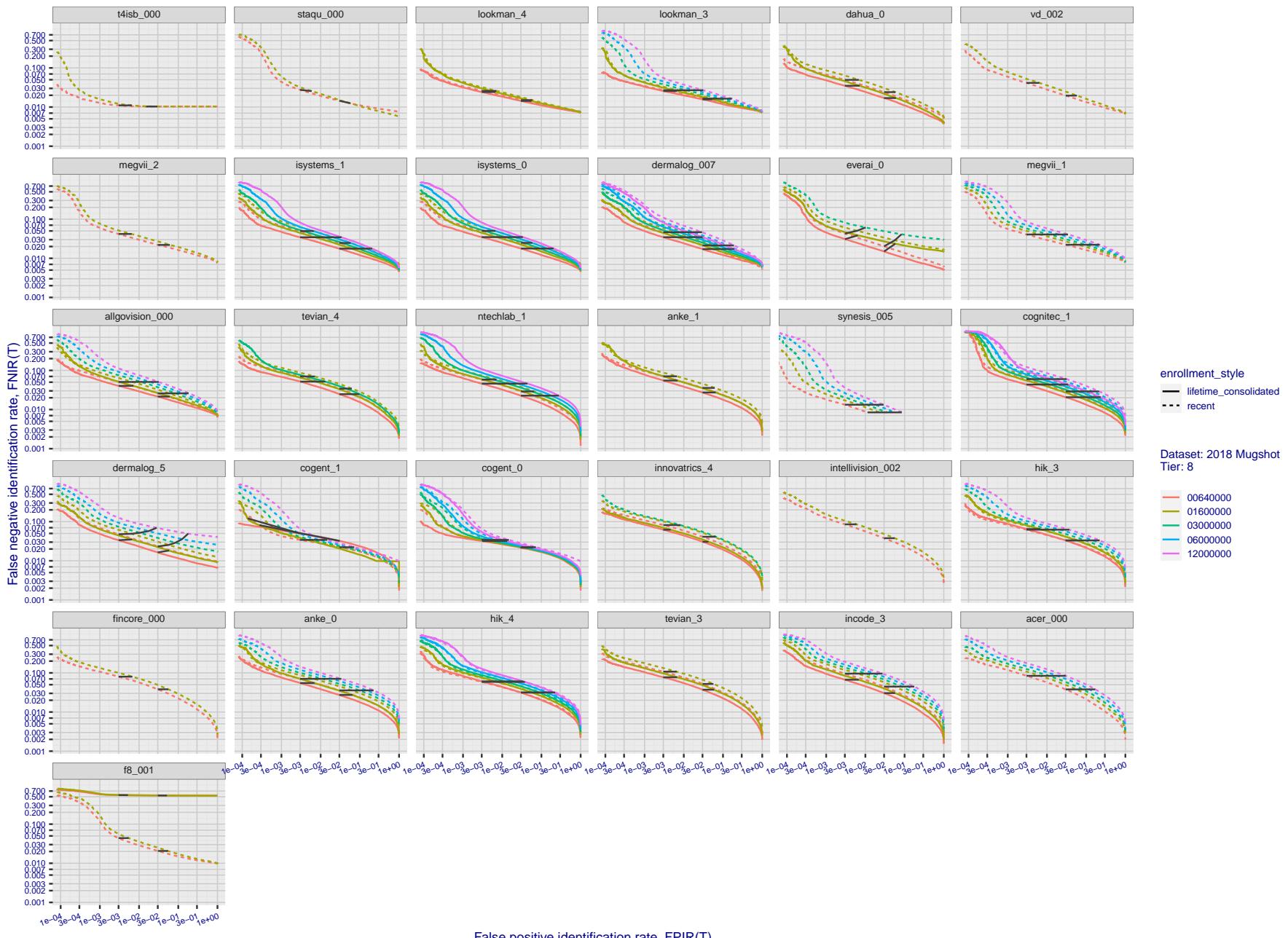


Figure 55: [FRVT-2018 Mugshot Dataset] Identification miss rates vs. false positive rates. The figure shows miss rates $\text{FNIR}(N, L, T)$ as a function of $\text{FPIR}(N, T)$, with N ranging from 640 000 to 12 000 000 as noted in rows 1-10 of Table 1. These error tradeoff characteristics are useful for applications where a threshold must be elevated to limit false positives, such as when human reviewer labor is not matched to the volume of searches. Dark lines join points of equal threshold: If horizontal, $\text{FPIR}(T)$ rises with N , and mate scores are independent of N . Other algorithms adjust scores in an attempt to make FPIR independent of N .

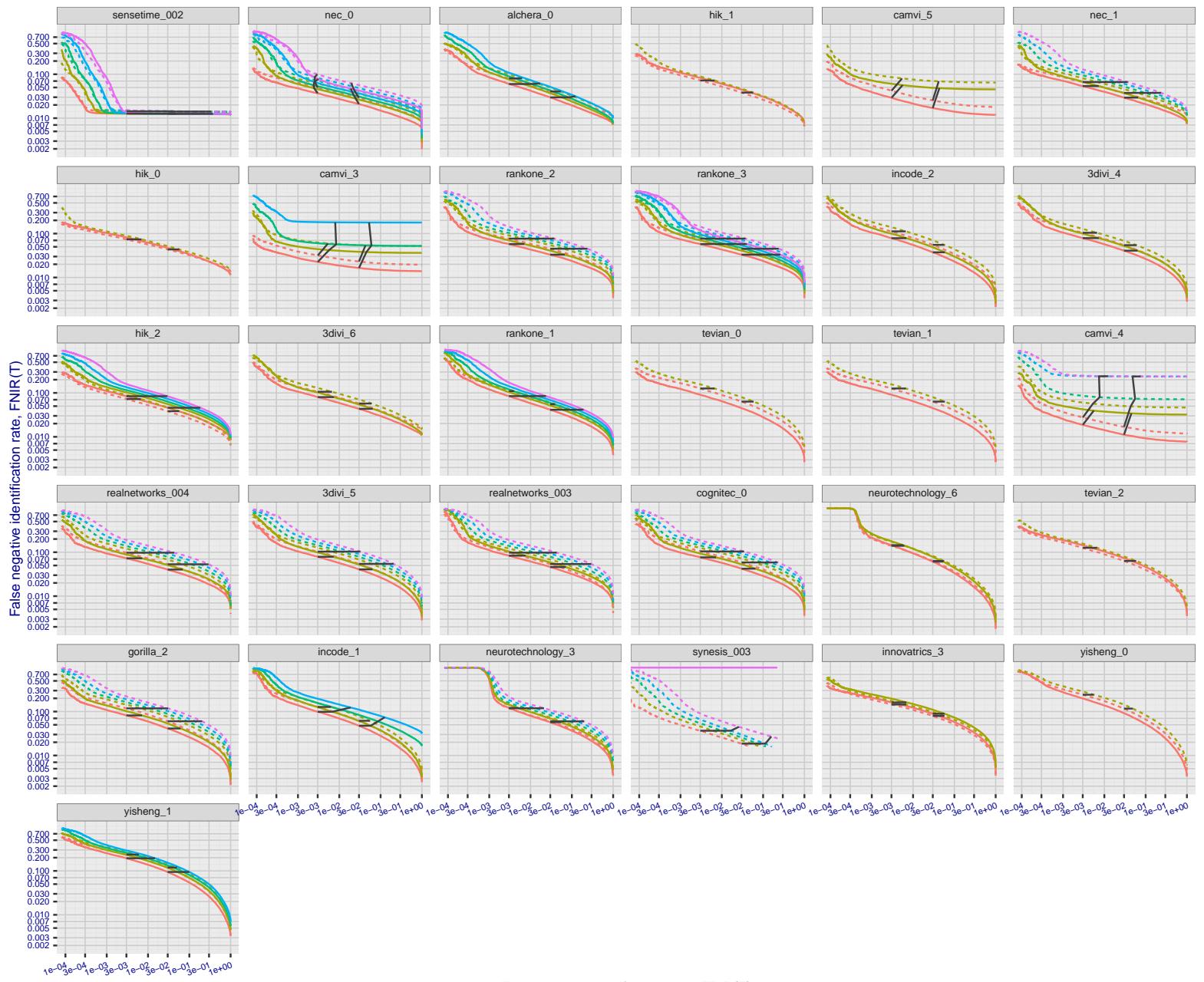


Figure 56: [FRVT-2018 Mugshot Dataset] Identification miss rates vs. false positive rates. The figure shows miss rates $\text{FNIR}(N, L, T)$ as a function of $\text{FPIR}(N, T)$, with N ranging from 640 000 to 12 000 000 as noted in rows 1-10 of Table 1. These error tradeoff characteristics are useful for applications where a threshold must be elevated to limit false positives, such as when human reviewer labor is not matched to the volume of searches. Dark lines join points of equal threshold: If horizontal, $\text{FPIR}(T)$ rises with N , and mate scores are independent of N . Other algorithms adjust scores in an attempt to make FPIR independent of N .

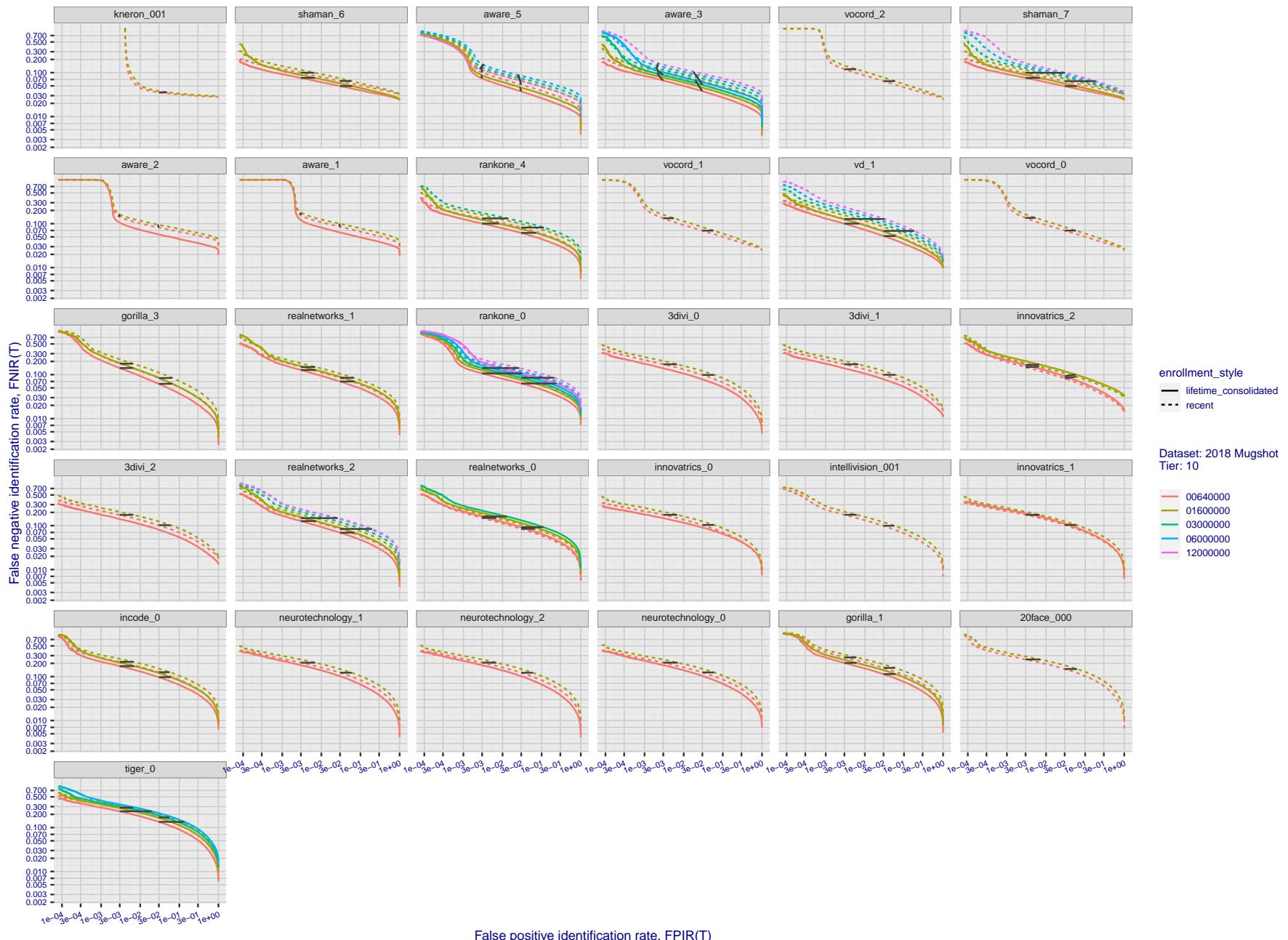


Figure 57: [FRVT-2018 Mugshot Dataset] Identification miss rates vs. false positive rates. The figure shows miss rates $\text{FNIR}(N, L, T)$ as a function of $\text{FPIR}(N, T)$, with N ranging from 640 000 to 12 000 000 as noted in rows 1-10 of Table 1. These error tradeoff characteristics are useful for applications where a threshold must be elevated to limit false positives, such as when human reviewer labor is not matched to the volume of searches. Dark lines join points of equal threshold: If horizontal, $\text{FPIR}(T)$ rises with N , and mate scores are independent of N . Other algorithms adjust scores in an attempt to make FPIR independent of N .

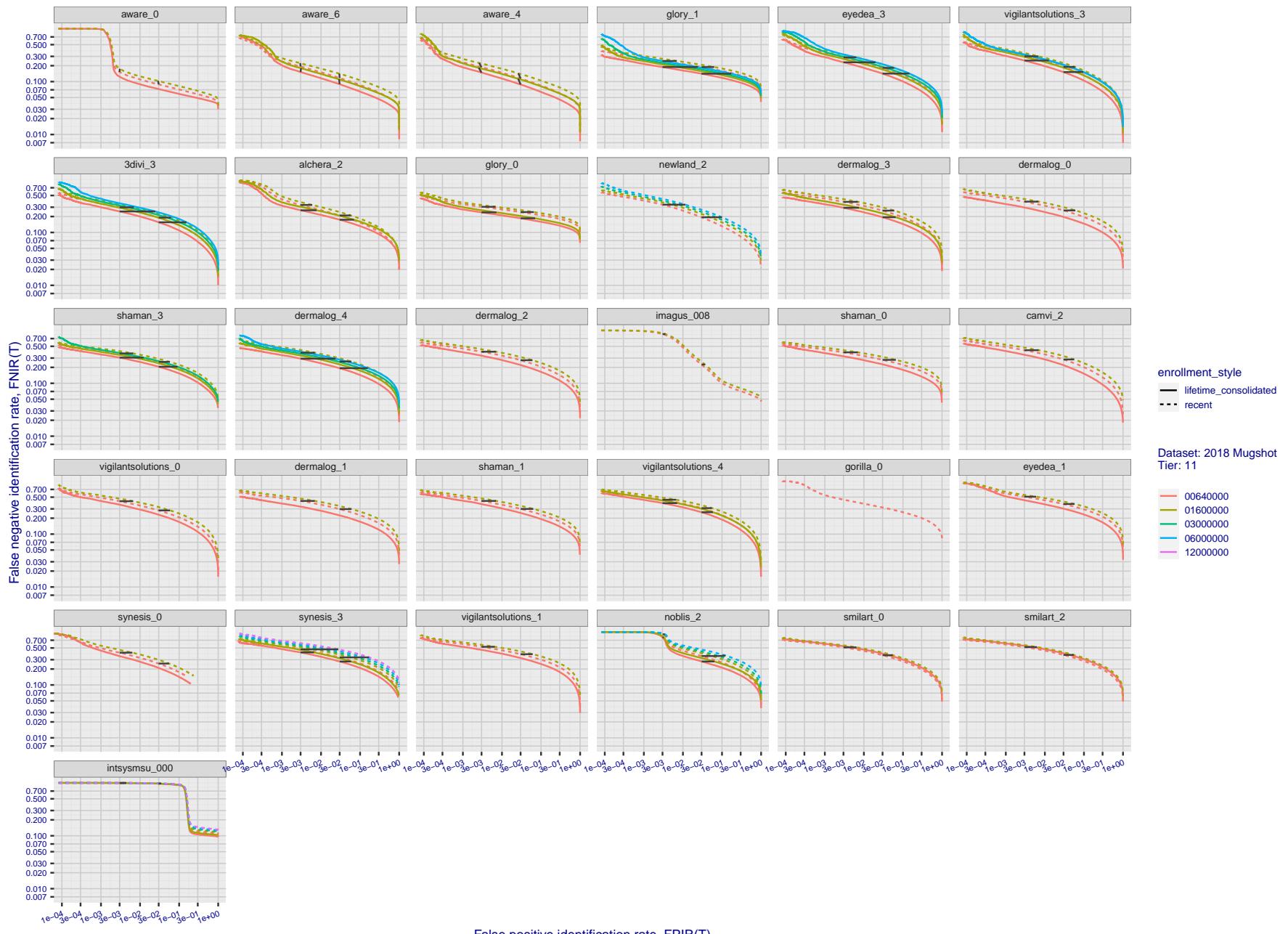


Figure 58: [FRVT-2018 Mugshot Dataset] Identification miss rates vs. false positive rates. The figure shows miss rates $\text{FNIR}(N, L, T)$ as a function of $\text{FPIR}(N, T)$, with N ranging from 640 000 to 12 000 000 as noted in rows 1-10 of Table 1. These error tradeoff characteristics are useful for applications where a threshold must be elevated to limit false positives, such as when human reviewer labor is not matched to the volume of searches. Dark lines join points of equal threshold: If horizontal, $\text{FPIR}(T)$ rises with N , and mate scores are independent of N . Other algorithms adjust scores in an attempt to make FPIR independent of N .

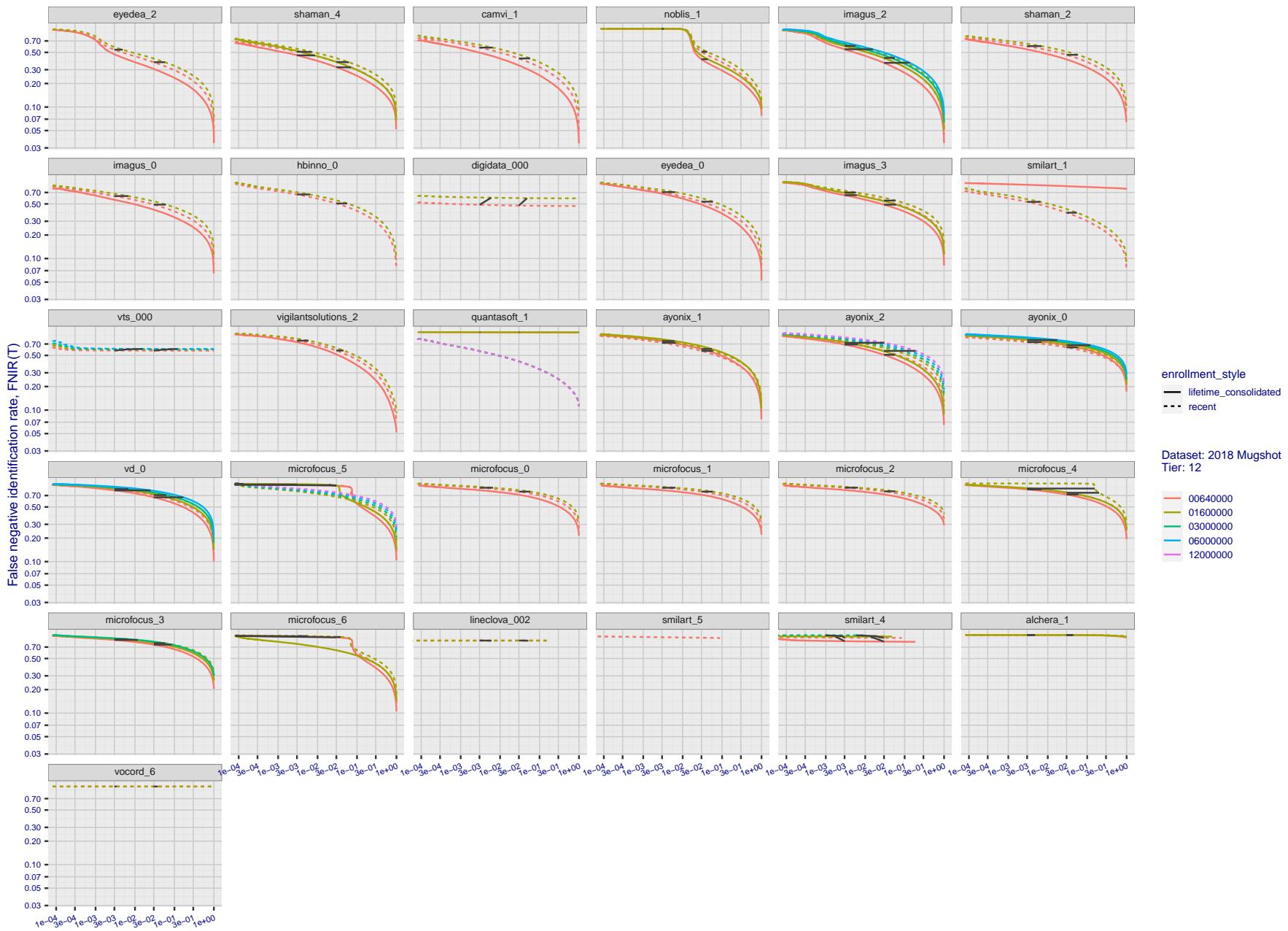


Figure 59: [FRVT-2018 Mugshot Dataset] Identification miss rates vs. false positive rates. The figure shows miss rates $\text{FNIR}(N, L, T)$ as a function of $\text{FPIR}(N, T)$, with N ranging from 640 000 to 12 000 000 as noted in rows 1-10 of Table 1. These error tradeoff characteristics are useful for applications where a threshold must be elevated to limit false positives, such as when human reviewer labor is not matched to the volume of searches. Dark lines join points of equal threshold: If horizontal, $\text{FPIR}(T)$ rises with N , and mate scores are independent of N . Other algorithms adjust scores in an attempt to make FPIR independent of N .

Appendix B Effect of time-lapse: Accuracy after face ageing

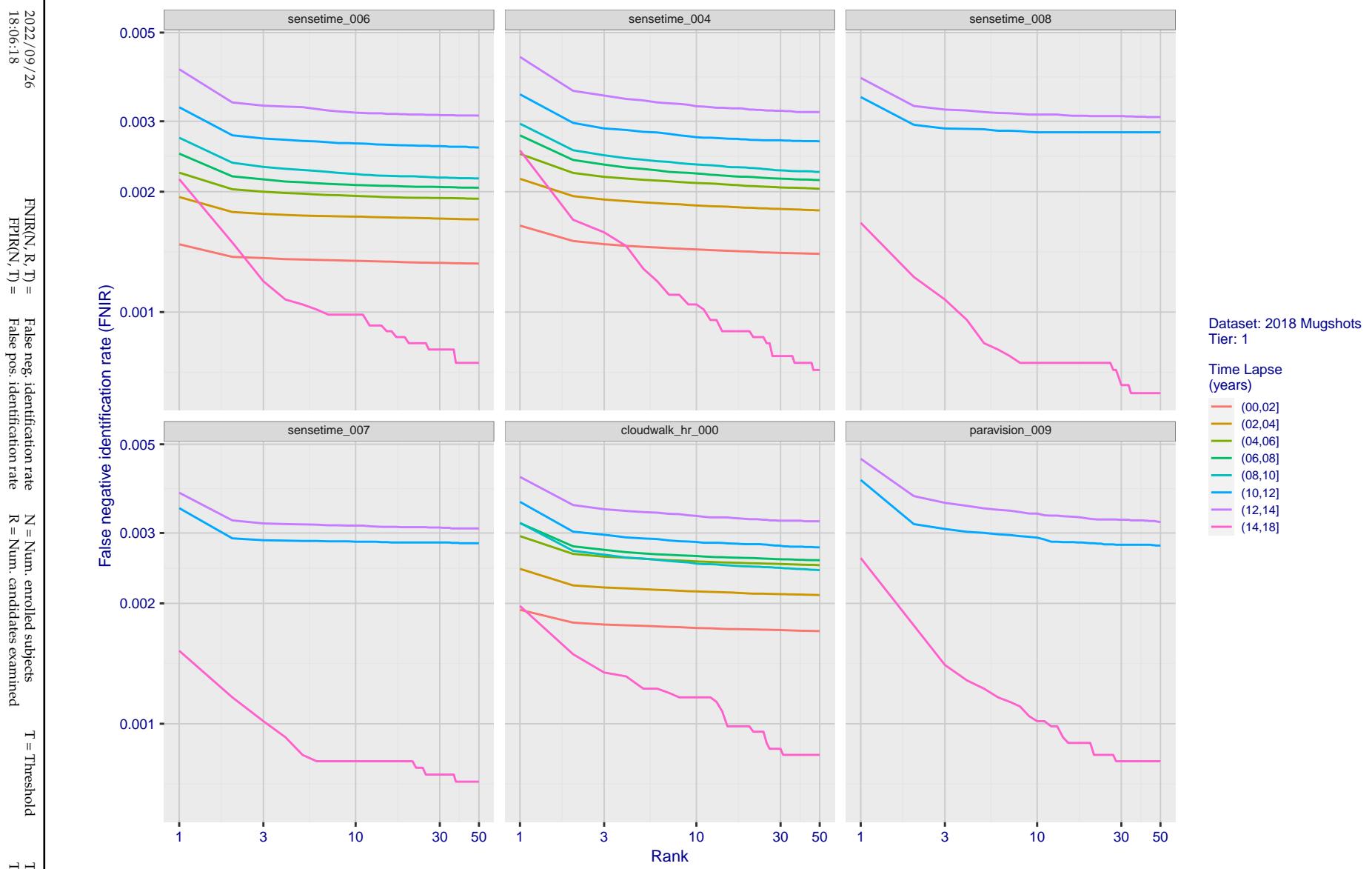


Figure 60: [FRVT-2018 Mugshot Ageing Dataset] Identification miss rates vs. rank by time-elapsed. The oldest image of each individual is enrolled. Thereafter, all more recent images are searched. Miss rates are computed over all searches noted in row 17 of Table 1 and binned by number of years between search and initial enrollment.

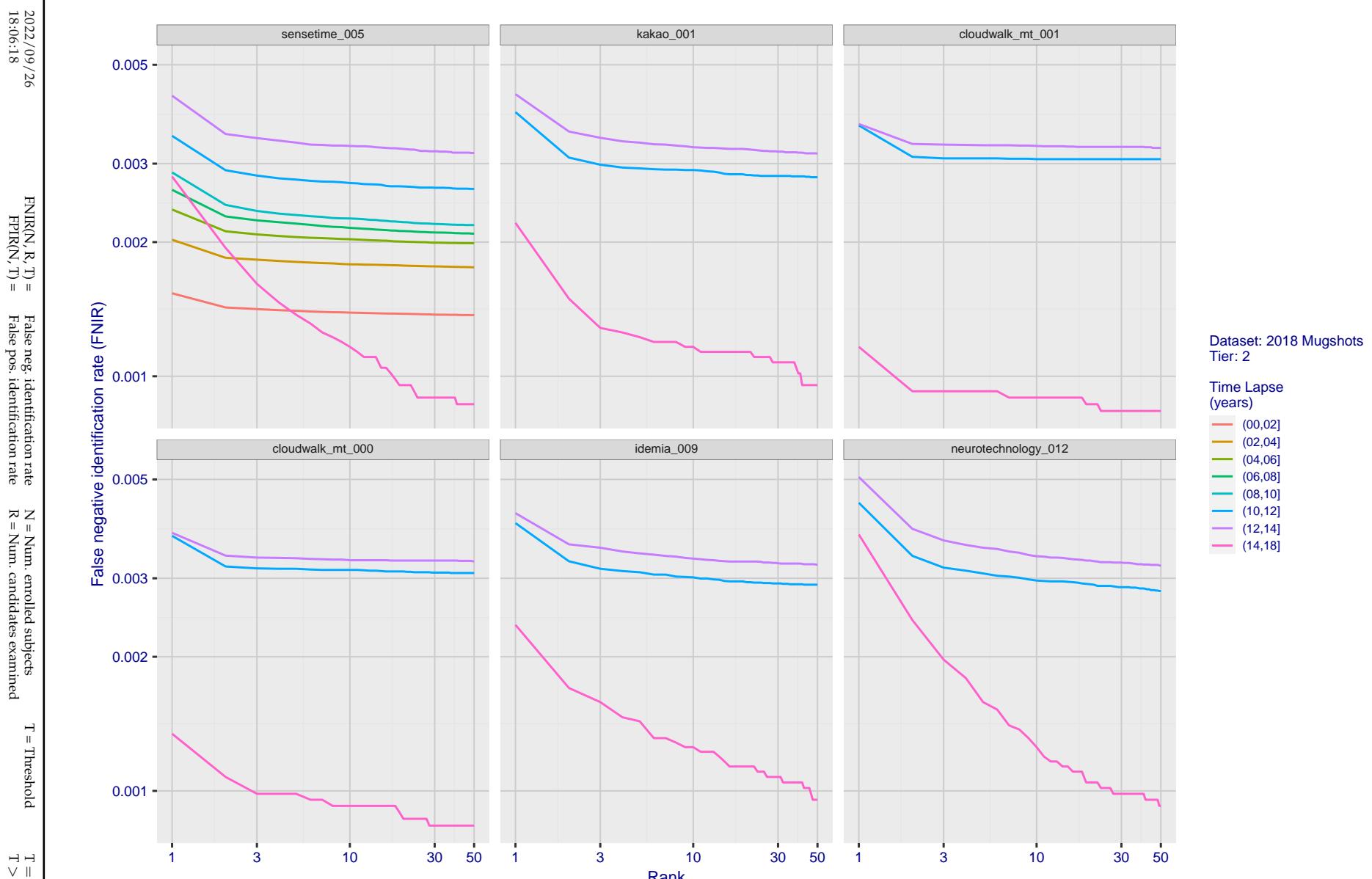


Figure 61: [FRVT-2018 Mugshot Ageing Dataset] Identification miss rates vs. rank by time-elapsed. The oldest image of each individual is enrolled. Thereafter, all more recent images are searched. Miss rates are computed over all searches noted in row 17 of Table 1 and binned by number of years between search and initial enrollment.

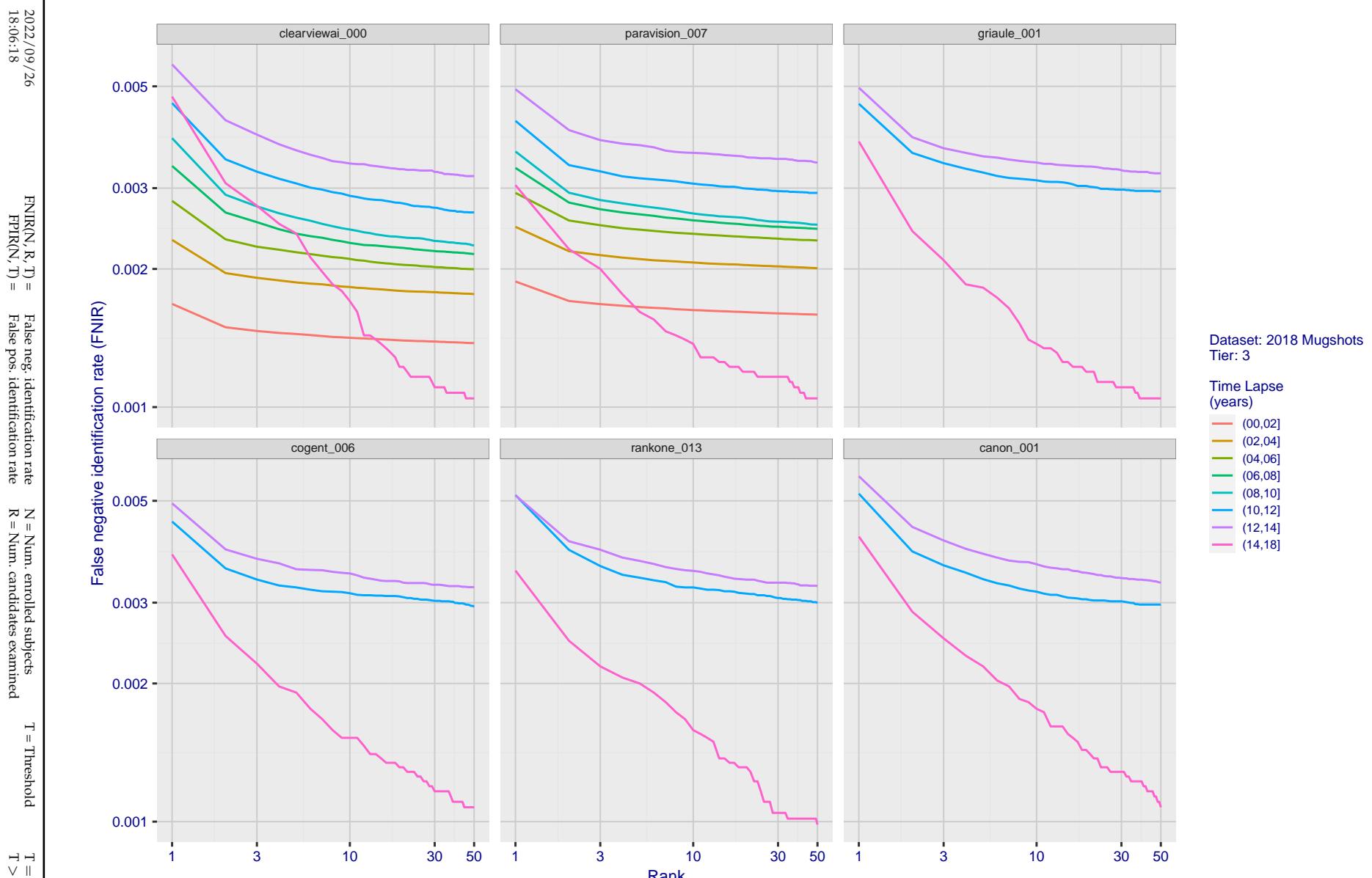


Figure 62: [FRVT-2018 Mugshot Ageing Dataset] Identification miss rates vs. rank by time-elapsed. The oldest image of each individual is enrolled. Thereafter, all more recent images are searched. Miss rates are computed over all searches noted in row 17 of Table 1 and binned by number of years between search and initial enrollment.

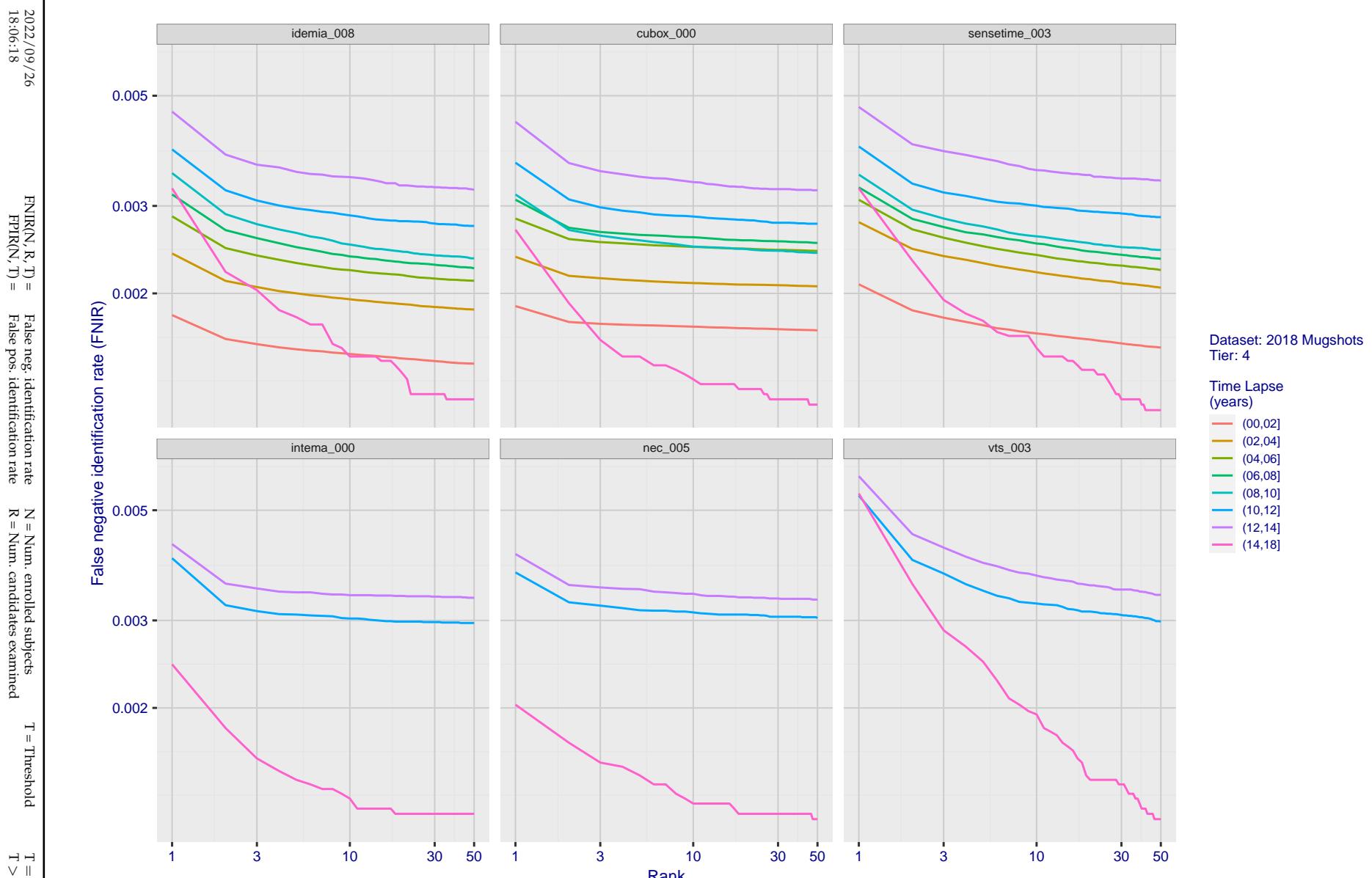


Figure 63: [FRVT-2018 Mugshot Ageing Dataset] Identification miss rates vs. rank by time-elapsed. The oldest image of each individual is enrolled. Thereafter, all more recent images are searched. Miss rates are computed over all searches noted in row 17 of Table 1 and binned by number of years between search and initial enrollment.

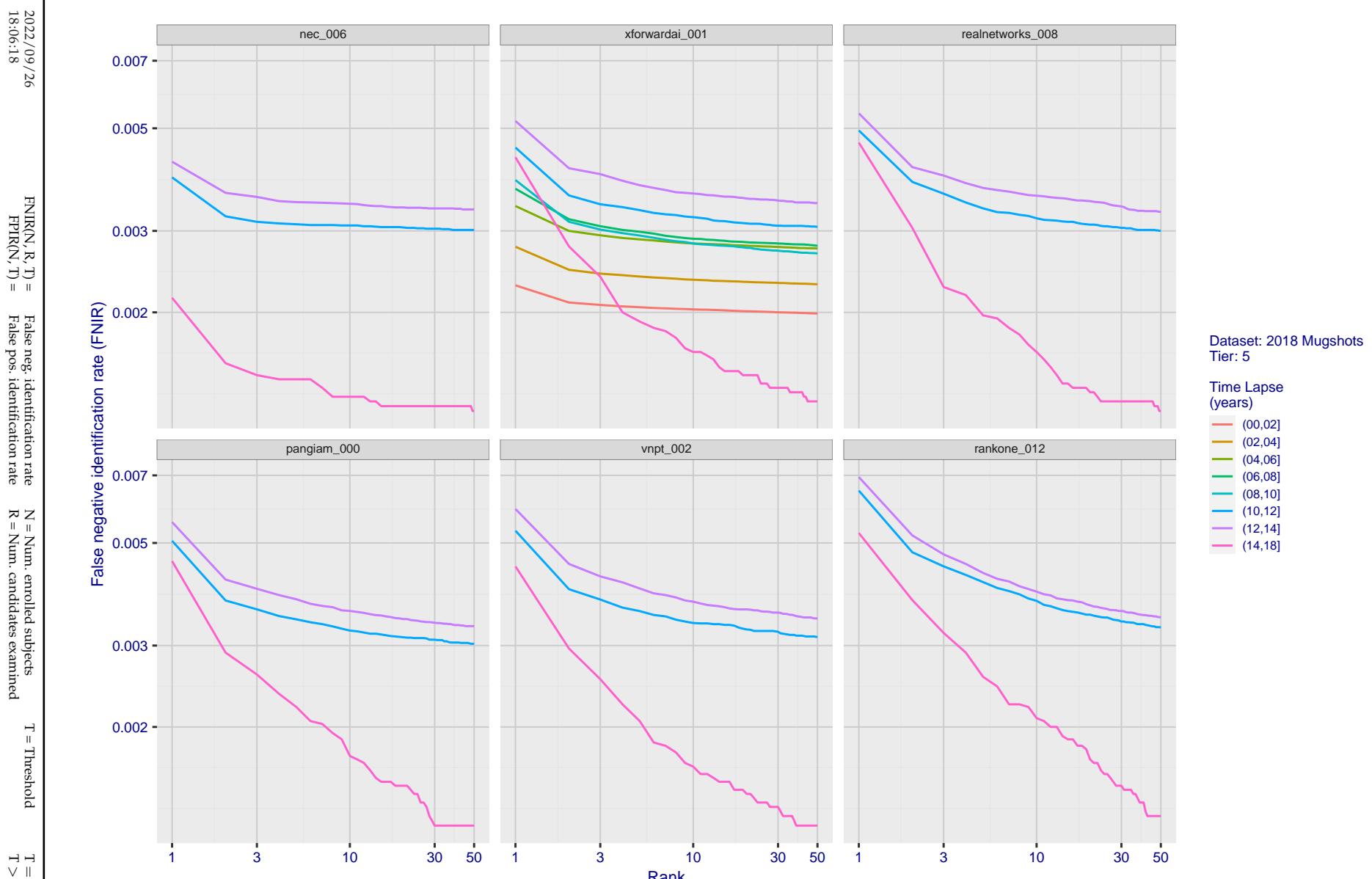


Figure 64: [FRVT-2018 Mugshot Ageing Dataset] Identification miss rates vs. rank by time-elapsed. The oldest image of each individual is enrolled. Thereafter, all more recent images are searched. Miss rates are computed over all searches noted in row 17 of Table 1 and binned by number of years between search and initial enrollment.

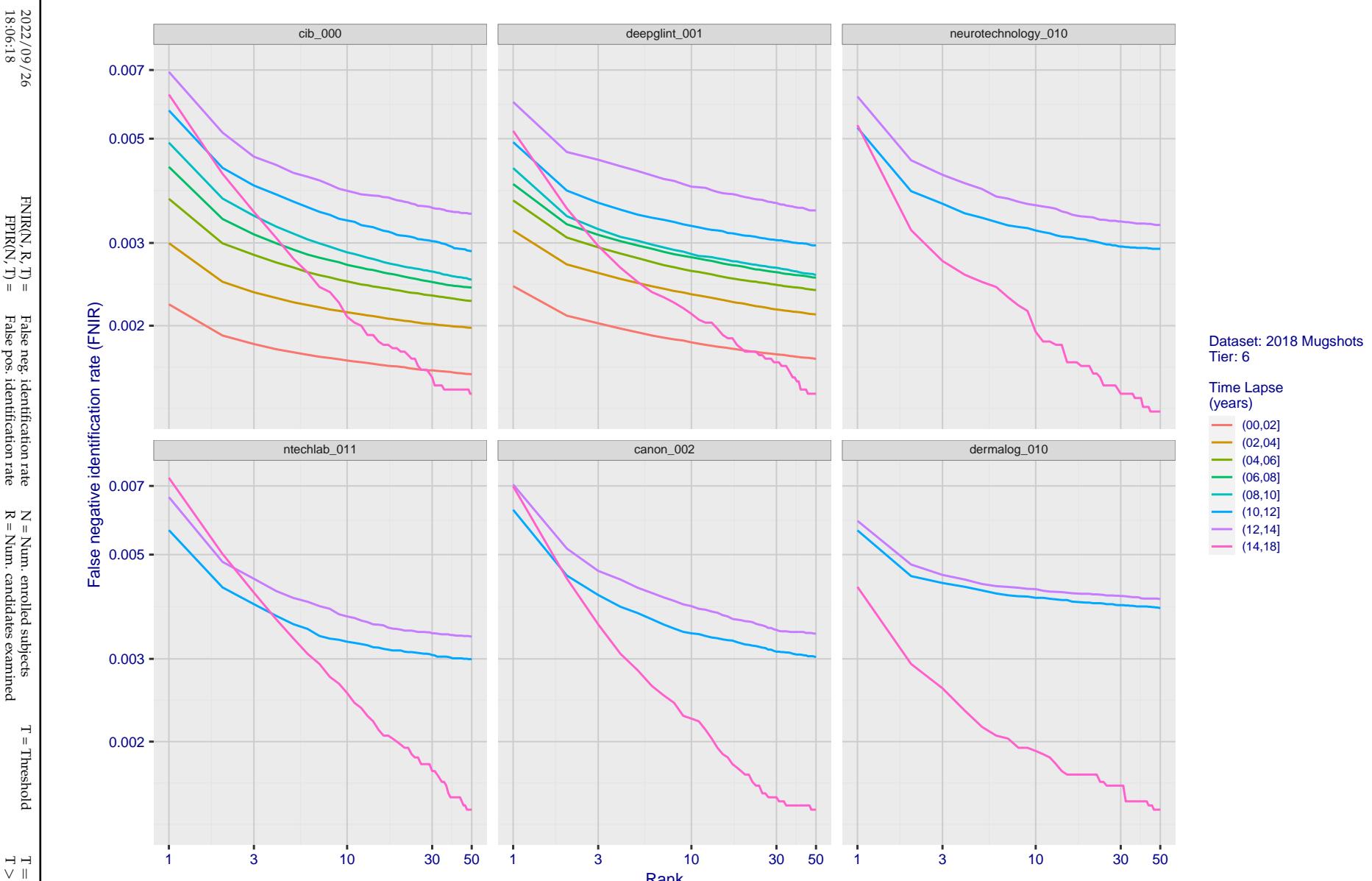


Figure 65: [FRVT-2018 Mugshot Ageing Dataset] Identification miss rates vs. rank by time-elapsed. The oldest image of each individual is enrolled. Thereafter, all more recent images are searched. Miss rates are computed over all searches noted in row 17 of Table 1 and binned by number of years between search and initial enrollment.

2022/09/26
18:06:18FNIR(N, R, T) = False neg. identification rate
FPIR(N, T) = False pos. identification rateN = Num. enrolled subjects
R = Num. candidates examinedT = Threshold
T = 0 → Investigation

T > 0 → Identification

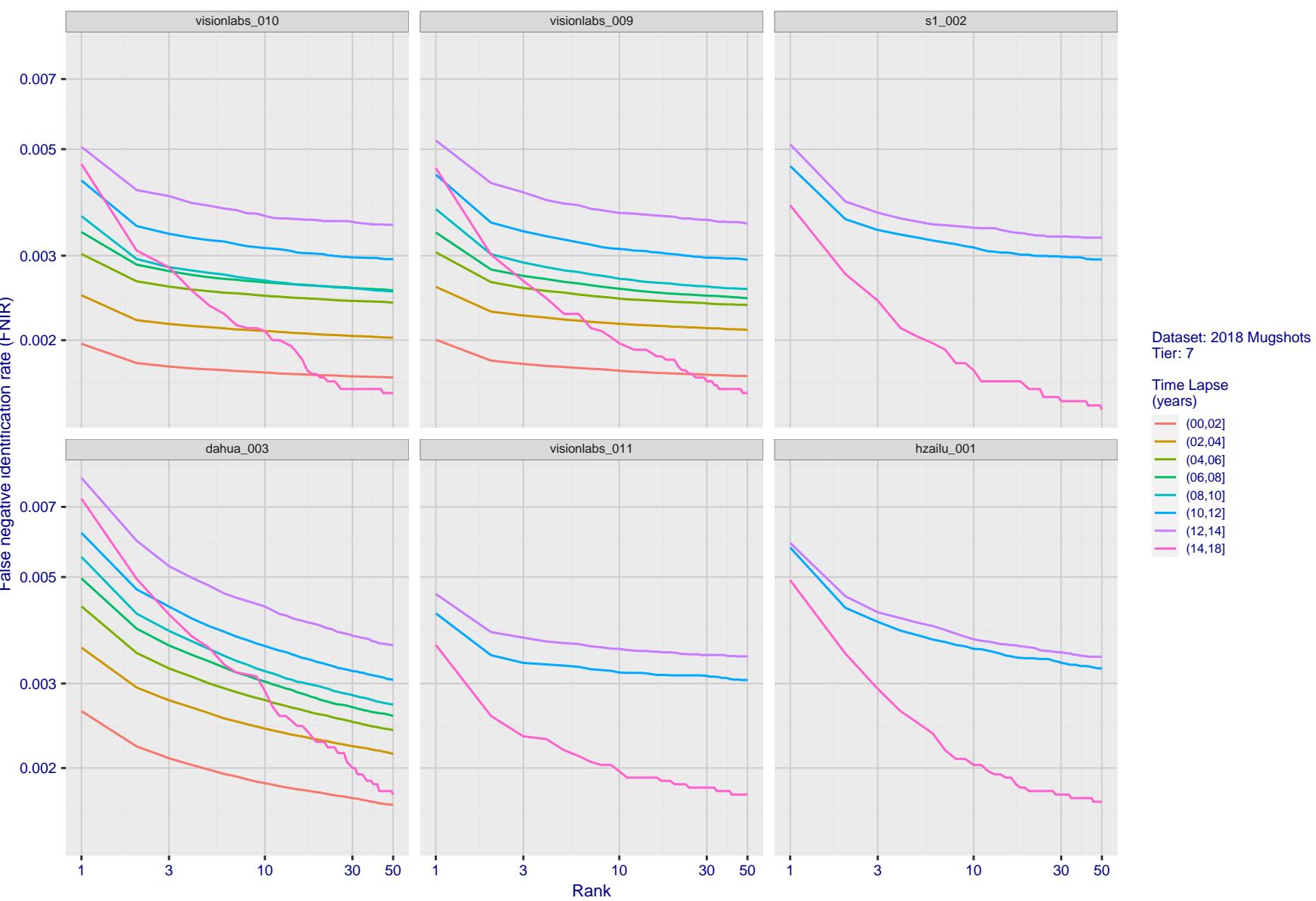


Figure 66: [FRVT-2018 Mugshot Ageing Dataset] Identification miss rates vs. rank by time-elapsed. The oldest image of each individual is enrolled. Thereafter, all more recent images are searched. Miss rates are computed over all searches noted in row 17 of Table 1 and binned by number of years between search and initial enrollment.

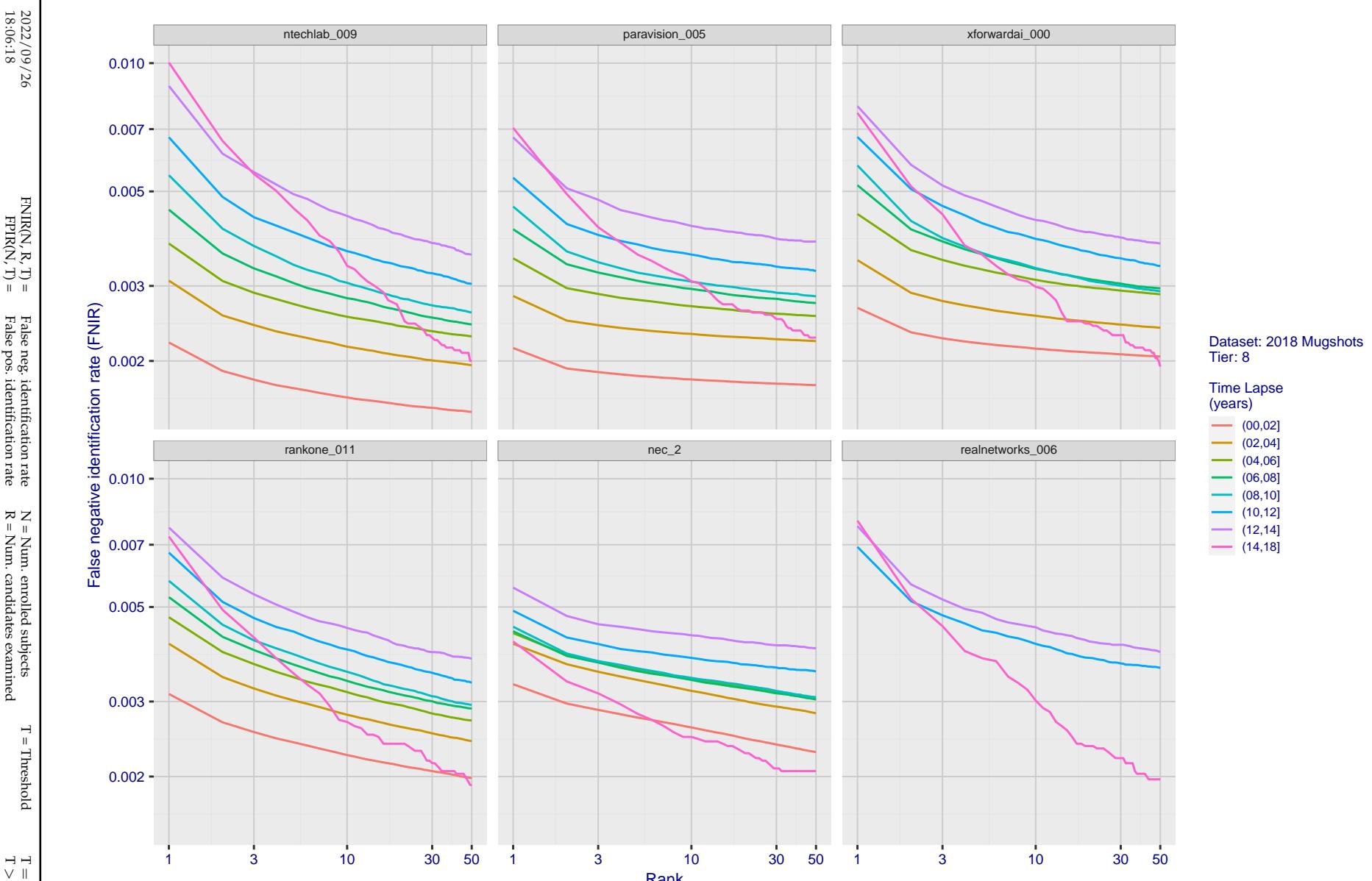


Figure 67: [FRVT-2018 Mugshot Ageing Dataset] Identification miss rates vs. rank by time-elapsed. The oldest image of each individual is enrolled. Thereafter, all more recent images are searched. Miss rates are computed over all searches noted in row 17 of Table 1 and binned by number of years between search and initial enrollment.

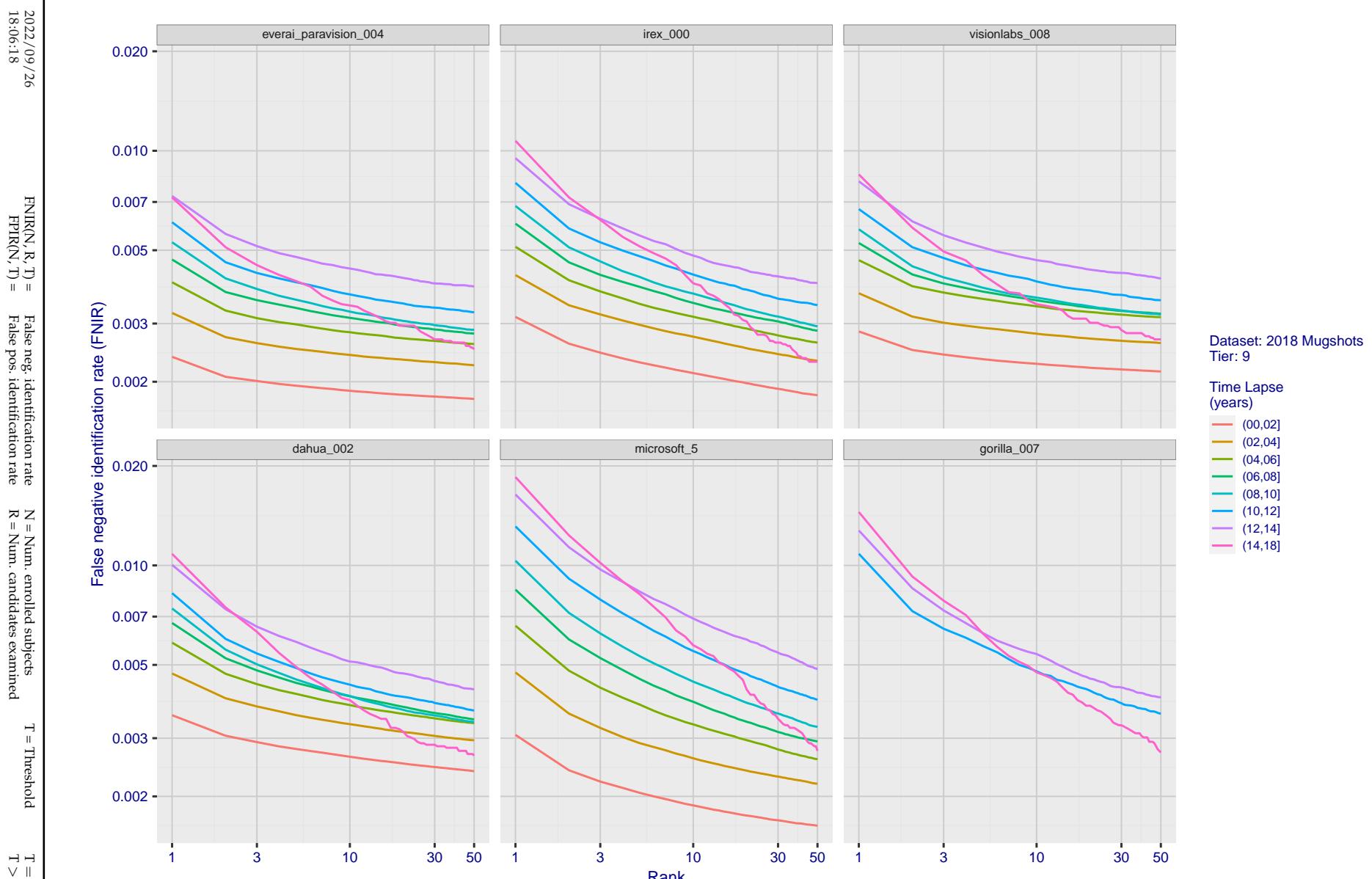


Figure 68: [FRVT-2018 Mugshot Ageing Dataset] Identification miss rates vs. rank by time-elapsed. The oldest image of each individual is enrolled. Thereafter, all more recent images are searched. Miss rates are computed over all searches noted in row 17 of Table 1 and binned by number of years between search and initial enrollment.

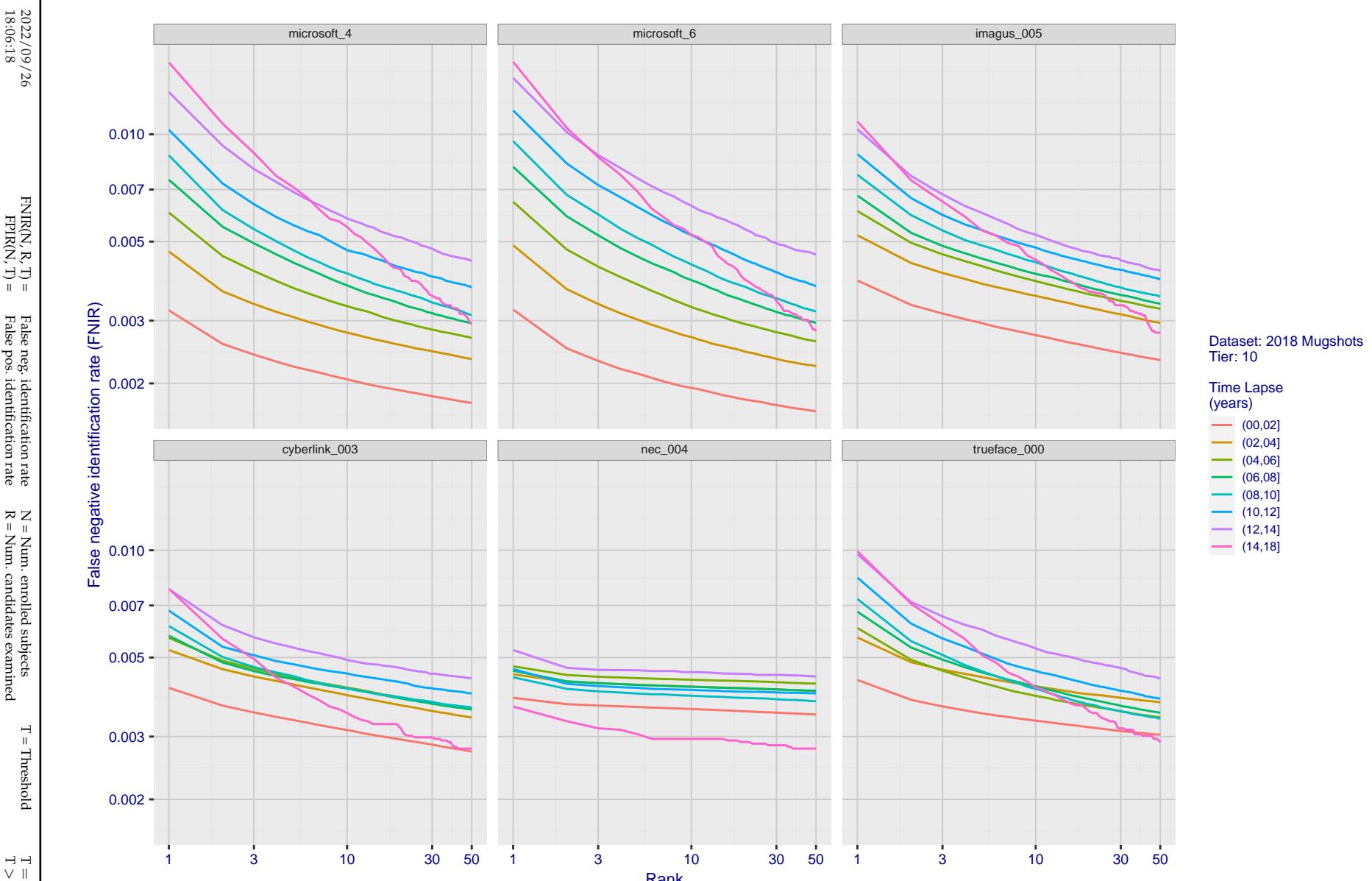


Figure 69: [FRVT-2018 Mugshot Ageing Dataset] Identification miss rates vs. rank by time-elapsed. The oldest image of each individual is enrolled. Thereafter, all more recent images are searched. Miss rates are computed over all searches noted in row 17 of Table 1 and binned by number of years between search and initial enrollment.

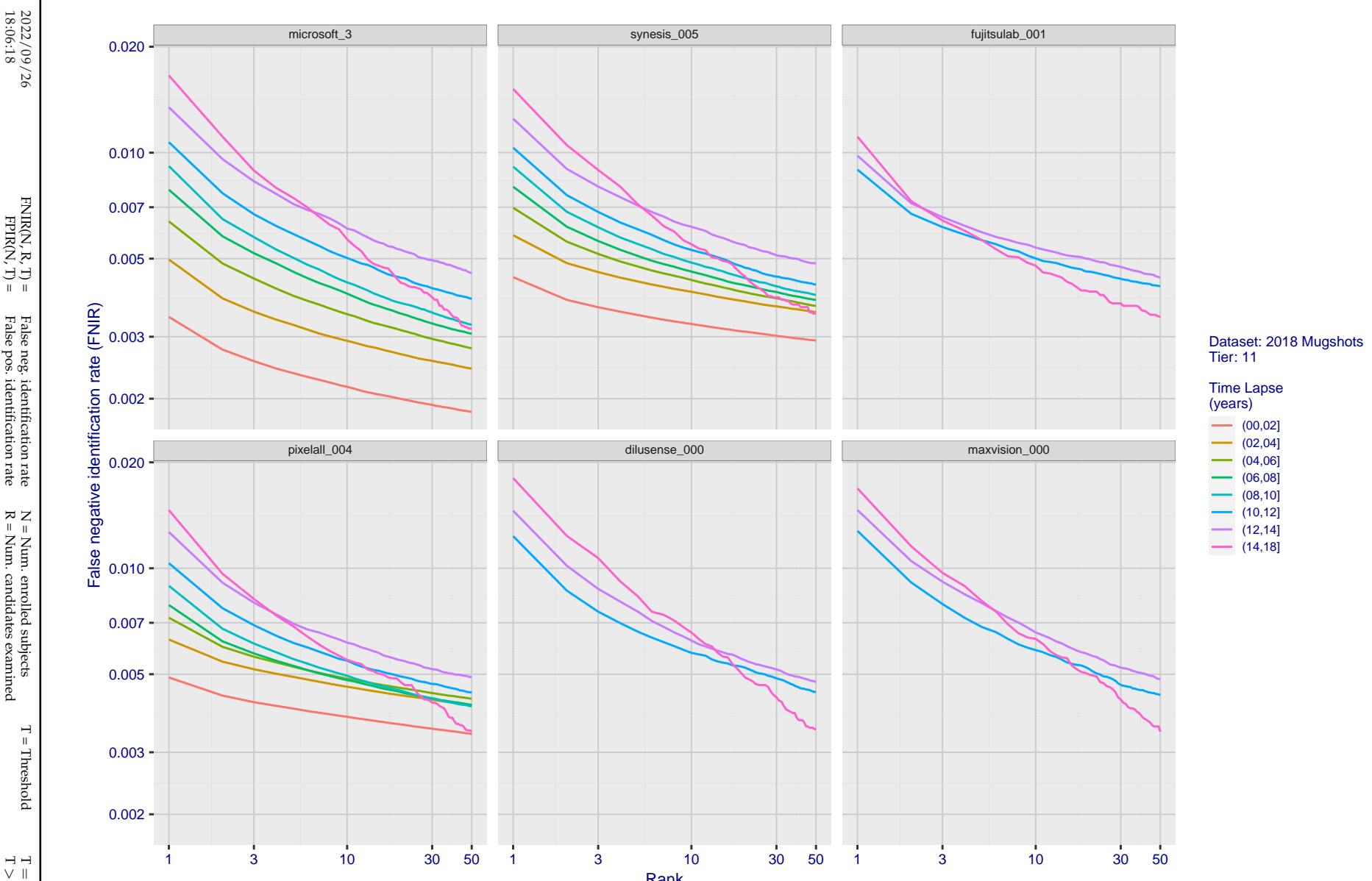


Figure 70: [FRVT-2018 Mugshot Ageing Dataset] Identification miss rates vs. rank by time-elapsed. The oldest image of each individual is enrolled. Thereafter, all more recent images are searched. Miss rates are computed over all searches noted in row 17 of Table 1 and binned by number of years between search and initial enrollment.

2022/09/26
18:06:18FNIR(N, R, T) = False neg. identification rate
FPIR(N, T) = False pos. identification rateN = Num. enrolled subjects
R = Num. candidates examinedT = Threshold
T = 0 → Investigation

T > 0 → Identification

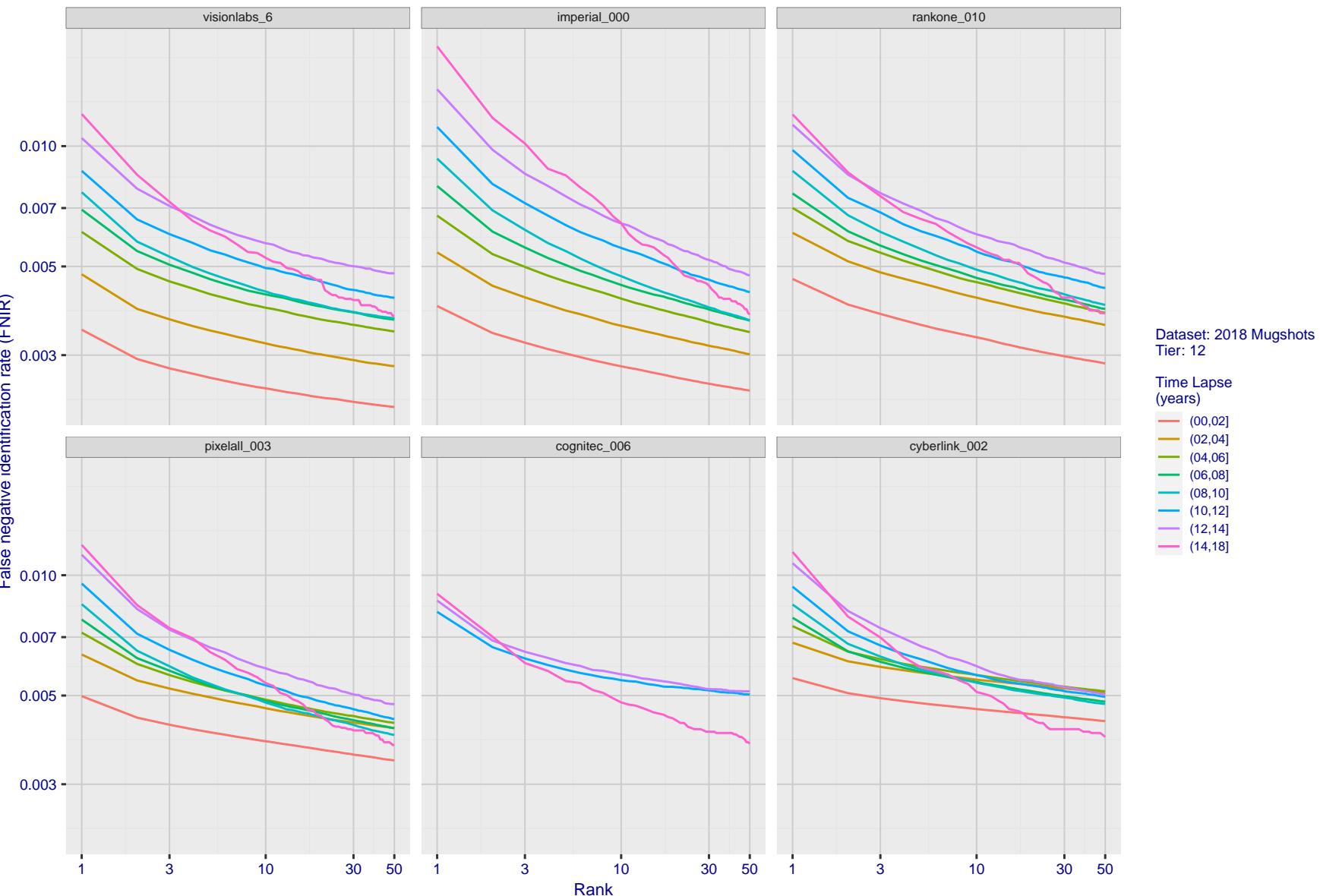


Figure 71: [FRVT-2018 Mugshot Ageing Dataset] Identification miss rates vs. rank by time-elapsed. The oldest image of each individual is enrolled. Thereafter, all more recent images are searched. Miss rates are computed over all searches noted in row 17 of Table 1 and binned by number of years between search and initial enrollment.

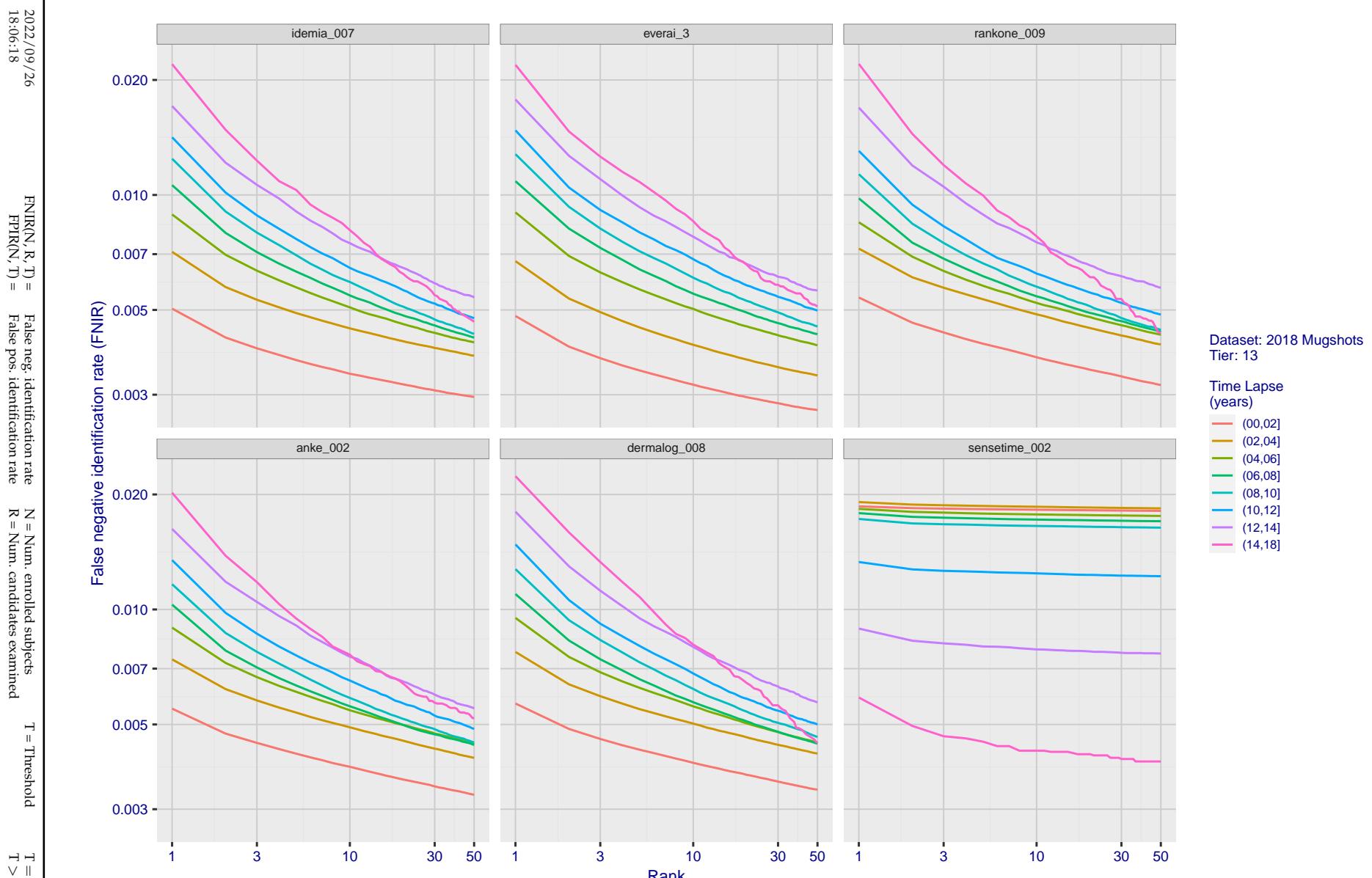


Figure 72: [FRVT-2018 Mugshot Ageing Dataset] Identification miss rates vs. rank by time-elapsed. The oldest image of each individual is enrolled. Thereafter, all more recent images are searched. Miss rates are computed over all searches noted in row 17 of Table 1 and binned by number of years between search and initial enrollment.

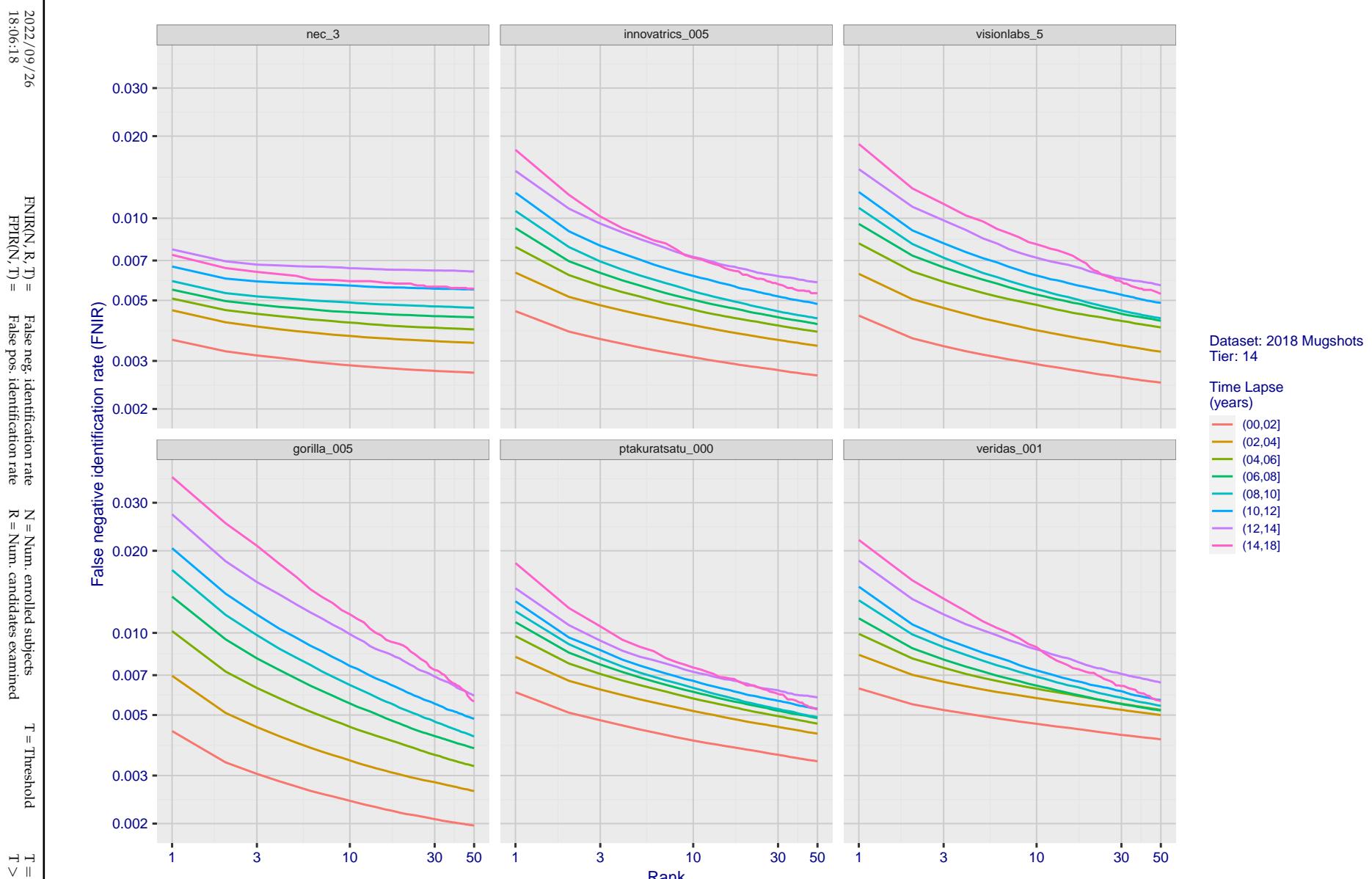


Figure 73: [FRVT-2018 Mugshot Ageing Dataset] Identification miss rates vs. rank by time-elapsed. The oldest image of each individual is enrolled. Thereafter, all more recent images are searched. Miss rates are computed over all searches noted in row 17 of Table 1 and binned by number of years between search and initial enrollment.

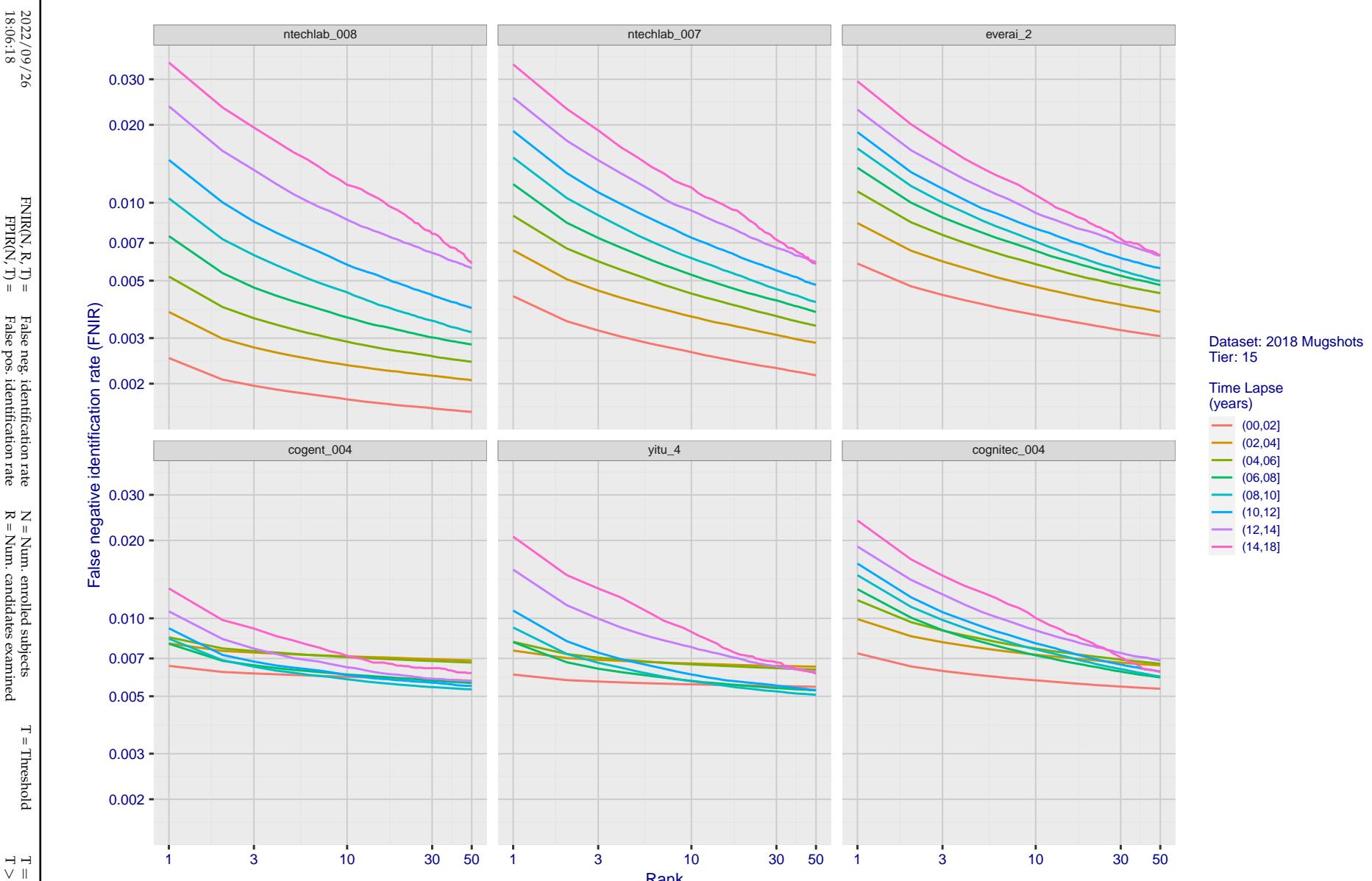


Figure 74: [FRVT-2018 Mugshot Ageing Dataset] Identification miss rates vs. rank by time-elapsed. The oldest image of each individual is enrolled. Thereafter, all more recent images are searched. Miss rates are computed over all searches noted in row 17 of Table 1 and binned by number of years between search and initial enrollment.

2022/09/26
18:06:18FNIR(N, R, T) = False neg. identification rate
FPIR(N, T) = False pos. identification rateN = Num. enrolled subjects
R = Num. candidates examined

T = Threshold

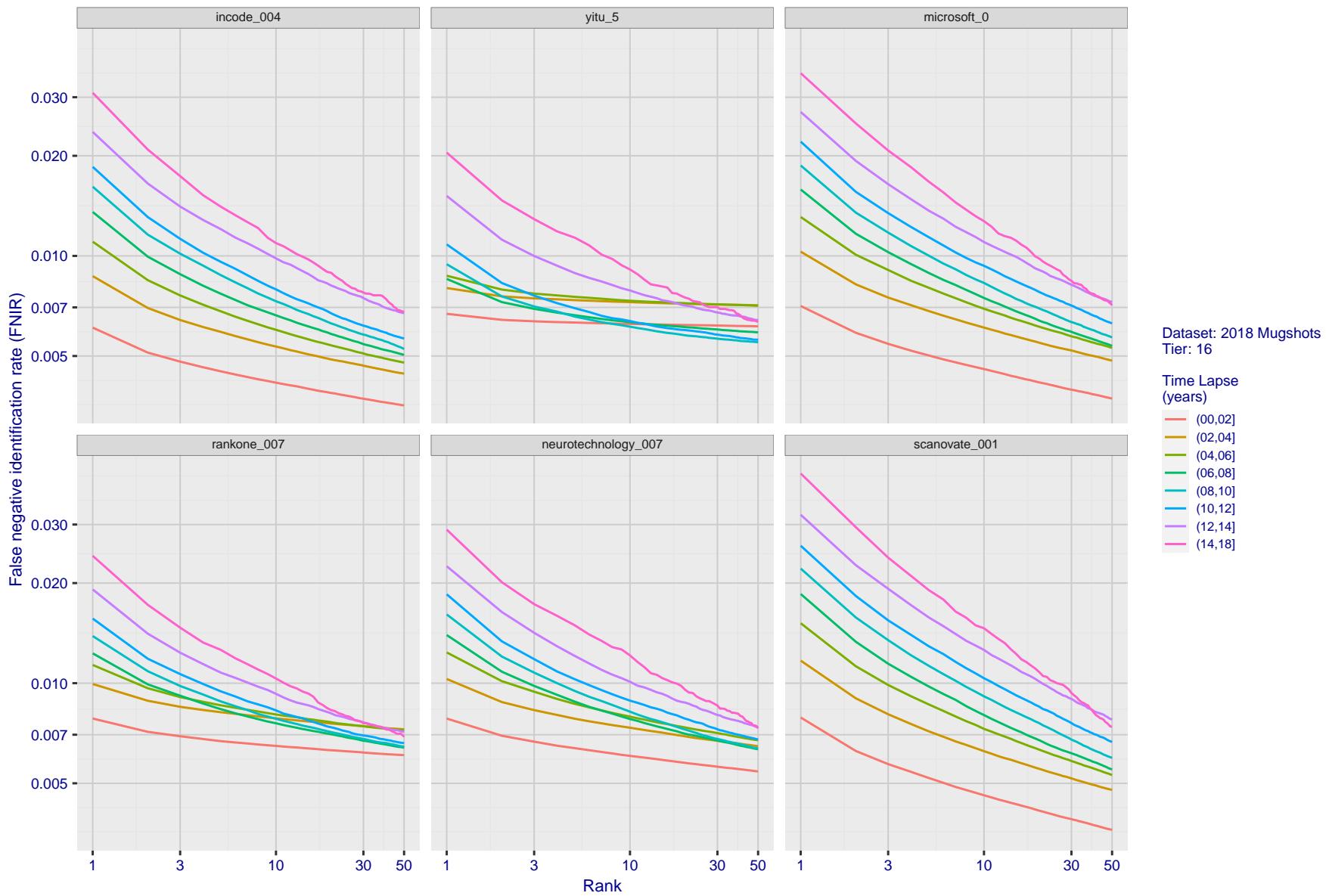
T = 0 → Investigation
T > 0 → Identification

Figure 75: [FRVT-2018 Mugshot Ageing Dataset] Identification miss rates vs. rank by time-elapsed. The oldest image of each individual is enrolled. Thereafter, all more recent images are searched. Miss rates are computed over all searches noted in row 17 of Table 1 and binned by number of years between search and initial enrollment.

2022/09/26
18:06:18FNIR(N, R, T) = False neg. identification rate
FPIR(N, T) = False pos. identification rateN = Num. enrolled subjects
R = Num. candidates examined

T = Threshold

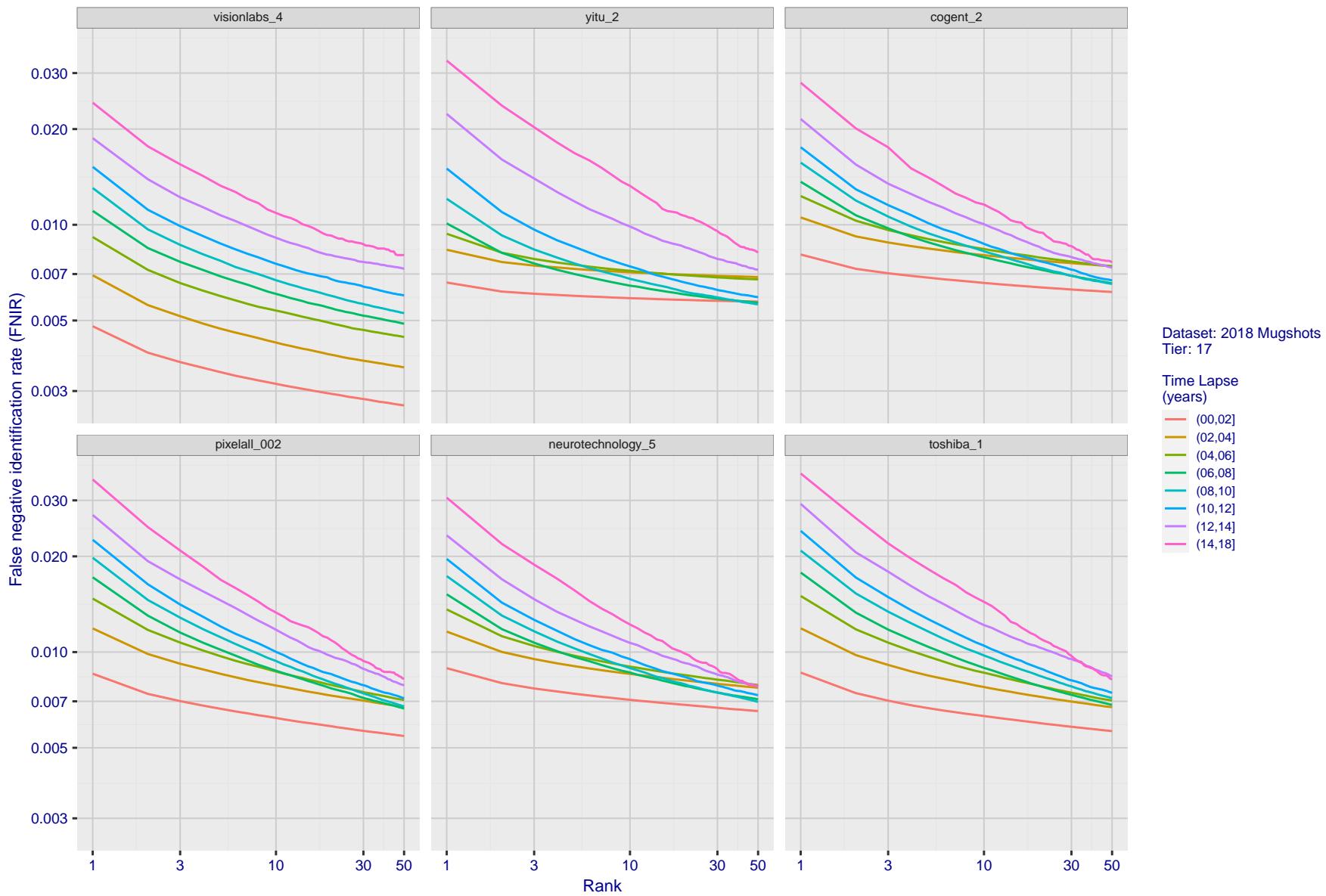
T = 0 → Investigation
T > 0 → Identification

Figure 76: [FRVT-2018 Mugshot Ageing Dataset] Identification miss rates vs. rank by time elapsed. The oldest image of each individual is enrolled. Thereafter, all more recent images are searched. Miss rates are computed over all searches noted in row 17 of Table 1 and binned by number of years between search and initial enrollment.

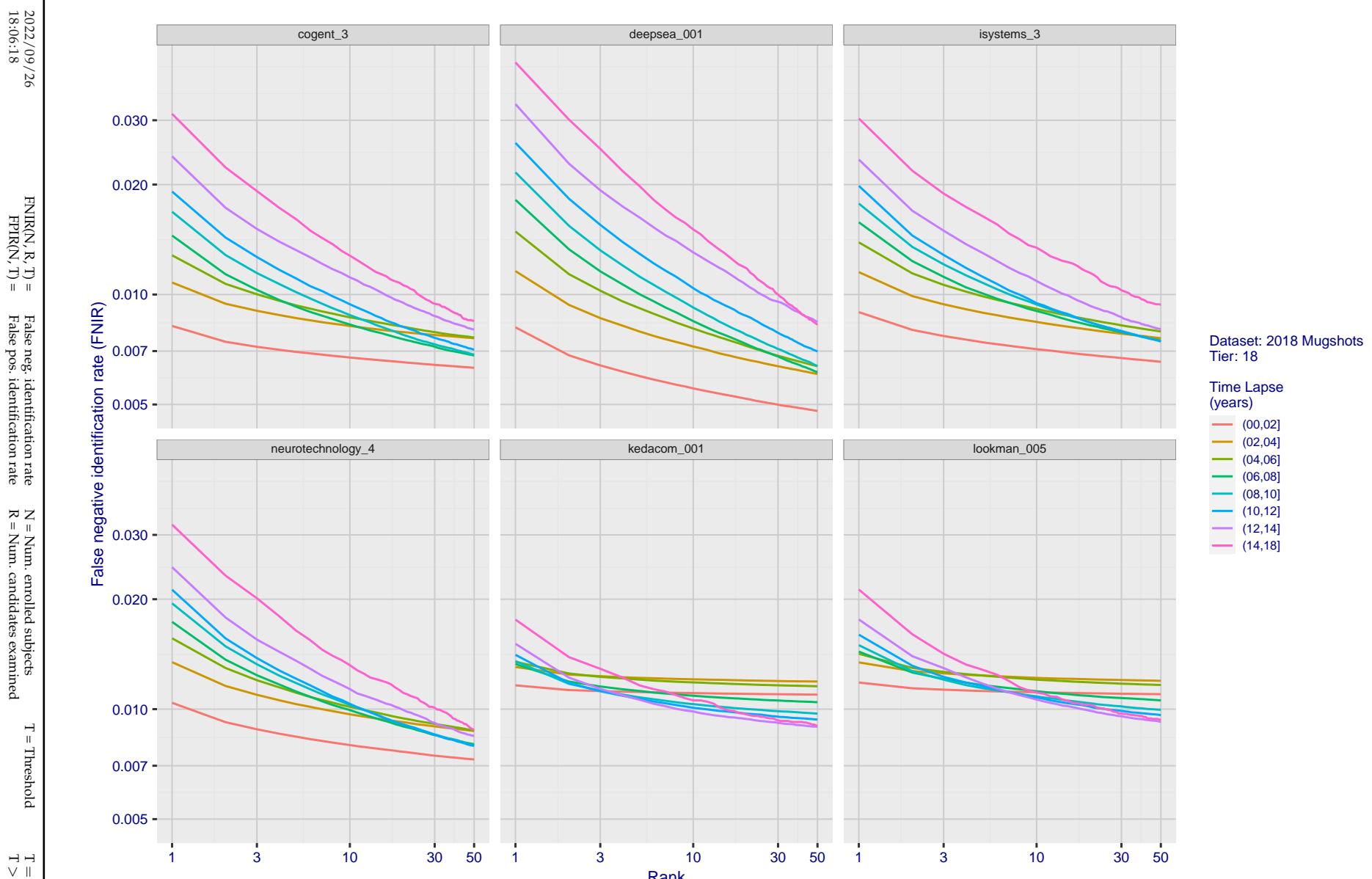


Figure 77: [FRVT-2018 Mugshot Ageing Dataset] Identification miss rates vs. rank by time-elapsed. The oldest image of each individual is enrolled. Thereafter, all more recent images are searched. Miss rates are computed over all searches noted in row 17 of Table 1 and binned by number of years between search and initial enrollment.

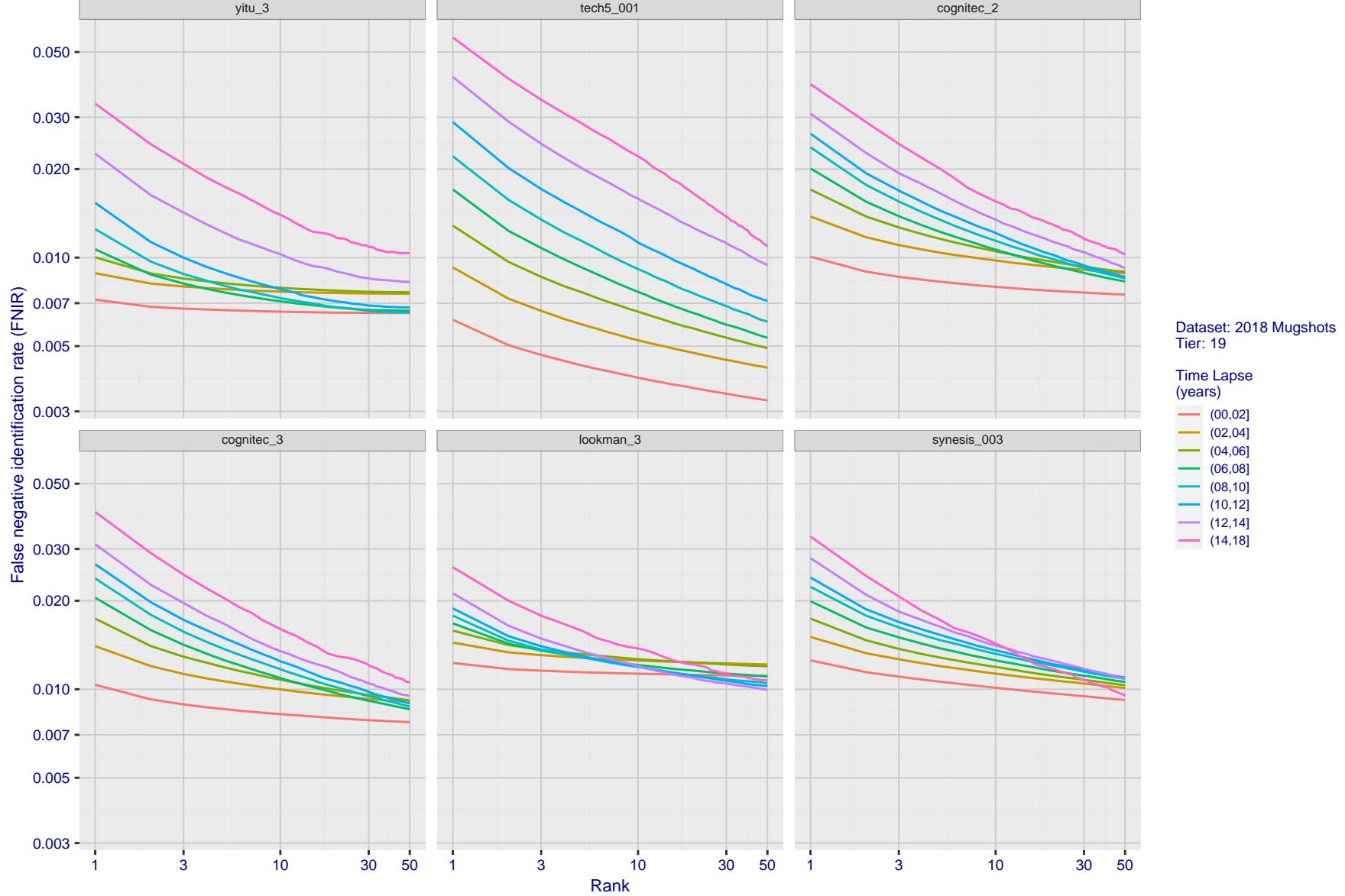


Figure 78: [FRVT-2018 Mugshot Ageing Dataset] Identification miss rates vs. rank by time-elapsed. The oldest image of each individual is enrolled. Thereafter, all more recent images are searched. Miss rates are computed over all searches noted in row 17 of Table 1 and binned by number of years between search and initial enrollment.

2022/09/26
18:06:18FNIR(N, R, T) = False neg. identification rate
FPIR(N, T) = False pos. identification rateN = Num. enrolled subjects
R = Num. candidates examinedT = Threshold
T = 0 → Investigation

T > 0 → Identification

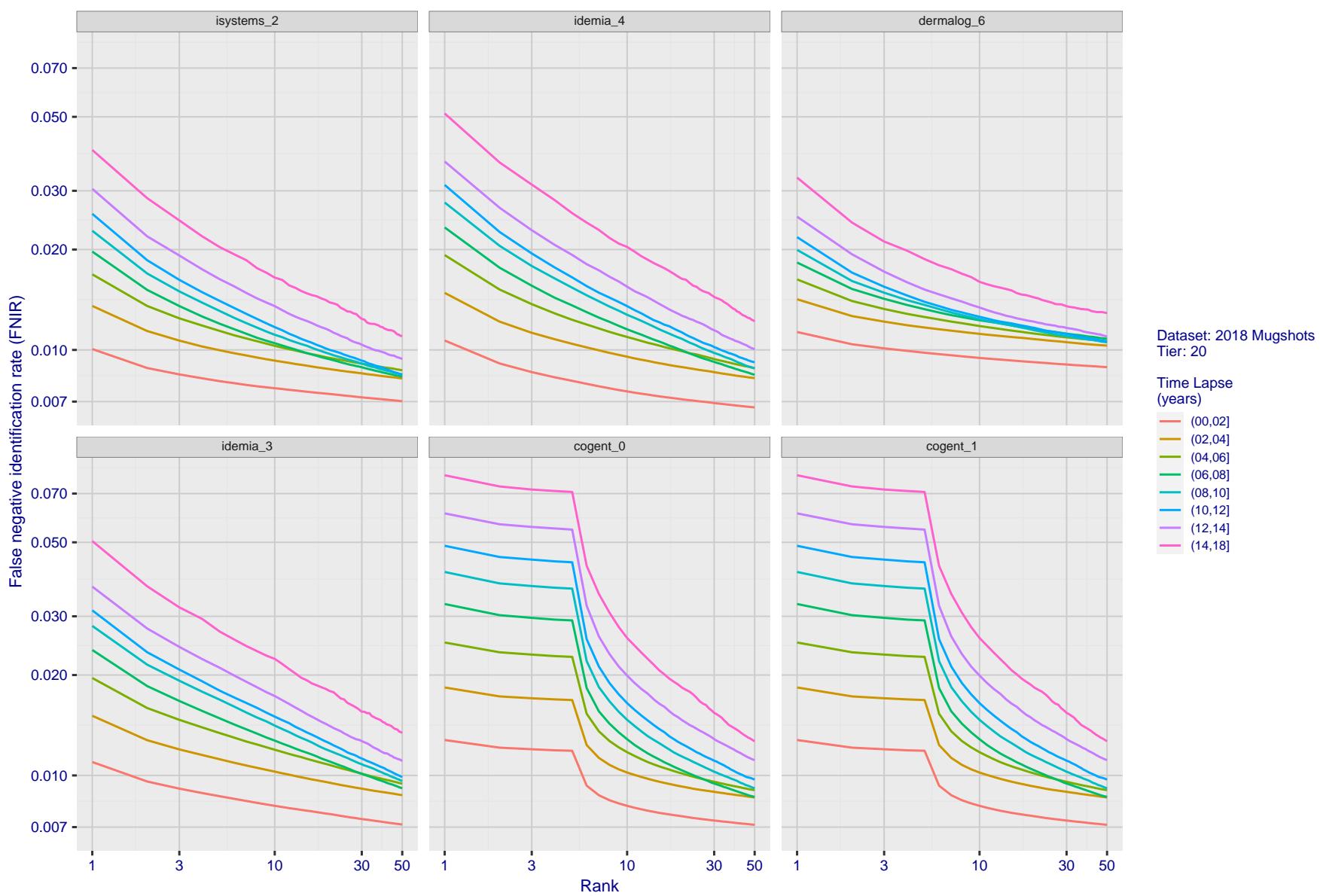


Figure 79: [FRVT-2018 Mugshot Ageing Dataset] Identification miss rates vs. rank by time elapsed. The oldest image of each individual is enrolled. Thereafter, all more recent images are searched. Miss rates are computed over all searches noted in row 17 of Table 1 and binned by number of years between search and initial enrollment.

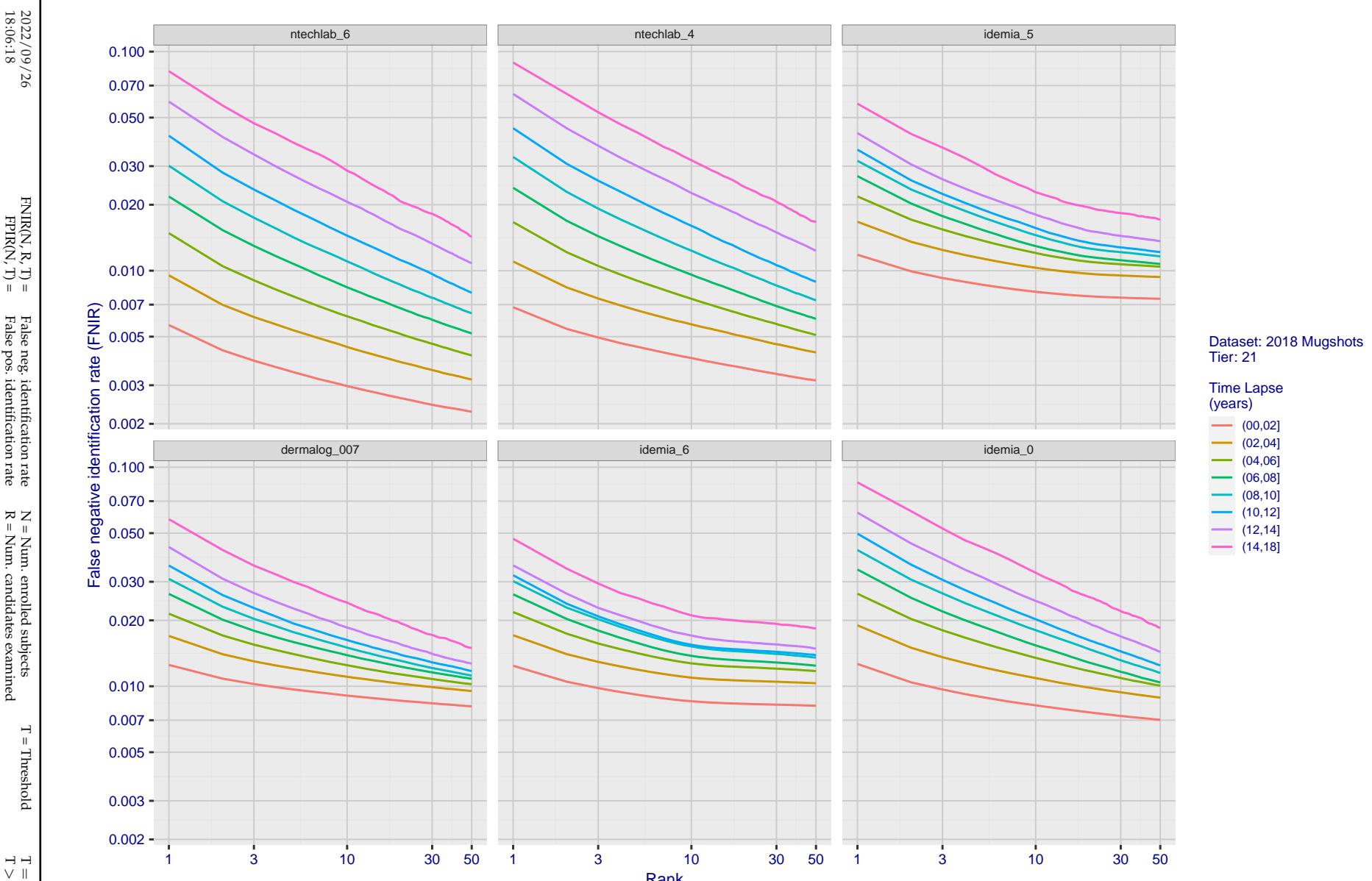


Figure 80: [FRVT-2018 Mugshot Ageing Dataset] Identification miss rates vs. rank by time-elapsed. The oldest image of each individual is enrolled. Thereafter, all more recent images are searched. Miss rates are computed over all searches noted in row 17 of Table 1 and binned by number of years between search and initial enrollment.

2022/09/26
18:06:18FNIR(N, R, T) = False neg. identification rate
FPIR(N, T) = False pos. identification rateN = Num. enrolled subjects
R = Num. candidates examined

T = Threshold

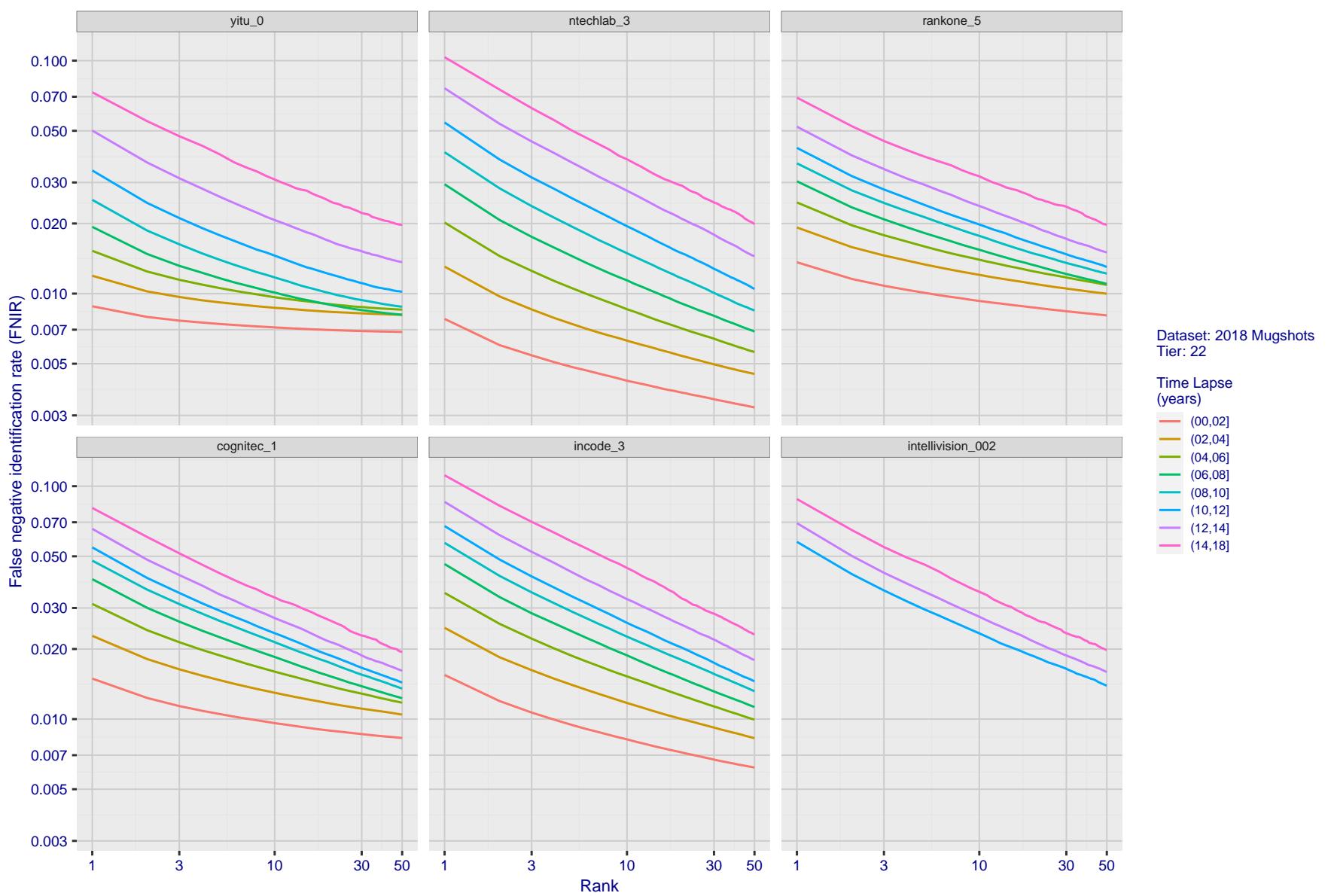
T = 0 → Investigation
T > 0 → Identification

Figure 81: [FRVT-2018 Mugshot Ageing Dataset] Identification miss rates vs. rank by time-elapsed. The oldest image of each individual is enrolled. Thereafter, all more recent images are searched. Miss rates are computed over all searches noted in row 17 of Table 1 and binned by number of years between search and initial enrollment.

2022/09/26
18:06:18FNIR(N, R, T) = False neg. identification rate
FPFR(N, T) = False pos. identification rateN = Num. enrolled subjects
R = Num. candidates examinedT = Threshold
T = 0 → Investigation

T > 0 → Identification

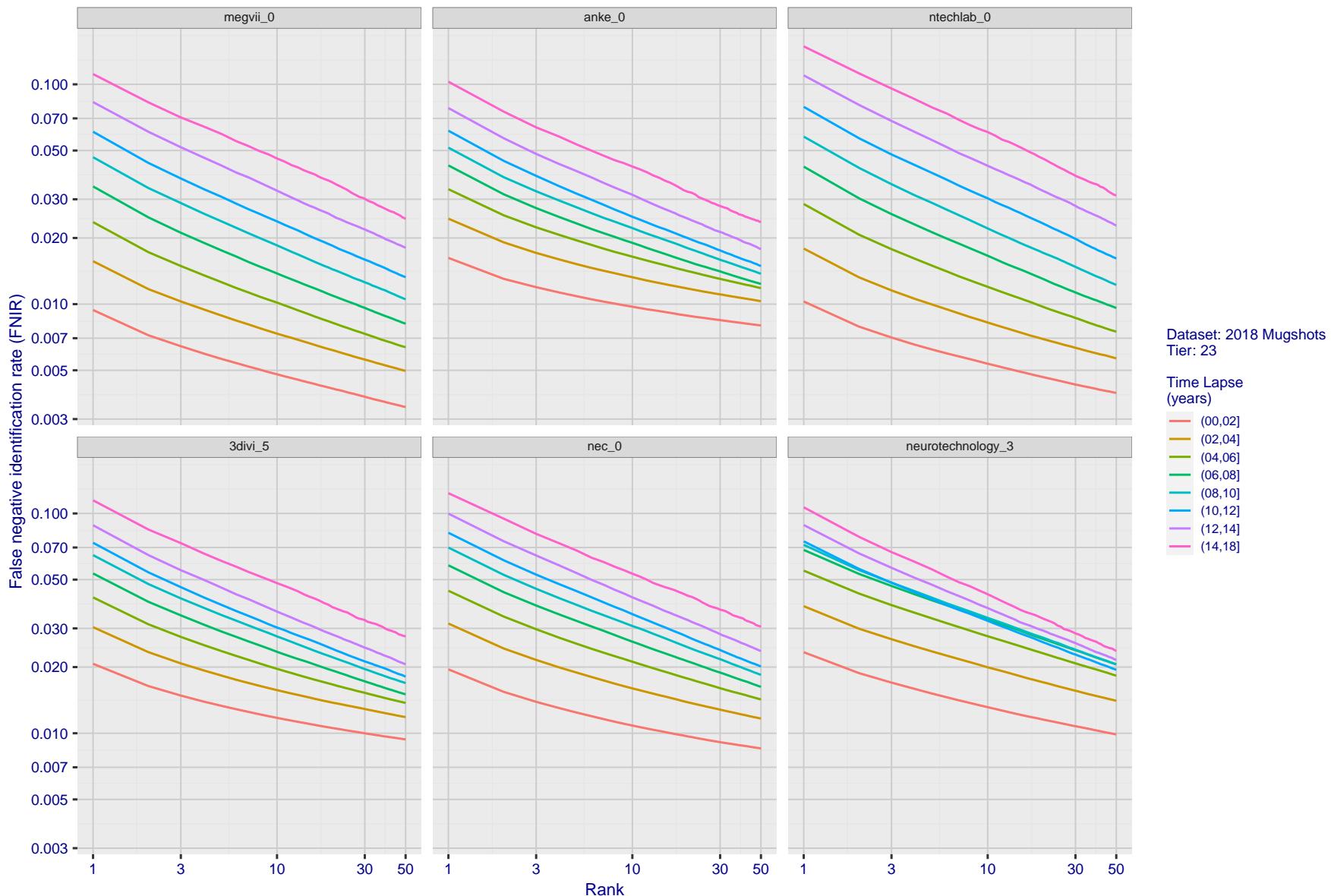


Figure 82: [FRVT-2018 Mugshot Ageing Dataset] Identification miss rates vs. rank by time-elapsed. The oldest image of each individual is enrolled. Thereafter, all more recent images are searched. Miss rates are computed over all searches noted in row 17 of Table 1 and binned by number of years between search and initial enrollment.

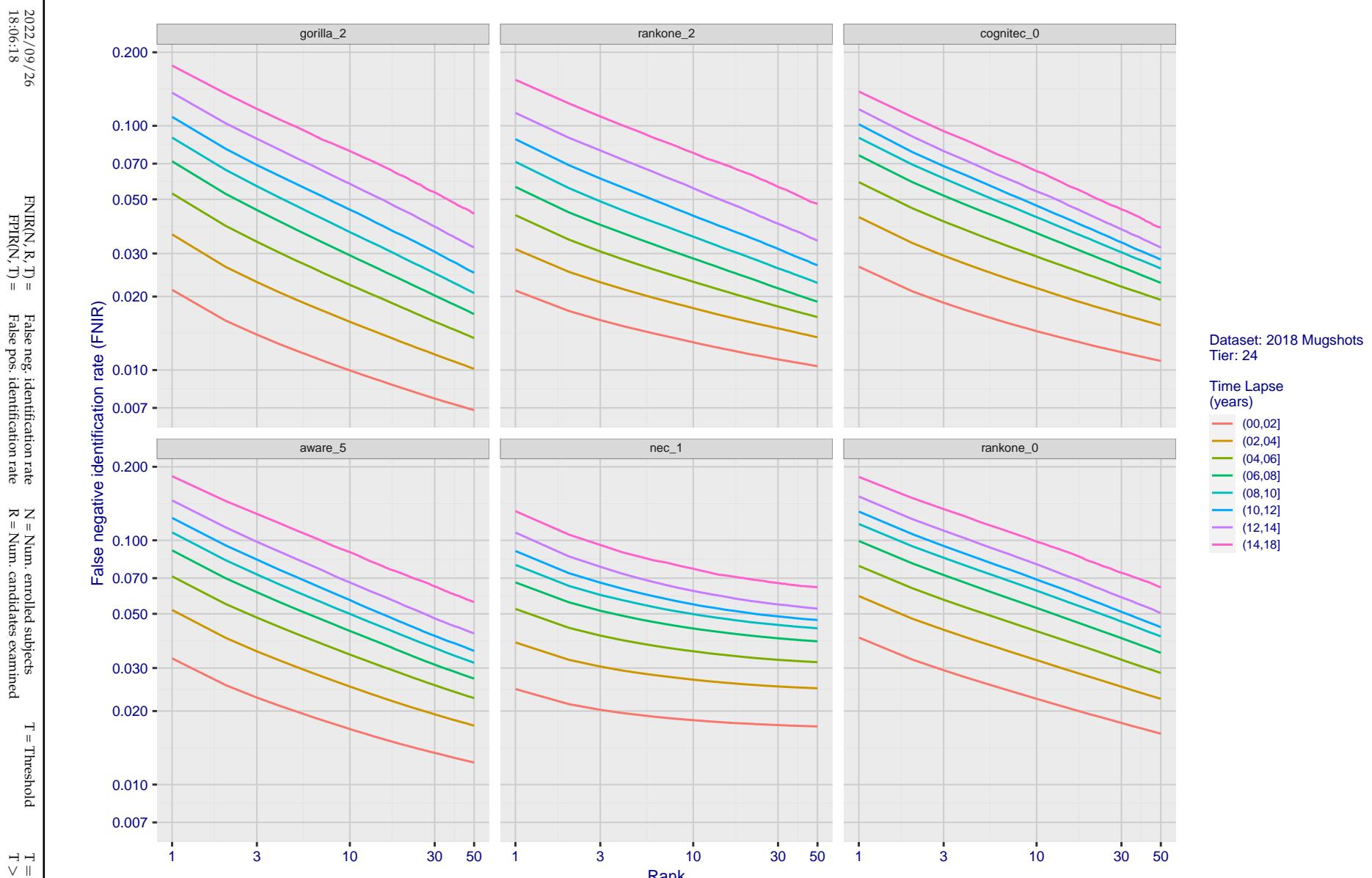


Figure 83: [FRVT-2018 Mugshot Ageing Dataset] Identification miss rates vs. rank by time-elapsed. The oldest image of each individual is enrolled. Thereafter, all more recent images are searched. Miss rates are computed over all searches noted in row 17 of Table 1 and binned by number of years between search and initial enrollment.

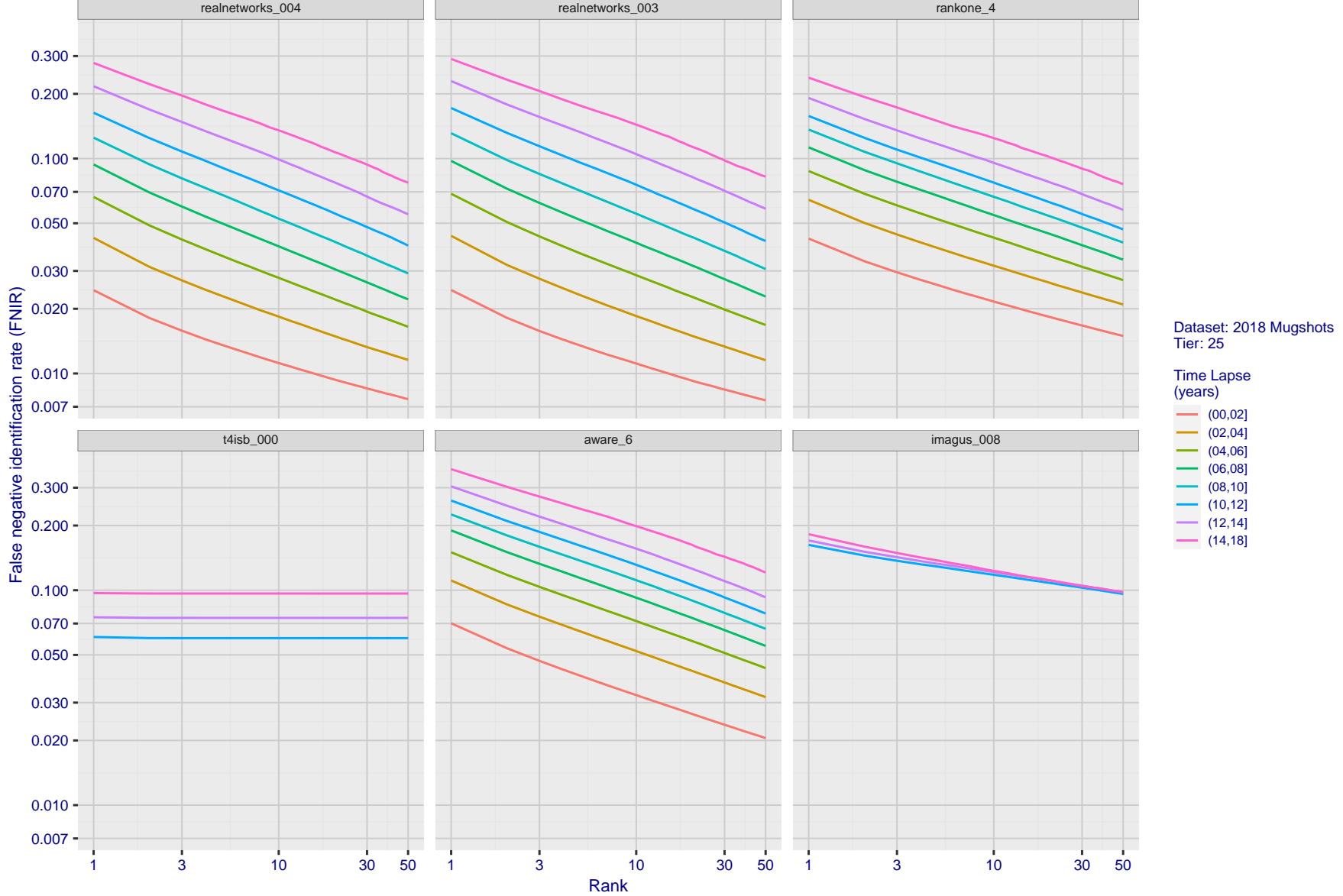


Figure 84: [FRVT-2018 Mugshot Ageing Dataset] Identification miss rates vs. rank by time-elapsed. The oldest image of each individual is enrolled. Thereafter, all more recent images are searched. Miss rates are computed over all searches noted in row 17 of Table 1 and binned by number of years between search and initial enrollment.

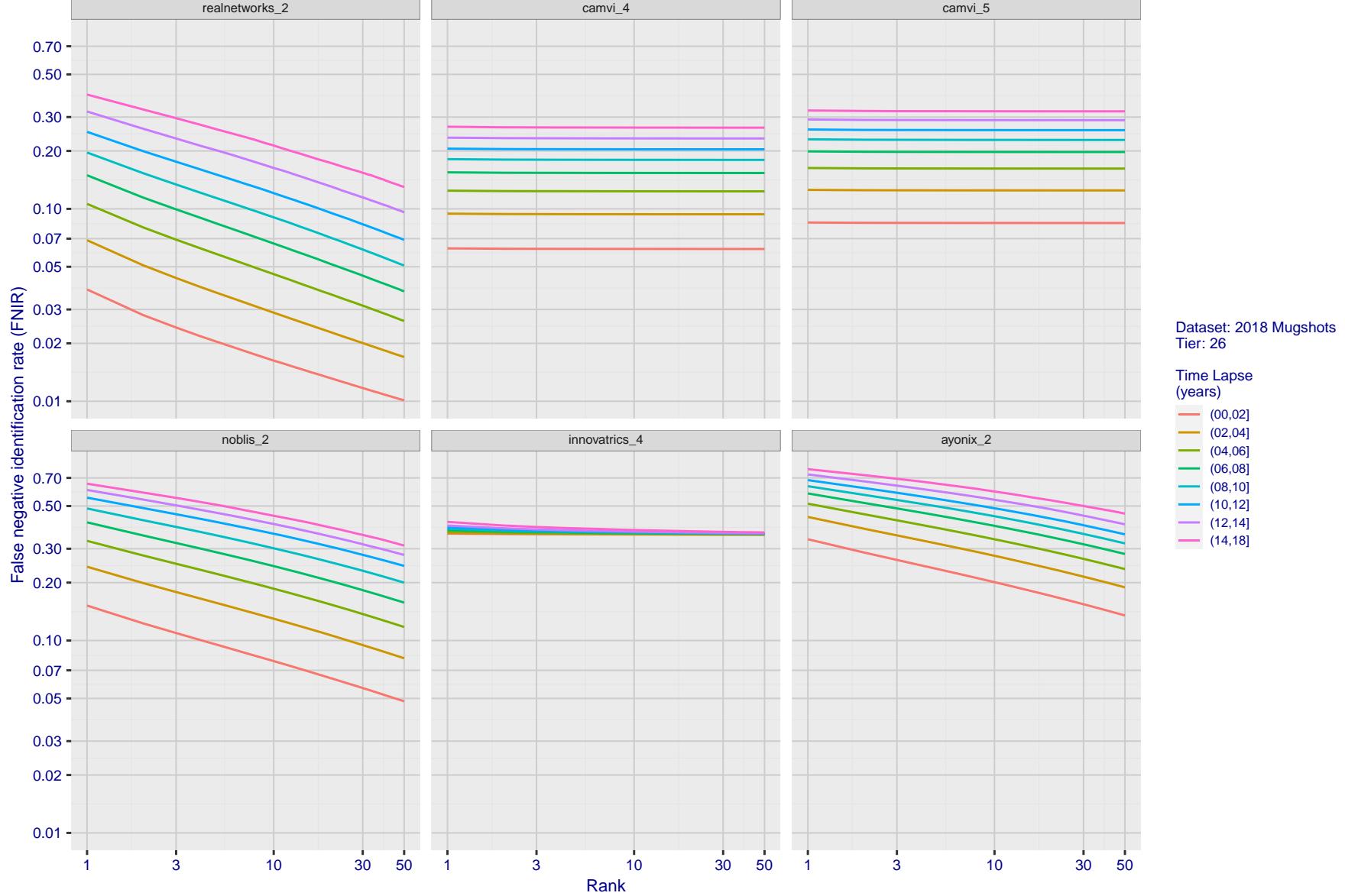


Figure 85: [FRVT-2018 Mugshot Ageing Dataset] Identification miss rates vs. rank by time-elapsed. The oldest image of each individual is enrolled. Thereafter, all more recent images are searched. Miss rates are computed over all searches noted in row 17 of Table 1 and binned by number of years between search and initial enrollment.

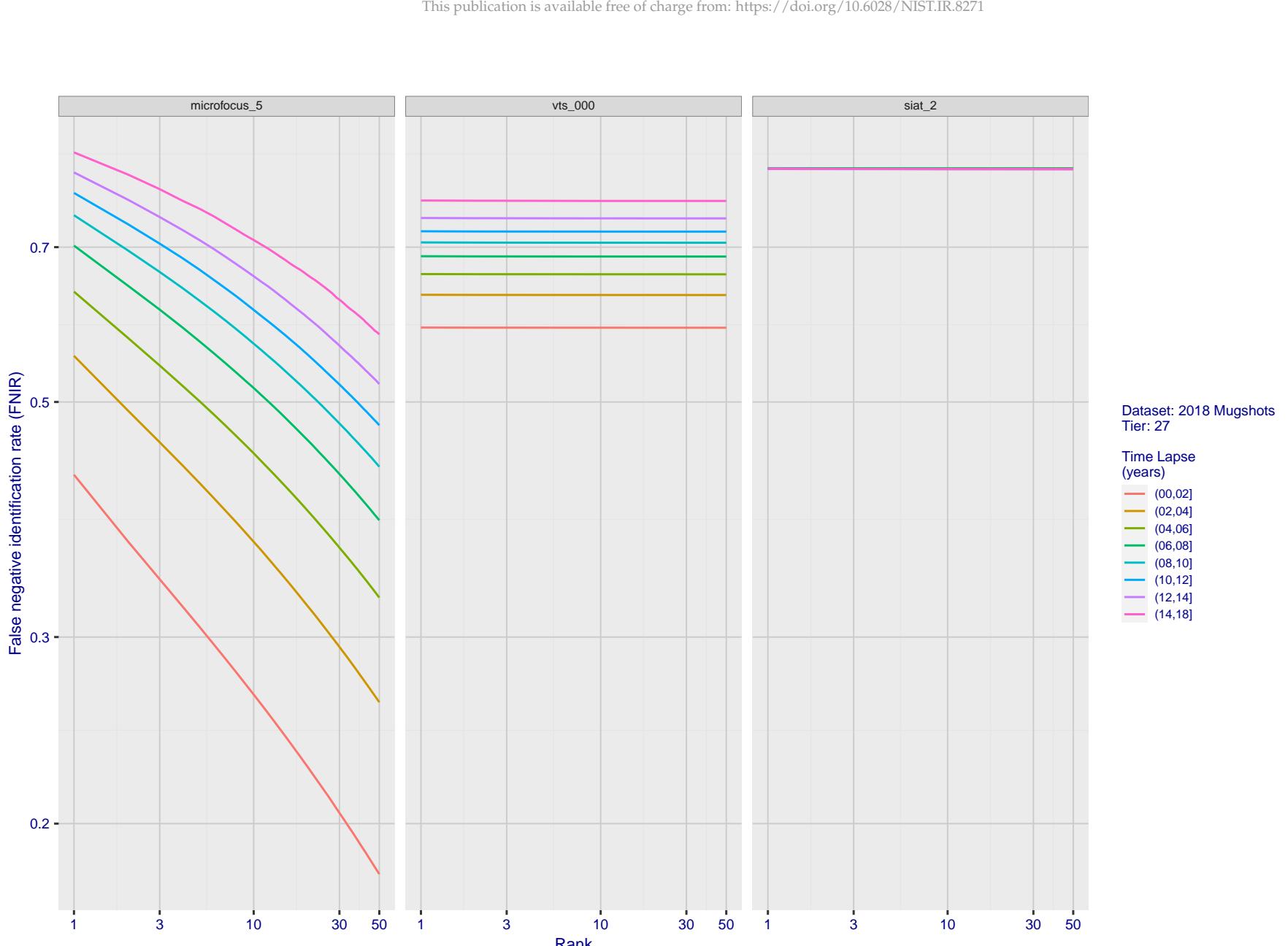


Figure 86: [FRVT-2018 Mugshot Ageing Dataset] Identification miss rates vs. rank by time-elapsed. The oldest image of each individual is enrolled. Thereafter, all more recent images are searched. Miss rates are computed over all searches noted in row 17 of Table 1 and binned by number of years between search and initial enrollment.

2022/09/26 18:06:18	$\text{FNIR}(N, R, T) =$ $\text{FPTR}(N, T) =$	False neg. identification rate False pos. identification rate	$N =$ Num. enrolled subjects $R =$ Num. candidates examined	$T =$ Threshold $T > 0 \rightarrow$ Identification	$T = 0 \rightarrow$ Investigation
------------------------	---	--	--	---	-----------------------------------

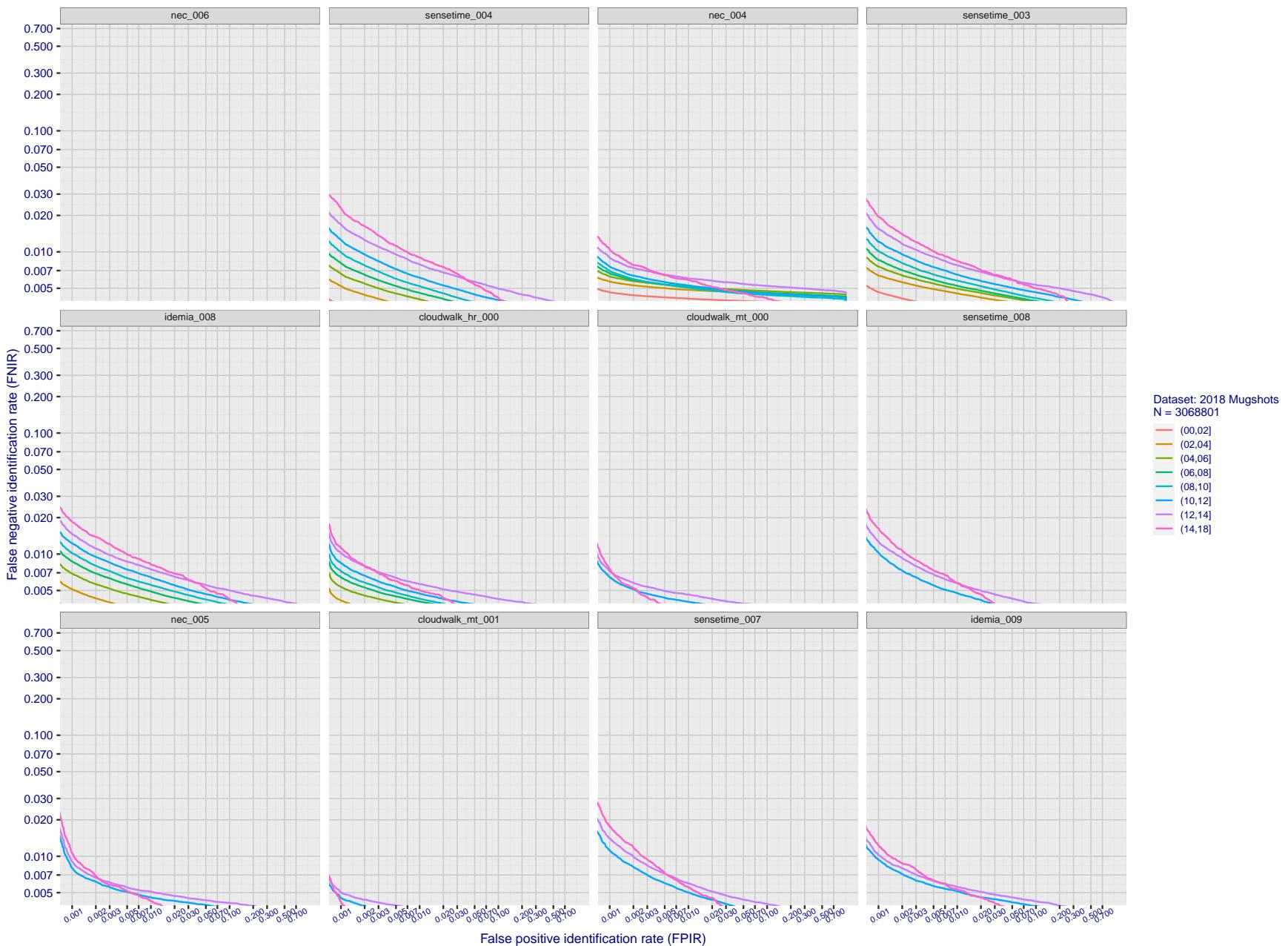


Figure 87: [FRVT-2018 Mugshot Ageing Dataset] Identification miss rates vs. FPIR by time-elapsed. The oldest image of each individual is enrolled. Thereafter, all more recent images are searched. Miss rates are computed over all searches noted in row 17 of Table 1 and binned by number of years between search and initial enrollment. FPIR is computed from the same FRVT 2018 non-mates noted in row 3 of Table 1 with $N = 3000000$.

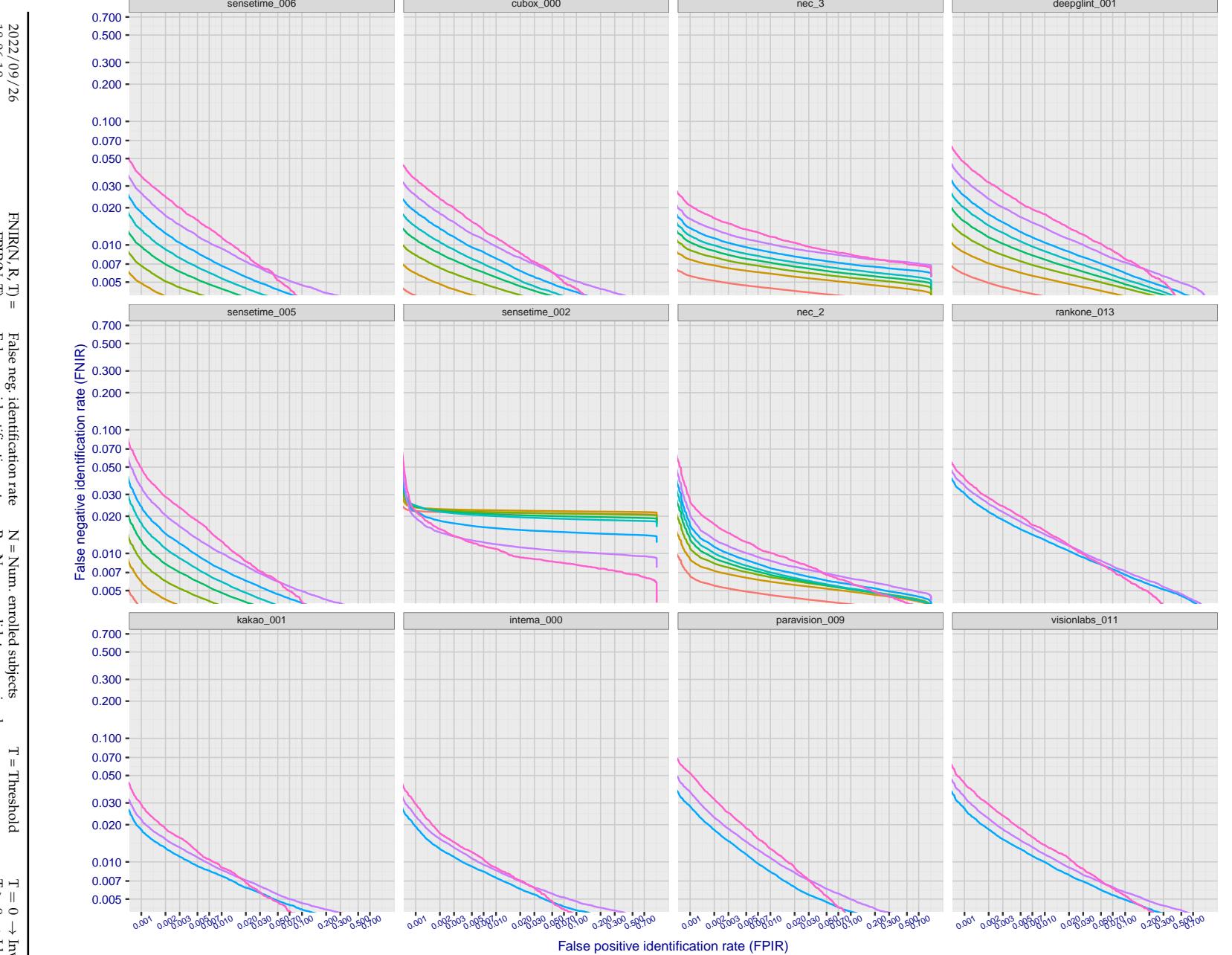


Figure 88: [FRVT-2018 Mugshot Ageing Dataset] Identification miss rates vs. FPIR by time-elapsed. The oldest image of each individual is enrolled. Thereafter, all more recent images are searched. Miss rates are computed over all searches noted in row 17 of Table 1 and binned by number of years between search and initial enrollment. FPIR is computed from the same FRVT 2018 non-mates noted in row 3 of Table 1 with $N = 3\,000\,000$.

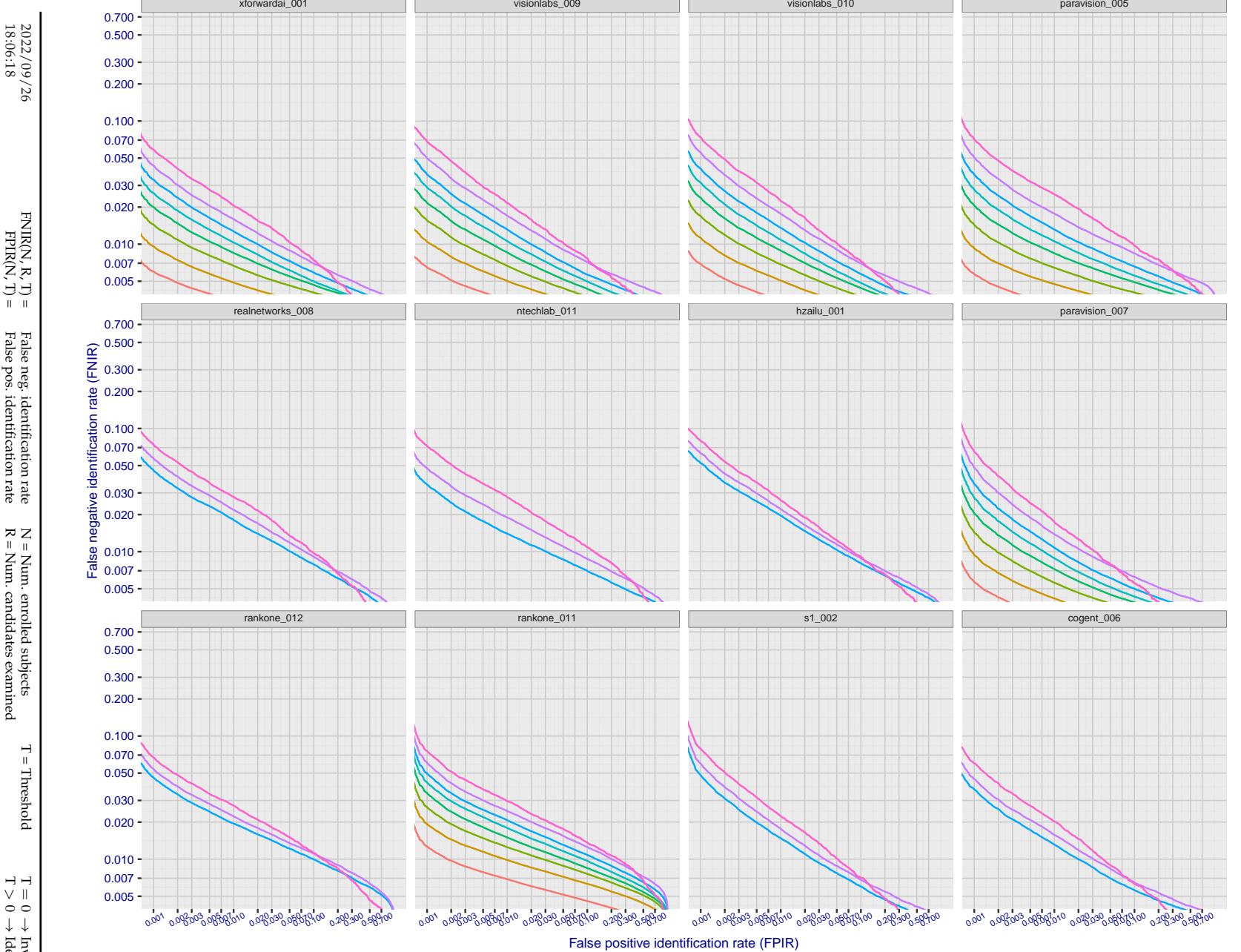


Figure 89: [FRVT-2018 Mugshot Ageing Dataset] Identification miss rates vs. FPIR by time-elapsed. The oldest image of each individual is enrolled. Thereafter, all more recent images are searched. Miss rates are computed over all searches noted in row 17 of Table 1 and binned by number of years between search and initial enrollment. FPIR is computed from the same FRVT 2018 non-mates noted in row 3 of Table 1 with $N = 3\,000\,000$.

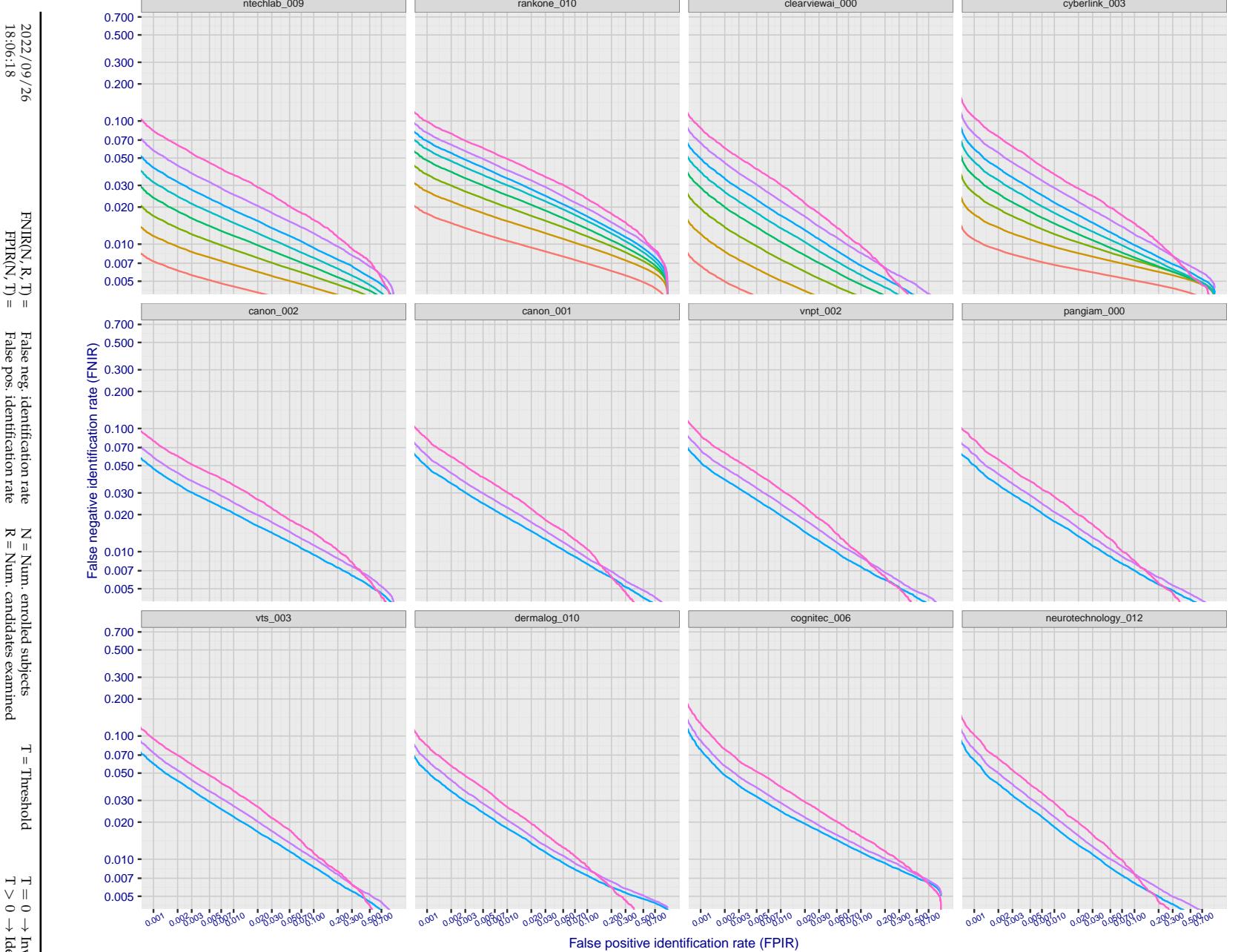


Figure 90: [FRVT-2018 Mugshot Ageing Dataset] Identification miss rates vs. FPIR by time-elapsed. The oldest image of each individual is enrolled. Thereafter, all more recent images are searched. Miss rates are computed over all searches noted in row 17 of Table 1 and binned by number of years between search and initial enrollment. FPIR is computed from the same FRVT 2018 non-mates noted in row 3 of Table 1 with $N = 3\,000\,000$.

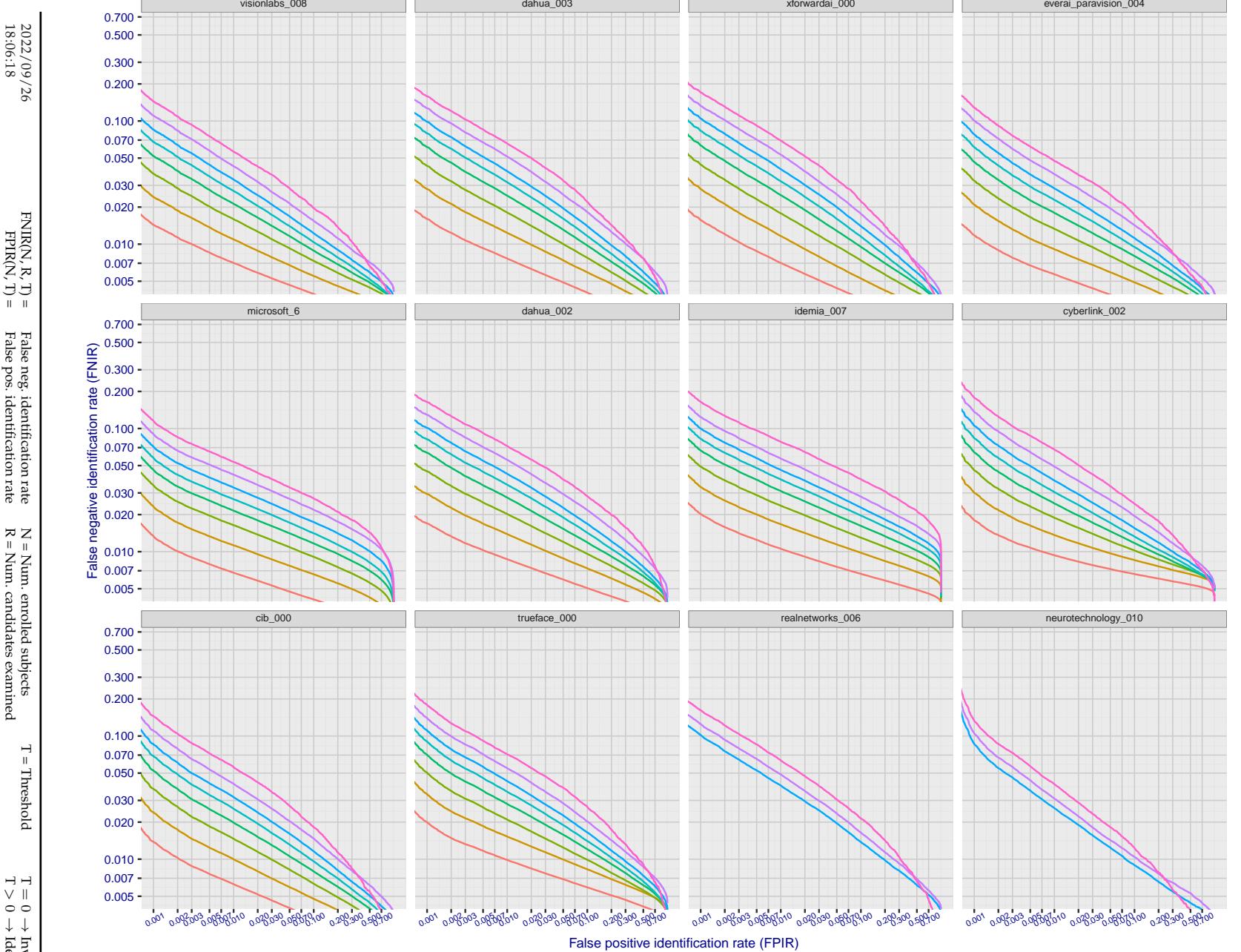


Figure 91: [FRVT-2018 Mugshot Ageing Dataset] Identification miss rates vs. FPIR by time-elapsed. The oldest image of each individual is enrolled. Thereafter, all more recent images are searched. Miss rates are computed over all searches noted in row 17 of Table 1 and binned by number of years between search and initial enrollment. FPIR is computed from the same FRVT 2018 non-mates noted in row 3 of Table 1 with N = 3 000 000.

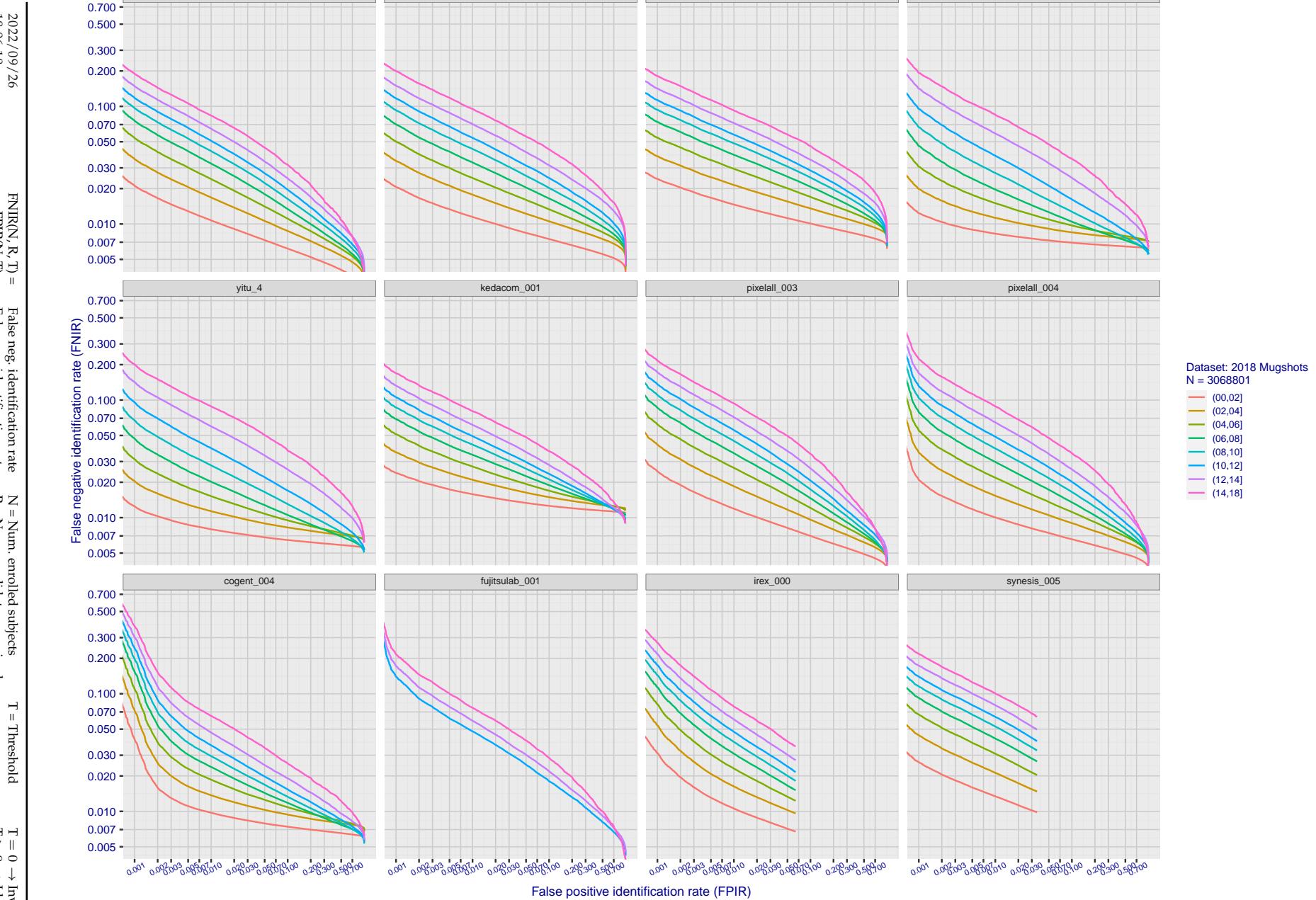


Figure 92: [FRVT-2018 Mugshot Ageing Dataset] Identification miss rates vs. FPIR by time-elapsed. The oldest image of each individual is enrolled. Thereafter, all more recent images are searched. Miss rates are computed over all searches noted in row 17 of Table 1 and binned by number of years between search and initial enrollment. FPIR is computed from the same FRVT 2018 non-mates noted in row 3 of Table 1 with $N = 3\,000\,000$.

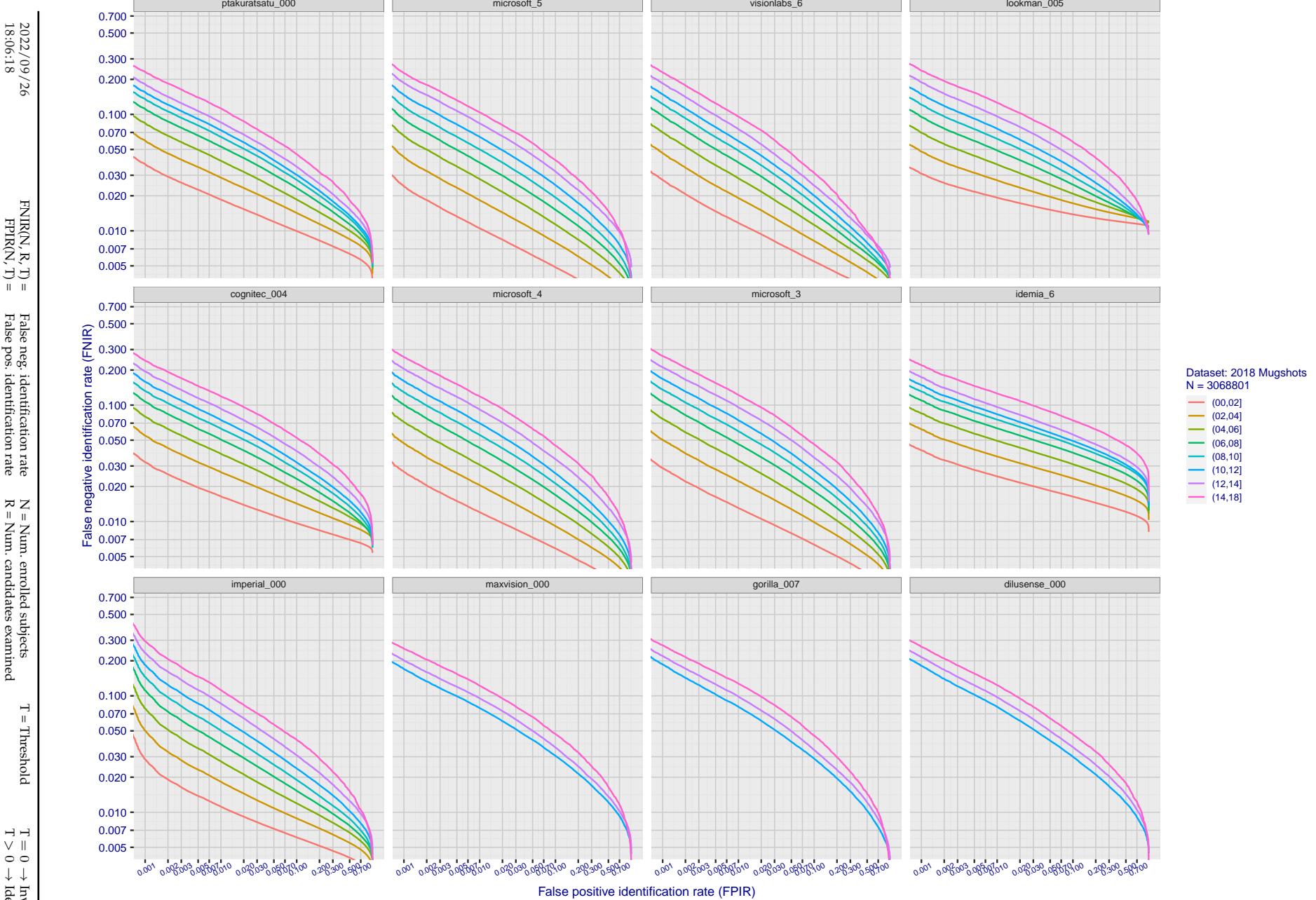


Figure 93: [FRVT-2018 Mugshot Ageing Dataset] Identification miss rates vs. FPIR by time-elapsed. The oldest image of each individual is enrolled. Thereafter, all more recent images are searched. Miss rates are computed over all searches noted in row 17 of Table 1 and binned by number of years between search and initial enrollment. FPIR is computed from the same FRVT 2018 non-mates noted in row 3 of Table 1 with N = 3 000 000.

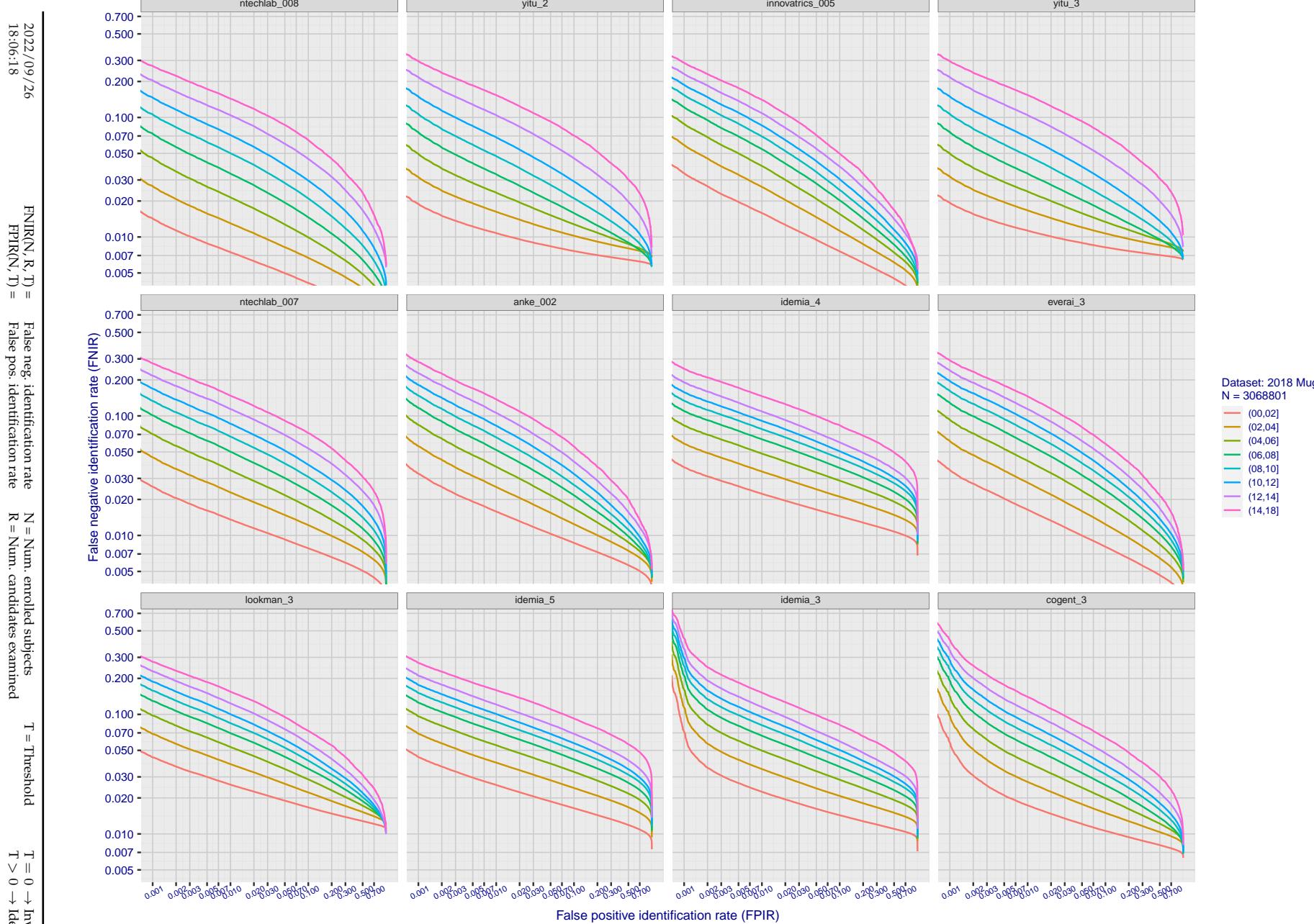


Figure 94: [FRVT-2018 Mugshot Ageing Dataset] Identification miss rates vs. FPIR by time-elapsed. The oldest image of each individual is enrolled. Thereafter, all more recent images are searched. Miss rates are computed over all searches noted in row 17 of Table 1 and binned by number of years between search and initial enrollment. FPIR is computed from the same FRVT 2018 non-mates noted in row 3 of Table 1 with $N = 3\,000\,000$.

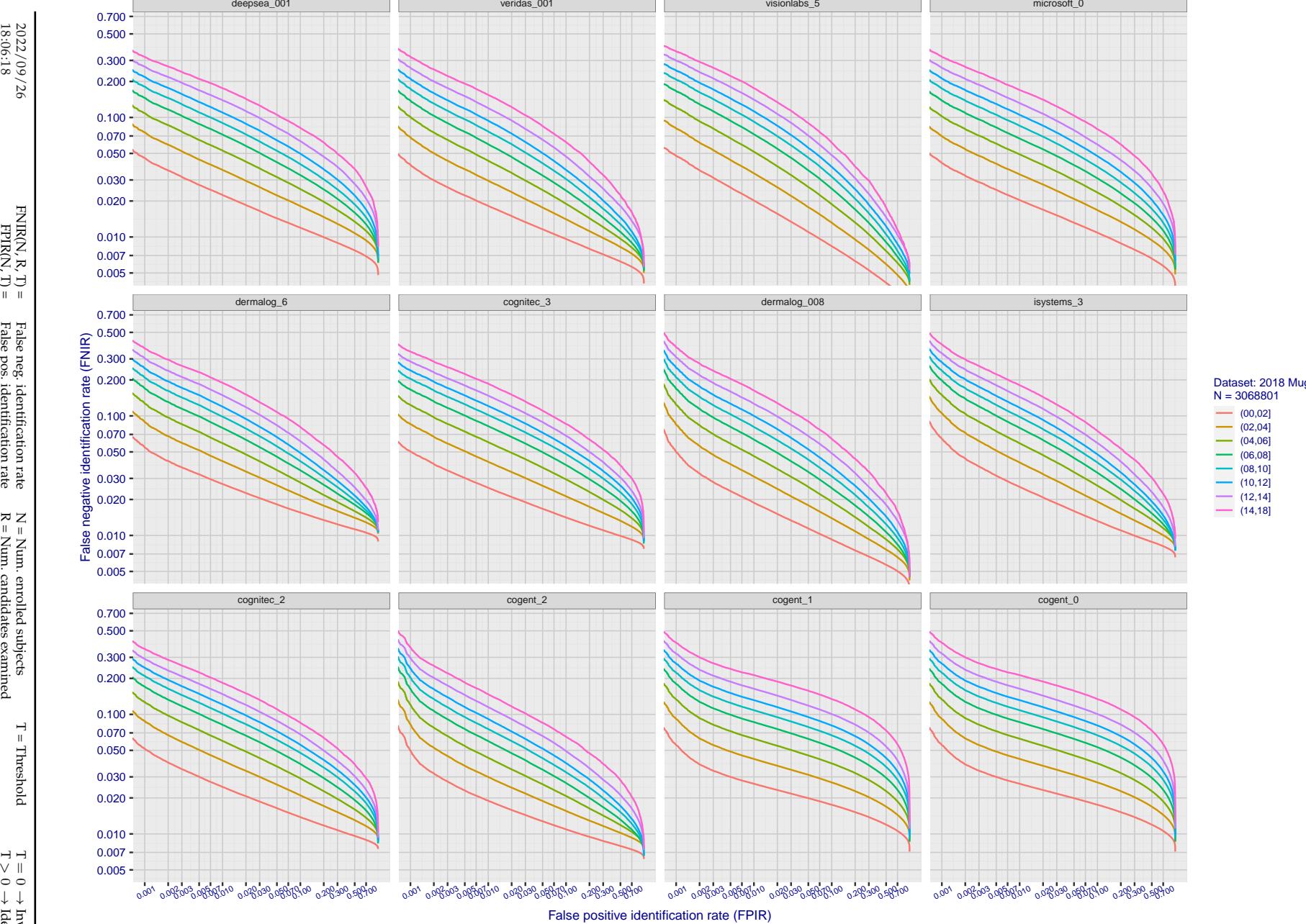


Figure 95: [FRVT-2018 Mugshot Ageing Dataset] Identification miss rates vs. FPIR by time-elapsed. The oldest image of each individual is enrolled. Thereafter, all more recent images are searched. Miss rates are computed over all searches noted in row 17 of Table 1 and binned by number of years between search and initial enrollment. FPIR is computed from the same FRVT 2018 non-mates noted in row 3 of Table 1 with $N = 3\,000\,000$.

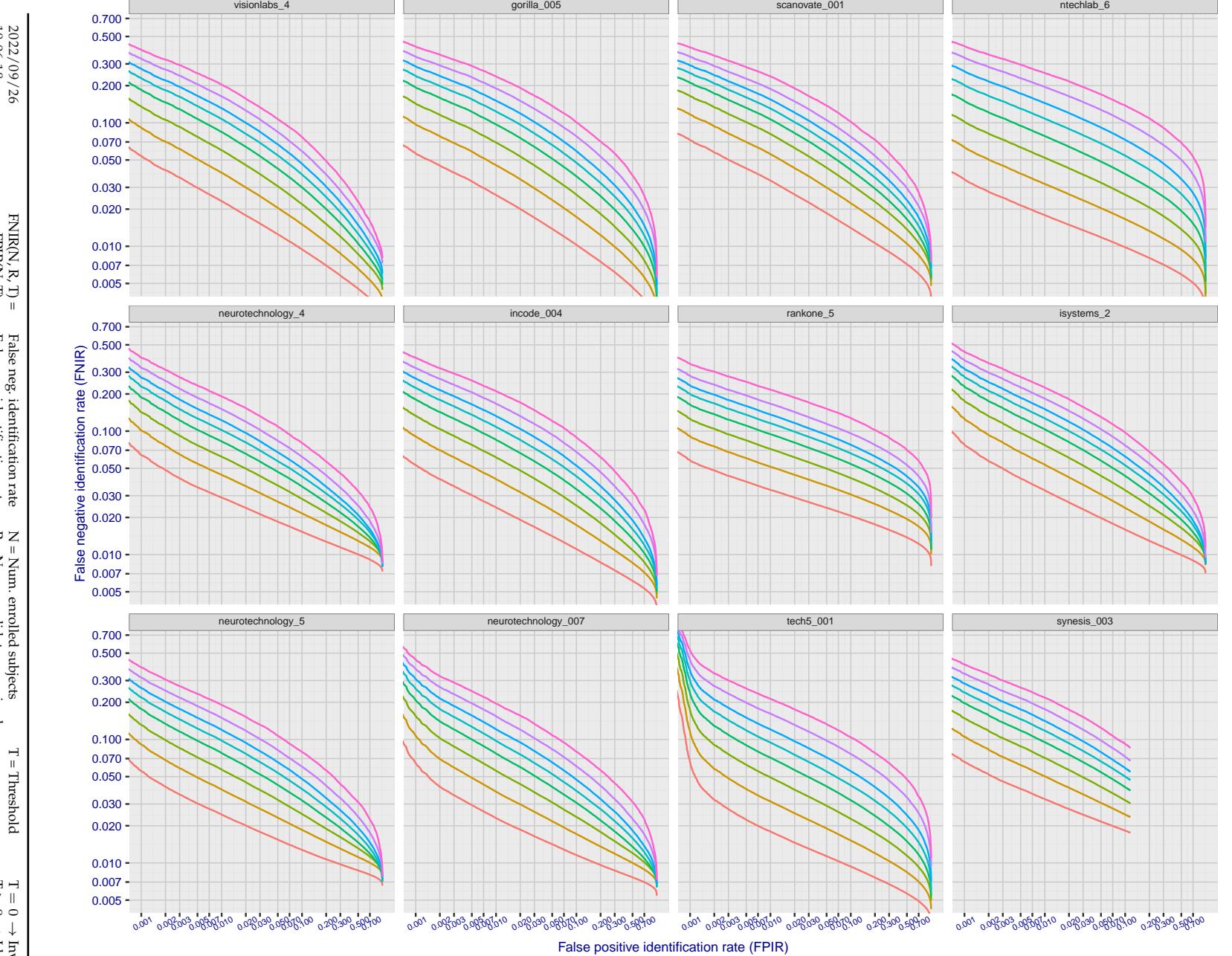


Figure 96: [FRVT-2018 Mugshot Ageing Dataset] Identification miss rates vs. FPIR by time-elapsed. The oldest image of each individual is enrolled. Thereafter, all more recent images are searched. Miss rates are computed over all searches noted in row 17 of Table 1 and binned by number of years between search and initial enrollment. FPIR is computed from the same FRVT 2018 non-mates noted in row 3 of Table 1 with $N = 3\,000\,000$.

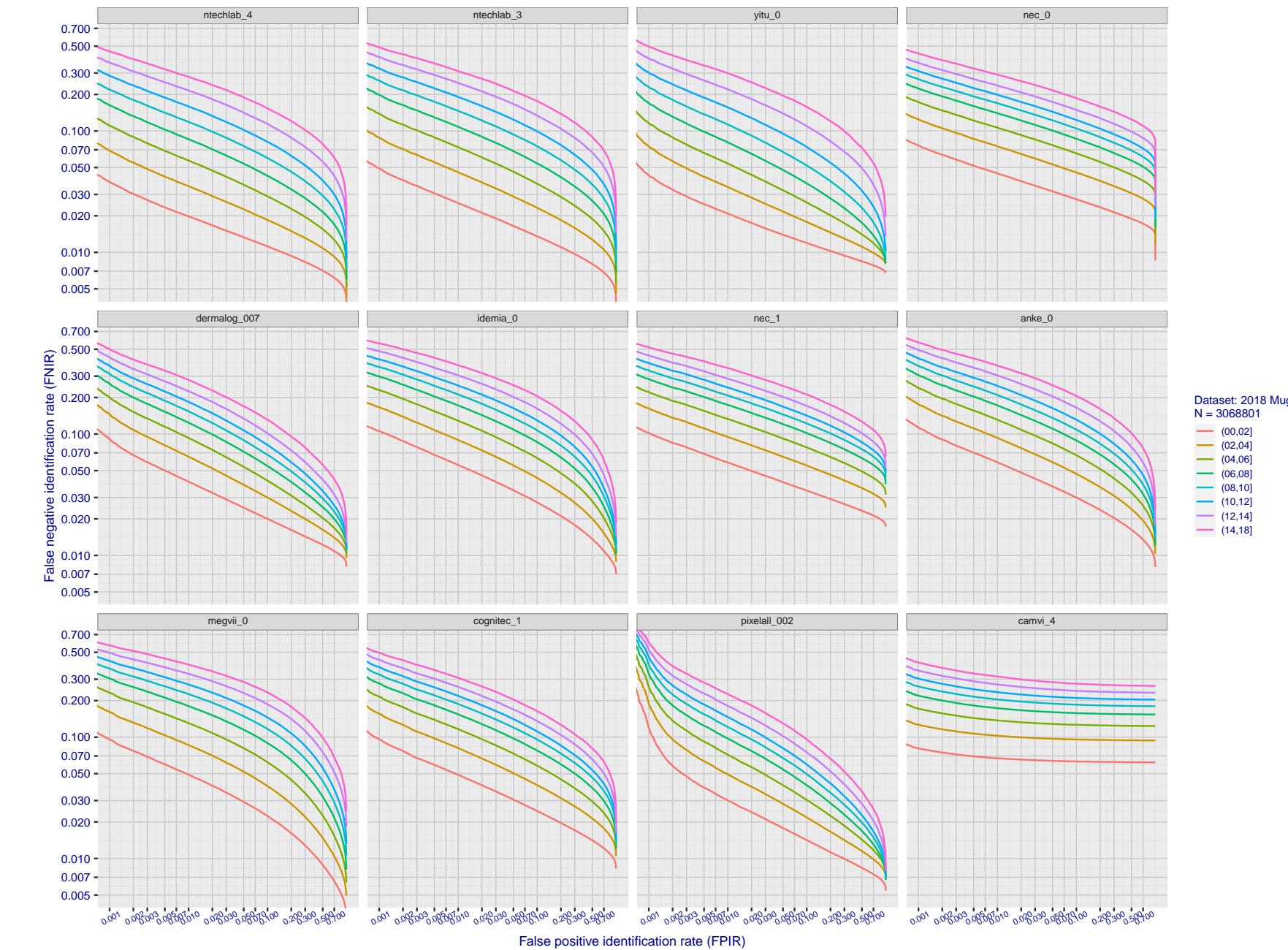


Figure 97: [FRVT-2018 Mugshot Ageing Dataset] Identification miss rates vs. FPIR by time-elapsed. The oldest image of each individual is enrolled. Thereafter, all more recent images are searched. Miss rates are computed over all searches noted in row 17 of Table 1 and binned by number of years between search and initial enrollment. FPIR is computed from the same FRVT 2018 non-mates noted in row 3 of Table 1 with $N = 3\,000\,000$.

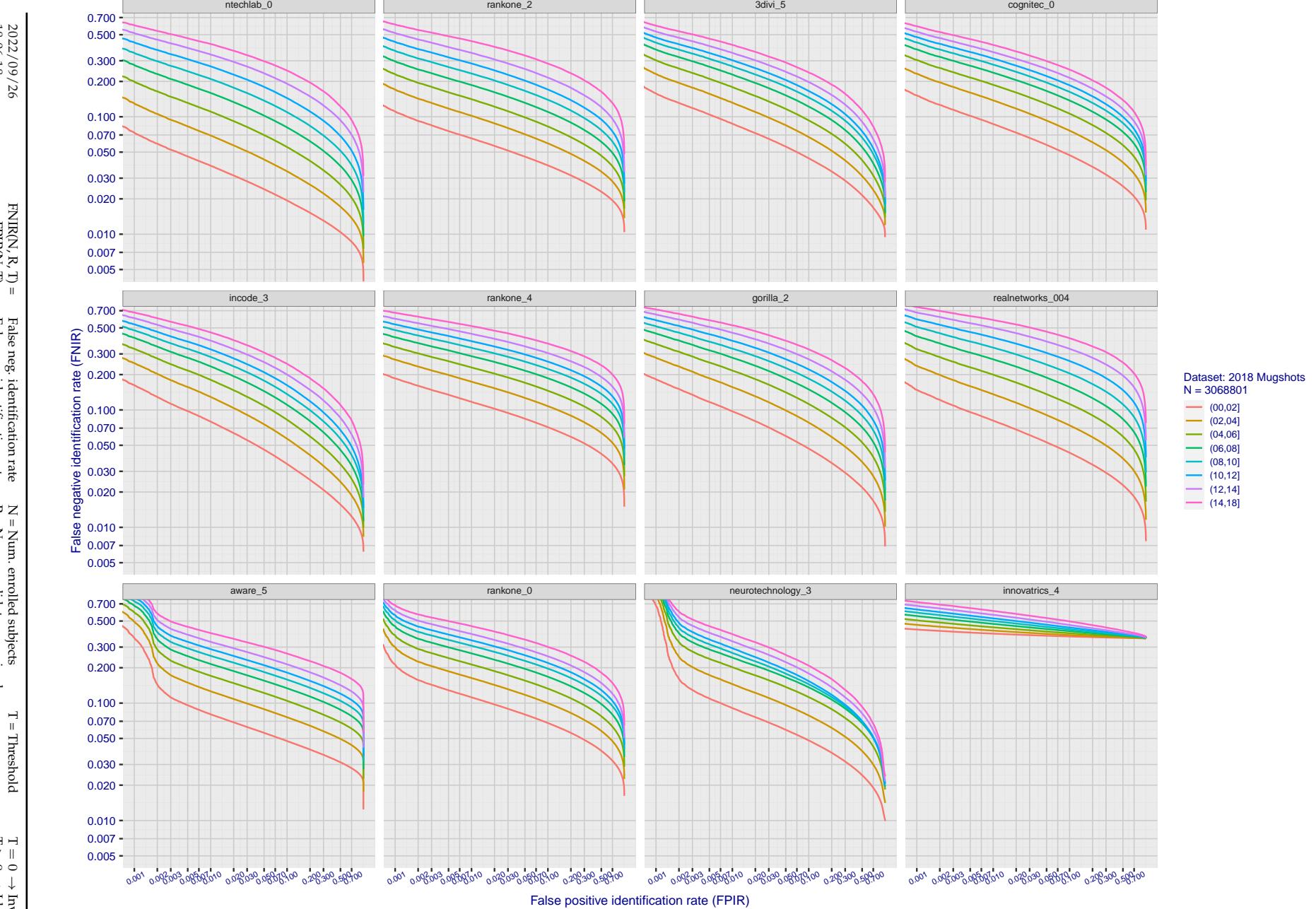


Figure 98: [FRVT-2018 Mugshot Ageing Dataset] Identification miss rates vs. FPIR by time-elapsed. The oldest image of each individual is enrolled. Thereafter, all more recent images are searched. Miss rates are computed over all searches noted in row 17 of Table 1 and binned by number of years between search and initial enrollment. FPIR is computed from the same FRVT 2018 non-mates noted in row 3 of Table 1 with $N = 3\,000\,000$.

2022 / 09 / 26
18:06:18FNIR(N, R, T) = False neg. identification rate
FPIR(N, T) = False pos. identification rateN = Num. enrolled subjects
R = Num. candidates examined

T = Threshold

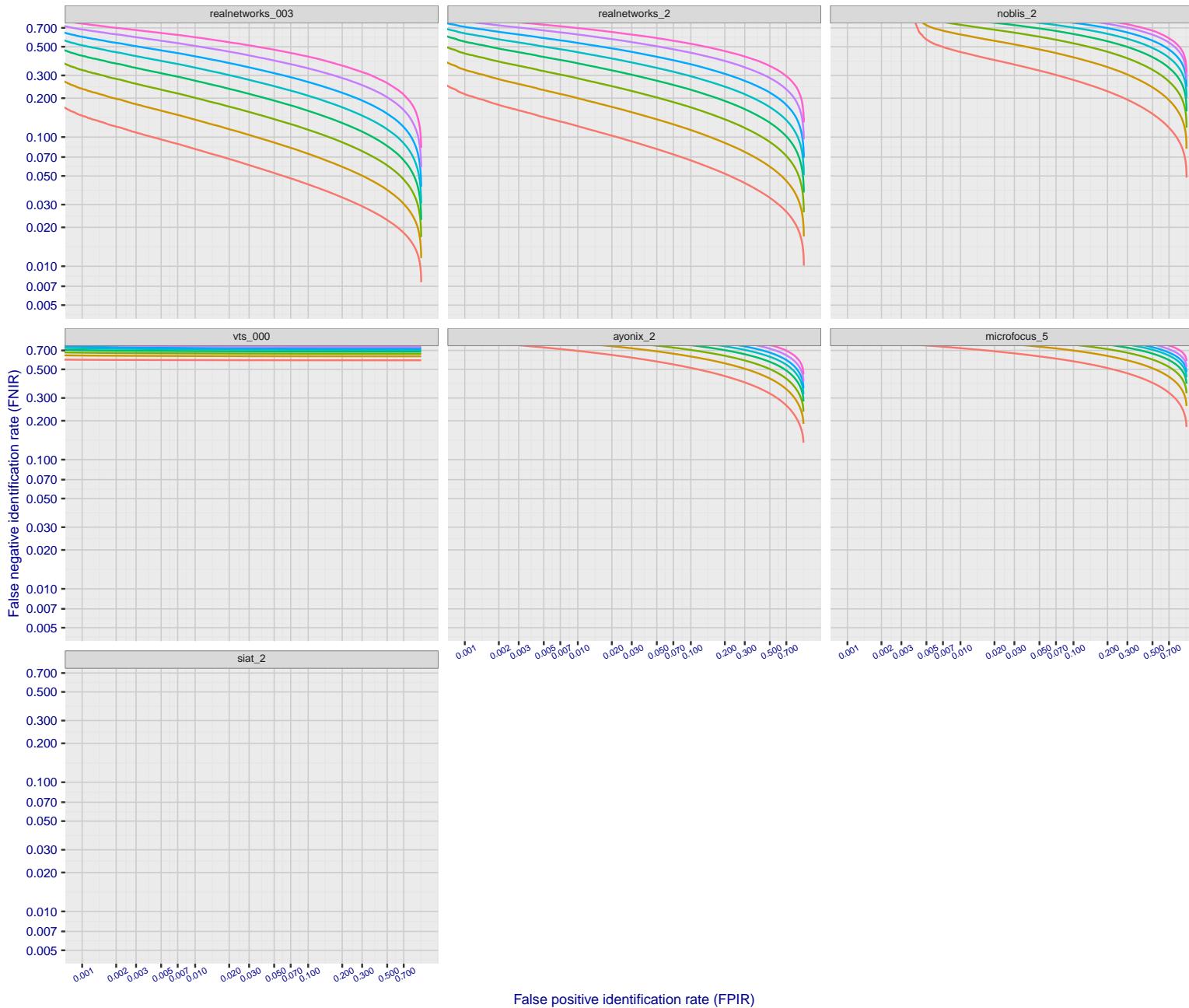
T = 0 → Investigation
T > 0 → Identification

Figure 99: [FRVT-2018 Mugshot Ageing Dataset] Identification miss rates vs. FPIR by time-elapsed. The oldest image of each individual is enrolled. Thereafter, all more recent images are searched. Miss rates are computed over all searches noted in row 17 of Table 1 and binned by number of years between search and initial enrollment. FPIR is computed from the same FRVT 2018 non-mates noted in row 3 of Table 1 with N = 3 000 000.

2022/09/26 18:06:18	$\text{FNIR}(N, R, T) =$ $\text{FPTR}(N, T) =$	False neg. identification rate False pos. identification rate	$N =$ Num. enrolled subjects $R =$ Num. candidates examined	$T =$ Threshold $T > 0 \rightarrow$ Identification	$T = 0 \rightarrow$ Investigation
------------------------	---	--	--	---	-----------------------------------

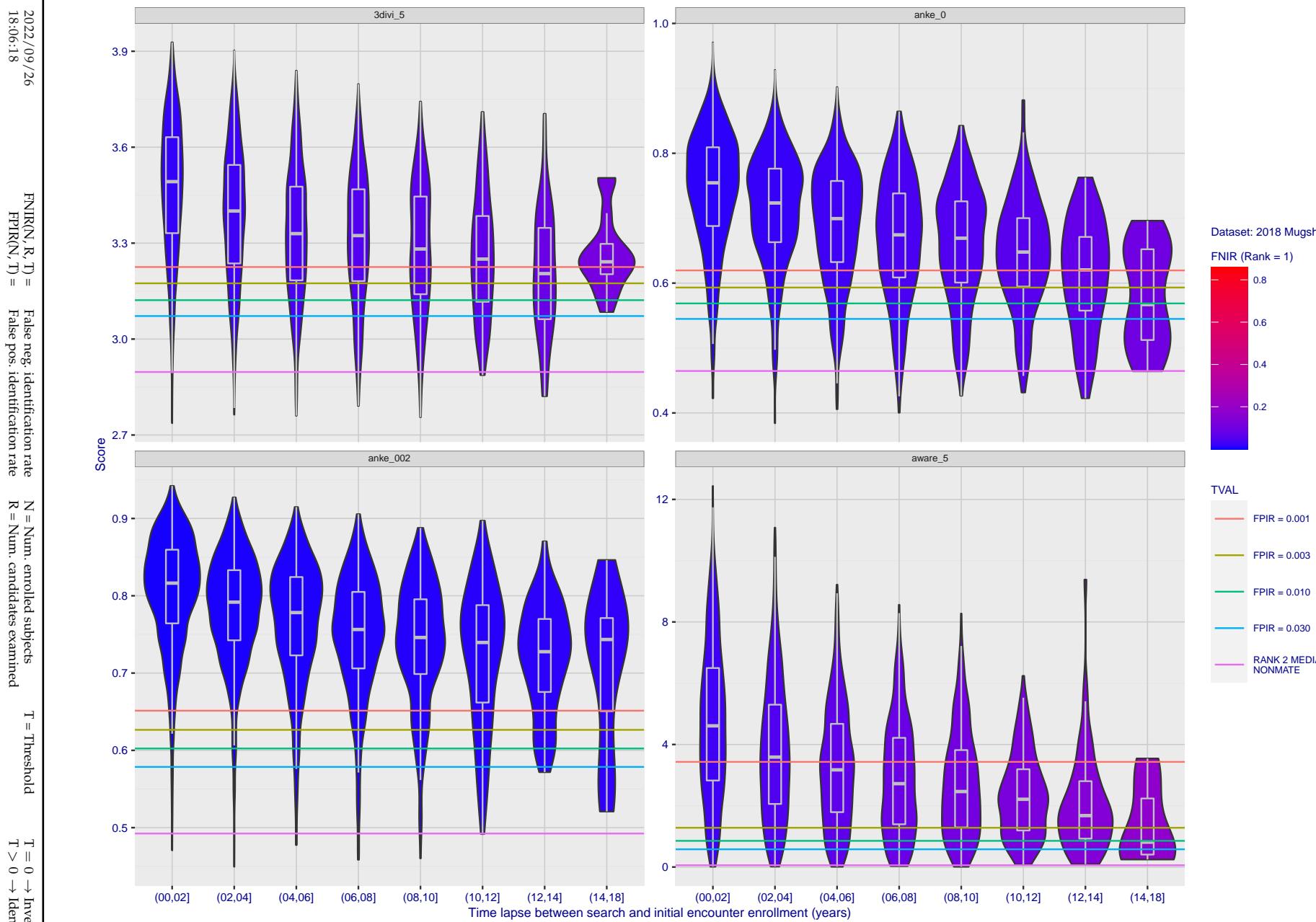


Figure 100: [FRVT-2018 Mugshot Ageing Dataset] Native mate scores vs. time-elapsed. The oldest image of each individual is enrolled. Thereafter, all more recent images are searched. Mated score distributions are computed over all searches noted in row 17 of Table 1 binned by number of years between search and initial enrollment.

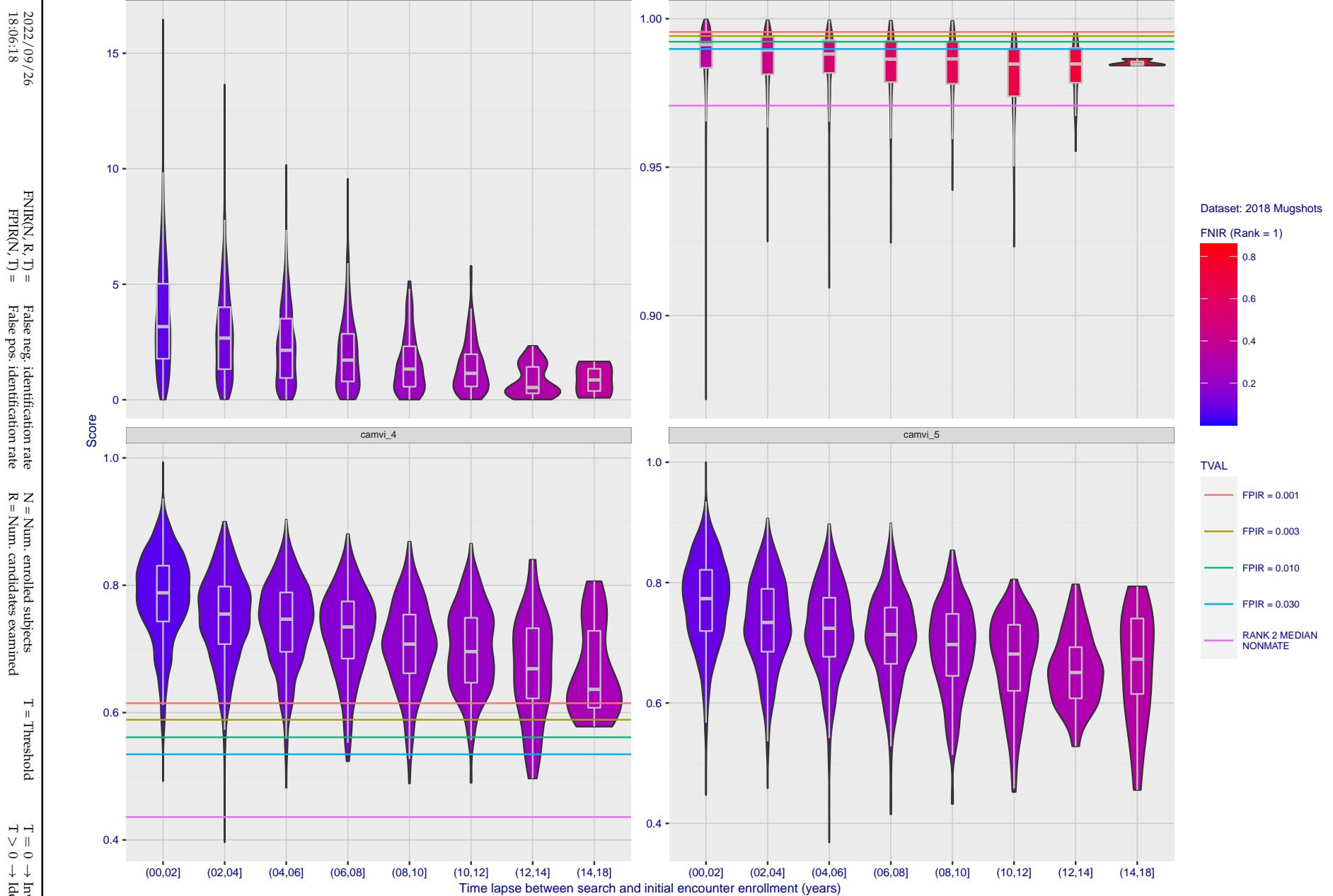


Figure 101: [FRVT-2018 Mugshot Ageing Dataset] Native mate scores vs. time-elapsed. The oldest image of each individual is enrolled. Thereafter, all more recent images are searched. Mated score distributions are computed over all searches noted in row 17 of Table 1 binned by number of years between search and initial enrollment.

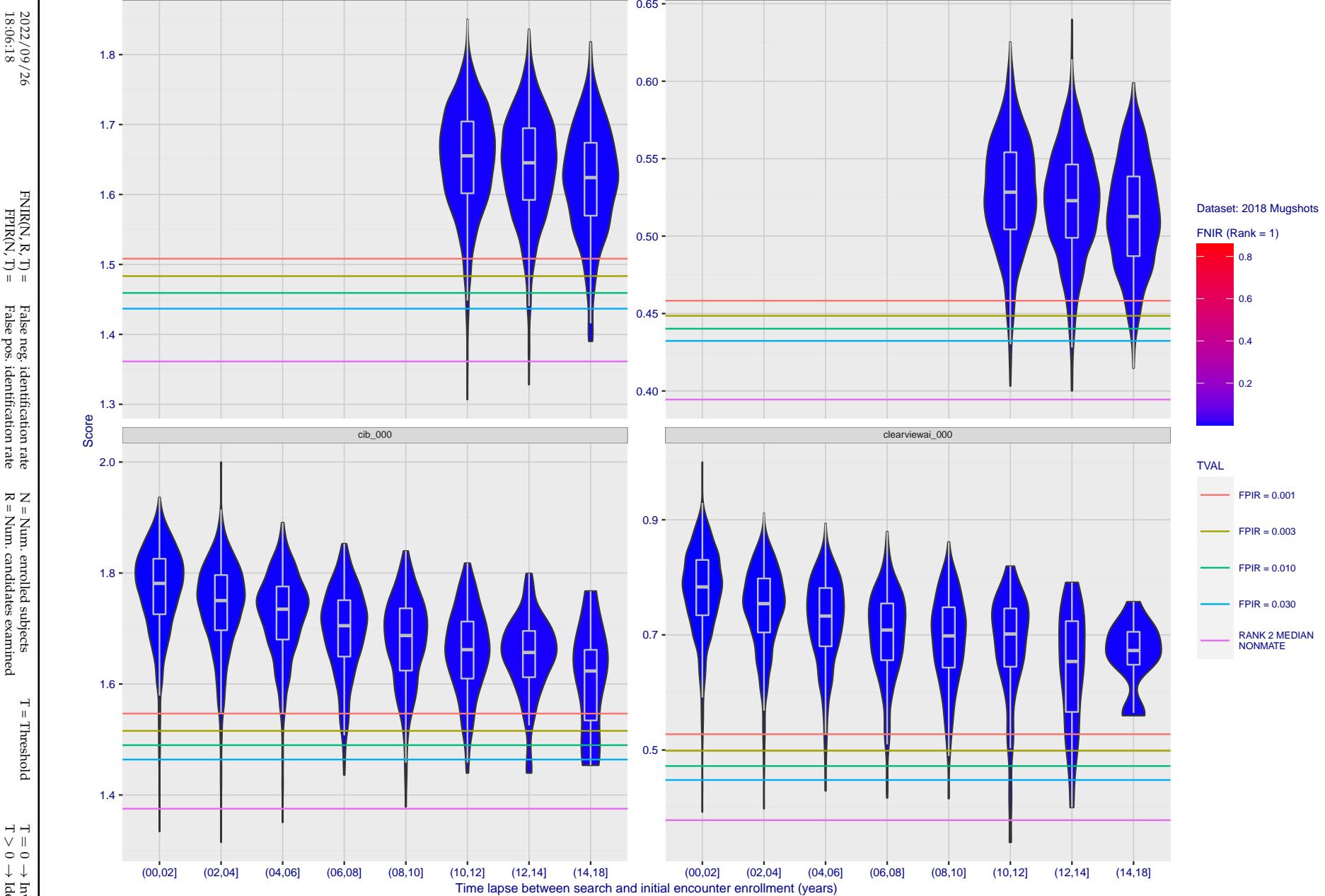


Figure 102: [FRVT-2018 Mugshot Ageing Dataset] Native mate scores vs. time-elapsed. The oldest image of each individual is enrolled. Thereafter, all more recent images are searched. Mated score distributions are computed over all searches noted in row 17 of Table 1 binned by number of years between search and initial enrollment.

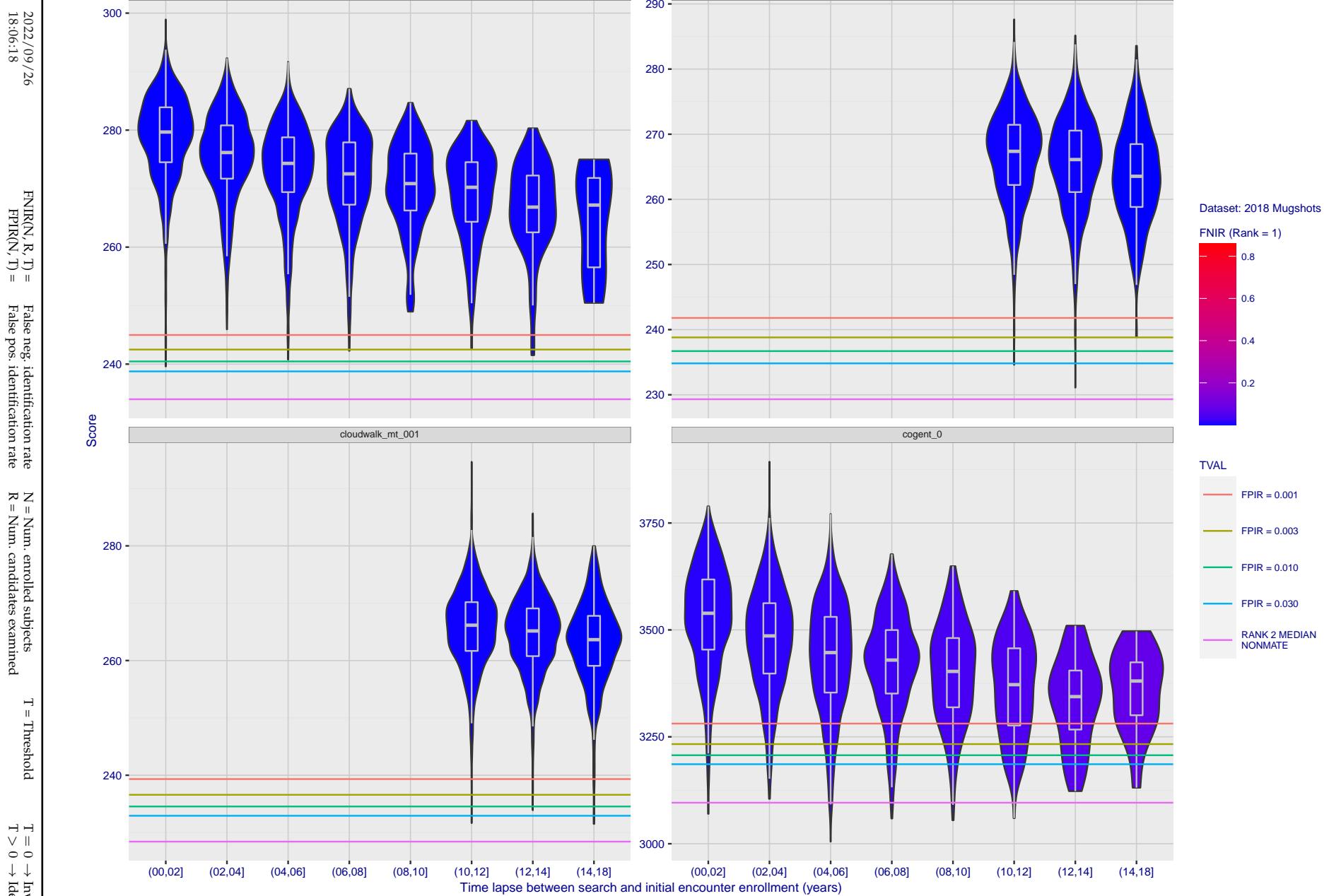


Figure 103: [FRVT-2018 Mugshot Ageing Dataset] Native mate scores vs. time-elapsed. The oldest image of each individual is enrolled. Thereafter, all more recent images are searched. Mated score distributions are computed over all searches noted in row 17 of Table 1 binned by number of years between search and initial enrollment.

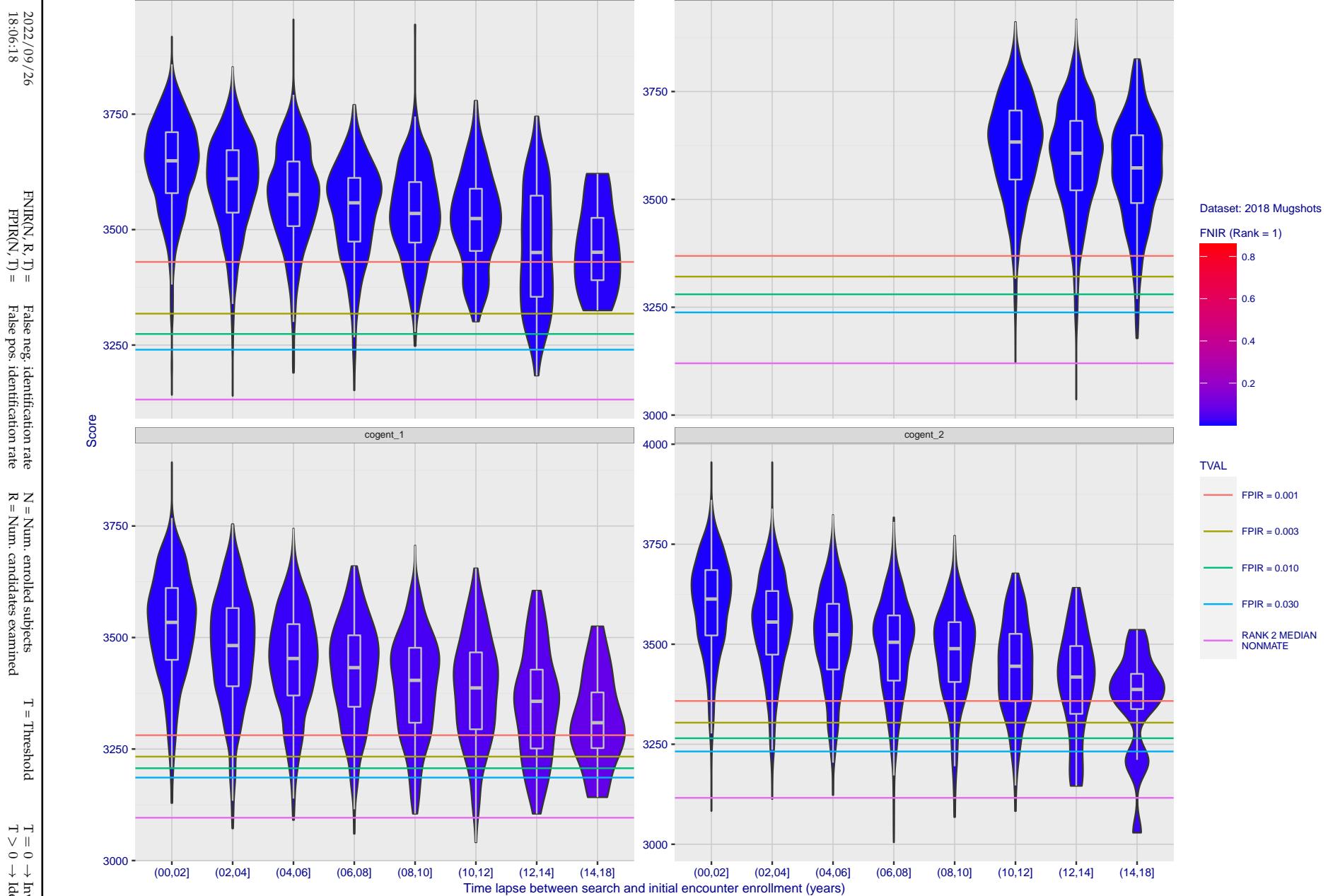


Figure 104: [FRVT-2018 Mugshot Ageing Dataset] Native mate scores vs. time-elapsed. The oldest image of each individual is enrolled. Thereafter, all more recent images are searched. Mated score distributions are computed over all searches noted in row 17 of Table 1 binned by number of years between search and initial enrollment.

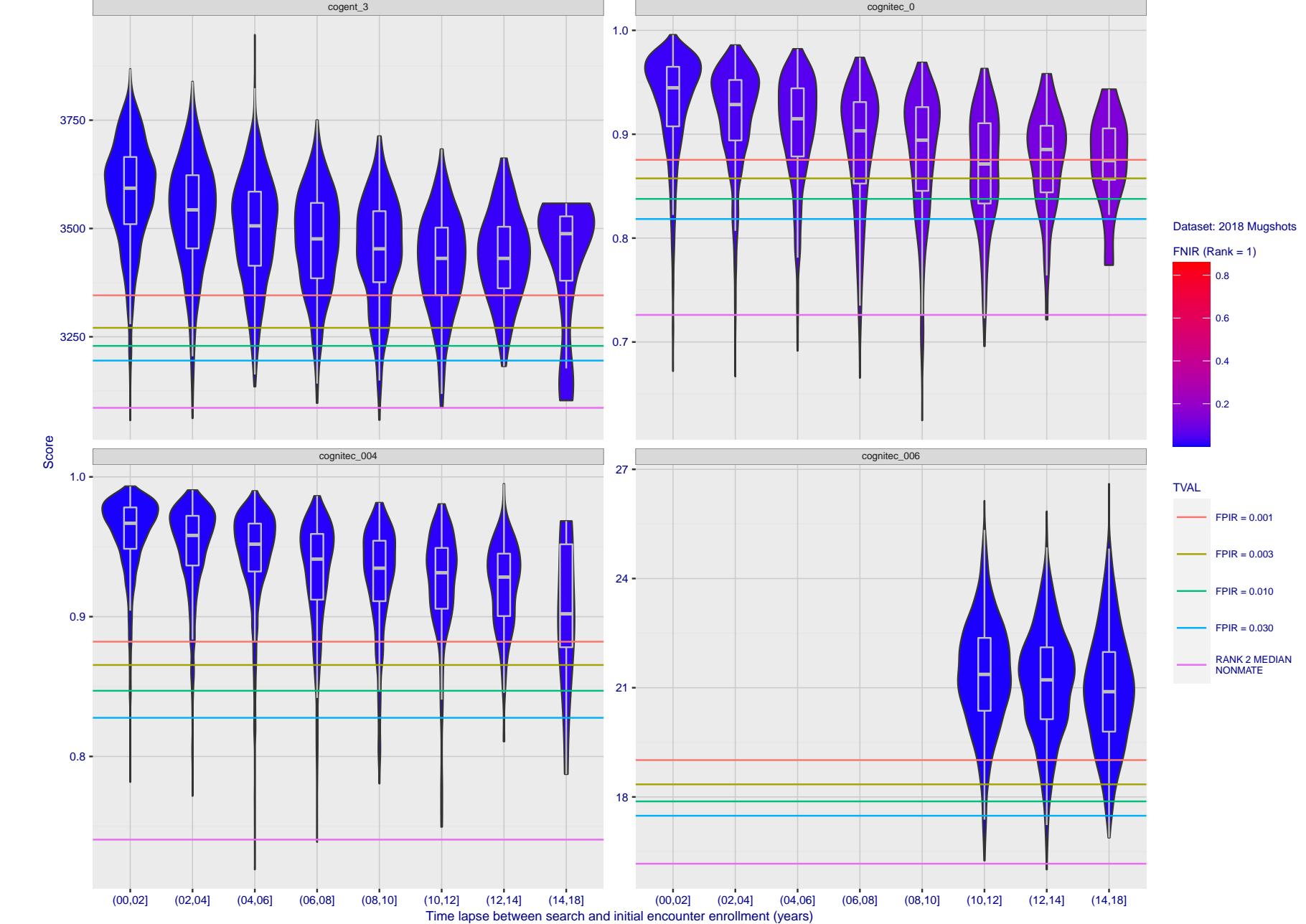


Figure 105: [FRVT-2018 Mugshot Ageing Dataset] Native mate scores vs. time-elapsed. The oldest image of each individual is enrolled. Thereafter, all more recent images are searched. Mated score distributions are computed over all searches noted in row 17 of Table 1 binned by number of years between search and initial enrollment.

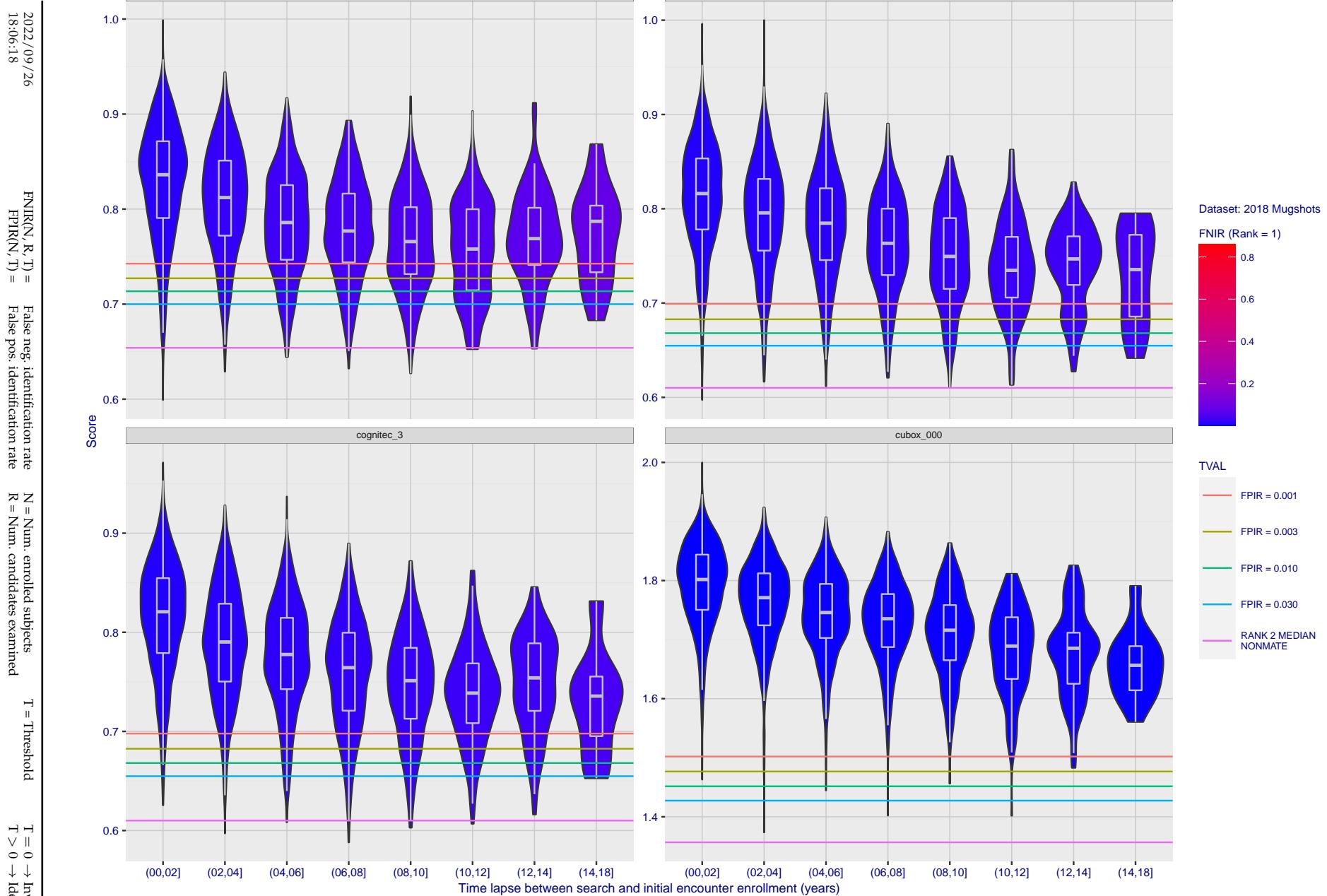


Figure 106: [FRVT-2018 Mugshot Ageing Dataset] Native mate scores vs. time-elapsed. The oldest image of each individual is enrolled. Thereafter, all more recent images are searched. Mated score distributions are computed over all searches noted in row 17 of Table 1 binned by number of years between search and initial enrollment.

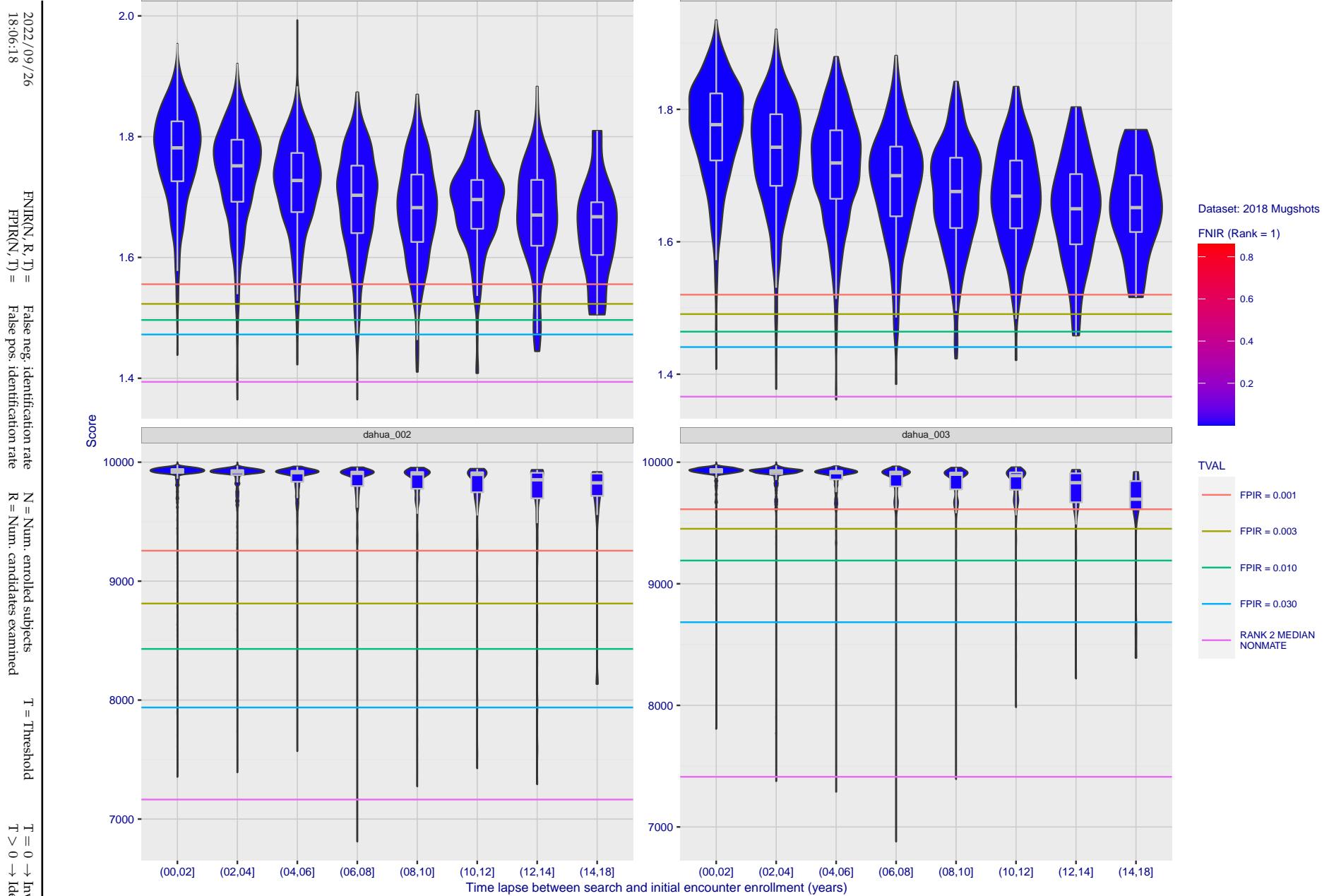


Figure 107: [FRVT-2018 Mugshot Ageing Dataset] Native mate scores vs. time-elapsed. The oldest image of each individual is enrolled. Thereafter, all more recent images are searched. Mated score distributions are computed over all searches noted in row 17 of Table 1 binned by number of years between search and initial enrollment.

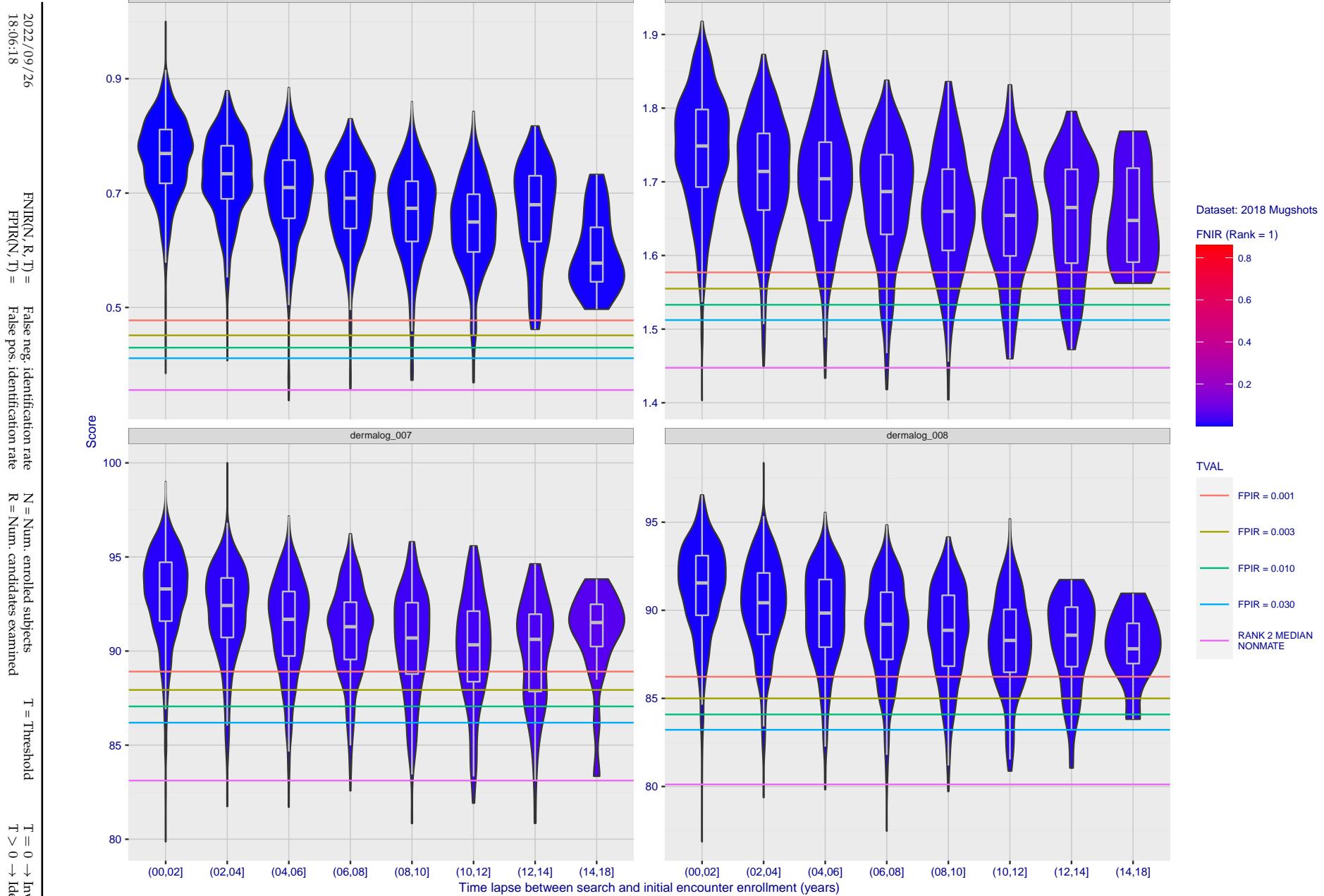


Figure 108: [FRVT-2018 Mugshot Ageing Dataset] Native mate scores vs. time-elapsed. The oldest image of each individual is enrolled. Thereafter, all more recent images are searched. Mated score distributions are computed over all searches noted in row 17 of Table 1 binned by number of years between search and initial enrollment.

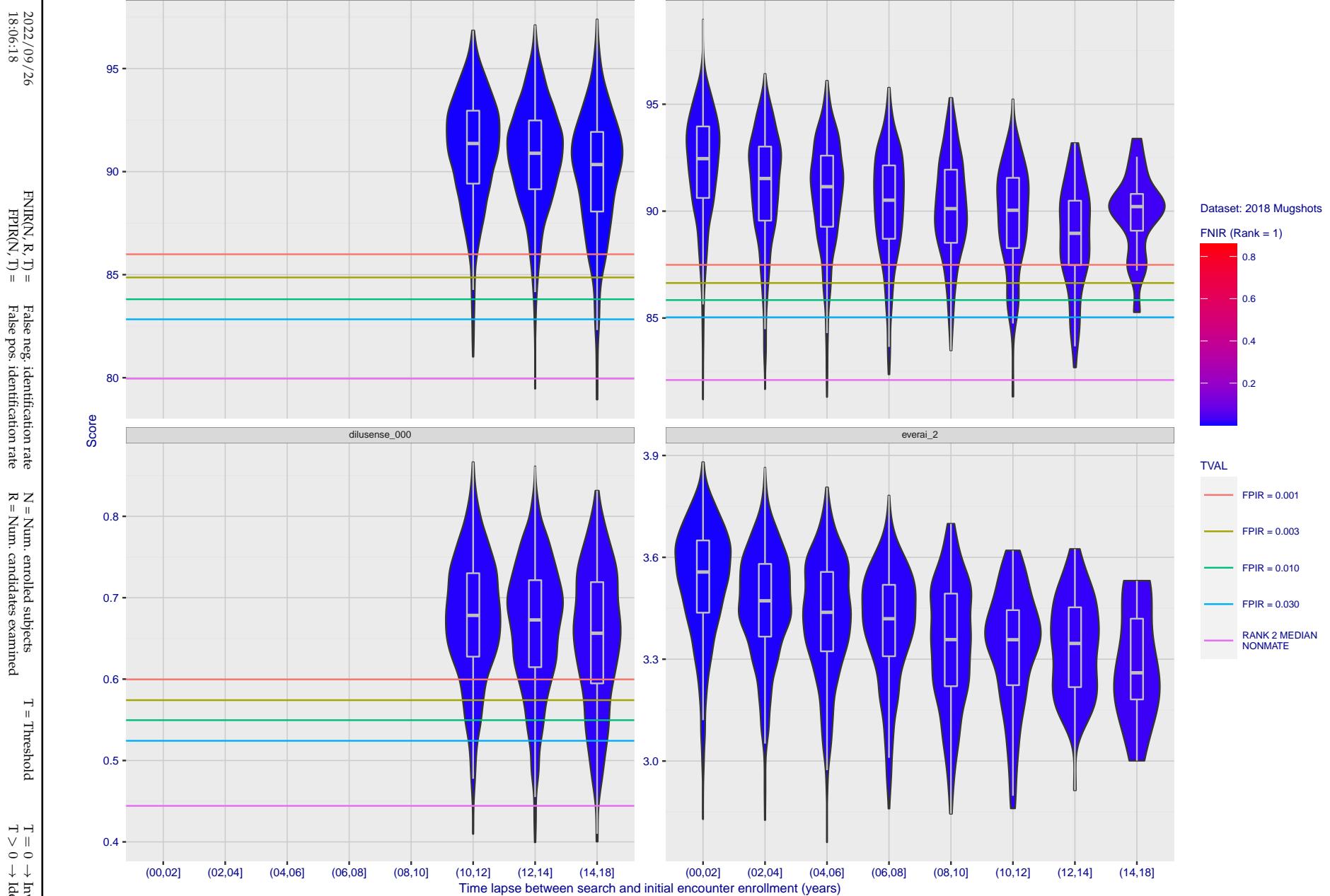


Figure 109: [FRVT-2018 Mugshot Ageing Dataset] Native mate scores vs. time-elapsed. The oldest image of each individual is enrolled. Thereafter, all more recent images are searched. Mated score distributions are computed over all searches noted in row 17 of Table 1 binned by number of years between search and initial enrollment.

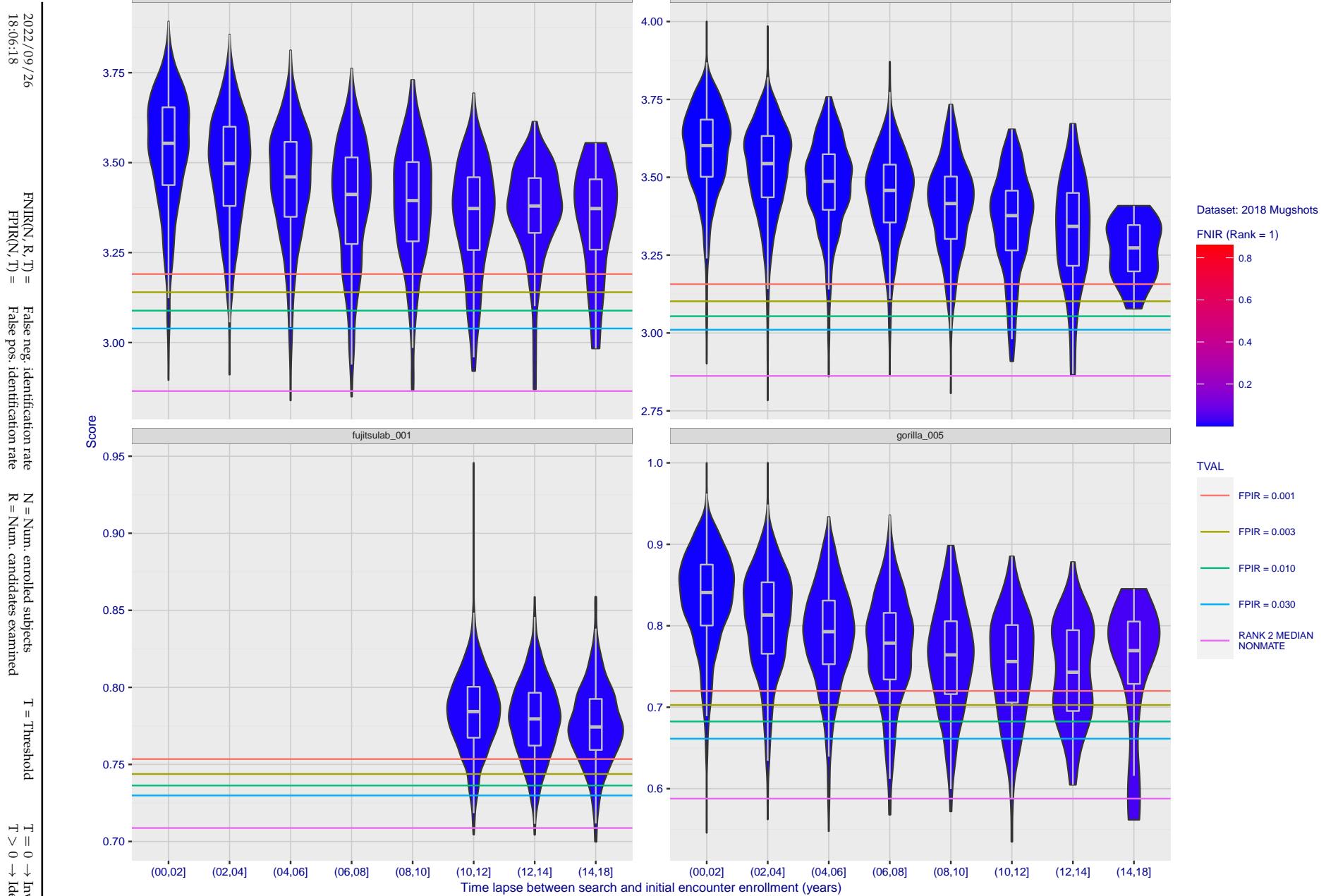


Figure 110: [FRVT-2018 Mugshot Ageing Dataset] Native mate scores vs. time-elapsed. The oldest image of each individual is enrolled. Thereafter, all more recent images are searched. Mated score distributions are computed over all searches noted in row 17 of Table 1 binned by number of years between search and initial enrollment.

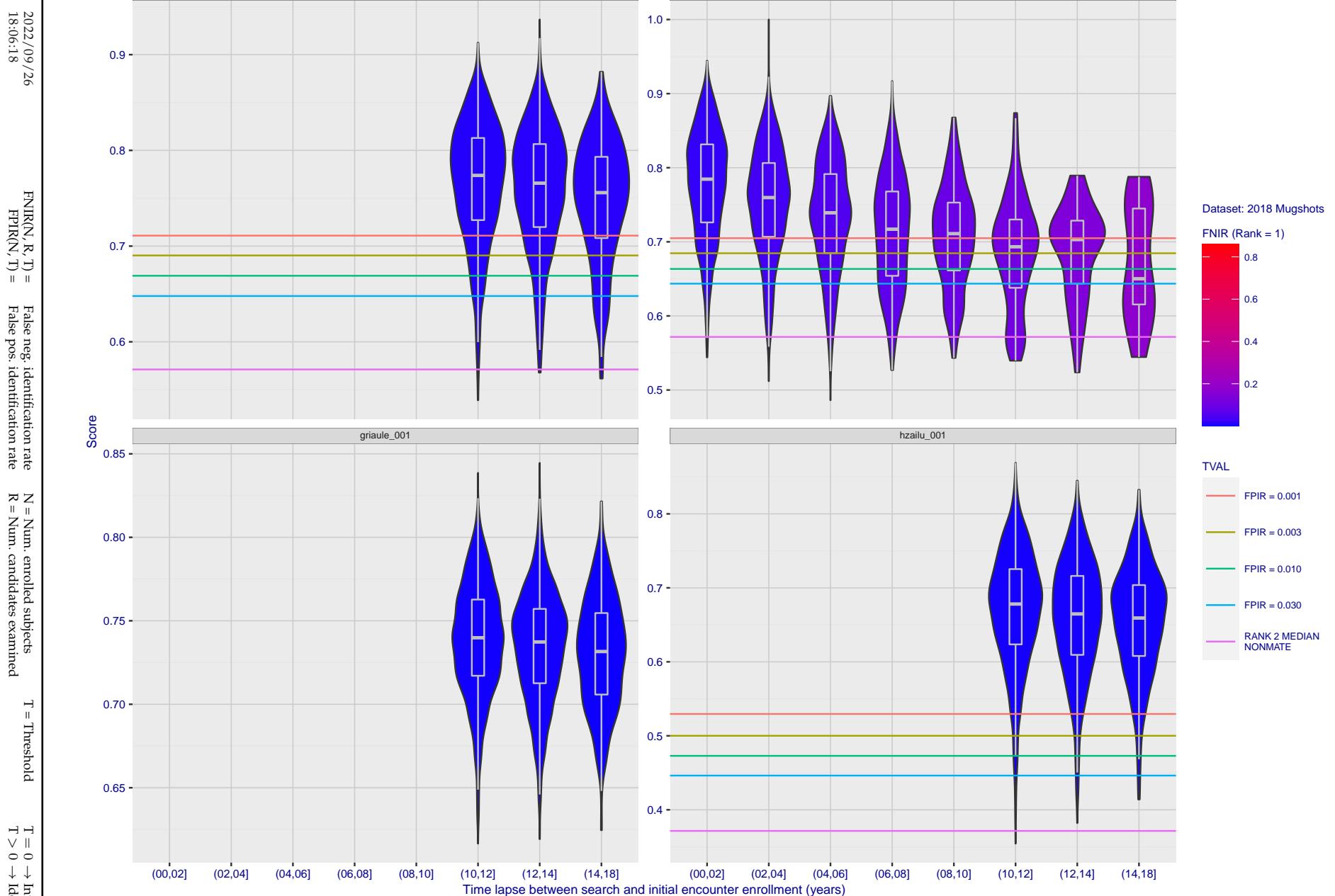


Figure 111: [FRVT-2018 Mugshot Ageing Dataset] Native mate scores vs. time-elapsed. The oldest image of each individual is enrolled. Thereafter, all more recent images are searched. Mated score distributions are computed over all searches noted in row 17 of Table 1 binned by number of years between search and initial enrollment.

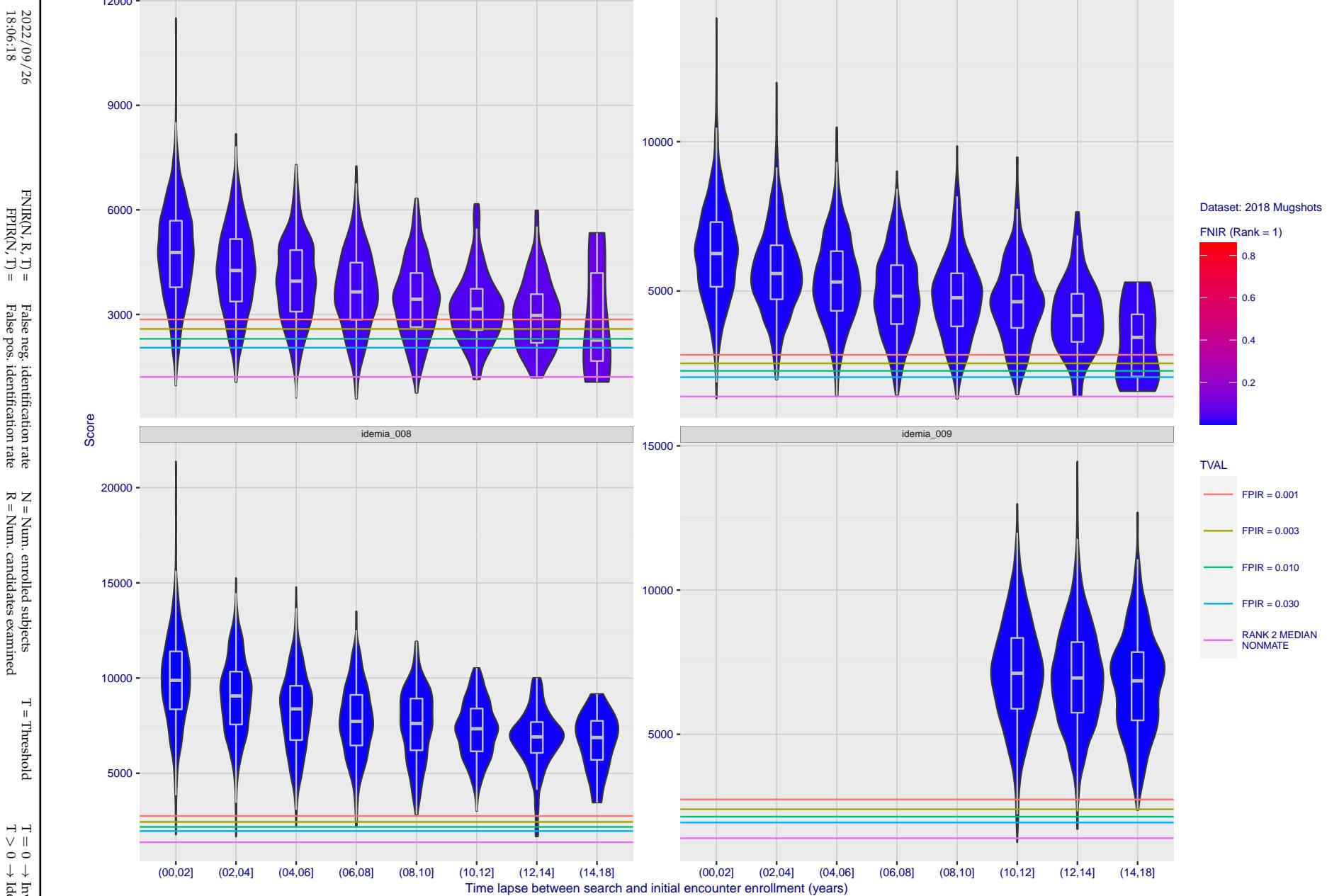


Figure 112: [FRVT-2018 Mugshot Ageing Dataset] Native mate scores vs. time-elapsed. The oldest image of each individual is enrolled. Thereafter, all more recent images are searched. Mated score distributions are computed over all searches noted in row 17 of Table 1 binned by number of years between search and initial enrollment.

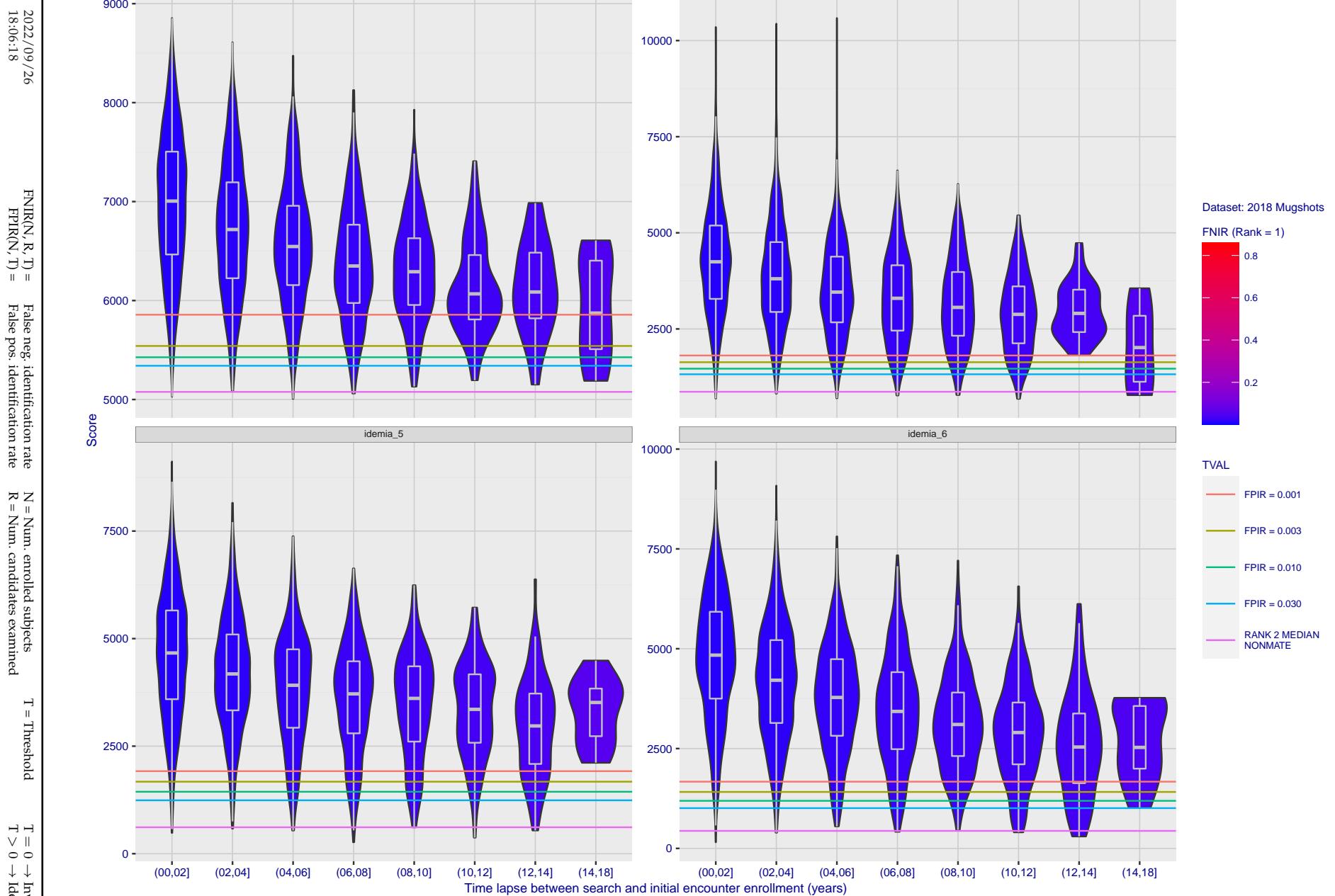


Figure 113: [FRVT-2018 Mugshot Ageing Dataset] Native mate scores vs. time-elapsed. The oldest image of each individual is enrolled. Thereafter, all more recent images are searched. Mated score distributions are computed over all searches noted in row 17 of Table 1 binned by number of years between search and initial enrollment.

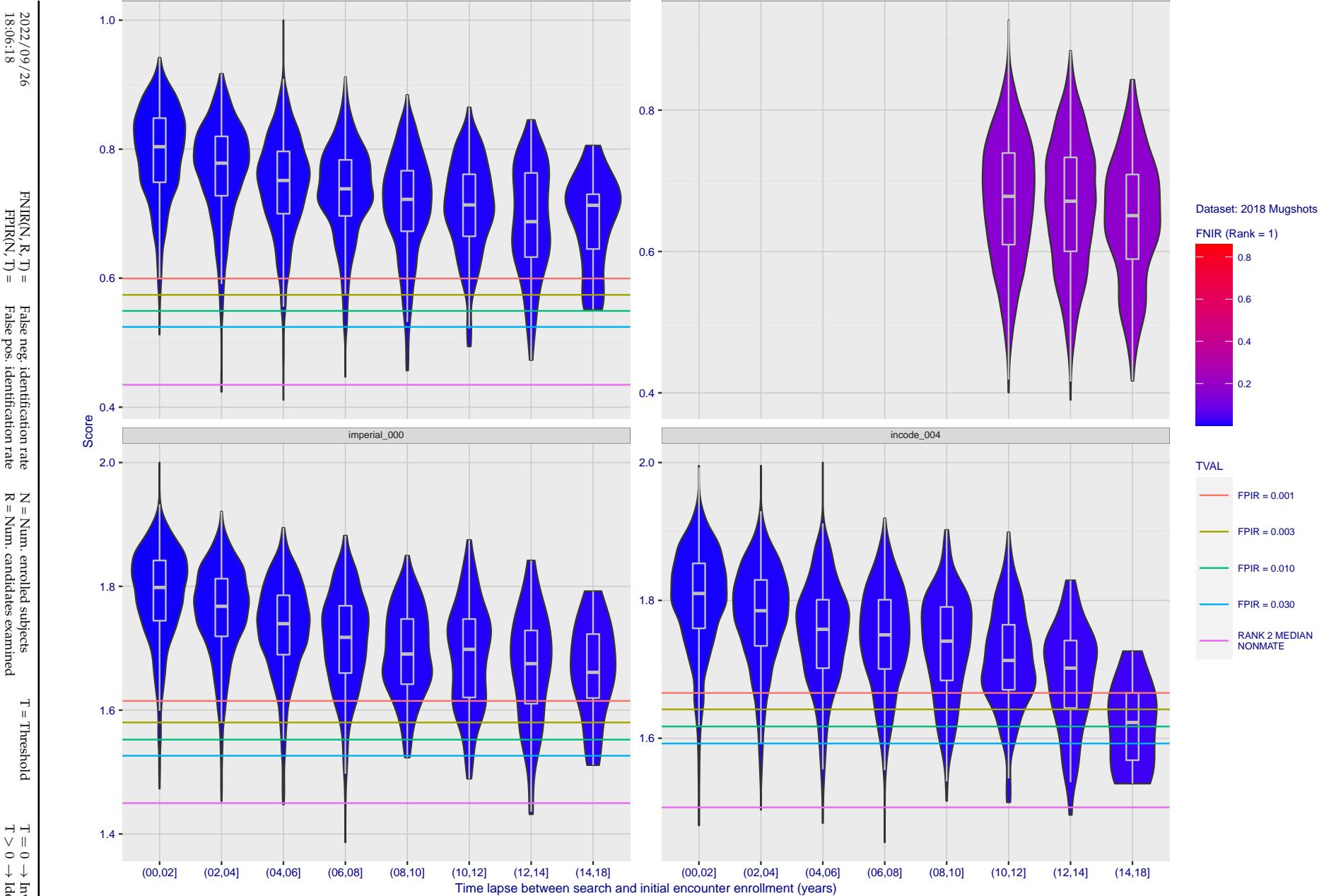


Figure 114: [FRVT-2018 Mugshot Ageing Dataset] Native mate scores vs. time-elapsed. The oldest image of each individual is enrolled. Thereafter, all more recent images are searched. Mated score distributions are computed over all searches noted in row 17 of Table 1 binned by number of years between search and initial enrollment.

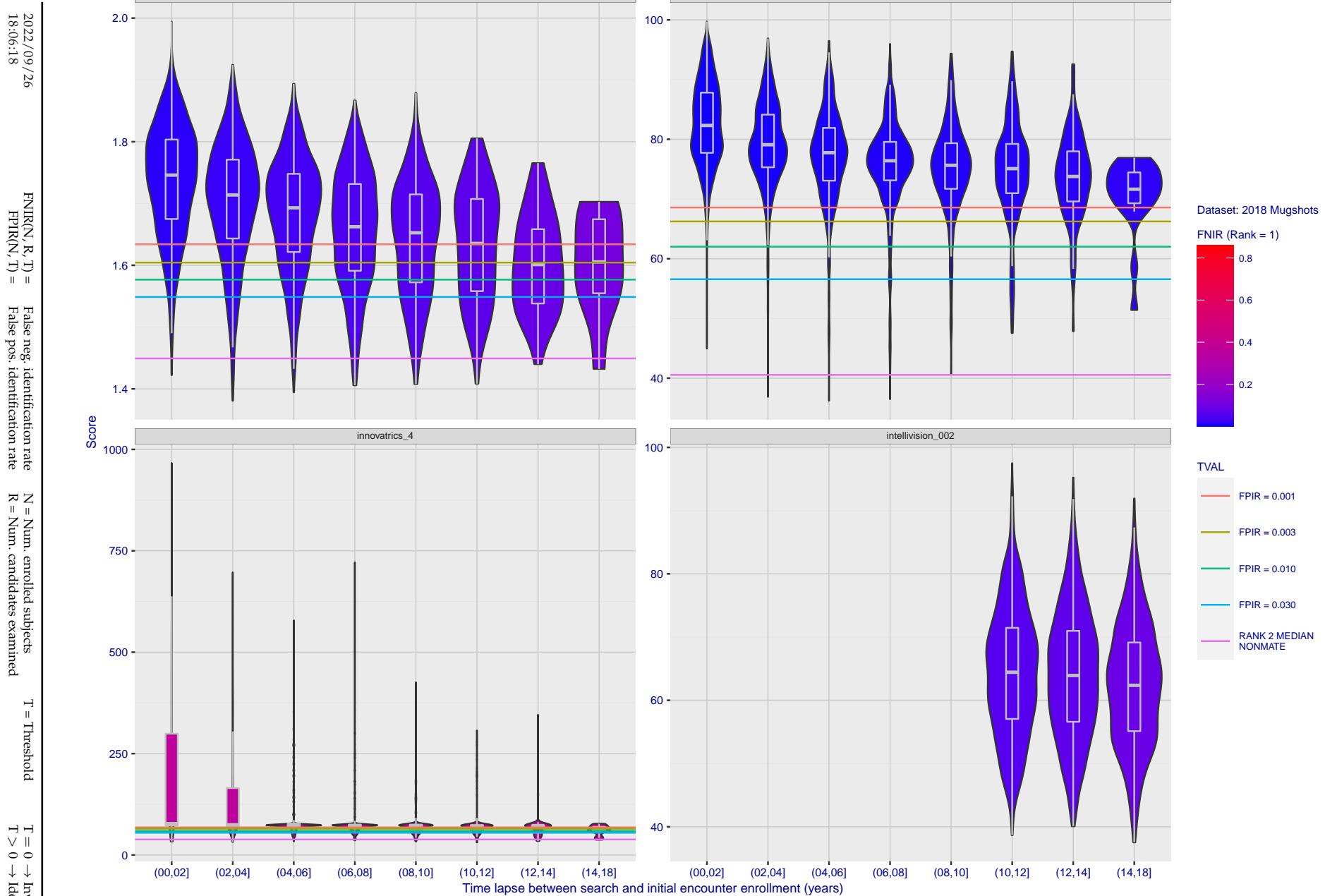


Figure 115: [FRVT-2018 Mugshot Ageing Dataset] Native mate scores vs. time-elapsed. The oldest image of each individual is enrolled. Thereafter, all more recent images are searched. Mated score distributions are computed over all searches noted in row 17 of Table 1 binned by number of years between search and initial enrollment.

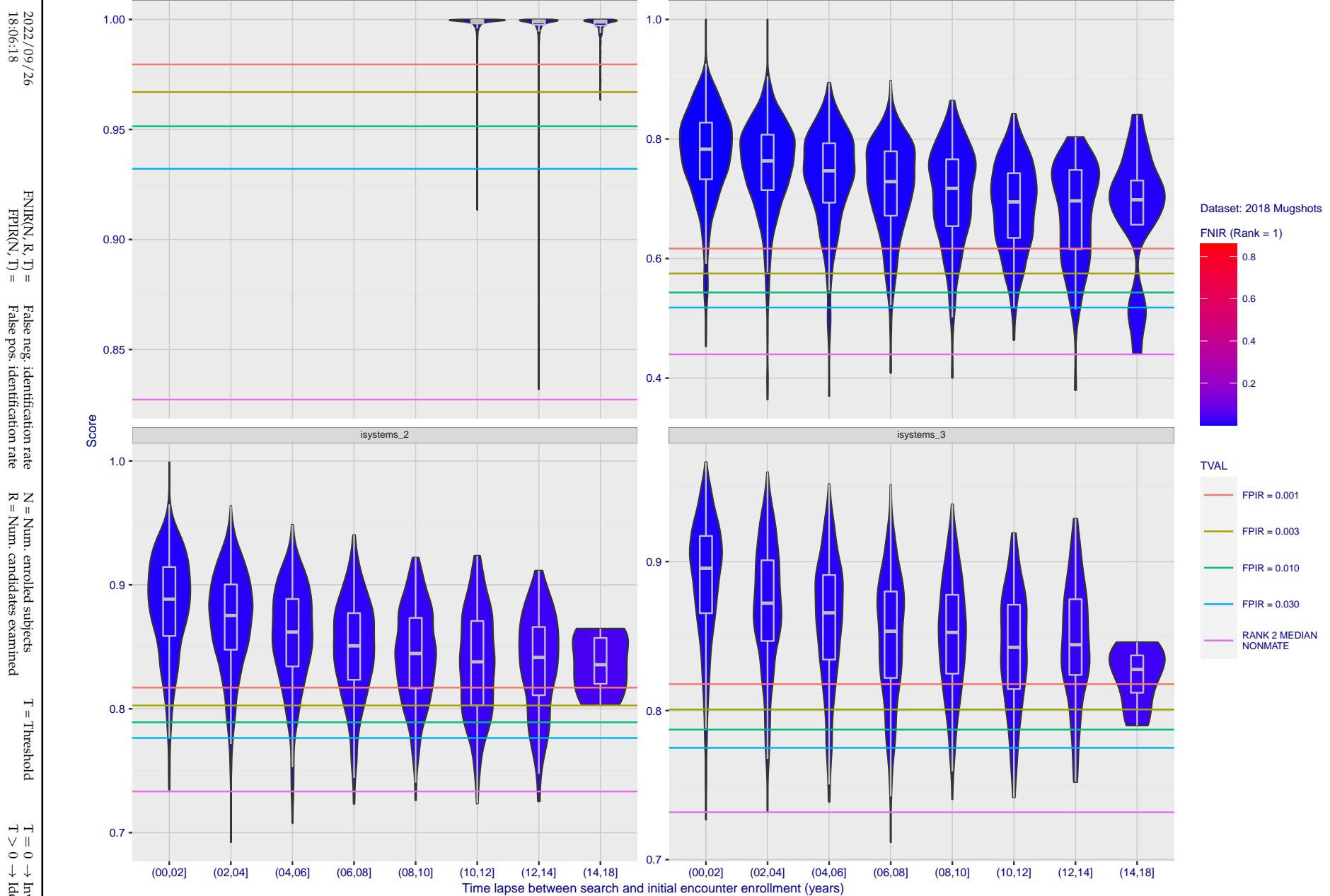


Figure 116: [FRVT-2018 Mugshot Ageing Dataset] Native mate scores vs. time-elapsed. The oldest image of each individual is enrolled. Thereafter, all more recent images are searched. Mated score distributions are computed over all searches noted in row 17 of Table 1 binned by number of years between search and initial enrollment.

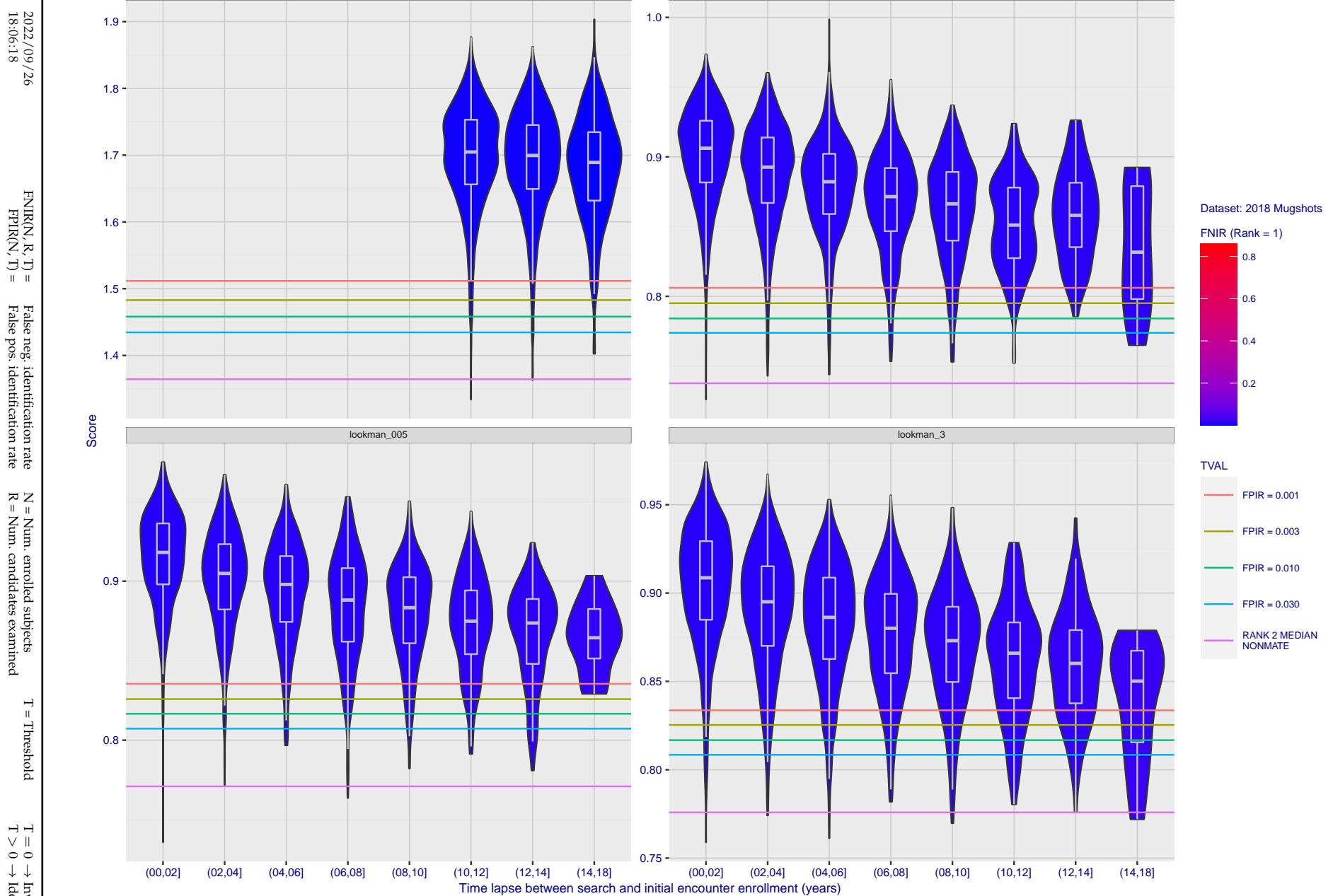


Figure 117: [FRVT-2018 Mugshot Ageing Dataset] Native mate scores vs. time-elapsed. The oldest image of each individual is enrolled. Thereafter, all more recent images are searched. Mated score distributions are computed over all searches noted in row 17 of Table 1 binned by number of years between search and initial enrollment.

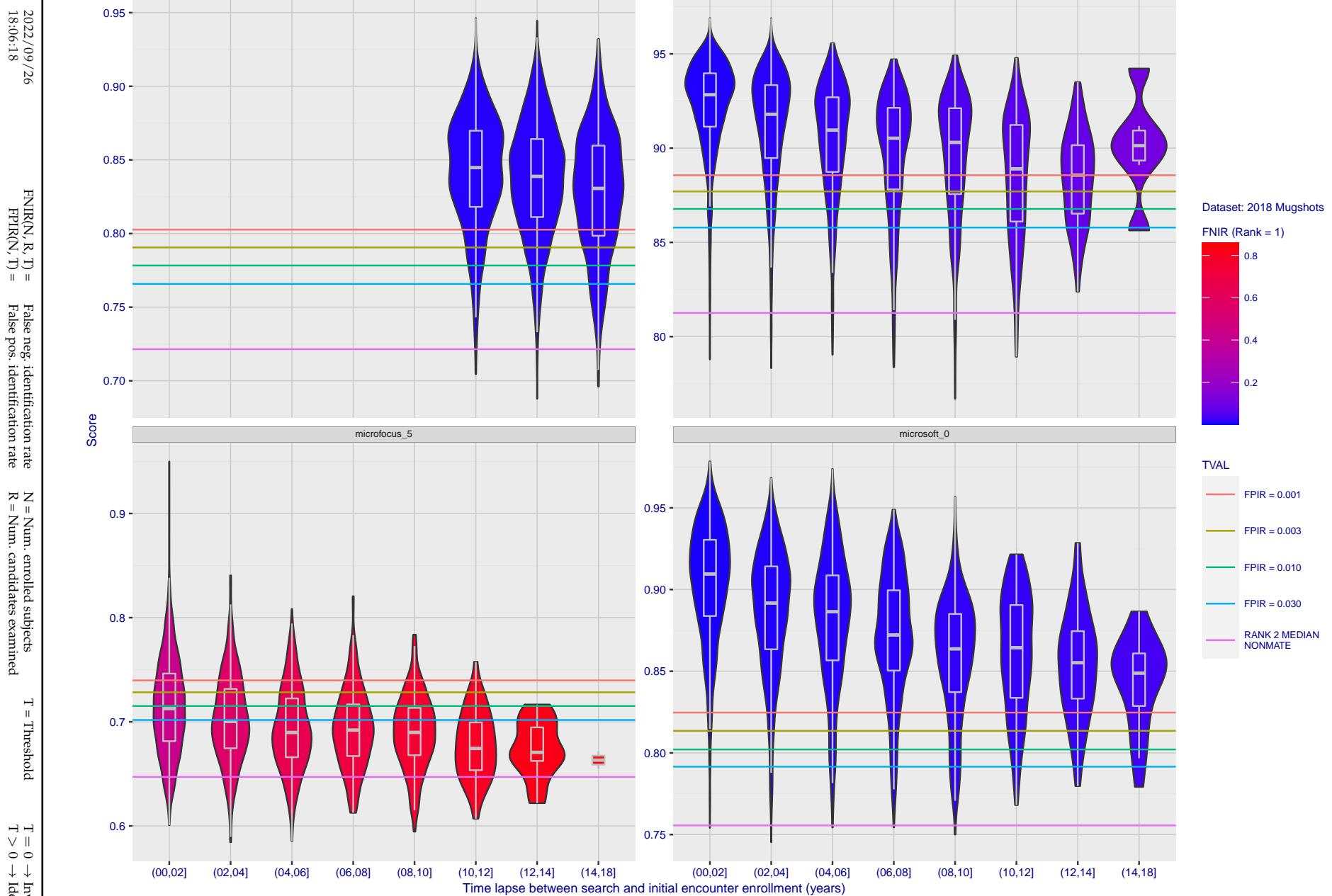


Figure 118: [FRVT-2018 Mugshot Ageing Dataset] Native mate scores vs. time-elapsed. The oldest image of each individual is enrolled. Thereafter, all more recent images are searched. Mated score distributions are computed over all searches noted in row 17 of Table 1 binned by number of years between search and initial enrollment.

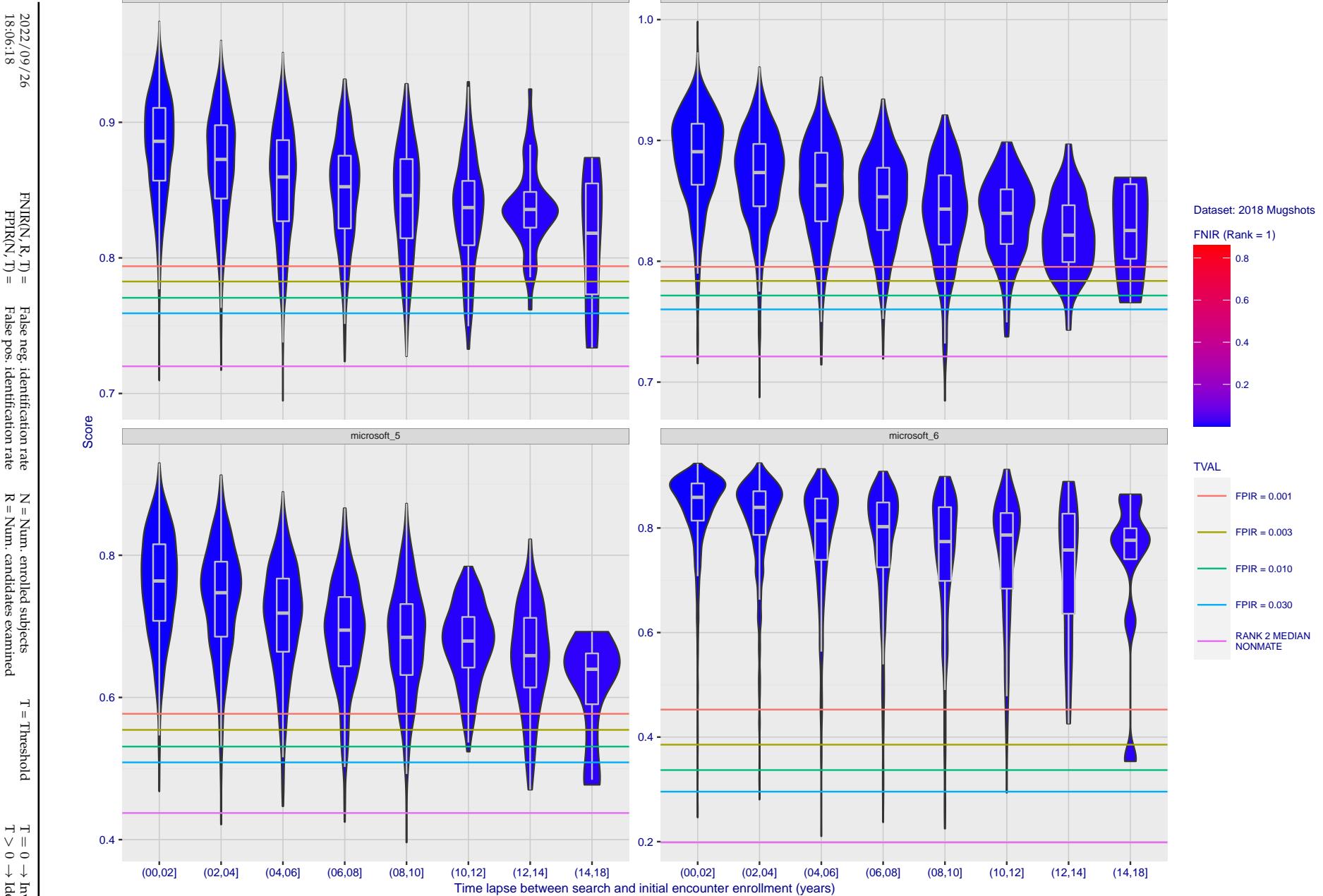


Figure 119: [FRVT-2018 Mugshot Ageing Dataset] Native mate scores vs. time-elapsed. The oldest image of each individual is enrolled. Thereafter, all more recent images are searched. Mated score distributions are computed over all searches noted in row 17 of Table 1 binned by number of years between search and initial enrollment.

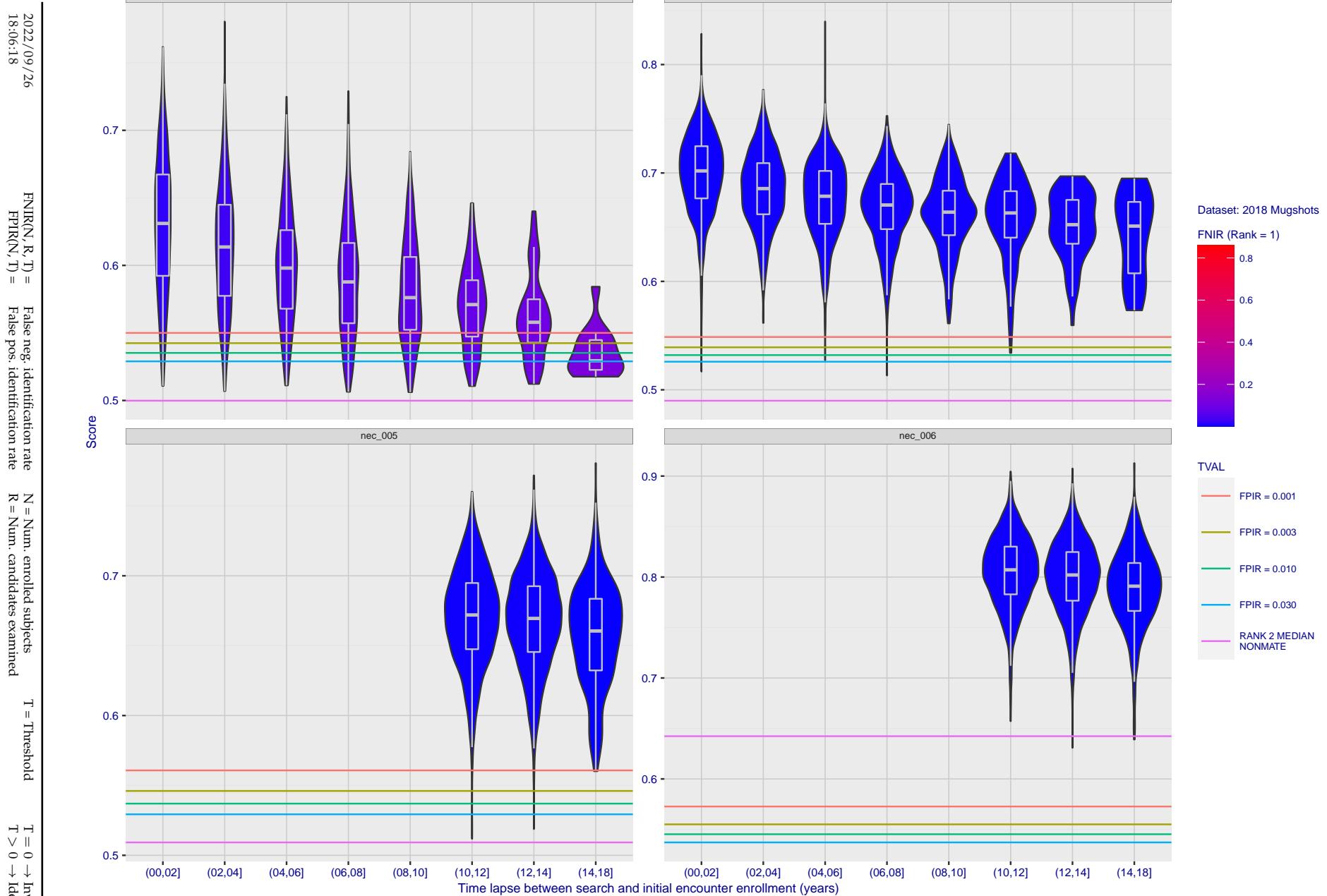


Figure 120: [FRVT-2018 Mugshot Ageing Dataset] Native mate scores vs. time-elapsed. The oldest image of each individual is enrolled. Thereafter, all more recent images are searched. Mated score distributions are computed over all searches noted in row 17 of Table 1 binned by number of years between search and initial enrollment.

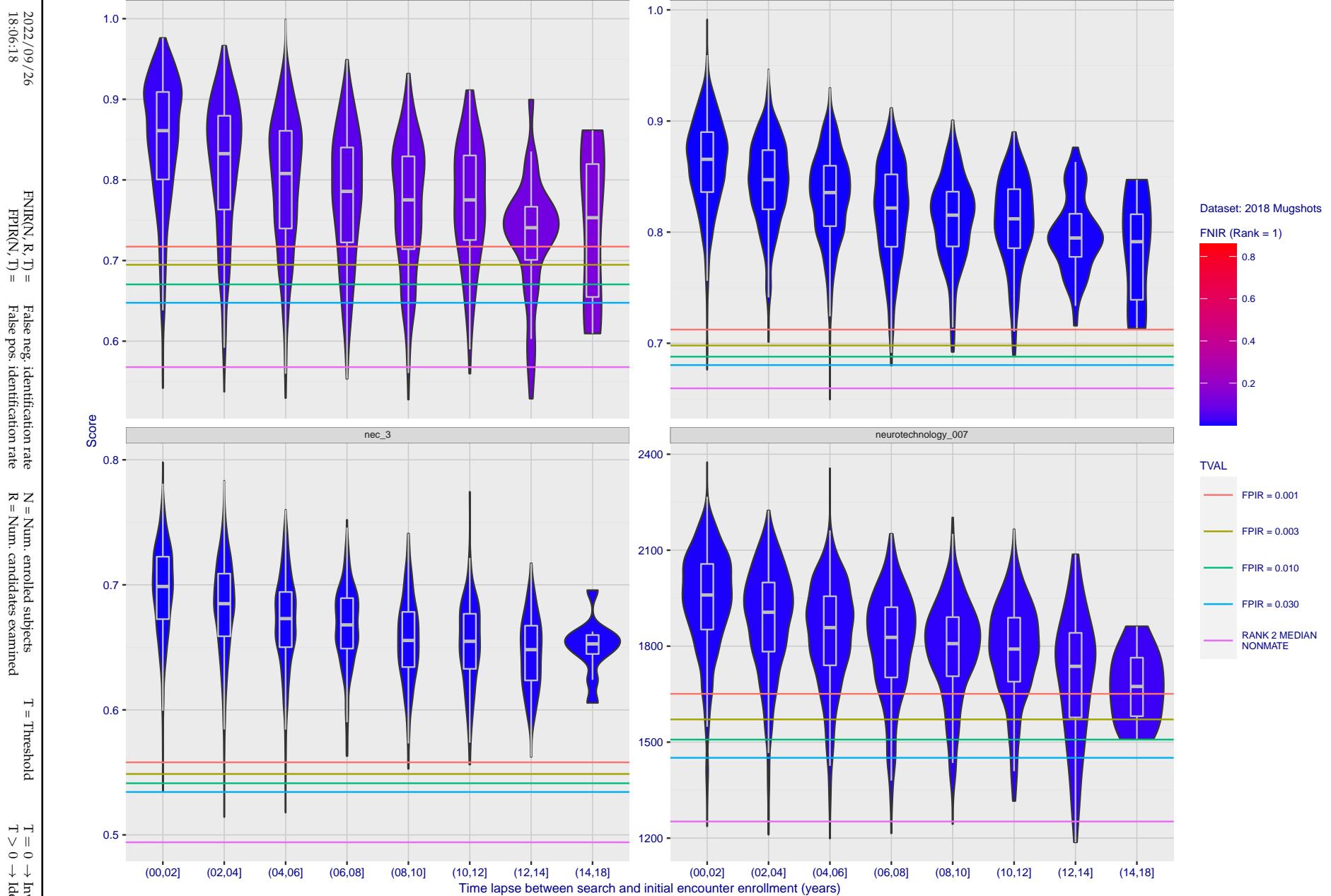


Figure 121: [FRVT-2018 Mugshot Ageing Dataset] Native mate scores vs. time-elapsed. The oldest image of each individual is enrolled. Thereafter, all more recent images are searched. Mated score distributions are computed over all searches noted in row 17 of Table 1 binned by number of years between search and initial enrollment.

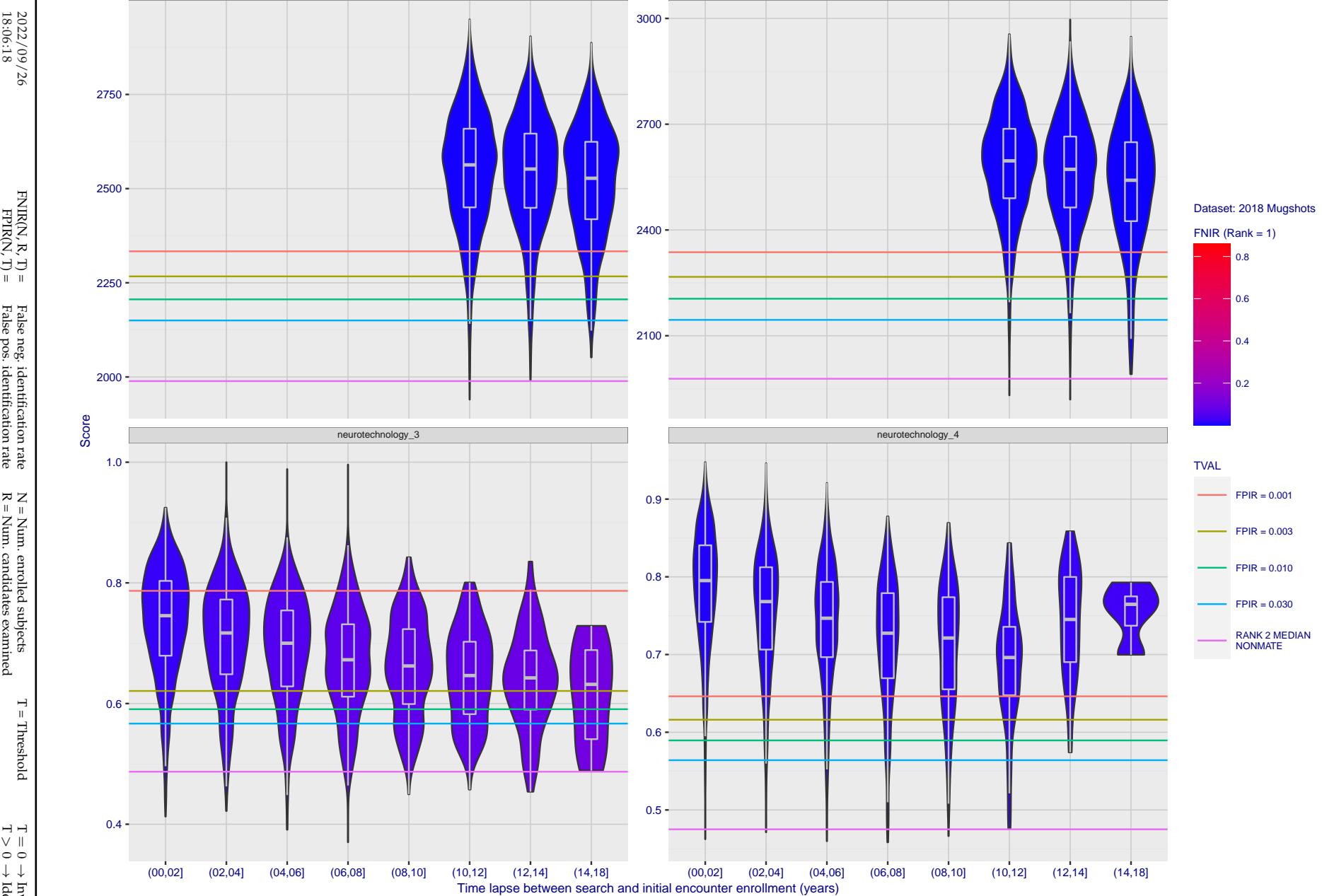


Figure 122: [FRVT-2018 Mugshot Ageing Dataset] Native mate scores vs. time-elapsed. The oldest image of each individual is enrolled. Thereafter, all more recent images are searched. Mated score distributions are computed over all searches noted in row 17 of Table 1 binned by number of years between search and initial enrollment.

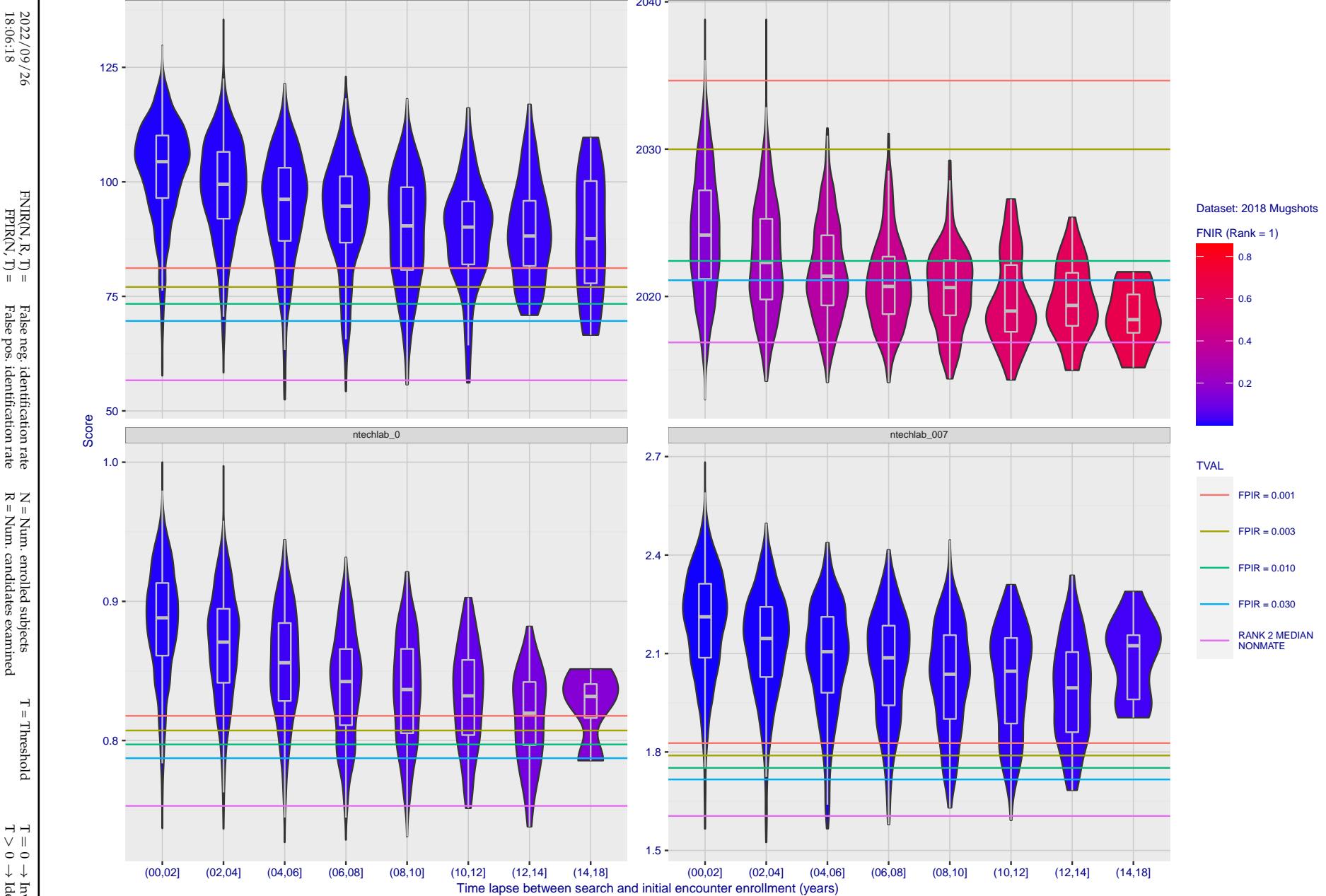


Figure 123: [FRVT-2018 Mugshot Ageing Dataset] Native mate scores vs. time-elapsed. The oldest image of each individual is enrolled. Thereafter, all more recent images are searched. Mated score distributions are computed over all searches noted in row 17 of Table 1 binned by number of years between search and initial enrollment.

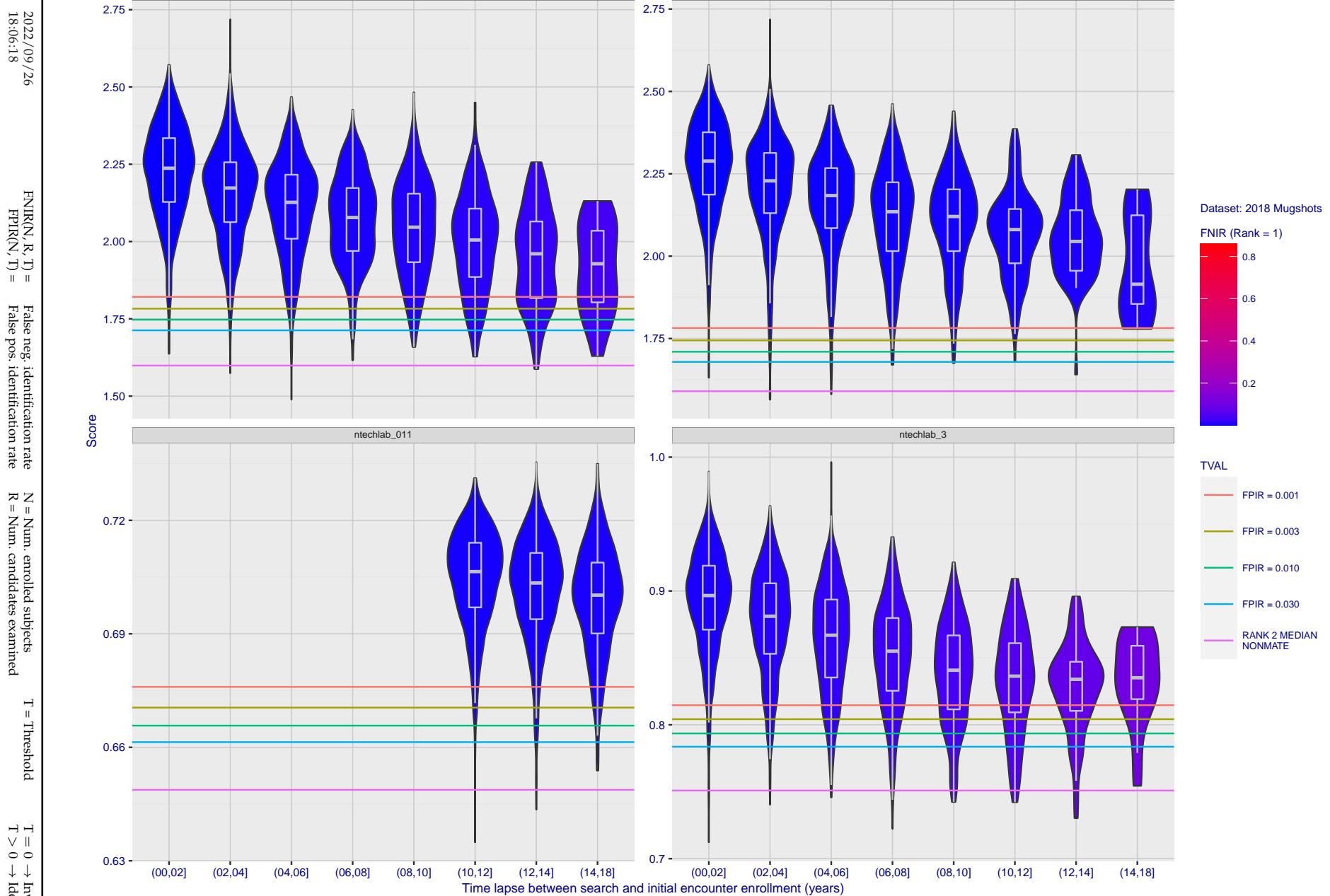


Figure 124: [FRVT-2018 Mugshot Ageing Dataset] Native mate scores vs. time-elapsed. The oldest image of each individual is enrolled. Thereafter, all more recent images are searched. Mated score distributions are computed over all searches noted in row 17 of Table 1 binned by number of years between search and initial enrollment.

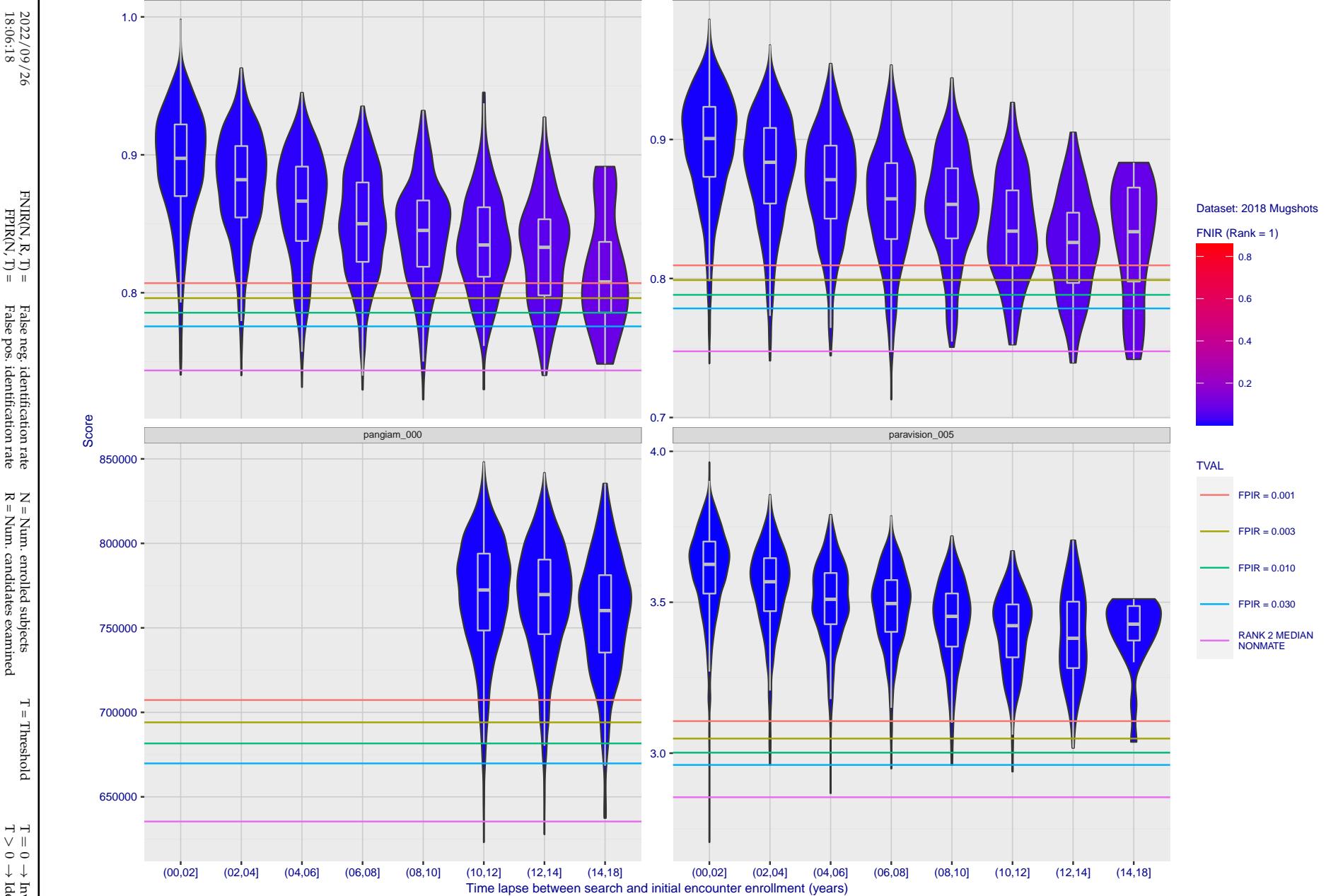


Figure 125: [FRVT-2018 Mugshot Ageing Dataset] Native mate scores vs. time-elapsed. The oldest image of each individual is enrolled. Thereafter, all more recent images are searched. Mated score distributions are computed over all searches noted in row 17 of Table 1 binned by number of years between search and initial enrollment.

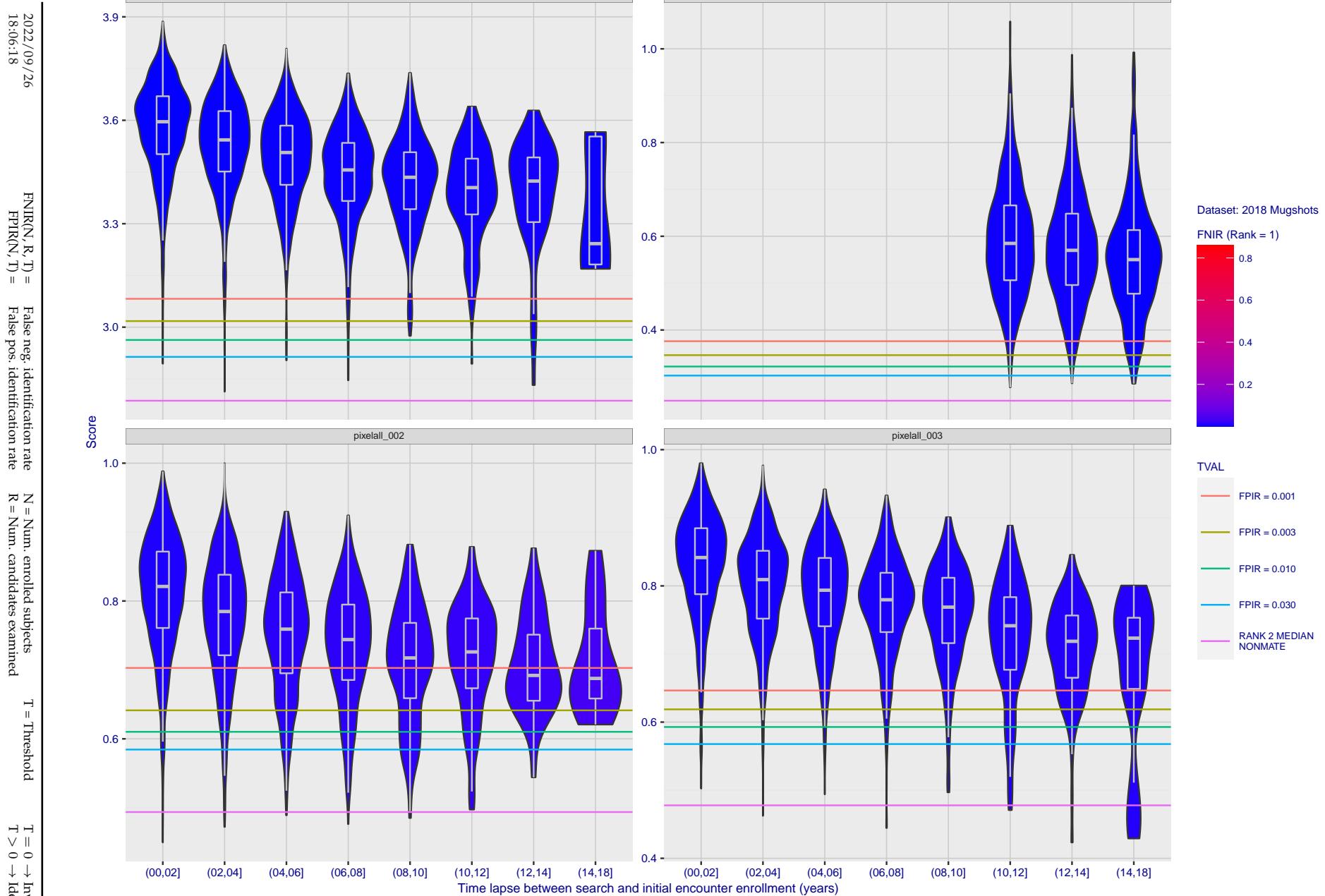


Figure 126: [FRVT-2018 Mugshot Ageing Dataset] Native mate scores vs. time-elapsed. The oldest image of each individual is enrolled. Thereafter, all more recent images are searched. Mated score distributions are computed over all searches noted in row 17 of Table 1 binned by number of years between search and initial enrollment.

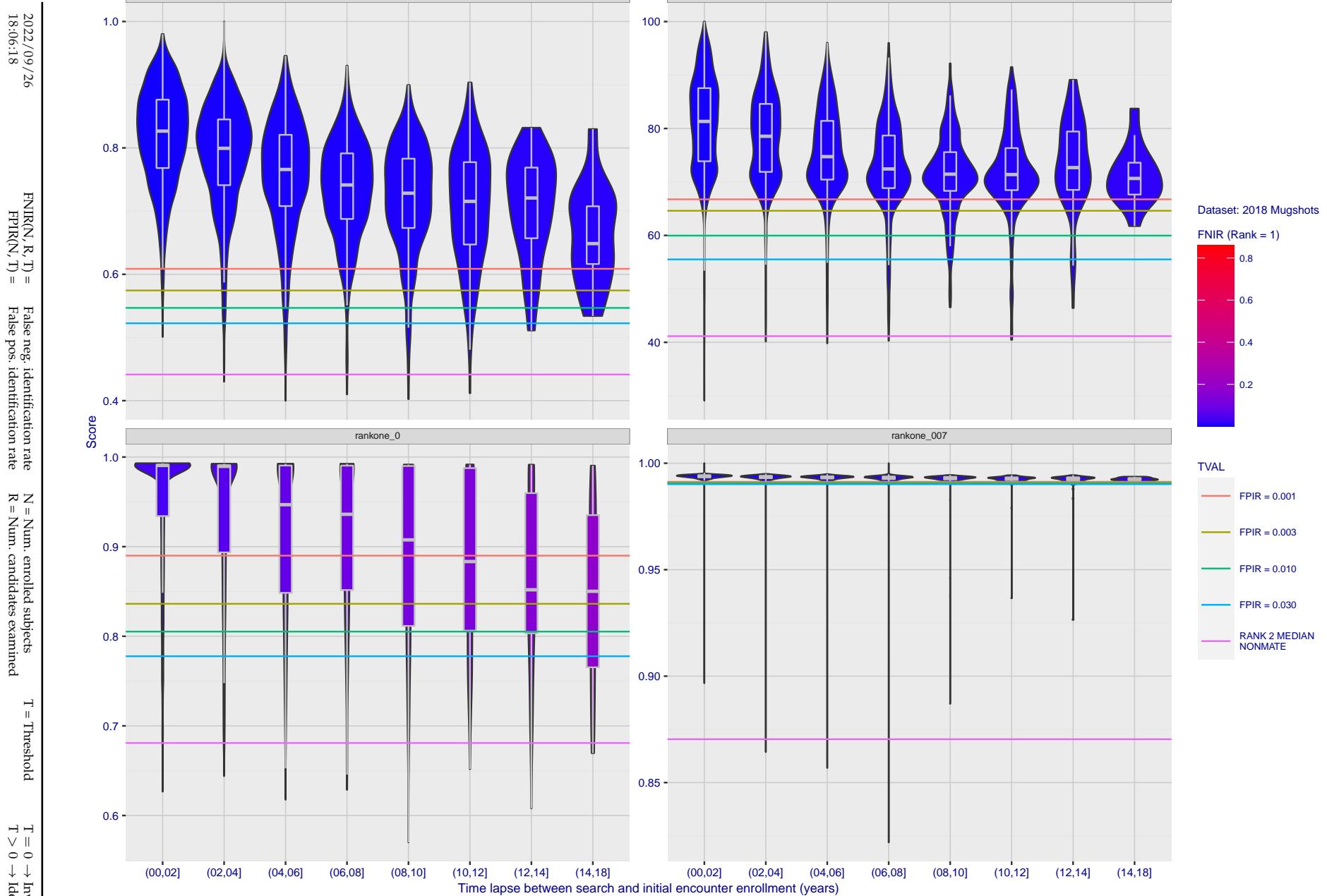


Figure 127: [FRVT-2018 Mugshot Ageing Dataset] Native mate scores vs. time-elapsed. The oldest image of each individual is enrolled. Thereafter, all more recent images are searched. Mated score distributions are computed over all searches noted in row 17 of Table 1 binned by number of years between search and initial enrollment.

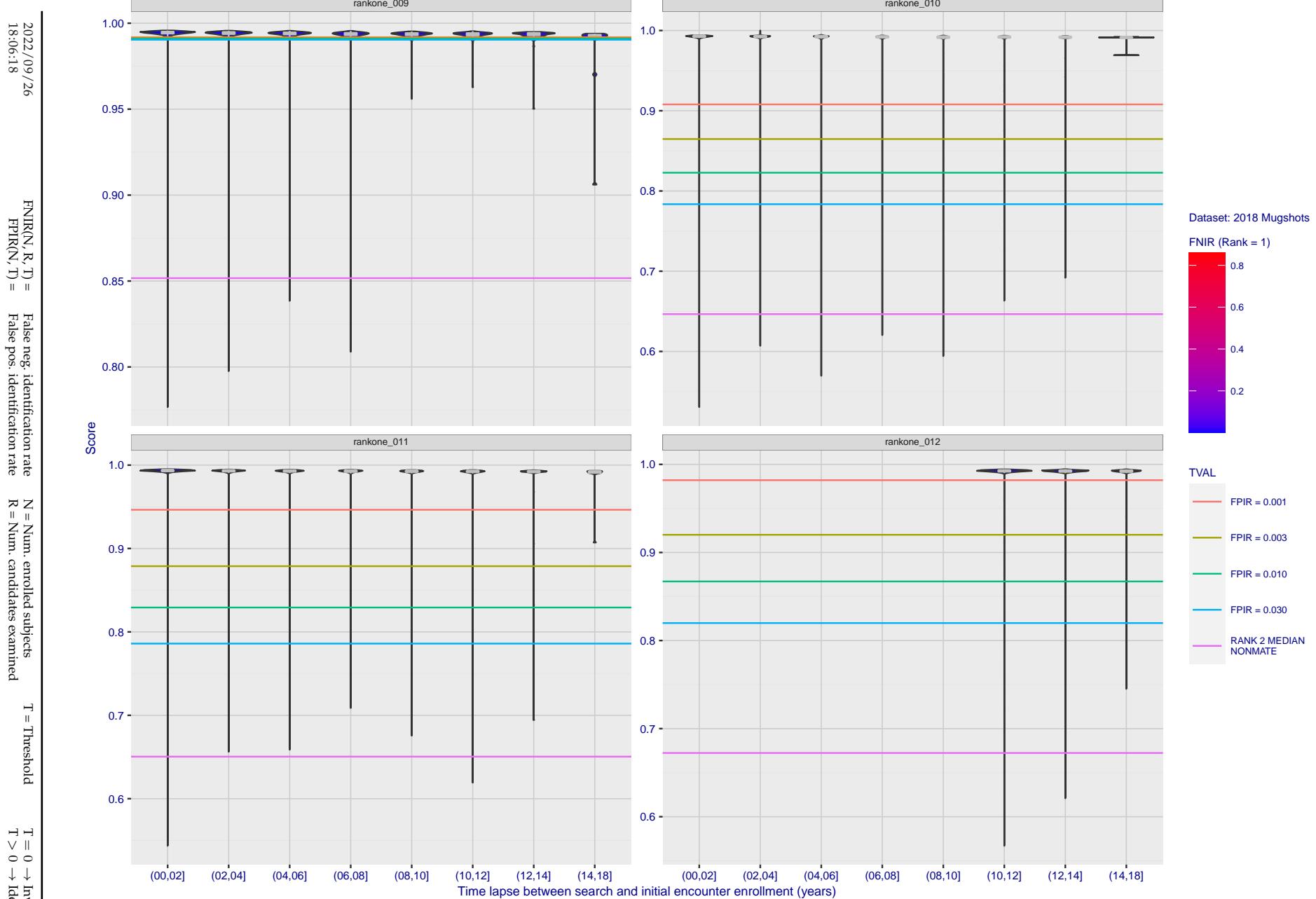


Figure 128: [FRVT-2018 Mugshot Ageing Dataset] Native mate scores vs. time-elapsed. The oldest image of each individual is enrolled. Thereafter, all more recent images are searched. Mated score distributions are computed over all searches noted in row 17 of Table 1 binned by number of years between search and initial enrollment.

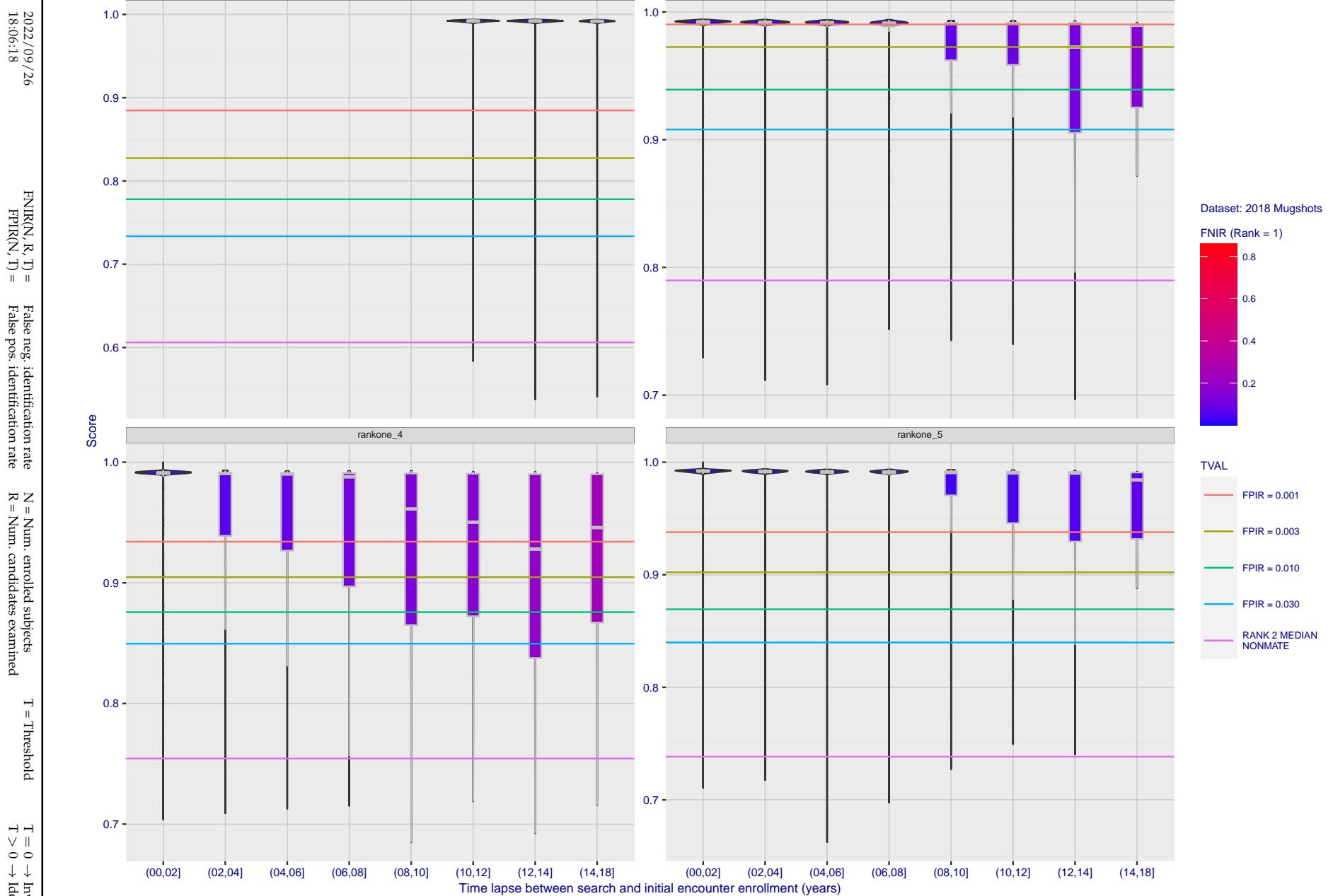


Figure 129: [FRVT-2018 Mugshot Ageing Dataset] Native mate scores vs. time-elapsed. The oldest image of each individual is enrolled. Thereafter, all more recent images are searched. Mated score distributions are computed over all searches noted in row 17 of Table 1 binned by number of years between search and initial enrollment.

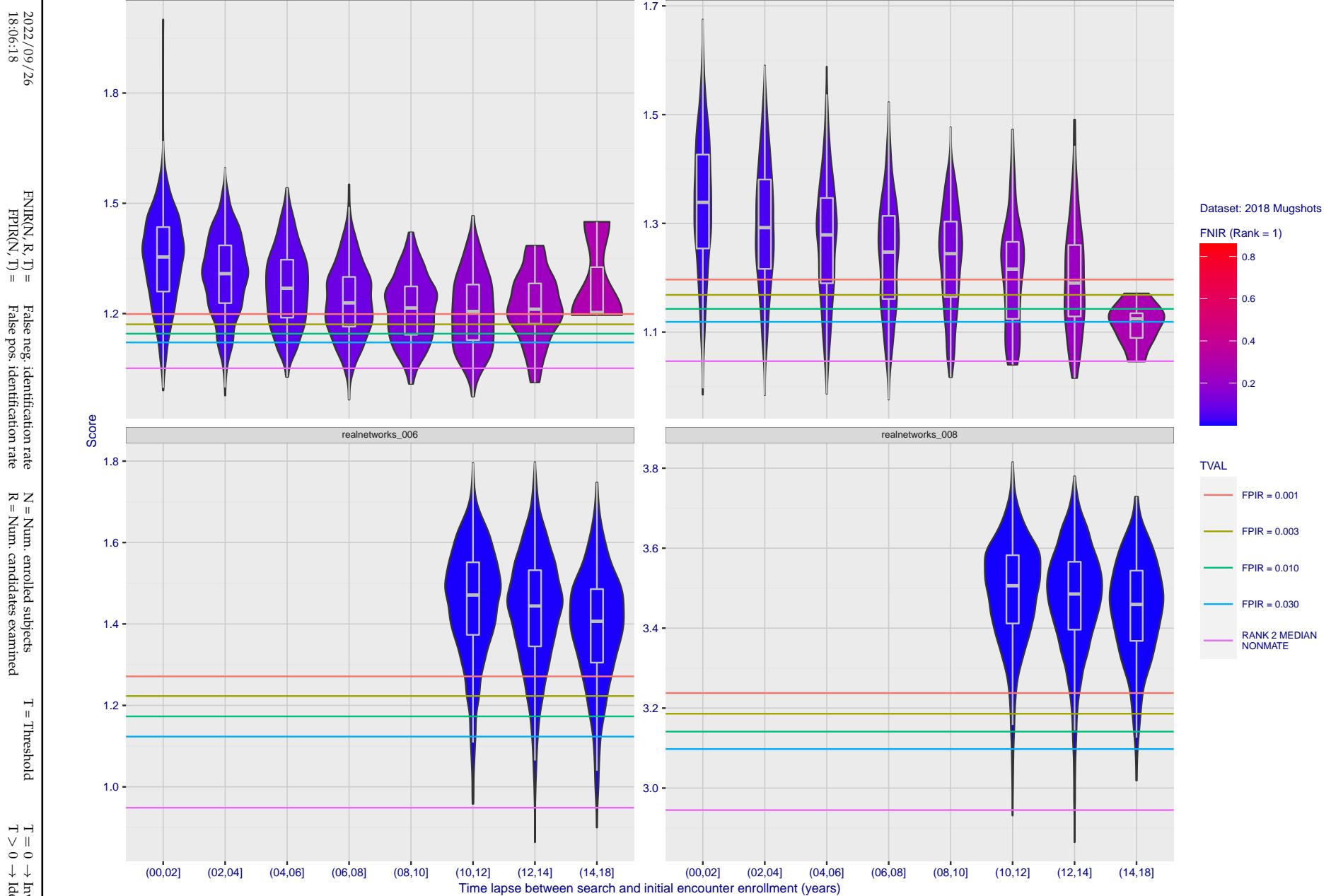


Figure 130: [FRVT-2018 Mugshot Ageing Dataset] Native mate scores vs. time-elapsed. The oldest image of each individual is enrolled. Thereafter, all more recent images are searched. Mated score distributions are computed over all searches noted in row 17 of Table 1 binned by number of years between search and initial enrollment.

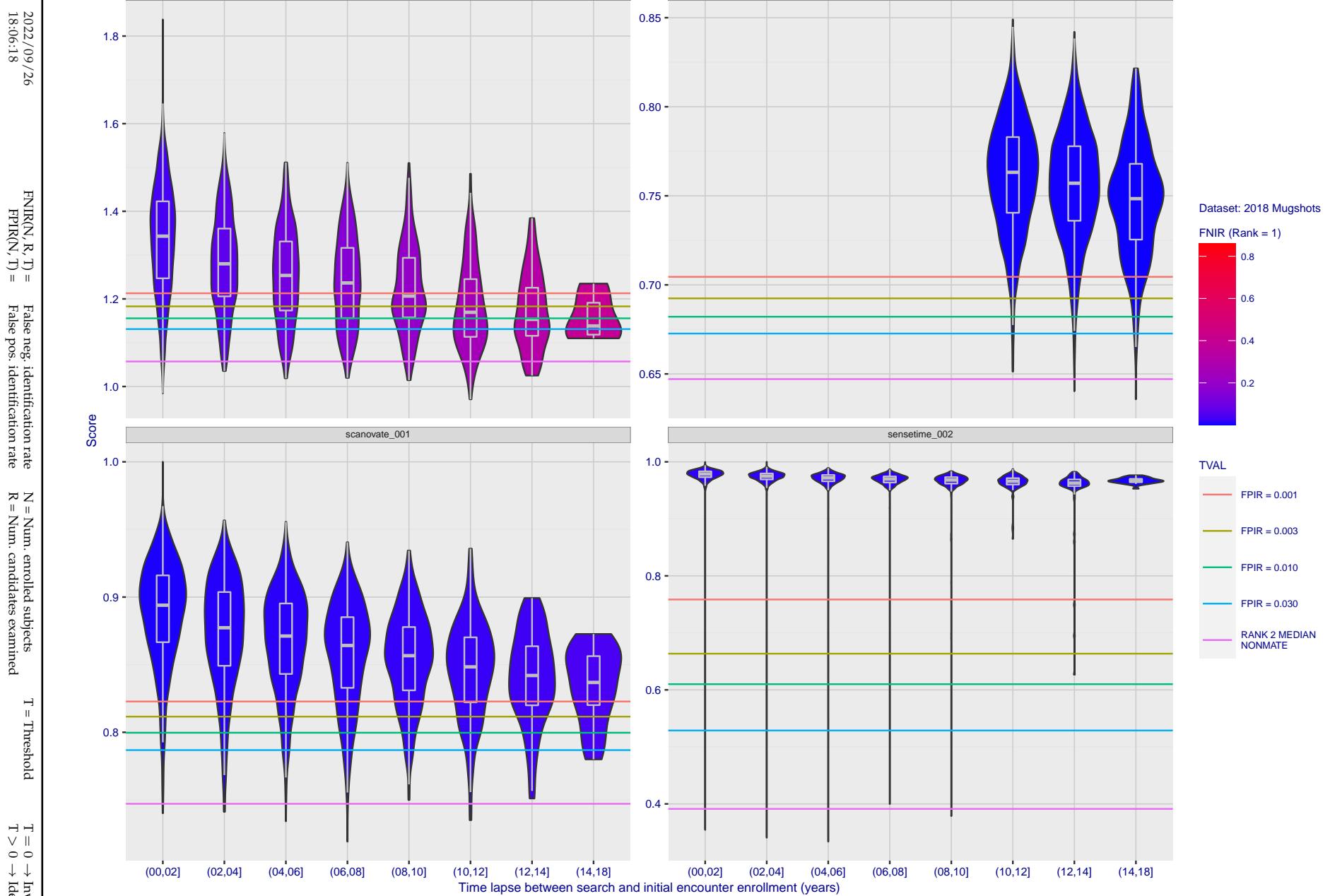


Figure 131: [FRVT-2018 Mugshot Ageing Dataset] Native mate scores vs. time-elapsed. The oldest image of each individual is enrolled. Thereafter, all more recent images are searched. Mated score distributions are computed over all searches noted in row 17 of Table 1 binned by number of years between search and initial enrollment.

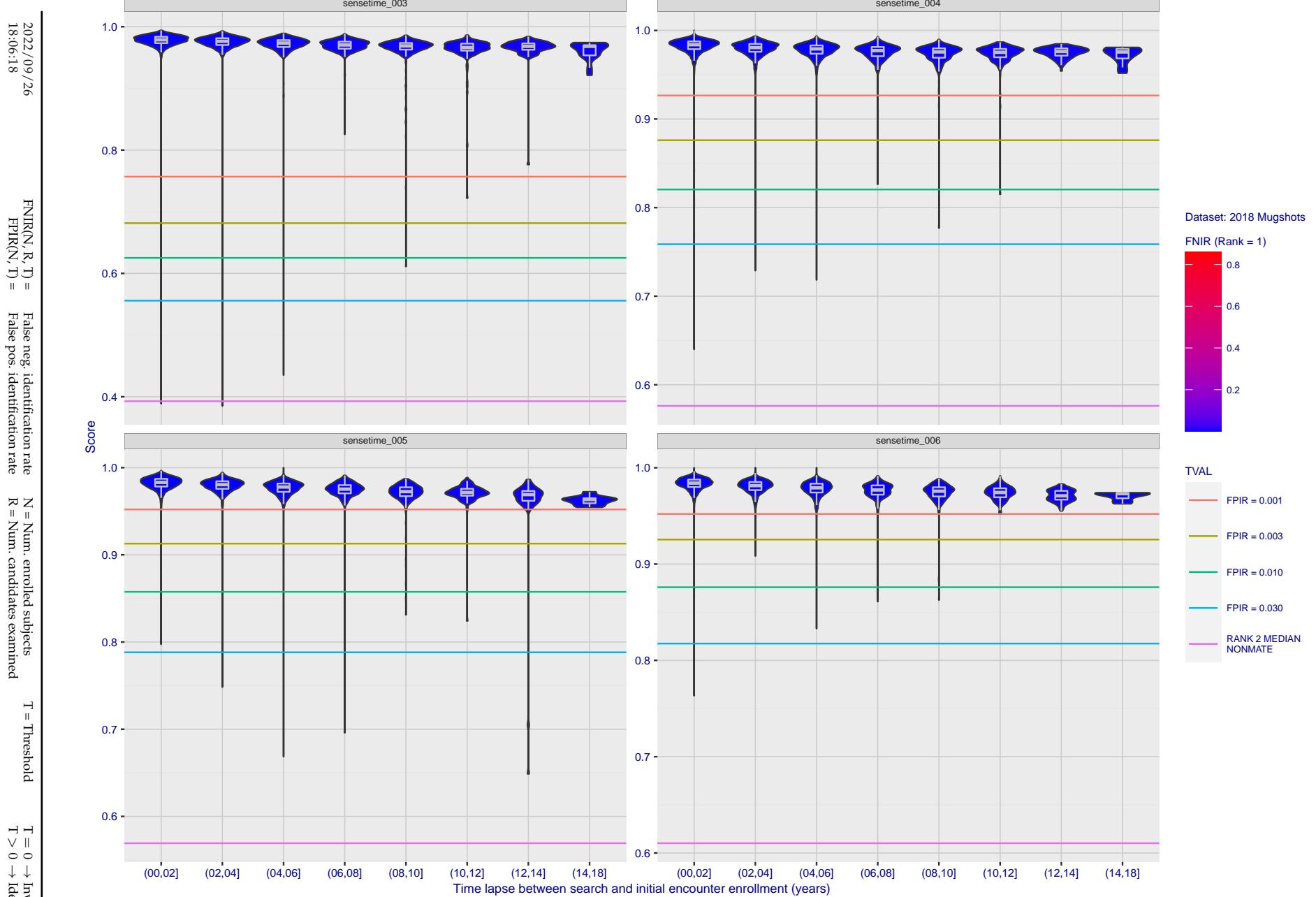


Figure 132: [FRVT-2018 Mugshot Ageing Dataset] Native mate scores vs. time-elapsed. The oldest image of each individual is enrolled. Thereafter, all more recent images are searched. Mated score distributions are computed over all searches noted in row 17 of Table 1 binned by number of years between search and initial enrollment.

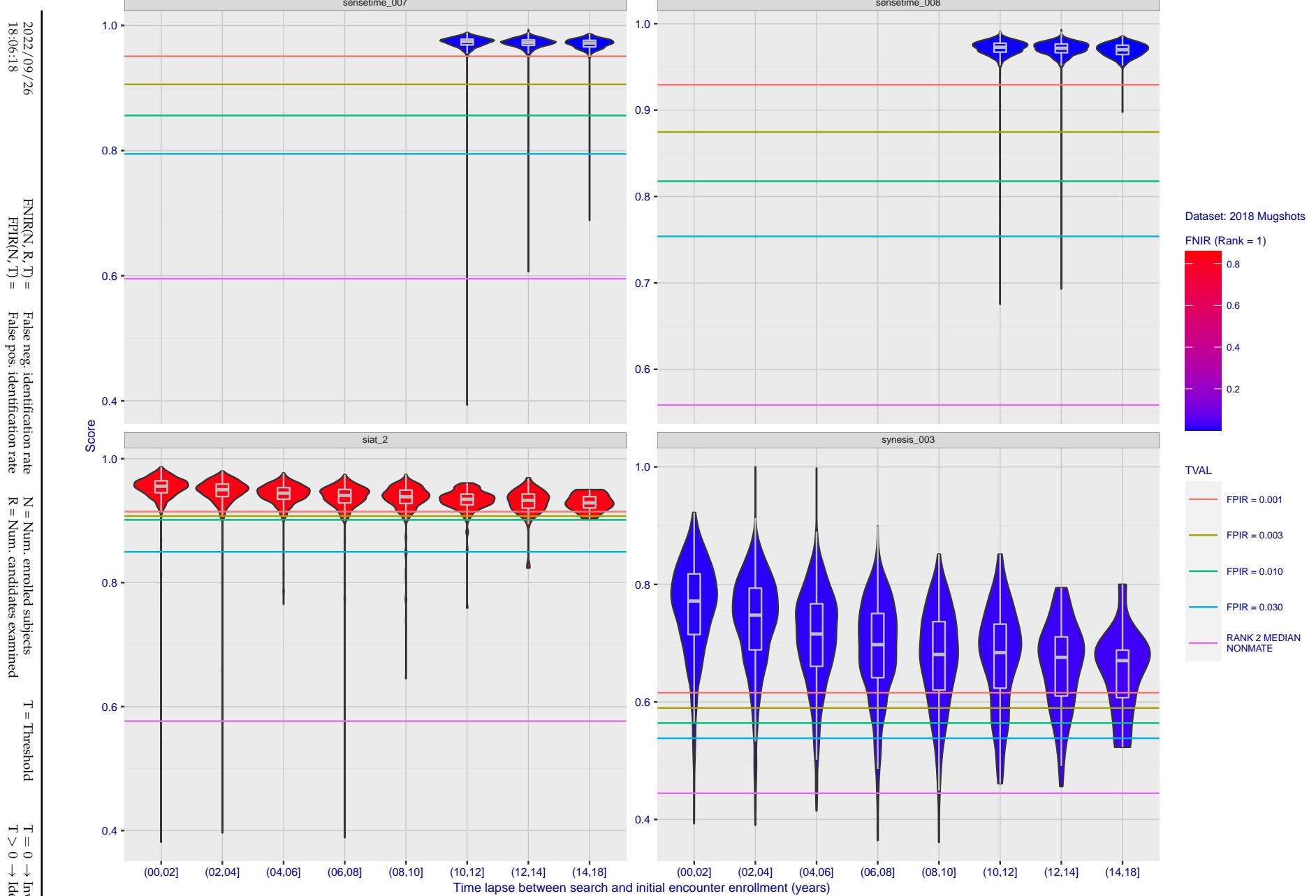


Figure 133: [FRVT-2018 Mugshot Ageing Dataset] Native mate scores vs. time-elapsed. The oldest image of each individual is enrolled. Thereafter, all more recent images are searched. Mated score distributions are computed over all searches noted in row 17 of Table 1 binned by number of years between search and initial enrollment.

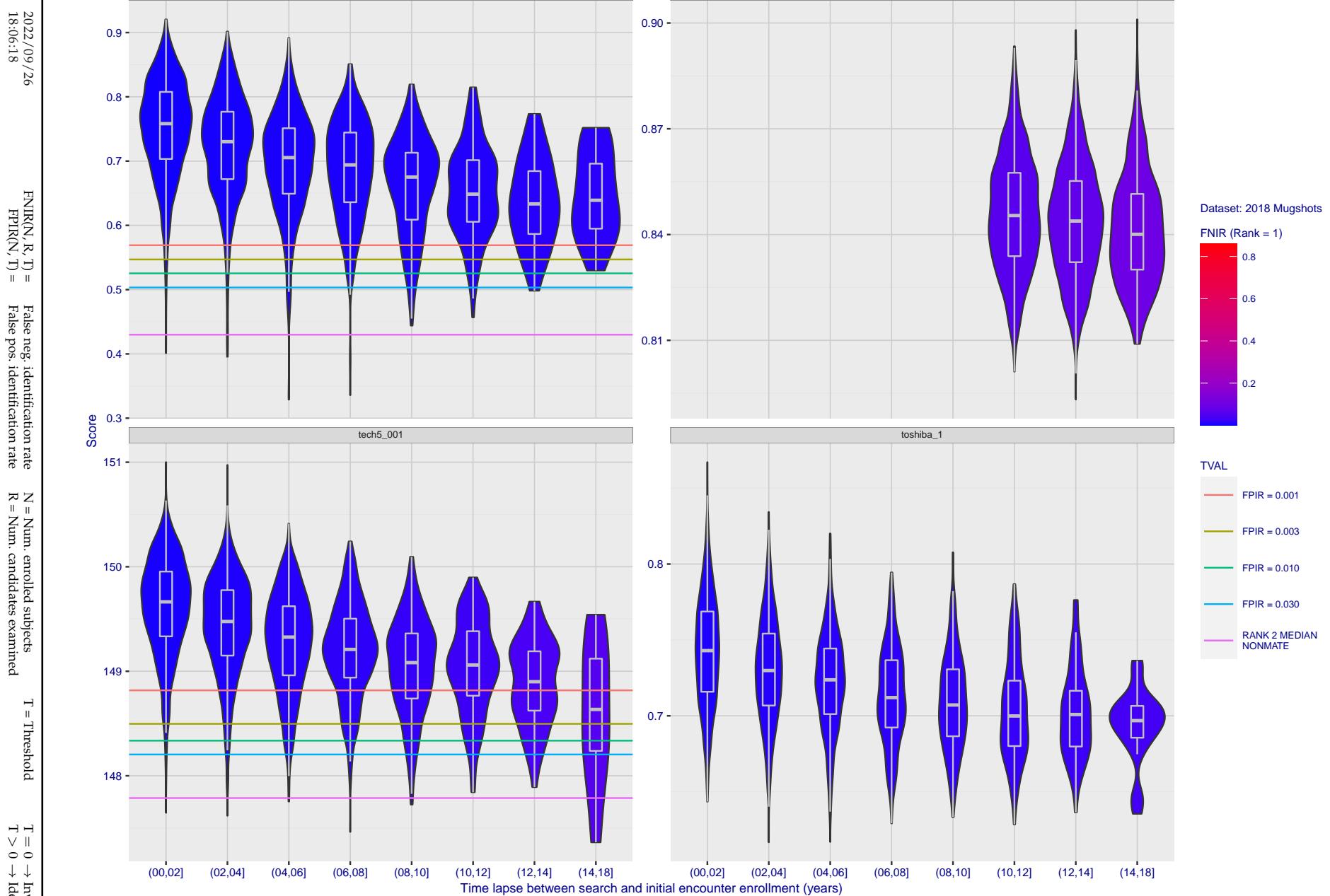


Figure 134: [FRVT-2018 Mugshot Ageing Dataset] Native mate scores vs. time-elapsed. The oldest image of each individual is enrolled. Thereafter, all more recent images are searched. Mated score distributions are computed over all searches noted in row 17 of Table 1 binned by number of years between search and initial enrollment.

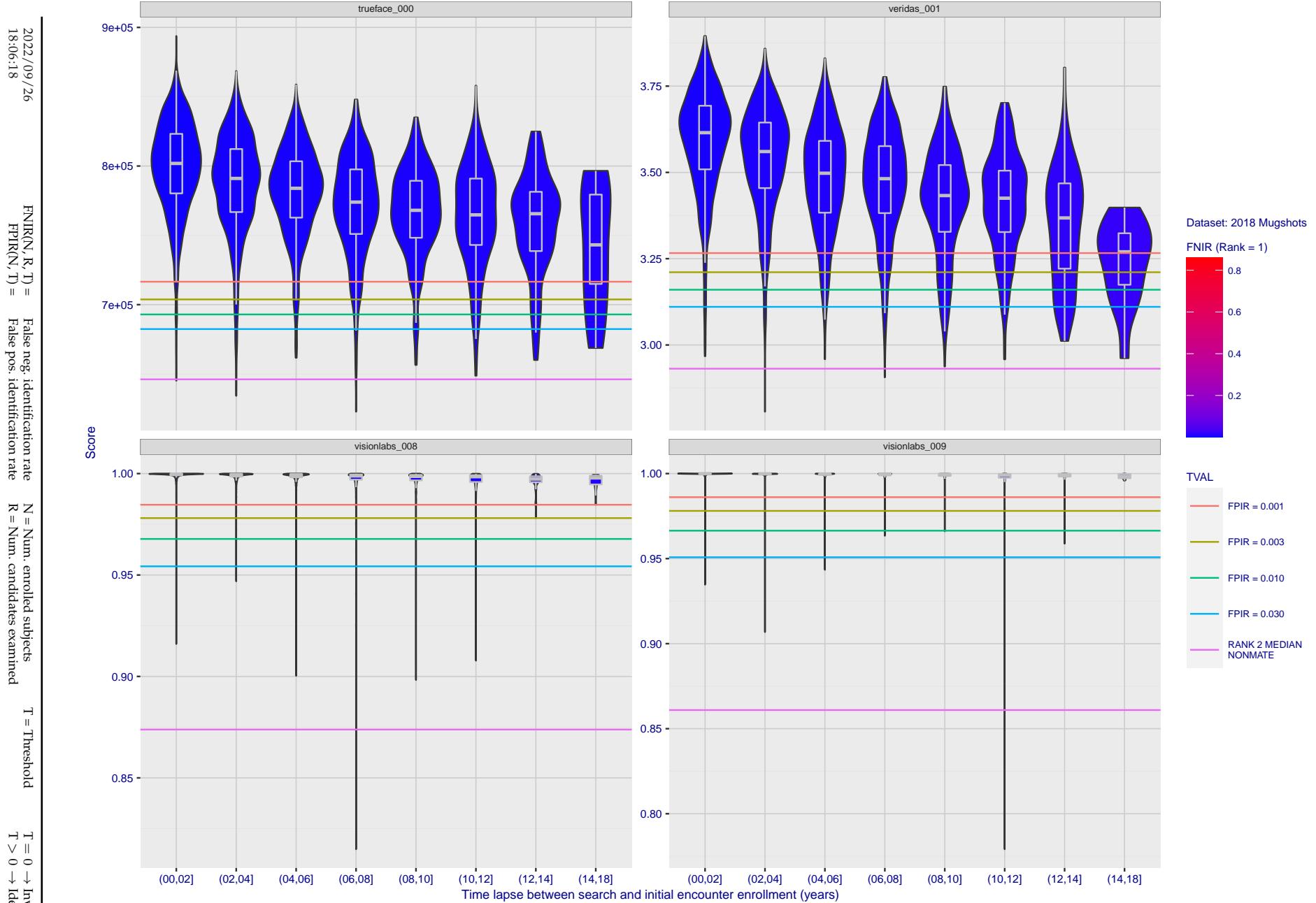


Figure 135: [FRVT-2018 Mugshot Ageing Dataset] Native mate scores vs. time-elapsed. The oldest image of each individual is enrolled. Thereafter, all more recent images are searched. Mated score distributions are computed over all searches noted in row 17 of Table 1 binned by number of years between search and initial enrollment.

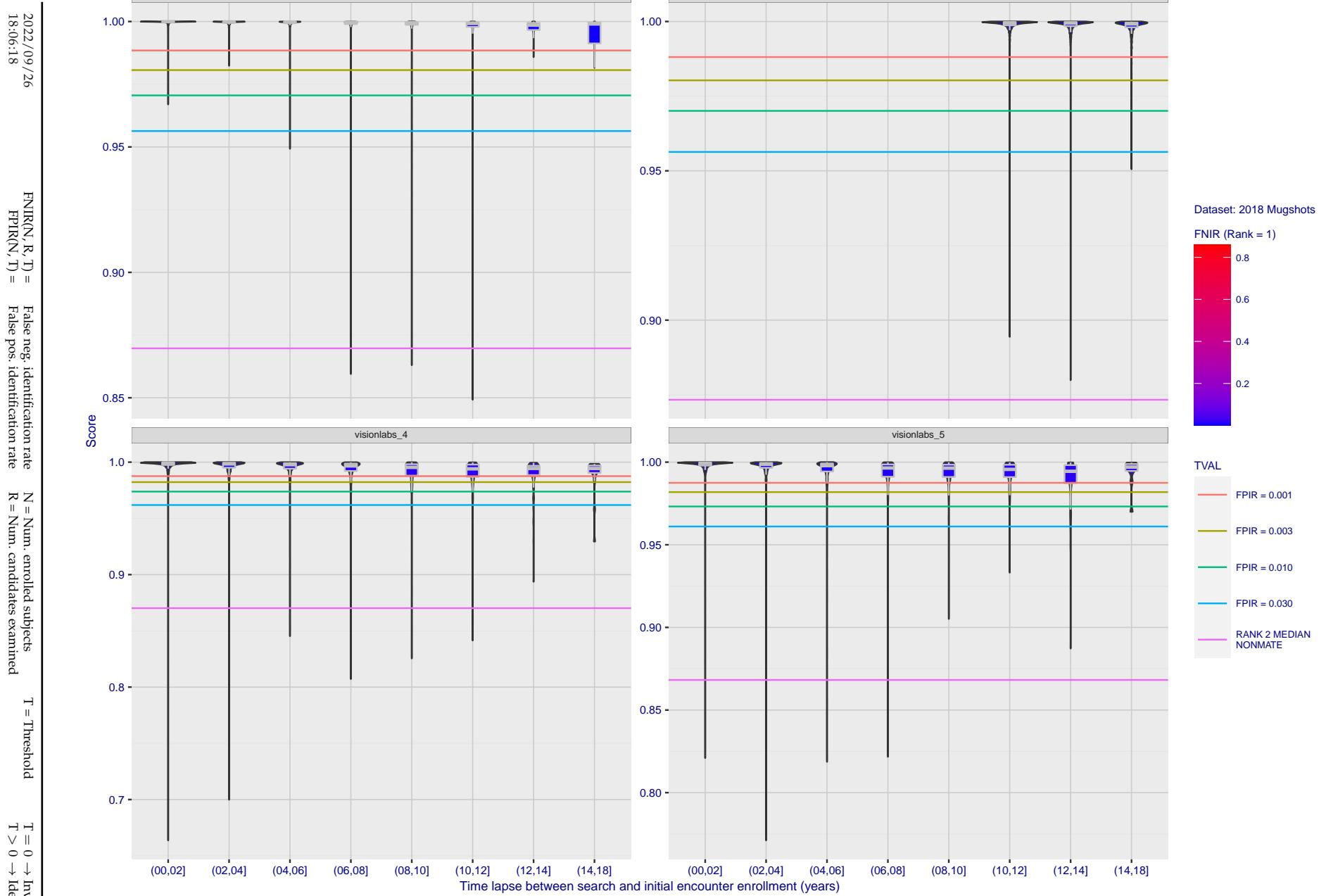


Figure 136: [FRVT-2018 Mugshot Ageing Dataset] Native mate scores vs. time-elapsed. The oldest image of each individual is enrolled. Thereafter, all more recent images are searched. Mated score distributions are computed over all searches noted in row 17 of Table 1 binned by number of years between search and initial enrollment.

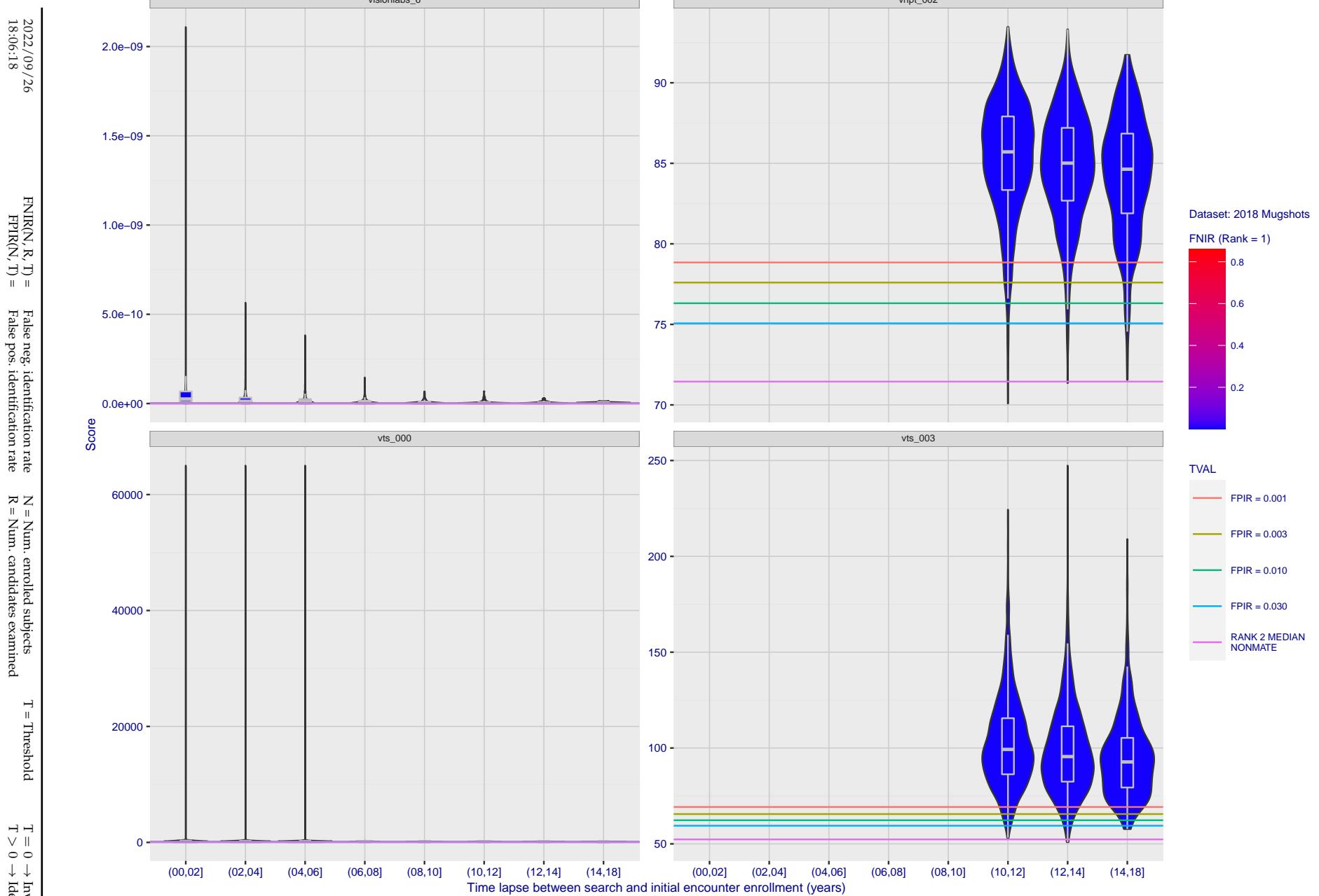


Figure 137: [FRVT-2018 Mugshot Ageing Dataset] Native mate scores vs. time-elapsed. The oldest image of each individual is enrolled. Thereafter, all more recent images are searched. Mated score distributions are computed over all searches noted in row 17 of Table 1 binned by number of years between search and initial enrollment.

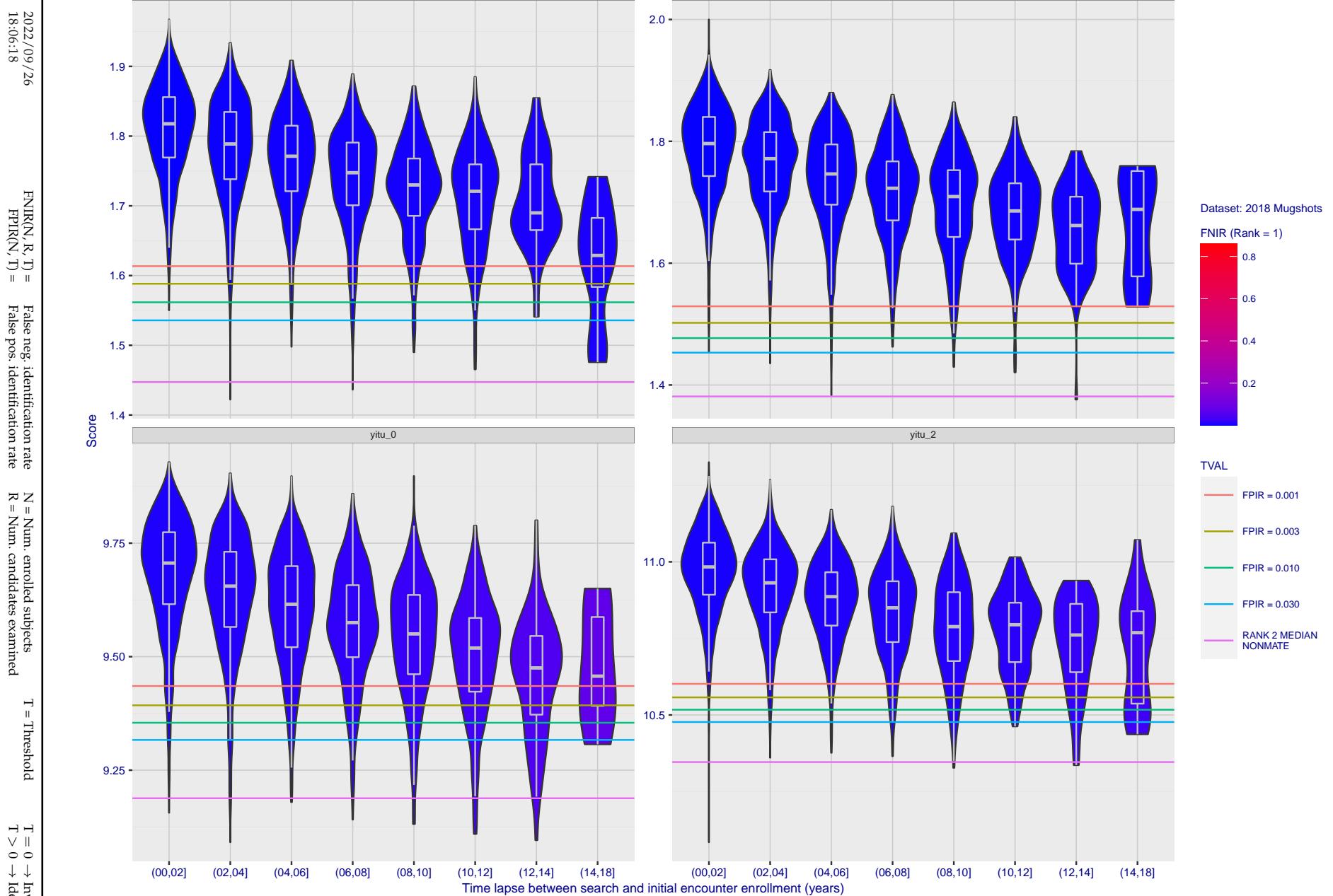


Figure 138: [FRVT-2018 Mugshot Ageing Dataset] Native mate scores vs. time-elapsed. The oldest image of each individual is enrolled. Thereafter, all more recent images are searched. Mated score distributions are computed over all searches noted in row 17 of Table 1 binned by number of years between search and initial enrollment.

2022/09/26
18:06:18FNIR(N, R, T) = False neg. identification rate
FPIR(N, T) = False pos. identification rateN = Num. enrolled subjects
R = Num. candidates examined

T = Threshold

T = 0 → Investigation
T > 0 → Identification

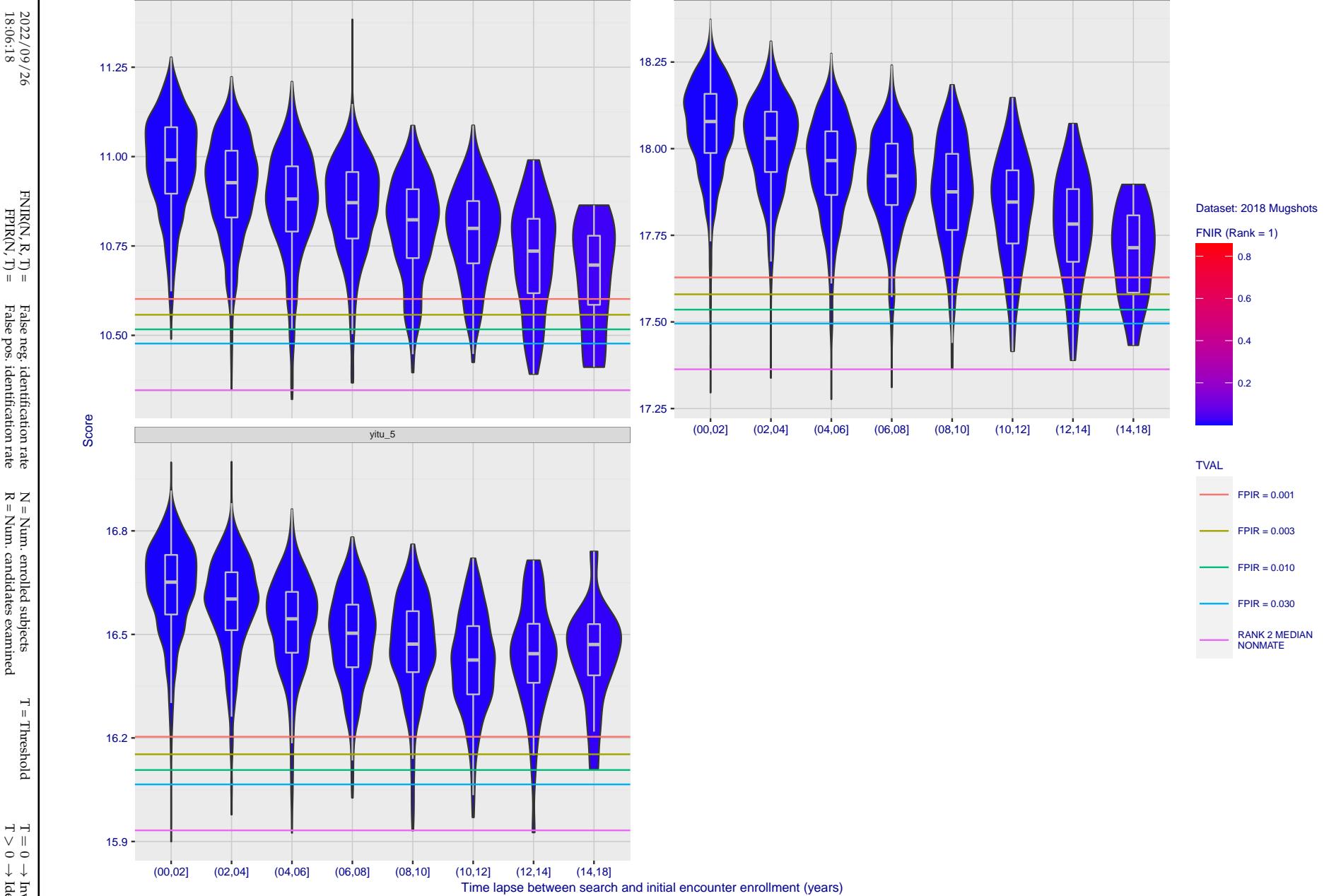


Figure 139: [FRVT-2018 Mugshot Ageing Dataset] Native mate scores vs. time-elapsed. The oldest image of each individual is enrolled. Thereafter, all more recent images are searched. Mated score distributions are computed over all searches noted in row 17 of Table 1 binned by number of years between search and initial enrollment.

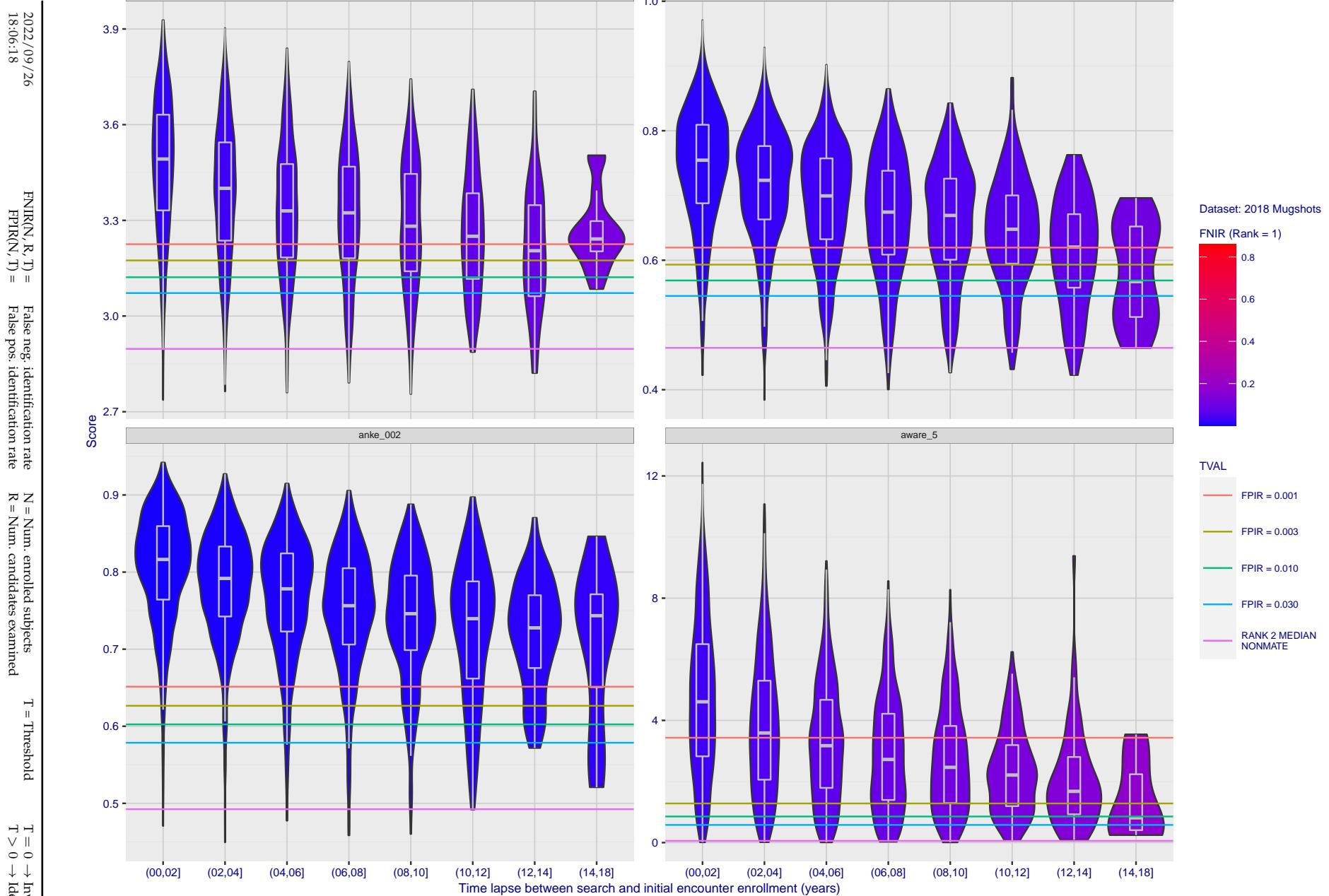


Figure 140: [FRVT-2018 Mugshot Ageing Dataset] Native mate scores vs. time-elapsed. The oldest image of each individual is enrolled. Thereafter, all more recent images are searched. Mated score distributions are computed over all searches noted in row 17 of Table 1 binned by number of years between search and initial enrollment.

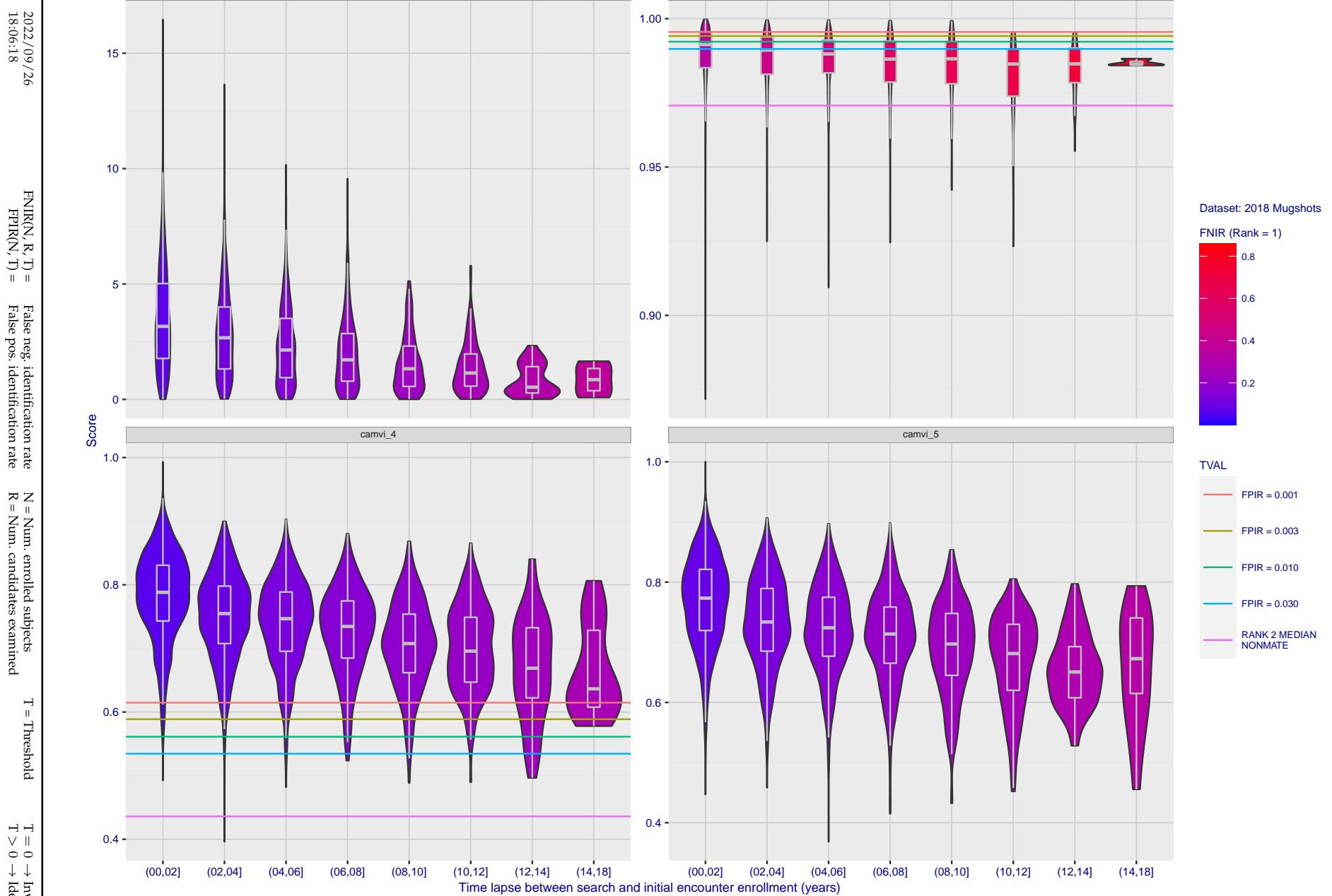


Figure 141: [FRVT-2018 Mugshot Ageing Dataset] Native mate scores vs. time-elapsed. The oldest image of each individual is enrolled. Thereafter, all more recent images are searched. Mated score distributions are computed over all searches noted in row 17 of Table 1 binned by number of years between search and initial enrollment.

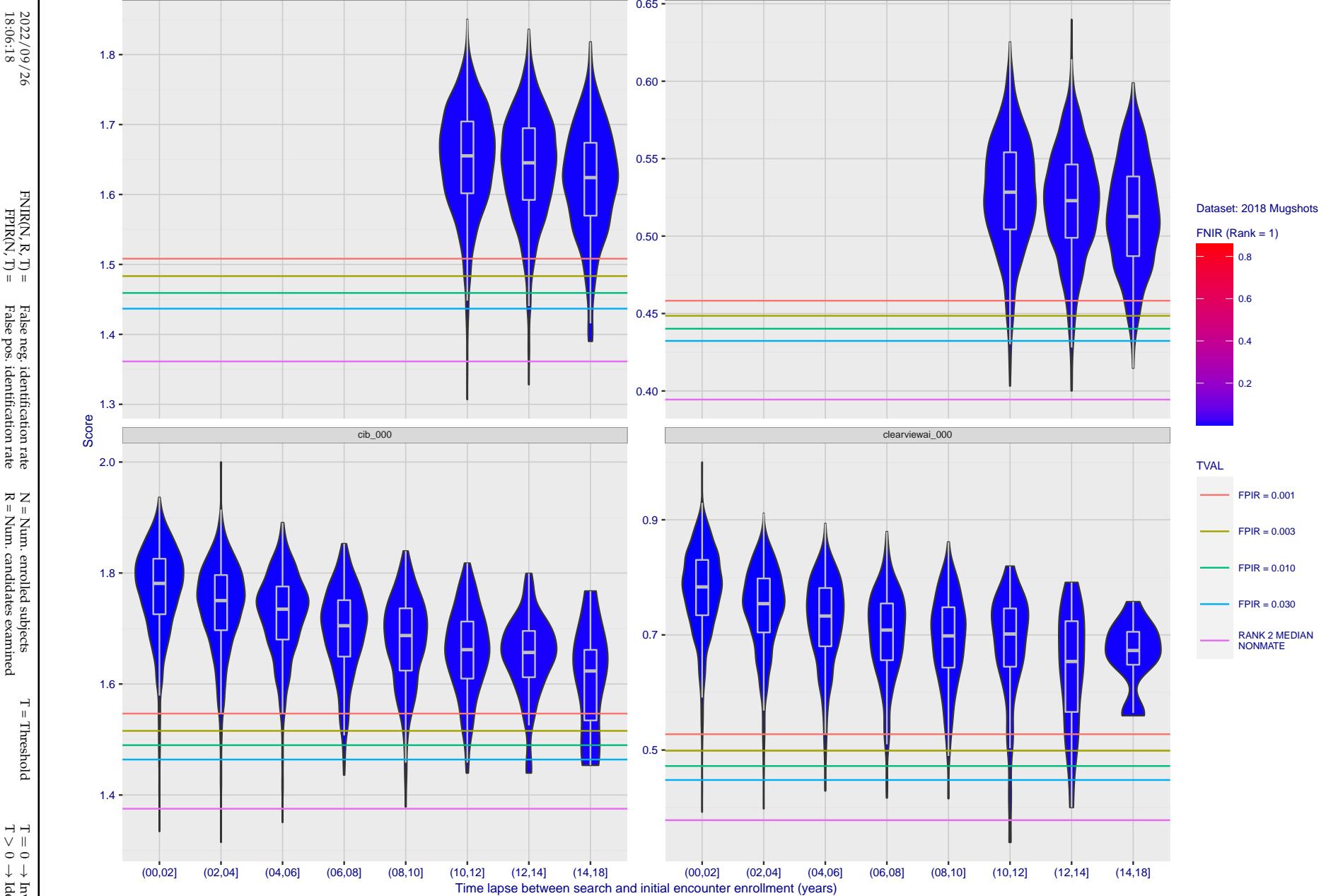


Figure 142: [FRVT-2018 Mugshot Ageing Dataset] Native mate scores vs. time-elapsed. The oldest image of each individual is enrolled. Thereafter, all more recent images are searched. Mated score distributions are computed over all searches noted in row 17 of Table 1 binned by number of years between search and initial enrollment.

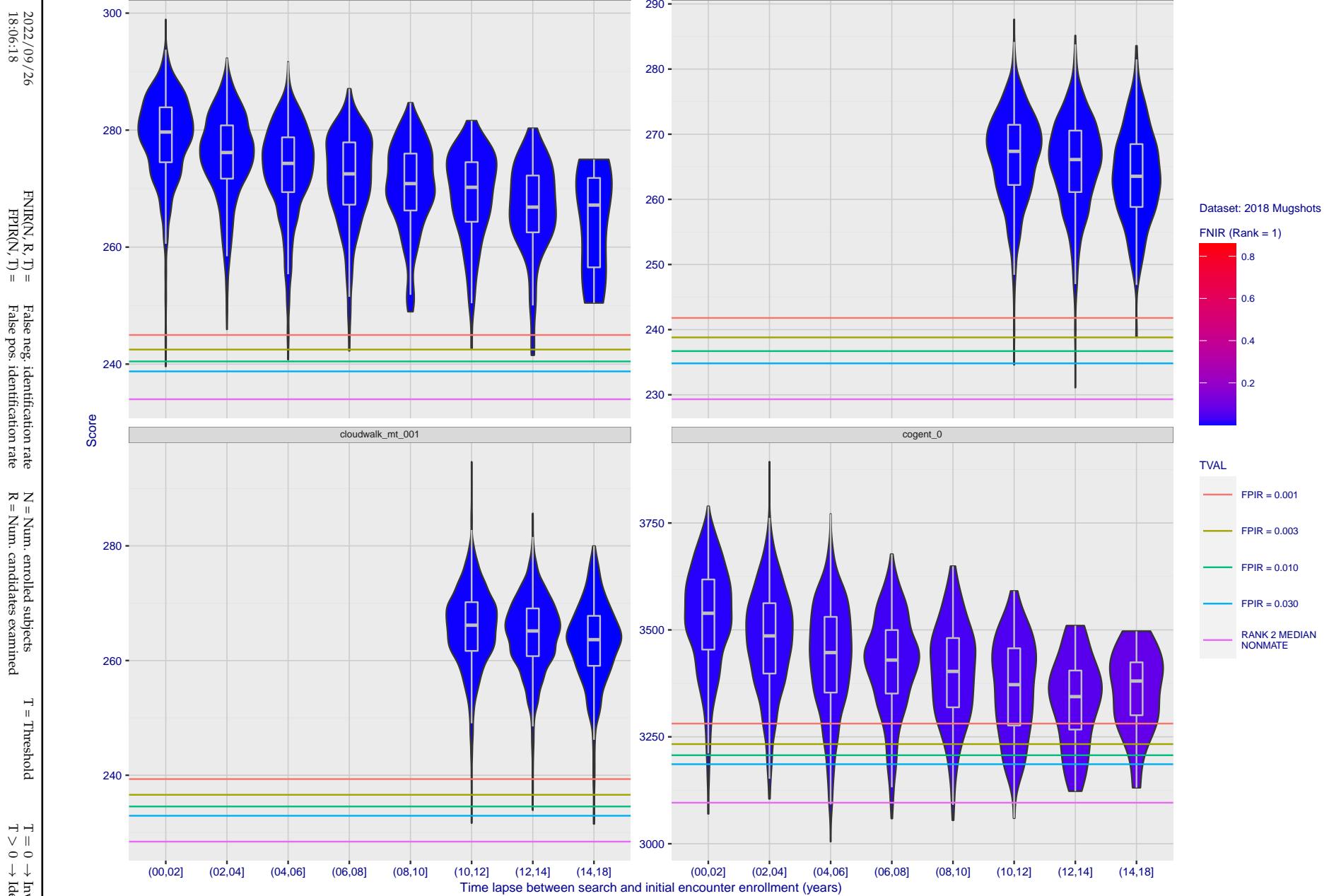


Figure 143: [FRVT-2018 Mugshot Ageing Dataset] Native mate scores vs. time-elapsed. The oldest image of each individual is enrolled. Thereafter, all more recent images are searched. Mated score distributions are computed over all searches noted in row 17 of Table 1 binned by number of years between search and initial enrollment.

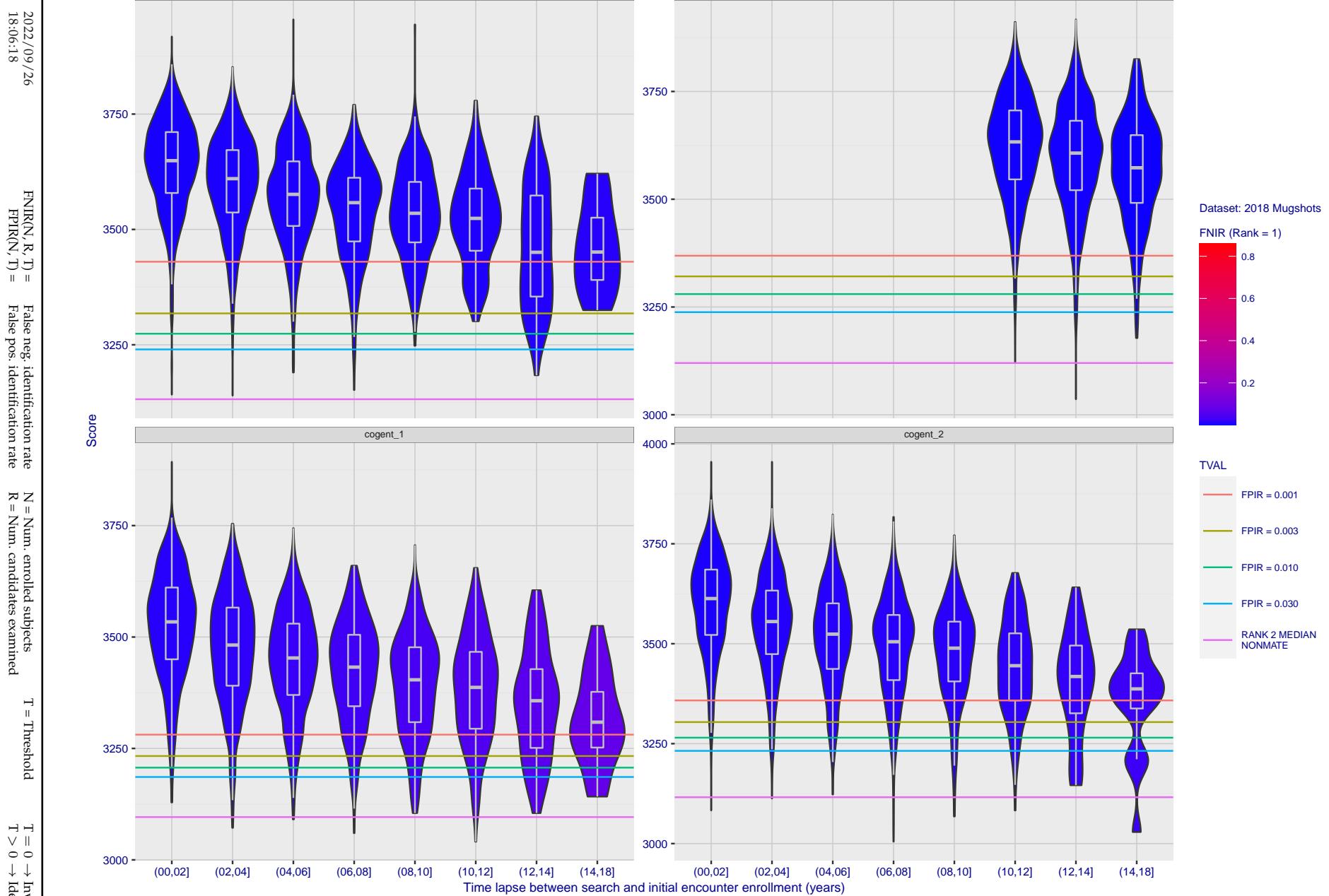


Figure 144: [FRVT-2018 Mugshot Ageing Dataset] Native mate scores vs. time-elapsed. The oldest image of each individual is enrolled. Thereafter, all more recent images are searched. Mated score distributions are computed over all searches noted in row 17 of Table 1 binned by number of years between search and initial enrollment.

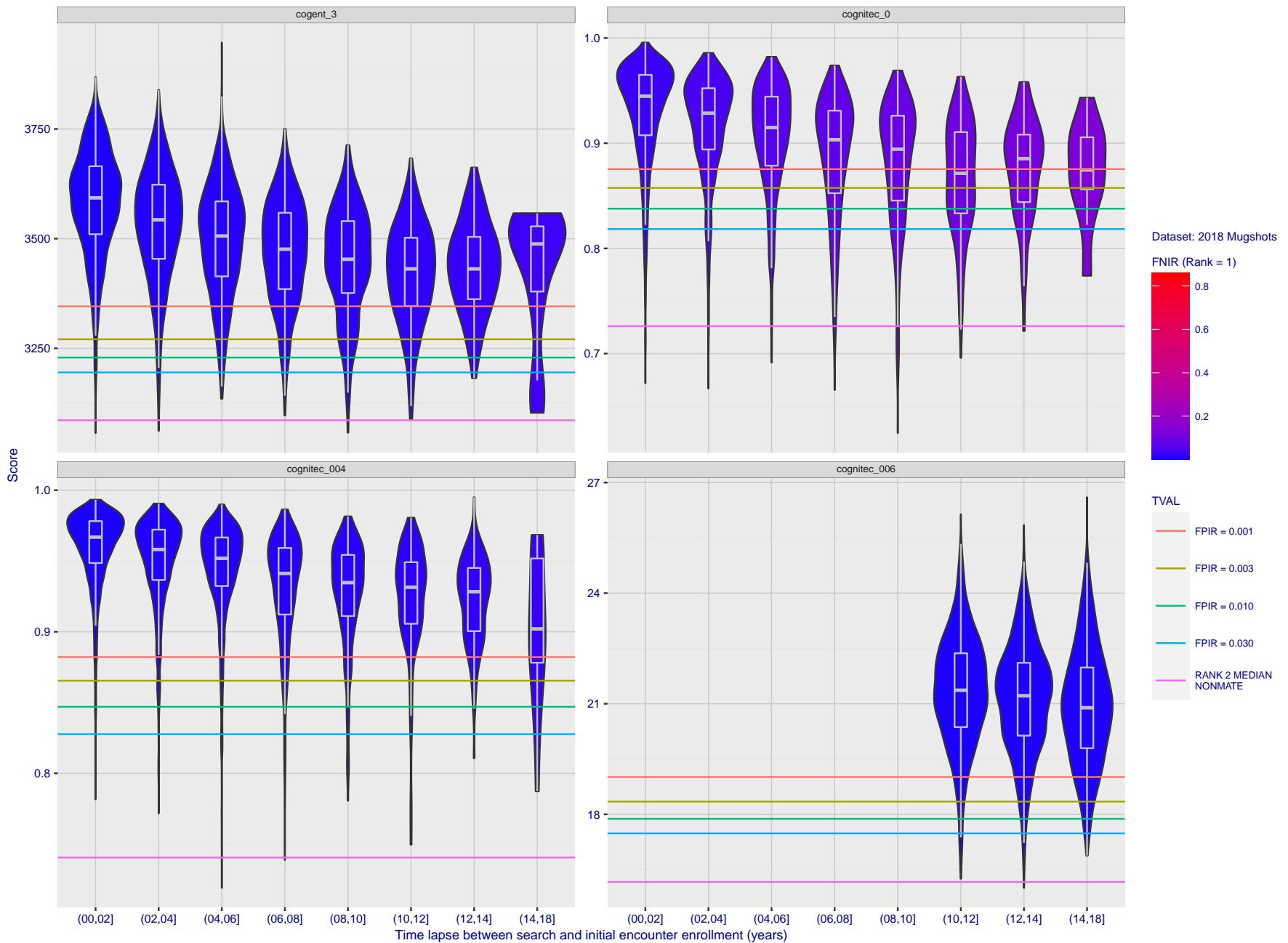


Figure 145: [FRVT-2018 Mugshot Ageing Dataset] Native mate scores vs. time-elapsed. The oldest image of each individual is enrolled. Thereafter, all more recent images are searched. Mated score distributions are computed over all searches noted in row 17 of Table 1 binned by number of years between search and initial enrollment.

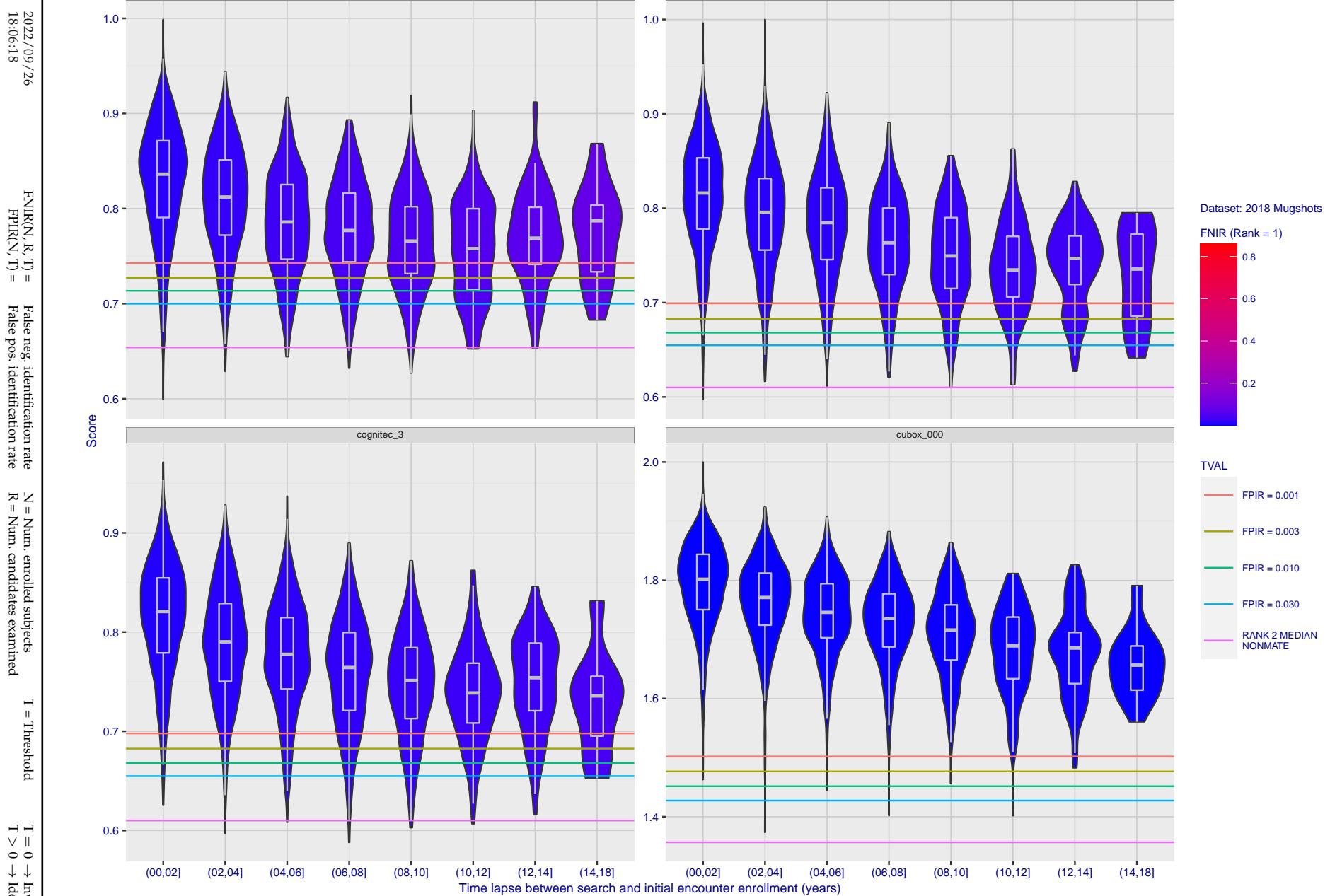


Figure 146: [FRVT-2018 Mugshot Ageing Dataset] Native mate scores vs. time-elapsed. The oldest image of each individual is enrolled. Thereafter, all more recent images are searched. Mated score distributions are computed over all searches noted in row 17 of Table 1 binned by number of years between search and initial enrollment.

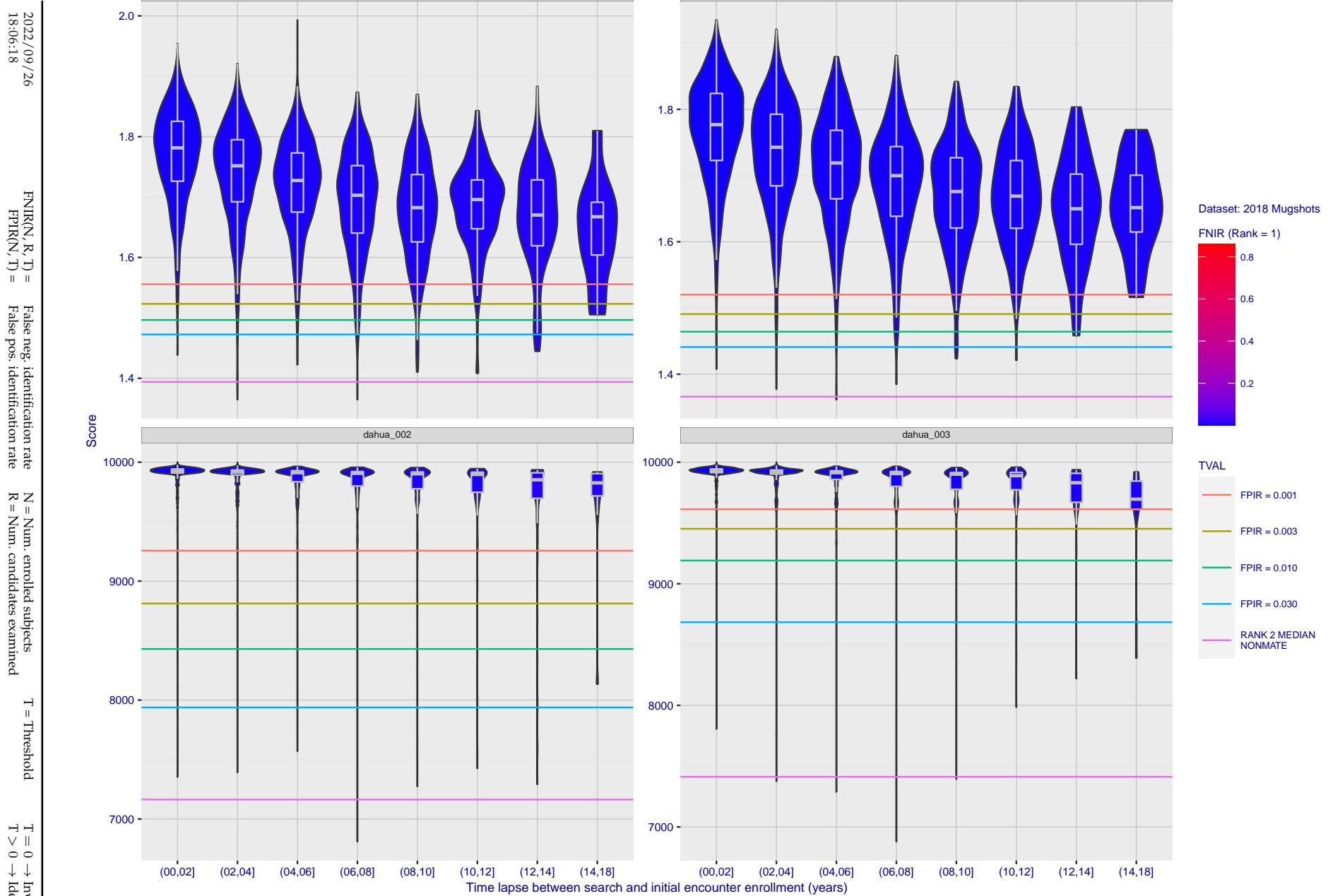


Figure 147: [FRVT-2018 Mugshot Ageing Dataset] Native mate scores vs. time-elapsed. The oldest image of each individual is enrolled. Thereafter, all more recent images are searched. Mated score distributions are computed over all searches noted in row 17 of Table 1 binned by number of years between search and initial enrollment.

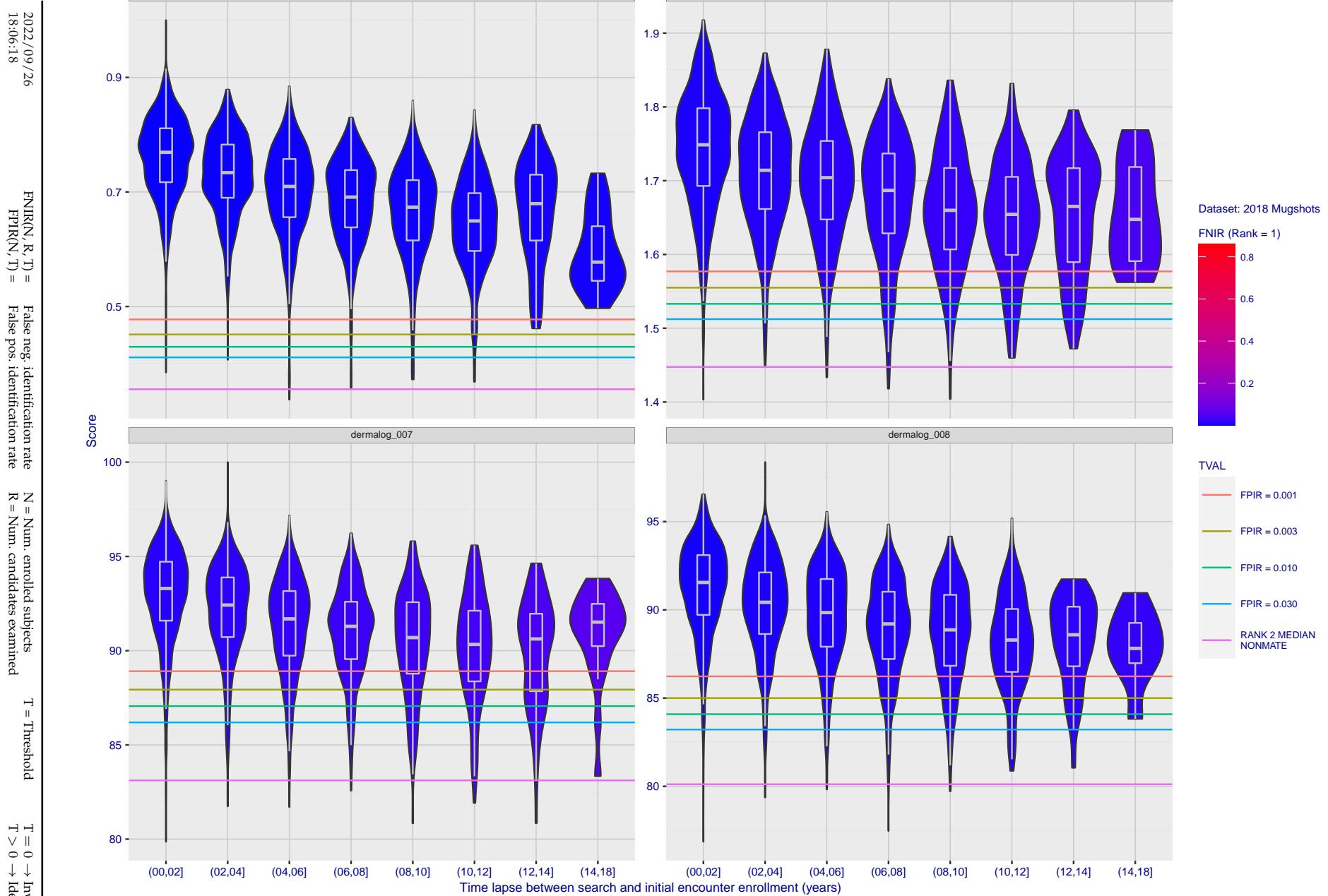


Figure 148: [FRVT-2018 Mugshot Ageing Dataset] Native mate scores vs. time-elapsed. The oldest image of each individual is enrolled. Thereafter, all more recent images are searched. Mated score distributions are computed over all searches noted in row 17 of Table 1 binned by number of years between search and initial enrollment.

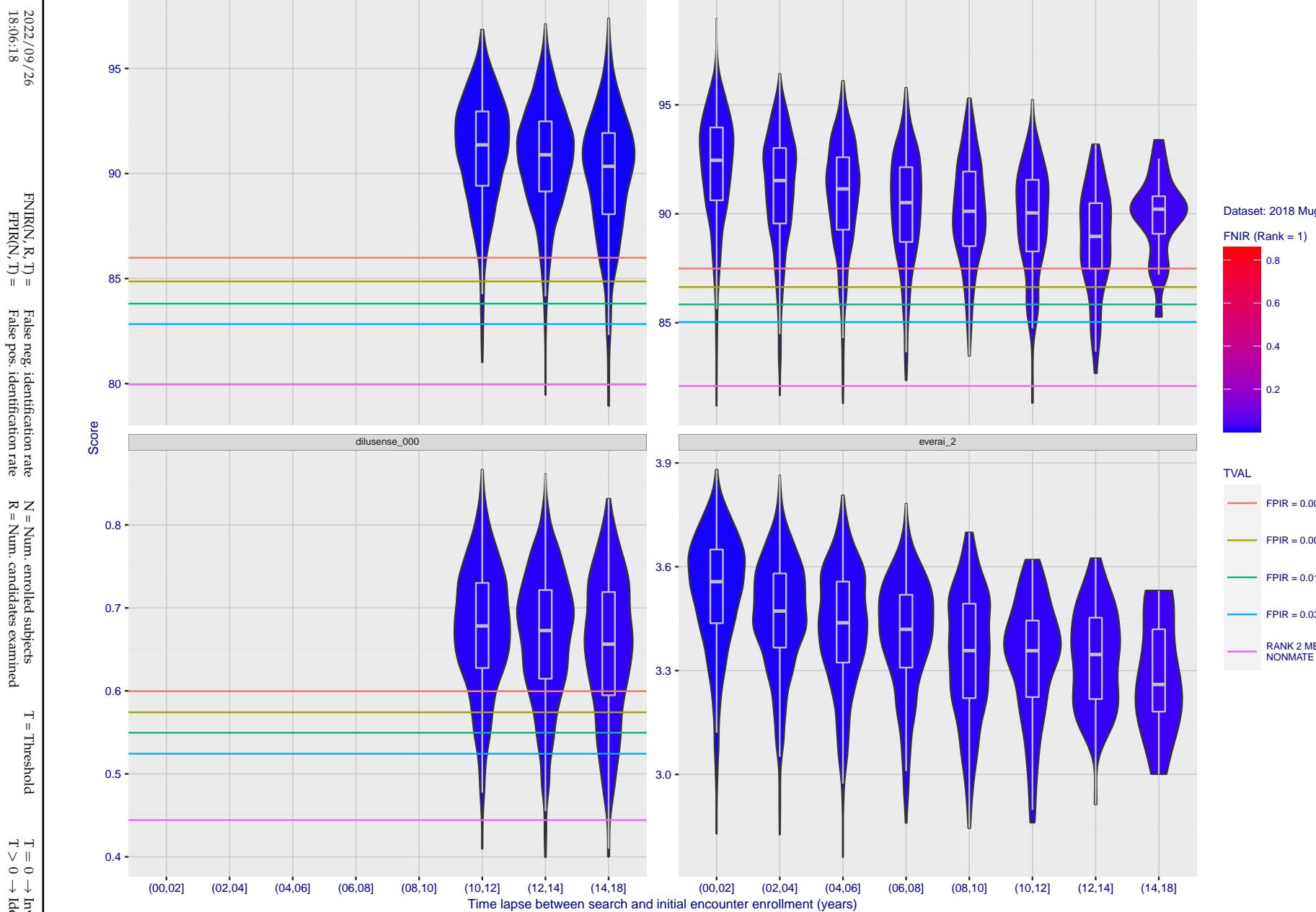


Figure 149: [FRVT-2018 Mugshot Ageing Dataset] Native mate scores vs. time-elapsed. The oldest image of each individual is enrolled. Thereafter, all more recent images are searched. Mated score distributions are computed over all searches noted in row 17 of Table 1 binned by number of years between search and initial enrollment.

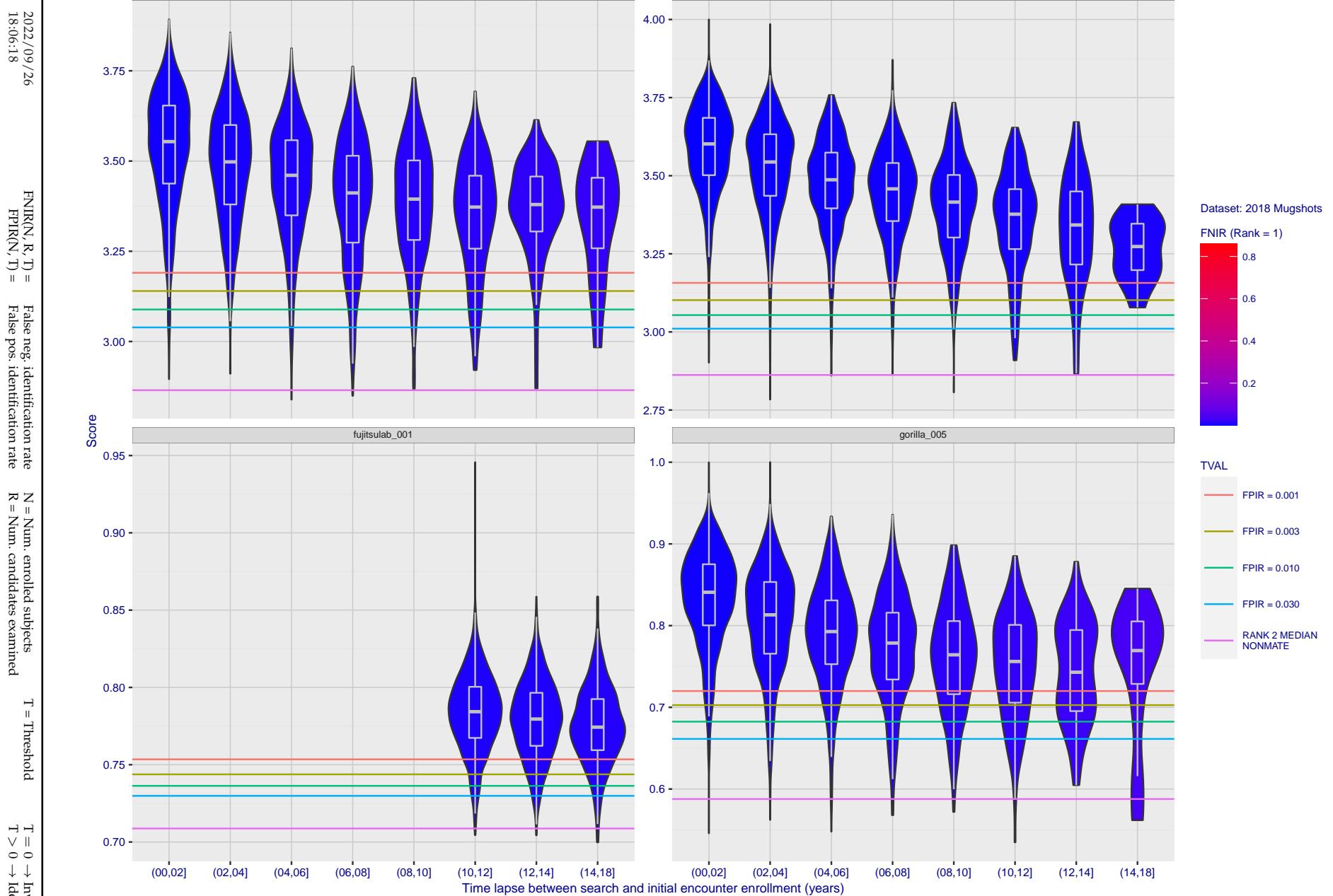


Figure 150: [FRVT-2018 Mugshot Ageing Dataset] Native mate scores vs. time-elapsed. The oldest image of each individual is enrolled. Thereafter, all more recent images are searched. Mated score distributions are computed over all searches noted in row 17 of Table 1 binned by number of years between search and initial enrollment.

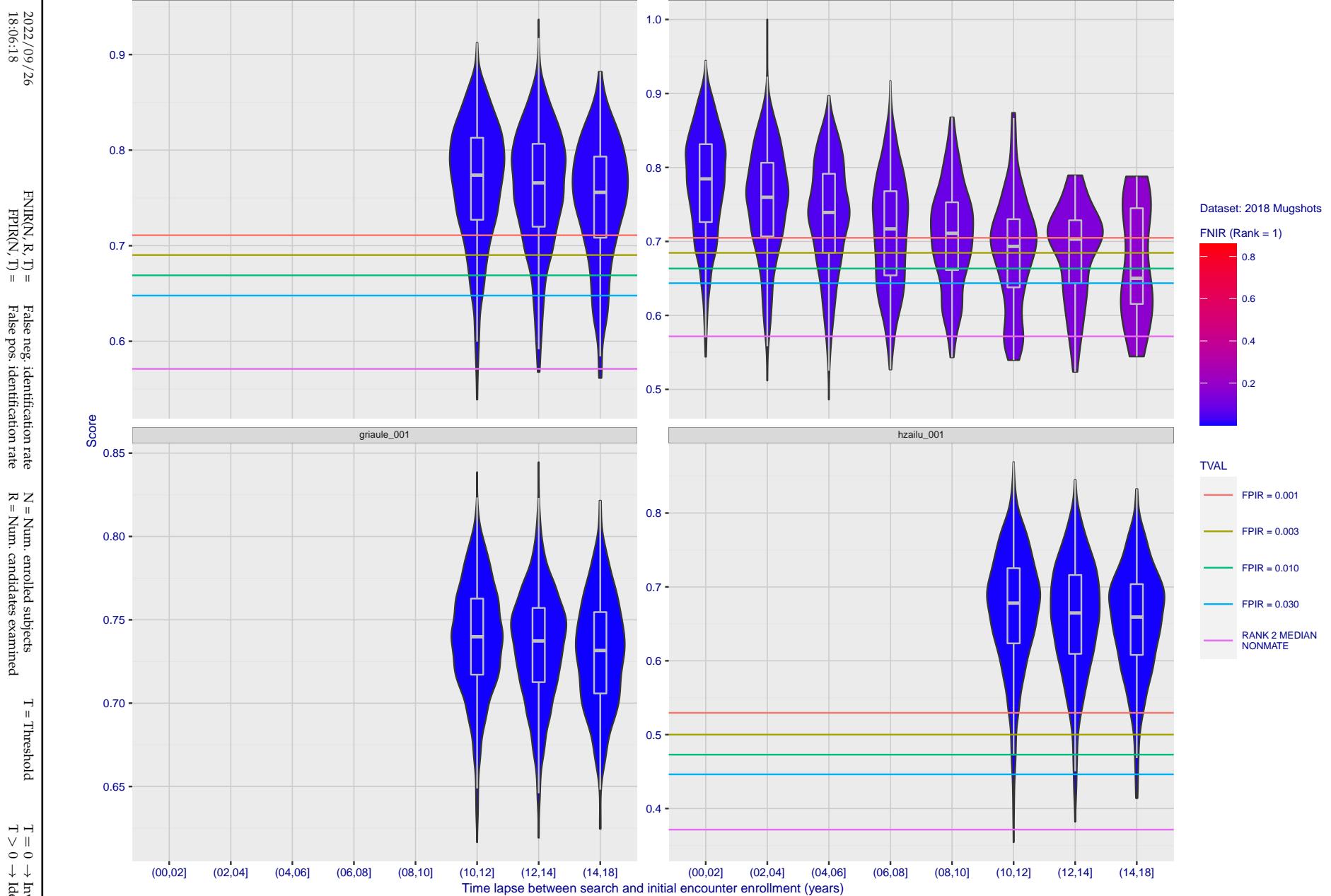


Figure 151: [FRVT-2018 Mugshot Ageing Dataset] Native mate scores vs. time-elapsed. The oldest image of each individual is enrolled. Thereafter, all more recent images are searched. Mated score distributions are computed over all searches noted in row 17 of Table 1 binned by number of years between search and initial enrollment.

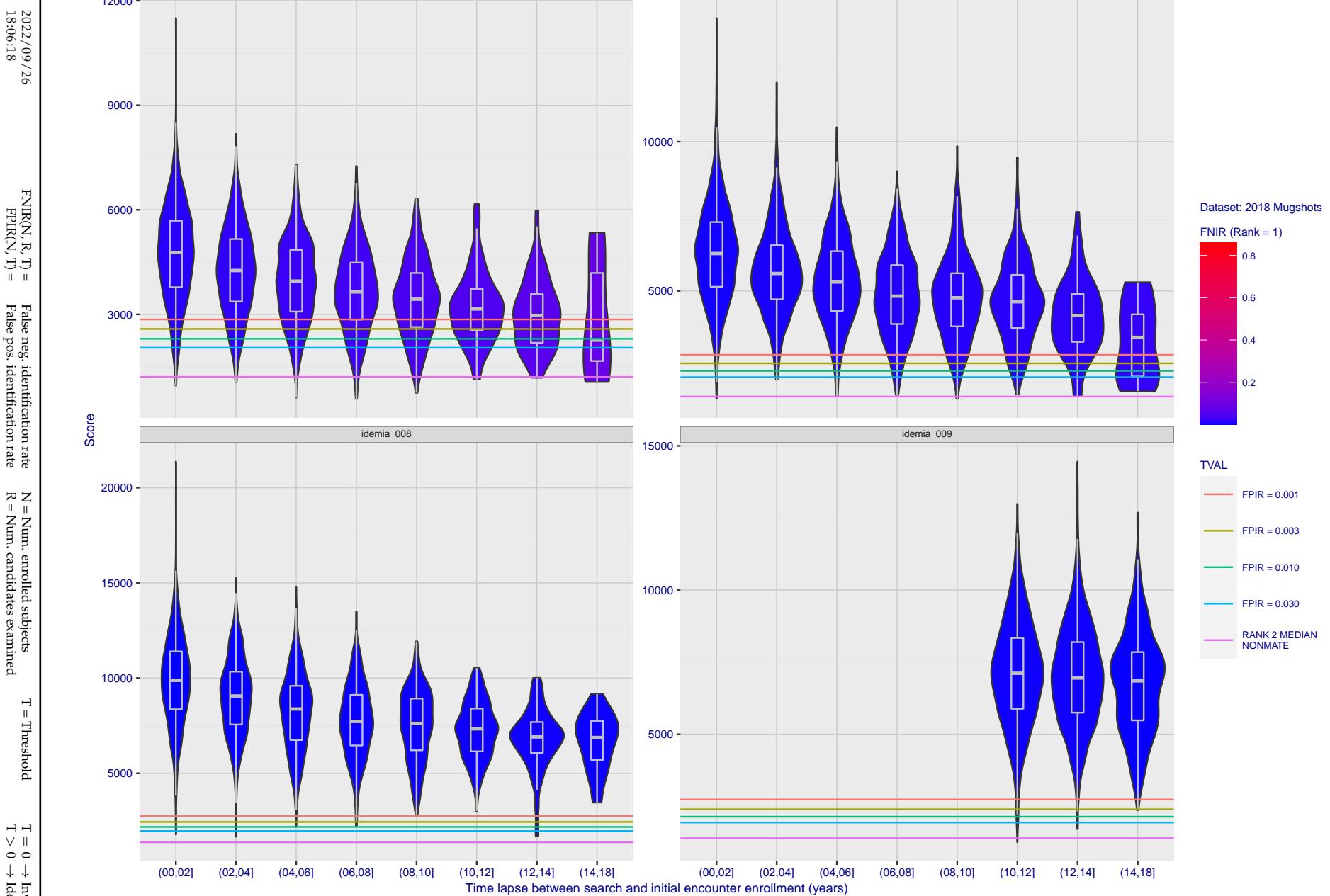


Figure 152: [FRVT-2018 Mugshot Ageing Dataset] Native mate scores vs. time-elapsed. The oldest image of each individual is enrolled. Thereafter, all more recent images are searched. Mated score distributions are computed over all searches noted in row 17 of Table 1 binned by number of years between search and initial enrollment.

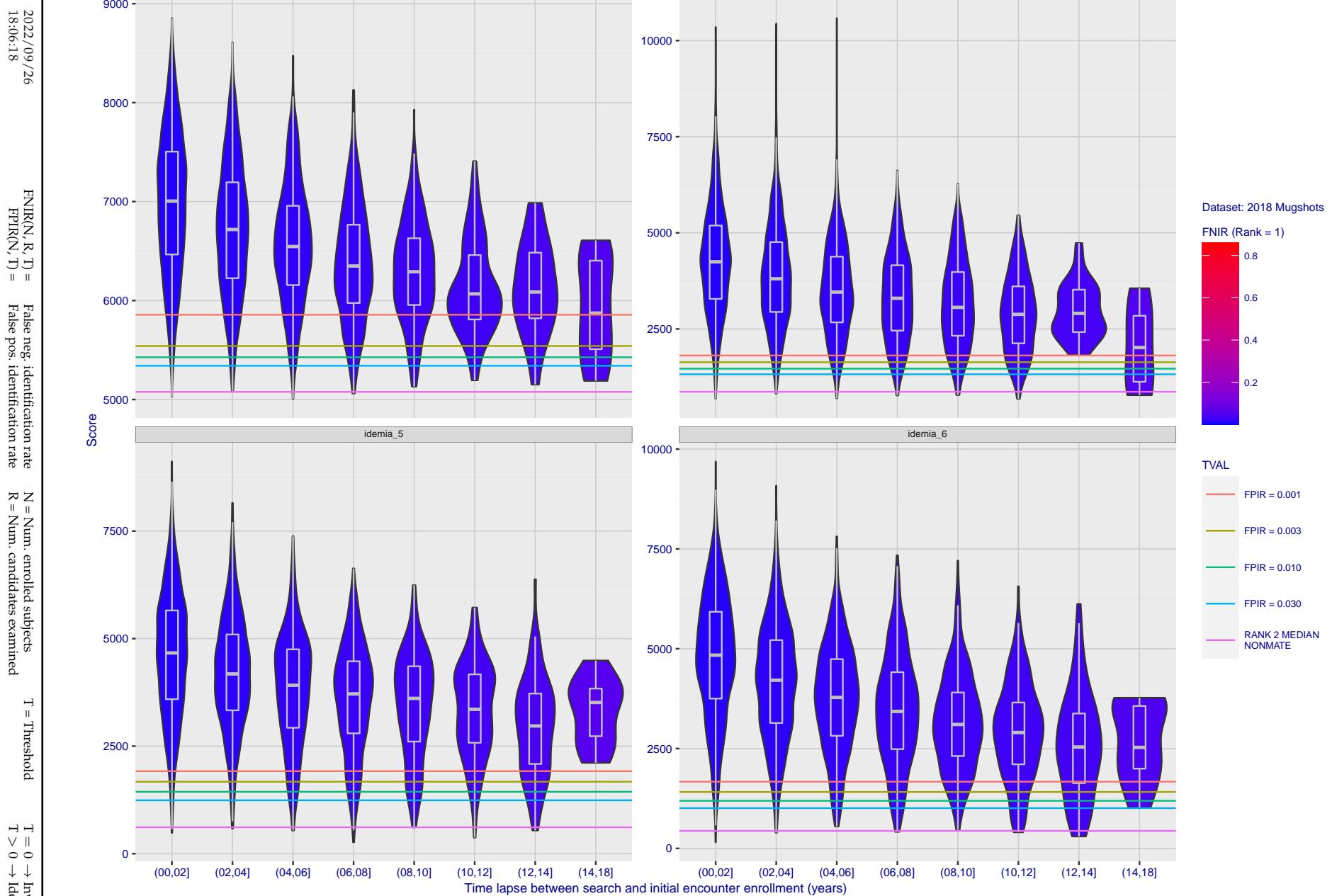


Figure 153: [FRVT-2018 Mugshot Ageing Dataset] Native mate scores vs. time-elapsed. The oldest image of each individual is enrolled. Thereafter, all more recent images are searched. Mated score distributions are computed over all searches noted in row 17 of Table 1 binned by number of years between search and initial enrollment.

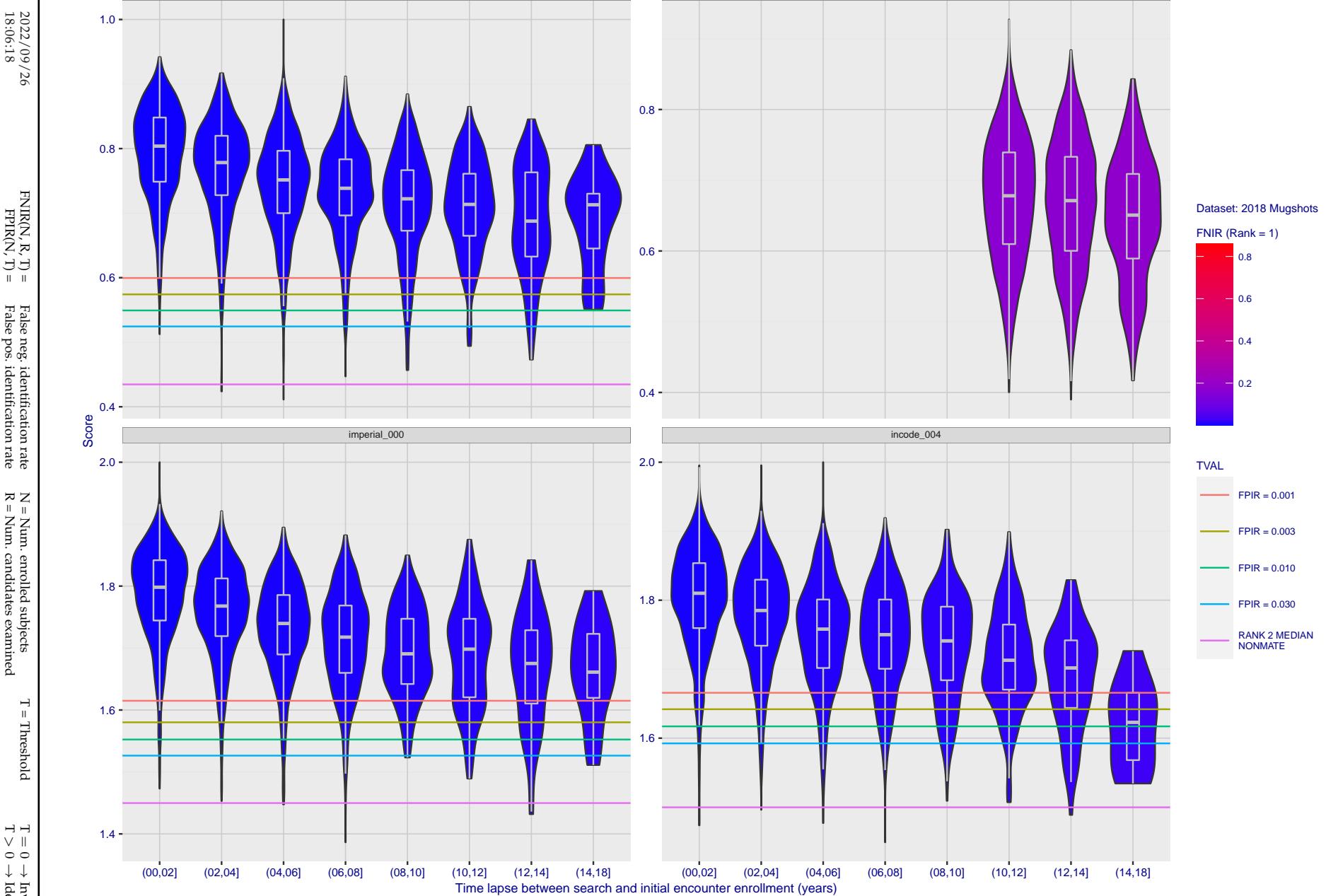


Figure 154: [FRVT-2018 Mugshot Ageing Dataset] Native mate scores vs. time-elapsed. The oldest image of each individual is enrolled. Thereafter, all more recent images are searched. Mated score distributions are computed over all searches noted in row 17 of Table 1 binned by number of years between search and initial enrollment.

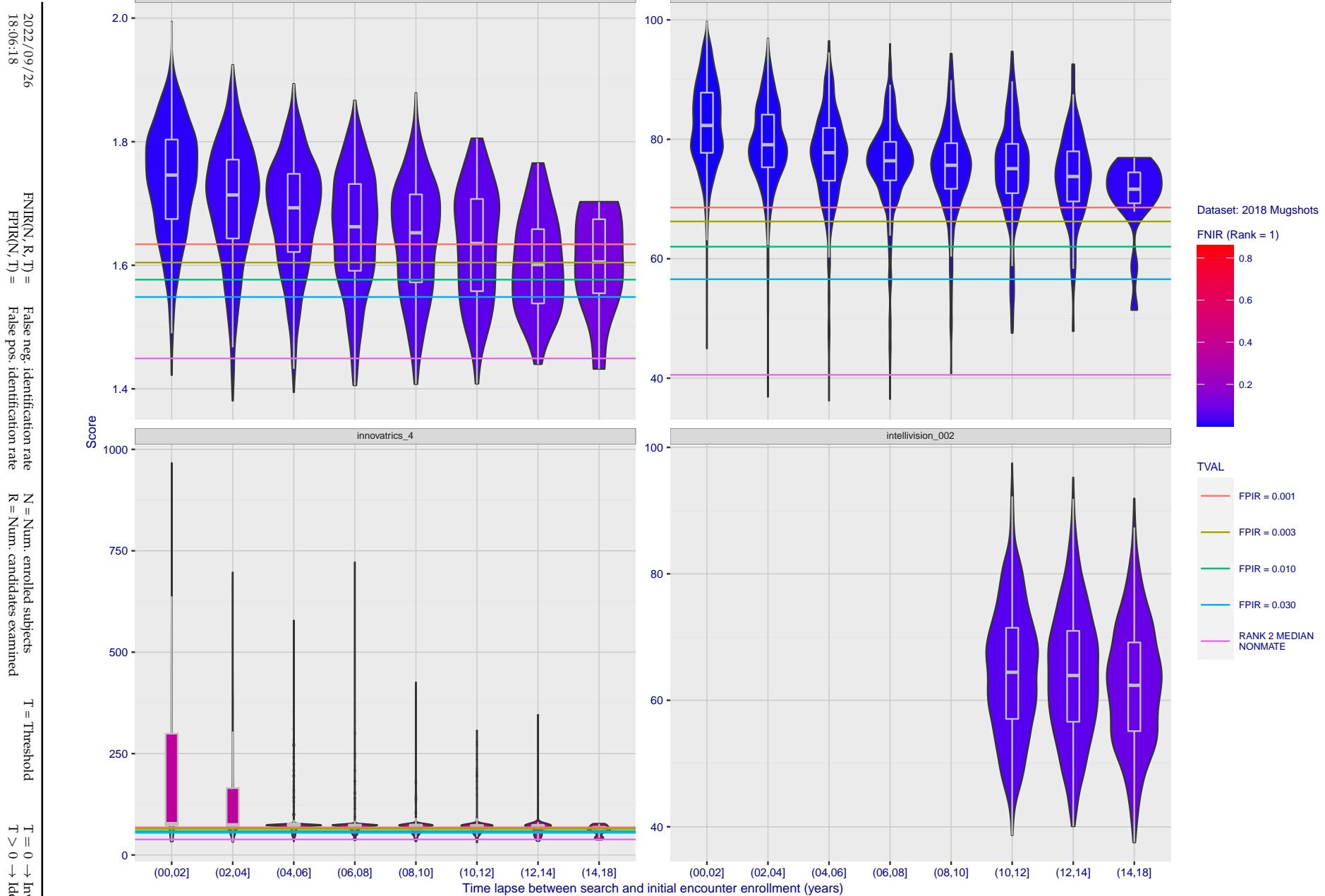


Figure 155: [FRVT-2018 Mugshot Ageing Dataset] Native mate scores vs. time-elapsed. The oldest image of each individual is enrolled. Thereafter, all more recent images are searched. Mated score distributions are computed over all searches noted in row 17 of Table 1 binned by number of years between search and initial enrollment.

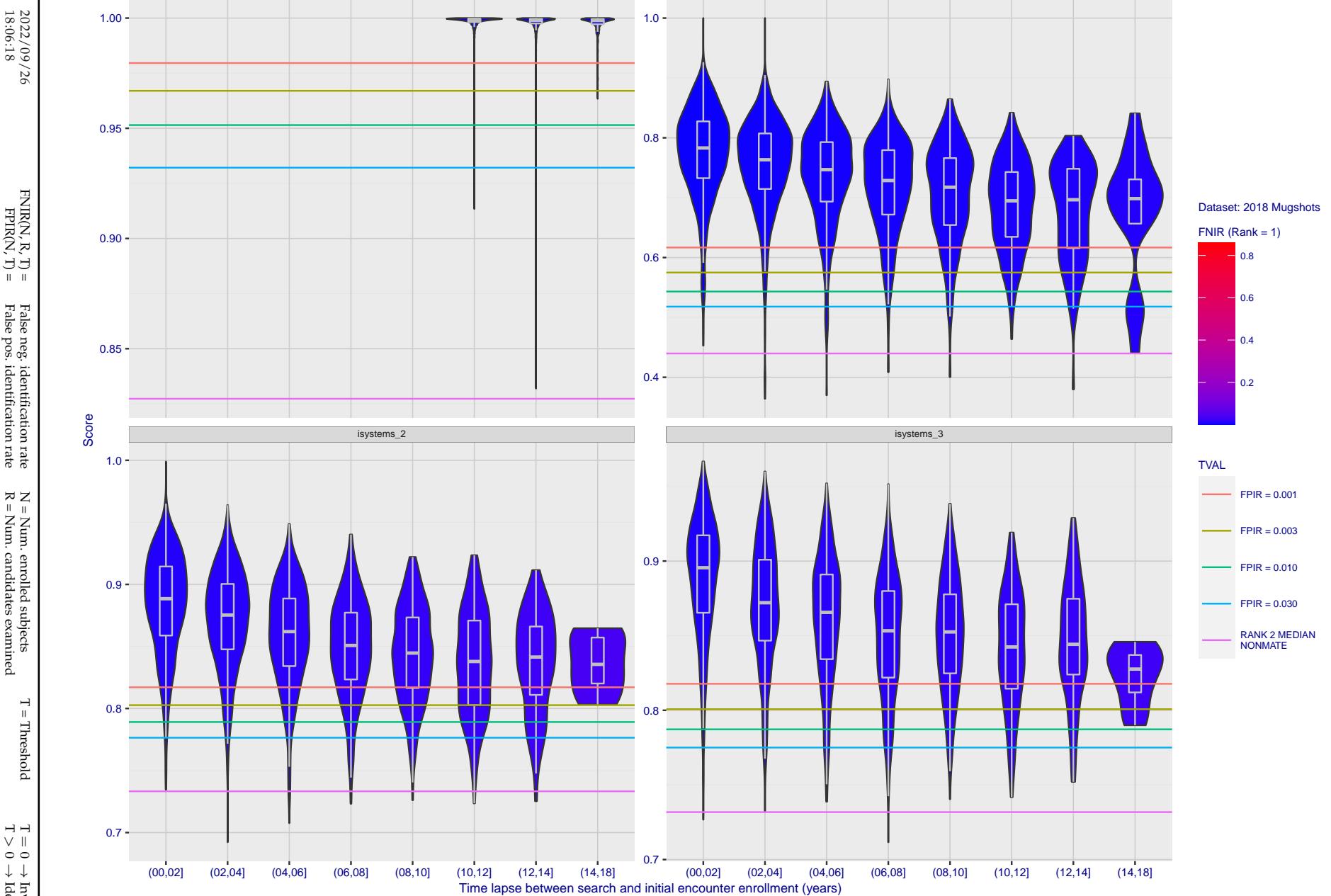


Figure 156: [FRVT-2018 Mugshot Ageing Dataset] Native mate scores vs. time-elapsed. The oldest image of each individual is enrolled. Thereafter, all more recent images are searched. Mated score distributions are computed over all searches noted in row 17 of Table 1 binned by number of years between search and initial enrollment.

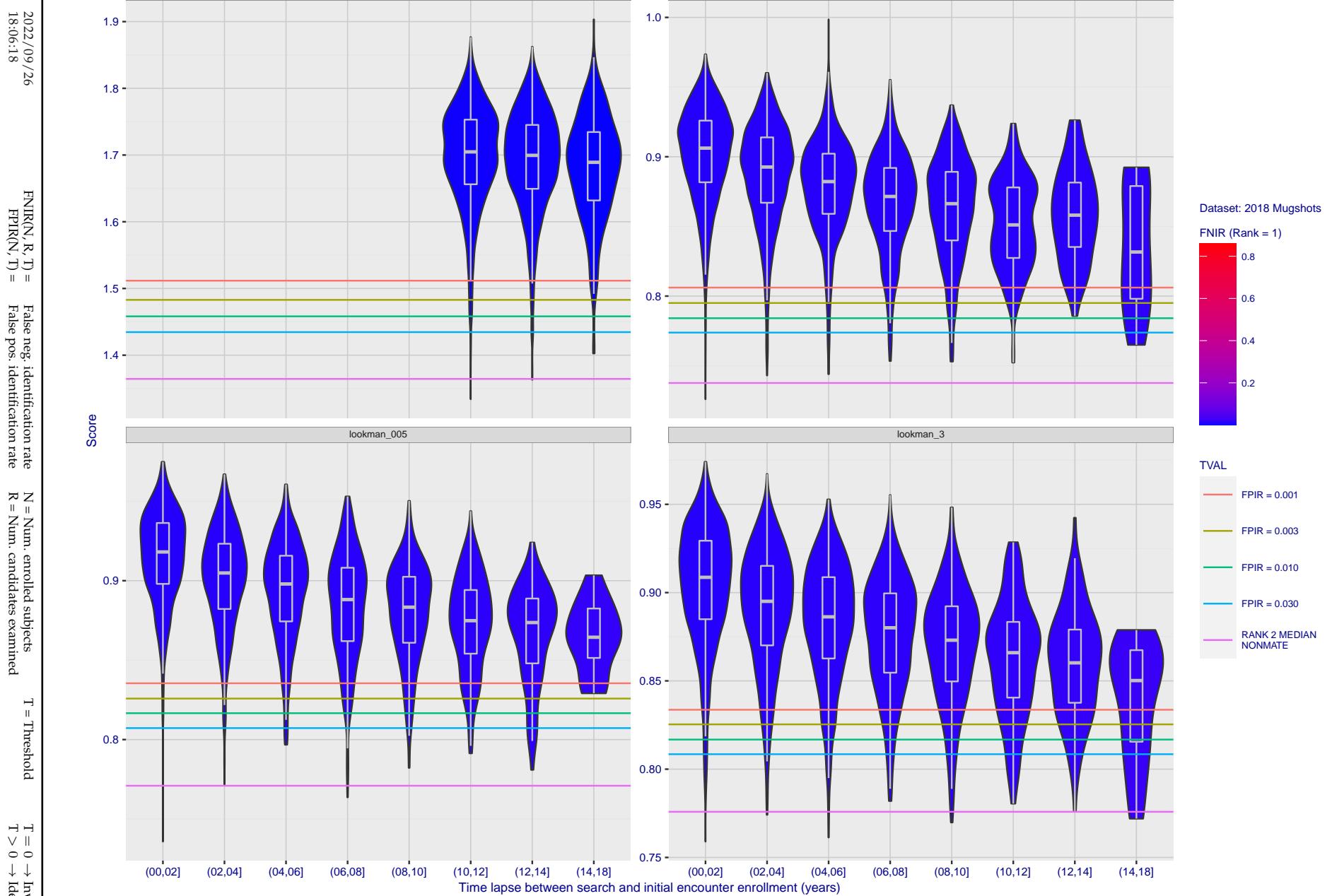


Figure 157: [FRVT-2018 Mugshot Ageing Dataset] Native mate scores vs. time-elapsed. The oldest image of each individual is enrolled. Thereafter, all more recent images are searched. Mated score distributions are computed over all searches noted in row 17 of Table 1 binned by number of years between search and initial enrollment.

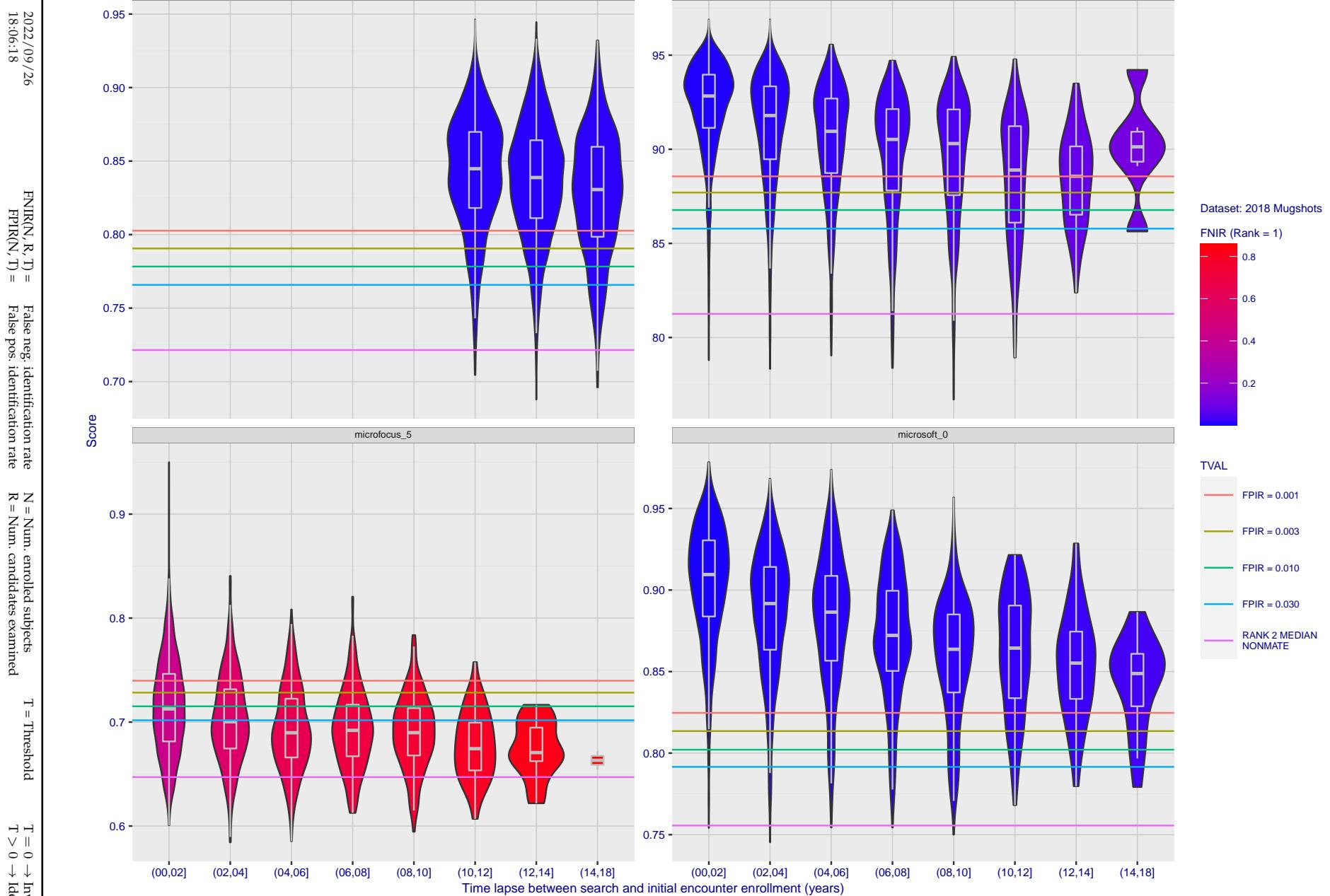


Figure 158: [FRVT-2018 Mugshot Ageing Dataset] Native mate scores vs. time-elapsed. The oldest image of each individual is enrolled. Thereafter, all more recent images are searched. Mated score distributions are computed over all searches noted in row 17 of Table 1 binned by number of years between search and initial enrollment.

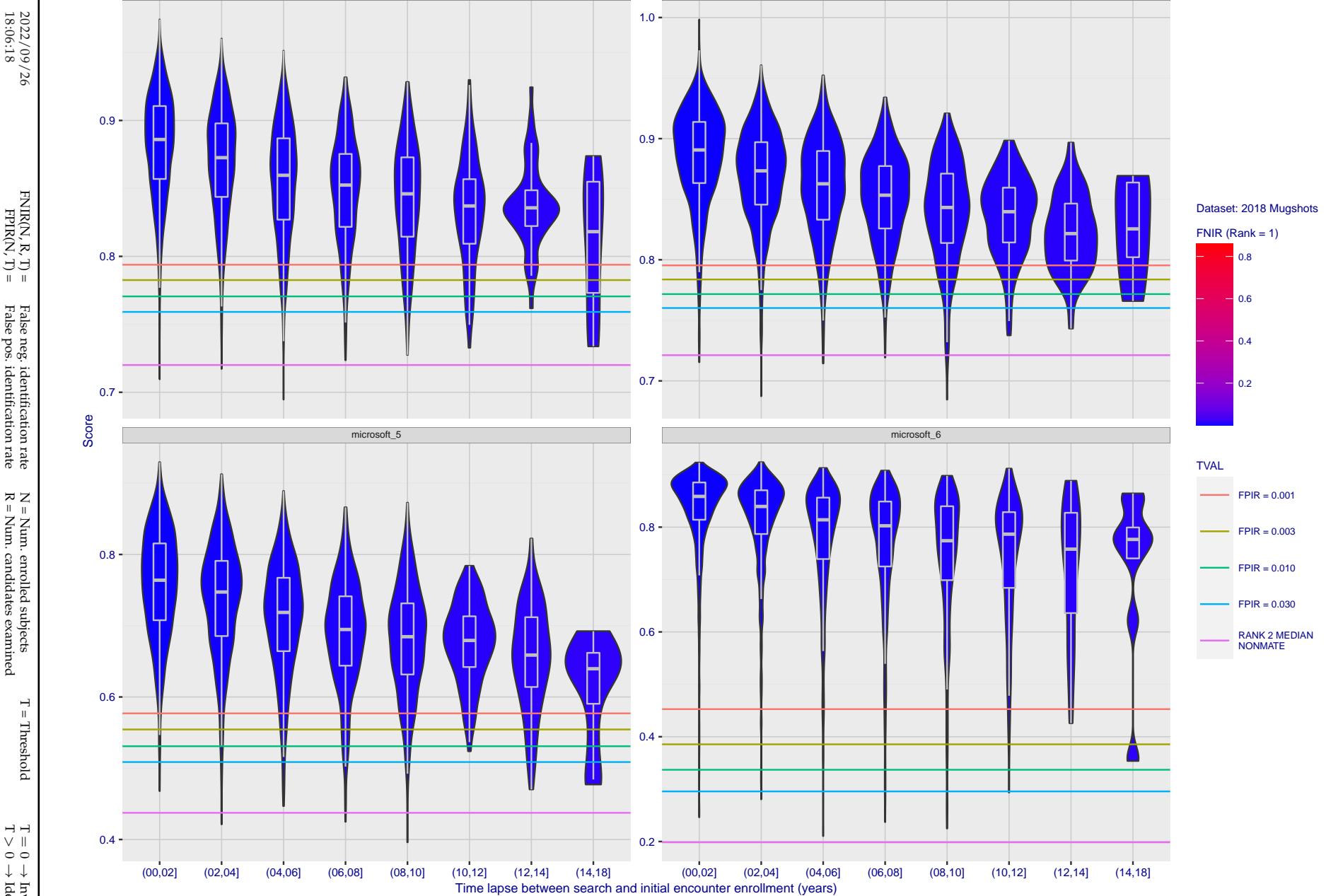


Figure 159: [FRVT-2018 Mugshot Ageing Dataset] Native mate scores vs. time-elapsed. The oldest image of each individual is enrolled. Thereafter, all more recent images are searched. Mated score distributions are computed over all searches noted in row 17 of Table 1 binned by number of years between search and initial enrollment.

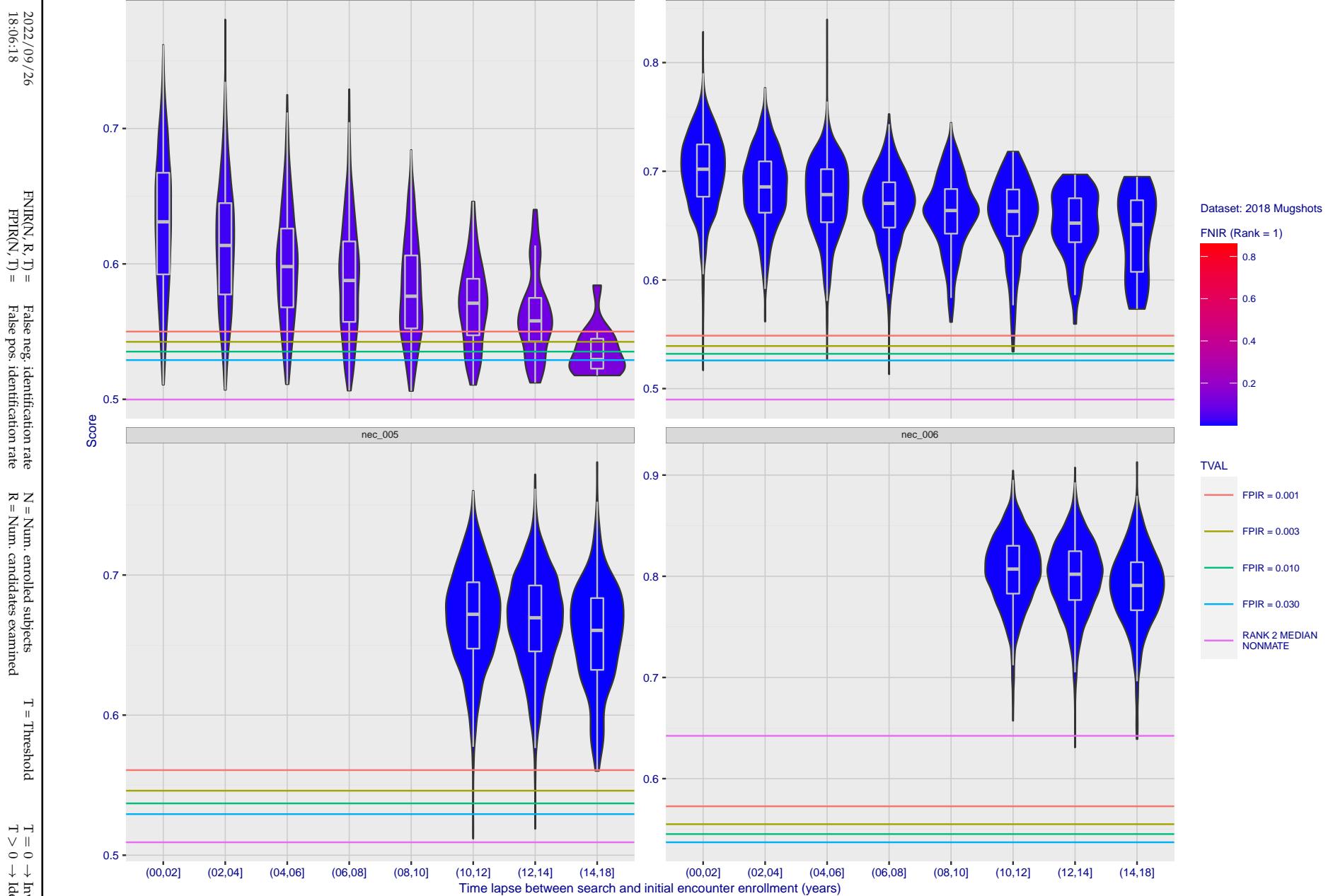


Figure 160: [FRVT-2018 Mugshot Ageing Dataset] Native mate scores vs. time-elapsed. The oldest image of each individual is enrolled. Thereafter, all more recent images are searched. Mated score distributions are computed over all searches noted in row 17 of Table 1 binned by number of years between search and initial enrollment.

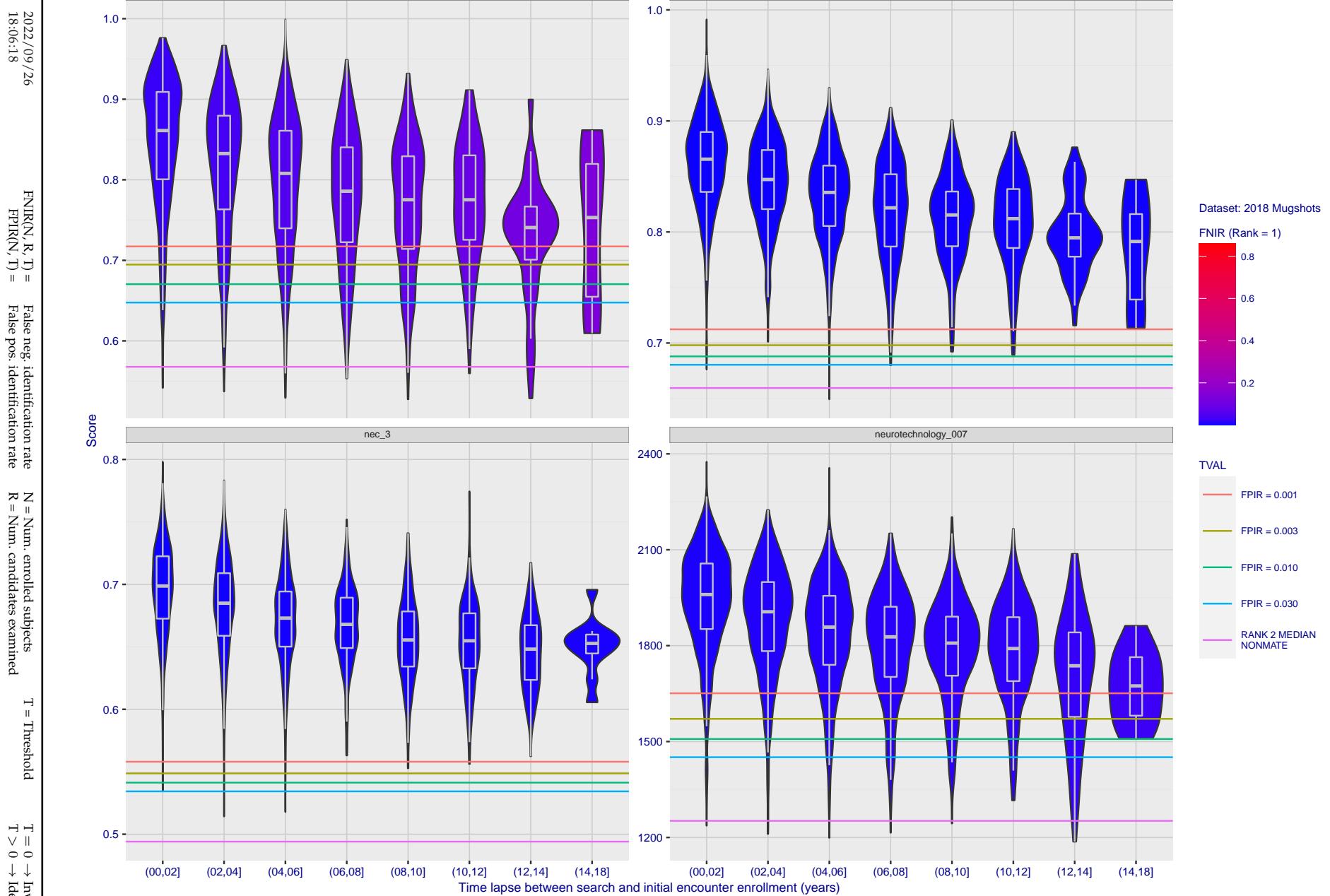


Figure 161: [FRVT-2018 Mugshot Ageing Dataset] Native mate scores vs. time-elapsed. The oldest image of each individual is enrolled. Thereafter, all more recent images are searched. Mated score distributions are computed over all searches noted in row 17 of Table 1 binned by number of years between search and initial enrollment.

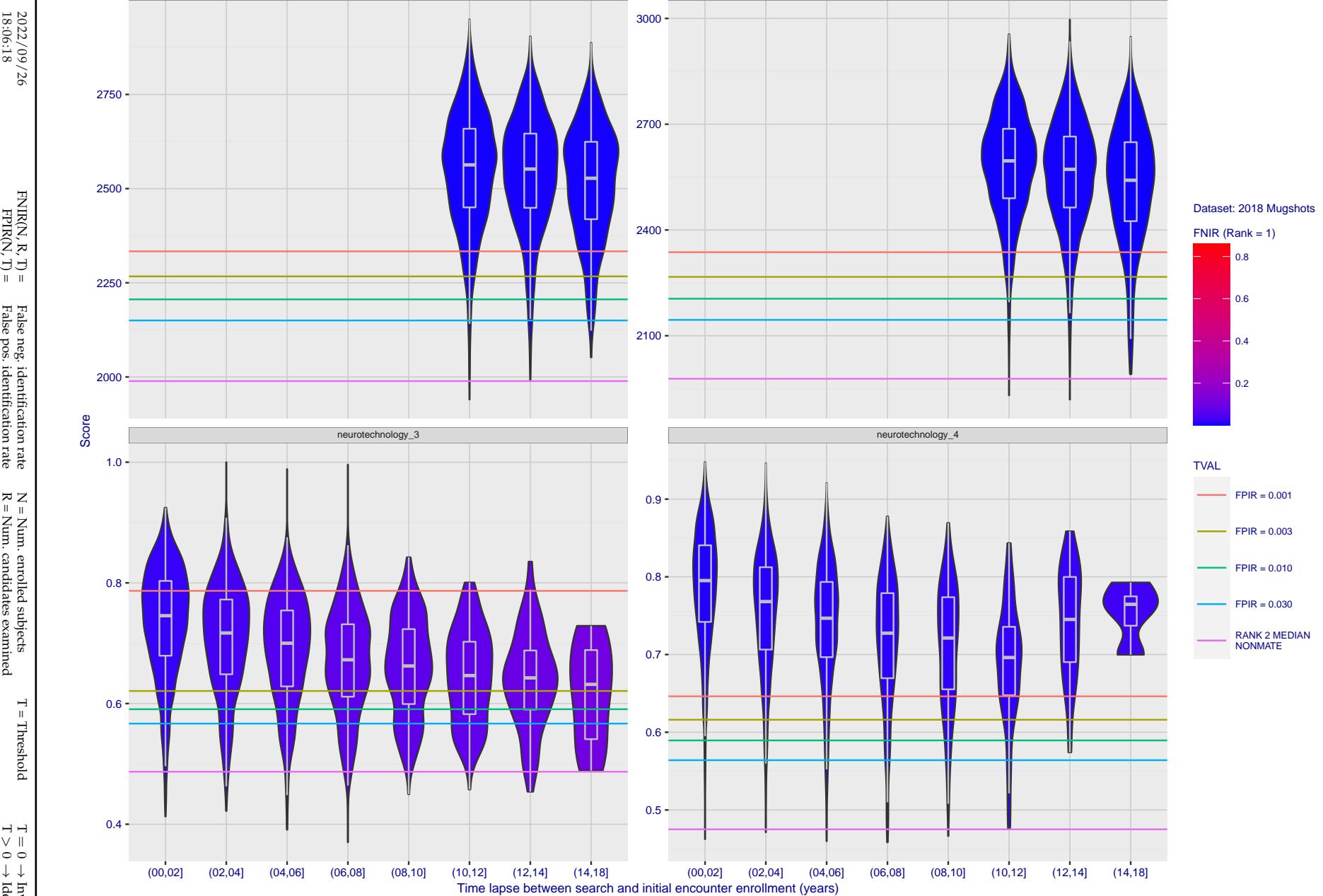


Figure 162: [FRVT-2018 Mugshot Ageing Dataset] Native mate scores vs. time-elapsed. The oldest image of each individual is enrolled. Thereafter, all more recent images are searched. Mated score distributions are computed over all searches noted in row 17 of Table 1 binned by number of years between search and initial enrollment.

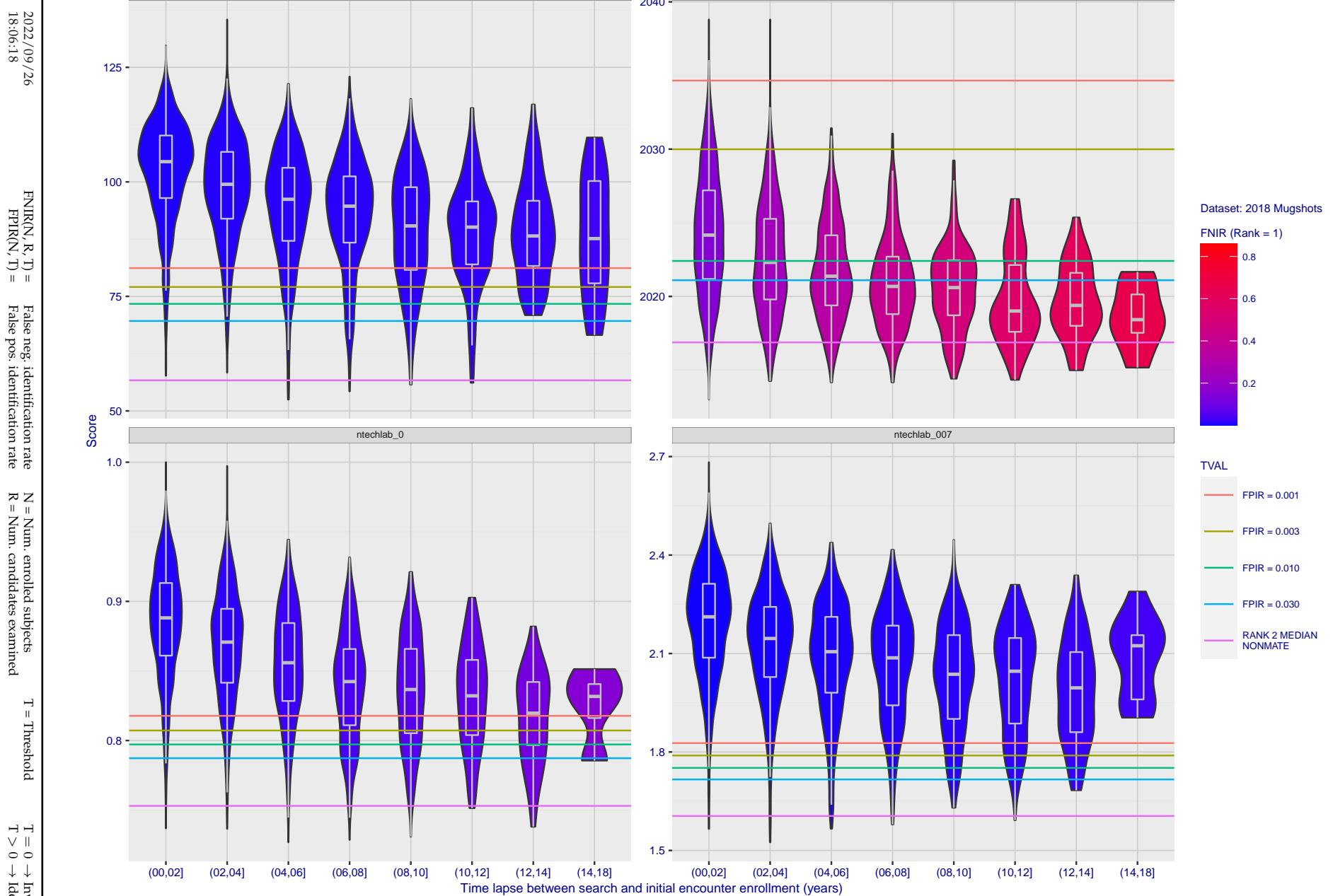


Figure 163: [FRVT-2018 Mugshot Ageing Dataset] Native mate scores vs. time-elapsed. The oldest image of each individual is enrolled. Thereafter, all more recent images are searched. Mated score distributions are computed over all searches noted in row 17 of Table 1 binned by number of years between search and initial enrollment.

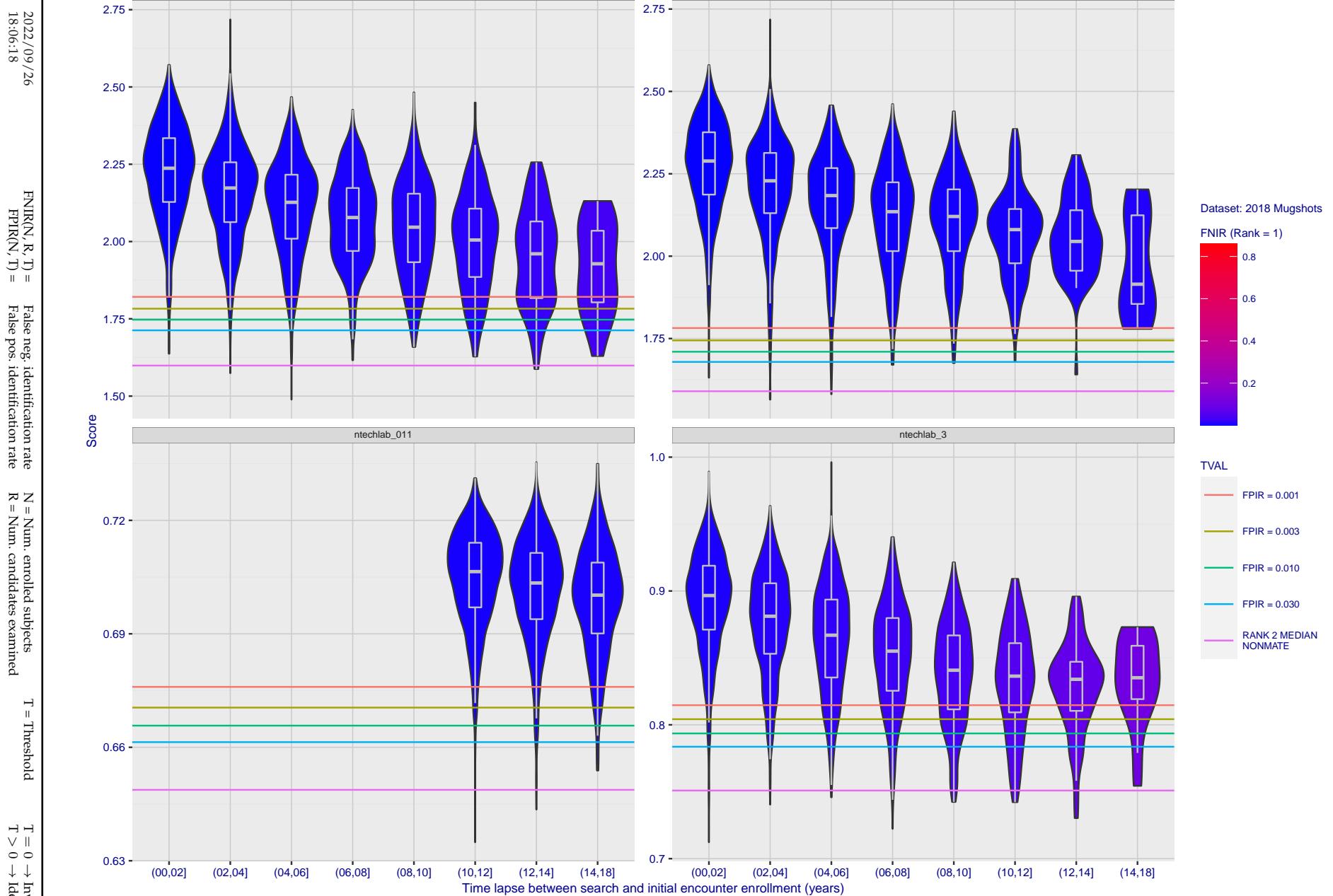


Figure 164: [FRVT-2018 Mugshot Ageing Dataset] Native mate scores vs. time-elapsed. The oldest image of each individual is enrolled. Thereafter, all more recent images are searched. Mated score distributions are computed over all searches noted in row 17 of Table 1 binned by number of years between search and initial enrollment.

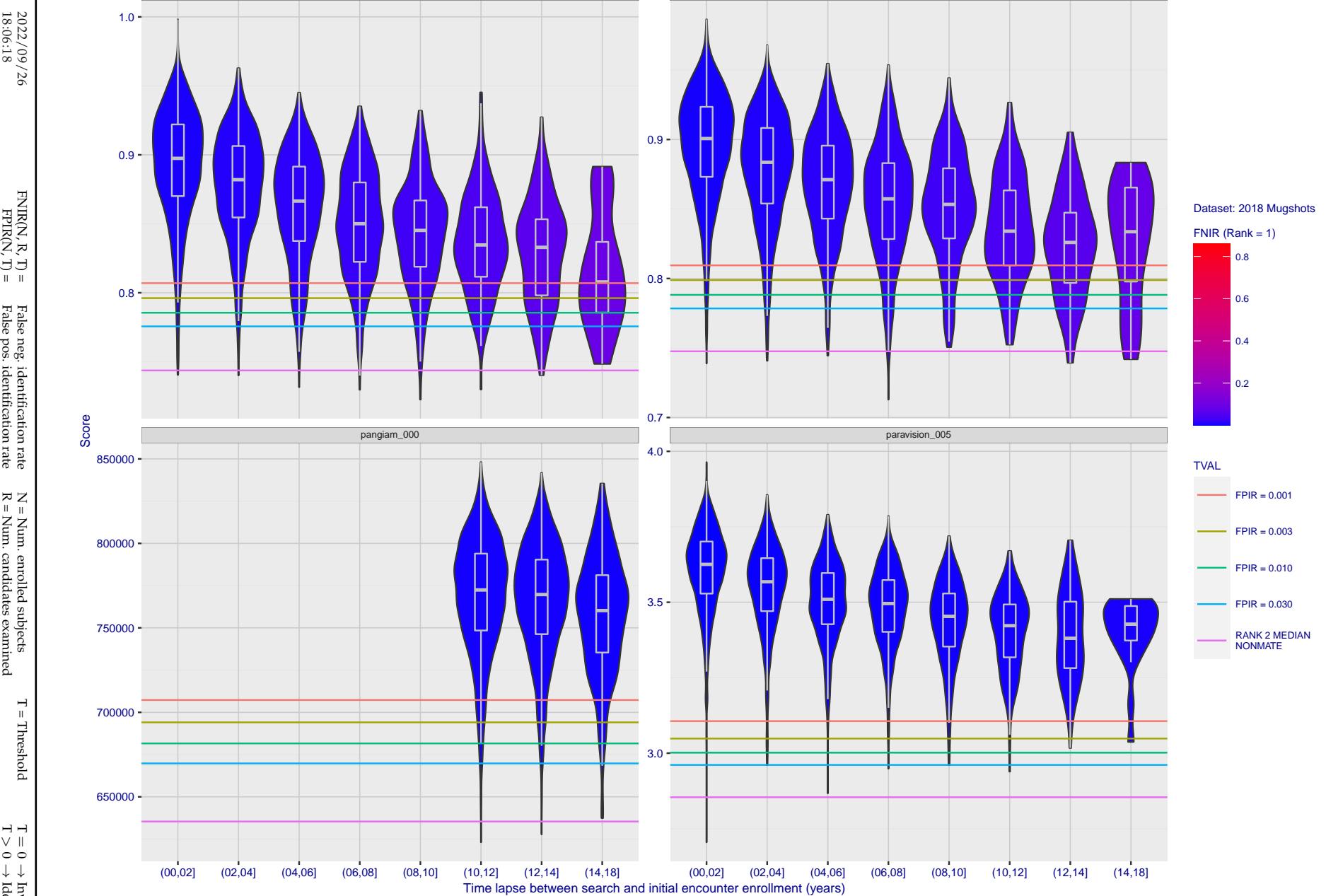


Figure 165: [FRVT-2018 Mugshot Ageing Dataset] Native mate scores vs. time-elapsed. The oldest image of each individual is enrolled. Thereafter, all more recent images are searched. Mated score distributions are computed over all searches noted in row 17 of Table 1 binned by number of years between search and initial enrollment.

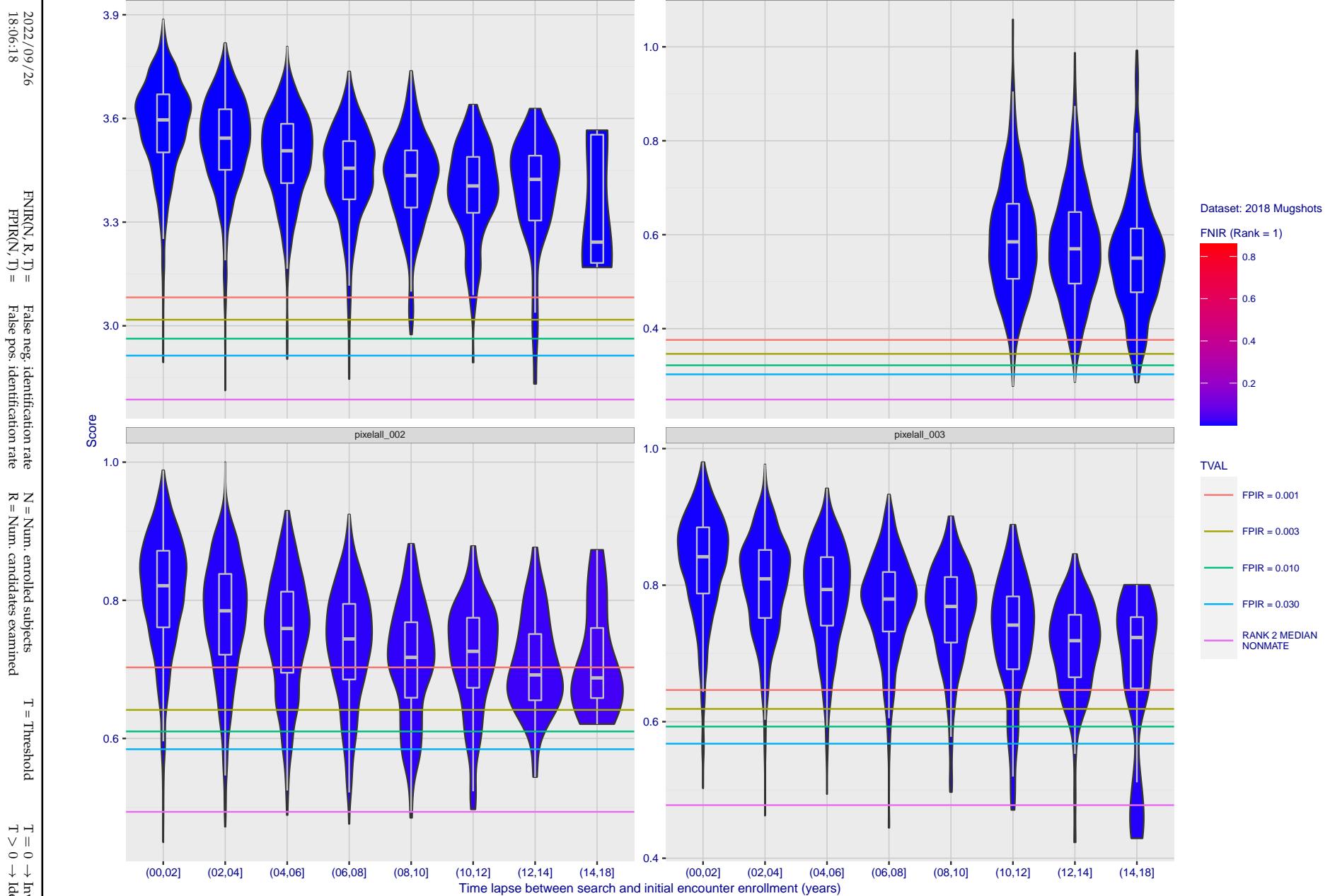


Figure 166: [FRVT-2018 Mugshot Ageing Dataset] Native mate scores vs. time-elapsed. The oldest image of each individual is enrolled. Thereafter, all more recent images are searched. Mated score distributions are computed over all searches noted in row 17 of Table 1 binned by number of years between search and initial enrollment.

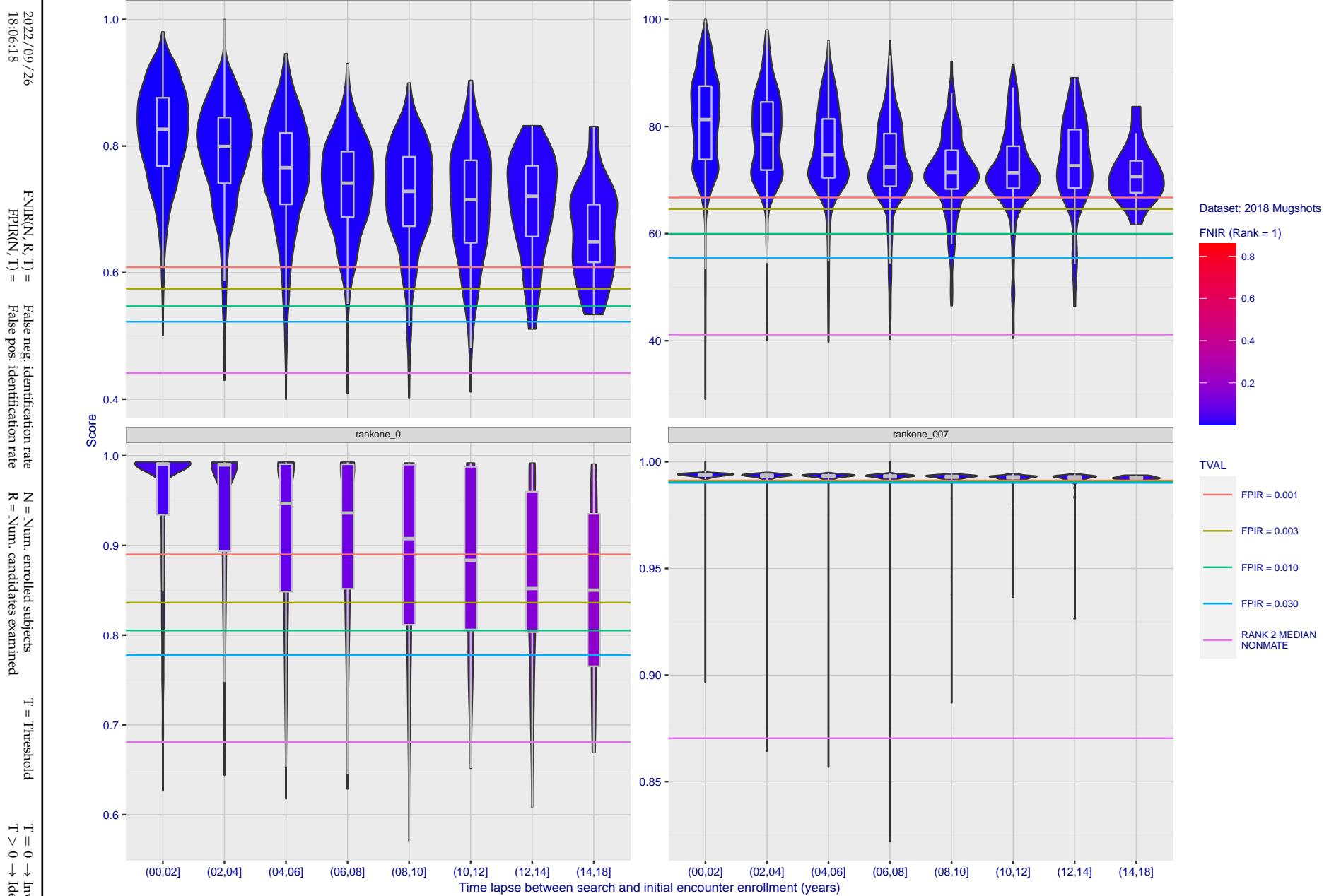


Figure 167: [FRVT-2018 Mugshot Ageing Dataset] Native mate scores vs. time-elapsed. The oldest image of each individual is enrolled. Thereafter, all more recent images are searched. Mated score distributions are computed over all searches noted in row 17 of Table 1 binned by number of years between search and initial enrollment.

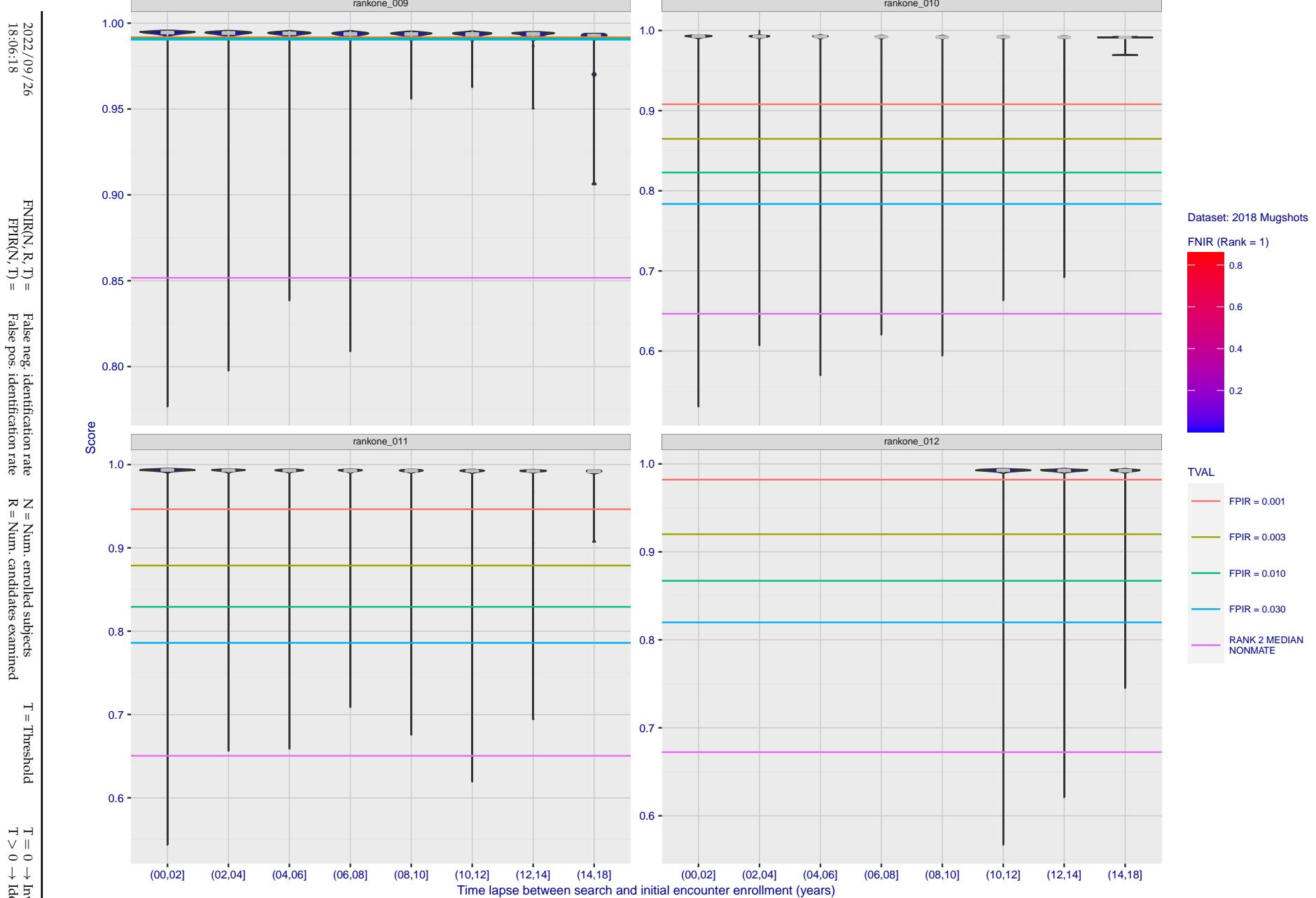


Figure 168: [FRVT-2018 Mugshot Ageing Dataset] Native mate scores vs. time-elapsed. The oldest image of each individual is enrolled. Thereafter, all more recent images are searched. Mated score distributions are computed over all searches noted in row 17 of Table 1 binned by number of years between search and initial enrollment.

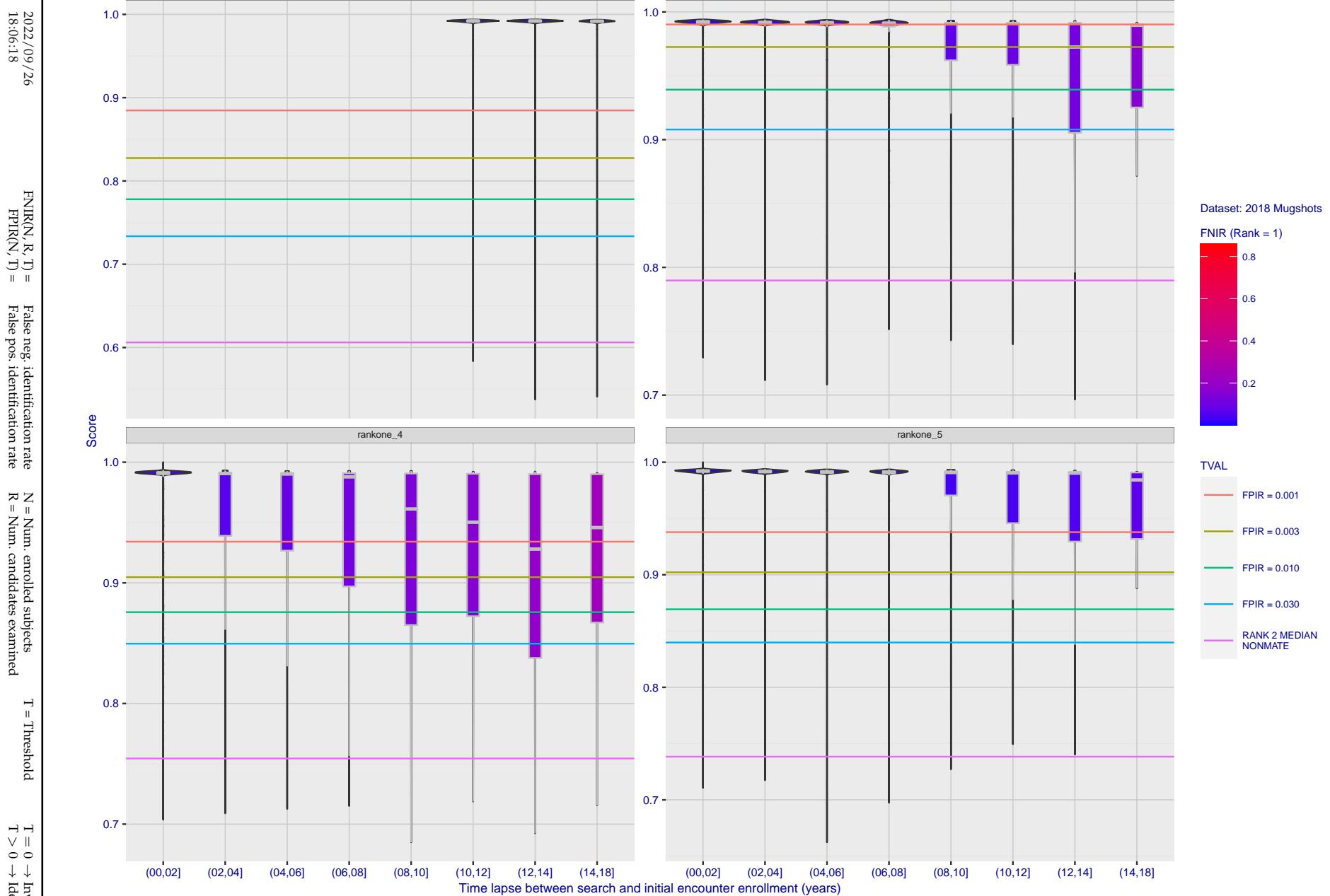


Figure 169: [FRVT-2018 Mugshot Ageing Dataset] Native mate scores vs. time-elapsed. The oldest image of each individual is enrolled. Thereafter, all more recent images are searched. Mated score distributions are computed over all searches noted in row 17 of Table 1 binned by number of years between search and initial enrollment.

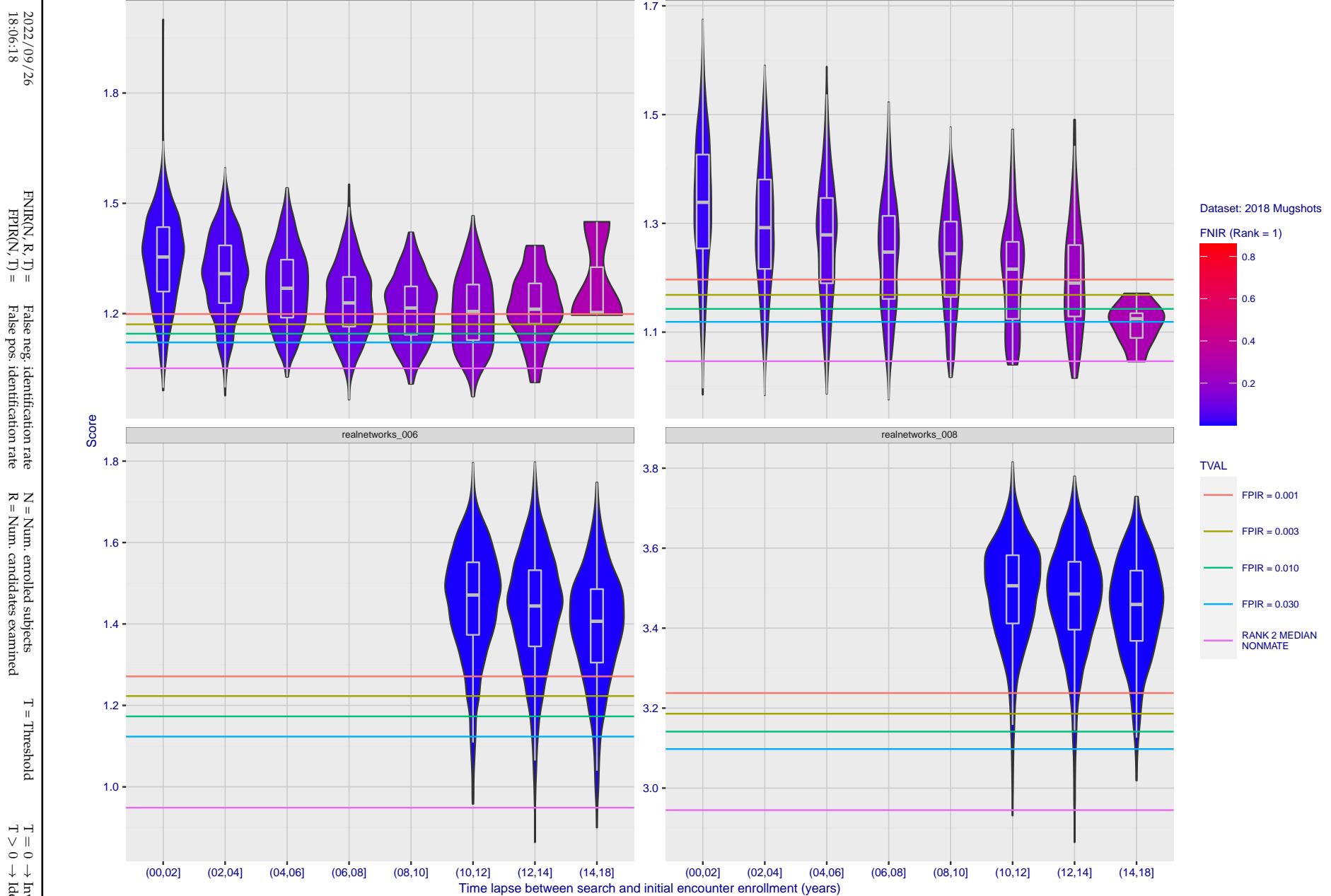


Figure 170: [FRVT-2018 Mugshot Ageing Dataset] Native mate scores vs. time-elapsed. The oldest image of each individual is enrolled. Thereafter, all more recent images are searched. Mated score distributions are computed over all searches noted in row 17 of Table 1 binned by number of years between search and initial enrollment.

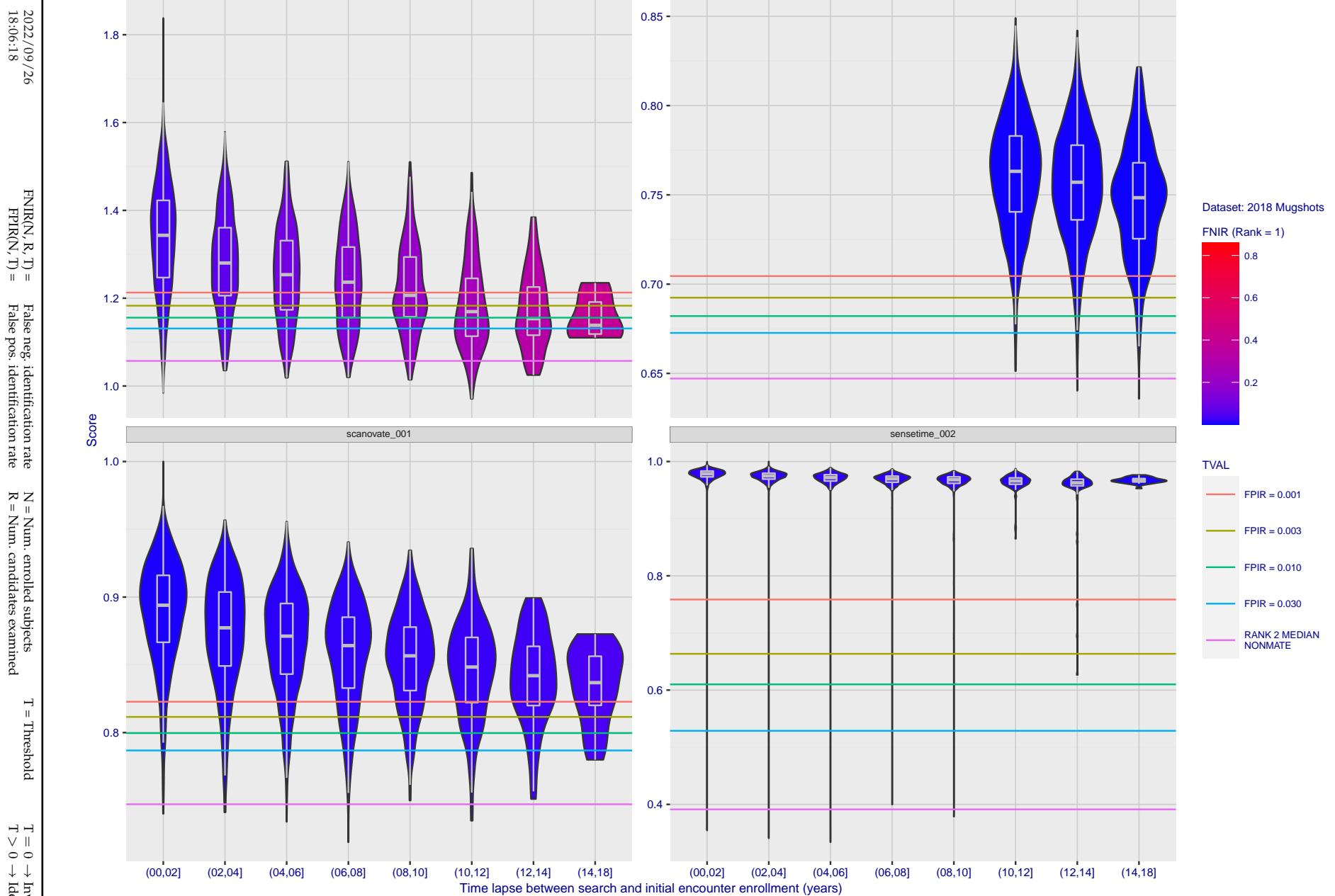


Figure 171: [FRVT-2018 Mugshot Ageing Dataset] Native mate scores vs. time-elapsed. The oldest image of each individual is enrolled. Thereafter, all more recent images are searched. Mated score distributions are computed over all searches noted in row 17 of Table 1 binned by number of years between search and initial enrollment.

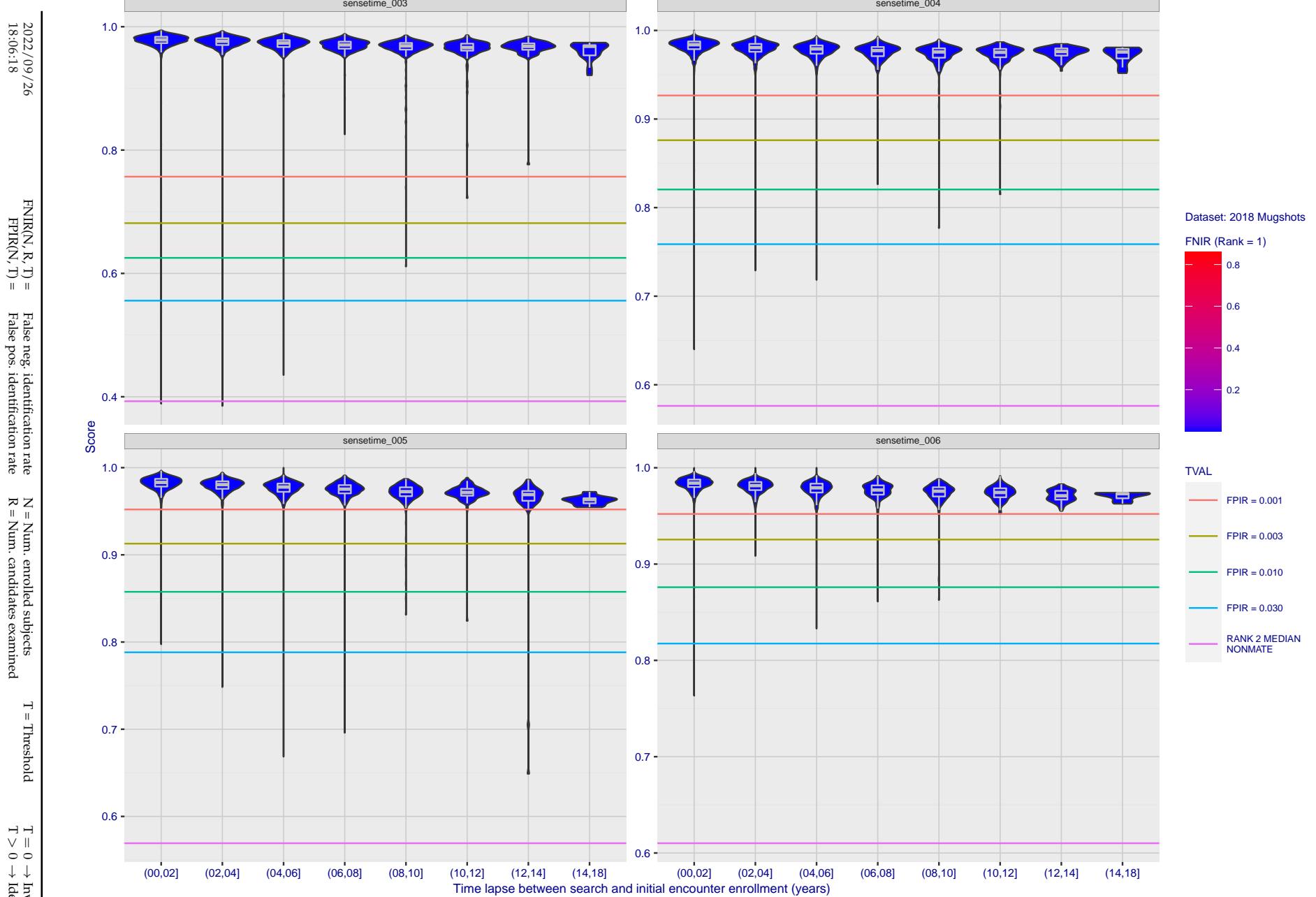


Figure 172: [FRVT-2018 Mugshot Ageing Dataset] Native mate scores vs. time-elapsed. The oldest image of each individual is enrolled. Thereafter, all more recent images are searched. Mated score distributions are computed over all searches noted in row 17 of Table 1 binned by number of years between search and initial enrollment.

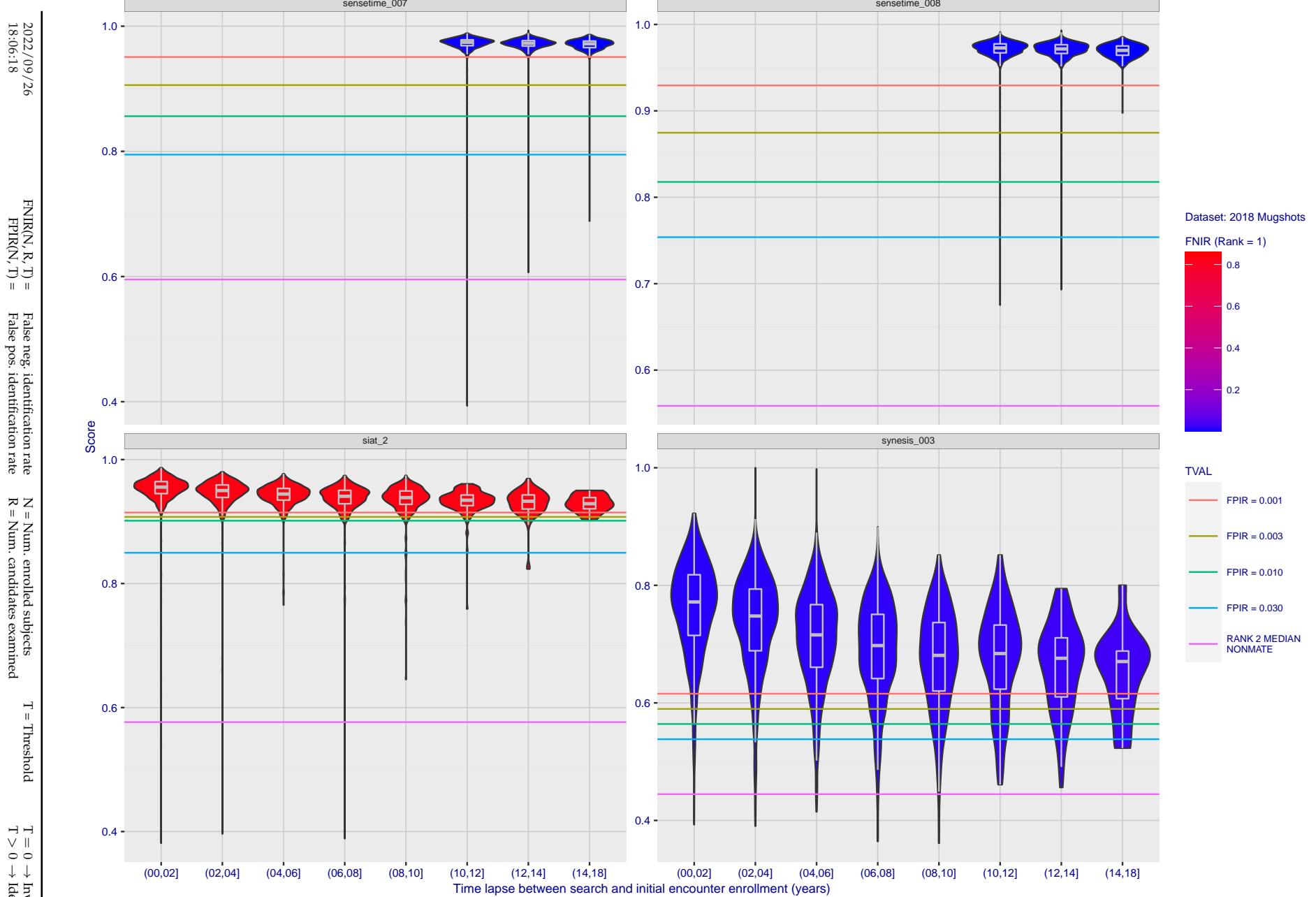


Figure 173: [FRVT-2018 Mugshot Ageing Dataset] Native mate scores vs. time-elapsed. The oldest image of each individual is enrolled. Thereafter, all more recent images are searched. Mated score distributions are computed over all searches noted in row 17 of Table 1 binned by number of years between search and initial enrollment.

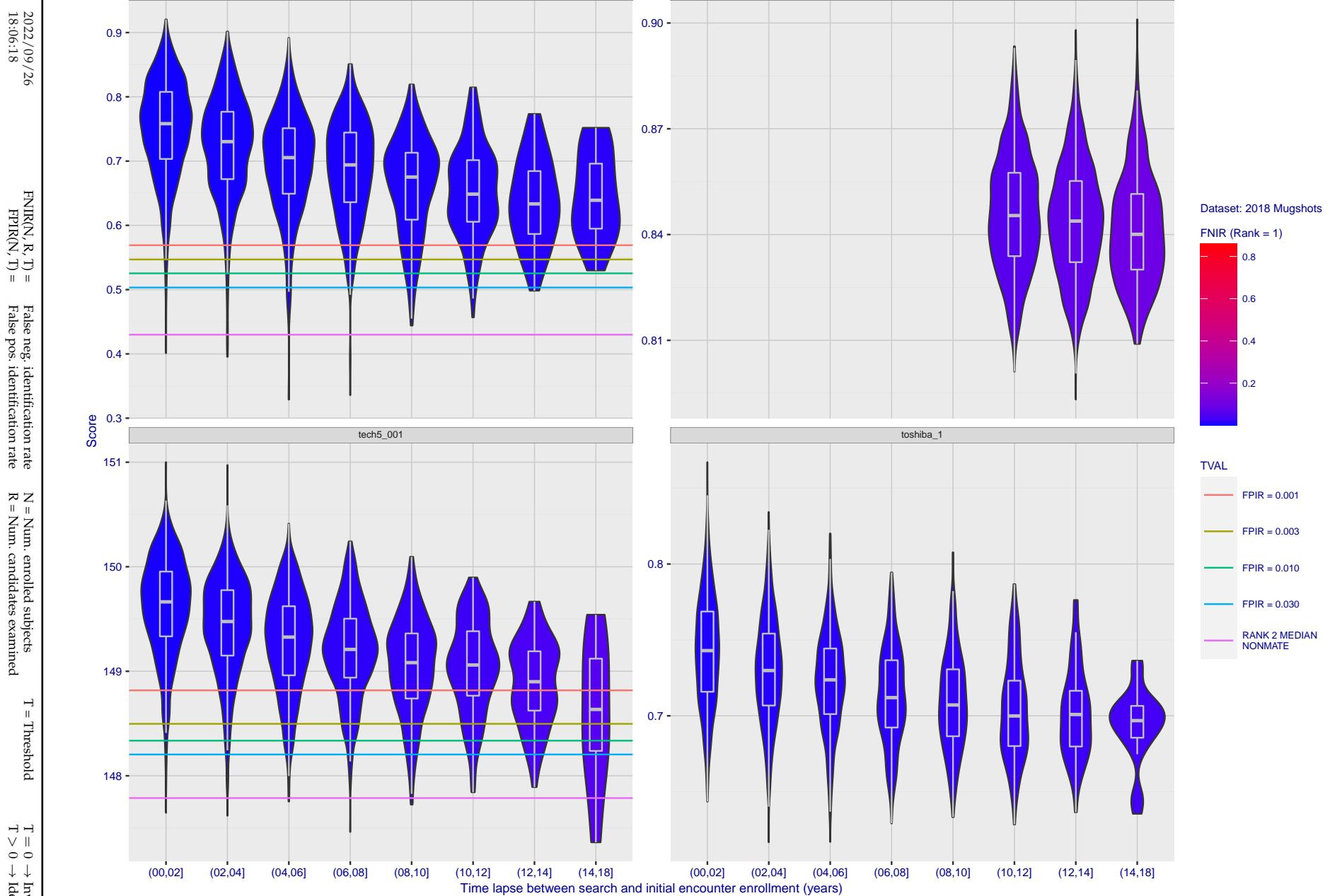


Figure 174: [FRVT-2018 Mugshot Ageing Dataset] Native mate scores vs. time-elapsed. The oldest image of each individual is enrolled. Thereafter, all more recent images are searched. Mated score distributions are computed over all searches noted in row 17 of Table 1 binned by number of years between search and initial enrollment.

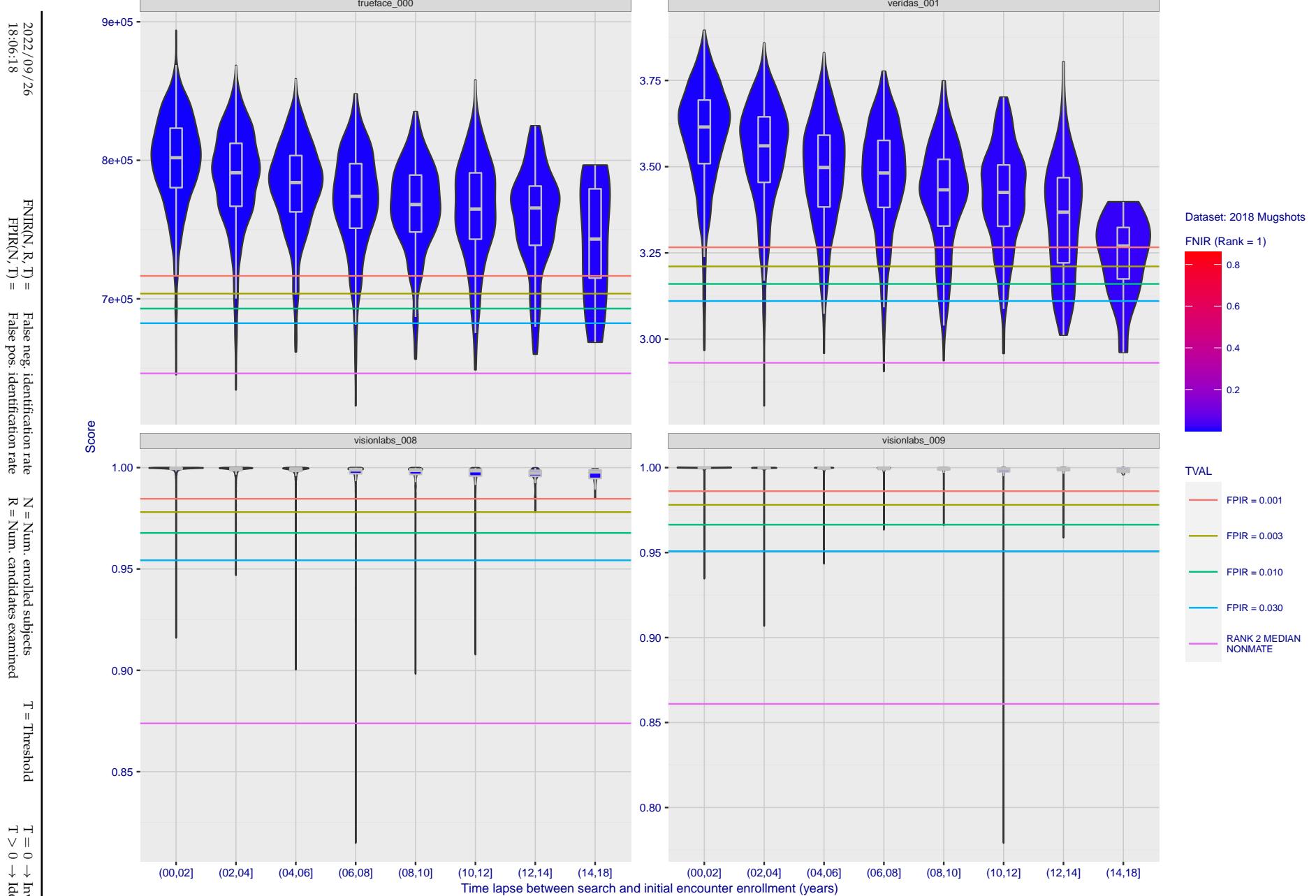


Figure 175: [FRVT-2018 Mugshot Ageing Dataset] Native mate scores vs. time-elapsed. The oldest image of each individual is enrolled. Thereafter, all more recent images are searched. Mated score distributions are computed over all searches noted in row 17 of Table 1 binned by number of years between search and initial enrollment.

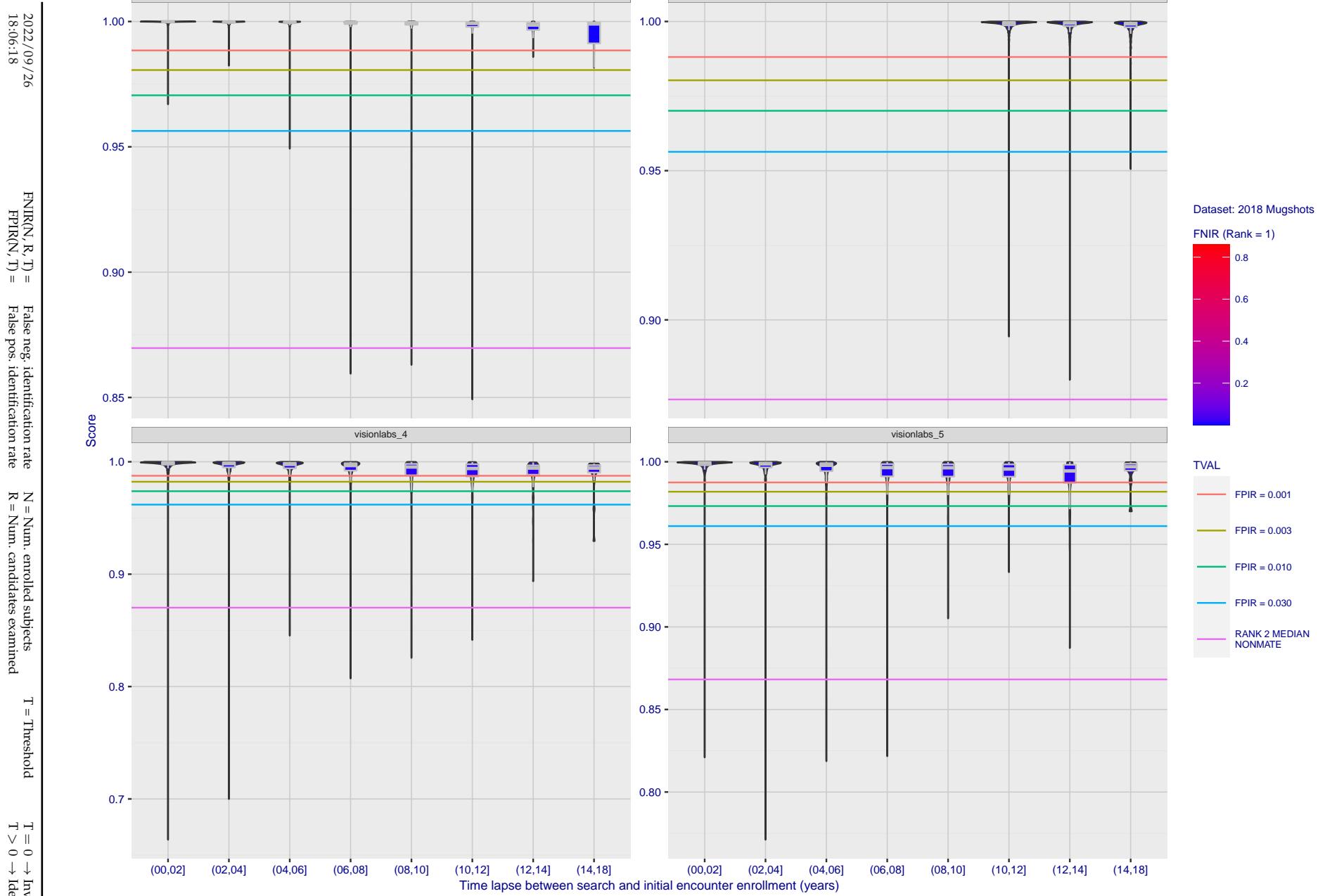


Figure 176: [FRVT-2018 Mugshot Ageing Dataset] Native mate scores vs. time-elapsed. The oldest image of each individual is enrolled. Thereafter, all more recent images are searched. Mated score distributions are computed over all searches noted in row 17 of Table 1 binned by number of years between search and initial enrollment.

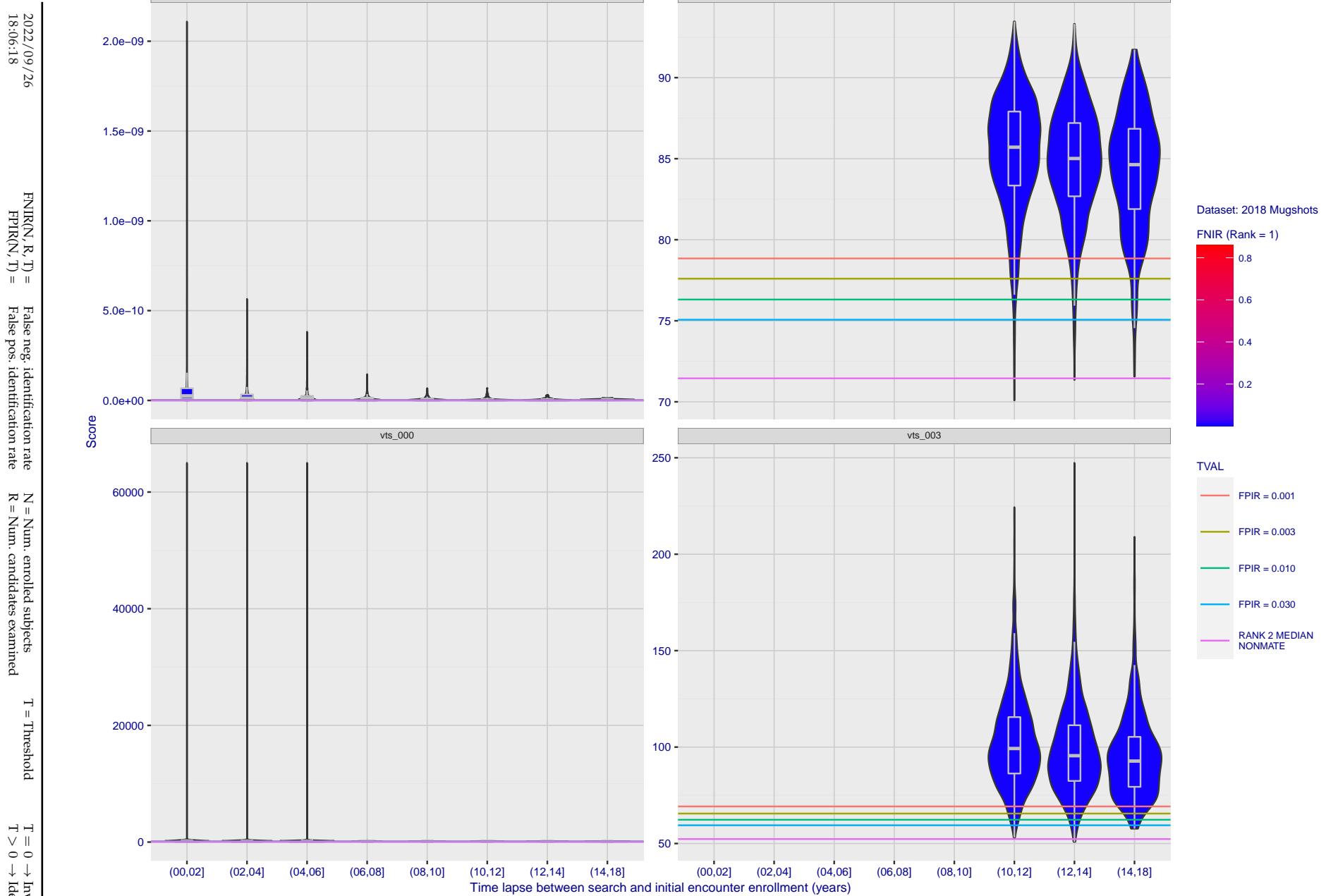


Figure 177: [FRVT-2018 Mugshot Ageing Dataset] Native mate scores vs. time-elapsed. The oldest image of each individual is enrolled. Thereafter, all more recent images are searched. Mated score distributions are computed over all searches noted in row 17 of Table 1 binned by number of years between search and initial enrollment.

2022/09/26
18:06:18FNIR(N, R, T) = False neg. identification rate
FPTR(N, T) = False pos. identification rateN = Num. enrolled subjects
R = Num. candidates examined

T = Threshold

T = 0 → Investigation
T > 0 → Identification

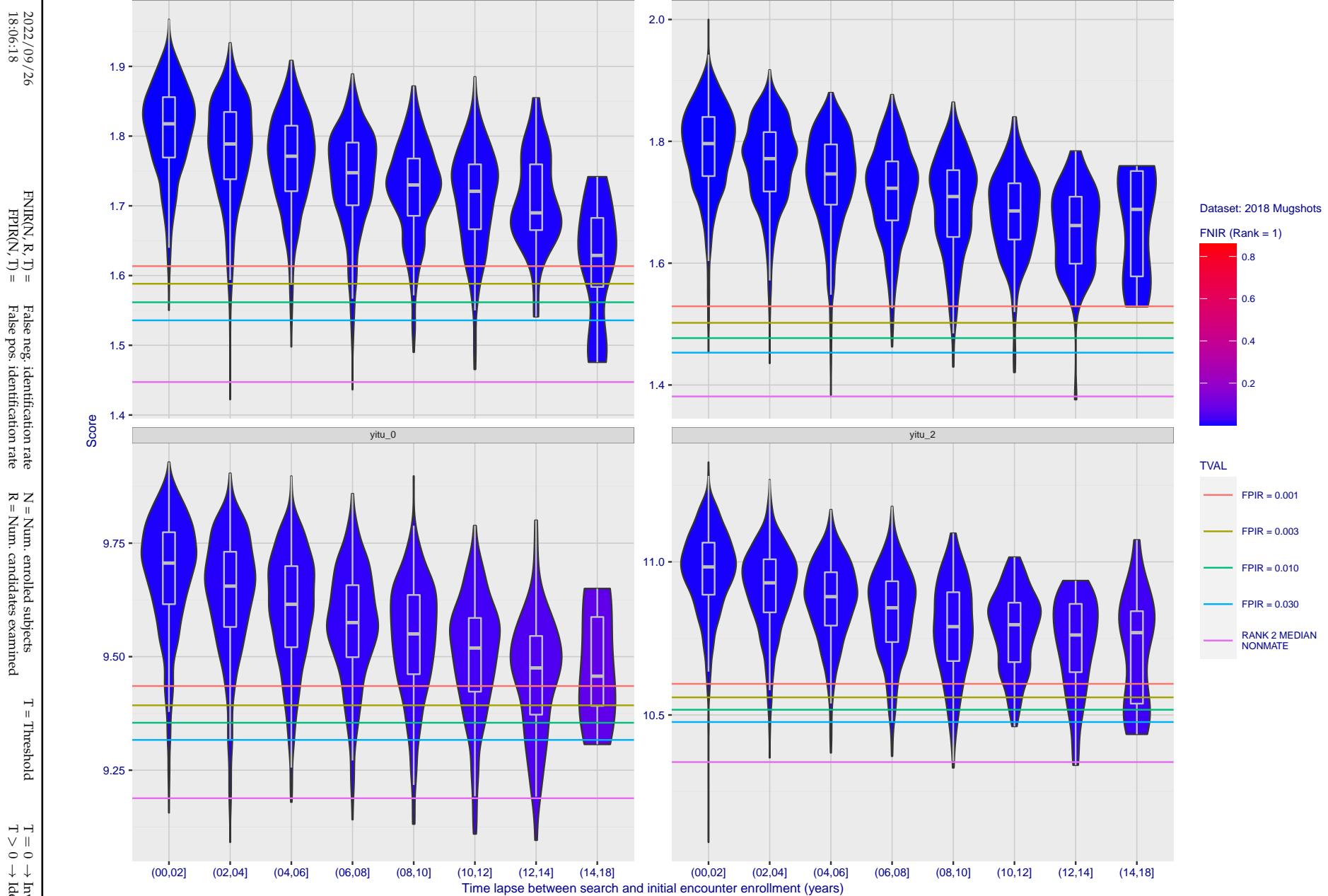


Figure 178: [FRVT-2018 Mugshot Ageing Dataset] Native mate scores vs. time-elapsed. The oldest image of each individual is enrolled. Thereafter, all more recent images are searched. Mated score distributions are computed over all searches noted in row 17 of Table 1 binned by number of years between search and initial enrollment.

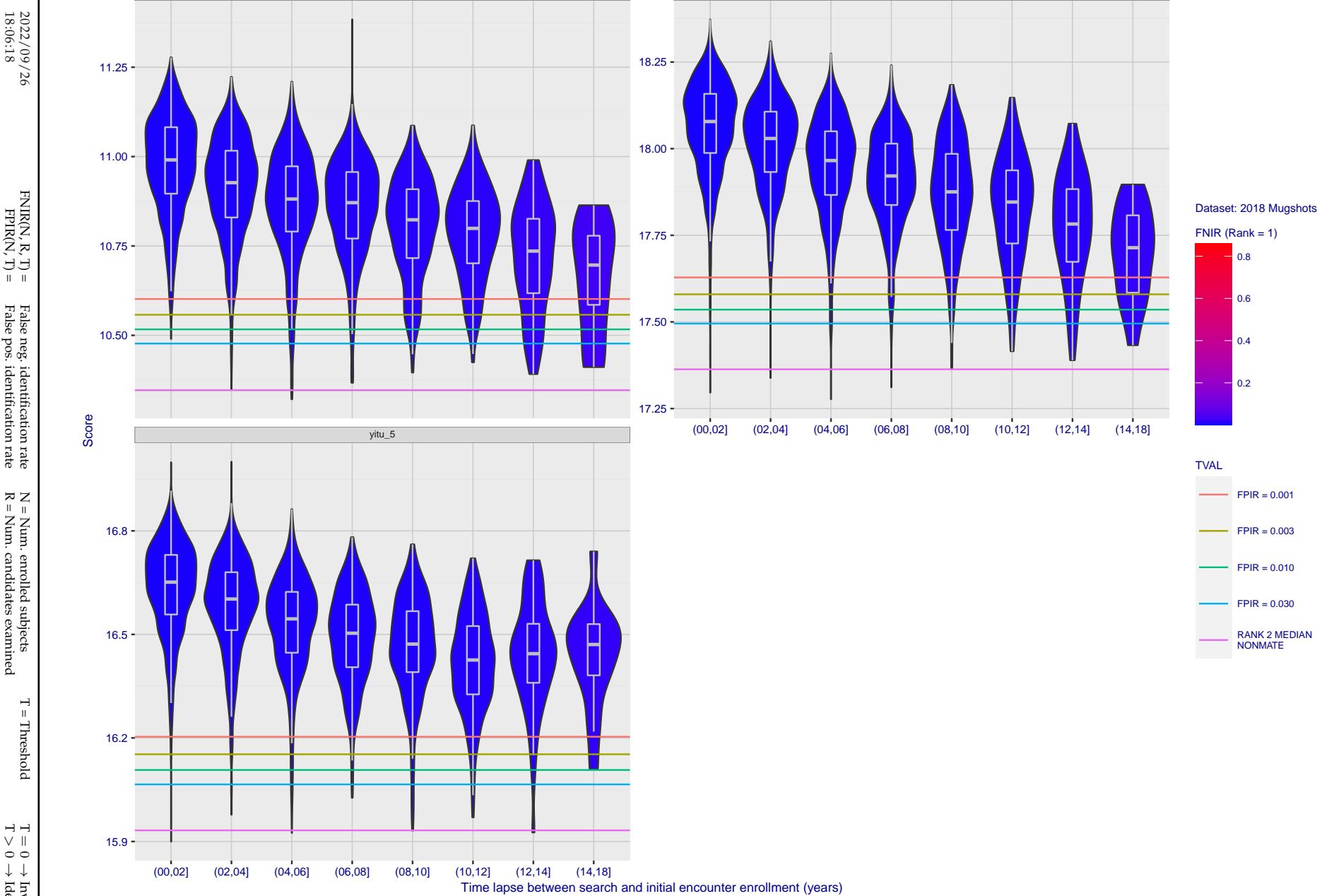


Figure 179: [FRVT-2018 Mugshot Ageing Dataset] Native mate scores vs. time-elapsed. The oldest image of each individual is enrolled. Thereafter, all more recent images are searched. Mated score distributions are computed over all searches noted in row 17 of Table 1 binned by number of years between search and initial enrollment.

Appendix C Effect of enrolling multiple images

2022/09/26
18:06:18FNIR(N, R, T) = False neg. identification rate
FPIR(N, T) = False pos. identification rateN = Num. enrolled subjects
R = Num. candidates examined

T = Threshold

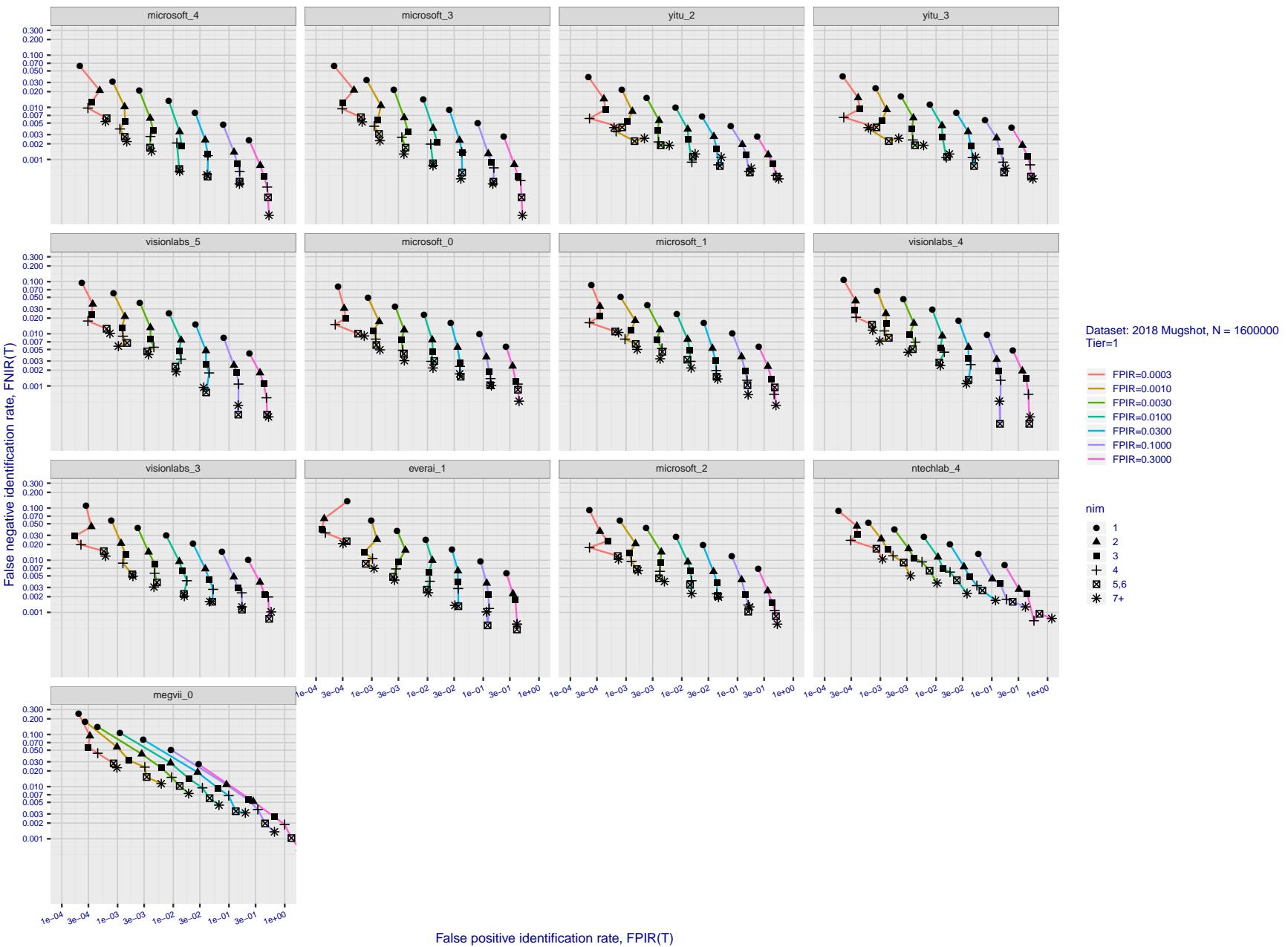
T = 0 → Investigation
T > 0 → Identification

Figure 180: [FRVT-2018 Mugshot Dataset] Effect of enrolling multiple images for each identity. The plot shows an identification miss rates vs. false positive rates, at seven operating thresholds. The enrolled population size is fixed. The images are enrolled with lifetime-consolidation - see section 2.3.

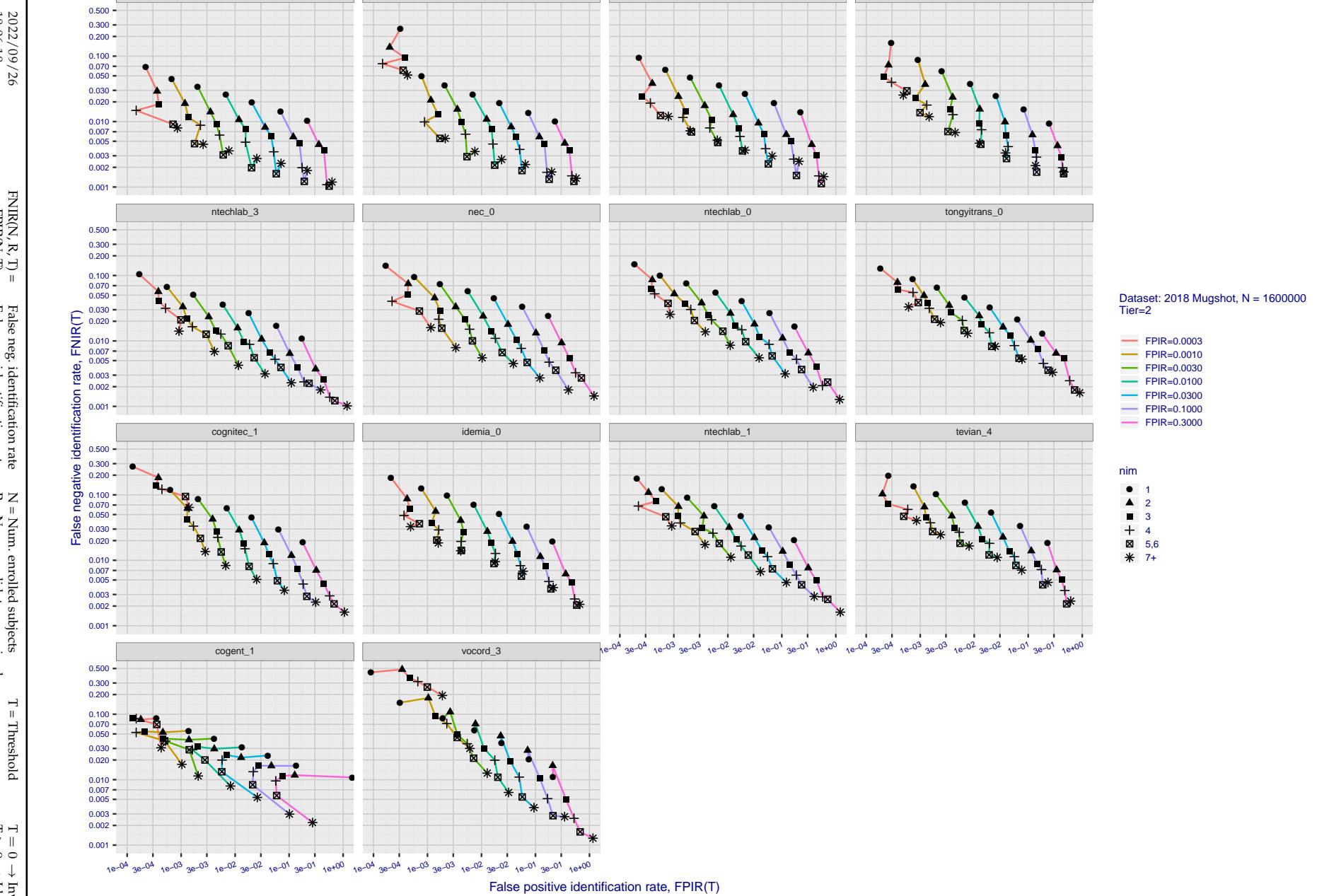


Figure 181: [FRVT-2018 Mugshot Dataset] Effect of enrolling multiple images for each identity. The plot shows an identification miss rates vs. false positive rates, at seven operating thresholds. The enrolled population size is fixed. The images are enrolled with lifetime-consolidation - see section 2.3.

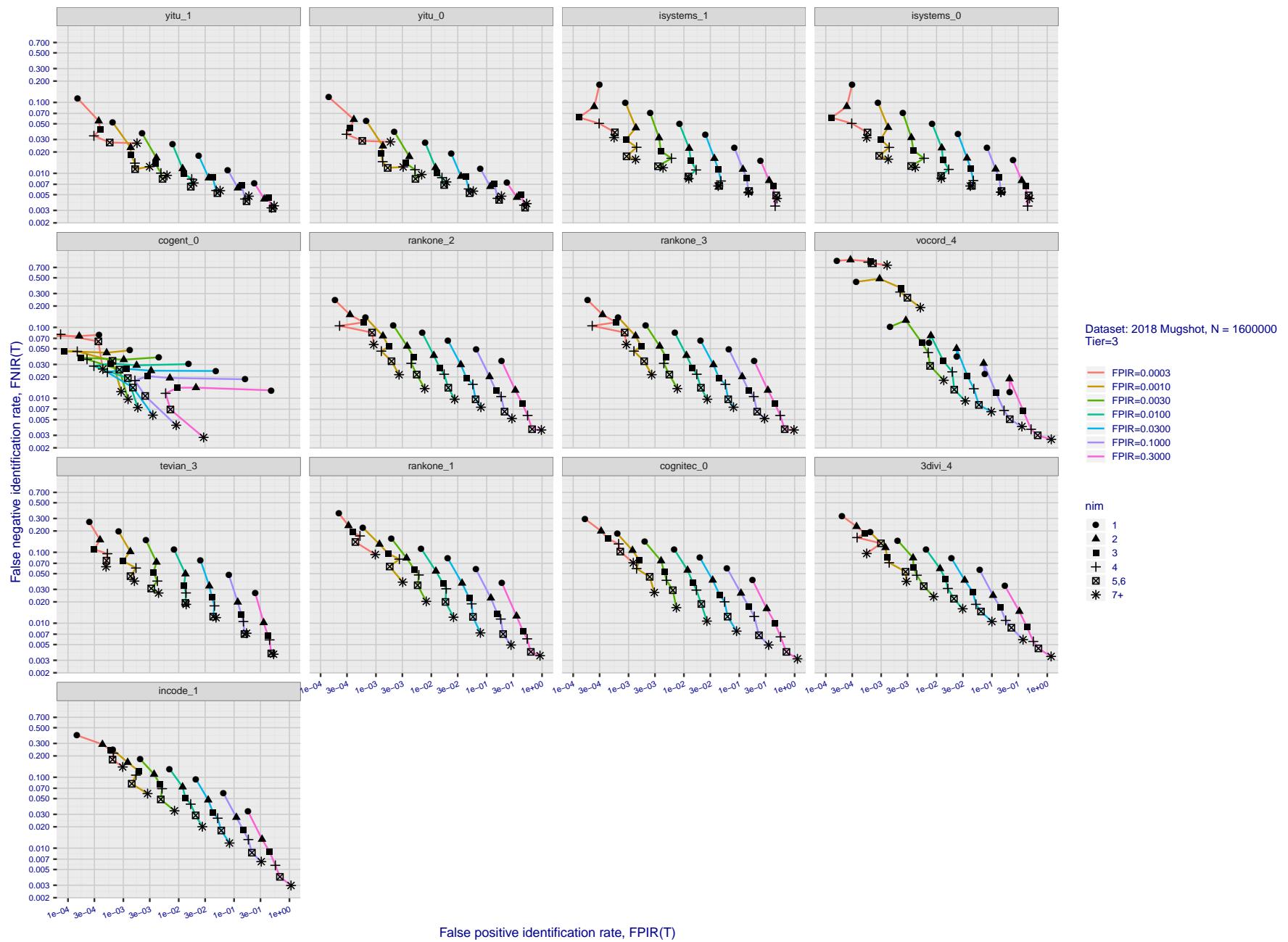


Figure 182: [FRVT-2018 Mugshot Dataset] Effect of enrolling multiple images for each identity. The plot shows an identification miss rates vs. false positive rates, at seven operating thresholds. The enrolled population size is fixed. The images are enrolled with lifetime-consolidation - see section 2.3.

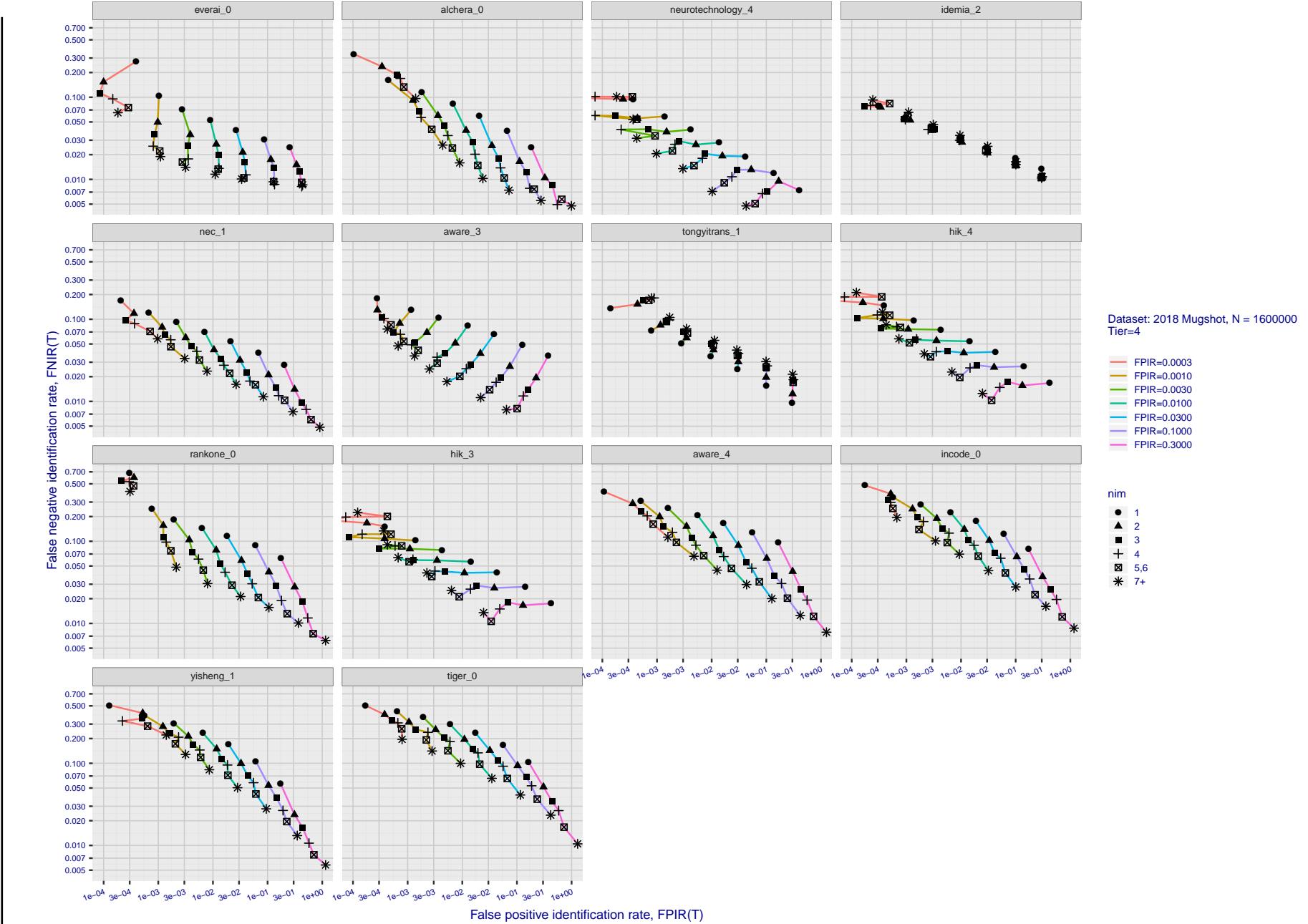


Figure 183: [FRVT-2018 Mugshot Dataset] Effect of enrolling multiple images for each identity. The plot shows an identification miss rates vs. false positive rates, at seven operating thresholds. The enrolled population size is fixed. The images are enrolled with lifetime-consolidation - see section 2.3.

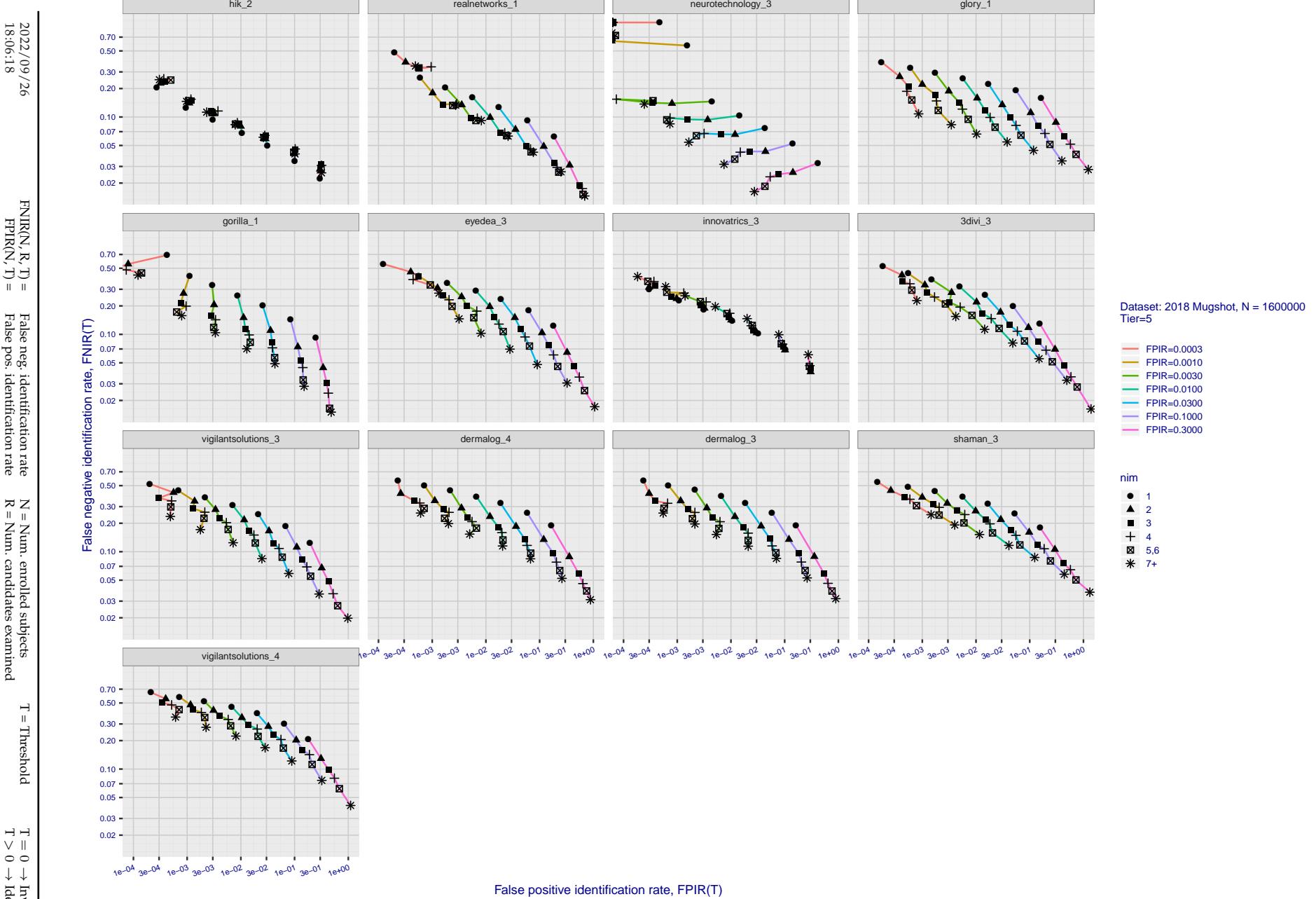


Figure 184: [FRVT-2018 Mugshot Dataset] Effect of enrolling multiple images for each identity. The plot shows an identification miss rates vs. false positive rates, at seven operating thresholds. The enrolled population size is fixed. The images are enrolled with lifetime-consolidation - see section 2.3.

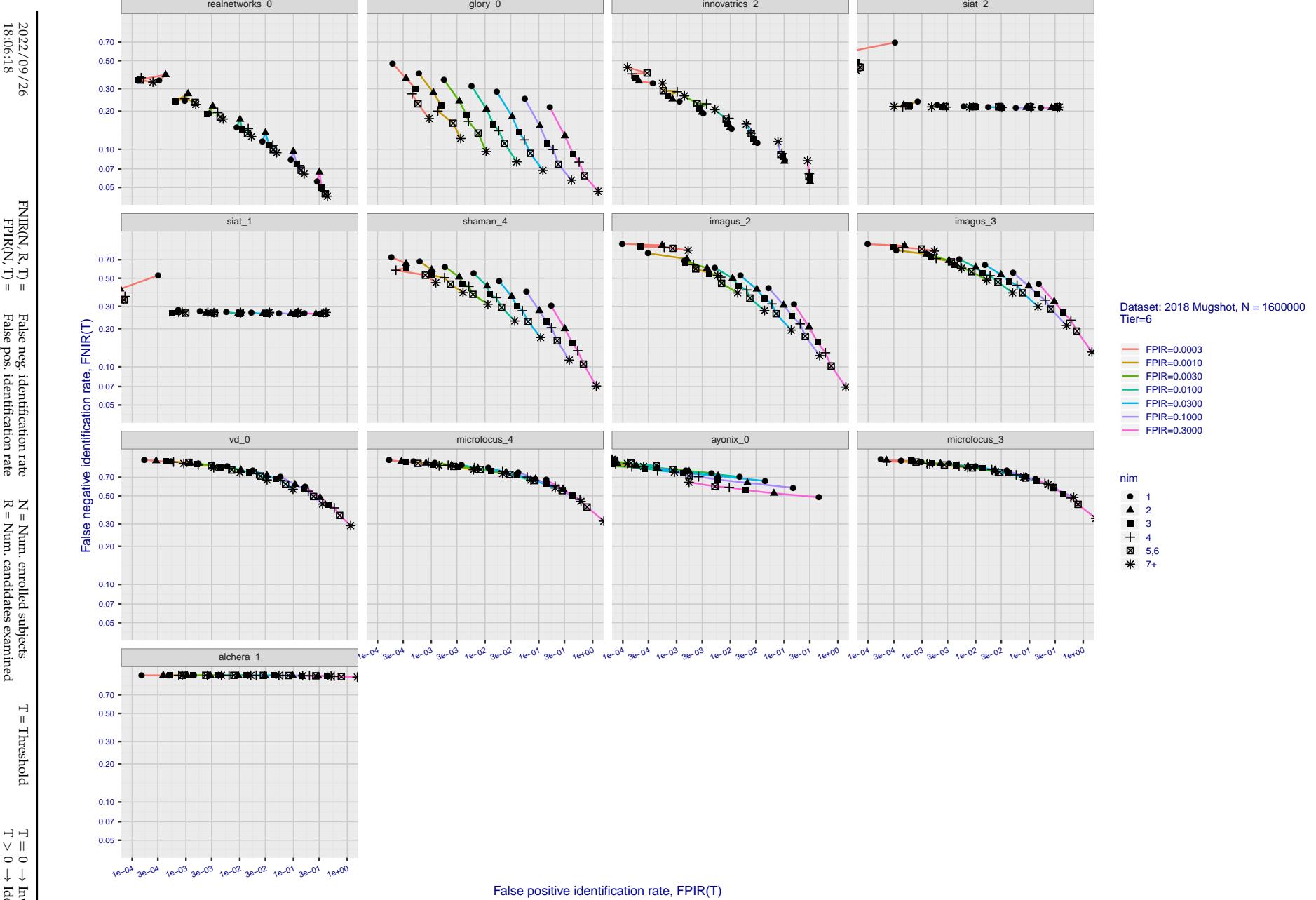


Figure 185: [FRVT-2018 Mugshot Dataset] Effect of enrolling multiple images for each identity. The plot shows an identification miss rates vs. false positive rates, at seven operating thresholds. The enrolled population size is fixed. The images are enrolled with lifetime-consolidation - see section 2.3.

Appendix D Accuracy with poor quality webcam images

2022/09/26 18:06:18	$\text{FNIR}(N, R, T) =$ $\text{FPTR}(N, T) =$	False neg. identification rate False pos. identification rate	$N =$ Num. enrolled subjects $R =$ Num. candidates examined	$T =$ Threshold $T > 0 \rightarrow$ Identification	$T = 0 \rightarrow$ Investigation
------------------------	---	--	--	---	-----------------------------------

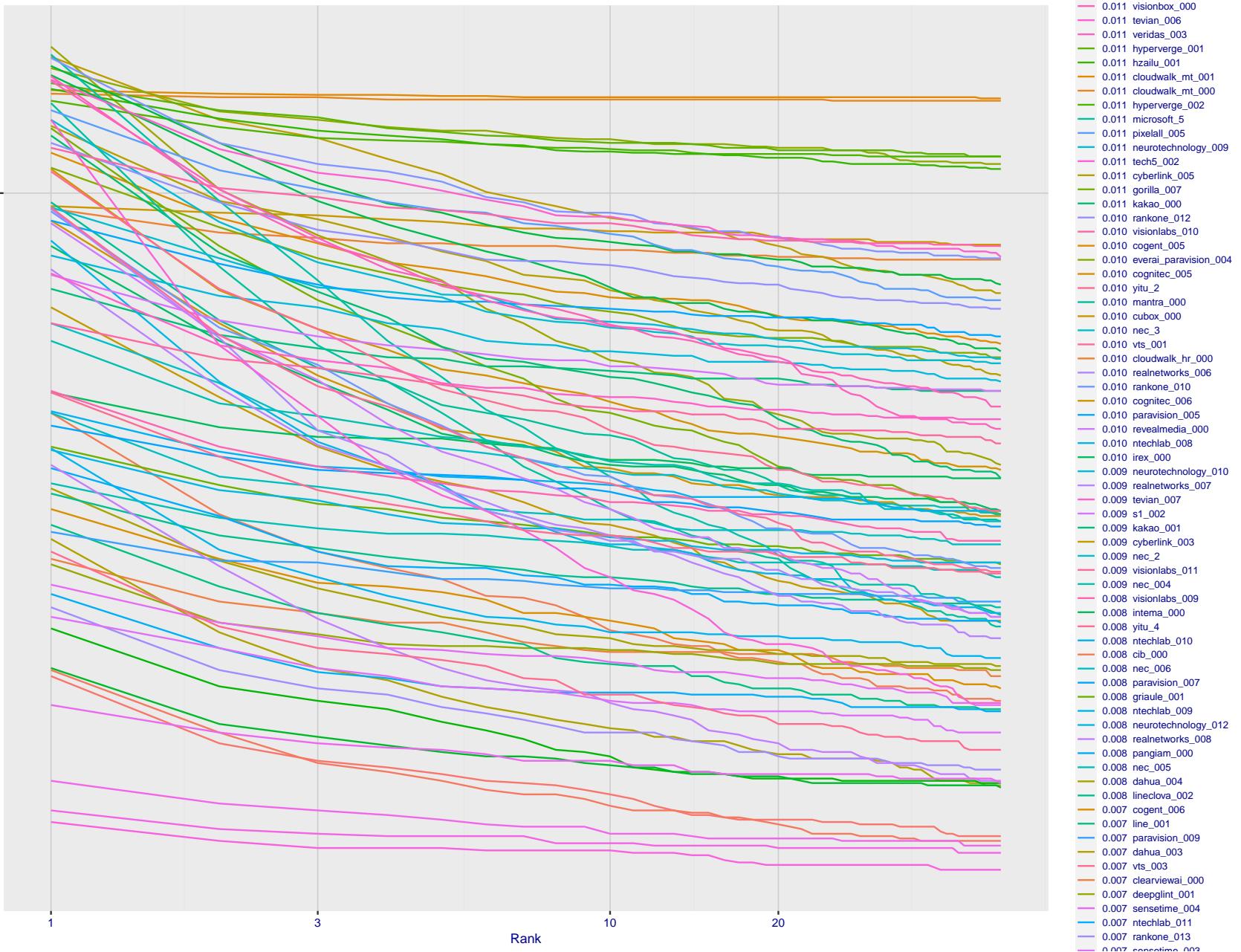


Figure 186: [Webcam Dataset] Identification miss rates vs. rank. The results apply to cross-domain recognition in which webcams are searched against enrolled mugshots. The FNIR values are higher than those for mugshot-mugshot identification due to low image resolution, lighting and less constrained subject pose in webcam images - see Figure 6.

2022/09/26
18:06:18

$\text{FNIR}(N, R, T) =$ False neg. identification rate
 $\text{FPIR}(N, T) =$ False pos. identification rate

$N =$ Num. enrolled subjects
 $R =$ Num. candidates examined

$T =$ Threshold
 $T = 0 \rightarrow$ Investigation
 $T > 0 \rightarrow$ Identification

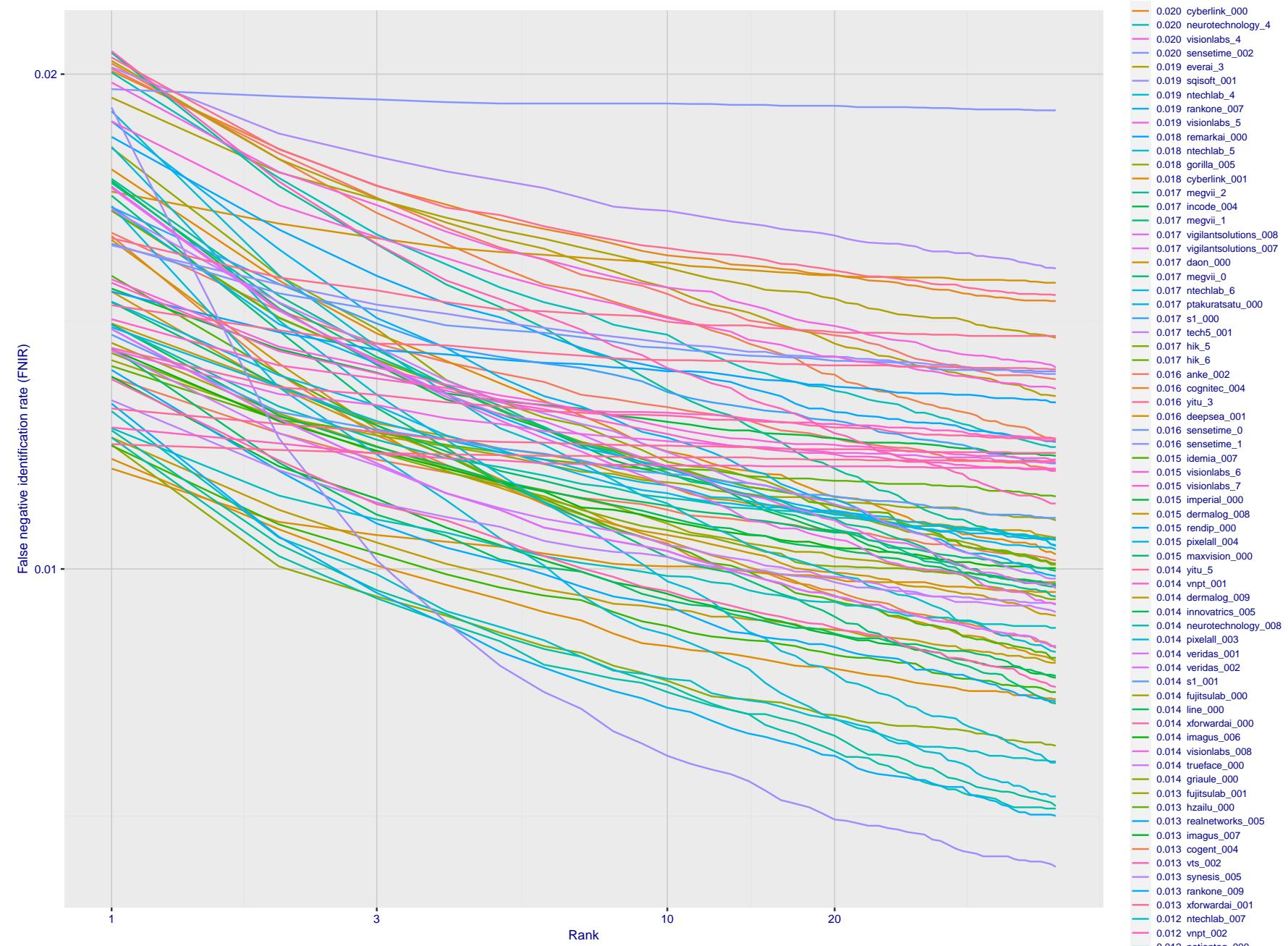


Figure 187: [Webcam Dataset] Identification miss rates vs. rank. The results apply to cross-domain recognition in which webcams are searched against enrolled mugshots. The FNIR values are higher than those for mugshot-mugshot identification due to low image resolution, lighting and less constrained subject pose in webcam images - see Figure 6.

2022/09/26

18:06:18

FNIR(N, R, T) = False neg. identification rate
FPTR(N, T) = False pos. identification rateN = Num. enrolled subjects
R = Num. candidates examinedT = Threshold
T = 0 → Investigation
T > 0 → Identification

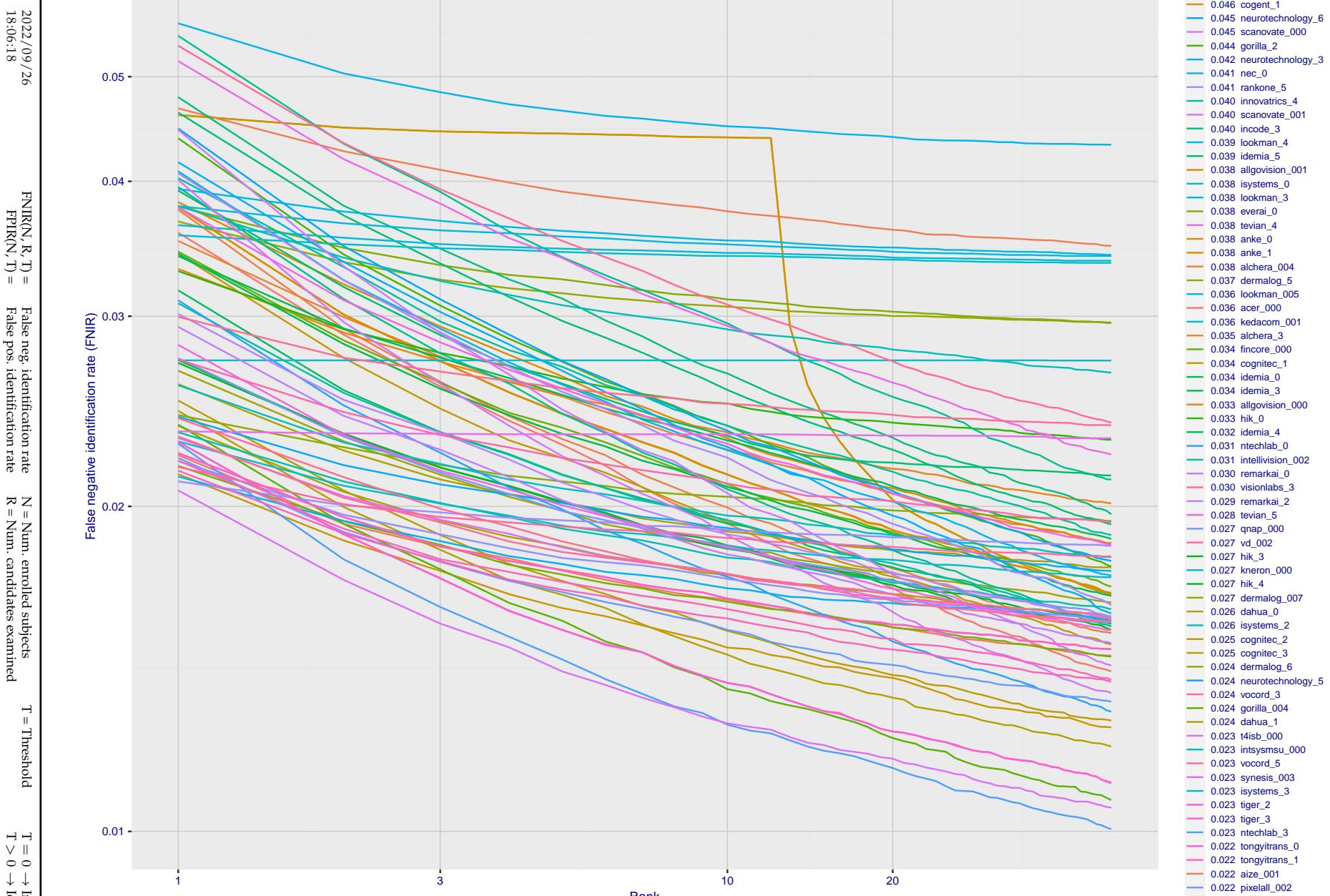


Figure 188: [Webcam Dataset] Identification miss rates vs. rank. The results apply to cross-domain recognition in which webcams are searched against enrolled mugshots. The FNIR values are higher than those for mugshot-mugshot identification due to low image resolution, lighting and less constrained subject pose in webcam images - see Figure 6.

2022/09/26

18:06:18

FNIR(N, R, T) = False neg. identification rate
FPIR(N, T) = False pos. identification rateN = Num. enrolled subjects
R = Num. candidates examined

T = Threshold

T = 0 → Investigation
T > 0 → Identification

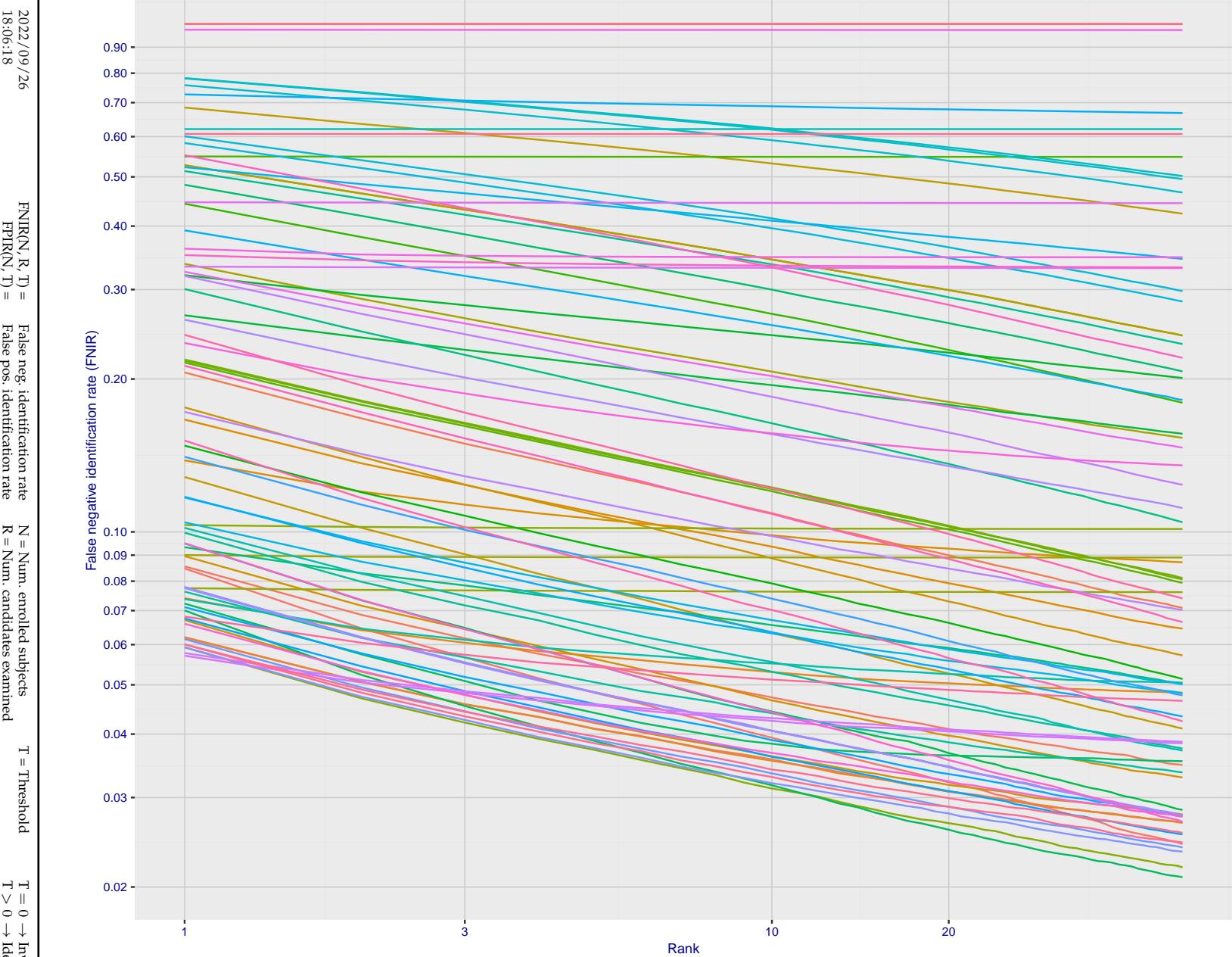


Figure 189: [Webcam Dataset] Identification miss rates vs. rank. The results apply to cross-domain recognition in which webcams are searched against enrolled mugshots. The FNIR values are higher than those for mugshot-mugshot identification due to low image resolution, lighting and less constrained subject pose in webcam images - see Figure 6.

2022/09/26 18:06:18	$FNIR(N, R, T) =$ $FPIR(N, T) =$	False neg. identification rate False pos. identification rate	$N =$ Num. enrolled subjects $R =$ Num. candidates examined	$T =$ Threshold $T > 0 \rightarrow$ Identification	$T = 0 \rightarrow$ Investigation
------------------------	-------------------------------------	--	--	---	-----------------------------------

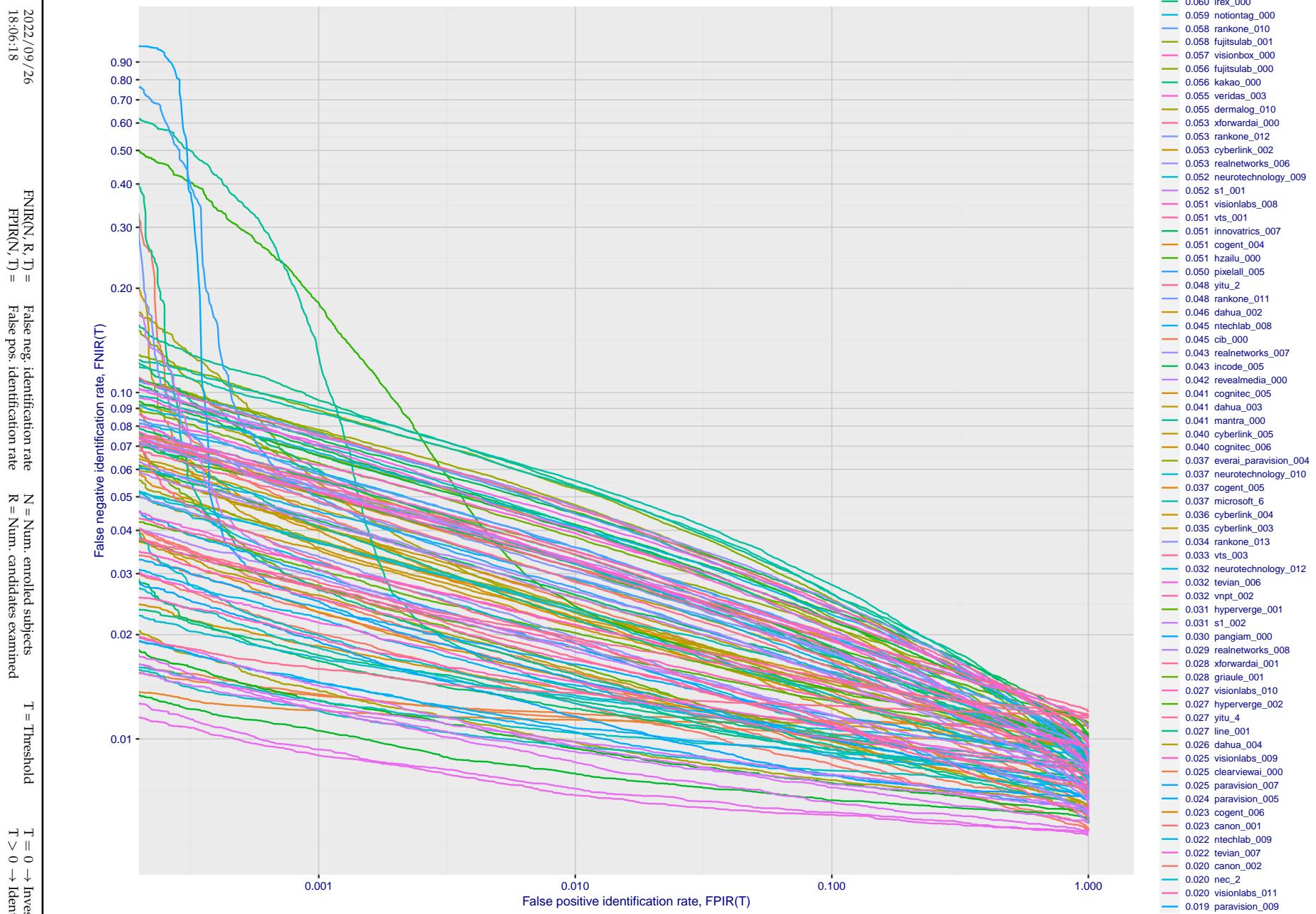


Figure 190: [Webcam Dataset] Identification miss rates vs. false positive rates. The results apply to cross-domain recognition in which webcams are searched against enrolled mugshots. The FNIR values are higher than those for mugshot-mugshot identification due to low image resolution, lighting and less constrained subject pose in webcam images - see Figure 6.

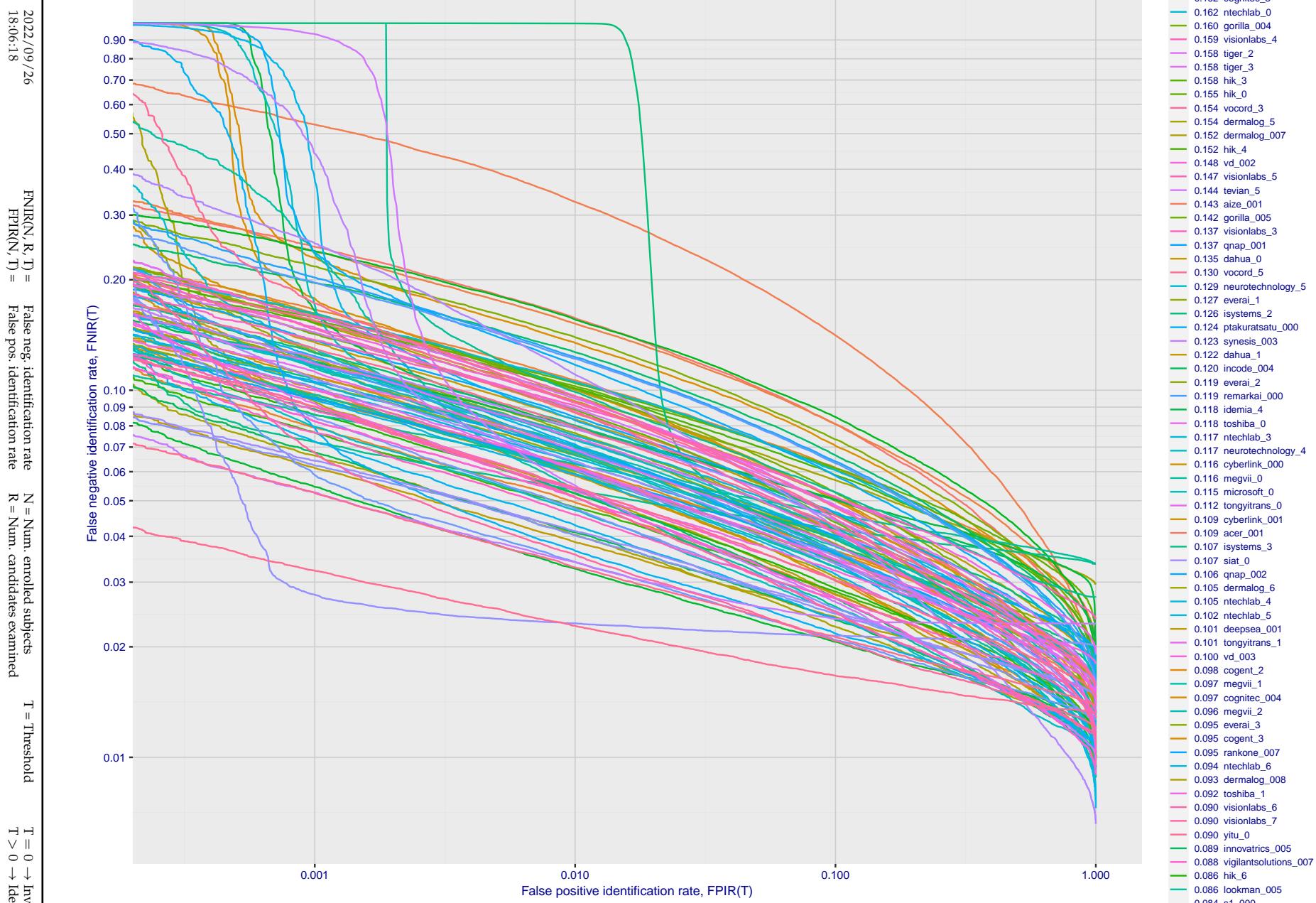


Figure 191: [Webcam Dataset] Identification miss rates vs. false positive rates. The results apply to cross-domain recognition in which webcams are searched against enrolled mugshots. The FNIR values are higher than those for mugshot-mugshot identification due to low image resolution, lighting and less constrained subject pose in webcam images - see Figure 6.

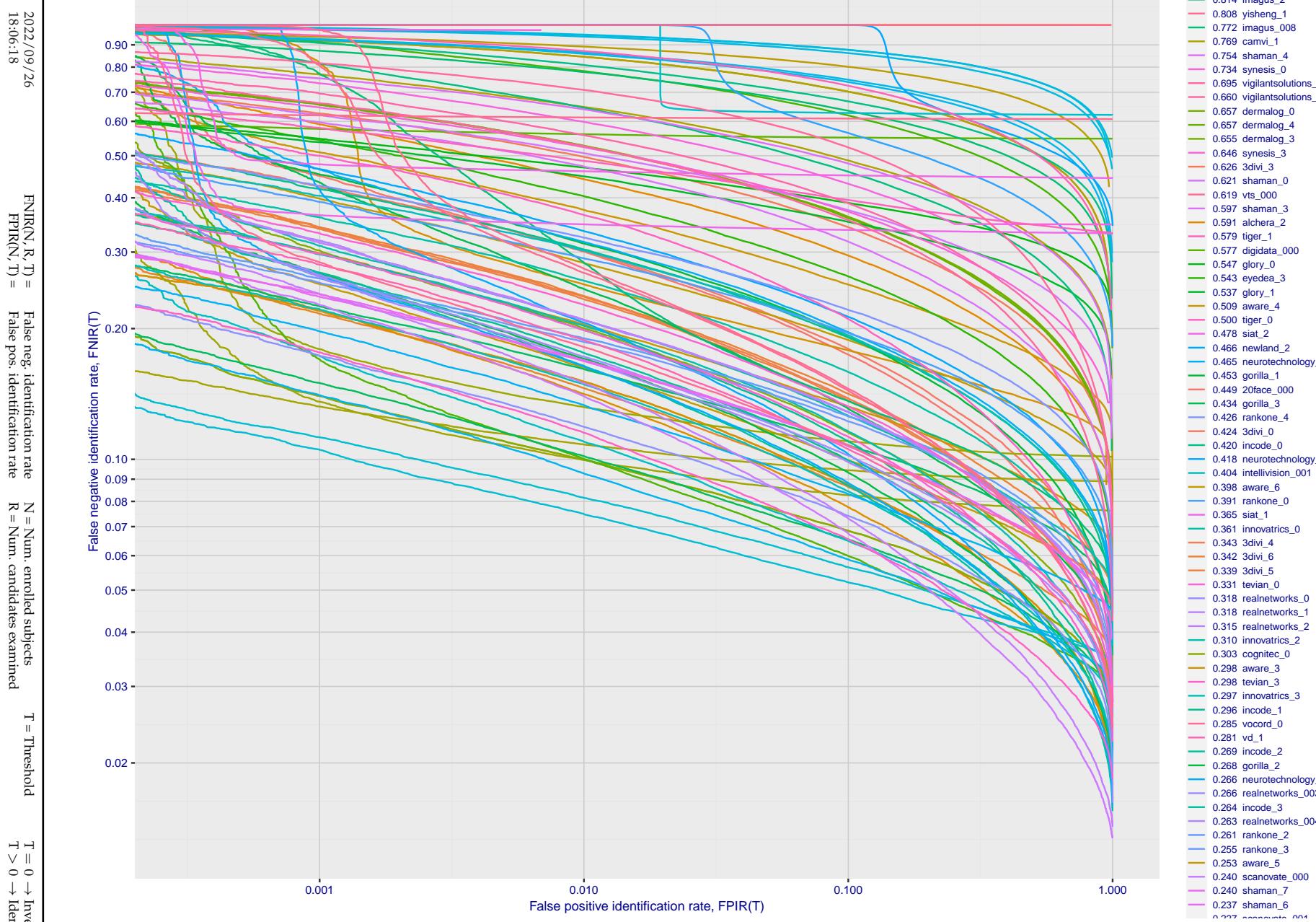


Figure 192: [Webcam Dataset] Identification miss rates vs. false positive rates. The results apply to cross-domain recognition in which webcams are searched against enrolled mugshots. The FNIR values are higher than those for mugshot-mugshot identification due to low image resolution, lighting and less constrained subject pose in webcam images - see Figure 6.

Appendix E Accuracy for profile-view to frontal recognition

Figures 193 - 195 gives accuracy results for searching 100 000 mated and 100 000 non-mated profile-view images against the same FRVT 2018 frontal enrollment dataset, $N = 1\,600\,000$, used in the main mugshot trials. This experiment corresponds to row-13 of Table 1. An example of profile-view image is given in Figure 7.

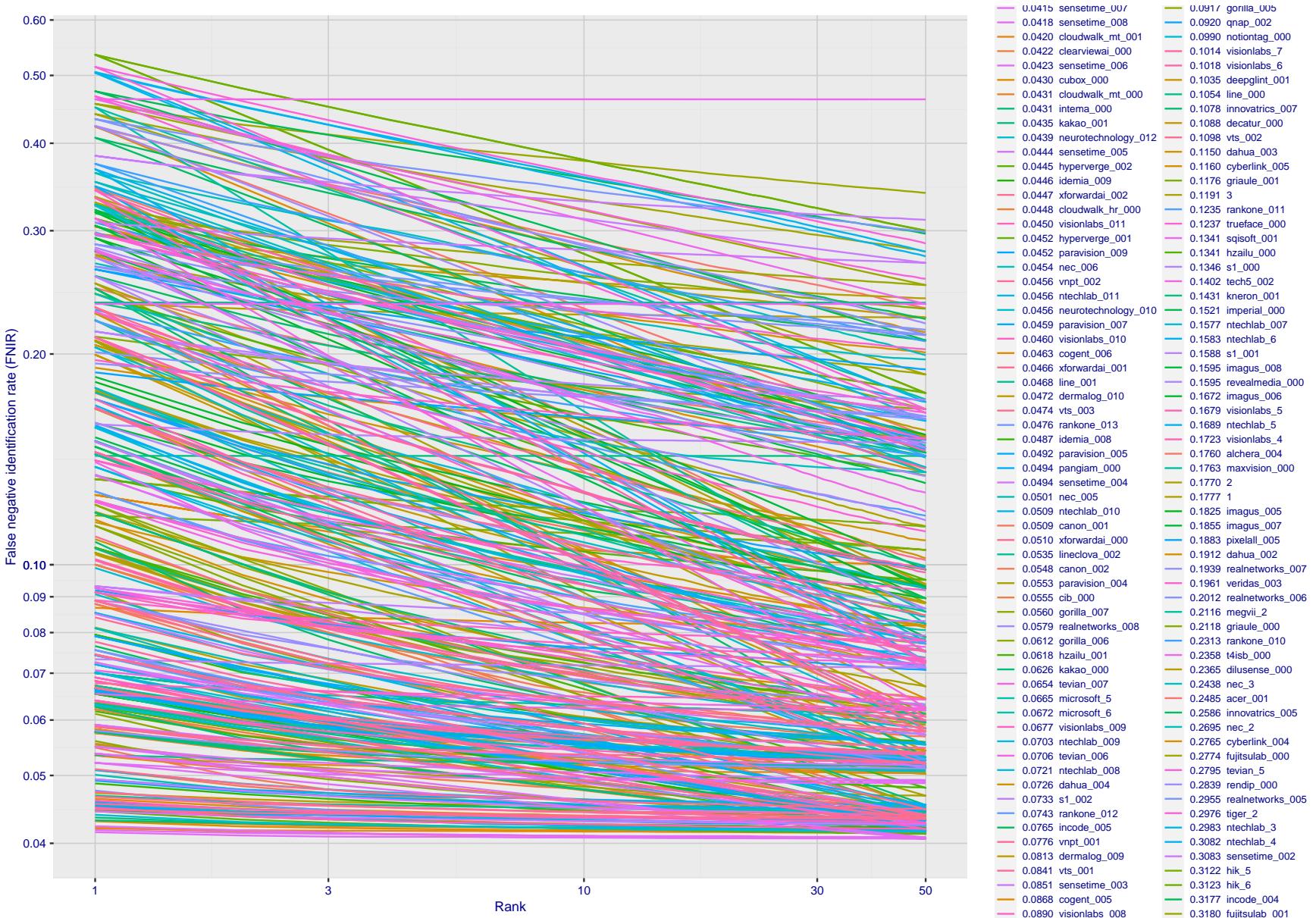
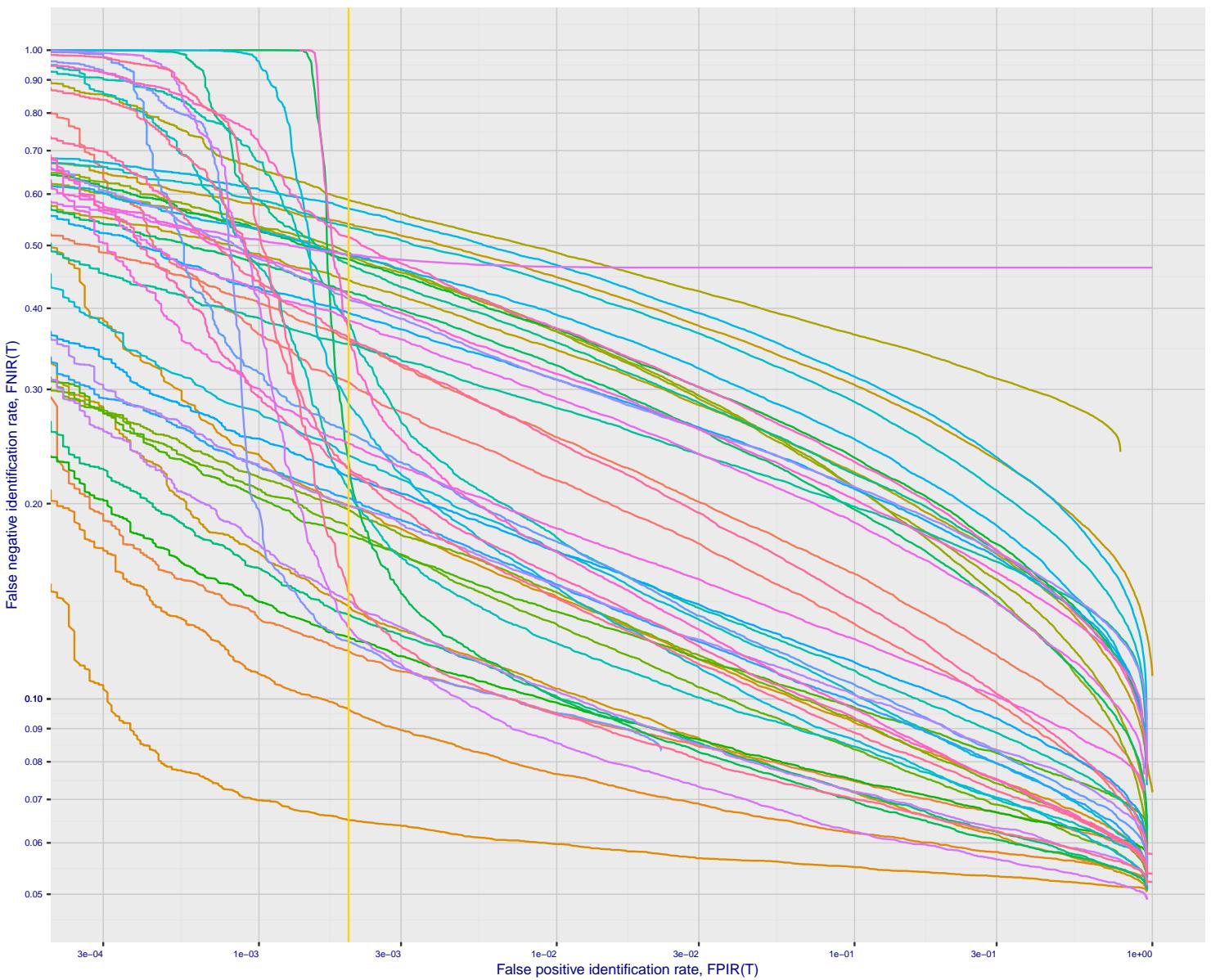


Figure 193: [Mugshot and profile-view dataset] Rank-based accuracy. For some of the more accurate Phase 3 algorithms the figure plots error tradeoff characteristics for frontal and profile-view searches into an enrolled set of $N = 1\,600\,000$ frontal images. Note that some algorithms fail on profile-view images with $\text{FNIR} \rightarrow 1$ - this evaluation did not ask developers to provide profile-view capability. Some algorithms, on the other hand, give FNIR approaching that for frontal-view searches using c. 2010 algorithms. The best result is that 91% of profile-view searches yield the correct mate at rank 1, and better than 94% in the top-50 candidates.

2022/09/26
18:06:18
 $\text{FNIR}(N, R, T) =$
False neg. identification rate
 $\text{FPIR}(N, T) =$
False pos. identification rate
 $N =$ Num. enrolled subjects
 $R =$ Num. candidates examined
 $T =$ Threshold
 $T = 0 \rightarrow$ Investigation
 $T > 0 \rightarrow$ Identification



Dataset: 2018 Mugshot–Profile
 $\text{FNIR} @ \text{FPIR} = 0.002$
 $N = 1600000$

- 0.0651 cloudwalk_mt_001
- 0.0963 cloudwalk_mt_000
- 0.1188 cloudwalk_hr_000
- 0.1226 s1_002
- 0.1247 idemia_009
- 0.1287 sensetime_008
- 0.1350 kakao_001
- 0.1390 cubox_000
- 0.1418 sensetime_005
- 0.1466 xforwardai_002
- 0.1786 idemia_008
- 0.1842 hyperverge_002
- 0.1957 hyperverge_001
- 0.1984 sensetime_004
- 0.1988 cogent_006
- 0.2039 ntechlab_011
- 0.2107 nec_006
- 0.2201 ntechlab_010
- 0.2265 vnppt_002
- 0.2271 xforwardai_001
- 0.2326 intema_000
- 0.2376 neurotechnology_010
- 0.2478 tevian_007
- 0.2579 pangiam_000
- 0.2854 neurotechnology_012
- 0.3078 canon_001
- 0.3523 microsoft_6
- 0.3560 canon_002
- 0.3596 xforwardai_000
- 0.3673 visionlabs_010
- 0.3810 nec_005
- 0.3829 tevian_006
- 0.3932 ntechlab_009
- 0.4137 sensetime_003
- 0.4184 visionlabs_008
- 0.4240 kakao_000
- 0.4420 dahua_004
- 0.4675 microsoft_5
- 0.4757 incode_005
- 0.4810 gorilla_006
- 0.4836 ntechlab_008
- 0.4844 t4ib_000
- 0.4880 gorilla_007
- 0.5150 vnppt_001
- 0.5339 neurotechnology_009
- 0.5396 dahua_003
- 0.5696 notiontag_000
- 0.5877 dilusense_000

Figure 194: [Mugshot and profile-view dataset] Threshold-based accuracy. For some of the more accurate Phase 3 algorithms the figure plots error tradeoff characteristics for frontal and profile-view searches into an enrolled set of $N = 1600000$ frontal images. Note that some algorithms fail on profile-view images with $\text{FNIR} \rightarrow 1$ - this evaluation did not ask developers to provide profile-view capability. Some algorithms, on the other hand, give FNIR approaching that for frontal-view searches using c. 2010 algorithms.

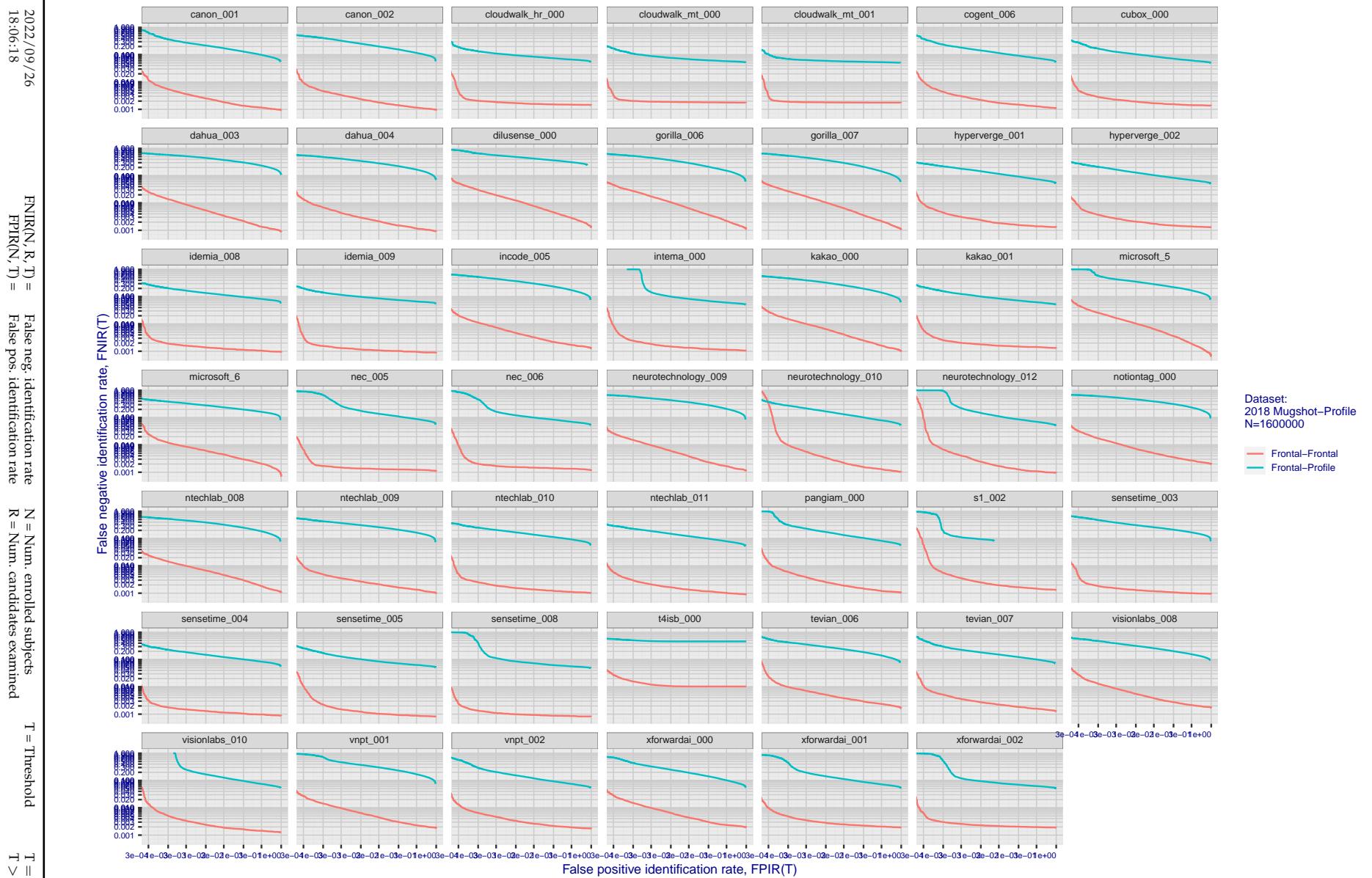


Figure 195: [Mugshot and profile-view dataset] Speed-accuracy tradeoff. For some of the more accurate Phase 3 algorithms the figure plots error tradeoff characteristics for frontal and profile-view searches into an enrolled set of $N = 1\,600\,000$ frontal images. Some algorithms fail on profile-view images with $\text{FNIR} \rightarrow 1$ - this evaluation did not ask developers to provide profile-view capability. Some algorithms, on the other hand, give FNIR approaching that for frontal-view searches using c. 2010 algorithms. Blue lines connect points of equal threshold from which it is evident that some algorithms would give markedly higher false positive outcomes if profile-view images were searched in a system configured for frontal searches. This would be a vulnerability in an access control system.

Appendix F Search duration

As in and prior tests, this section documents search speeds spanning three orders of magnitude. In applications where search volumes are high enough, this will have implications for hardware requirements especially for large N or when search duration is appreciably larger than the time it takes to prepare a template from the search image(s). Further, given very large (and growing) operational databases, the scalability of algorithms is important. It has been reported previously [8] that search duration can scale sublinearly with enrolled population size N. Further there has been considerable recent research on indexing, exact [13] and approximate nearest neighbor search [1,13] and fast-search [14,16].

Figure 196 charts the search duration measurements presented earlier in Tables 2 - 4.

- ▷ Most algorithms scale linearly. For those in that category, there is a wide range in speed with search durations ranging from 82 milliseconds for a 12 million gallery (for NEC-3) to more than 40 seconds (for Yitu-3, Toshiba-2) and even higher for less accurate algorithms.
- ▷ Some developers (Camvi, Dermalog, EverAI, Innovatrics, and Visionlabs) provide algorithms whose template search durations grow approximately logarithmically i.e. $T(N) \sim \log N$ with the constant a varying between implementations. In the figure this model is fit using the point $T(1) = 0$, and $T(640\,000)$. This very sublinear behaviour affords extremely fast search times in very large galleries. One caveat for the sublinear algorithms is that their fast-search data structures can require considerable computation time - on the order of hours - for N in the millions, and this scales mildly super-linearly, i.e. $O(N^b)$, $b > 1$. There are exceptions: the Camvi algorithms take minutes; and Innovatrics' scale sublinearly.

2022/09/26 18:06:18	$FNIR(N, R, T) =$ $FPIR(N, T) =$	False neg. identification rate False pos. identification rate	$N =$ Num. enrolled subjects $R =$ Num. candidates examined	$T =$ Threshold $T > 0 \rightarrow$ Identification	$T = 0 \rightarrow$ Investigation
------------------------	-------------------------------------	--	--	---	-----------------------------------

2022 / 09 / 26
18:06:18FNIR(N, R, T) = False neg. identification rate
FPIR(N, T) = False pos. identification rateN = Num. enrolled subjects
R = Num. candidates examined

T = Threshold

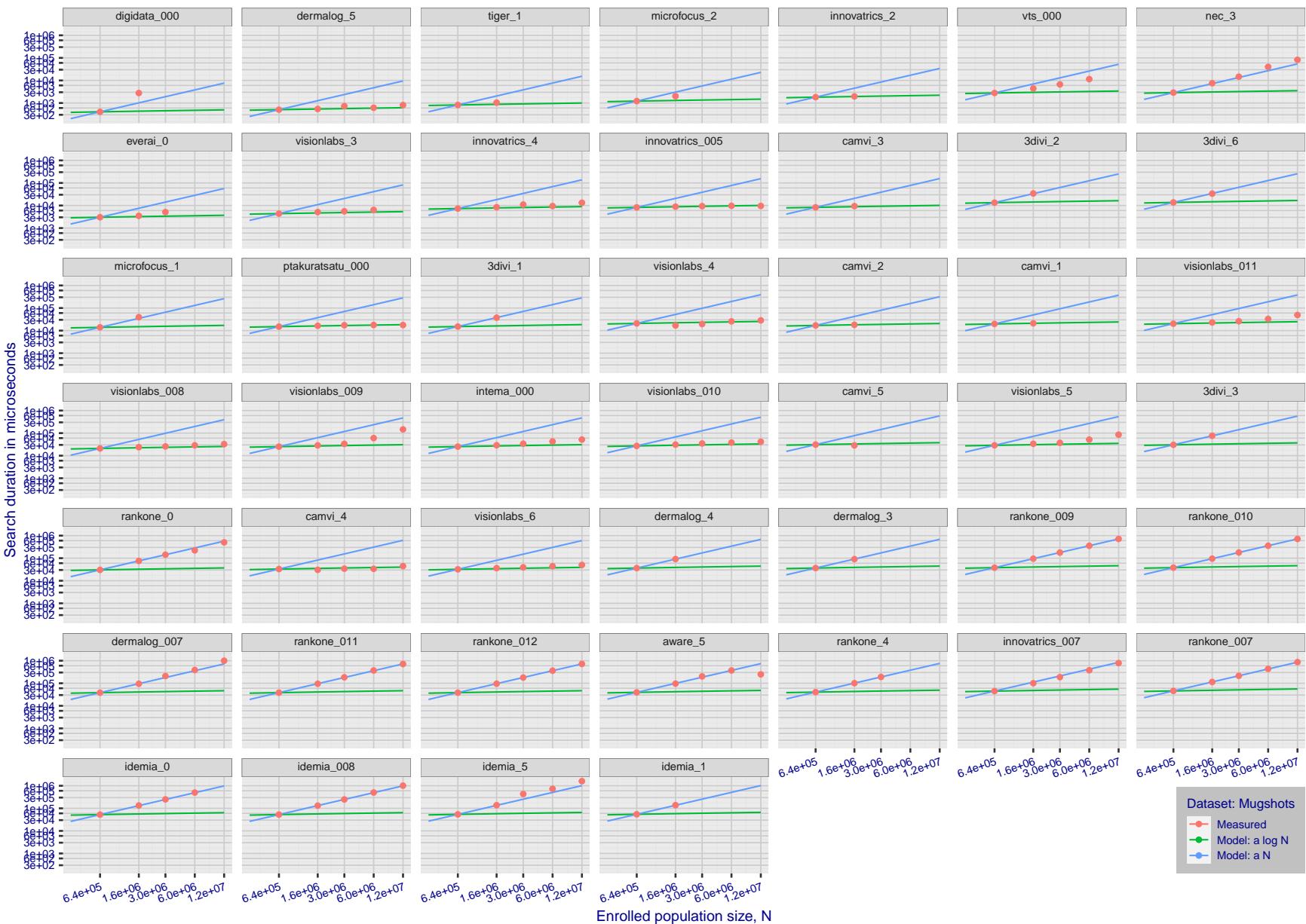
T = 0 → Investigation
 $T > 0 \rightarrow$ Identification

Figure 196: [Mugshot Dataset] Search duration vs. enrolled population size. In red are the actual point durations measured on a single c. 2016 core. The blue shows linear growth from $N = 640\,000$. The green line shows logarithmic growth from that point to $N = 1\,600\,000$. Note the sublinear growth from algorithms from Camvi, Dermalog, EverAI, Innovatrics, and Visionlabs. The tiger_1 algorithm is also sublinear, but inaccurate and inoperable at $N \geq 3000000$. This capability sometimes comes at the additional expense of converting a linear gallery data structure into whatever fast-search data structure is used. Note that search times are sometimes dominated by the template generation times shown in Table 25.

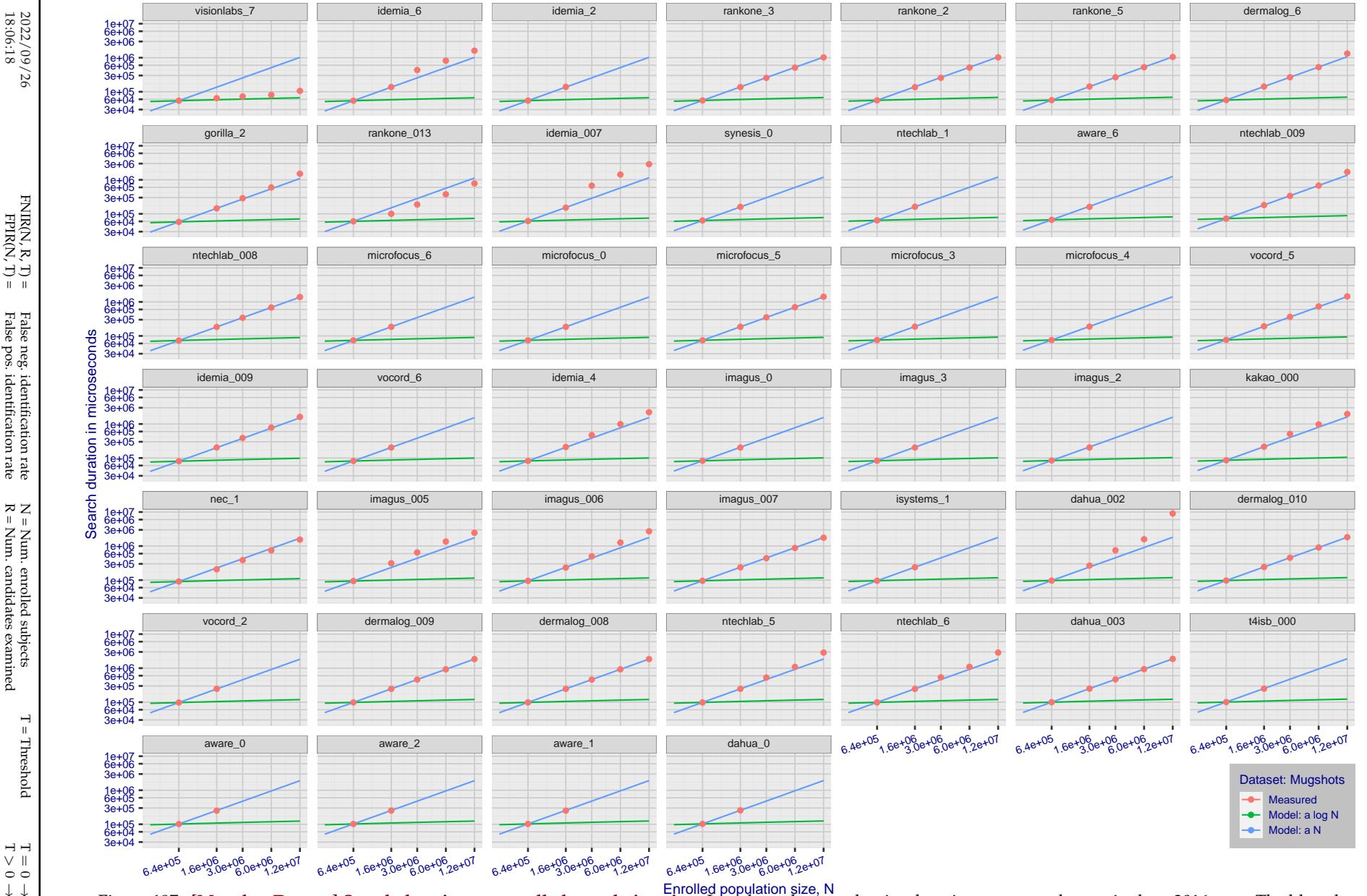


Figure 197: [Mugshot Dataset] Search duration vs. enrolled population size. In red are the actual point durations measured on a single c. 2016 core. The blue shows linear growth from $N = 640\,000$. The green line shows logarithmic growth from that point to $N = 1\,600\,000$. Note the sublinear growth from algorithms from Camvi, Dermalog, EverAI, Innovatrics, and Visionlabs. The tiger_1 algorithm is also sublinear, but inaccurate and inoperable at $N \geq 3000000$. This capability sometimes comes at the additional expense of converting a linear gallery data structure into whatever fast-search data structure is used. Note that search times are sometimes dominated by the template generation times shown in Table 25.

2022 / 09 / 26
18:06:18FNIR(N, R, T) = False neg. identification rate
FPFR(N, T) = False pos. identification rateN = Num. enrolled subjects
R = Num. candidates examined

T = Threshold

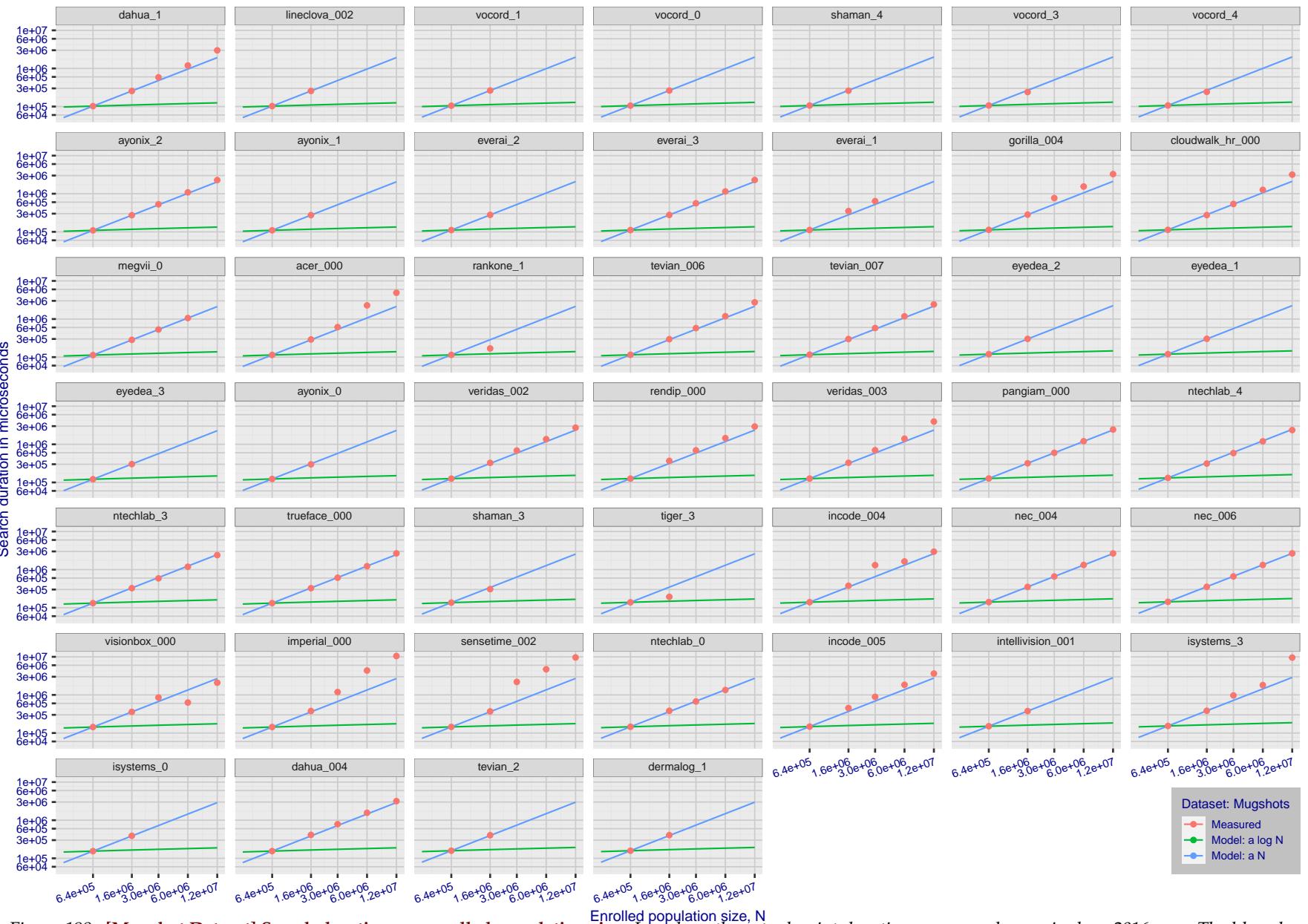
T = 0 → Investigation
 $T > 0 \rightarrow$ Identification

Figure 198: [Mugshot Dataset] Search duration vs. enrolled population size. In red are the actual point durations measured on a single c. 2016 core. The blue shows linear growth from $N = 640\,000$. The green line shows logarithmic growth from that point to $N = 1\,600\,000$. Note the sublinear growth from algorithms from Camvi, Dermalog, EverAI, Innovatrics, and Visionlabs. The tiger_1 algorithm is also sublinear, but inaccurate and inoperable at $N \geq 3000000$. This capability sometimes comes at the additional expense of converting a linear gallery data structure into whatever fast-search data structure is used. Note that search times are sometimes dominated by the template generation times shown in Table 25.

2022 / 09 / 26
18:06:18FNIR(N, R, T) = False neg. identification rate
FPFR(N, T) = False pos. identification rateN = Num. enrolled subjects
R = Num. candidates examined

T = Threshold

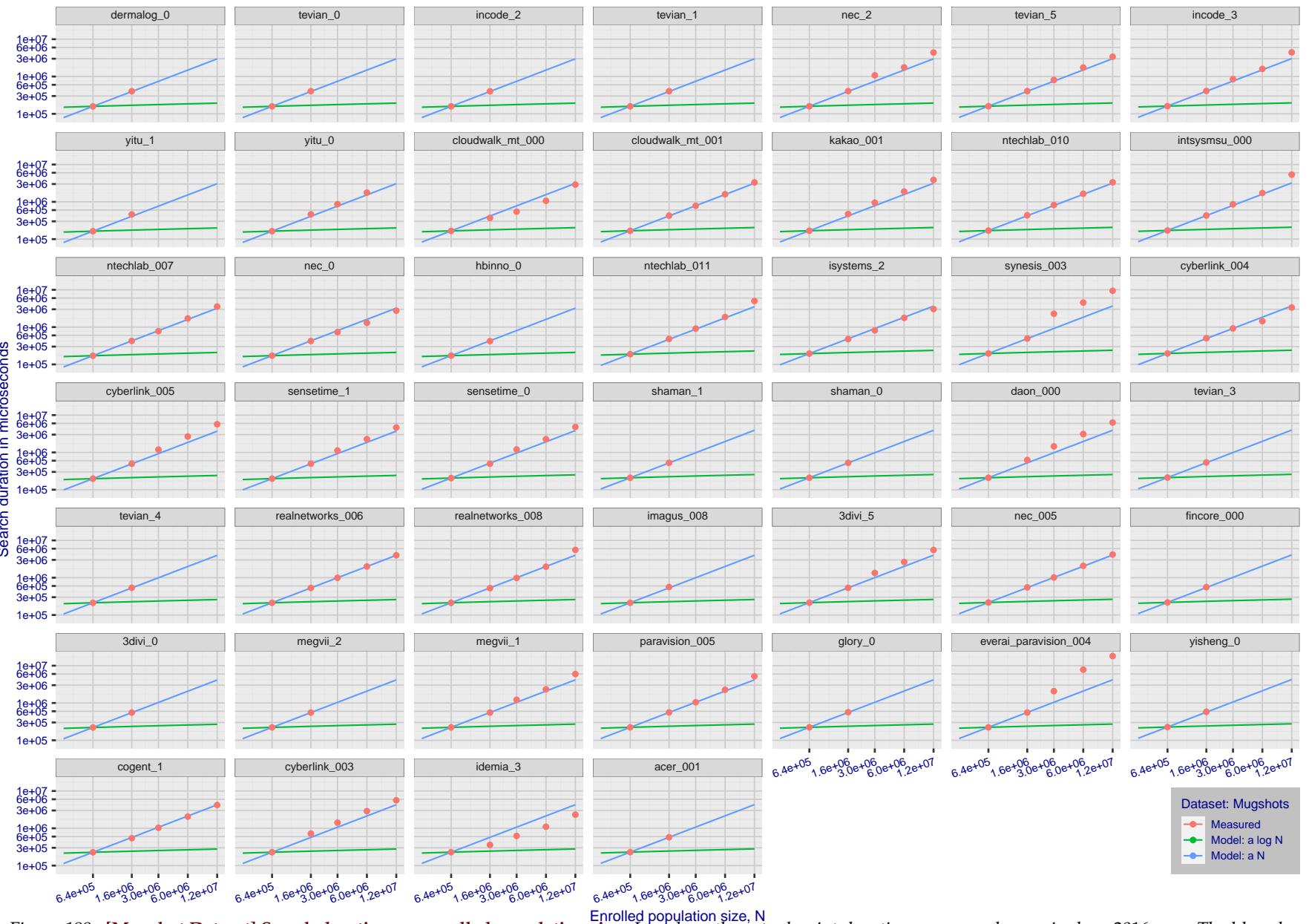
T = 0 → Investigation
 $T > 0 \rightarrow$ Identification

Figure 199: [Mugshot Dataset] Search duration vs. enrolled population size. In red are the actual point durations measured on a single c. 2016 core. The blue shows linear growth from $N = 640\,000$. The green line shows logarithmic growth from that point to $N = 1\,600\,000$. Note the sublinear growth from algorithms from Camvi, Dermalog, EverAI, Innovatrics, and Visionlabs. The tiger_1 algorithm is also sublinear, but inaccurate and inoperable at $N \geq 3000000$. This capability sometimes comes at the additional expense of converting a linear gallery data structure into whatever fast-search data structure is used. Note that search times are sometimes dominated by the template generation times shown in Table 25.

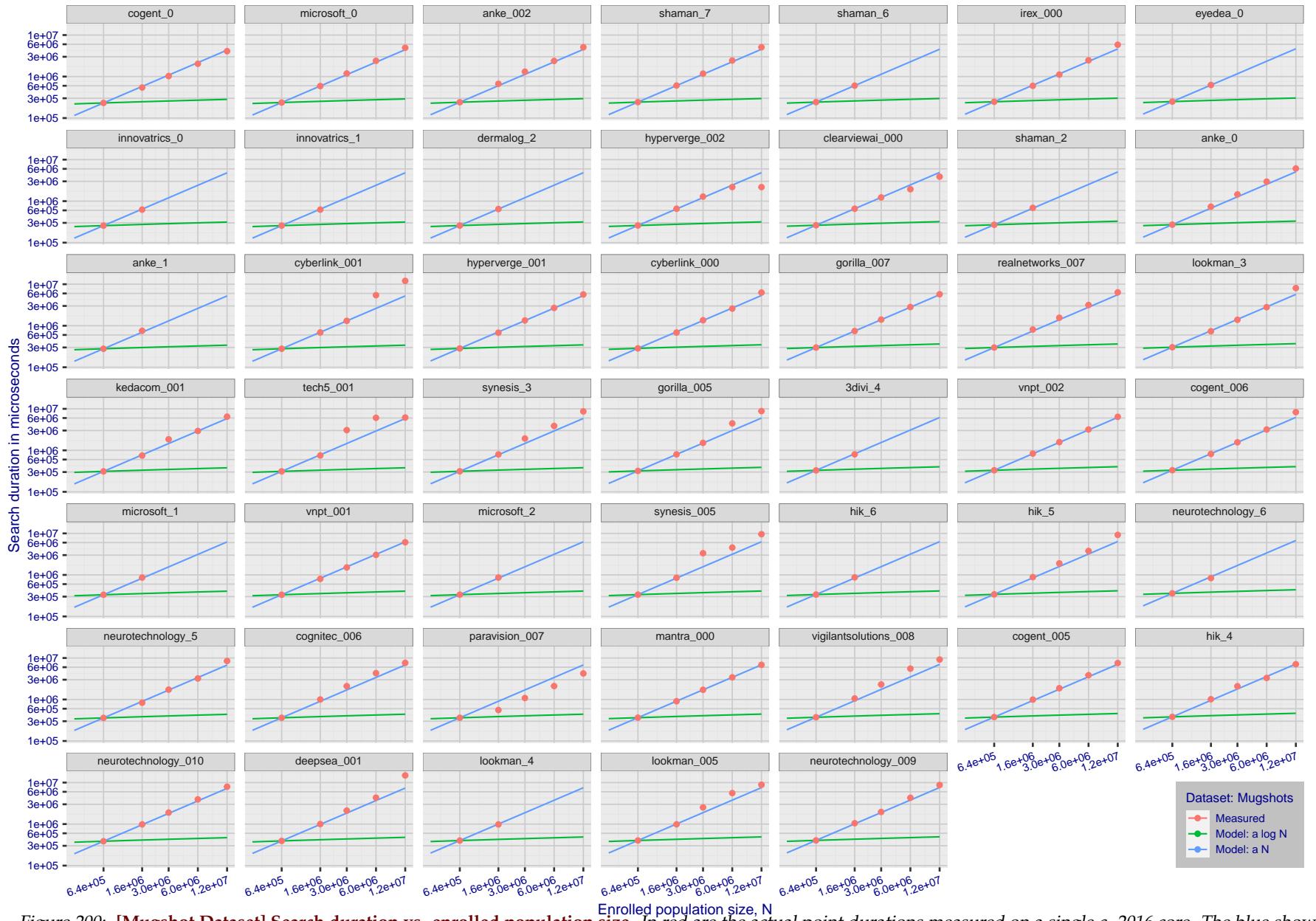


Figure 200: [Mugshot Dataset] Search duration vs. enrolled population size. In red are the actual point durations measured on a single c. 2016 core. The blue shows linear growth from $N = 640\,000$. The green line shows logarithmic growth from that point to $N = 1\,600\,000$. Note the sublinear growth from algorithms from Camvi, Dermalog, EverAI, Innovatrics, and Visionlabs. The tiger_1 algorithm is also sublinear, but inaccurate and inoperable at $N \geq 3000000$. This capability sometimes comes at the additional expense of converting a linear gallery data structure into whatever fast-search data structure is used. Note that search times are sometimes dominated by the template generation times shown in Table 25.

2022 / 09 / 26
18:06:18FNIR(N, R, T) = False neg. identification rate
FPIR(N, T) = False pos. identification rateN = Num. enrolled subjects
R = Num. candidates examined

T = Threshold

T = 0 → Investigation
 $T > 0 \rightarrow$ Identification

2022 / 09 / 26
18:06:18FNIR(N, R, T) = False neg. identification rate
FPIR(N, T) = False pos. identification rateN = Num. enrolled subjects
R = Num. candidates examined

T = Threshold

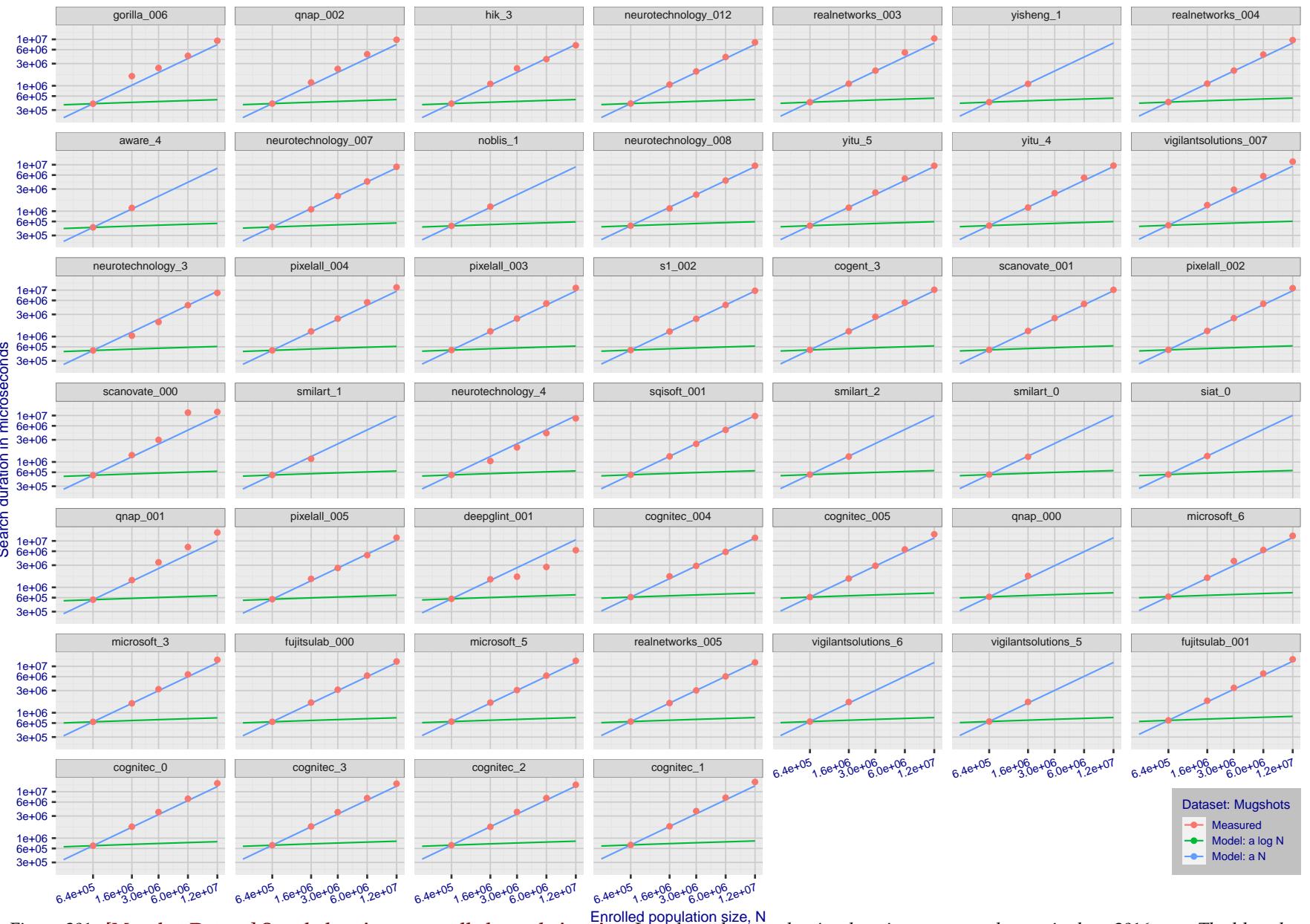
T = 0 → Investigation
 $T > 0 \rightarrow$ Identification

Figure 201: [Mugshot Dataset] Search duration vs. enrolled population size. In red are the actual point durations measured on a single c. 2016 core. The blue shows linear growth from $N = 640\,000$. The green line shows logarithmic growth from that point to $N = 1\,600\,000$. Note the sublinear growth from algorithms from Camvi, Dermalog, EverAI, Innovatrics, and Visionlabs. The tiger_1 algorithm is also sublinear, but inaccurate and inoperable at $N \geq 3000000$. This capability sometimes comes at the additional expense of converting a linear gallery data structure into whatever fast-search data structure is used. Note that search times are sometimes dominated by the template generation times shown in Table 25.

2022 / 09 / 26
18:06:18FNIR(N, R, T) = False neg. identification rate
FPIR(N, T) = False pos. identification rateN = Num. enrolled subjects
R = Num. candidates examined

T = Threshold

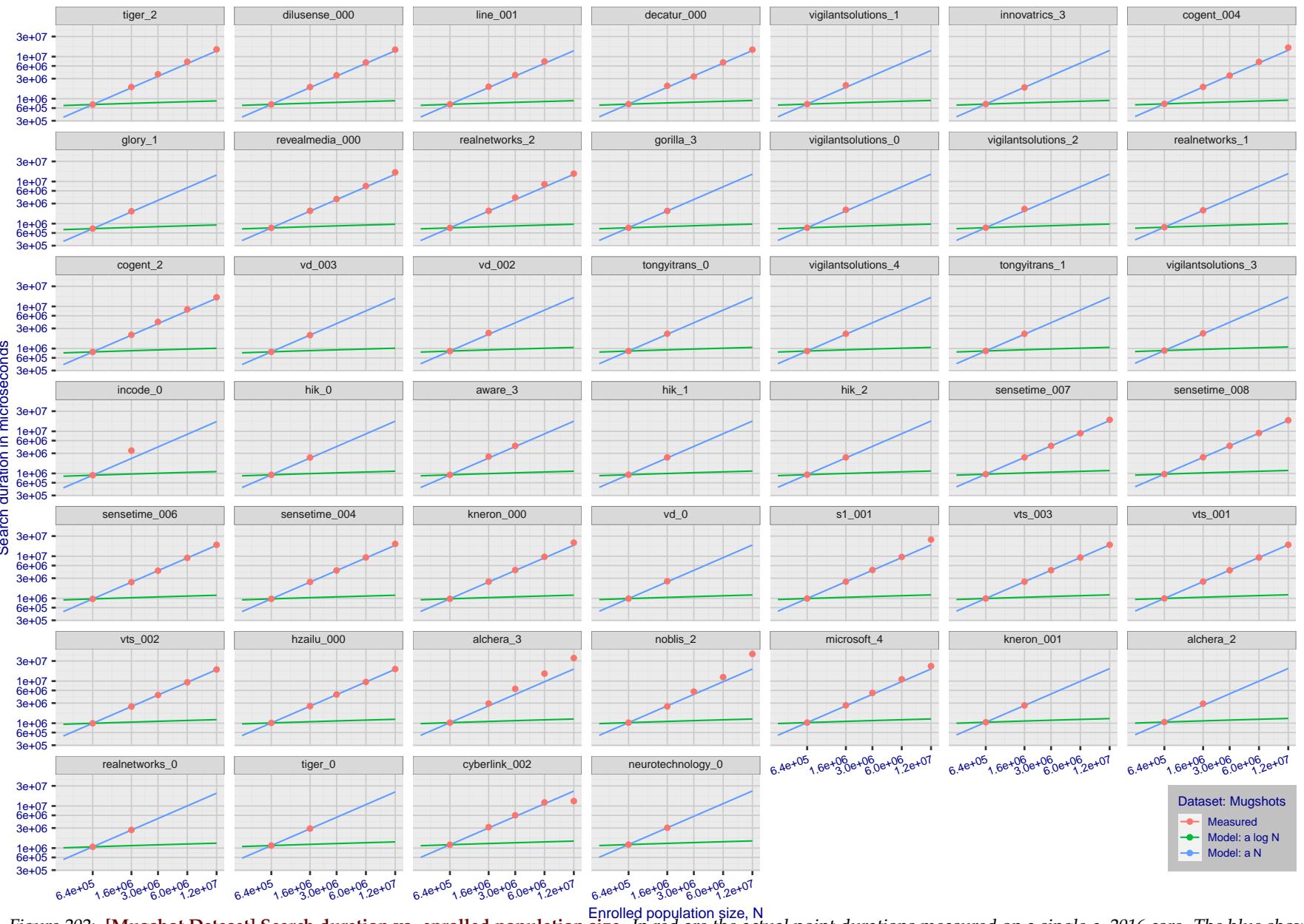
T = 0 → Investigation
T > 0 → Identification

Figure 202: [Mugshot Dataset] Search duration vs. enrolled population size. In red are the actual point durations measured on a single c. 2016 core. The blue shows linear growth from $N = 640\,000$. The green line shows logarithmic growth from that point to $N = 1\,600\,000$. Note the sublinear growth from algorithms from Camvi, Dermalog, EverAI, Innovatrics, and Visionlabs. The tiger_1 algorithm is also sublinear, but inaccurate and inoperable at $N \geq 3000000$. This capability sometimes comes at the additional expense of converting a linear gallery data structure into whatever fast-search data structure is used. Note that search times are sometimes dominated by the template generation times shown in Table 25.

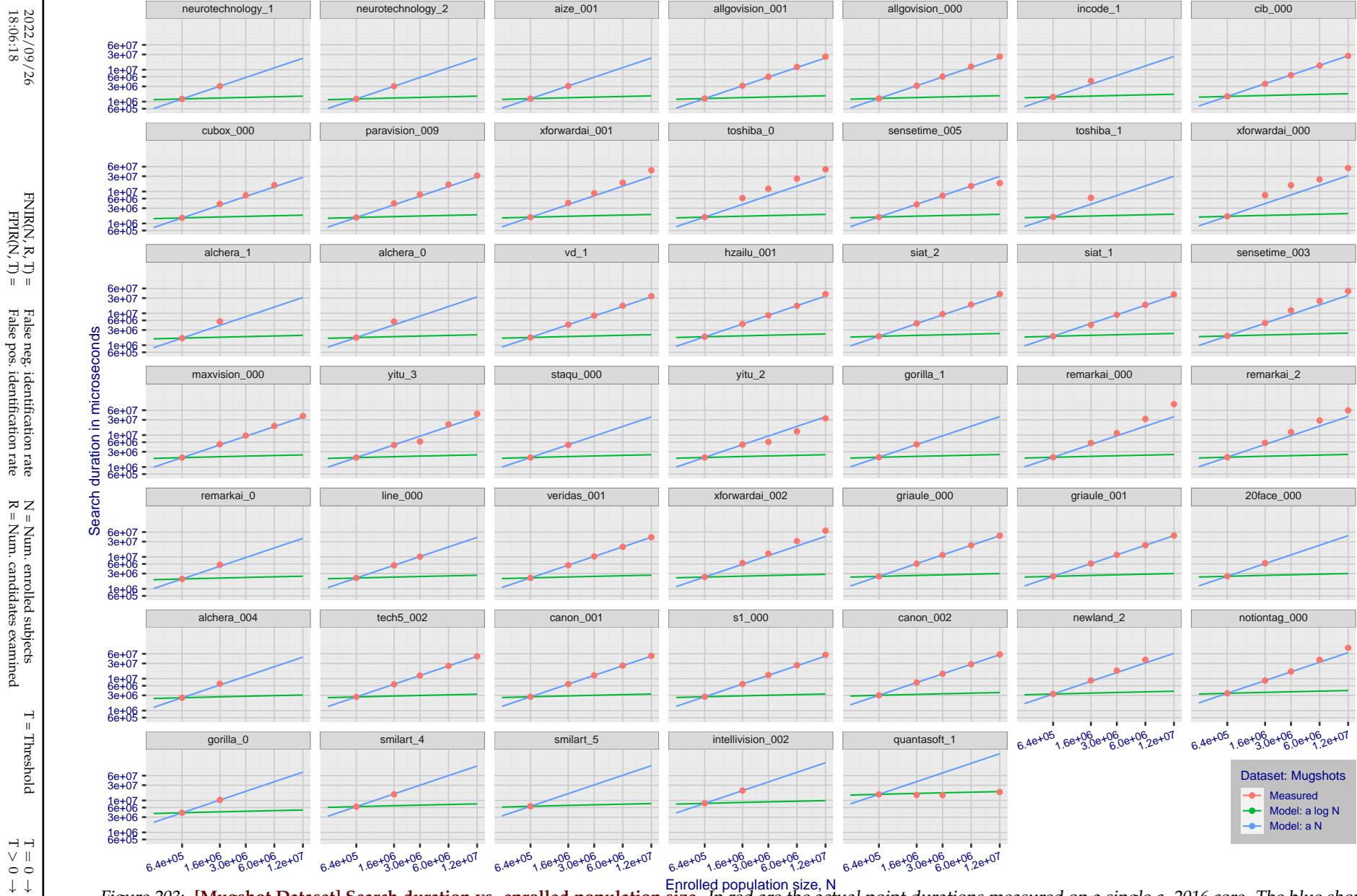


Figure 203: [Mugshot Dataset] Search duration vs. enrolled population size. In red are the actual point durations measured on a single c. 2016 core. The blue shows linear growth from $N = 640\,000$. The green line shows logarithmic growth from that point to $N = 1\,600\,000$. Note the sublinear growth from algorithms from Camvi, Dermalog, EverAI, Innovatrics, and Visionlabs. The tiger_1 algorithm is also sublinear, but inaccurate and inoperable at $N \geq 3000000$. This capability sometimes comes at the additional expense of converting a linear gallery data structure into whatever fast-search data structure is used. Note that search times are sometimes dominated by the template generation times shown in Table 25.

Appendix G Gallery Insertion Timing

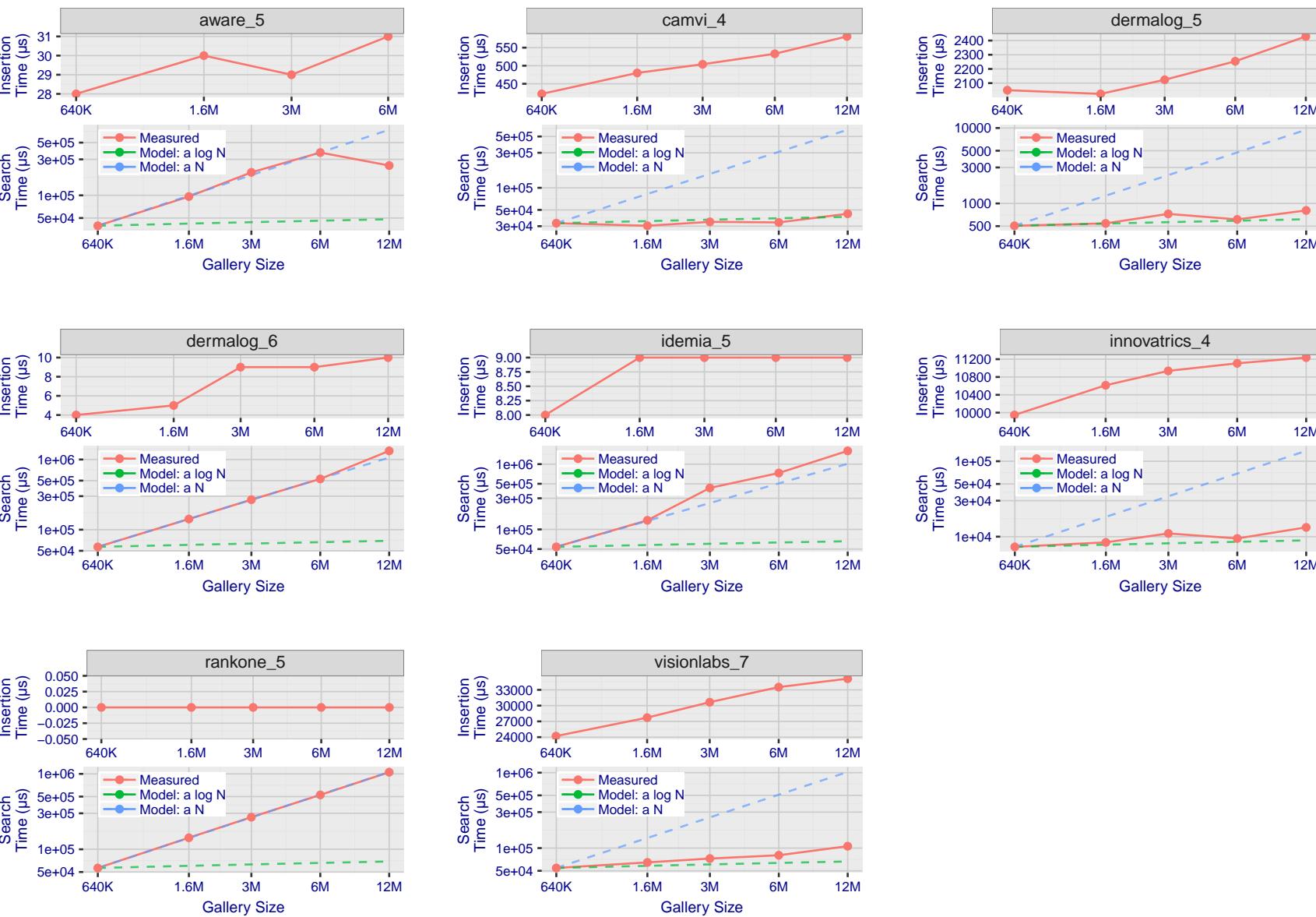
2022/09/26
18:06:18FNIR(N, R, T) = False neg. identification rate
FPIR(N, T) = False pos. identification rateN = Num. enrolled subjects
R = Num. candidates examinedT = Threshold
T = 0 → Investigation
T > 0 → Identification

Figure 204: [Mugshot Dataset] Gallery insertion duration vs. enrolled population size. This chart plots the time it takes to insert a single template into a finalized gallery, illustrated over increasing gallery sizes. For reference, search times on finalized galleries of corresponding sizes are plotted right underneath. Gallery insertion time plots were generated on algorithms that 1) successfully implemented gallery insertion with no errors and 2) that were run on galleries with N up to 12 000 000. Generally, only the more accurate algorithms were run on galleries with N up to 12 000 000.

2022 / 09 / 26
18:06:18FNIR(N, R, T) = False neg. identification rate
FPFR(N, T) = False pos. identification rateN = Num. enrolled subjects
R = Num. candidates examinedT = Threshold
T = 0 → Investigation

T > 0 → Identification

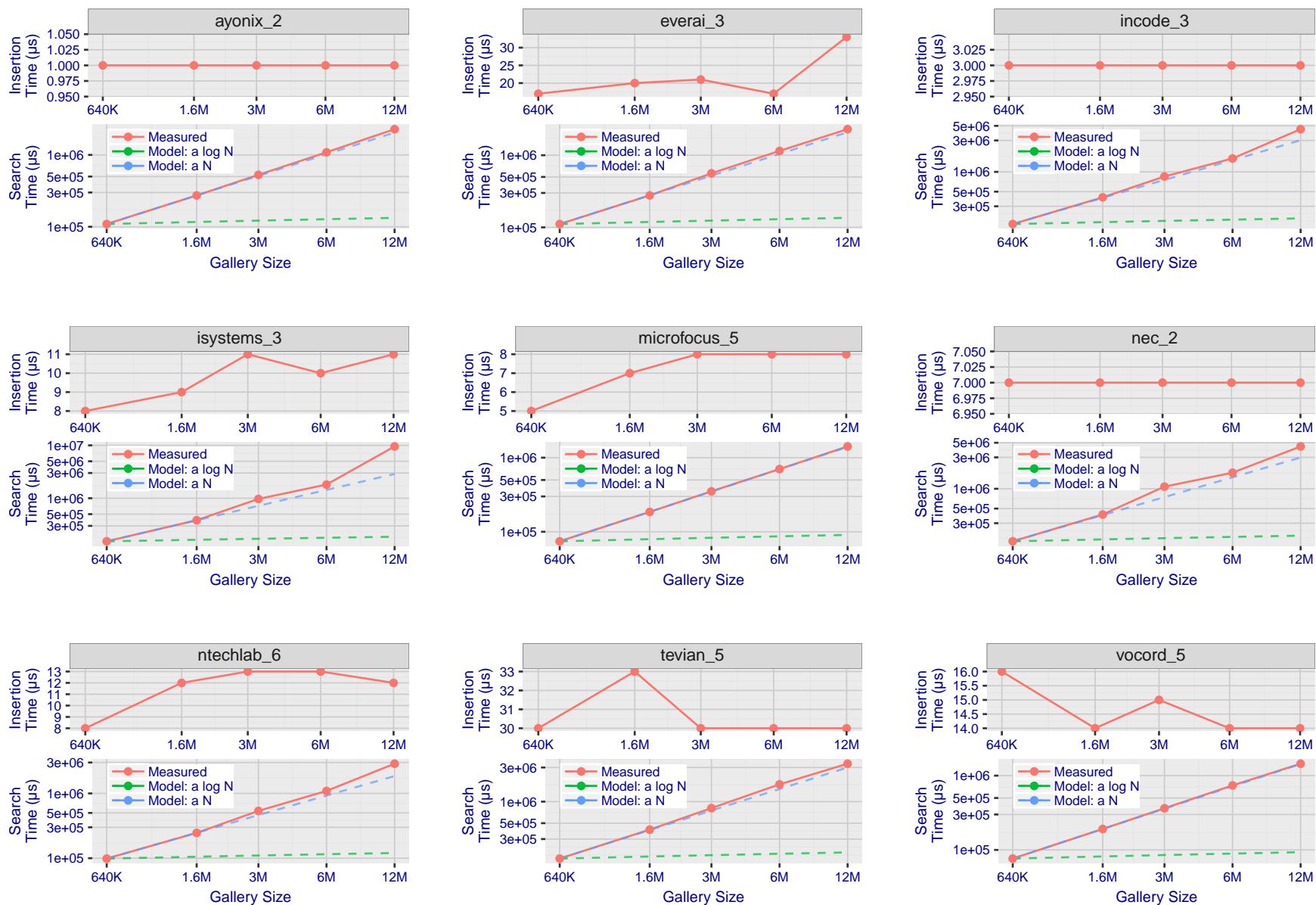


Figure 205: [Mugshot Dataset] Gallery insertion duration vs. enrolled population size. This chart plots the time it takes to insert a single template into a finalized gallery, illustrated over increasing gallery sizes. For reference, search times on finalized galleries of corresponding sizes are plotted right underneath. Gallery insertion time plots were generated on algorithms that 1) successfully implemented gallery insertion with no errors and 2) that were run on galleries with N up to 12 000 000. Generally, only the more accurate algorithms were run on galleries with N up to 12 000 000.

2022 / 09 / 26
18:06:18FNIR(N, R, T) = False neg. identification rate
FPIR(N, T) = False pos. identification rateN = Num. enrolled subjects
R = Num. candidates examined

T = Threshold

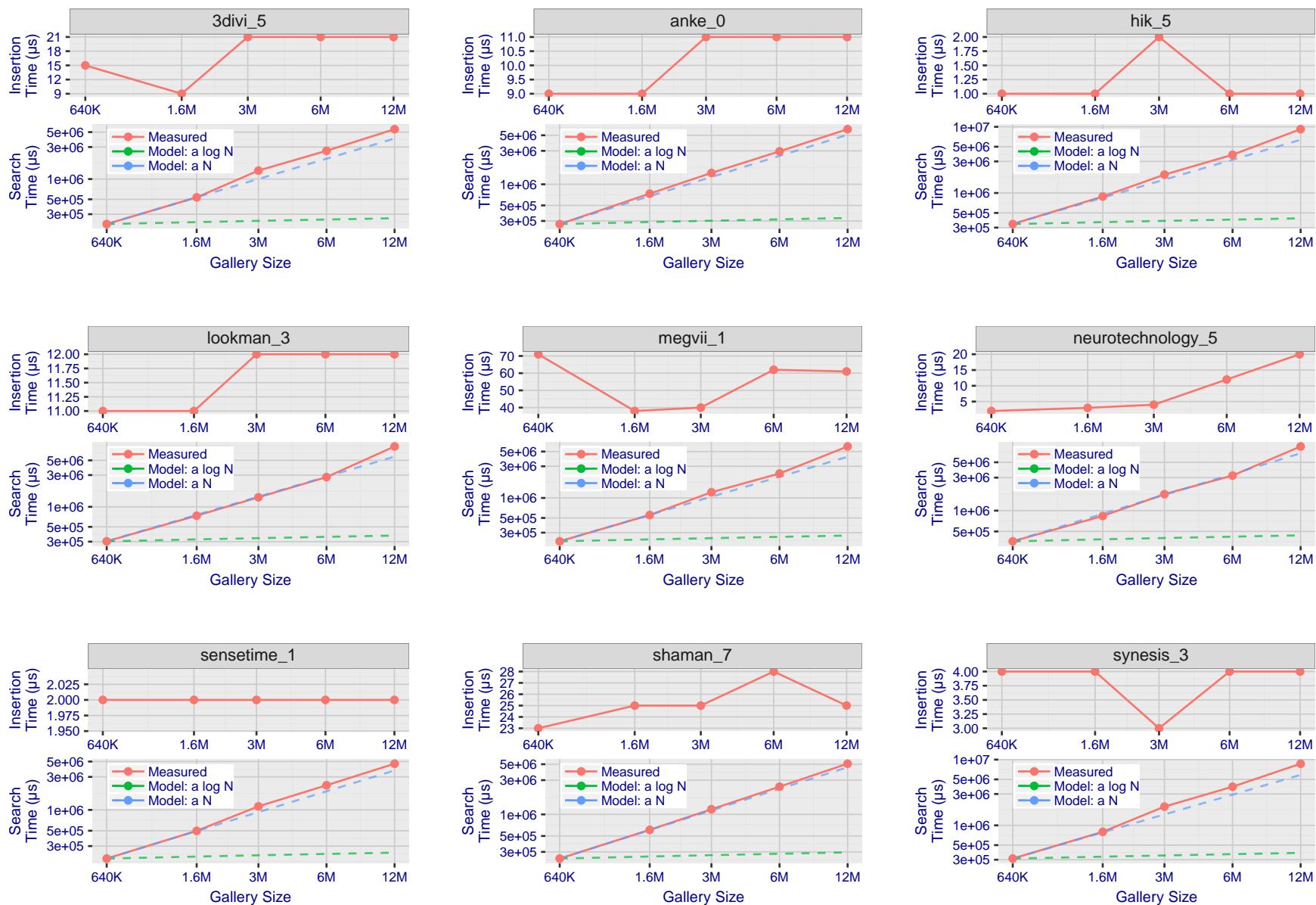
T = 0 → Investigation
 $T > 0 \rightarrow$ Identification

Figure 206: [Mugshot Dataset] Gallery insertion duration vs. enrolled population size. This chart plots the time it takes to insert a single template into a finalized gallery, illustrated over increasing gallery sizes. For reference, search times on finalized galleries of corresponding sizes are plotted right underneath. Gallery insertion time plots were generated on algorithms that 1) successfully implemented gallery insertion with no errors and 2) that were run on galleries with N up to 12 000 000. Generally, only the more accurate algorithms were run on galleries with N up to 12 000 000.

2022 / 09 / 26
18:06:18FNIR(N, R, T) = False neg. identification rate
FPTR(N, T) = False pos. identification rateN = Num. enrolled subjects
R = Num. candidates examinedT = Threshold
T = 0 → Investigation

T > 0 → Identification

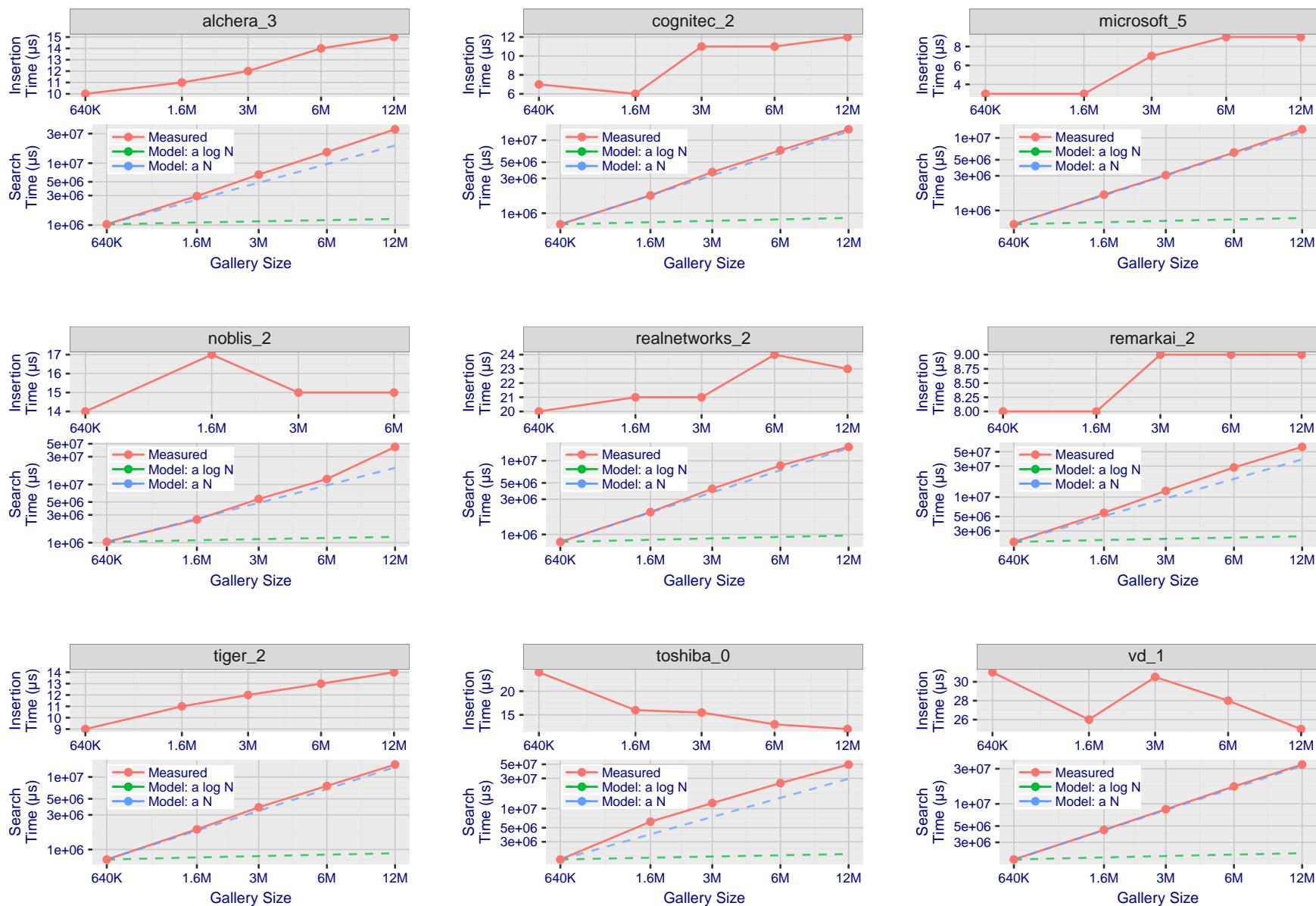


Figure 207: [Mugshot Dataset] Gallery insertion duration vs. enrolled population size. This chart plots the time it takes to insert a single template into a finalized gallery, illustrated over increasing gallery sizes. For reference, search times on finalized galleries of corresponding sizes are plotted right underneath. Gallery insertion time plots were generated on algorithms that 1) successfully implemented gallery insertion with no errors and 2) that were run on galleries with N up to 12 000 000. Generally, only the more accurate algorithms were run on galleries with N up to 12 000 000.

References

- [1] Artem Babenko and Victor Lempitsky. Efficient indexing of billion-scale datasets of deep descriptors. In *The IEEE Conference on Computer Vision and Pattern Recognition (CVPR)*, June 2016.
- [2] L. Best-Rowden and A. K. Jain. Longitudinal study of automatic face recognition. *IEEE Transactions on Pattern Analysis and Machine Intelligence*, 40(1):148–162, Jan 2018.
- [3] Blumstein, Cohen, Roth, and Visher, editors. *Random parameter stochastic models of criminal careers*. National Academy of Sciences Press, 1986.
- [4] Thomas P. Bonczar and Lauren E. Glaze. Probation and parole in the united statesm 2007, statistical tables. Technical report, Bureau of Justice Statistics, December 2008.
- [5] White D., Kemp R. I., Jenkins R., Matheson M, and Burton A. M. Passport officers' errors in face matching. *PLoS ONE*, 9(8), 2014. e103510. doi:10.1371/journal.pone.0103510.
- [6] P. Grother, G. W. Quinn, and P. J. Phillips. Evaluation of 2d still-image face recognition algorithms. NIST Interagency Report 7709, National Institute of Standards and Technology, 8 2010. <http://face.nist.gov/mbe> as MBE2010 FRVT2010.
- [7] P. J. Grother, R. J. Micheals, and P. J. Phillips. Performance metrics for the frvt 2002 evaluation. In *Proceedings of Audio and Video Based Person Authentication Conference (AVBPA)*, June 2003.
- [8] Patrick Grother and Mei Ngan. Interagency report 8009, performance of face identification algorithms. *Face Recognition Vendor Test (FRVT)*, May 2014.
- [9] Patrick Grother, George Quinn, and Mei Ngan. Face in video evaluation (five) face recognition of non-cooperative subjects. Interagency Report 8173, National Institute of Standards and Technology, March 2017. <https://doi.org/10.6028/NIST.IR.8173>.
- [10] Patrick Grother, George W. Quinn, and Mei Ngan. Face recognition vendor test - still face image and video concept, evaluation plan and api. Technical report, National Institute of Standards and Technology, 7 2013. http://biometrics.nist.gov/cs.links/face/frvt/frvt2012/NIST_FRVT2012.api_Aug15.pdf.
- [11] K. He, X. Zhang, S. Ren, and J. Sun. Deep residual learning for image recognition. In *2016 IEEE Conference on Computer Vision and Pattern Recognition (CVPR)*, pages 770–778, June 2016.
- [12] Gary B. Huang, Manu Ramesh, Tamara Berg, and Erik Learned-Miller. Labeled faces in the wild: A database for studying face recognition in unconstrained environments. Technical Report 07-49, University of Massachusetts, Amherst, October 2007.
- [13] Masato Ishii, Hitoshi Imaoka, and Atsushi Sato. Fast k-nearest neighbor search for face identification using bounds of residual score. In *2017 12th IEEE International Conference on Automatic Face & Gesture Recognition (FG 2017)*, pages 194–199, Los Alamitos, CA, USA, May 2017. IEEE Computer Society.
- [14] Jeff Johnson, Matthijs Douze, and Hervé Jégou. Billion-scale similarity search with gpus. *CoRR*, abs/1702.08734, 2017.

- [15] Ira Kemelmacher-Shlizerman, Steven M. Seitz, Daniel Miller, and Evan Brossard. The megaface benchmark: 1 million faces for recognition at scale. *CoRR*, abs/1512.00596, 2015.
- [16] Yury A. Malkov and D. A. Yashunin. Efficient and robust approximate nearest neighbor search using hierarchical navigable small world graphs. *CoRR*, abs/1603.09320, 2016.
- [17] Joyce A. Martin, Brady E. Hamilton, Michelle J.K. Osterman, Anne K. Driscoll, , and Patrick Drake. National vital statistics reports. Technical Report 8, Centers for Disease Control and Prevention, National Center for Health Statistics, National Vital Statistics System, Division of Vital Statistics, November 2018.
- [18] O. M. Parkhi, A. Vedaldi, and A. Zisserman. Deep face recognition. In *British Machine Vision Conference*, 2015.
- [19] P. Jonathon Phillips, Amy N. Yates, Ying Hu, Carina A. Hahn, Eilidh Noyes, Kelsey Jackson, Jacqueline G. Cava-zos, Géraldine Jeckeln, Rajeev Ranjan, Swami Sankaranarayanan, Jun-Cheng Chen, Carlos D. Castillo, Rama Chellappa, David White, and Alice J. O'Toole. Face recognition accuracy of forensic examiners, superrecognitioners, and face recognition algorithms. *Proceedings of the National Academy of Sciences*, 115(24):6171–6176, 2018.
- [20] Florian Schroff, Dmitry Kalenichenko, and James Philbin. Facenet: A unified embedding for face recognition and clustering. *CoRR*, abs/1503.03832, 2015.
- [21] Jeroen Smits and Christiaan Monden. Twinning across the developing world. *PLOS ONE*, 6(9):1–5, 09 2011.
- [22] Yaniv Taigman, Ming Yang, Marc'Aurelio Ranzato, and Lior Wolf. Deepface: Closing the gap to human-level performance in face verification. In *Proceedings of the 2014 IEEE Conference on Computer Vision and Pattern Recognition, CVPR '14*, pages 1701–1708, Washington, DC, USA, 2014. IEEE Computer Society.
- [23] A. Towler, R. I. Kemp, and D White. *Unfamiliar face matching systems in applied settings*. Nova Science, 2017.
- [24] Working Group 3. Ed. M. Werner. *ISO/IEC 19794-5 Information Technology - Biometric Data Interchange Formats - Part 5: Face image data*. JTC1 :: SC37, 2 edition, 2011. <http://webstore.ansi.org>.
- [25] David White, James D. Dunn, Alexandra C. Schmid, and Richard I. Kemp. Error rates in users of automatic face recognition software. *PLoS ONE*, 10:1–14, October 2015.
- [26] Bradford Wing and R. Michael McCabe. Special publication 500-271: American national standard for information systems data format for the interchange of fingerprint, facial, and other biometric information part 1. Technical report, NIST, September 2015. ANSI/NIST ITL 1-2015.
- [27] Andreas Wolf. Portrait quality - (reference facial images for mrtd). Technical report, ICAO, April 2018.
- [28] D. Yadav, N. Kohli, P. Pandey, R. Singh, M. Vatsa, and A. Noore. Effect of illicit drug abuse on face recognition. In *2016 IEEE Winter Conference on Applications of Computer Vision (WACV)*, pages 1–7, Los Alamitos, CA, USA, mar 2016. IEEE Computer Society.